AGARD-LS-43-71

AGARD

ADVISORY GROUP FOR AEROSPACE RESEARCH & DEVELOPMENT

7 RUE ANCELLE 92 NEUILLY SUR SEINE FRANCE

LECTURE SERIES No. 43

on

Assessment of Lift Augmentation Devices

NORTH ATLANTIC TREATY ORGANIZATION

DISCLAIMER NOTICE

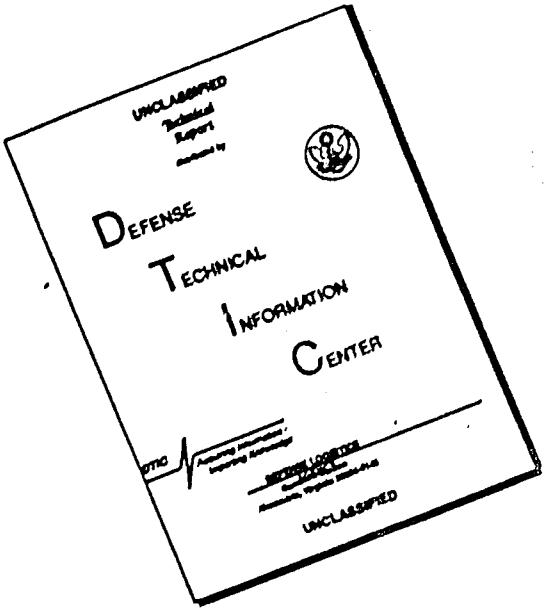

THIS DOCUMENT IS BEST QUALITY AVAILABLE. THE COPY FURNISHED TO DTIC CONTAINED A SIGNIFICANT NUMBER OF PAGES WHICH DO NOT REPRODUCE LEGIBLY.

Lecture Series 43

NORTH ATLANTIC TREATY ORGANIZATION

ADVISORY GROUP FOR AEROSPACE RESEARCH AND DEVELOPMENT

(ORGANISATION DU TRAITE DE L'ATLANTIQUE NORD)

ASSESSMENT OF LIFT AUGMENTATION DEVICES

These Papers were presented at a Lecture Series jointly sponsored by AGARD and the von Kármán Institute, held at the Institute, Rhode-Saint-Genèse, Belgium, April 20-24, 1970

Published February 1971

629.7.075:533.6.013.13

Printed by Technical Editing and Reproduction Ltd
Harford House, 7-9 Charlotte St. London, W1P 1HD

FOREWORD

This publication contains edited versions of the lecture notes and complementary discussions from the AGARD – VKI Lecture Series on "Assessment of Lift Augmentation Devices", at the von Kármán Institute for Fluid Dynamics during the week 20-24 April 1970.

The lecture series was designed to provide an up-to-date account of special aerodynamic problems and applications of lift-augmentation devices; including appraisals of the present state of knowledge, novel aerodynamic advances, experimental and theoretical treatments, applications for transport and combat aircraft, important areas for research and development. It was primarily intended for aeronautical engineers with a need to acquire a more adequate background on lift-augmentation devices. But short discussions were held after most of the lectures, together with a final Discussion Seminar, to take advantage of participants with specialised knowledge as appropriate.

The Course was well supported as regards both the number of attendees (about 100) and their technical quality. The organisation was carried out under the auspices and with the support of AGARD, in collaboration with the von Kármán Institute who had the responsibility for the general administration and local organisation.

A special tribute must be paid to the lecture staff, for the quality of their presentations, the valuable analysis contained in their lecture notes provided for distribution during the Course, and their cooperative participation in discussions. Our thanks also go to the official and private organisations through whose courtesy it was possible to offer such technical experts as lecturers.

Paul E.Colin
Associate Director,
von Kármán Institute, Brussels.

John Williams
Aerodynamics Department,
Royal Aircraft Establishment, UK.

The Course Directors and Editors

September, 1970

CONTENTS

	Page
FOREWORD by J.Williams and P.E.Colin (Editors)	iii
	Reference
AERODYNAMICS OF MECHANICAL HIGH-LIFT DEVICES by D.M.McRae (UK)	1
AERODYNAMICS OF PNEUMATIC HIGH-LIFT DEVICES by J.von der Decken (Germany)	2
AERODYNAMICS OF VARIABLE SWEEP by Ph.Poisson-Quinton (France)	3
FUNDAMENTAL ASPECTS OF FLOW SEPARATION UNDER HIGH-LIFT CONDITIONS by H.P.Horton (VKI)	4
SOME NOTES ON TWO-DIMENSIONAL HIGH-LIFT TESTS IN WIND-TUNNELS by B.van den Berg (Netherlands)	5
MODEL TESTING REQUIREMENTS AND TECHNIQUES FOR HIGH-LIFT SCHEMES; THREE-DIMENSIONAL ASPECTS by C.Russell (UK)	6
ANALYSIS OF TRANSPORT APPLICATIONS FOR HIGH-LIFT SCHEMES by L.B.Gratzer (USA)	7
ANALYSIS OF COMBAT AIRCRAFT APPLICATIONS FOR LIFT-AUGMENTATION DEVICES by R.Taisseire (France)	8
FLIGHT TESTING MILITARY TRANSPORT AIRCRAFT FOR CLEARANCE IN THE STOL ROLE by K.P.Eyre (UK)	9
LIFT-AUGMENTATION DEVICES AND THEIR EFFECT ON THE ENGINE by J.A.Hooper, E.A.White and H.C.Hillier (UK)	10
OPTIMISING THE PROPULSIVE/LIFT SYSTEM FOR TURBOFAN STOL AIRCRAFT CONSIDERING COST EFFECTIVENESS by H.T.Bowling (USA)	11
SEMINAR CONTRIBUTIONS	
A NEW TECHNIQUE FOR AEROFOIL LEADING-EDGE STUDIES by J.Monnerie (France)	12
SOME COMMENTS ON CHARACTERISTICS OF HIGH-LIFT WINGS by D.N.Foster (UK)	13
THE HUNTING H.126 JET-FLAP RESEARCH AIRCRAFT by K.D.Harris (UK)	14
AERODYNAMIC RESEARCH ON HIGH-LIFT SYSTEMS by F.Mavriplis (Canada)	15

AERODYNAMICS OF MECHANICAL HIGH-LIFT DEVICES

by

D.M.McRae

Aerodynamics Dept, Hawker Siddeley Aviation Ltd
Hatfield, UK

SUMMARY

The empirical correlations used in the estimation of maximum lift of single aerofoils are described and the use of pressure distribution calculations to augment these correlations is discussed. Examples are given of Reynolds Number and Mach Number on maximum lift at low Mach Number.

The use of such correlations is extended to flapped aerofoils by use of a simple method involving plotting maximum lift against lift increment due to flap at zero incidence. This is shown to follow logically from a description of the flow field and its effect on the boundary layer. Empirical correlation for the estimation of the lift increment ΔC_L to flap at constant incidence is shown.

Comments are made on the effect of various leading-edge devices especially fixed leading-edge shape modifications and Handley Page slats. Examples are given of adverse interaction between leading-edge slats and trailing-edge flaps.

Mechanical details of flap support systems are described and the considerations involved in the best choice for various applications are discussed.

Drag estimation at high lift is discussed and attention drawn to the increasing difficulty of this problem, as lift is increased.

Finally the development of satisfactory stalling behaviour in three dimensions, including the use of fences and spoilers is described.

NOTATION

C_L		lift coefficient
ΔC_L		increment in C_L due to flap at constant α, usually $\alpha = 0$
$C_{L\,max}$		lift coefficient at stall
$\Delta C_{L\,max}$		increment in $C_{L\,max}$ due to high-lift device
C_p		pressure coefficient
C_μ		momentum coefficient of "blowing" air
$C_{\mu\,crit}$		minimum C_μ for attached flow
A		aspect-ratio
$a_{0\,T}$		wing-lift curve slope in two-dimensional potential flow
$a_{2\,0\,T}$		flap-lift curve slope in two-dimensional potential flow
b/2		semi-span
c or c_w		chord with devices retracted
c_f		flap chord
E	=	c_f/c
H		total head in boundary-layer
H_0		free-stream total head
h		distance from surface
M		Mach number
p_0		free-stream static pressure
Re		Reynolds number
t		aerofoil maximum thickness
$y_{5\,u}/c$		aerofoil upper-surface ordinate at 5% chord
α		angle of incidence measured to datum chord of section with devices closed
δ		flap angle
$\Lambda_{H\,L}$		sweep-back angle of Hinge Line
$\Lambda_{c/4}$		sweep-back angle of Quarter-Chord Line
λ		defined in text
κ		defined in text
ψ		defined in text
′ (prime)		refers to quantities defined using chord
″ (double prime)		or area with devices extended (omitted when sense is obvious)

AERODYNAMICS OF MECHANICAL HIGH-LIFT DEVICES

D.M.McRae

1. INTRODUCTION

The purpose of this lecture is to describe in fairly general terms the stalling of conventional aerofoils and the effects of mechanical high-lift devices thereon. The factors affecting maximum lift coefficient are discussed in the context of estimation methods. Drag is also discussed.

2. SIMPLE AEROFOILS

Various empirical correlations of maximum lift coefficient of aerofoils have been made in the past. The classic works of this nature centred on the era 1936 to 1946, a time when the calculation of potential flow pressure distributions was not generally possible for "the average aerodynamicist". At the end of this period the potential flow pressure distributions were however available for the NACA aerofoils, tests of which formed the main part of the empirical data. Nevertheless the most successful correlations were in terms of simple geometric parameters rather than in terms of pressure distributions. Some of the most significant of these empirical analyses are those of References 1 and 2.

Dating from about 10 years later, Reference 3 by Gault gives a classification of the three main classes of stalling behaviour which, for conventional aerofoils, has not been improved upon. The omission of any mention of Mach number, even though all the data is probably for Mach number less than about 0.18, is a feature which may be regretted.

These correlations were based almost entirely on data measured on the NACA digit, 5 digit and 6 series aerofoils, these aerofoils providing then the only large body of high Reynolds number data. Whilst computerised pressure distribution methods, both "forward" and "inverse" have now enabled design aerodynamicists to depart from these families of aerofoils, there has been no corresponding expansion in published high Reynolds number data. The coming of computerised boundary-layer calculations might be expected to improve the situation by releasing us from this straight jacket of geometric correlations: however, though attempts had undoubtedly been made I am unable to report any improved method of estimation based thereon.

The general availability of the pressure distribution method has contributed, however, to the improvement of maximum lift, particularly by the use of leading-edge modifications. It must be pointed out that this application has largely been to aerofoils basically designed to a combination of structural and cruise considerations, that is to sections of somewhat limited overall camber such as are common on high subsonic aircraft.

Thus, the methods available to us for determination of maximum lift of clean aerofoils can be summarised in Figure 1. This is presentation of the test results published by Abbott and Von Doenhoff[4]. Figure 1 in fact uses the data for a Reynolds number of 6×10^6, in order to be comparable with another Figure to be presented later: a very similar diagram would be produced by using the 9×10^6 Reynolds number data.

The steeply sloping left-hand part of the diagram corresponds to rather sudden stalls, described in Reference 3 as being associated with separation near the leading-edge. When dealing with some new aerofoil likely to fall in this class, one could attempt to ensure that it lay near the top of the scatter band by using the calculation of pressure distribution to ensure that some lack of smoothness of other peculiarity of design did not cause an unnecessarily high peak of negative pressure.

It should be noted that in some respects the USAF handbook[1] on the one hand, and on the other hand the British Royal Aeronautical Society Data sheets[2] and Figure 1, can give conflicting results for some types of departure from the standard families of thickness distribution. For instance, blunting of the leading-edge causes a modest reduction of $C_{L\,max}$ according to the USAF handbook, based as it is on the increase in thickness between 6% and 15% whereas the others would predict a fairly dramatic improvement, being based on the ordinate at 5% chord, one using thickness and the other upper surface.

There is probably inadequate test data published to resolve which is correct. The present author can only recommend recourse to calculated pressure distributions to suggest which is the more likely effect in any particular

case under investigation. But this is still not proof. It is to be remarked that Reference 3 is based on yet another criterion, the upper surface ordinate at 1.25%.

The apparently more scattered right-hand part of the diagram (Fig.1) corresponds to cases with progressive separation from the trailing-edge, and can be sorted out by labelling the points with thickness-chord ratio and some camber parameter such as "design" lift coefficient. The use of "design" lift coefficient is however likely to be misleading if the camber line of the aerofoil for which one is trying to produce an estimate is not of the same family as those of the test data.

We must now come to the effect of Reynolds number. Figure 17 shows the results of varying tunnel speed in an atmospheric tunnel, on a number of swept wing half-models of 20 inches chord. The low slope region on the left corresponds to "thin aerofoil" stalls, the so called "long bubble" case. The steep rise corresponds to sudden leading-edge stalls, that is of bursting short bubbles.

The low slope region on the right does not necessarily correspond, however, to progressive trailing-edge stall; in some cases at least, the onset of Mach number effects is thought to be involved. Certainly Mach number effects can extend down to quite low Mach numbers. Figure 15 shows flight results on an aircraft in the clean configuration; these results show no sign of the variation of $C_{l\,max}$ with Mach number stopping in the range covered.

The value of $\delta C_{l\,max}/\delta M = 1.5$ shown in Figure 15 is not untypical though rather higher values are sometimes found, and of course, in case where the stall is of the thin aerofoil type, the effect of Mach number is small.

It will be seen from the preceding that the state of estimation methods for clean aerofoils is still somewhat unsatisfactory and not much better than 20 years ago. However, the work on pressure distribution methods and boundary-layer methods, where considerable progress has been made in the last 10 years, may be expected to lead to improvement ultimately, and can already be used to indicate whether relatively small changes are good or bad.

3. TRAILING-EDGE DEVICES

After the somewhat dismal situation on the estimation of $C_{L\,max}$ on clean aerofoils, we will start this section with a rather startling assertion that trailing-edge devices, at least at large angular settings such as those used for landing, make the estimation of $C_{L\,max}$ easier than for the clean aerofoil.

Figure 2 shows an analysis of all the 60° split-flap data given in Reference 4. The choice of ordinate will be explained later, but the improvement in correlation with the single parameter $y_{s\,u}/c$ compared with Figure 1 is immediately apparent. It will also be noted that the majority of the aerofoils fall on the steeply sloping part of the diagram. This sensitivity to leading-edge geometry is, in the case of clean aerofoils, generally typical of stalls involving separation from close to the leading-edge.

Examination of the shape of the lift-curve peak in the flapped cases fails to reveal any that are typical of trailing-edge stalls as categorised in Reference 3. In particular, the aerofoils in that band $3½\% > y_{s\,u}/C < 5½\%$ have much sharper peaks in the flapped cases than in the clean cases, and may be presumed to have changed from a trailing-edge type stall when clean, to a leading-edge type stall when flapped. It has to be admitted that the three aerofoils on the extreme right have moderately sharp peaks when flapped. This is slightly surprising in view of the lack of sensitivity of $C_{L\,max}$ to leading-edge geometry as between these three aerofoils which are NACA 4415, 4418 and 4424.

The fact that almost all the aerofoils in Figure 2 have stalls which are dominated by the leading-edge characteristics forms the justification of the choice of ordinate. This sensitivity suggests that the load carried near the leading-edge is an important feature. Thin aerofoil theory shows that, in two-dimensional flow, for vanishingly small values of $E = c_f/c$, the load carried across the leading-edge is the same for an unflapped aerofoil at a value of C_L and for a flapped aerofoil when $(C_L - ½\Delta C_L)$ has the same value; where ΔC_L is the increment of C_L at constant incidence due to flap rotation. The factor of ½ decreases for increasing values of E, but not very much in the usual working range. Of course, as the flap is in all cases in Figure 2 a split flap of $E = 0.2$ at 60°, there is not much variation in ΔC_L; the values lie mostly between 1.2 and 1.5. The use of this ordinate is thus not fundamental to obtaining a reasonable correlation for one particular flap configuration.

Figure 3 shows the envelope of Figures 1 and 2 superimposed. It will be seen that, for the regions where the stall is leading-edge dominated, i.e. where the slope against $y_{s\,u}/c$ is high and positive, this concept of leading-edge loading has gone a long way towards forcing the flapped data to correlate with the unflapped data. The difference in $(C_{l\,max} - ½\Delta C_L)$ is only between zero and 0.3. We will see later, when we consider the pressure distributions and their effects on the boundary-layer, that it is not unreasonable that even in leading-edge dominated cases the flapped aerofoil should show a greater benefit than $½\Delta C_L$ over the unflapped. This is because the flap has also reduced the subsequent adverse gradient. It might also be postulated that this effect would be expected to be reduced in cases where $C_{l\,max}$ has become sensitive to Mach number; since in that case it is to be supposed that the value of C_p min, that is its relation to C_p for $M_L = 1$, would be of significance; whereas in the other situation it is the pressure gradient which is important in determining boundary-layer separation.

When assessing the $C_{L\,max}$ of clean wings it is fairly common practice to carry out spanwise load distribution calculations and then to compare the sectional $C_{l\,max}$ available at the various positions across the span with the C_l demanded by the spanwise load distribution. The use of this procedure on wings with part-span flaps is not very meaningful, as, at a section just beyond the end of the flap the C_l demanded will commonly be greater than two-dimensional unflapped data would suggest is likely to be available.

The author proposes to ignore this difficulty for the moment, and to show that quite often good correlation can thereby be obtained. If for $y_{su}/c < 3\frac{1}{2}\%$, Figure 3 had shown a perfect collapse of the flapped data onto the unflapped, then in finite aspect-ratio cases, at any rate for full-span flaps, one might expect $\delta C_{l\,max}/\delta C_L$ to equal $\frac{1}{2}(A + 2)/A$. This results directly from the independence of $C_{l\,max}$ from variation of aspect-ratio and the dependence of lift curve slope, both $a_1 = \partial C_L/\partial\alpha$ and $a_2 = \partial C_L/\partial\delta_F$ on aspect-ratio, approximately as $A/(A + 2)$. The independence of $C_{l\,max}$ from aspect-ratio is of course restricted to cases where aspect-ratio is greater than about 4 and leading-edge sweep is not excessive. That is, restricted to cases where neither leading-edge separation vortices, nor tip-edge separation vortices, contribute any appreciable extra lift.

We will now compare this proposition with a number of test results and it will be seen that it fits the test data no less well in the case of part-span flaps than for full-span flaps. Some data is shown for cases with leading-edge slats. Whether wings with slats stall in a leading-edge dominated fashion, or what the parameters are which determine this, we will not discuss at this stage.

Figure 4 shows a collection of four finite aspect-ratio wings. Of these, the one clean leading-edge of $y_{su}/c \approx 4\%$ fits $\frac{1}{2}(A + 2)/A$ very well, in spite of having only part-span flaps. The other clean leading-edge has a y_{su}/c of about 5¼ and displays a slope of rather over unity (about 1.07). The correlation is all the more remarkable when it is realised that both of these cases include a point for which ΔC_L has collapsed owing to excessive flap angle. The Reynolds number in these two cases is between 1 and 1.4×10^6.

The curve at the top left is something of a rogue for which the author can offer no explanation.

Figure 5 shows the corresponding plotting for a full-span blown flap. The example again includes cases of both separated flow on the flaps and of attached flow on the flaps. Correcting the lift for the direct jet momentum produces only a very small improvement in the already good correlation. This shows that a blown flap is "just another flap". The blow serves to improve ΔC_L due to flap, but the effect on $C_{L\,max}$ is practically no different from that due to any other flap that produces the same ΔC_L. Of course, there may not be any other such flap; hence the advantage of the blown flap.

Figure 7 shows another case, this time with a leading-edge slat. In this example the slope is rather lower than $\frac{1}{2}(A + 2)/A$. This has been observed on other occasions on slotted wings. It is suggested that this might be associated with a growth in the slat wake between the C_L at which ΔC_L is determined and $C_{L\,max}$ causing in effect a decrease in ΔC_L as incidence is increased. It is also to be noted that the full-span flap case does slightly less well than the part-span cases.

From the preceding description we can postulate the general shape of relation between $C_{L\,max}$ and $\Delta C_l(\alpha = 0)$. We can also postulate the steps which must be gone through in order to estimate $C_{L\,max}$ of a flapped wing. See Table IV (Fig.19). Figure 20 shows this diagramatically. It should be noted that, whilst Figures 1 and 2 give some sort of correlation of $C_{L\,max}$ and the notional leading-edge stall $C_{l\,max}$, it is not suggested by the author that these figures should be used if any other data on more closely related configurations is available. It is also desirable to use theoretical pressure distribution calculations to determine whether the section in question is likely to be near the top edge of the scatter band.

The procedure outlined in Table IV (Fig.19) will seem to lead to the possibility of $C_{L\,max}$ vs C_l diagrams with a distinct bend partway through the flap angle range. The examples so far shown do not obviously reveal such a case, but Figure 18 does show a case which seems might fall into this category. Having postulated from the observed behaviour of the $C_{L\,max}$ vs C_L plots that there are two distinct modes of operation, we will now see how this deduction is supported by considerations of boundary-layer behaviour and observed pressure distributions.

Figure 6 shows a typical pressure distribution measured in a low-speed wind-tunnel at a lift coefficient a little below the maximum. It is in fact on a wing with a leading-edge slat.

The upper-surface pressure distribution is typical, characterised by a high suction peak near the leading-edge followed by a rapid pressure rise. Without a slat these features would be even more marked. Without a flap and without an incipient trailing-edge stall, this pressure rise would end at the trailing-edge with a pressure coefficient of about +0.1 to +0.2. The flap, in this case at 40% causes the trailing-edge pressure on the main element to be more negative by about $\Delta C_p \approx 1.0$.

If pressure distributions with and without flap are compared, not at constant incidence but at constant leading-edge peak heigh, then, and can also be shown by theoretical pressure distribution calculation there is not much effect on pressure gradient immediately behind the leading-edge peak, but the pressure gradient further back is considerably reduced thereby reducing the tendency to progressive boundary-layer separation from the trailing-edge.

Thus in cases without trailing-edge stall, the effect of flap may be expected to follow roughly the "constant leading-edge load" criterion, but if the stall without flap was progressive from the trailing-edge a larger improvement may be expected.

Thus we can summarise the effect of the flap:

(a) By producing an increment of lift at constant incidence compared with the unflapped case, an increment of lift of about half this amount is produced when the loading and tendency to separate near the leading-edge is the same in the two cases.

(b) If without flap there is a separation associated with the pressure gradient on the rear part of the aerofoil, then by producing a local suction at the rear of the main element, and hence less adverse pressure gradients, the flap may delay or eliminate the trailing-edge stall.

The function under heading (a) is common to all types of trailing-edge flap, but the aerodynamic means of producing function (b) differs according to the type of flap and is tabulated in Figure 8. I have in this Table gone outside the terms of reference of this lecture and included blown and jet flaps. I have felt it desirable to do this since the overall programme for the week might at first sight, by separating them into separate lectures, give the impression that they have little in common with "mechanical" flaps. I think that the similarities in their effect of the main wing cannot be over emphasised.

The various types of flap also differ in the way the main aerofoil boundary layer passes downstream from the flap knuckle. These differences are tabulated in Figure 9. These differences will of course lead to differing ΔC_L vs flap angle relations.

The estimation of ΔC_L is a subject on which a fair amount of empirical analysis has been done over the years. One method used by the author is due to D.H.Wilkinson and takes the form:

$$\psi'' = \frac{\Delta C_L''(\alpha = 0)(A'' + 2)}{(1 + t/c'')A''\lambda''\kappa \cos \Lambda_{HL}},$$

where the double prime signifies the use of chords and areas which include the extension due to leading and trailing-edge devices and ΔC_L is the lift increment due to the extending and deflecting the trailing-edge device. κ is part-span factor taken from Royal Aeronautical Society Data Sheets[2]. λ is the potential flow value of $a_{2D T}/a_{0T}$ for a thin aerofoil from the same source. Λ_{HL} is the sweep angle of the flap hinge line. A is the Aspect-Ratio. $(1 + t/c'')$ is an approximation to the effect of thickness on the potential flow lift curve slope.

Thus ψ'' is the lift curve of a hypothetical full-chord flap on a thin aerofoil in two dimensions but with the boundary-layer effects of the actual case. In the absence of such effects, the slope of ψ'' against flap angle would be expected to be 2π. Figure 10 shows such a ψ'' flow obtained for a Fowler flap. No doubt each worker in high lift has his favoured set of such curves, or their equivalent, for each type of flap with which he is concerned. One has more confidence in using such a method for scaling for small changes from a closely related case, so the author has not here attempted to produce a completely general correlation and has only shown one typical such curve. For those without data on "Closely Related" cases, there are curves in both USAF handbook and the RAeS data sheets which can be used for the same purpose though they are presented in slightly transformed fashions.

The index of the cosine term is entirely empirical and would differ according to whether the flap angle used is a rotation of the flap about a swept axis or is the angle in a line-of-flight section. The value of unity is slightly surprising on theoretical grounds.

All that is claimed is that it seems to work better than a value of 2 for flaps with attached flow.

A word of warning must be inserted here on the subject of $\Delta C_{L\,max}$ due to flaps. Firstly, for plain flaps with separated flow, some analyses show less benefit for large values of c_F/c than the theoretical C_L benefits would suggest. Figure 21 compares these. Secondly other analyses of the effect of sweep on $\Delta C_{L\,max}$ due to flap have given, for various types of flap, losses worse than $\cos^3 \Delta c/4$ compared with $\cos \Lambda_{HL}$ suggested above. The author's data does not extend over a sufficiently wide range of sweep to be conclusive, but have not so far suggested such severe losses.

Returning to the ψ'' plot of Figure 10 for an attached flow flap, the slope of ψ'' versus flap angle is markedly less than 2π. Contributions to the deficit are presumably:

(a) Nonlinear effects in potential flow; whilst these may be appreciable on multi-slotted flaps achieving attached flow with about 90° deflection on the last element (as on the Breguet 941) and on blown flaps with angles of about 60° and over, such effects are not important at $\alpha = 0°$ and $\delta = 40°$.

(b) The potential flow effects of the flow through the various slots.

(c) Boundary layer and wake displacement thickness effects.

Figure 11 shows some total-head profiles measured on a wing with a slat and a Fowler flap. These are measured on the same models as Figure 6. The highest incidence shown is just before the stall and is the same as that for Figure 6. At mid flap chord the wake from the main element is still fairly separate from the flap boundary layer. However, the slat wake appears to be well mixed with the main aerofoil boundary layer before the shroud point is reached. Just before the stall there is a very large thickening of this combined slat wake and main aerofoil boundary layer, although as far as it was possible to judge the flow was still unseparated.

The thinness of the flap boundary layer shown (or rather not shown as the experiment has failed to measure it) in Figure 11 makes it seem unlikely that the displacement thickness of this boundary layer is the sole reason for the ψ'' slope being less than 2π. The flow through the slots will cause some loss of this slope in a potential flow situation, but the thickening of the wake of the main element (and slat in the case illustrated) is likely to be the main cause. Hence, a method of calculating this wake flow is needed in any attempt to calculate flap characteristics from a combination of potential flow and boundary-layer calculations.

3. LEADING-EDGE DEVICES

Tabulated in Figure 23 are the principle types of leading-edge device. They have been separated into three groups. Group 1 functions by modifying the pressure distribution. Group 2 by improving the state of the boundary layer without much effect on the pressure distribution, and Group 3 by both means.

We will now comment on each of these in turn.

3.1 Leading-Edge Flaps

A chart for the effect of leading-edge flaps is given in the USAF handbook[1] based on a premise that the increment $C_{L\,max}$ is determined by the pressure distribution close to the leading-edge: this of course is rather similar to the present author's suggestions for the effect of trailing-edge flaps on aerofoils which are not too thick. The chart is presented together with a suggestion that it should be used for nose flap angles not exceeding 25°. At some angle typically of this order, the suction near the knuckle and the subsequent pressure recovery will take over the production of the separation. Whilst the value quoted is in close agreement with the lecturer's experience, it is to be expected that the knuckle radius will be a factor in determining the maximum useful angle. Reynolds number is also a factor; whilst 25° is probably about the best angle at high Reynolds number, model tests at about 10^6 Re, often indicate about 35° as being the best angle, therby giving a falsely optimistic increment in $C_{l\,max}$. It is also necessary to call attention to the mechanical difficulties of manufacturing a smooth knuckle, and the combination of such irregularities, gaps and leaks will often lead to a significant reduction in the increment in $C_{l\,max}$. It should also be noted that at thickness-chord ratio of about 13% and above, it becomes very difficult to produce a geometry which looks attractive, and presumably at these thicknesses there can be little gain in $C_{l\,max}$.

3.2 Fixed Leading-Edge Droop

The effect of fixed leading-edge droop can be assessed by a similar concept. This is by calculation of pressure distributions with and without the modification and then finding the increase in C_l to give the same peak suction value near the leading-edge. It has been common practice in the UK to use a peak suction of $C_p = -10$ for such calculations, as suggested by the late Miss Bradfield of the Royal Aircraft Establishment, Farnborough. However, it seems to be necessary to scale down the calculated improvement in $C_{l\,max}$ by a factor typically between 0.5 and 1.0. Such calculation requiring detailed knowledge of the sections is rather inconvenient for early project assessment. A cruder form of assessment would be to use the y_{su}/c correlation presented at the beginning of the lecture, but this does not really help much, since the question immediately arises of how large a modification is acceptable and only detailed calculations will show up what the limit is.

At this point, whilst we are discussing pressure distributions, it is appropriate to call attention to what may well be a limitation to most if not all the suggested methods of evaluating $C_{l\,max}$. This restriction is that they are arrived at from experience on aerofoils which in general have been designed with some degree of restriction in thickness and camber due to considerations of high-speed flight: if not from Mach number considerations, then at least due to structural considerations. It seems quite possible that, if an aerofoil was designed solely for maximum lift in the clean configuration, the subsequent effect of high-lift devices may not follow the description very closely. Put another way, the experience is based on aerofoils which have either leading-edge or trailing-edge stalls. Whilst Reference 3 has a further category termed "combined" stall of which the prime example is NACA 23012, a section of moderate thickness and rather low camber, it is reasonable to suppose such aerofoils are included. However, it seems possible there might be aerofoils perhaps of high camber and low thickness which might give very good values of $C_{L\,max}$ for which, owing to a total lack of data, no such assurance can be given.

Returning to the question of the factor typically of 0.5 for $C_{l\,max}/(C_l$ for $C_p = -10)$, it must be pointed out that tests at low Reynolds number may give wildly optimistic results for this factor. Figure 17 shows the variation of $C_{L\,max}$ with Reynolds Number for an aerofoil with a series of leading-edge modifications. The tests are in an atmospheric tunnel and wind speed is changed to obtain the variation of Reynolds Number: thus Mach Number

is also varying and may be starting to affect the results at the right-hand side of the diagram. It will be seen that, where the values of $C_{l\,max}$ are rising very steeply there are very large differences between the various cases, but at the right-hand edge the differences appear to be settling down to much more modest values. This is presumably due to changes in the distance between the stagnation point and the laminar separation point differing; the larger values, resulting from the larger values of leading-edge radius, causing the steep part of the curve to be at lower values of Re, based on chord.

3.3 Krueger Flap

Whilst very crude generalisations may be possible, there are many detailed variables, such as the leading-edge radius of the flap, the curvature between there and the basic nose, and the fit and leaks between the flap and the main aerofoil, these variables seem likely to have a profound effect on the $C_{L\,max}$. The lecturer would be generally unhappy to rely on anything other than model tests conducted, at adequate Reynolds Number, on an adequately detailed representation including the leaks.

3.4 Slat Without Slot

Since, as with the leading-edge flap, the leading-edge geometry of the device is the same as the leading-edge geometry of the basic aerofoil, this device can be expected to correlate in the same way as the leading-edge flap. There will be a different set of irregularities at the knuckle, but some evidence exists to suggest that the limiting useful angles are similar.

3.5 Tangential Blowing and Boundary-Layer Suction

These topics will be left to the lecturer on Pneumatic Devices.

3.6 "Letter Box" Slot

Only a very limited amount of data is thought to be available in NACA work from the early 1930 era. Reference 5 is typical and shows a value of $C_{l\,max}$ of about 0.47 at a rather low Reynolds Number (0.6×10^6). As mentioned in section 3.8, I would guess this may well reduce to about 0.3 at full scale. Different basic sections may well give different results.

3.7 Vortex Generators

The lecturer has included this item for completeness but is unaware of any data.

3.8 Handley-Page Slat

Figure 25 shows some typical results for the $\Delta C_{L\,max}$ due to slats. These results of course depend on spending a considerable effort on optimising the "cut line profile", gap, overlap and rotation angle. The Reynolds Number of these results is low. There are some indications that at full scale the effect may well be rather less. Put another way, there are indications that there is rather less scale effect with slats than on plain aerofoils. It is not clear why this should be so.

It is common practice to think of slats in terms of the slot rejuvenating the boundary layer. The author considers that this approach is not very helpful in understanding the features that are involved in optimising the configuration. Figure 11 shows some total-head surveys carried out on a wing with a slat; it shows that the slat wake has passed fairly far back before becoming mixed with the main element boundary layer. To that extent, keeping the slat (that is the leading-edge) boundary layer out of the main element boundary layer has helped the state of the latter. However, there are additional benefits and these may be seen in Figure 12 which tabulates the features that effect the pressure distribution. It will be realised that for optimum performance a balance must be struck between items 1 and 3 to get optimum rotation; also the correct balance between items 3 and 4 on the one hand and the need to keep the slat wake separate from the main element boundary layer until far enough downstream will determine the correct gap.

As will be explained in the section on interaction between leading and trailing-edge devices there is a reduction of $\Delta C_{L\,max}$ due to slat with flaps down; or rather, as Figure 25 is for flaps down cases, an improvement flaps up.

Just as with leading-edge flaps attention must be paid to mechanical details, such as the step in the upper surface step where the slat trailing-edge stows, and also in this case the various supports between the slat and the main element.

3.9 Krueger Slat

As there are more variables available to the designer, there is the possibility of producing a better performance than with the orthodox slat. For a given front spar position, a larger area extension can be obtained especially if a

folding knuckle is used. The leading-edge radius may be made larger than that of the basic aerofoil. These features are perhaps offset by a too flat profile of the part forming the lower surface of the basic aerofoil. In the case of the flexible device used by Boeing on the 747, this area can also be optimised.

3.10 Combined Leading-Edge Flap and Vortex Generators

There is only one known example of this ad hoc combination (on the Hawker Siddeley Trident 1): the vortex generators retract for cruising flight. Obviously any such ad hoc combination would have to be the subject of a detailed model investigation before committing a project to using it.

4. INTERACTION BETWEEN LEADING AND TRAILING-EDGE DEVICES

The examples given of the $C_{l\,max}$ vs C_l relation in the presence of slats (two in Figure 4 and all of Figure 7) show a variety of slopes. Whilst the top-left curve in Figure 4 seems to be a complete rogue for which the author has no explanation, the other slotted case on that figure looks as though it may fall into the category of trailing-edge stall changing to leading-edge stall part-way up. The case in Figure 7 is clearly of the leading-edge limited type. With slats extended, this could just as well be a stall near the upper surface discontinuity as on the slat. The slope, only 80% of the $\frac{1}{2}(A'' + 2)/(A'')$ value, is about the lowest the lecturer has come across.

It seems likely that this relatively poor performance is associated with the gross thickening of the combined slat and main element wake passing over the flap. Figure 11 seems to give some indication of this, though a traverse further aft would have been more definitive. This thickening would reduce the $\Delta C_l''$ due to flap as when the stall is approached, whereas the $\Delta C_L''$ plotted is either that at zero incidence or sometimes that obtained by extrapolating the linear part of the C_L vs α curve back to $\alpha = 0°$. An alternative statement of exactly the same effect is that made in the section on slats, that the increment in $C_{l\,max}$ due to adding a slat is commonly less with flaps extended than with flaps retracted. It seems likely that the use of larger gaps, especially the flap gap may well alleviate this loss, but would at the same time restrict the maximum usable flap angle by reducing the action listed number 3 in Figure 12 when applied to the main element and the flap, thereby worsening the state of the flap boundary layer.

In making an estimate it is of course important not to include this effect twice. The estimator must make up his mind whether he is going to reduce the $\Delta C_{L\,max}$ due to flap in the presence of the slat, or to reduce the $\Delta C_{L\,max}$ due to the slat in the presence of the flap. In practice it is often convenient to follow the sequence of opening of the devices in deciding which way to choose. It is rare to deploy the trailing-edge devices before the leading-edge devices: therefore it is recommended to regard the effect as one of the slat causing a loss of flap effectiveness.

The construction of the $C_{L\,max}$ vs C_L for a slotted wing will pose the problem of whether, slat-open the stall is a leading-edge stall or a trailing-edge stall, and if the latter, what the hypothetical $C_{l\,max}$ for a leading-edge stall would be. At this stage, one must have recourse to model tests and thus one can really only scale between closely related configurations.

Figure 13 shows some data which at first sight contradicts the general trend of adverse interaction between slats and flaps; the $\Delta C_{L\,max}$ due to slat is marginally greater flaps down than flaps up. The only obvious indication of any interaction is the slightly more rounded lift curve peak. However, when this data is replotted as in Figure 14 with lift coefficients based on the appropriate extended area and with the incidences reduced by the appropriate $57.3\,C_L/\pi A$, to remove approximately the effect of varying finite aspect-ratio, it becomes more obvious that there is adverse interaction. First, the flap in the absence of the slat has caused a loss of lift slope, even though as is to be expected there is less rounding of the peak of the curve. Secondly, the rounding of the peak (caused by the slat) of 2½° departure from the straight line is doubled in the case of slat and flap combined.

5. MECHANICAL DETAILS

The effect of mechanical imperfections on the effectiveness of leading-edge flaps and slats has been mentioned in the appropriate sections, as has the effect of slat tracks and jacks.

Slotted flaps, including multi-slotted and Fowler types can be supported in a number of ways. Some of these methods interrupt the upper surface of the flap, some principally the leading-edge of the flap, and some the lower surface only. Broadly speaking, interruptions in the leading-edge or upper surface may be expected to cause local separations and hence loss of lift at any substantial flap angle. Associated with this loss of lift will be a drag penalty but, if take-off flap angles are small, this may not be very serious. The choice of support scheme must of course be a "trade-off" exercise between cruise drag, flap performance and weight. The principal schemes are listed: tracked schemes may of course give circular movement or non-circular according to choice. The comments are made in the context of conventional transport aircraft.

(a) **Simple Hinge on Under Wing Brackets**

This is used on the DC9 and on the H.S.125. This is attractive because of its mechanical simplicity and is light in weight. If the flap travels are not large, the cruise drag is fairly small. However, it becomes much less attractive at Mach numbers of about 0.8 and over. The higher sweeps of the flap hinge line combine with difficulty the making the bracket t/c ratio sufficiently low, and made it difficult to avoid excessive drag due to local Mach number problems.

(b) **Swinging Links**

These are used on the DC4, 6, 7 series. It may well be even lighter than the simple hinge so far as the mechanism is concerned, but it interrupts the flap upper surface and leading-edge, probably leading to aerodynamic losses and possibly some weight penalty in the flap structure. However, as the motion is normal to hinge line, large flap travels at high sweeps will cause difficulties with fairing alignment and hence cruise drag.

(c) **Underwing Tracks**

These can leave the flap leading-edge and upper surface uninterrupted. At high sweep-back angles, line-of-flight tracks carry a considerable sideload and may become rather heavy or bulky as this must be carried as sideways bending in the track. As the aerodynamic benefits of the clean flap leading-edge and upper surface, together with large flap rearward travel, are most significant at landing, the use of underwing tracks is most appropriate on aircraft with a high ratio of landing weight to take-off weight, that is on short range aircraft.

(d) **Tracks within the Wing Profile**

Though only capable of giving a limited rearward movement without protruding outside the profile, size for size they are probably only lighter than underwing tracks by saving the weight of the fairing and, by keeping them normal to flap leading-edge, the side load problem at large sweeps can be avoided. Because of their zero cruisedrag penalty combined with loss of landing flap performance their application would seem to be on long range aircraft with a low ratio of landing weight to take-off weight.

(e) **Tracks with Overwing Fairings**

These avoid the lateral support problems at high sweep as support can be provided outside the fairing, but within the wing profile from the upper shroud skinning. There will of course be aerodynamic losses of landing flap performance. There may be a case for their use intermediate between underwing tracks and within the profile tracks. The fairings will usually be rather smaller than the corresponding underwing track scheme, since a considerable part of the track depth may be contained within the wing profile above the flap stowed leading-edge.

There is another feature, aimed at maintaining the quality of flow through the slot of the flap. This is the deflected lower shroud. Often, for a variety of reasons, there is a portion of wing profile between the rear spar and the stowed flap leading-edge. This piece of skin may be rotated trailing-edge up, in order to give a less tortuous path to the air that will later pass through the slot. In the case of slotted and multi-slotted flaps, with an upper shroud point at about 80% chord there may be benefits at both take-off and landing. The F.28 with a Fowler-type flap has a more elaborate arrangement. The author is of course unaware of Messrs.Fokkers reasons for this device, but would assume that the principal benefit is likely to be a drag reduction with take-off flap settings.

6. DRAG AT HIGH LIFT

Over the recent years, two considerations have seriously increased the aerodynamicist's problem in the estimation of the drag of transport aircraft with high-lift devices extended. The foremost of these is the increasingly competitive climate in which take-off performance guarantees have to be given in advance of flight test. The other is the increase in C_L at which the drag estimate is required. This has shifted the emphasis from terms that are relatively easy to estimate, to terms which are less easy to estimate from first principles and at the same time are difficult to extract from empirical analysis of model tests.

Figure 26 shows, roughly to scale, a typical drag breakdown in a take-off case. This has been drawn up on the assumption that $C_{L\,max}$ in the take-off confirguration is of the order of 2, whereas 10 years ago $\sqrt{2}$ was a more likely figure. It will be seen that the modulus of the terms stepped off within the circled area now predominate over those stepped off at $C_L = 0$, whereas in the case for an earlier era the reverse is the case.

The terms stepped off at the left-hand side are:

(a) Clean aircraft low-lift profile drag.

(b) Flap low-lift drag which will increase somewhat with flap size.

(c) Slat low-lift drag if appropriate.

(d) Vortex Drag term in $(\Delta C_L)^2$ in which the increase in ΔC_L will be roughly offset by the effect of increased flap span.

The terms that are indicated at the right-hand side of the diagram and which have increased markedly, include:

(a) Vortex drag terms in C_L^2 in excess of $C_L^2/\pi A$.

(b) Vortex drag term in $C_L \Delta C_L$.

(c) Lift-dependent profile drag, slats and flaps extended.

(d) Excess of wing lift over weight owing to download on tailplane.

(e) C_{LT}^2 terms in tailplane drag.

(f) Wing to tailplane interaction.

(g) Rudder drag in engine-out case.

There are too many terms in this group to allow formal separation from flight tests. One therefore must rely considerably on model tests either of the aircraft in question, or generalised model tests, as a basis of estimation; however, several of the terms are likely to be Reynolds number dependent. Also, at high lift the corrections that have to be applied to model results for constraint, support interference etc. are sufficiently important to make the general correlation of a wide range of model tests a rather dubious procedure; since, except for "in house" testing, sufficient confidence in the corrections used may be lacking. Tunnel to flight comparisons on existing aircraft are therefore extremely important in the assessment of new projects.

7. STALL "FIXING" AND LEADING-EDGE INTERRUPTIONS

In the last part of this lecture we will describe typical patterns of flow breakdown in three dimensions. This is in the context of conventional transport aircraft for which the handling requirements are, in effect, that at the stall there shall be a nose-down pitch which is sufficiently strong as to be unmistakable, that any lateral disturbance shall be readily controllable to within about 30° of roll, and that there shall be warning to the pilot of the approach of the stall in the form of buffet.

In fact, a considerable number of modern aircraft types do not have adequate pre-stall buffet from aerodynamic sources, and it is provided by means of an electrically-driven stick shaker. Historically, before the coming of the jet engine it was much more common for aircraft to have adequate pre-stall buffet, though even in the late 1930 era single-engined aircraft using NACA 23012 had started the trend. The buffet was commonly caused by flow separation emanating from nacelle-to-wing junctions or from the rear of the wing-to-fuselage junction on thick wings. In either case, it seems likely that adequate development work in these areas could have increased C_{Lmax} and at the same time reduced or eliminated the pre-stall buffet. Thus it can be argued that absence of such buffet should now become almost a design aim, when striving for high values of C_{Lmax} .

Similarly, the nose-down pitch on a small number of aircraft has been produced or augmented by artificial means, that is by "stick pushers". However, recourse to "stick pushers" poses a much more serious problem from the point of view of safety and system reliability than does the shaker, and it seems to be worth considerable effort on the part of the aerodynamicist to provide the nose-down pitch by aerodynamic means.

The lateral requirement is in effect a requirement for nothing to happen, and the author is unaware of any artificial aid capable of making up for aerodynamic short-comings in this respect.

Figure 16 shows the wings of some Hawker Siddeley aircraft developed during the last 15 years. All four of these have stick shakers to avoid the necessity of providing pre-stall buffet. All four, if flown without fences (or in the case of the Comet 4C without the pinion tank) and without deliberate degradation of the inboard leading-edge, would have an outboard wing stall and unsatisfactory lateral and longitudinal characteristics. With the configurations illustrated, the flow separations during normal stall demonstrations for certification purposes are confined to the inboard wing; the wing in the region of the aileron does not suffer separated flow during these stalls. In all these cases a spoiler of some sort is provided to produce an inboard stall before the tip would otherwise have stalled, and a fence or other device is used to prevent the spread of this stall to the aileron and tip region. In the case of the Comet 4C the pinion tank serves instead of a fence, but it must be noted that considerable development effort was

required to suppress premature separations associated with the tank-to-wing junction. A large fillet is needed on the inboard side; this fillet has considerable nose-down camber and also a fixed "letter box" slot. The use of spoiler type devices that are adjustable during development flying, rather than relying on basic aerofoil section variation to promote the inboard wing stall, ensures that only a minimum loss of $C_{L\,max}$ is suffered below the value defined by the outer wing stall.

This minimised "stall fixing" loss can on occasion get hidden in the effect of Reynolds number when comparing wind-tunnel results with flight results. The chord near the tip is typically about one-third of the foot chord of the wing. At flight Re number, the resulting change of Reynolds number has but a small effect on $C_{L\,max}$ available on the outboard wing relative to the inboard wing. At model Reynolds numbers, if these are sufficiently low, this ratio will cause a much more serious degradation of the tip. If then a model of the aircraft including the "stall fix" devices is being tested at a low Reynolds number, the model may well have an outboard wing stall. The model with the "stall fix" devices removed would show substantially the same value of $C_{L\,max}$, but the corresponding full-scale value, if it could be measured in such a configuration, would have increased; thus the "stall unfixed" configuration might have the scale effect suggested by section data for the outer wing section, whilst the "stall fixed" configuration would have rather less scale effect

While suppression of the outboard wing stall is a necessary requirement for satisfactory lateral behaviour it is not sufficient; when $C_{L\,max}$ is sufficiently high for there to be a substantial loss of lift after the stall, it is also necessary for the inboard wing stall to develop symmetrically. There are indications that this becomes more difficult to ensure as $C_{L\,max}$ is increased.

REFERENCES

1. USAF Stability and Control Datcom.

2. Royal Aeronautical Society Data Sheets.

3. Gault, D.E. *A Correlation of Low Speed, Airfoil-Section Stalling Characteristics with Reynolds Number and Airfoil Geometry.* NACA T.N.3963.

4. Abbott, I.H. von Doenhoff, A.E. *Theory of Wing Sections.* McGraw Hill & Dover Publications, New York.

5. Weick, Shortal, *The Effect of Multiple Fixed Slots and a Trailing-Edge Flap on the Lift and Drag of a Clark Y Airfoil.* NACA T.R.427.

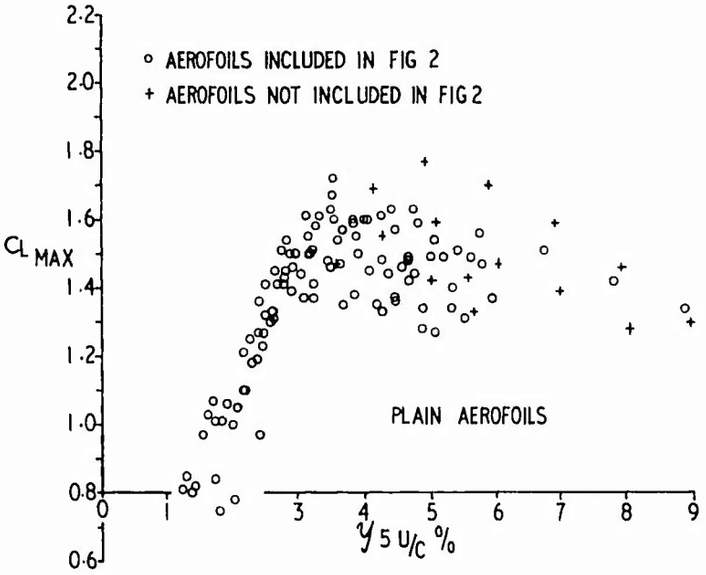

Figure 1

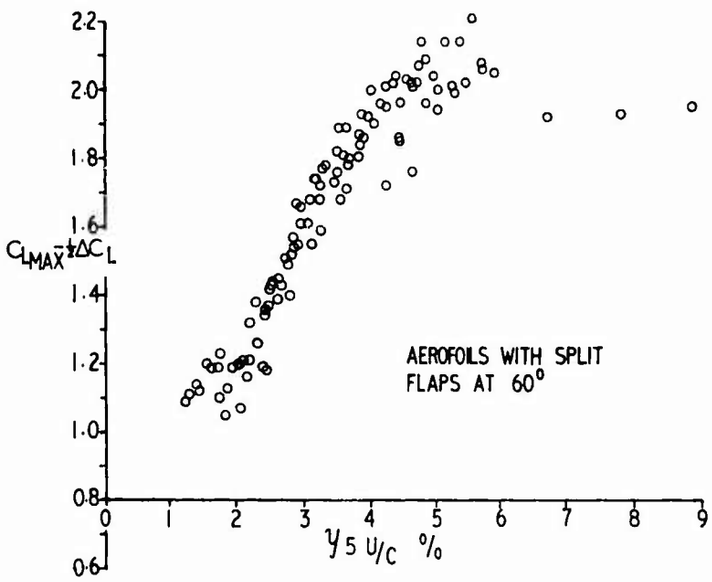

Figure 2

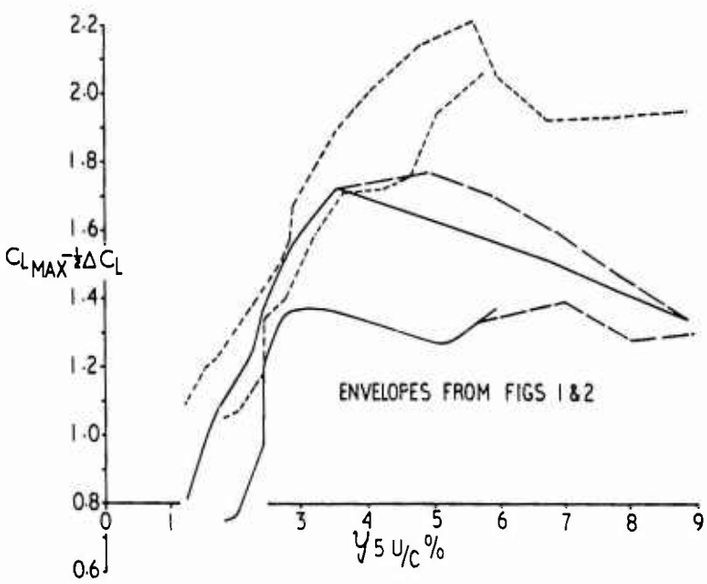

Figure 3

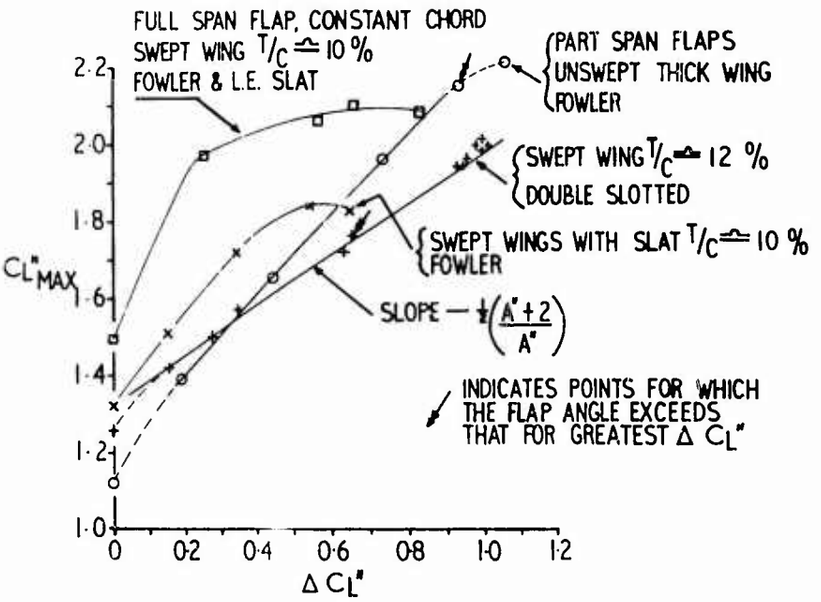

Figure 4

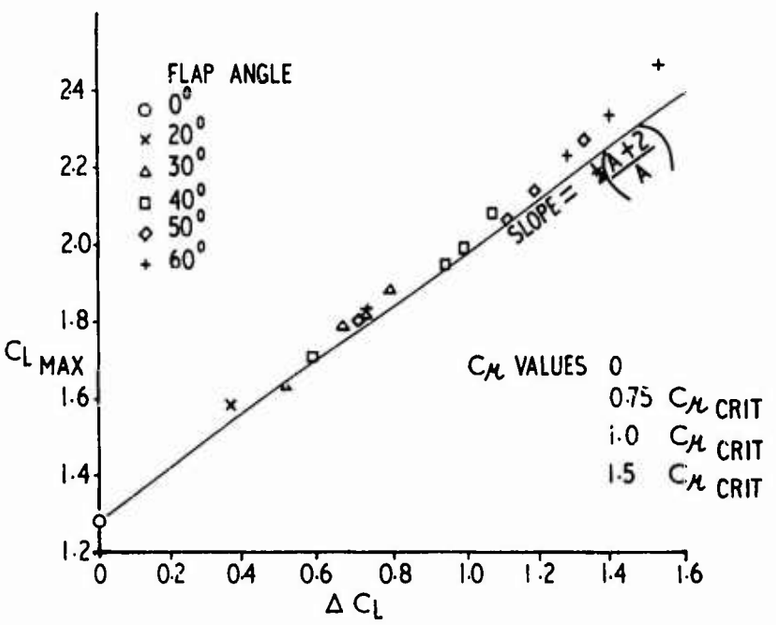

Figure 5

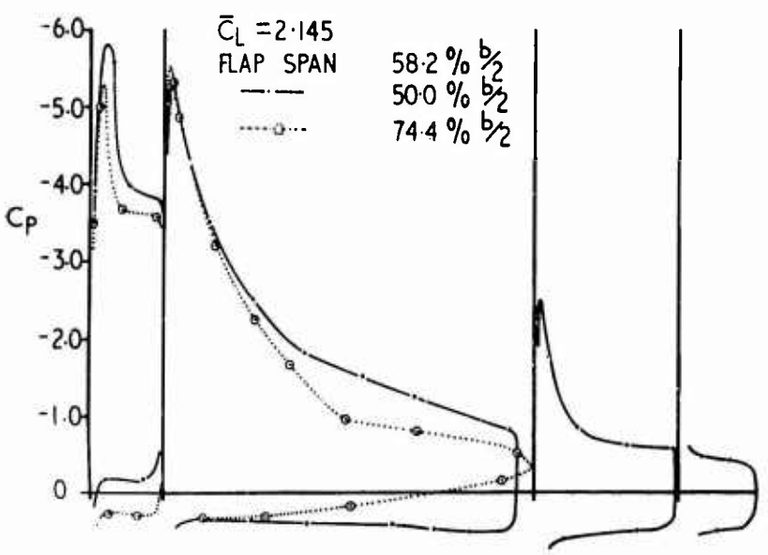

Figure 6

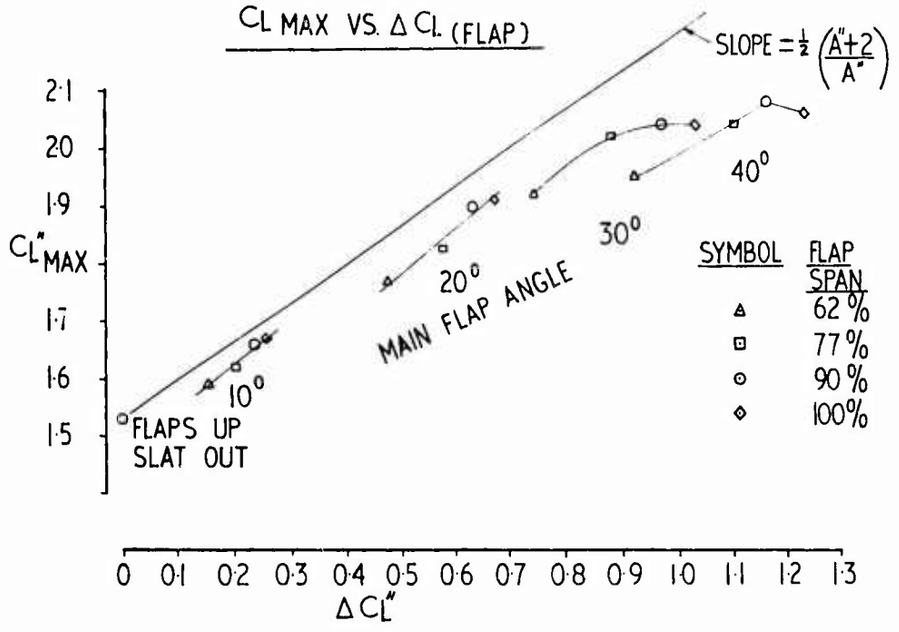

Figure 7

Figure 8

TABLE I

Type of Flap	Method of producing low pressure at rear of main surface.
Plain flap with attached flow (small angles)	Substantially potential flow round knuckle.
Plain flap with separated flow	Analogous to base pressure.
Split flap	Base pressure.
Blown flap	Substantialiy potential flow round knuckle with small entrainment sink effects.
Jet flap	Substantially potential flow round knuckle plus appreciable entrainment sink effect.
Slotted flap (all types)	Suction field associated with suctions on forward part of flap.

TABLE II

Type of Flap	Treatment of main surface boundary - layer downstream of flap knuckle.
Plain flap with attached flow (small angles)	Ordinary entrainment of external stream into boundary - layer enables small pressure rises to be traversed.
Plan flap with separated flow	Boundary layer separates: resulting bubble causes considerable loss in the lift increment – flap angle relation.
Split flap	"Knuckle" is at trailing-edge : poor lift increment flap angle relation as only one surface is deflected.
Blown flap and Jet flap	Jet momentum keeps boundary-layer unseparated.
Slotted flap (all types)	Boundary - layer becomes a wake which is better able to traverse pressure gradient owing to absence of zero velocity (wall) point. Thickening of wake by pressure gradient causes some loss in lift increment – flap angle relation.

Figure 9

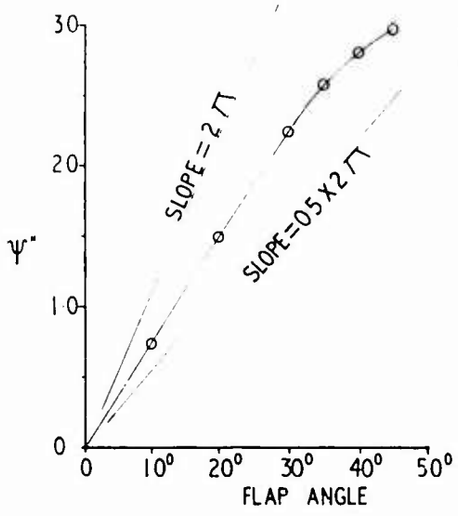

TYPICAL FOWLER FLAP
ON SLATTED WING

Figure 10

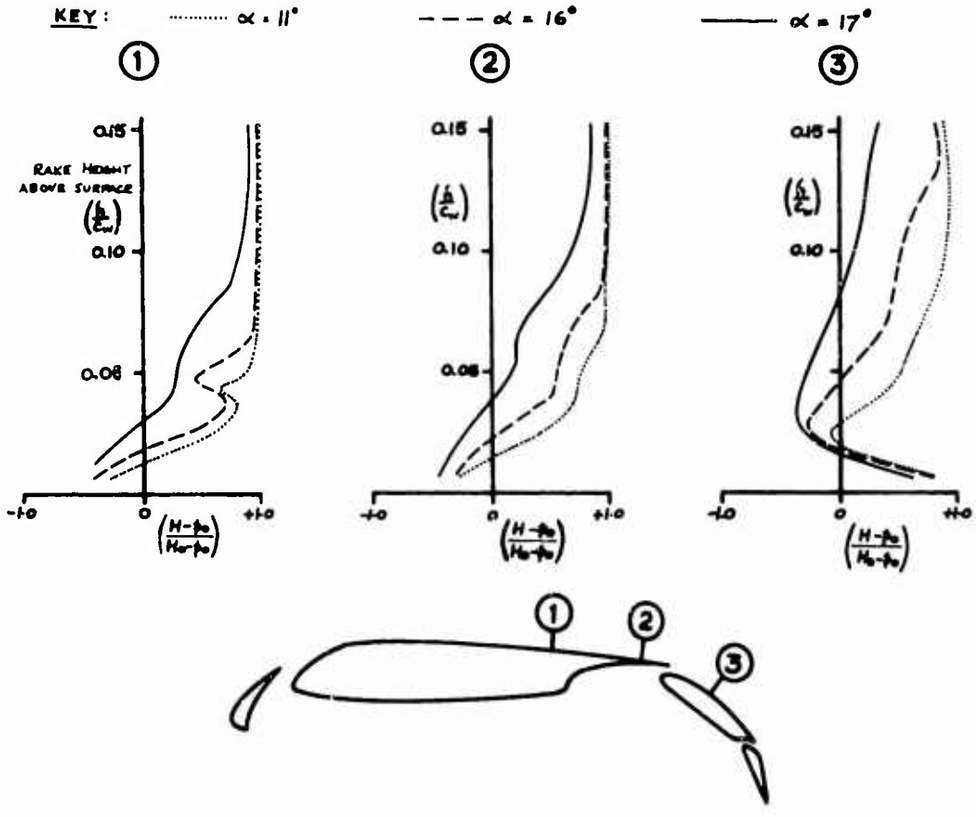

Figure 11

TABLE III

Effects of Slat on Pressure Distribution

1.	Nose-down rotation of slat reduces peak suction on slat for given C_L.
2.	Flow through slot reduces peak suction on slat for given C_L.
3	Presence of slat trailing-edge reduces peak suction on main element provided slat is not too nose down.
4.	Presence of main element leading-edge produces suction at slat trailing-edge.

Figure 12

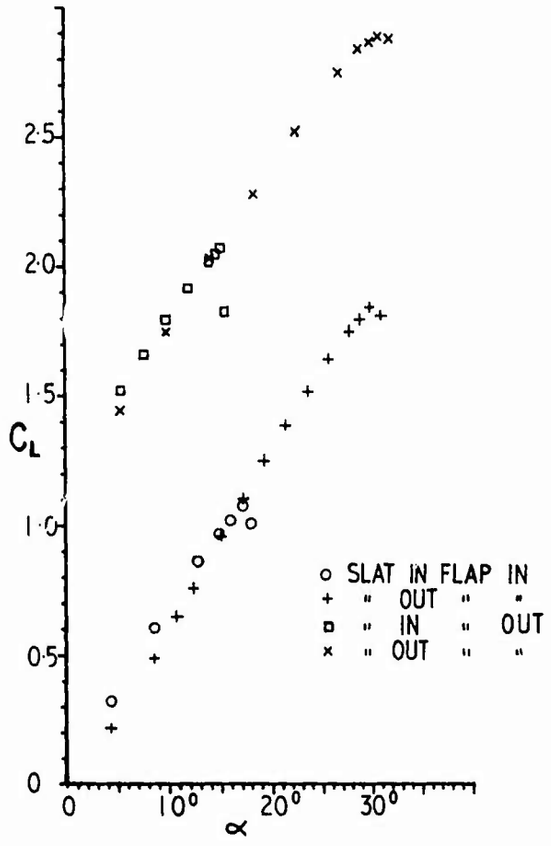

Figure 13

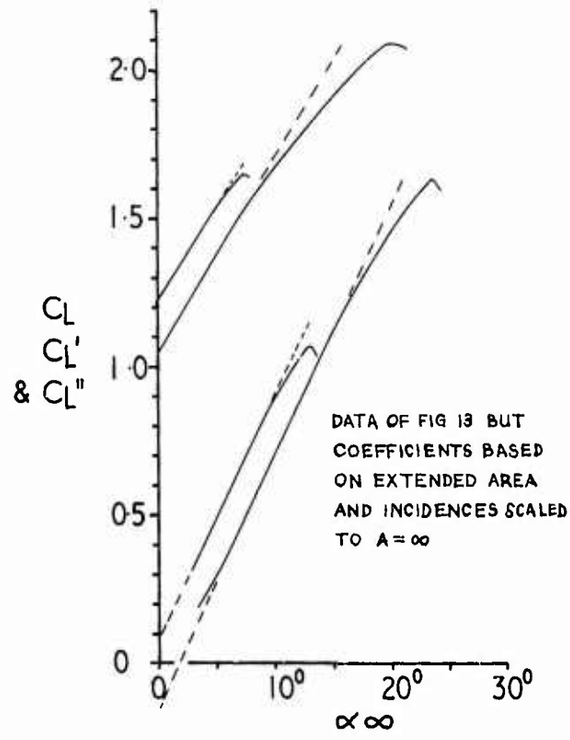

Figure 14

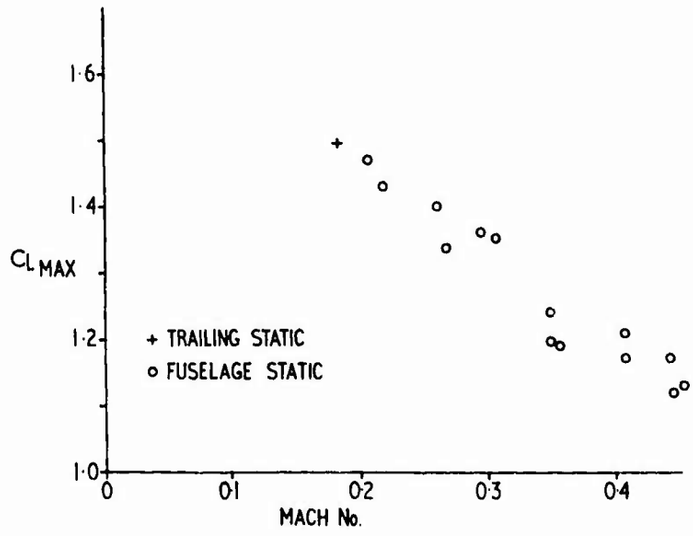

Figure 15

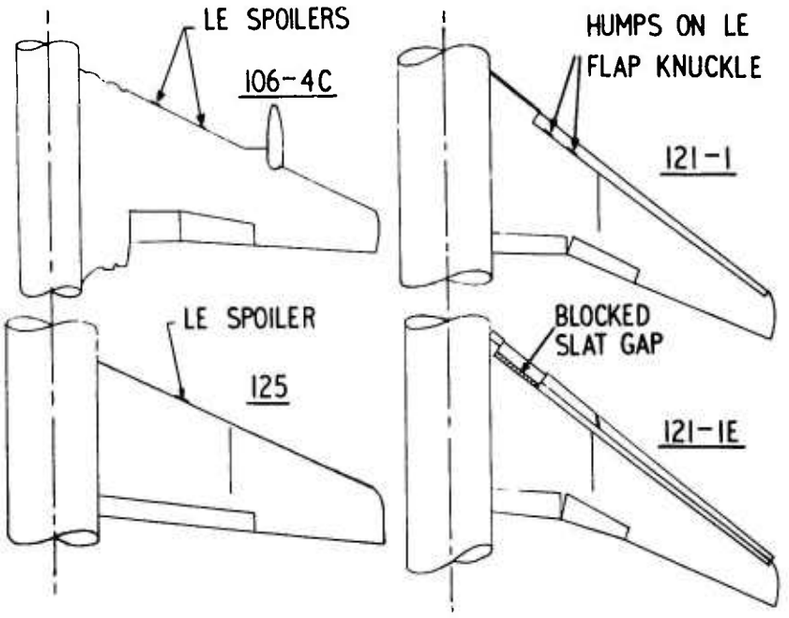

Figure 16

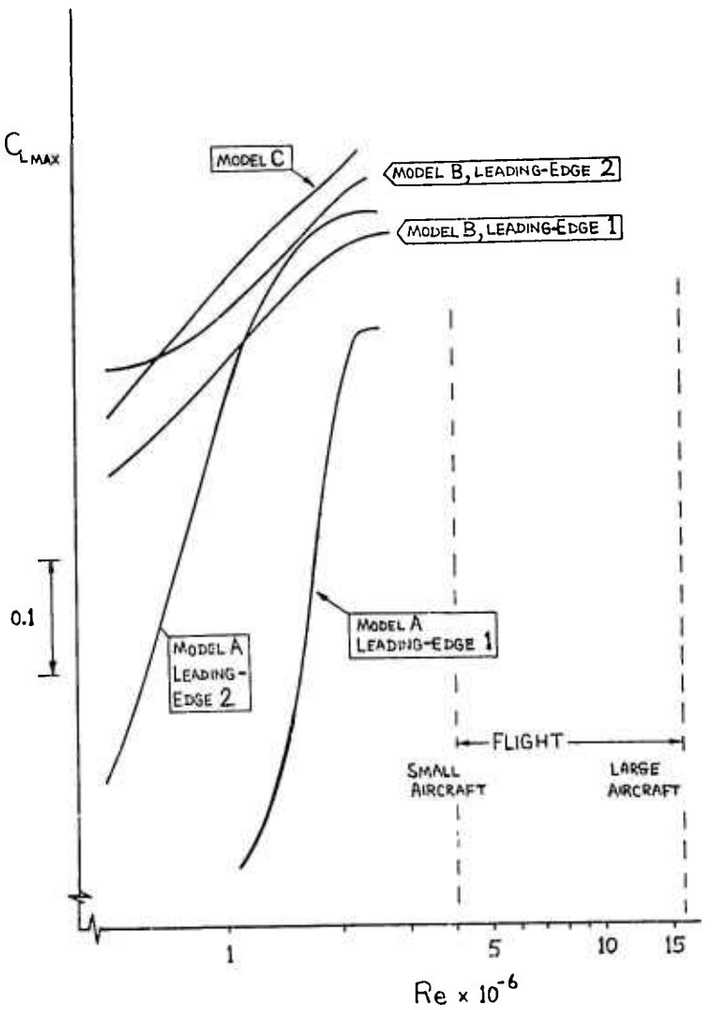

Figure 17

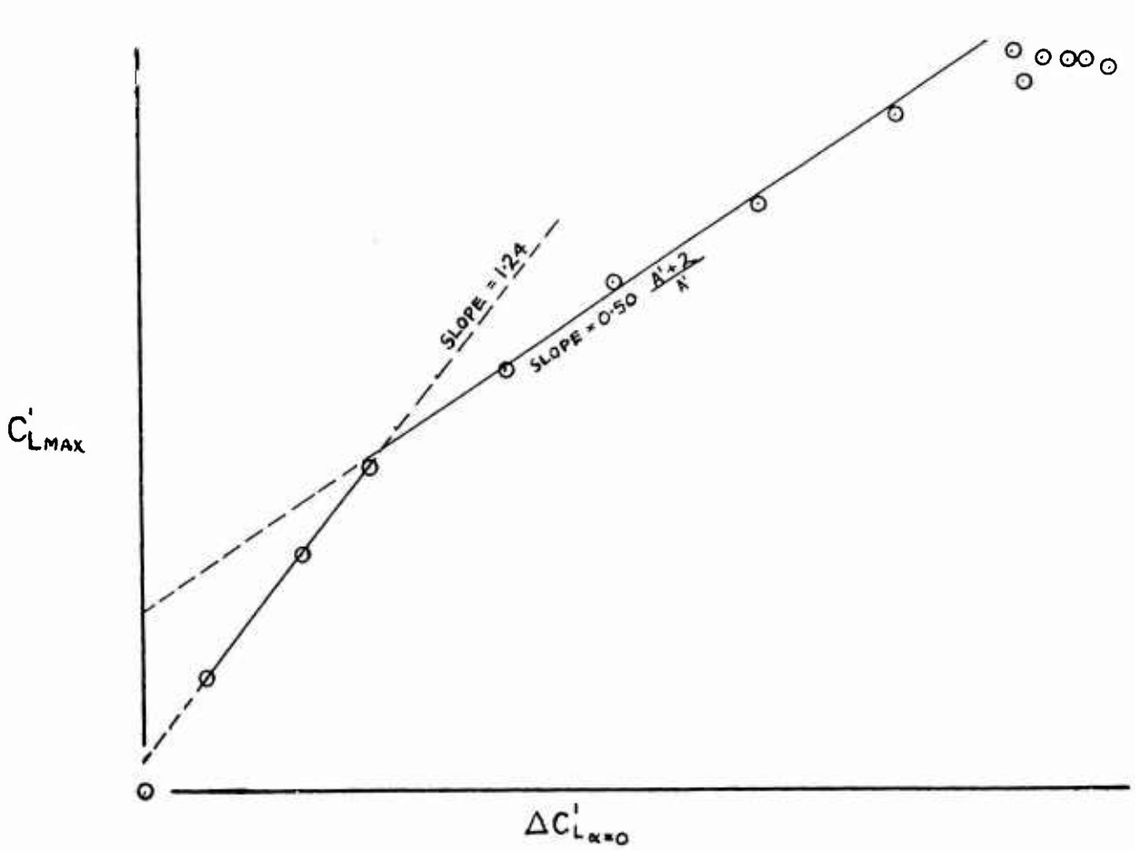

Figure 18

Table IV

1. Determine sectional C_L max. of clean aerofoil.
2. Adjust for sweep and spanwise load distribution.
3. Determine sectional C_L max. of section as if it were a leading stall case.
4. Adjust as in 2.
5. Determine $\Delta C_L''(\alpha = o)$ for various flap angles.
6. By some means assess whether $\partial C''_{L\,max.}/\partial \Delta C''_L$ for the leading edge limited case should differ appreciably from $\frac{1}{2}(A''+2)/A''$.
7. Assess any further losses near maximum useable flap angle.
8. Through clean wing C_L max. draw $\partial C_L''$ max./$\partial \Delta C_L''$ at value of about 1.05.
9. Through notional "leading-edge stall C_L max." draw $\partial C_L''$ max./$\partial \Delta C''_L$ C_L'' at value of $\frac{1}{2}(A''+2)/A''$ or slightly less, from experience of similar configurations.
10. Draw in further rounding near maximum flap angle.

Figure 19

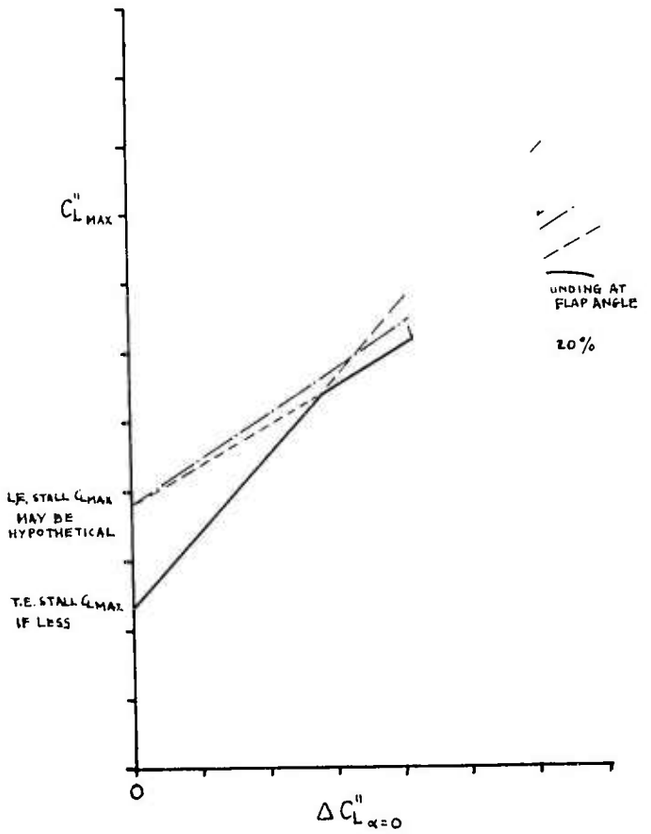

Figure 20

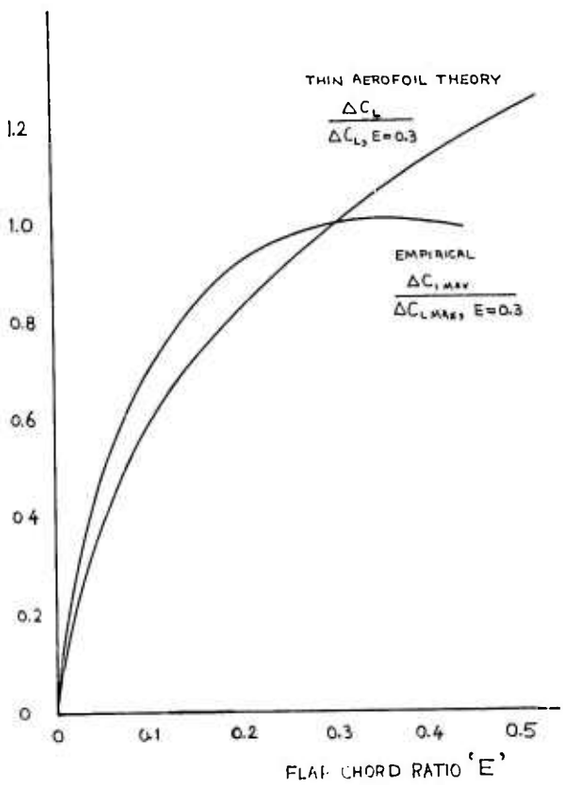

Figure 21/22

Table V

Leading-Edge Devices

Group 1 Acts by changing the pressure distribution.

1. Leading-Edge Flap
2. Fixed Leading-Edge Shape Modification
3. Krueger Flap
4. "Slat without Slot"

Group 2 Acts on Boundary-Layer

5. Tangential Blowing
6. Boundary-Layer Suction
7. "Letter Box" Slot
8. Vortex Generators

Group 3 Combined Action

9. Handley Page Slat
10. Krueger Slat
11. Leading-Edge Flap with Vortex Generators on Knuckle.

Figure 23

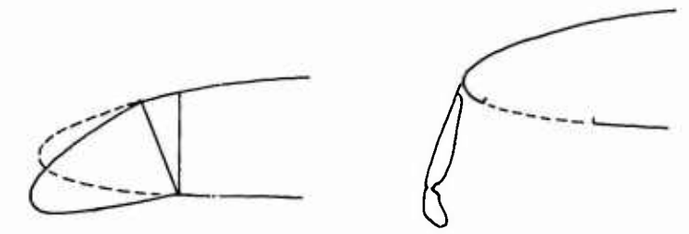

1. LEADING-EDGE FLAP

2. KRUEGER FLAP

3. FIXED LEADING-EDGE MODIFICATION

4. SEALED SLAT

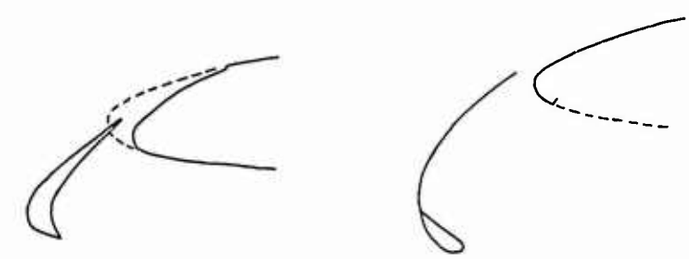

5. HANDLEY PAGE SLAT

6. KRUEGER SLAT

Figure 24

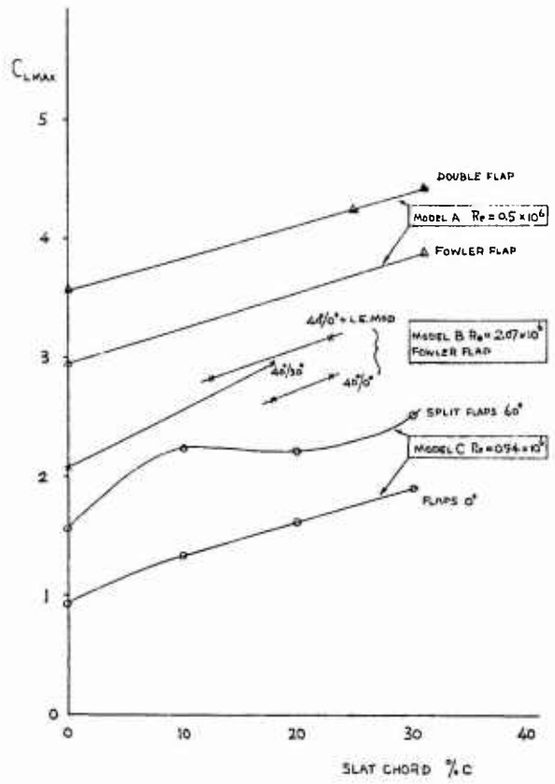

Figure 25

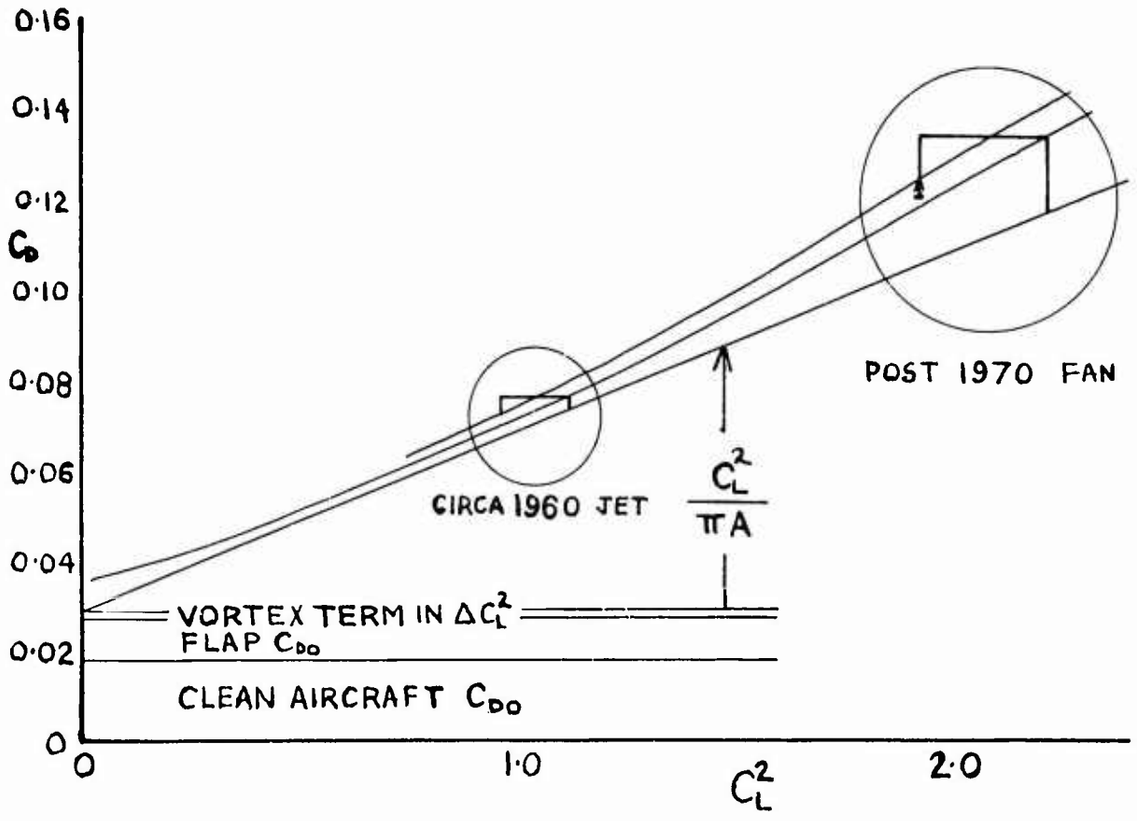

Figure 26

SUMMARY OF DISCUSSION

relating to

AERODYNAMICS OF MECHANICAL HIGH-LIFT DEVICES

1. Basis and Extrapolation of Figure 19 of Paper

The curves were not measured at constant Mach number, since the measurements were made in an unpressurised tunnel. If the curves were extended to even higher Reynolds number by further increasing tunnel velocity, then the Mach number effect would become predominant and the curves would turn down. If, however, they could be extended without increase in Mach number (either by chord increase or tunnel density increase), the lecturer was confident that C_{Lmax} would continue to increase, though possibly at a fairly modest rate.

2. Effect of Surface Discontinuity on the Main Element Upper Surface of a Wing with Handley-Page Slat

The lecturer had no data to quote on this, but noted that three different aircraft manufacturers have adopted three different solutions. The BAC VC10 has no discontinuity when the slats are extended, accepting a penalty in cruise drag. A version of the Boeing 737 has a step of about 0.060 in., while the H.S.121-2E has a sloping ramp at about 30° to the adjacent surface and about 0.20 in higher. This divergence of approach could probably be taken as indicating that the losses are neither negligible nor enormous.

3. Application of Lifting-Surface Theory for Investigation of High-Lift Devices

In the calculation of the lift in the unstalled case due to incidence and flap angle, improved lifting surface theory might result in some small increase in accuracy, especially at low aspect-ratio. However, in the estimation of C_{Lmax} at moderate and high aspect-ratios, there are so many other items of doubt that a small improvement in the estimation of the unstalled potential flow does not seem to be of prime importance.

4. Value of ΔC_{Lmax} due to Vortex Generators on the H.S.121-1 Aircraft

The lecturer though the ΔC_{Lmax} was of the order 0.1.

AERODYNAMICS OF PNEUMATIC HIGH-LIFT DEVICES

by

J. von der DECKEN

Institut fur Strömungsmechanik, Technische Hochschule Braunschweig;

Braunschweig, Germany.

SUMMARY

High-lift devices have achieved a great signifance for take-off and landing of modern aircraft because of the steadily increasing wing-loadings and the limitations of the runway lengths. An introductory survey of pneumatic boundary-layer and circulation control schemes for increasing maximum lift is given. The physical background of boundary-layer control by suction and blowing, and of supercirculation and slipstream effects, is described; also the aerodynamic efficiency of the different devices is estimated by theoretical approaches. Finally, practical applications and performance evluation of pneumatic devices are discussed.

1. INTRODUCTION

As we learned in the preceding lecture from Mr. McRae, mechanical high-lift devices have been developed very thoroughly, so that mechanical flaps are in widespread use on all production aircraft of today. Often the mechanical flaps are arranged in a very sophisticated manner, with a system of flaps located at the leading-edge as well as at the trailing-edge of the wing, producing remarkable gains in lift. Although lift coefficients up to 3.0 and more have been achieved, the efficiency of such mechanical flaps is limited. The well-known reason is, that steep adverse pressure gradients in the pressure distribution lead to boundary-layer separation, if the angle of attack or the angle of flap deflection is increased too much. But there exists a still greater need for additional lift, because of the steadily increasing wing loadings of modern aircraft on the one hand and the take-off and landing requirements on the other. A low minimum speed during landing demands a high value of C_{Lmax}, when the wing loading is prescribed:

$$V = \sqrt{\frac{2}{\rho}\frac{W}{S}\frac{1}{C_L}} \qquad (1)$$

(V = speed, ρ = air density, W/S = wing loading, C_L = lift coefficient)

The influence of the higher wing loading has to be compensated by higher maximum lift values, in order to keep the lengths of the runways within reasonable limits. Especially for STOL (Short Take Off and Landing) aircraft, high maximum lift values are needed during the starting and landing phases.

So further methods have been developed for increasing lift by artificial means, based on pneumatic devices; namely boundary-layer control (BLC), circulation control and the jet-flap principle. These methods have become of special interest because aircraft now commonly incorporate jet-engines for propulsion.

A rough idea of the effect of boundary-layer control may be seen in Fig. 1, which shows the flow patterns around three body shapes; namely (a) circular cylinder, (b) aerofoil, (c) diffuser. On the upper Figures the real separated flow is illustrated and on the lower ones the artificially attached flow is described. In all three cases the steep adverse pressure gradient at the rear part of the body causes the flow to separate from the wall, which leads to a considerable pressure drag for the cylinder, to a loss of lift for the aerofoil and to a loss of pressure for the diffuser. By suction through a slot the separation is avoided.

In Fig. 2 a review is given on some remarkable dates in the history of boundary-layer control. The idea of BLC is as old as the concept of boundary-layer itself, since L. Prandtl (1) showed already in his fundamental work of 1904 that on a circular cylinder the inviscid flow with corresponding lift force can be realized by boundary-layer suction. Besides suction there are other effective methods for boundary-layer control, as for instance moving of the wall and tangential jet ejection. A comprehensive review of the early German contributions on this field has been given by A. Betz in his article to the most important Handbook of "Boundary-Layer and Flow Control" edited by G.V. Lachmann (2). As a first aeronautical application of BLC, the slat (after Betz, Lachmann and Handley Page) became known in 1922. Only a few years later the problems of lift augmentation on aerofoils by means of suction were investigated very successfully by J. Ackeret, O. Schrenk and B. Regenscheit at the AVA in Göttingen. On the basis of this research work, two suction aeroplanes AF1 and AF2 were built by the AVA Göttingen in the year 1940. As we shall see later, the slotted wings of these research aircraft were tested in flight with great success. From about 1940, the increase of lift by means of blowing a thin jet over the trailing-edge flap was investigated by W. Schwier at the AVA, also.

After the war, BLC investigations were continued in England by J. Williams (2) and his collaborators at the NPL and RAE, in France by R. Legendre, Ph. Poisson-Quinton (2) and M. Roy from ONERA, and in USA where for instance continuously distributed suction was investigated by A. Raspet. But in Europe, as well as in USA, more and more emphasis was put on BLC by blowing instead of suction, because the jet engine readily provided a supply of high pressure air.

At the third ICAS-Congress in Stockholm in 1962, H. Schlichting (3) gave a survey of the research work which had been done so far in Germnay, in the field of increasing high-lift by artificial means. F. Thomas (4), (5) has also given another lecture about the same subject here at the von Karman Institute in 1967 and 1968. It should be mentioned that most of the figures presented in this lecture are taken directly from H. Schlichting and F. Thomas, to whom I wish to express my thanks.

Detailed lists of references of the very extensive literature in this wide field of research may be found in Refs. 2, 3, 4, 5, and in the Proceedings of the NASA Conference on V/STOL Aircraft (6); as well as in "A Review of the Jet-Flap" compiled by G.K. Korbacher and K. Sridhar (7).

2. PHYSICAL BACKGROUND OF BOUNDARY-LAYER CONTROL

In order to adjust the wing section of an aeroplane to the changing flight conditions, the angle of attack can be increased and the trailing-edge flap can be deflected. There are two regions on an aerofoil where, at high angles of attack or flap deflection, flow separation becomes imminent; near the wing nose (especially for thin profiles) and close to the flap hinge (Fig. 3). Because of frictional losses, the kinetic energy of the boundary-layer fluid is not sufficient to overcome the strong adverse pressure gradients, so the flow separates from the wing surface. The flow separation indicates an upper limit for the greatest attainable lift coefficients. There are two basic methods available for preventing separation and augmenting maximum lift by pneumatic means:-

(a) Removing the low energy fluid from the boundary by suction through slots or holes.

(b) Accelerating the low energy fluid by blowing high energy flow into the boundary-layer.

This is demonstrated in Fig. 4.

3. BOUNDARY-LAYER CONTROL BY SUCTION

As already mentioned, the earliest method to avoid flow separation consists of sucking the decelerated fluid from the boundary-layer through slots into the interior of the wing. In this way the mainstream flow from outside the boundary-layer is drawn near to the wall (Fig. 4b), and the lift coefficients predicted by potential flow theory can thus be achieved. As the energy for the suction has to be supplied by a separate power unit, we must find the most effective arrangement for the suction system, so that the required power is as small as possible. This means, we are looking for the minimum suction quantity of air which is just great enough to avoid separation completely. The intensity of the suction is usually given by the volume parameter

$$C_Q = \frac{Q}{S.U_\infty} , \qquad (2)$$

where Q is the total suction quantity of air, U_∞ is the velocity of the mainstream and S the wing area.

Wind-tunnel tests have shown that:-

(a) Continuously distributed suction through the porous surface of an aerofoil is more effective than sucking through single slots (8).

(b) The suction zone should be situated very close to the nose of the wing or knee of the flap, where at large angles of incidence or flap deflection a steep pressure minimum occurs.

3.1 Nose suction

In Fig. 5 and Fig. 6 the superiority of continuously distributed suction is demonstrated on a swept wing with a thin profile, which was tested in a wind-tunnel by E.D. Poppleton (10). A gain in lift of $\Delta C_{Lmax} \approx 0.7$ is achieved in the case of continuously distributed suction with a volume coefficient of $C_Q = 0.003$, whereas in the case of suction through a single slot $C_Q = 0.012$ is needed (Fig. 5a). By deflecting the trailing-edge flap, the two effects of nose suction and flap deflection can be added and a still higher maximum lift is produced (Fig. 5b). In Fig. 6, the lift gains due to suction are plotted against the volume parameter C_Q. Here, it turns out again that continuously distributed suction is superior to the suction through single slots. Moreover, a wide slot seems to be better than a small one.

Another example for nearly continuously distributed nose-suction is given in Fig. 7. In the region of 15% of the chord length c, the wing surface is perforated by a large number of closely-spaced holes of 0.5 mm diameter and of density 13 holes per square centimeter. For the wing without flap deflection, the maximum lift is increased from 0.8 to 1.65 with a volume coefficient of only $C_Q = 0.006$; while with flap deflection $\eta_F = 45^\circ$, the C_{Lmax} increases from 1.7 to 2.5 with the same C_Q.

The pressure distributions, presented in Fig. 8 for an angle of attack $\alpha = 23^\circ$, show the strong influence of BLC by suction near the nose of the profile. Furthermore, it is clearly seen that the volume parameter C_Q can be the smaller the closer the suction zone lies to the pressure minimum. Fig. 9 illustrates how the position of the suction zone, on a very thin symmetrical profile with continuously distributed suction, affects the value of C_Q required to achieve a certain lift.

An analytical method for calculating the turbulent boundary-layer with continuously distributed suction has been developed by W. Pechau (11). Certain empirical assumptions in this method, particularly the dependence of the skin friction of the turbulent boundary-layer with suction on the nature of the porous wall as well as on the volume coefficient C_Q, has been obtained from systematic measurements by W. Wuest (9).

3.2 Trailing-edge suction

An example of suction through one discrete slot at the hinge of a flap is shown in Fig. 10; typical results of this very thick wing are shown in Fig. 11. The effective camber of the wing with deflected flap is increased by suction and a considerable gain in the maximum lift coefficient ($\Delta C_{Lmax} = 1.4$) is achieved with a volume parameter $C_Q = 0.035$. The efficiency of the flap with and without suction is demonstrated by Fig. 12. Separation could be avoided for flap angles up to 75° and the theoretical lift predicted by Glauert's method was reached for flap angles up to 40°. The critical (minimum) volume coefficient C_{QA}, which is required for complete boundary-layer control, is plotted versus the flap angle in Fig. 13. The experimental curve is compared with a simple analytical method, following K.O. Arnold (12). This method is based on the same concept elaborated by F. Thomas for blowing over the trailing-edge of a wing, which will be discussed in more detail later.

4. BOUNDARY-LAYER CONTROL BY BLOWING

For jet propelled aircraft, boundary-layer control by blowing has obvious advantages over BLC by suction, since the high pressure air supply for such a blowing device is directly available from the compressor of the jet engine. A very thin jet of high velocity is blown out of a narrow slot parallel to the wall into the boundary-layer. The slots are situated either near the wing nose or close to the knee of the trailing-edge flap, as is shown in Fig. 14. The intensity of the blowing jet is here expressed by the momentum coefficient

$$C_\mu = \frac{m_j v_j}{q_\infty S} = 2 \frac{\rho_j}{\rho_\infty} \left(\frac{v_j}{U_\infty}\right)^2 \frac{s}{c}, \qquad (3)$$

rather than by volume coefficient C_Q.

(m_j = mass flow per second, v_j = jet velocity, q_∞ = mainstream dynamic head, s = width of blowing slot, c = chord length).

Fig. 15 shows the effect of blowing over the trailing-edge flap and the velocity distribution, which can be expected in the boundary-layer down stream of the blowing slot. The jet discharged tangentially to the curved wall of the flap knee remains attached to the rigid surface according to the so called Coanda-effect. Turbulent mixing and entrainment problems are of great importance in this connection. The high velocity jet accelerates the fluid near the boundary and, by mixing processes, a boundary-layer profile is developed which is able to withstand the adverse pressure gradient for a considerable distance.

4.1 Trailing-edge blowing

A typical example of the lift increments obtained by blowing over the trailing-edge flap of a thin aerofoil is shown in Fig. 16 (from Ref. 13). When the flap is deflected by 45°, a maximum lift coefficient $C_{L\max}$ of nearly 2.5 is achieved with a momentum coefficient $C_\mu = 0.13$. The smaller the jet momentum is made, the smaller becomes the effective camber of the aerofoil, because the flow is no longer completely attached.

There are various possibilities as to how the flow will behave under the influence of the strength of the jet momentum blown over the trailing-edge flap. This is illustrated in Fig. 17 (from Ref. 16). When the flap is deflected, we move from curve (1) ($\eta_F = 0°$) to curve (2) ($\eta_F = 60°$). But the lift curve predicted by potential theory is reached only if we blow with a certain momentum C_μ over the trailing-edge flap. Here the required minimum momentum to avoid separation completely is $C_{\mu A} = 0.09$ (independent of the angle of attack). Going from curve (1) to curve (3) we observe that the maximum lift is still increased, but the corresponding angle of attack is reduced. The reason is that for high angles of flap deflection the flow already separates at the nose of the aerofoil at low angles of attack. By increasing the jet momentum beyond the value $C_{\mu A}$ needed for complete attachment the lift is increased, too (curve (5)). This state is called supercirculation or jet-flap effect, because the jet of high velocity is now projected beyond the trailing-edge of the flap and thus operates like an extended flap. For small values of the momentum coefficient the lift increase is produced through BLC and for large ones through supercirculation. Though for large values of C_μ the flow separates at the nose of the aerofoil, it is forced to reattach towards the rear by the influence of the jet, so that a large separation bubble is established. As the curves of the pitching moment show, the lift increase by means of blowing at the trailing-edge is coupled with large nose-down pitching moments. This difficulty leads to a concept of combined blowing at the nose as well as at the trailing-edge, which is discussed later.

In Fig. 18 the increase in lift by blowing is plotted against the momentum parameter C_μ for the same aerofoil as in Fig. 17. In the plotting two different ranges for each curve are to be distinguished: at first a very steep ascent of ΔC_L versus C_μ until the theoretically predicted lift (Glauert) is reached, and then a much slighter increase of lift beyond $\Delta C_{L\text{th}}$. In the first part of the curves we have boundary-layer control, in the second part supercirculation.

4.2 Analytic Assessment of the Critical Momentum Coefficient for Complete Boundary-Layer Control

Because of the large differences of lift slopes in these two parts, it is very important to know the critical momentum coefficient $C_{\mu A}$ for complete boundary-layer control giving the theoretically predicted lift. First of all $C_{\mu A}$ depends on the flap angle η_F, as shown in Fig. 18. The plotting of the measurements of different authors indicate that, besides the flap angle, other parameters such as the slot width have obviously a strong influence on the quantity $C_{\mu A}$. The most favourable $C_{\mu A}$ - values, i.e. the smallest are achieved with small slot widths and hence with large blowing velocities. In order to arrive at an analytical prediction of the momentum coefficient required to avoid separation, F. Thomas (14) carried out detailed measurements in the boundary-layer behind a blowing slot with the aid of a special experimental set-up. In these experiments, the ratio of jet velocity v_j to external velocity U_∞ as well as the slot width were varied. Fig. 19 shows typical boundary-layer profiles measured at various positions downstream of the blowing slot.

In order to provide an analytical treatment, the integral values of the boundary-layer theory are formed for the measured velocity profiles in the usual way. This means that we obtain the momentum loss thickness $\vartheta(x)$ as a function of the distance x along the wall:

$$\vartheta \rho_k w_k^2 = \int_0^\infty \rho u \, (w_k - u) \, dy. \qquad (4)$$

Here, $w_k(x)$ = velocity outside the boundary-layer or contour velocity predicted by potential theory, respectively;

while, $u(y;x)$ = velocity inside the boundary-layer.

Forming also the momentum loss thickness for the jet at the slot leads to the following negative value:

$$\vartheta_j = -\frac{1}{2} c_\mu \left(1 - \frac{w_{kj}}{v_j}\right) c \ , \tag{5}$$

with $$w_{kj} = v_k(x = x_j)$$

Hence at the slot, the momentum loss thickness jumps by the amount of ϑ_j. A typical example of the development of the measured function $\vartheta(x)$ is given in Fig. 20. The curve for the undisturbed flow without separation is indicated by $\vartheta_o(x)$. The curve with blowing follows the undisturbed curve at first, then at the slot it falls abruptly by the amount ϑ_j. Immediately downstream of the slot there follows a strong increase in momentum loss thickness due to very strong wall friction. Beyond a distance of about x = 150 s behind the slot, the curve $\vartheta(x)$ runs again parallel to the non-separated curve $\vartheta_o(x)$ without blowing. As a measure of the loss in momentum immediately behind the slit, a "momentum efficiency" is defined by

$$\eta_\vartheta = \frac{\vartheta(x) - \vartheta_o(x)}{\vartheta_j} \tag{6}$$

Thus, the quantity $(1-\eta\vartheta)$ corresponds to the loss in momentum caused by the strongly increased wall friction shortly behind the slot. This lost momentum quantity does not contribute in accelerating the boundary-layer tending to separate. Only the following momentum quantity,

$$\vartheta_B = \vartheta(x) - \vartheta_o(x) = \eta_\vartheta \vartheta_j, \tag{7}$$

serves the original aim.

The ratio $\eta\vartheta$ is clearly dependent on the velocity ratio v_j/U_∞. F. Thomas has found the following empirical law from these measurements (Fig. 20):-

$$\eta_\vartheta = 0.85 \left(1 - \frac{w_{kj}}{v_j}\right) \text{ for } v_j \geq 2U_\infty \tag{8}$$

With Equations (5), (7), (8) we obtain for the momentum coefficient:

$$c_\mu = \frac{2\,\vartheta_j/c}{1 - w_{jk}/v_j} = \frac{2\,\vartheta_B/c}{0.85(1 - w_{kj}/v_j)^2} \tag{9}$$

Substituting for the velocity ratio v_j/U_∞ in terms of the momentum coefficient

$$c_\mu = 2 \frac{\rho_j}{\rho_\infty} \left(\frac{v_j}{U_\infty}\right)^2 \frac{s}{c} \ ,$$

and solving the quadratic Equation with respect to c_μ, we finally find the simple result:

$$c_{\mu A} = \left(1.53\ \vartheta_B/c + \frac{w_{kj}}{U_\infty} \sqrt{2 \frac{\rho_j}{\rho_\infty} \frac{s}{c}}\right)^2 \tag{10}$$

This Equation shows clearly the importance of the slot-width ratio s/c and of the velocity ratio w_{kj}/U_∞ of the potential flow at the slot. In order to get as small values of c_μ as possible, the following requirements should be observed:-

(a) small slot width ratio s/c

(b) weak pressure minimum at the nose or flap knee to make the velocity ratio w_{kj}/U_∞ as small as possible.

The procedure of estimating the critical momentum coefficient $c_{\mu A}$ is demonstrated in Fig. 21. First, one has to calculate the pressure distribution on the contour of the flapped wing by a method, which is able to reproduce the pressure peaks near the flap knee, as for instance the panel method of J.L. Hess and A.M.O. Smith (15). From this calculation the velocity ratio at the slot w_{kj}/U_∞ is achieved. Then the separation point due to the calculated pressure distribution is found by known methods of boundary-layer theory. The separation point usually is situated very close behind the suction peak. The thick boundary-layer arriving from ahead of the separation point is now supplied with new momentum by the jet, so that the separation point is shifted rearwards. If the separation point is to be situated just at the trailing-edge of the profile, then a momentum ϑ_B is necessary, which follows from the theory of the turbulent boundary-layer:

$$\frac{\vartheta_B}{c} = 0.037 \left(\frac{U_\infty c}{\nu}\right)^{-0.2} \left(\frac{w_{kTE}}{U}\right)^{-3} \left[\int_{x_{sep}}^{x_{TE}} \left(\frac{w_k(x)}{U_\infty}\right)^{3.5} d\frac{x}{c}\right]^{0.8}$$

(sep = separation point, TE = trailing edge)

This momentum loss must be compensated by the net input of the jet, if separation is to be avoided.

The comparison of the results of this calculation shows a fairly good agreement with experimental results up to the flap angle $\eta_F = 45^\circ$ (Fig. 21).

4.3 Combined Blowing over the Nose and the Trailing-Edge Flap

As already mentioned, the lift increase by means of blowing over the trailing-edge of a wing is coupled with strong nose-down pitching moments, which are very objectionable. Besides this, a certain reduction in the range of usable angles of attack is caused by an early separation of the flow near the nose, especially if thin aerofoils are used. Attempts to overcome these difficulties lead naturally to the concept of combined blowing at the nose as well as over the trailing-edge flap. Even in the range of supercirculation combined blowing is advantageous, because the same lift coefficient can be achieved with a smaller total jet momentum. This is shown in Fig. 22, where the different possibilities of additional BLC at the wing nose are demonstrated.

Combined blowing has been investigated for instance by K. Gersten and R. Löhr (16). A typical result of the wind-tunnel tests is given in Fig. 23. The momentum coefficient at the flap has been fixed to $C_{\mu k} = 0.10$, because this amount had turned out to be the critical momentum coefficient C_{μ_A} for the simple blown flap (Fig. 17). Now the momentum coefficient at the nose has been varied. Though a certain gain in lift was registered, the curves do not follow the theoretical predicted curve, because the flow now tends to separate at the knee of the trailing-edge flap. This means that the critical momentum coefficient $C_{\mu kA}$ for the trailing-edge is not only dependent on the angle of flap deflection, but here $C_{\mu kA}$ is increased by increasing the momentum coefficient $C_{\mu N}$ at the nose. This leads to the following two questions:

(a) What amount of $C_{\mu NA}$ is required for a given configuration, to avoid separation at the nose?

(b) By what amount is the value $C_{\mu kA}$ raised due to the blowing at the nose?

Before answering these questions we should have another glance at Fig. 23. For angles of attack smaller than $\alpha = 0$, blowing at the nose is not required at all. However, if there is blowing at the nose at such small angles of attack, one obtains an increase in lift by means of supercirculation, which can be interpreted as an addition camber.

In Fig. 24 the pressure distributions shown have been calculated for the given aerofoil with a flap deflection of $\eta_k = 60^\circ$, on the assumption of inviscid flow. The curves are plotted for three angles of attack ($\alpha = -5^\circ, 5^\circ, 15^\circ$). It is surprising that the pressure distributions along the flap surface are almost independent of the angle of attack. This is the reason, why the critical momentum coefficient $C_{\mu kA}$ of simple flap blowing is also independent of α. Mainly, the minimum pressure peak at the nose is increased by increasing the angle of attack. Thus we must expect that the critical value $C_{\mu NA}$ at the nose also will increase with α.

Next, the method for predicting the critical values of C_μ (following F. Thomas) is applied to this case of combined blowing. The procedure is demonstrated again in Fig. 25 and may be explained once more for better understanding. From the computed velocity distribution w_k/U_∞ the momentum loss thickness $\vartheta(x)$ is calculated in the usual way. At the slot the curve jumps by the amount of ϑ_j due to the momentum of the jet, see Equation (5). Immediately behind the slot, ϑ ascends steeply due to the strong friction at the wall. After a distance of about 150 s, ϑ runs again parallel to the original curve, so that only a certain amount ϑ_G of the blown in momentum is left. ϑ_G corresponds to the wanted momentum coefficient C_μ, see Equation (10). The results of theory and experiment are compared in Fig. 26. Though there are only two measured points, we can state the following:

(a) the $C_{\mu NA}$ curve is in good agreement with the two measured points

(b) the $C_{\mu kA}$ values are obviously dependent on $C_{\mu NA}$ and approximately the following relation holds

$$C_{\mu kA} = (C_{\mu kA})_{won} + \frac{1}{3} C_{\mu NA} \qquad (11)$$

(Note:- won = without nose blowing)

This is astonishing indeed, because one would have expected a decrease of the $C_{\mu kA}$-value according to the additional blowing momentum at the nose. The explanation for this strange behaviour is that an additional power is obviously required in order to pull the nose jet around the deflected trailing-edge flap.

In Fig. 27 the two momentum coefficients are varied systematically for the configuration of $\eta_k = 60^\circ$, $\alpha = 10^\circ$, and a certain distance h of the wing above the ground. The typical behaviour of the lift and pitching moment as a function of the momentum ratio $C_{\mu N}/C_{\mu G}$ is shown, where $C_{\mu G} = C_{\mu N} + C_{\mu k}$. The lift curve for $C_{\mu G} = \text{const}$ obviously have a maximum. If the C_A - value is prescribed, as for instance $C_L = 2.2$, then we find that with blowing at the nose

(a) a much smaller total momentum is required,

(b) a much smaller pitching moment is produced.

In the following Fig. 28 the corresponding conditions of flow are illustrated, as obtained by tests with a tuft probe. We must differentiate between four ranges:-

(1) nose and trailing-edge separation

(2) nose separation (bubble), attached flow at TE

(3) completely attached flow

(4) attached flow at the nose, separated flow at TE.

The two optimal points obtained in these two graphs for $\alpha = 5^{\circ}$ and 10° are used for the comparison with the theory in Fig. 26. For $C_{\mu G}$-values less than these optimal ones we are in the range of boundary-layer control, and for those stronger than the optimal $C_{\mu G}$-values we are in the range of supercirculation. The broken curves in Fig. 28 indicate the optimal blowing ratio in the range of supercirculation and show clearly that, with increasing the total momentum, the part which is blown out at the nose must be increased likewise more and more. Obviously, it is favourable to blow out at the nose as much as possible, so that a separation at the trailing-edge just is avoided.

4.4 Forward-Facing Flap

Another possibility, to avoid the strong nose-down pitching moments associated with trailing-edge blowing, is the forward-facing flap having a single blowing slot in its leading-edge, as suggested by D.G. Hurley (2). Fig. 29 shows typical results of this high-lift device, which is especially suitable for a thin wing having a sharp leading-edge. Then, the flow separates from the leading-edge of the wing and reattaches to the leading-edge of the flap establishing a flow of the free stream-line type. As the curves of lift against momentum coefficient show, there are large lifts obtained for moderate blowing quantities, while the total drag associated with this scheme is not very large. But it would be very dangerous if the pneumatic device were to fail after the spoiler flap is raised.

4.5 External Jet-Augmented Flaps and Slipstream Effects

Besides the possibility to conduct the high pressure air from the compressor of the jet engine inside the wing in spanwise direction, in order to discharge it from the interior of the wing over the trailing-edge flaps, there exists an alternative method; the hot jet exhausted by the jet engines is deflected by auxiliary flaps onto the trailing-edge flap system, generating by that means boundary-layer and circulation control effects. This arrangement, which may be denoted as an external jet-augmented flap, is illustrated in Fig. 30, which shows some modifications of jet deflection systems. Apart from the pure jet flap and the internal jet-augmented flap, two examples for external jet-augmented flaps are presented; firstly the wing with a pod-mounted jet engine, where the jet exhaust is deflected upwards; and secondly a configuration, where the jet engine is mounted on the upper side of the wing. In addition, the deflection of the propeller slipstream by means of trailing-edge flaps is shown schematically. A comparison between the efficiency of an 'upwards-deflected' jet exhaust of a pod-mounted jet engine ($\tau = -30^{\circ}$) on the one hand and a straight-downwards deflected jet of the same configuration on the other is given in Fig. 31 (based on wind-tunnel measurements, which have been reported by Ph. Poisson-Quinton in (2)). In both cases, the double-slotted trailing-edge flaps of the swept wing were deflected by an amount of $\eta_F = 45^{\circ}$ and the momentum coefficient was $C_{\mu} = 1.1$. It turns out that the straight-forward concept of deflecting the engine exhaust downwards, in order to obtain a lift increment due to the reaction force of the thrust ($C_L = C_T \sin \tau$), is less effective than ducting the exhausted jet through the flap system, because in the latter case the boundary-layer and circulation control effects generate much higher gains in lift. Moreover, in the first case, the super-velocities induced by the jet on the lower wing surface destroy a certain amount of lift. For example, at zero incidence and with a deflection angle $\tau = 90^{\circ}$, only 65 per cent of the thrust of $C_{\mu} = 1.1$ could be recovered in form of lift. Supercirculation is superior not only in respect of lift but also of drag, as is clearly to be seen from the lift coefficients corresponding to $C_D = 0$:

(a) external-flow jet flap ($\tau = -30^{\circ}$) : $C_L = 2.7$

(b) deflected jet ($\tau = 60^{\circ}$) : $C_L = 1.8$

Concluding this subject the two arrangements of blowing, either over a flap from the interior of the wing or against a double-slotted flap by directing the efflux of a pod-mounted engine upwards, are compared in Fig. 32. In this case, a canard equipped with the internal jet-augmented flap and a conventional aeroplane equipped with the external one were tested, both models having the same swept wing. The efficiency is equivalent for both configurations regarding the lift over momentum as well as the drag over momentum plots. - In this connection two recent investigations may be mentioned, carried out on a specific STOL transport aircraft model at the NASA Langley Research Center (17), (18). The externally-blown jet-augmented flap is the most promising concept of boundary-layer and circulation control, there is no doubt.

The most advanced attempt in the field of deflecting the propeller slipstream by means of powerful flaps was undertaken by Louis Breguet, who applied this idea in the STOL transport aircraft Breguet 940 "Integral" and the corresponding production aircraft Breguet 941, which has proved very successful (see Fig. 33). In this case the wing of the aeroplane is immersed almost completely in the slipstream of four propellers, which are coupled with each other because of safety requirements. The outer flap portions are less deflected than the inner ones and also act as ailerons.

4.6 Jet-Flap

4.6.1 Two-dimensional jet-flap theory

It has already been mentioned that the lift coefficient of an aerofoil can be increased beyond the theoretical value of the potential flow theory, if the momentum coefficient becomes higher than the critical value C_{μ_A}. This additional lift increase is much higher than the reaction force of the jet because of the supercirculation effect. The surplus momentum is equivalent to an extension of the mechanical flap in the form of a "fluid flap". Of course, it is also possible to produce a lift increment due to supercirculation by blowing a thin jet sheet with high velocity directly out of a slot in the trailing-edge of a wing section without using a mechanical flap at all. This principle is shown in Fig. 34, together with a typical pressure distribution generated on the wing surface and in the jet behind the trailing-edge. The jet reaction force (J) may be split up into a lift component (J sin η_j), which is smaller than the lift produced by supercirculation (Γ_∞), and a thrust component (J cos η_j). In principle, it is possible to blow the whole thrust-efflux of the engines through the trailing-edge slot of a jet-flapped aircraft.

The jet sheet, which is inclined downwards at a certain angle η_j to the chord of the aerofoil, is bent parallel to the mainstream direction by the external flow. According to the resulting curvature of the jet sheet, there exists a pressure difference between the upper and the lower side of the jet layer. For the theoretical calculation of the lift due to supercirculation, this pressure difference is assumed to be equivalent to a vorticity distribution. Hence, on the mean camber line of the wing section ($0 \leq x \leq c$) and of the jet sheet ($c \leq x \leq \infty$), vortices are distributed. The strength of these vorticity distributions can be calculated by extending the aerofoil theory due to W. Birnbaum and H. Glauert. But, contrary to simple aerofoil theory, one has to choose for the jet-flapped wing a vorticity distribution, which does not satisfy Kutta's condition at the trailing-edge. As the flow direction changes discontinuously by the angle η_j at the trailing-edge of the aerofoil, the vorticity becomes singular at this point - quite similar to the singularity which occurs at the hinge of a hinged flap.

In this manner, the jep-flap theory for two-dimensional aerofoils finally has been formulated by D.A. Spence (19), who related the unknown curvature of the jet sheet with the corresponding strength of the vortex distribution. Spence has made two assumptions

(1) no mixing of the jet sheet with the external flow

(2) irrotational flow within the jet sheet.

Besides this, he showed that to a good approximation the thickness effects of the jet sheet could be neglected. As in the case of the blown flap, the dominant parameters are the momentum coefficient C_μ and the angle η_j of the jet deflection. Now the theory supposes the vorticity distribution and hence the lift to be linearly dependent on the angle of attack α and the jet angle η_j, whereas the dependence of the momentum coefficient is a non-linear one. This leads to the following statement for the vorticity K(x):

$$K(x) = U_\infty \left[\eta_j f_1(x,C_\mu) + \alpha f_2(x,C_\mu)\right].$$

The functions f_1 and f_2, which have been determined once for all by Spence, have different analytical expressions on the wing and in the jet. The function f_2 has a singularity at the leading-edge and f_1 at the trailing-edge of the wing. In order to calculate these two functions, the flow condition must be satisfied along the chord of the wing and the jet. This concept has been extended to the case of cascade flow recently by U. Stark of Braunschweig (not yet published).

4.6.2 Three-dimensional jet-flap theory

A first approximation for the three-dimensional jet-flap theory was given also by D.A. Spence. But the full theory to treat the general case of jet-flaps at wings with finite span was developed by A. Das (20). This theory allows the calculation of the lift distribution along chord and span for wings with arbitrary plan forms and distributions of jet momentum as well as jet angles, by extending H. Multhopp's or E. Truckenbrodt's lifting surface theory. The concept of a continuous vorticity distribution along the chord and span of the wing is demonstrated in Fig. 35.

In the three-dimensional case the vorticity distribution along the chord is taken from the two-dimensional theory of Spence, but the functions are generalized with respect to the spanwise co-ordinate (Fig. 35):

$$K(x,y) = U_\infty \left[\eta_j f_1(x,y,C_\mu) + \alpha f_2(x,y,C_\mu)\right].$$

This vorticity distribution must be determined by satisfying the flow condition on the whole wing:

$$\alpha(x,y) + \alpha_i(x,y) = 0 .$$

Here $\alpha(x,y)$ is the local incidence given by the geometry of the wing and α_i is the incidence induced by the vorticity distribution. Far behind the wing the condition is to be satisfied that the direction of the jet sheet agrees with the local flow direction, which is given by the induced angle of attack in the jet sheet:

$$\frac{dz_j}{dx}\,(x=\infty,y) = -\,\alpha_{i\infty}(y)\ ,$$

with z_j as vertical location of the jet sheet. In the two-dimensional case the induced angle $\alpha_{i\infty} = 0$, whereas for a wing of finite span the jet sheet far behind the wing is no longer parallel to the mean flow direction, but inclined downwards by the angle $\alpha_{i\infty}$. The connection between the vorticity distribution and the induced angle is given by Biot-Savart's law, which leads to an integral equation for the vorticity distribution $K(x,y)$ of the wing surface. With these statements adapted to Multhopp's lifting surface theory, the solution is obtained.

A. Das has calculated numerous examples in 15 sections along the wing span, by solving a corresponding system of 24 equations with 24 unknowns. In Fig. 36 the lift and pitching moment along the span of a rectangular wing with jet-flap is presented (aspect-ratio 2.75). In Fig. 36a the overall values of C_L against C_μ and in Fig. 36b the local values along span for different values of C_μ are given; in the latter case only the contributions due to supercirculation (c_{lr} and c_{mr}) are plotted over the span. In all cases, the theory is in good agreement with the experiment. Furthermore in Fig. 37 some results for delta wings are given. Fig. 37a again shows the overall values of lift as a function of C_μ for two wings which differ only slightly in their geometry. The wing number 1 has been computed by A. Das and the other with the aid of the electrolytical analogy method of L. Malavard; the agreement is good. Fig. 37b shows the distribution of the local lift coefficient along the span of the delta wing number 1. Here, two different distributions of momentum along the span are compared:

(i) constant distribution of the jet momentum $J = \rho_j v_j^2 \cdot s \cdot b$

(ii) constant distribution of the local C_μ- distribution, i.e. $C_\mu = (\rho_j v_j^2/q_\infty)(s/c) = \text{const}$ with $c(\eta)$ and $v_j(\eta)$.

For large values of C_μ the two different distributions lead to almost the same curve C_L.

5. PRACTICAL APPLICATIONS OF PNEUMATIC HIGH-LIFT DEVICES

The pneumatic high-lift devices described in the previous chapters are of different values if their practical application is considered. Low weight and power requirements, high reliability and simplicity in design and maintenance, and last but not least low cost, are of great importance. In this respect, the mechanical high-lift devices have so many advantages that they are still used exclusively in all civil production aircrafts. Today one can find pneumatic methods for lift augmentation only in a large number of research aircraft and in military aircraft; see Refs (21) to (25).

Boundary-layer and circulation control by suction and blowing are quite different in their practical application. Several suction systems have been investigated in flight tests already since the late thirties. A typical example is shown in Fig. 38. These flight tests were performed by F. Schwarz with the aeroplane RW 3a (gross weight = 800 kp, aspect-ratio = 7,6). In order to keep the wing clear of disturbance due to the propeller, a pusher airscrew was mounted in the empennage. The suction zone ranged from 0.04 c to 0.22 c and was extended over the whole span. The total perforated area with 8600 drilled holes of 0.5 mm diameter covered only 1.2% of the upper surface.

Although considerable reductions in take-off and landing distances were obtained, the suction system has never been applied to production aircraft, because there are several disadvantages compared with the blowing system. A separate pump is required, the pressures are low and hence very thick ducts are needed, the proper distribution of suction intensity is difficult to achieve, perforations are difficult to be manufactured and are sensitive to rough treatment.

However, blowing devices do not show so many disadvantages, especially for jet propelled aircrafts. There is no need of a special pump for the air supply, the highly compressed blowing air needs only thin ducts, the high temperatures of the air can be used for de-icing and the proper momentum distribution along the span is easily obtained by applying choked slots. The simplicity and effectiveness of this reliable system have led to a progressive use in the field of military aircraft.

A practical example for the improvement in the take-off and landing distance, depending on the total thrust to weight ratio $(S + S_B)/G$, is shown in Fig. 39 for an aircraft with conventional double-slotted flaps compared with an aircraft with blown plain flaps (amount of blown momentum quantity $S_B = 0.05\ G$). The distances have been calculated by G. Streit and F. Thomas (26) for a constant wing loading of 300 kp/m^2. It turns out that a certain required distance for take-off and landing is achieved with much less total thrust for an airplane with blown flaps than is possible for conventional airplanes. Suggestions have even been made to apply the jet-flap principle to helicopters, which would require a continually changing deflection angle due to the changing flow conditions during one cycle. Some possibilities as to how the jet deflection angle τ can be changed are shown in Fig. 40.

Another serious problem connected with each high-lift system is a fluctuation or breakdown of the high lift due to a failure in the pneumatic device. Then corresponding to the loss in lift the induced drag is reduced in the same manner so that the thrust usually is not able to follow. With a jet-flap configuration blowing nearly the full thrust out of the trailing-edge of the wing, then the thrust, the lift increment due to supercirculation and the induced drag are coupled with one another. A fully-integrated jet-flap design would even control all manoeuvre actions by means of changing either the jet deflection angle or the thrust as shown in Fig. 41.

6. CONCLUDING REMARKS

It was intended to give an introduction into the rather wide field of pneumatic high-lift devices within a single lecture. Of course there are many problems which have not been mentioned at all, for instance noise problems. Only the following topics are briefly described in this paper:

(1) Boundary-layer control by suction (nose suction and trailing-edge suction)

(2) Boundary-layer and circulation control by blowing over the trailing-edge flap

(3) Combined blowing over the trailing-edge flap and at the wing nose

(4) Two-dimensional and three-dimensional jet-flap theory.

REFERENCES

1. Prandtl, L. — Ueber Flussigkeitsbewegung bei sehr kleiner Reibung. Verh. III. Intern. Math. Kongress, Heidelberg; 1904.

2. Lachmann, G. V. (Ed.) — Boundary Layer and Flow Control. Vol. I and II, London, Pergamon Press; 1961.

3. Schlichting, H. — Aerodynamische Probleme des Hochstauftriebes. Proc. 3rd ICAS-Congress (Stockholm, 1962), pp 275-303; 1964.

4. Thomas, F. — Some German contributions to the research on boundary layer and circulation control. AGARD-VKI Lecture Series on boundary-layer and circulation control, April 10-14; 1967.

5. Colin, P. E. Williams, J. (Ed.) — The Aerodynamics of V/STOL Aircraft. AGARDograph 126; 1968.

6. - — NASA Conference on V/STOL Aircraft; a compilation of the papers presented at Langley Research Center; November 17-18, 1960.

7. Korbacher, G. K. Sridhar, K. — A Review of the Jet Flap. University of Toronto, UTIA Review No. 14; 1960.

8. Raspet, A. Cornish, J. J. Bryant, G. D. — Delay of the stall by suction through distributed perforations. Aeron. Eng. Review, Vol. 15, pp 32-39; 1956.

9. Wuest, W. — Experimental investigation on boundary layer suction by series of slits and holes. AVA Research Report 60-01; 1960. Also, AGARD-Report No. 258; 1960.

10. Poppleton, E. D. — Boundary layer control for high lift by suction at the leading-edge of a 40 degree sweptback wing. ARC R&M 2900; 1955.

11. Pechau, W. — Ein Naherungsverfahren zur Berechnung der ebenen und rotationssymmetrischen turbulenten Grenzschicht mit beliebiger Absaugung oder Ausblasung. WGL-Jahrbuch 1958, pp 81-92. Also, AGARD-Report No. 259; 1960.

12. Arnold, K. O. — Untersuchung uber die Auftriebserhohung eines Tragflugels durch Schlitzabsaugung. Dissertation T.H. Braunschweig 1965. Z. Flugwiss, Vol. 15, pp 37-56; 1967.

13. Williams, J. — British research on boundary layer and flow control for high lift by blowing. Z. Flugwiss. 6, pp 143-160; 1958.

14. Thomas, F. — Untersuchungen uber die Erhohung des Auftriebes von Tragflugeln mittels Grenzschichtbeeinflussung durch Ausblasen. Z. Flugwiss., Vol. 10, pp 46-65; 1962.

15. Hess, J. L. Smith, A. M. O. — Calculation of potential flow about arbitrary bodies. Progress in Aeron. Sci. Vol. 8, pp 1-138; 1967. Pergamon Press, Oxford.

16. Gersten, K. Lohr, R. — Untersuchungen uber die Auftriebserhohung eines Tragflugels bei gleichzeitigem Ausblasen an der Hinterkantenklappe und an der Profilnase. DFL-Bericht 189; 1962. Also, Proc. 5th European Aeronautical Congress (Venice, Sept. 1962).

REFERENCES (continued)

17. Parlett, P.
Fink, M. P.
Freeman, D. C.
Wind-Tunnel Investigation of a Large Jet Transport Model Equipped with an External-Flow Jet Flap.
NASA TN D-4928; 1968.

18. Parlett, P.
Shivers, J. P.
Wind-Tunnel Investigation of an STOL Aircraft Configuration Equipped with an External-Flow Jet Flap.
NASA TN D-5364; 1969.

19. Spence, D. A.
The lift coefficient of a thin jet-flapped wing.
Proc. Roy. Soc. (A) 238, pp 46-68; 1956.

20. Das, A.
Tragflachentheorie fur Tragflugel mit Strahlklappen.
Jahrb. der WGL 1960, pp 112-133.
A lifting surface theory for jet-flapped wings.
Readers' Forum, J. Aero. Space Sci., pp 499-500; April 1962.

21. Cornish, J. J.
Some Aerodynamic and Operational Problems of STOL Aircraft with Boundary Layer Control.
J. Aircraft, Vol. 2, pp 78-86; 1965.

22. Williams, J.
Butler, S. F. J.
Aerodynamic Aspects of Boundary Layer Control for High Lift at Low Speeds.
AGARD Rep. 414; 1963.

23. Wimpress, J. K.
Shortening the Takeoff and Landing Distances of High Speed Aircraft.
AGARD Rep. 501; 1965.

24. Clark, D. G.
Flight Development of a High Lift Research Aircraft Using Distributed Suction.
AGARD Rep. 502; 1965.

25. Anderson, S. B.
Quigley, H. C.
Innis, R. C.
Stability and Control Considerations for STOL Aircraft.
AGARD Rep. 504; 1965.

26. Streit, G.
Thomas, F.
Experimentelle und theoretische Untersuchungen an Ausblaseflugeln und ihre Anwendung beim Flugzeugentwurf.
Jahrb. der WGL 1962, pp 119-132.

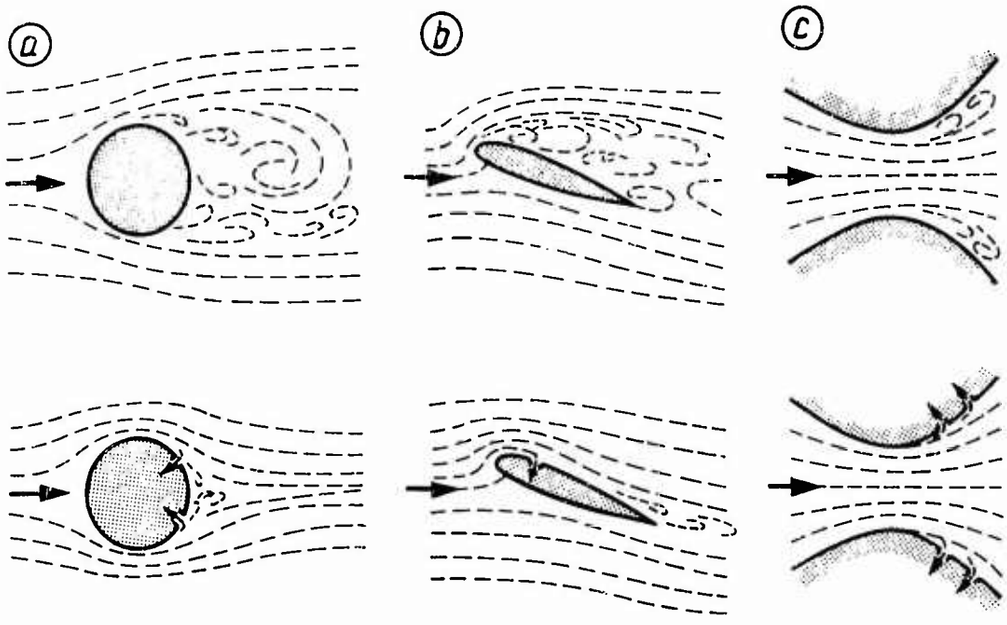

Fig.1 Flow pattern with and without boundary-layer control by suction
(a) circular cylinder
(b) aerofoil
(c) diffuser

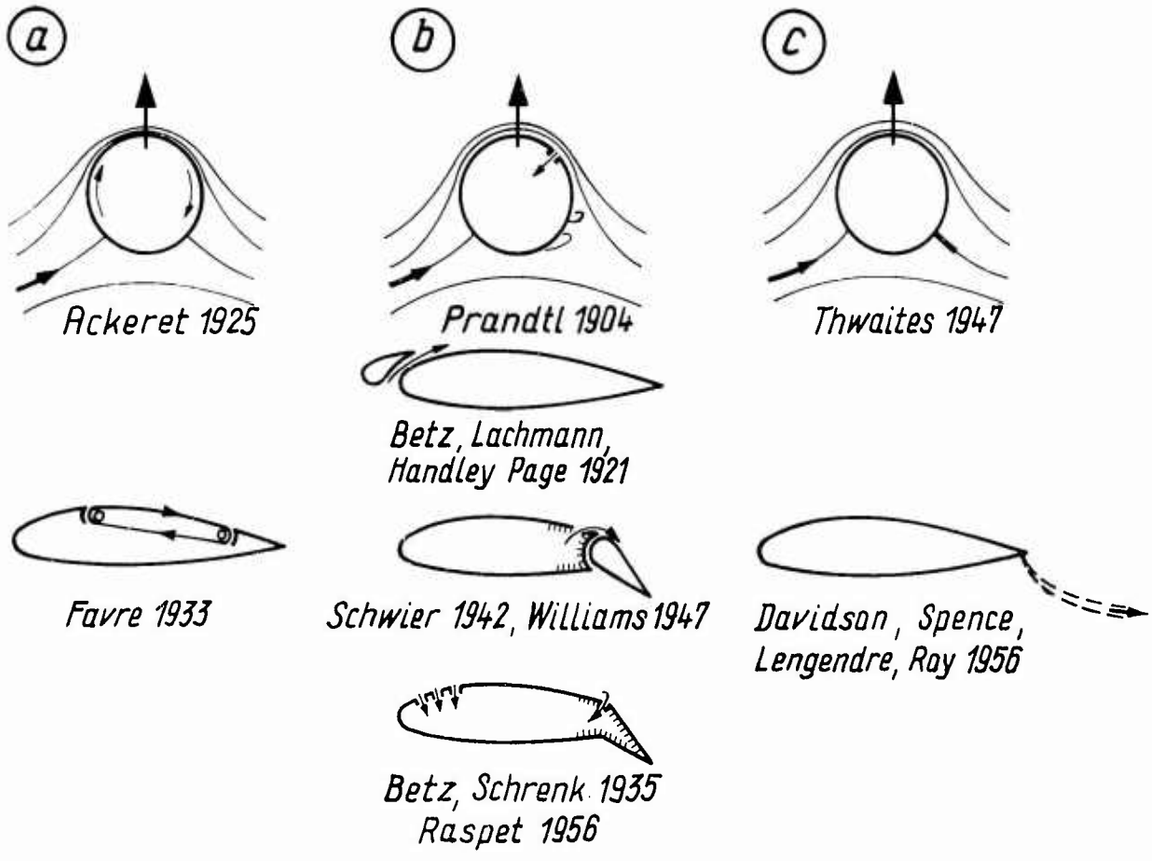

Fig.2 Dates in the history of boundary-layer control (BLC)
(a) BLC by moving wall
(b) BLC by suction or blowing
(c) circulation control (Thwaites-flap, jet-flap)

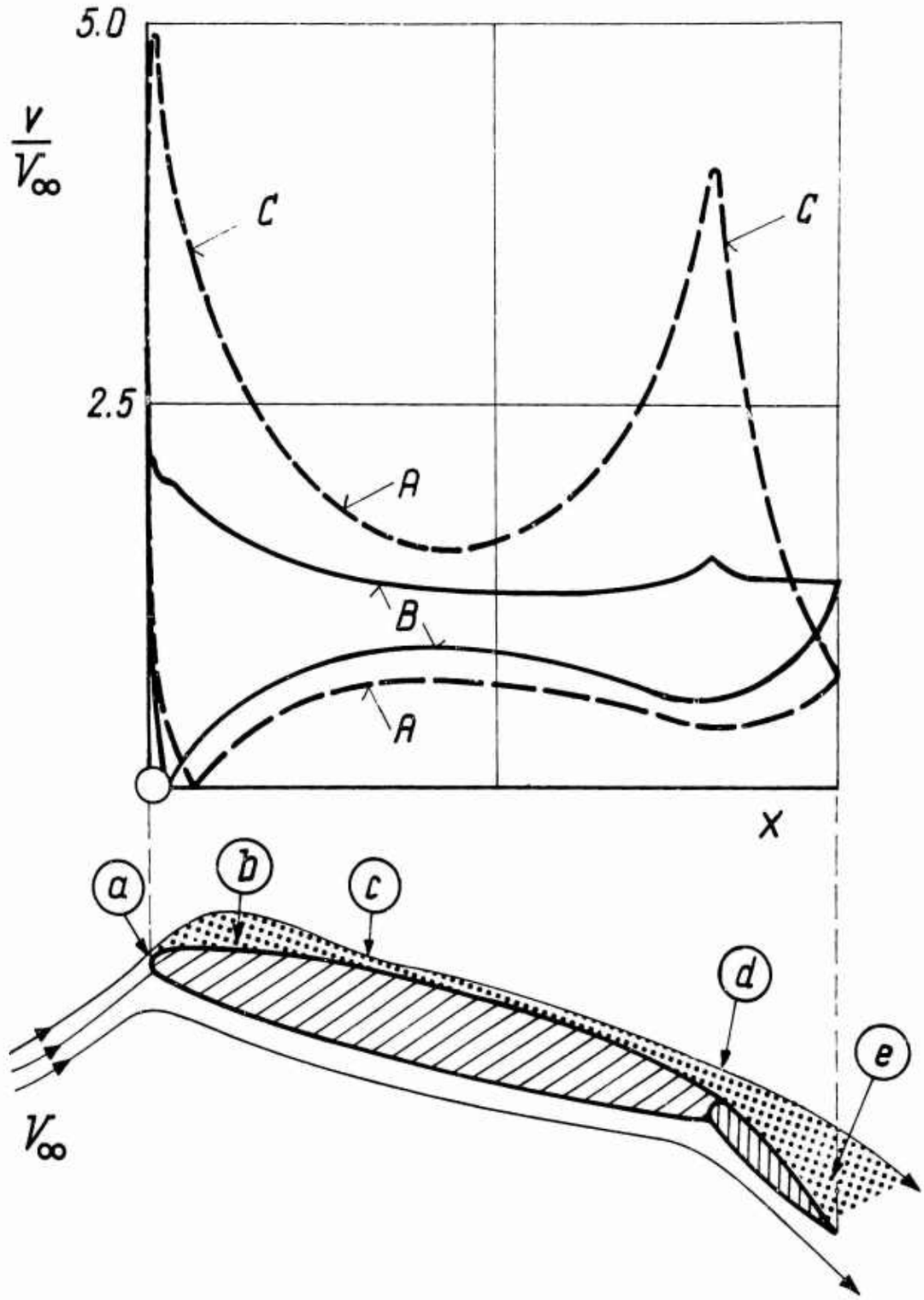

Fig.3 Velocity distribution of an aerofoil with trailing-edge flap

A = distribution for attached flow
B = distribution for separated flow
C = deceleration region
a = laminar separation point
b = separation bubble
c = turbulent reattachment point
d = turbulent separation point
e = reversed flow, wake

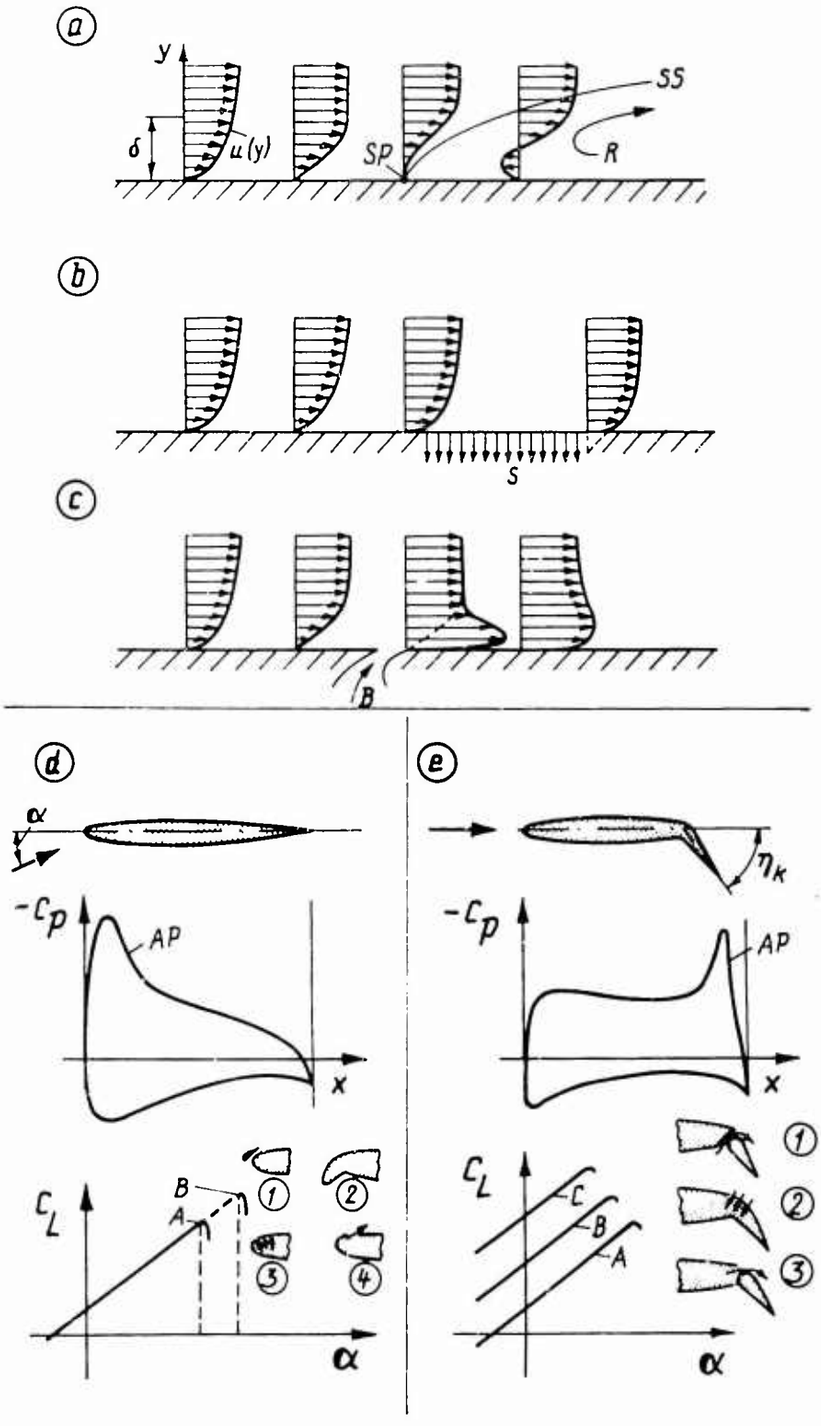

Fig 4 BLC methods for prevention of flow separation

(a) Boundary layer in the vicinity of a separation point
δ boundary layer thickness
SP separation point, $(\partial u/\partial y)_w = 0$
SS separation streamline
R reversed flow

(b) Prevention of separation by suction (S)

(c) Prevention of separation by blowing (B)

(d) Aerofoil at high angle of attack
A imminent at the nose
B without high lift aids
C with high lift aids
Methods: 1) Fix. nose flap,
2) BLC by suction, 3) BLC by blowing

(e) Aerofoil at high angle of trailing-edge flap, separation imminent at the flap knee.
A without flap, without BLC
B with flap, without BLC
C with flap, with BLC
Methods: 1) slotted flap, 2) BLC by suction, 3) BLC by blowing
AP adverse pressure gradient.

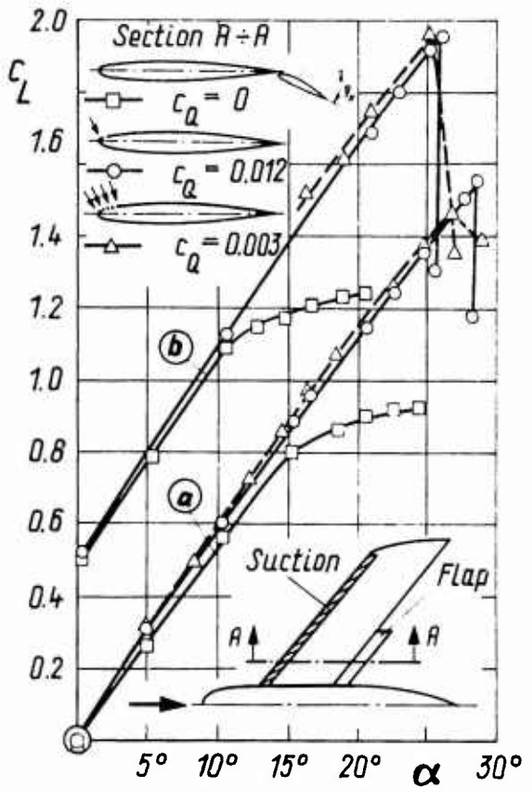

Fig.5 Effect of nose suction on the lift coefficient of a 40 deg swept-back wing
Wind-tunnel tests after E.D.Poppleton [10]
a = without flap, b = with flap deflected (η_k = 40°).
(1) without suction, (2) suction through leading-edge slot,
(3) suction through porous leading-edge

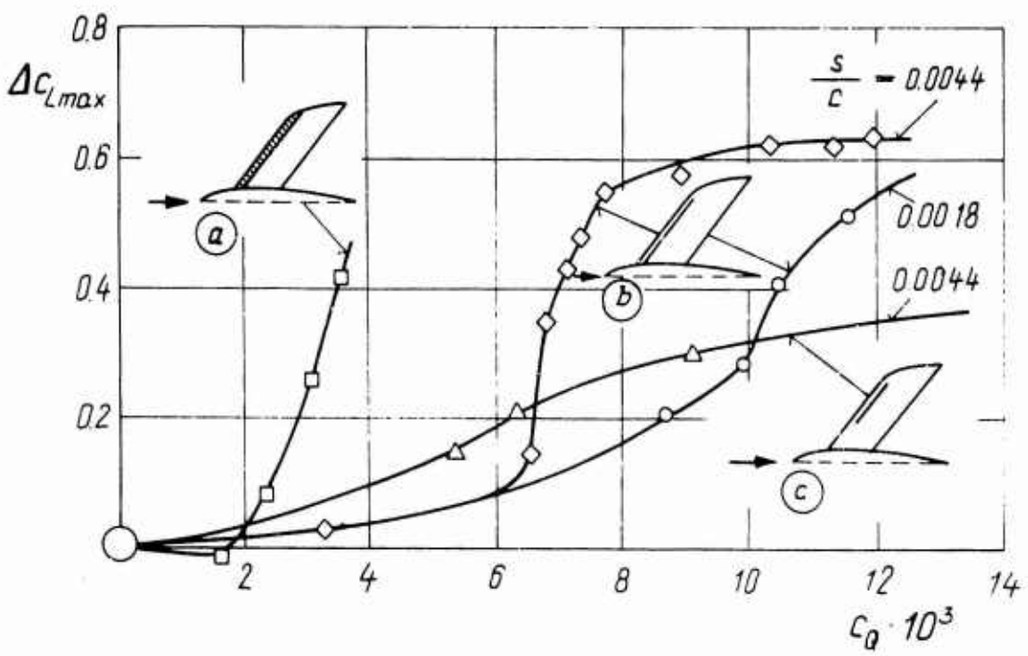

Fig.6 "Increment in $C_{L\,max}$ due to nose suction for a 40 deg swept-back wing"
Wind-tunnel tests after E.D.Poppleton [10]
(a) porous leading-edge, (b) leading-edge slot (full span)
(c) leading-edge slot (half span)

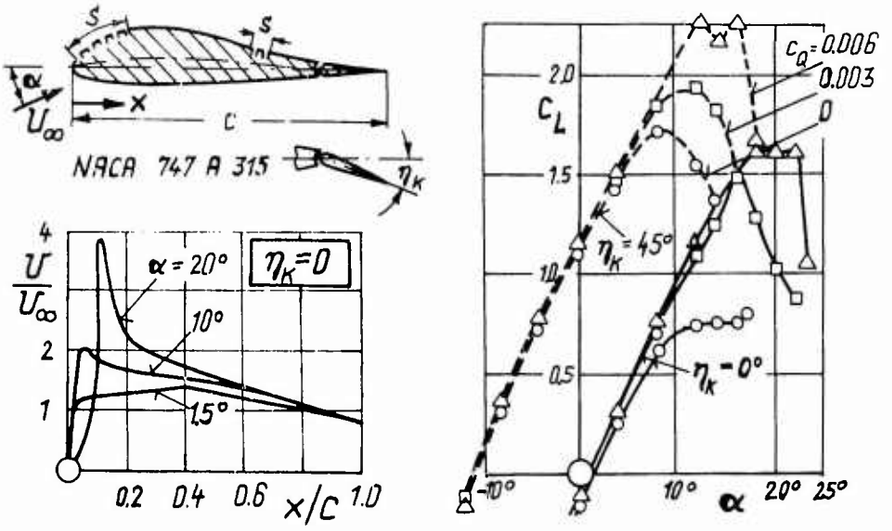

Fig.7 Effect of nose suction on the lift coefficient of an aerofoil with trailing-edge flap
Wind-tunnel tests after W.Wuest [9]

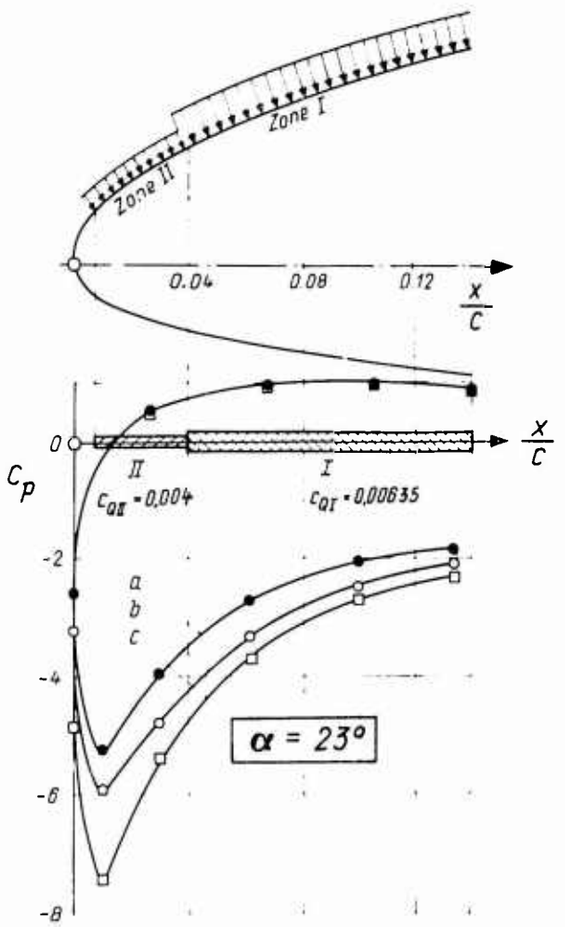

Fig.8 Effect of position of suction area on the pressure distribution
Wind-tunnel tests on wing section of experimental
aeroplane RW3 after W.Wuest [9]

(a) without suction, (b) suction in zone I
(c) suction in zone II

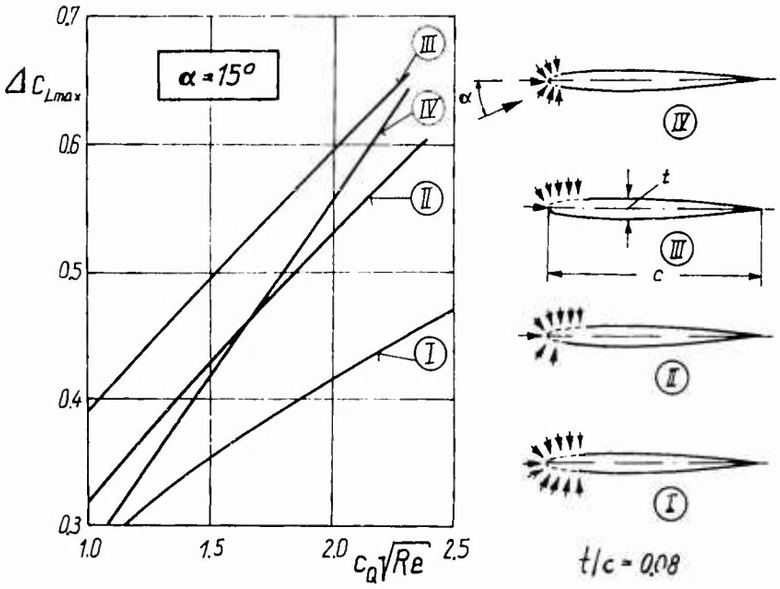

Fig.9 Increment in $c_{l\,max}$ due to various positions of suction area
Suction through porous surface at the nose of the aerofoil
Ref.: ARC R+M 2666

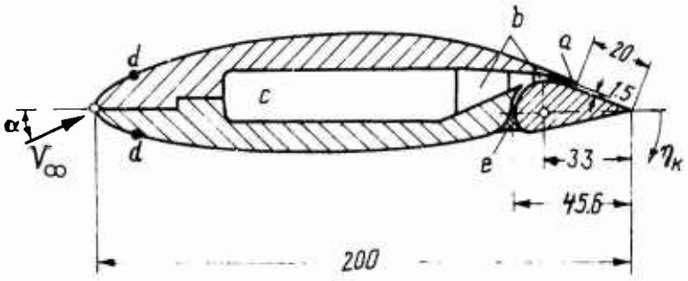

Fig.10 Wing section of NACA 66_4 A421 with suction device at the trailing-edge flap
Wind-tunnel model after K.O.Arnold [12]
(a) interchangeable trailing edge,
(b) spacer,
(c) suction chamber
(d) transition wire,
(e) sealing
(dimensions in mm)

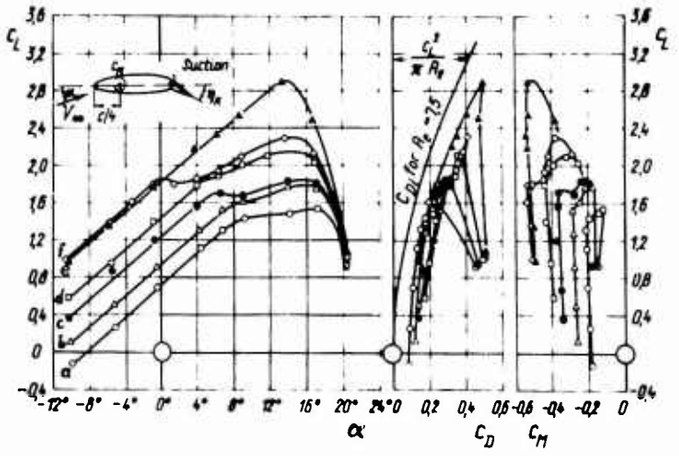

Fig.11 Three-component measurements on a wing with suction BLC at the trailing-edge flap
Wind-tunnel tests after K.O.Arnold [12]
(a) $c_Q = 0$ (d) $c_Q = 0{,}0262$
(b) $c_Q = 0{,}0144$ (e) $c_Q = 0{,}0292$
(c) $c_Q = 0{,}0180$ (f) $c_Q = 0{,}0351$

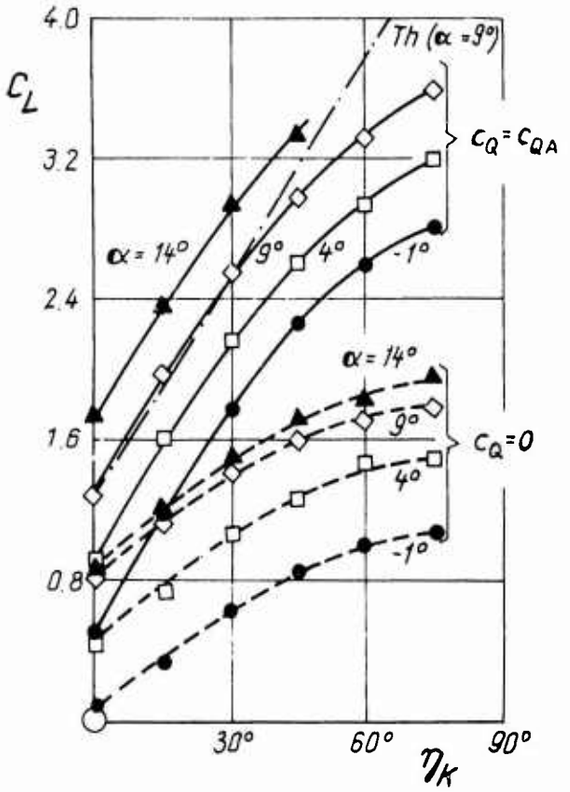

Fig.12 Lift coefficient versus trailing-edge flap angle with and without suction BLC . Wind-tunnel tests after K.O.Arnold [12] c_{QA} = minimum volume parameter, required for attached flow

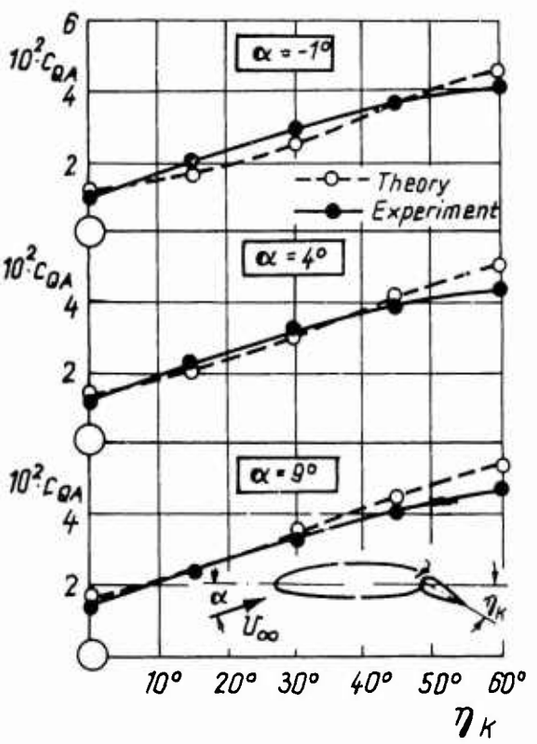

Fig.13 Comparison of theoretical and experimental results for the minimum suction coefficient Wind-tunnel tests at Re = $3.3 \cdot 10^5$ after K.O.Arnold [12]

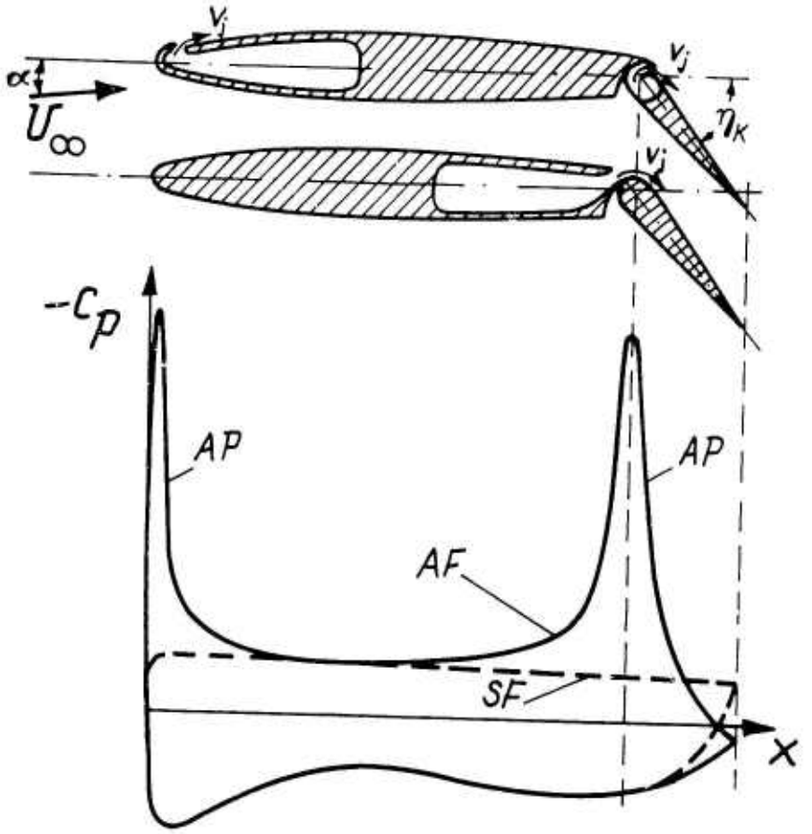

$$c_Q = \frac{m_j}{\varrho_\infty U_\infty S} = \frac{\varrho_j v_j s}{\varrho_\infty U_\infty c}$$

$$c_\mu = \frac{m_j v_j}{q_\infty S} = \frac{\varrho_j v_j^2 s}{q_\infty c}$$

$$q_\infty = \frac{\varrho_\infty}{2} U_\infty^2$$

Fig.14 Typical installation of blowing slots

AF = attached flow, SF = separated flow
AP = adverse pressure gradient
c_Q = volume parameter
m_j = mass flow of blowing jet
c_μ = momentum coefficient
q_∞ = pressure head
s = slot width, S = wing area

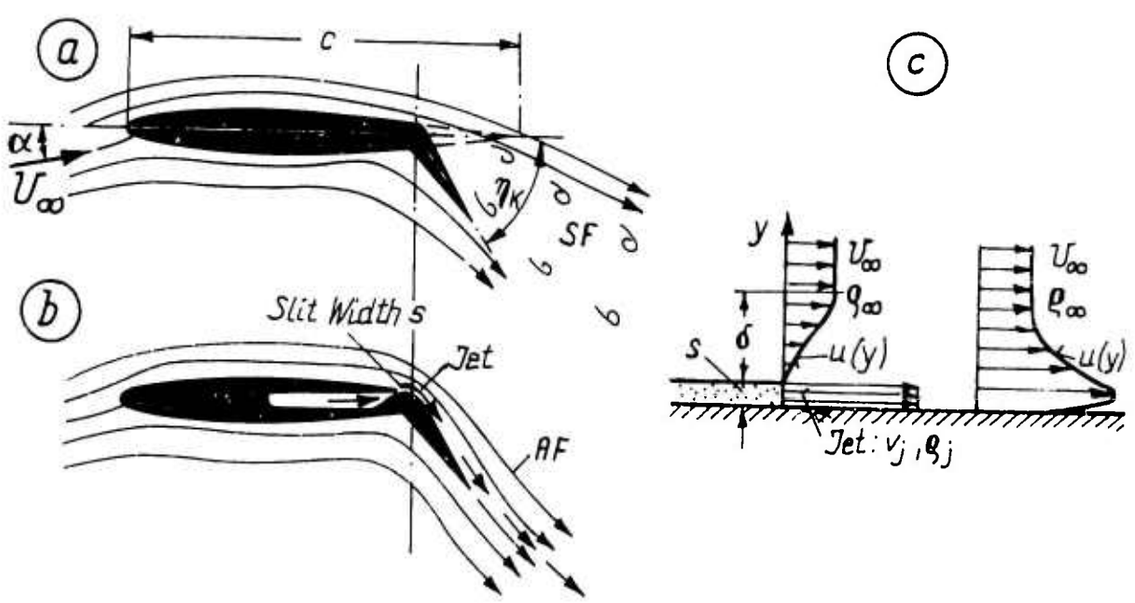

Fig.15 Flapped wing with blowing jet attached to the flap by Coanda effect

(a) separated flow (SF)

(b) attached flow (AF)

(c) velocity distribution for wall jet configuration

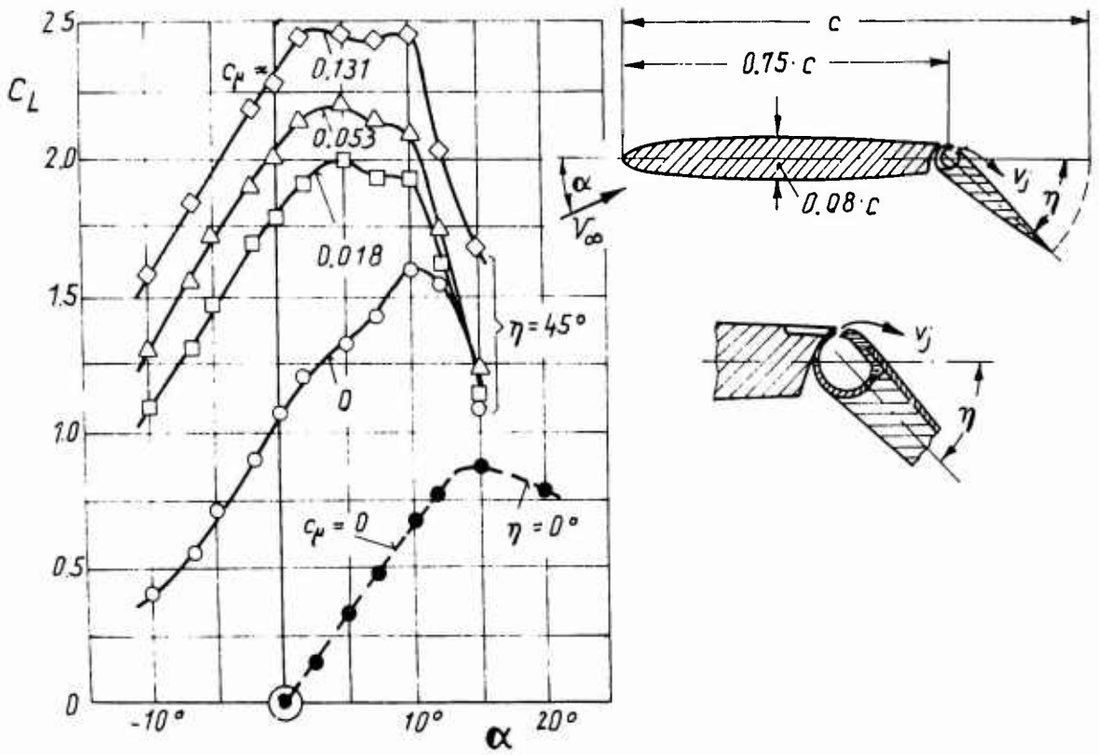

Fig.16 Effect of blowing over the trailing-edge flap on the lift coefficient
Wind-tunnel tests after J.Williams [13]

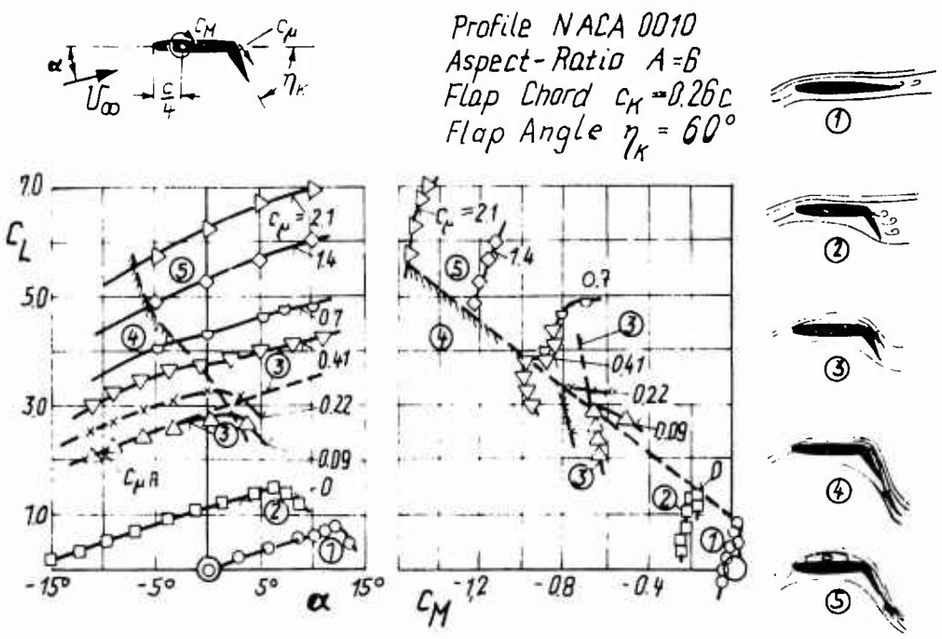

Fig.17 Lift and pitching moment of a profile with blowing over the trailing-edge flap
Wind-tunnel tests after R.I.ohr [16]
(1) without flap deflection, attached flow
(2) without blowing, separated flow at the flap
(3) minimum momentum coefficient $c_{\mu A}$ for complete BLC
(4) supercirculation
(5) separation bubble at the wing

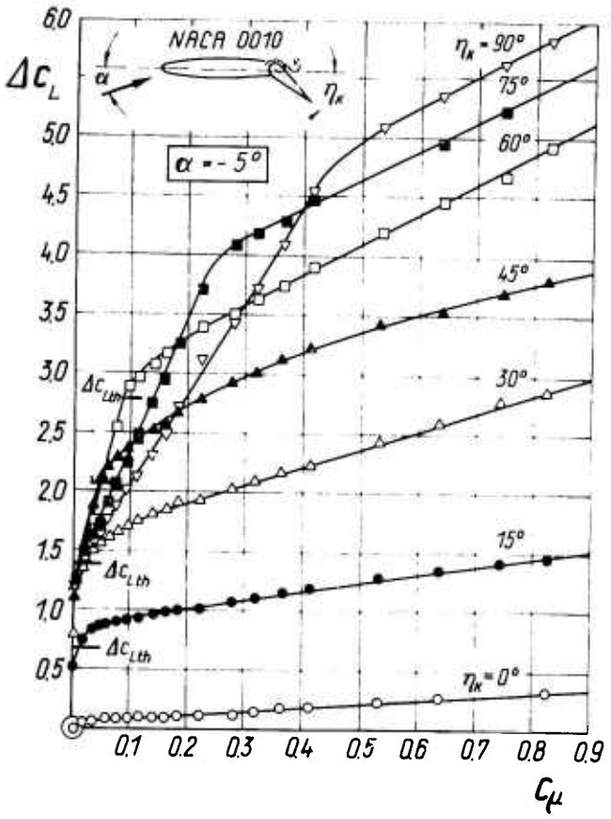

Fig.18 Lift increment due to blowing over the trailing-edge flap
Wind-tunnel tests after F.Thomas [14]

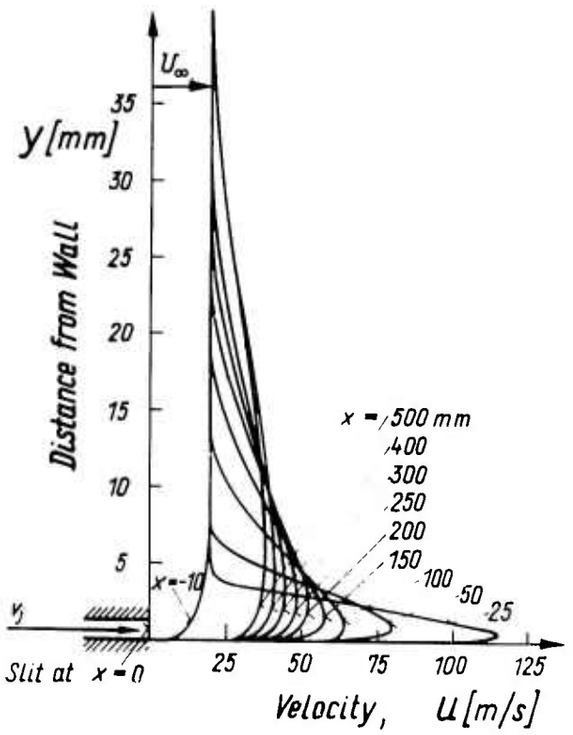

Fig.19 Velocity profiles in the boundary layer [ ] and a blowing slit
Wind-tunnel tests at a jet velocity ratio $v_j / U_\infty = 8$ by F.Thomas [14]

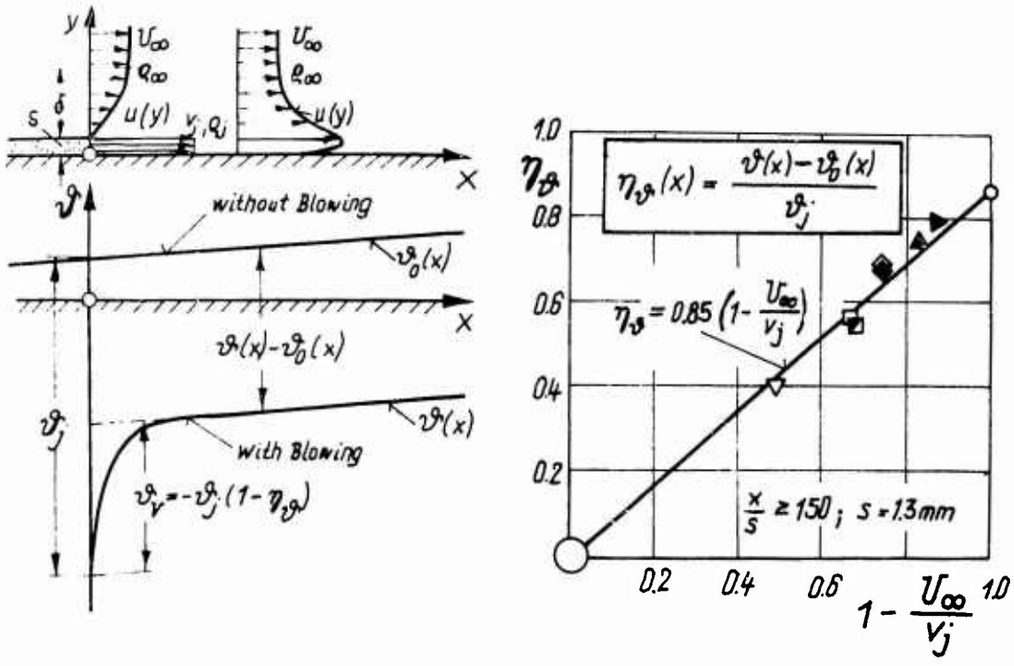

Fig.20 Momentum efficiency η_ϑ of the blowing jet as a function of the velocity ratio v_j/U_∞

Empirical formula after F.Thomas [14] ϑ_j = input of MLT by blowing jet
ϑ = momentum loss thickness (MLT)

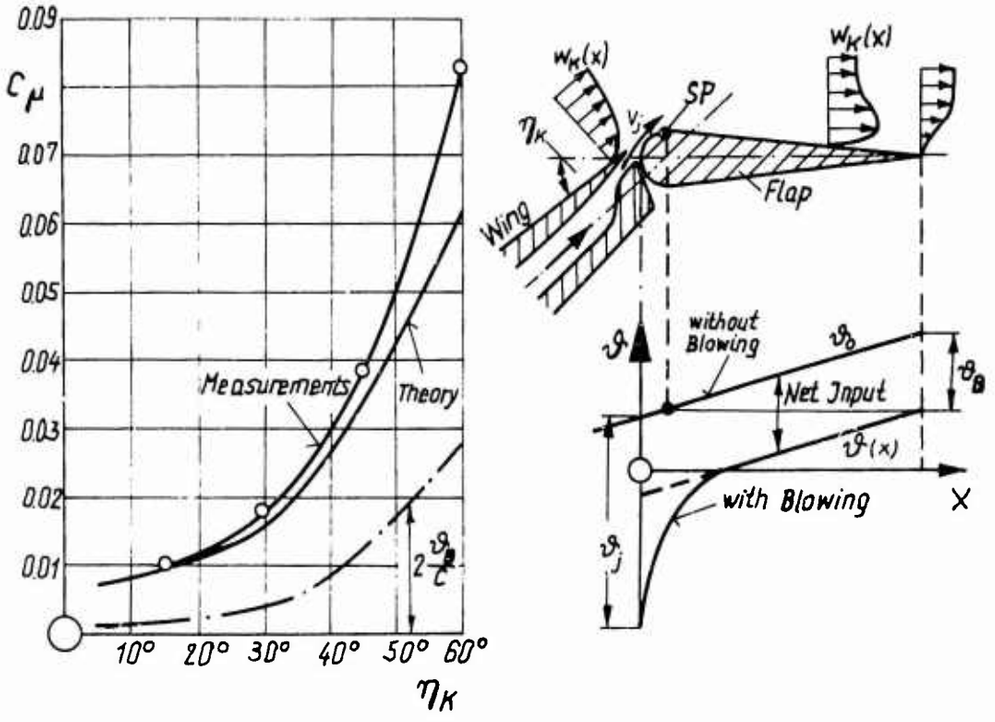

Fig.21 Estimation of minimum momentum coefficient $c_{\mu A}$ for avoiding separation on the flap after F.Thomas [14]

SP = separation point in case without blowing $\vartheta_B = \vartheta_0 - \vartheta$ = net input of MLT
ϑ = momentum loss thickness (MLT) with blowing ϑ_j = total input of MLT by blowing jet
ϑ_0 = MLT without blowing

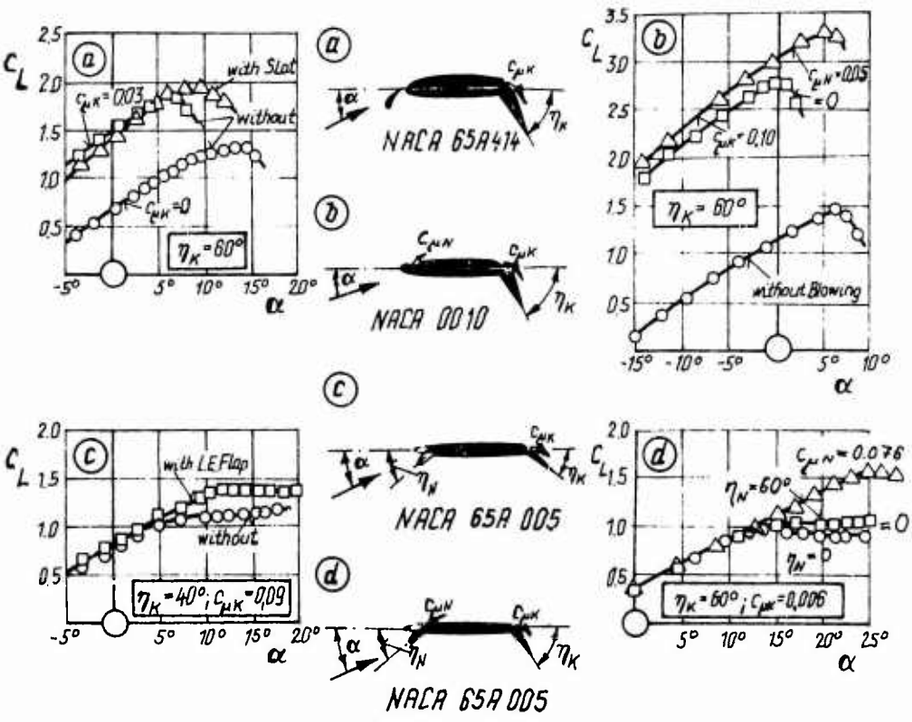

Fig.22 Various possibilities of BLC at the wing nose
(a) slat, Ref.: NASA TND 333
(b) blowing at the nose, Ref.: R.Lohr [16]
(c) leading-edge flap, Ref.: NASA TND 16
(d) blowing at leading-edge flap, Ref.: NACA RMA 58A09

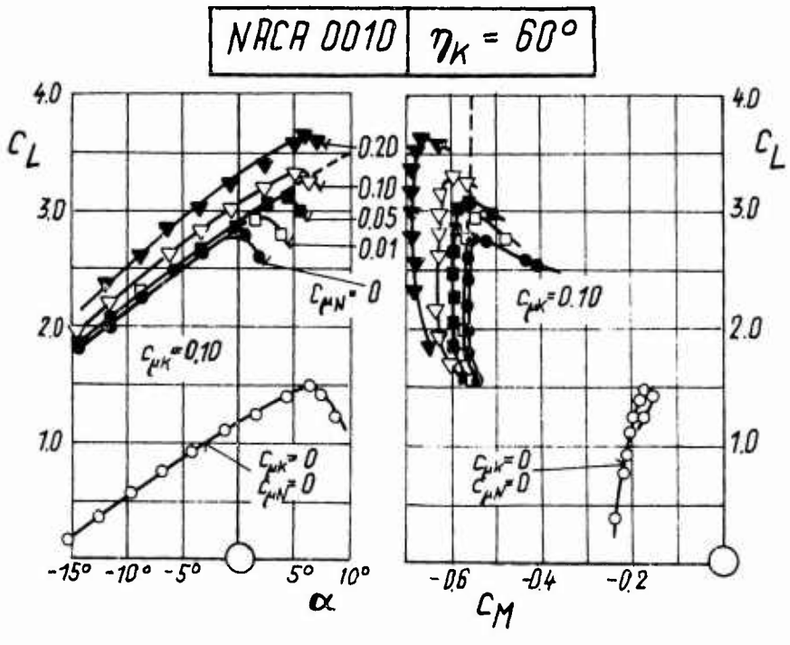

Fig.23 Effect of blowing at nose and trailing-edge flap on lift and pitching moment [16]

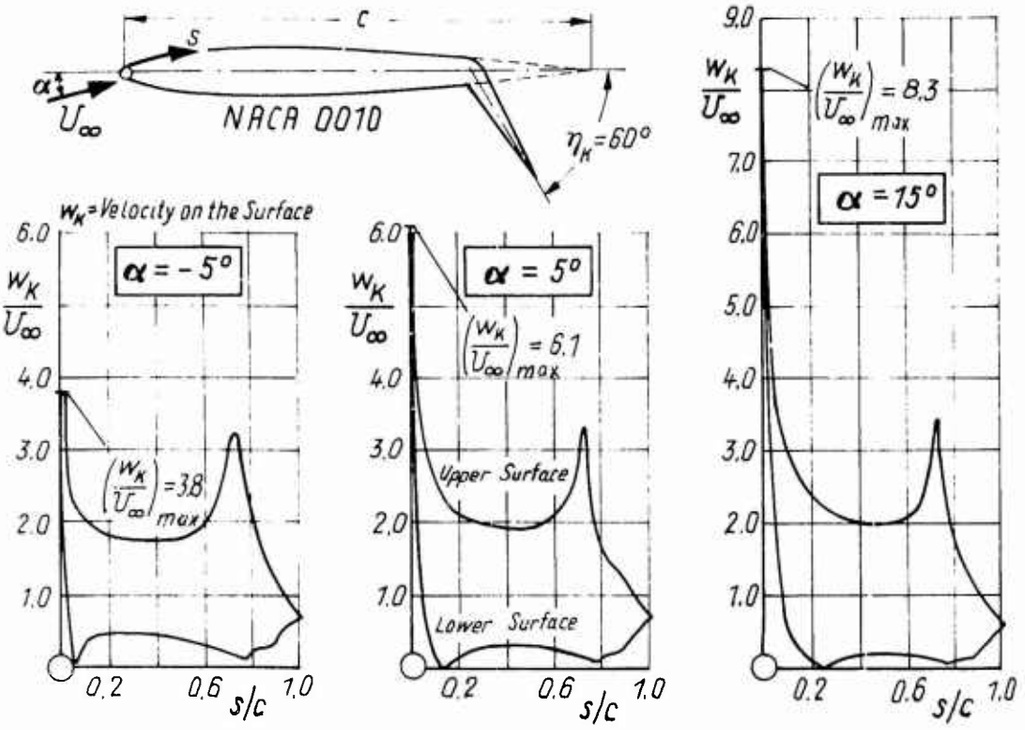

Fig.24 Velocity distributions over profile surface for inviscid potential flow

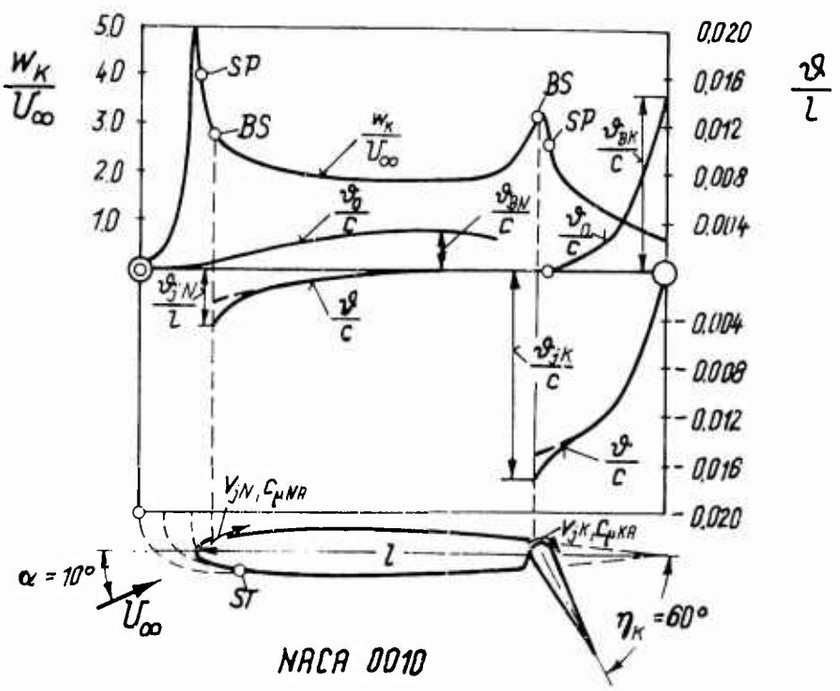

Fig.25 Estimation of minimum momentum coefficients at the nose $c_{\mu NA}$ and at the flap knee $c_{\mu KA}$

SP = separation point, BS = blowing slit
ST = stagnation point
ϑ = momentum loss thickness (MLT) with blowing
ϑ_0 = MLT without blowing
$\vartheta_B = \vartheta_0 - \vartheta$ = net input of MLT
ϑ_j = total input of MLT by blowing jet

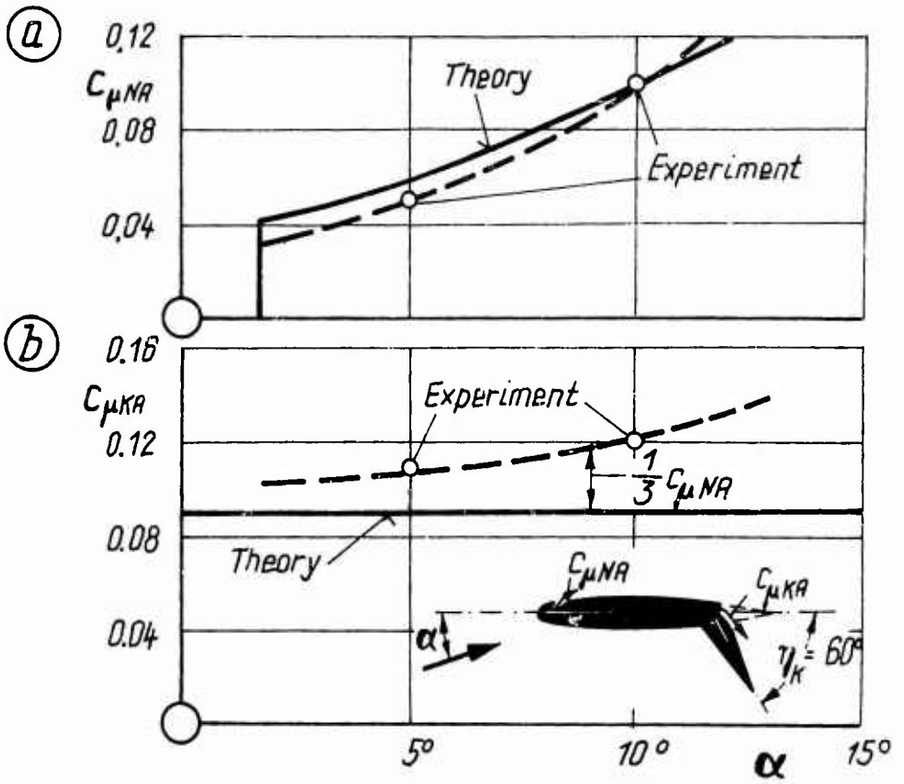

Fig.26 Minimum momentum coefficients preventing flow separation [16]
(a) momentum coefficient blown at the nose
(b) momentum coefficient blown over the flap

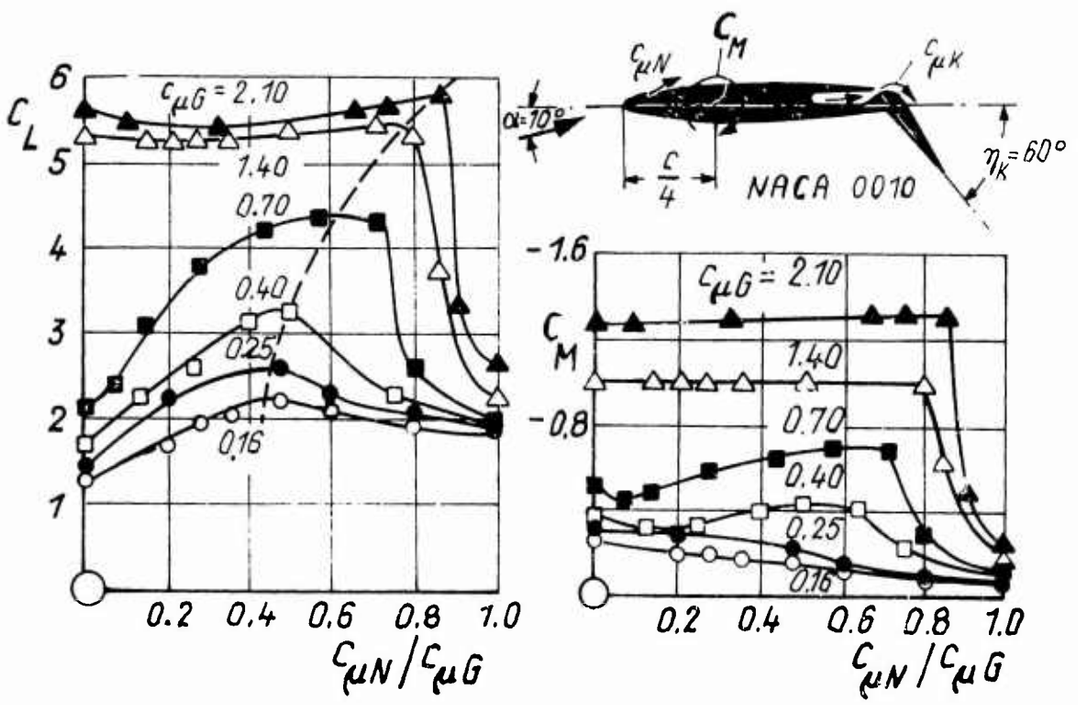

Fig.27 Effect of momentum ratio on lift and pitching moment [16]
$c_{\mu G} = c_{\mu N} + c_{\mu K}$ = total momentum coefficient
blown at the nose and over the flap

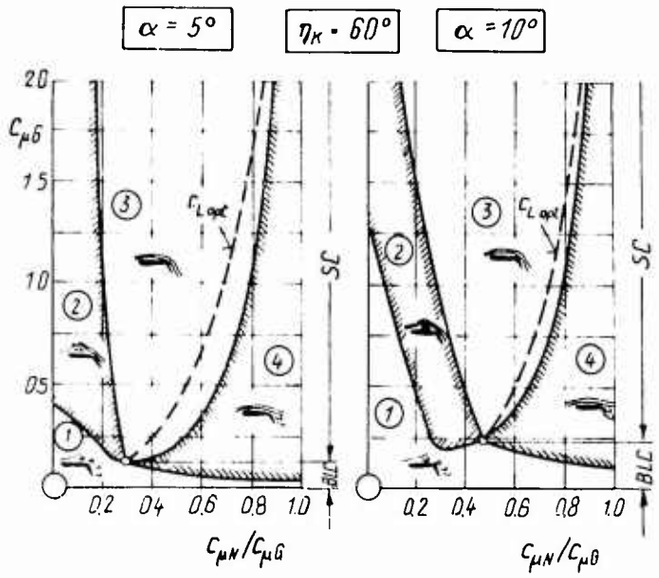

Fig.28 Flow condition on a flapped wing under the influence of different momentum ratios of blowing [16]

wing	flap
(1) separated	separated
(2) bubble	attached
(3) attached	attached
(4) attached	separated

BLC = boundary-layer control, SC = supercirculation
$c_{\mu G} = c_{\mu N} + c_{\mu K}$ = total momentum coefficient blown at the nose and over the flap

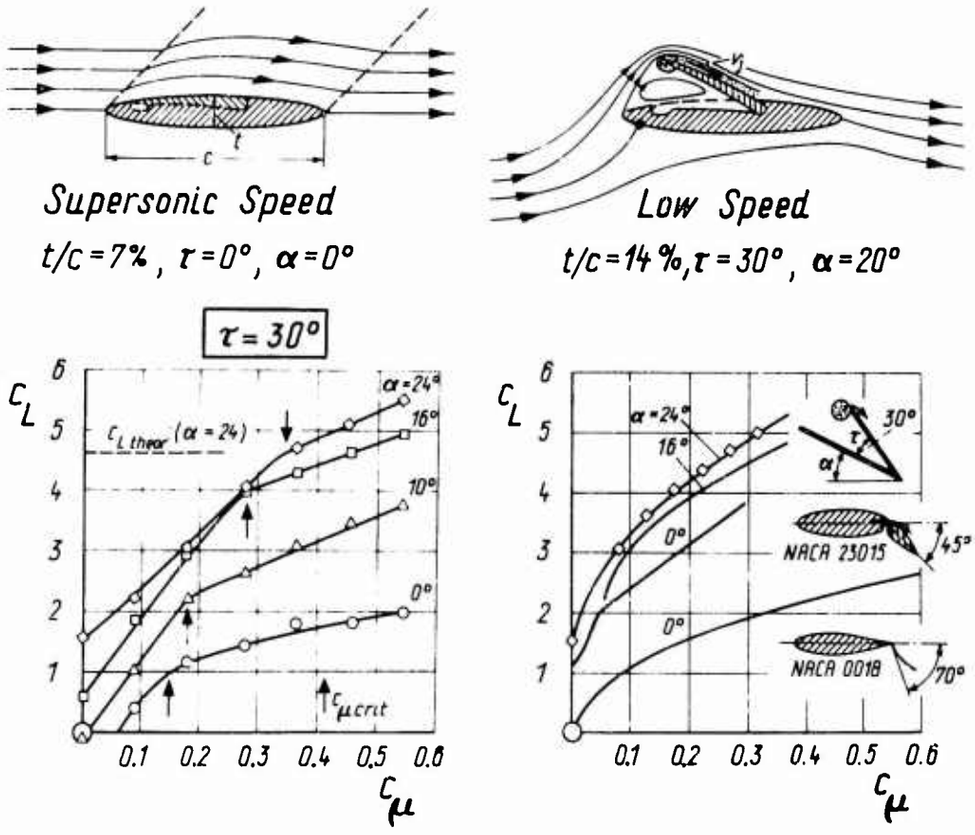

Fig.29 Forward facing flap after D.G.Hurley [2]
Free stream-line flow established by forward facing flap with blowing device

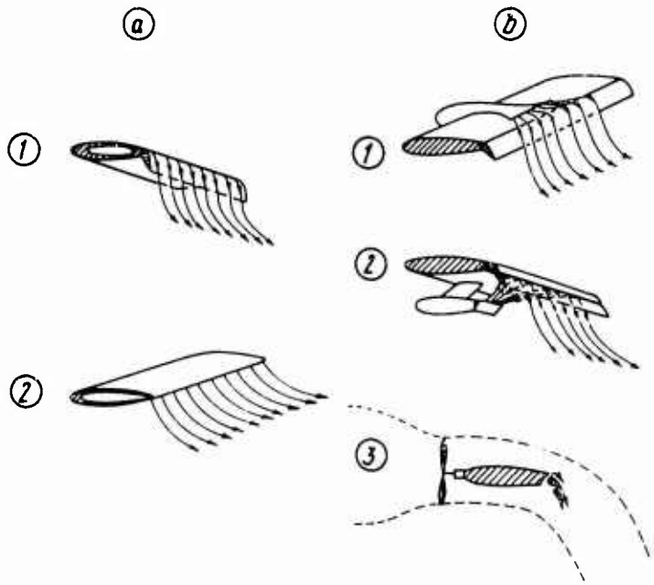

Fig.30 Various configurations of jet deflection
(a) Internal jet arrangement
(1) internal jet augmented flap
(2) pure jet-flap
(b) External jet arrangement
(1) external jet augmented flap with jet engine mounted on top of the wing
(2) external jet augmented flap with pod-mounted jet engine
(3) deflection of propeller slipstream by means of double-slotted trailing-edge flap

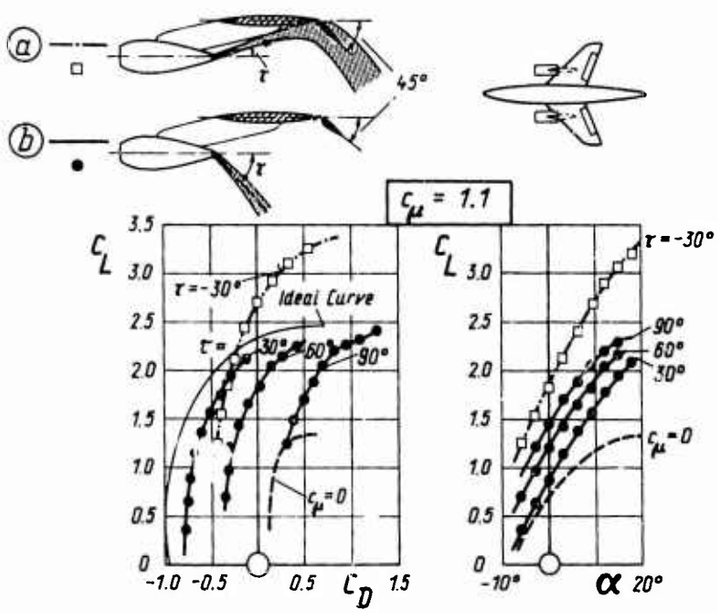

Fig.31 Effect of jet deflection on lift and drag
Comparison between two arrangements
(a) Upwards deflected jet exhaust (τ = -30°) impinging on double-slotted flaps
(b) downwards deflected jet exhaust (τ = 30°, 60°, 90°)
Wind tunnel results of 45 deg swept-back aircraft model with pod-mounted jet engine after Ph.Poisson-Quinton [2]

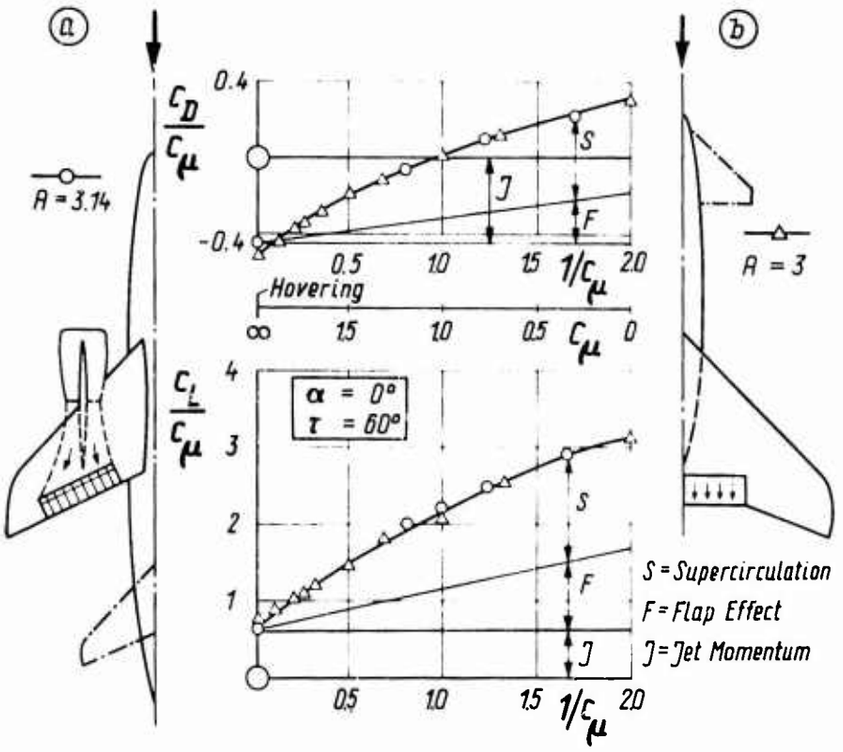

Fig.32 Comparison between external and internal jet augmented flaps

(a) external jet for conventional aircraft model with swept-back wing and pod-mounted engines
(b) internal jet for canard aircraft model with the same swept-back wing

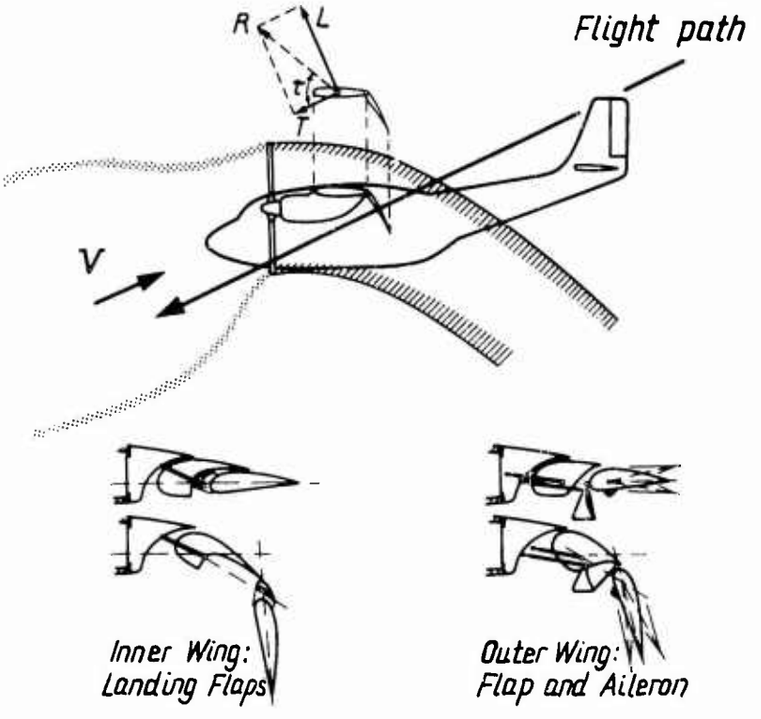

Fig.33 Vectored deflection of propeller slipstream. Application at Breguet 941
L = lift, T = thrust, R = resultant force

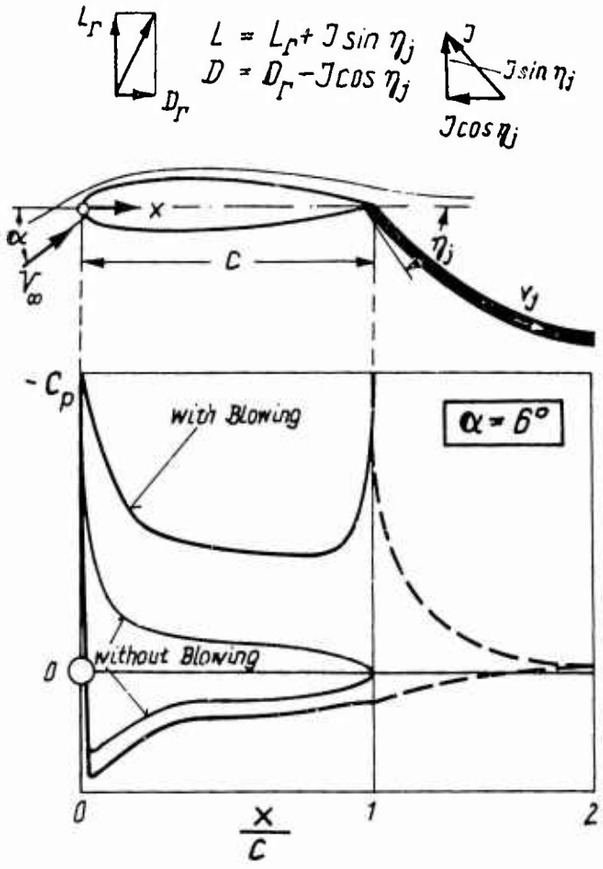

Fig.34 Pressure distribution of a jet-flapped aerofoil
L = lift due to circulation
D = lift induced drag due to circulation
J = jet reaction force

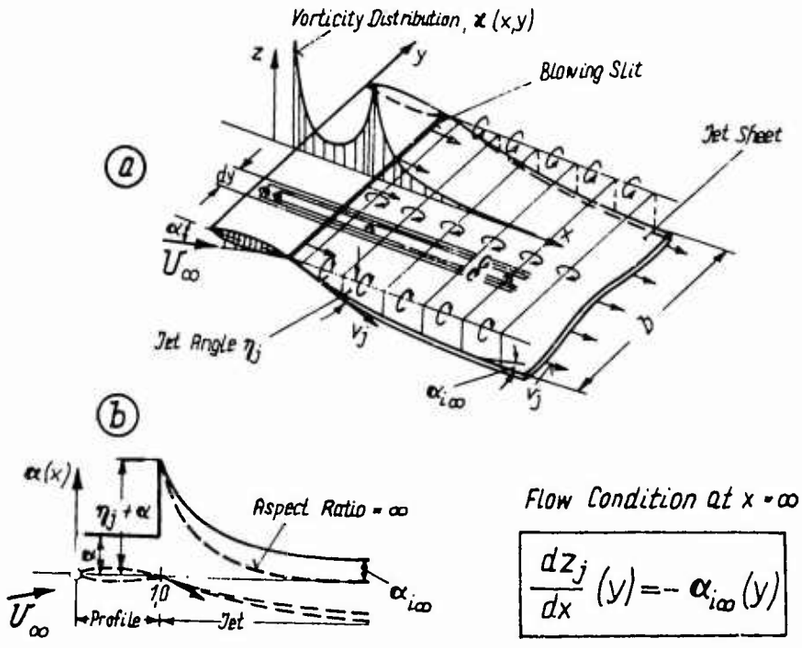

Fig.35 Vortex system of three-dimensional jet-flap theory after A.Das [20]
Adaptation of Multhopp's lifting surface theory to jet-flapped wings of finite span

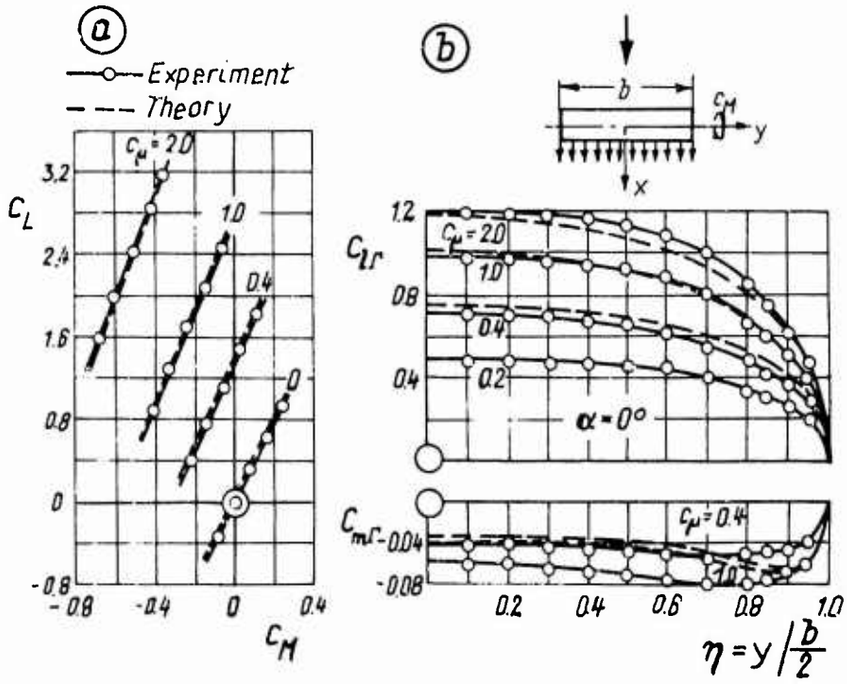

Fig.36 Lift and pitching moment for rectangular wing with jet-flap after A.Das [20]

(a) overall forces of lift versus pitching moment
(b) local forces of lift and pitching moment versus semispan (aspect ratio of the wing = 2.75)

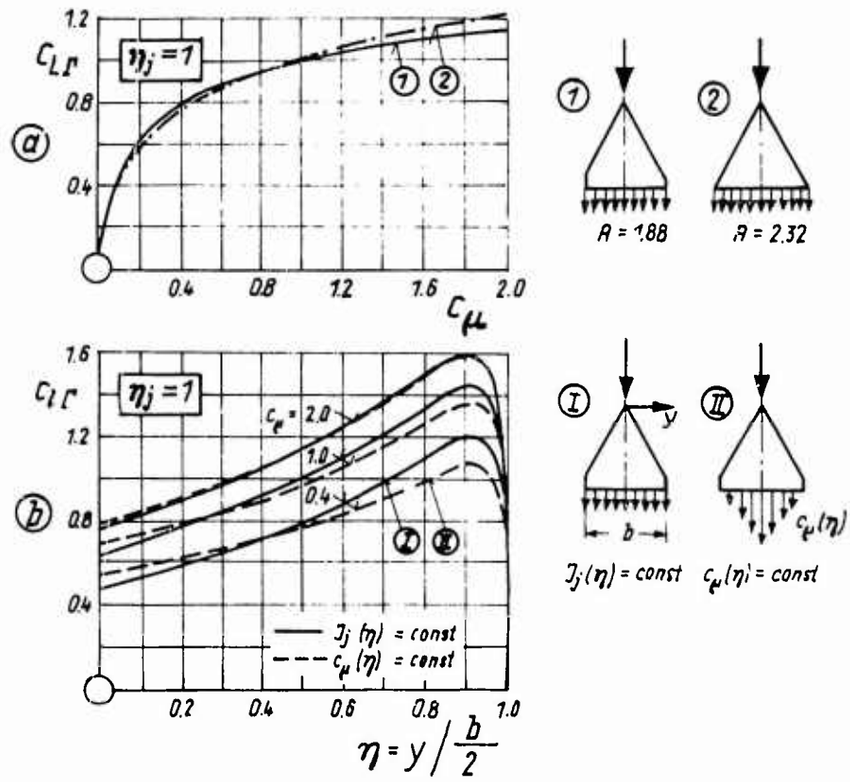

Fig.37 Lift distribution of a jet-flapped delta wing

(a) overall lift as a function of the momentum coefficient
(1) calculated by A.Das [20]
(2) electrolytical analogy by L.Malavard

(b) distribution of lift over semispan
I constant distribution of jet momentum over span
II constant distribution of momentum coefficient over span

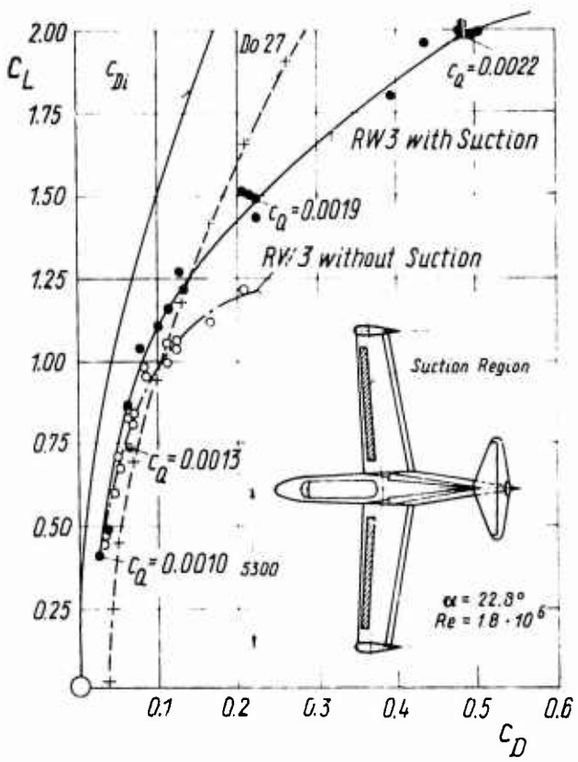

Fig.38 Polar curve of the experimental aircraft RW3A with nose suction
Flight tests by F.Schwarz

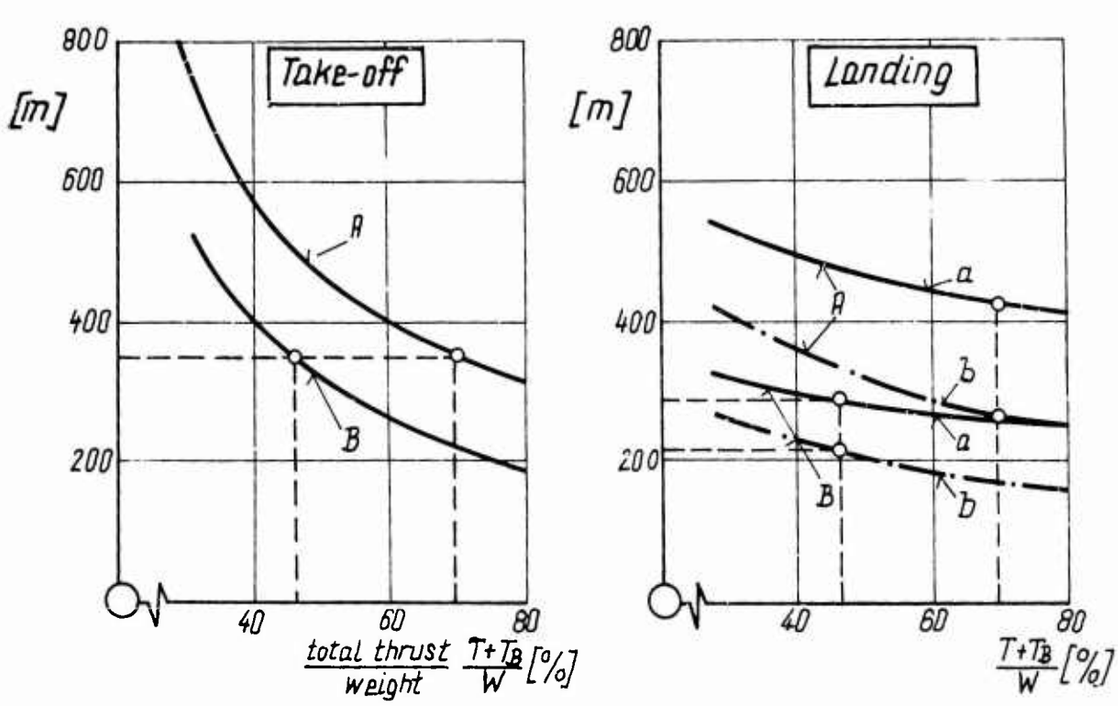

Fig.39 Take-off and landing distance as a function of total thrust
Calculated for an aircraft of 300 kp/m² wing loading, aspect-ratio 8 and 10.5 m obstacle by F.Thomas [26]
(A) double-slotted flaps without blowing
(B) plain flaps with blowing
(a) with flare out T = 0
(b) no flare out T ≠ 0

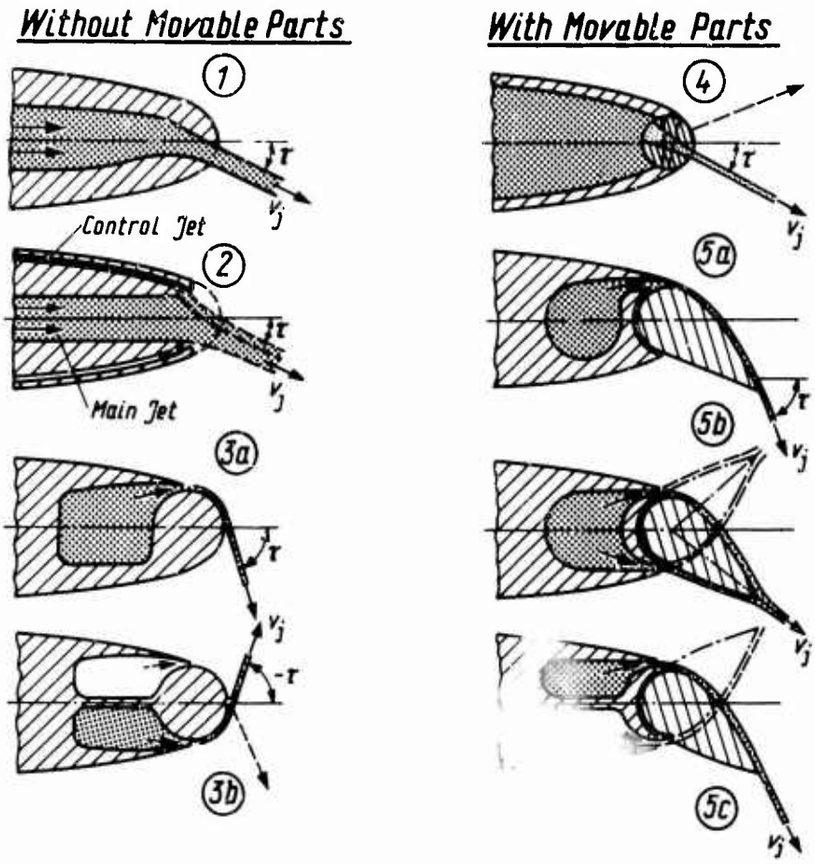

Fig.40 Design features of jet augmented flaps
(1) pure jet-flap with fixed jet angle
(2) jet-flap with chargeable jet angle: control jets
(3) jet-flap with changeable jet angle: Coanda effect
(4) jet-flap with changeable jet angle: rotary nozzle
(5) jet augmented flap with changeable flap angle

Maneuver Action	High Speed	Low Speed
Trim (Horizontal Flight)	Straight Jet Sheet	Jet-Flap Down
Elevator (Climb, Descent)	Change Angle	Change Thrust
Aileron	Change Angle	Change Thrust and/or Angle
Airbrake	Change Angle	Change Angle

Fig.41 Control forces and moments produced by jet-flaps
after I.M.Davidson [2]

SUMMARY OF DISCUSSION

relating to

AERODYNAMICS OF PNEUMATIC HIGH-LIFT DEVICES

1. Theoretical Methods for Predicting the Critical Momentum Coefficient

A theoretical method for predicting the critical momentum coefficient $C_{\mu A}$ for complete boundary-layer control in the case of a two-dimensional aerofoil has of course been given in the paper. However, an exact method of calculating the minimum blowing momentum needed to prevent flow separation in the three-dimensional case is still beyond the scope of boundary-layer theory. Nevertheless, the two-dimensional method put forward by F. Thomas, which is based on the integral relationships of boundary-layer theory, gives a first estimate for $C_{\mu A}$. Then, for example in the case of a swept-back wing of finite span, one has to chose some arbitrary higher value.

2. Use of Supersonic Blowing Speeds

It has been pointed out that the most favourable condition, giving the smallest momentum coefficient $C_{\mu A}$ for avoiding separation of the boundary-layer, is achieved with very small slot widths and hence with high blowing velocities. However, overall, it would not be advantageous to blow with supersonic speeds. The structural complication to ensure a good jet sheet of supersonic speed would be considerable, and it is already difficult to manufacture a simple convergent slot with constant slot width and uniform momentum distribution in the spanwise direction. Moreover, the maximum blowing velocity can be limited by the pressure ratio available from the compressor of the jet engine. In fact, the lecturer's opinion is that the highest blowing velocity which seems reasonable for practical application is the speed of sound.

3. Noise Produced by BLC or Jet-flap

Turbulent mixing and entrainment processes are the main reason for the generation of noise, and the noise energy grows proportionally to the eighth power of the jet velocity. However, the shape of the jet has also some influence; the noise generated decreases with increase of the ratio of actual jet circumference to the circumference of the equivalent circular jet of the same cross-sectional area. In this sense, the thin jet sheet blown out for boundary-layer control or in the form of a jet-flap has a favourable circumference ratio (i.e. very large). Thus, with BLC and jet-flaps the noise generation is low in comparison with the noise produced by a conventional jet nozzle, which usually has a circumference ratio near unity.

4. Variation of Optimum Momentum Ratio with $C_{\mu G}$ in Fig. 27 of the Paper and Possible Dependence on Reynolds Number

For combined blowing at the nose and at the trailing-edge flap of a NACA 0010 aerofoil, Fig. 27 shows the lift plotted against the momentum ratio $C_{\mu N}/C_{\mu G}$, where $C_{\mu N}$ is the momentum coefficient blown out at the nose and $C_{\mu G}$ is the total blow momentum coefficient at the nose and the flap knee. Each lift curve (for $C_{\mu G}$ = constant) shows a maximum at a certain momentum ratio, so that the optimum blowing ratio can be identified (see dotted line). For example, with small $C_{\mu G}$ - coefficients ($C_{\mu G} = 0.15$), the best efficiency is obtained at low momentum ratios ($C_{\mu N}/C_{\mu G} = 0.4$). i.e. more momentum is blown out at the rear than at the nose of the aerofoil; whereas, for high $C_{\mu G}$ - coefficients ($C_{\mu G} = 1.5$), the optimum is obtained at high ratios ($C_{\mu N}/C_{\mu G} = 0.8$). This dependence of the optimum momentum ratio on $C_{\mu G}$ can be interpreted with the help of Fig. 28. In Fig. 27, a configuration is represented having a high angle of incidence ($\alpha = 10^{\circ}$) in addition to the very high angle of flap deflection ($\eta_K = 60^{\circ}$). In this case, the danger of a flow separation at the nose in the form of a local bubble is imminent, apart from the separation at the trailing-edge flap. Thus, in order to achieve completely attached flow at $\alpha = 10^{\circ}$, it is necessary to blow out 50 per cent of the total jet momentum ($C_{\mu G} = 0.24$) at the nose, whereas at $\alpha = 5^{\circ}$ only 30 per cent of $C_{\mu G} = 0.12$ needs to be blown at the nose. These two points are marked in Fig. 28. When increasing the total momentum beyond the BLC into the

the supercirculation regime, it is more effective with respect to the lift to increase the percentage of the nose momentum too, blowing at the flap knee only as much as necessary to avoid separation at the trailing-edge. This is illustrated by the dotted lines in Fig. 28. The influence of the blowing at the nose in the supercirculation regime may be interpreted as an increase in the effective camber of the aerofoil. Attention should be paid to the fact that here, as in the whole lecture, mainly very severe momentum coefficients are considered and the range of weak blowing (say $C_\mu \prec 0.1$) is not treated very thoroughly. Naturally, Reynolds number has some influence on the whole mechanism, but this influence again is more important in the case of weak blowing.

AERODYNAMICS OF VARIABLE SWEEP

by

Ph. POISSON-QUINTON

Adjoint au Chef du Département des Etudes de Synthèse, O.N.E.R.A.

Chatillon-sous-Bagneux, France

1. INTRODUCTION

As you know, variable geometry has been applied to aircraft design in various forms for over 30 years. Typical examples are the undercarriage, flaps, airbrakes, variable-pitch propellers, and variable intakes and nozzles for engines. From an airframe point of view, we show in Fig. 1 some other examples where the wing or tailplane geometry is changed, as follows.

(A) The first configuration is a telescopic wing tested in France before the war by Makhonine; but this idea was not profitable because of the very small performance gain for the very complicated mechanism to translate the telescopic wing.

(B) The second example concerns the well-known extension of the wing surface by means of the rearward and downward movements of a slotted flap (Fowler-flap type); this system has become more and more sophisticated with recent transport aircraft, the most impressive being the tri-slotted flap used on the Boeing 727.

(C, D) The next two examples of variable geometry were proposed to improve some supersonic characteristics of high-speed aircraft, mainly their yawing stability (auxiliary fins) and their longitudinal manoeuvrability (by static margin reduction); the first one is the well-known wing-folding-tip as used on the American B70, an experimental Mach 3 bomber; the other is a folding tailplane tested in a wind-tunnel some years ago by ONERA, the unfolded tailplane being also used to trim some high-lift devices at a low speed.

(E) Lastly, the most interesting variable-geometry scheme is the variable-sweep wing, which is the subject of this paper.

It is perhaps worth recalling that the original concept for a variable-sweep wing is generally attributed to the well-known British engineer of the Vickers Company, Dr. Barnes Wallis, as early as 1944. By 1951, in the United States, Bell Aircraft had built and NACA had flown the X-5 subsonic experimental aircraft, while in 1952 the Grumman XF-10-F aircraft was completed for the US Navy. By 1958, Dr. Barnes Wallis produced designs of variable-sweep aircraft where only the outer portion of the wing was moved, the presence of the fixed delta-shaped inner wing alleviating the changes of both centre of gravity and centre of pressure with sweep; the aerodynamic centre variation was much less than with earlier designs in which the whole wing moved.

This new concept was discussed with NASA, who then began extensive wind-tunnel and analytical investigations. Their primary aim was to develop stable and controllable configurations, with near-optimum performance at both high-speed and low-speed. As you know, these American researches led to the military TFX programme culminating in the F111 multi-mission combat aircraft, and also to Boeing supersonic transport projects.

In 1963, the French Air Ministry asked O.N.E.R.A. to make a general study (both theoretical and experimental) on the variable-sweep principle, and asked the BREGUET Company to begin a feasibility study of a multi-mission fighter; in the mean time, DASSAULT Company undertook a project, with preliminary tests in various O.N.E.R.A. facilities. Finally, in October 1965, the DASSAULT Company was asked by the French Defense Department to build a prototype of a variable-sweep aircraft, namely the Mirage G; the first flight took place only two years afterwards, in November 1967, and a large part of the flight envelope was explored two months later.

Contemporary project studies led in Britain to the BAC advanced combat aircraft concepts (P45/ACA), and in Germany to the MPB Neuen Kampfflugzeug (NKF). These have of course now developed into the British/German/Italian multi-role combat aircraft project (Panavia MRCA).

Before beginning with my subject proper, namely high-lift performance for a variable-sweep aircraft, I must stress that it was quite difficult to prepare this paper, because a large part of the results on variable-sweep aircraft development is still classified in most countries. However, I shall try to explain some specific aerodynamic problems encountered in variable-sweep applications for:-

(a) Multi-mission military aircraft.

(b) Supersonic transport aircraft.

(c) Lifting bodies for re-entry from space.

2. AERODYNAMIC GOALS OF THE VARIABLE-SWEEP WING

2.1

Our goal some seven years ago, was to define an aircraft having, at the same time:-

The low-speed characteristics of a transport aircraft, with its very high aerodynamic efficiency at sub-critical Mach numbers;

the high-speed manoeuvrability of a modern fighter in transonic flight;

the good aerodynamic efficiency of a slender wing in supersonic flight.

Today, we shall speak mainly about this first requirement; but it is important to recall that, for a multi-mission aircraft, the fully-swept wing configuration with 70-75° sweepback angle is also very favorable for transonic low-level attack, because of the low gust sensitivity associated with the small

lift gradient of this slender wing. On the other hand, the high aspect-ratio of the unswept wing, with a leading-edge sweepback of 15-25°, offers a favorable condition for good aerodynamic efficiency in subsonic missions (surveillance, loiter, ferry missions, etc), together with high-lift capability for short take-off and landing.

2.2

First, we must discuss the choice of the pivot location, which plays a very important role as regards the aerodynamic and the flying qualities of a project. As shown on Fig. 2(a), with an inboard pivot location at the edge of the fuselage, the aerodynamic centre moves rearward as the sweep angle is increased. When the pivot is located at a selected outboard position, however, the aerodynamic centre for the swept configuration may be at the same location as that for the unswept configuration. From Fig. 2(b), it is evident that the static margin becomes very significant with the wing swept when the pivot is inboard. However, we shall see that a compromise must be adopted for the outboard location, to preclude the risk of a longitudinal instability (pitch-up) at large incidence arising from the up-load on a large fixed apex.

2.3

At the beginning of our work in ONERA, we treated this pivot problem theoretically (Fig. 3), making a systematic study of a family of wings having the same unswept planform (trapezoidal wing of aspect-ratio 7.5 taken as reference area, with leading-edge sweepback 15°, taper-ratio 1/3) and a fully-swept position with 70° sweep-back. We have analysed various locations of the pivot along the span and also along the local chord, six locations being tested in detail for three or four sweep angles by the rheo-electric analogy method in a three-dimensional tank. The main conclusion of this theoretical approach, now well confirmed by wind-tunnel tests, is summarised in Fig. 4. The centre of pressure shift between the two extreme sweep angles (15° and 70°) varies almost linearly with the spanwise location of the pivot. With an outboard pivot located at about 30 per cent of the span of the trapezoidal wing, the centre of pressure is exactly at the same position for these two extreme sweep angles. On the same Figure, the lift gradient $C_{L\alpha}$ of the slender configurations is seen to be about half the value obtained in the unswept wing position. It is also important to notice that the fixed-apex surface, on the front of the trapezoidal wing, grows when the pivot is more outboard along the span.

These same trends on the influence of the pivot location have been found in a British study (Fig. 5), where the aerodynamic centre position is plotted against the sweep angle with the Mach number increasing to give always a subsonic leading-edge.

Next, it is interesting to examine the shift of the aerodynamic centre with sweep angle in the case of two complete configurations, the tailplane being located just at the rear of the trailing-edge of the 70° wing (Fig. 6). Again, there is a very large difference of aerodynamic centre shift between an inboard and an outboard pivot. Also the amount of stability provided by the tailplane remains almost constant when the sweep angle increases from 15° to 70°, as shown at the bottom of this Figure.

3. HIGH-LIFT DEVICES

As in the pivot location analysis, we have made our theoretical study of trailing-edge flap effectiveness using the electric analogy method, on a typical extended wing configuration (A.25, $\phi = 15°$) with a 30 per cent chord flap over 75 per cent of the span. Fig. 7 gives the 'reduced circulation' ($\gamma = \Gamma/U_0 b$) along the span, both for angle-of-attack effect and for unit flap deflection; also, the integration of the local centres of pressure due to the flap effect giving the mean value on the reference chord.

For the combination of 11° angle-of-attack and 45° flap deflection, $C_L = 3$ is theoretically obtained; in fact, such a value can be realised only with boundary-layer control, both on the wing leading-edge and on the flap, or with a sophisticated slotted-flap system. Fig. 8 shows that, on a wind-tunnel model of this configuration equipped with a single-slotted flap, only 65 per cent of the theoretical flap effectiveness is obtained, while a simple Krüger flap at the leading-edge of this 10 per cent symmetrical profile appreciably increases stalling incidence and delays the pitch-up problem, as we shall see later.

The flap efficiency is reduced progressively when the wing sweep increases (Fig. 9), as predicted theoretically; but, between 15° and 25° sweepback the loss of lift is very small, so it is feasible to make use of this sweep flexibility to adjust the static margin of the aircraft at its best value during take-off and landing.

For this low-speed configuration, it is also interesting to examine the important problem of roll control (Fig. 10). A differential tailplane deflection, as used during high-speed flight ($\phi = 45°$ to $70°$) is not efficient enough for roll control at low speeds, where a spoiler system is probably the best solution permitting the flaps to be retained over the whole wing span. On Fig. 10, it is also shown that the spoilers (65° deflection, between 35 per cent and 95 per cent of the span) lose a large part of their effectiveness when the wing sweep is increased. Their efficiency is much improved at ($\phi = 15°$) when the flaps are deflected, because a large part of the lift increment ΔC_{LF} from the relevant flap is then destroyed by rear separation, giving a strong rolling moment. Finally, the spoiler effectiveness remains quite large near the stalling incidence, as evident from the right-hand diagram of Fig. 10.

Another very interesting aspect of this variable-sweep aircraft is shown on Fig. 11, where the lower diagram gives the yawing stability curves and the induced roll in side-slip for the two extreme configurations with 15° and 70° sweep angles. The same tailplane differential deflection ($\Delta\beta_t = 14°$) gives almost the same roll effectiveness in both cases; the upper curves show also that the yawing stability is almost the same for these two extreme configurations, even at this large angle-of-attack of 10°.

4. WING CAMBER

Leading-edge camber all along the span of a wing is well known to improve both the stall conditions at low speeds and the cruise efficiency (L/D); such application is very interesting for a variable-sweep aircraft. For the configuration already mentioned (A.25), we have calculated a conical camber distribution by slender wing theory (M = 1) on quasi-delta shaped wing with 70° sweep (Fig. 12); this very narrow camber (on 10 per cent span only) is quite pronounced when the wing is unswept to 15° sweep. In this case, such a camber allows a very high local C_L with the theoretical stagnation point located at the nose leading-edge, as shown in Fig. 13 by the streamlines obtained from electric analogy studies on a two-dimensional section at 90 per cent of the wing span. Fig. 13 also gives the theoretical lift distribution along the span with flaps deflected at 45° and with 6° angle-of-attack (mean C_L = 2.46). The efficiency of this cambered leading-edge was then proved by wind-tunnel tests; the leading-edge separation on the extended wing is removed up to high angles-of-attack, and also the leading-edge vortex on the fixed apex is greatly reduced (pitch-up problems delayed).

Another advantage of this camber, both on the apex and on the moveable wing, is the induced drag reduction as shown on Fig. 14. Here, for various sweep angles, the experimental values of C_L^2 vs C_D are plotted to show the large gain in L/D given by this camber for all the sweep values. Note that this camber improves the L/D of the 70° sweep configuration in the whole Mach number spectrum, up to M = 2.5. Moreover, the tuft flow visualisation patterns (Fig. 15) on the two extreme configurations, at the 8° angle-of-attack giving the best L/D, indicate that the vortex lift on the leading-edge of the arrow wing begins only above this incidence and that the flow is still very smooth in both cases.

5. THE PITCH-UP PROBLEM

The main problem encountered on variable-sweep configurations with a large fixed apex is a longitudinal instability near the stall, due to the increasing load on the apex while the movable wing is already stalled. One solution is to find a tailplane location which can compensate this nose-up tendency, as illustrated on Fig. 16, where the longitudinal stability curves for two horizontal tailplane locations are plotted (on the left). With a tailplane just in the same plane as the wing, there is a quite sharp nose-up pitching moment at the stall whereas, with a low-tailplane location, the aircraft stalls with a good nose-down pitching moment. For an intermediate tailplane position, shown on the right of Fig. 16, the longitudinal instability zone is very narrow and followed by a nose-down tendency after the stall. This behaviour is well explained on Fig. 17, where the mean downwash at the tailplane is plotted against angle-of-attack; the sudden loss of downwash due to the wing flow separation reduces the nose-up pitching moment given by the tailplane, and so balances the pitch-up tendency due to the wing apex.

Many large models of supersonic transport projects have been tested at high Reynolds numbers in the full-scale 40 x 80 ft wind-tunnel at the NASA Ames Research Center. In analysing the results from US laboratories, it should be noted that the swept wing (high-speed configuration) is usually taken as reference area. On the model shown in Fig. 18, NASA have studied the influence of the horizontal-tailplane location on longitudinal stability. Without horizontal tail, there is a strong pitch-up tendency well before the C_{Lmax} and a high tailplane location does not improve this instability very much; but a low tailplane is much more favorable and, in this case, the pitch-up appears only at the stall. On this configuration, the fixed apex of 70° sweep has a sharp leading-edge, which therefore exhibits a strong vortex flow at high angle-of-attack giving a nose-up trend at the stall.

Various flap configurations have also been tested by NASA on the same model, as summarised on Fig. 19. The diagram on the left shows that the outboard flap deflection gives some extra lift, but that the gain in C_{Lmax} is quite small. The second diagram shows that a double-slotted flap is more efficient than a simple one, but here again there is no gain in C_{Lmax}. The third diagram, on the right, confirms that it is possible to increase the sweep of the movable wing from 13.5° to 25° without loss of flap effectiveness.

Another configuration, very similar to the first Boeing SST project, has also been tested by the NASA in the same wind-tunnel (Fig. 20); here, the main aim was to control the flow on the fixed apex (or strake) to delay the vortex formation and hence the pitch-up. In fact, a round leading-edge (R_3) on the original sharp strakes (R_1) improves the longitudinal stability, but it is necessary to incorporate also some vortex generators on the strake, and the wing fence, to remove completely the pitch-up tendency. Of course, such devices are not easily stored during high-speed flight. Again on the same model, NASA made some tests with a blown flap having the same span as a conventional double-slotted flap. Fig. 21 shows that, for 50° flap deflection, flow attachment over the blown flap is obtained with a C_μ value of about 0.05, but a very strong pitch-up appears at the stall, despite the incorporation of a Krüger flap on the fixed apex to delay the vortex formation. In fact, the blown flap does not give a better C_{Lmax} than a conventional double-slotted flap, because of the premature separation on the movable wing and the vortex interaction on the apex.

In the case of the first Boeing SST project (Fig. 22), it was impossible to choose a low position for the horixontal-tailplane, because of the proximity of the engine jets. Hence, the longitudinal stability was not satisfactory at high angles-of-attack. Fig. 22 shows some typical results obtained by Boeings on a small model of this first project. The lifting effectiveness of the trailing-edge flaps was very good, but the behaviour of the pitching-moment was judged unsatisfactory, in spite of the very large slot on the apex leading-edge.

In the second Boeing SST project (Fig. 23), the four turbo-jets were put under a very large horizontal-tailplane, but in this case the tail arm was greatly reduced; thus a large part of the lift from the very efficient flap system was lost by the longitudinal trim. In the last version of this configuration, Boeing tried to improve the longitudinal trim by using a canard surface, but the aerodynamic gains were not sufficient to compensate for the increase of structural weight.

Clearly, it is much more difficult to design a civilian variable-sweep aircraft than a military one, because it is not acceptable to put jet engines inside the fuselage instead of the passengers. Already, in various countries, many variable-sweep applications to military aircraft are in a production phase (American F111), in a flight evaluation phase (French Mirage G, Russian Mikoyan), or in the design phase (French Mirage G4, Anglo-German-Italian MRCA, American fighter F14, American bomber B1); currently, this variable-sweep concept appears to be the only acceptable solution for multi-mission purposes.

6. VARIABLE-SWEEP APPLICATION TO RE-USABLE SPACECRAFT

To conclude, it is interesting to look at some applications for the space shuttle programme (NASA). Variable-sweep concepts can be applied both for the first-stage booster (return after the first-stage separation at Mach 10, to a conventional airport), and for the orbiter stage (return from a low orbit mission to a chosen airport). For the latter, NASA and General Dynamics have made an interesting optimisation study, summarised in Fig. 24, where three different configurations are shown differing from one another in their hypersonic efficiency (L/D = 1, 2 and 3) during the first part of the re-entry from space.

All of them have $(L/D)_{max}$ greater than 5 at low speed, with their wings extended, but the best configuration seems to be the second, shown in detail on Fig. 25. During ascent, orbital flight and hypersonic re-entry, the wings are folded at the top of the lifting body, to preclude any kinetic heating problems with them in the Newtonian shadow of the body during the re-entry; in this configuration, the maximum value of the subsonic trend L/D is about 3. With the wings at 45° sweep, the L/D increases to about 5. With the extended wing at 15° sweep, the trimmed L/D is about 8. (Better than most of our fighters). A plain flap at 30° deflection is easily trimmed by the tailplane surface to give a usable C_L of about 0.9 at the end of the flare, with a lift/drag ratio greater than 4.5. The main problem in choosing this concept for an orbiter spacecraft, is to balance the low-speed performance gains and the penalty of added wing weight which has to be put in orbit.

REFERENCES

1. Poisson-Quinton, Ph. Enselme, M. — Etude aerodynamique d'une famille d'ailes a flèche variable. 6th European Aeronautical Congress (Munich, Sept. 1965). Jahrbuch der WGLR 1965.

2. - — Design aspects of variable sweep aircraft. The Engineer, July 21 & 28, 1967.

3. Cook, A. M. Greif, R. K. Aoyagi, K. — Large-scale wind-tunnel investigation of the low-speed aerodynamic characteristics of a supersonic transport model having variable-sweep wings. NASA TN D-2824; May 1965.

4. Cook, A. M. Jones, D. G. — Large-scale wind-tunnel investigation to improve the low-speed longitudinal stability at high lift of a supersonic transport with variable-sweep wings. NASA TN D-5005; Jan. 1969.

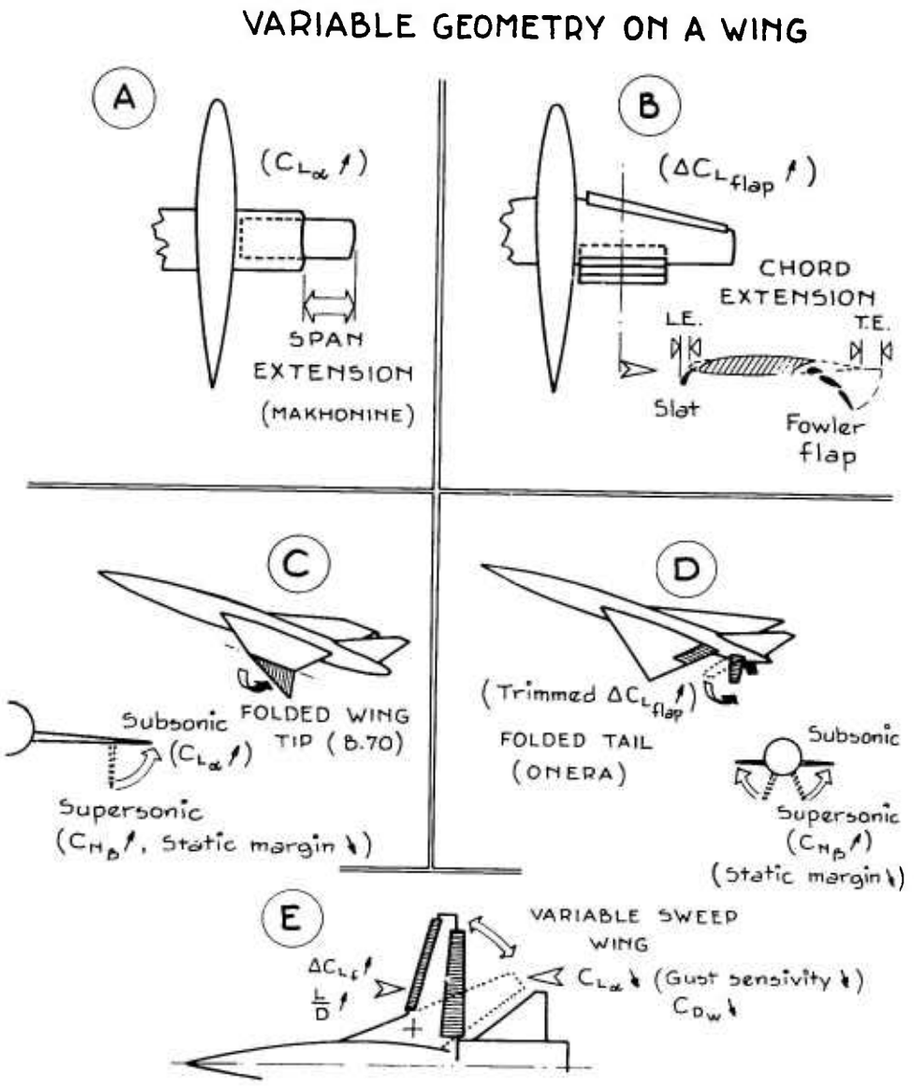

Figure 1.

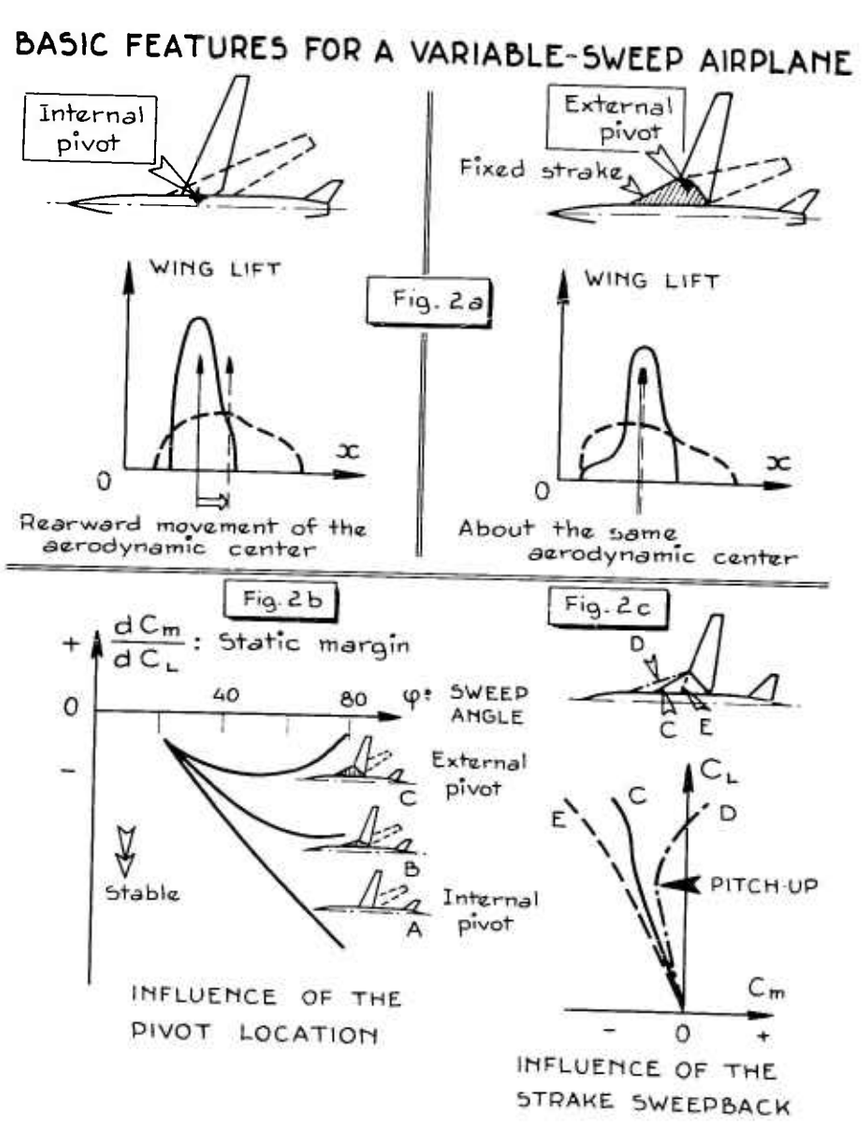

Figure 2.

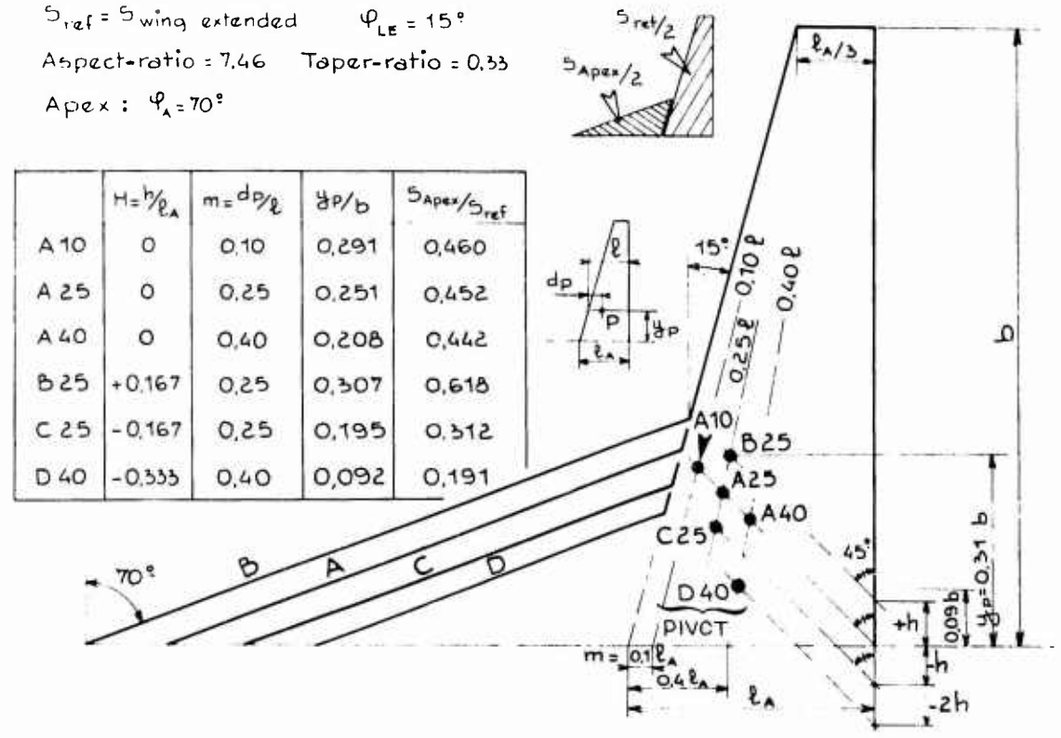

	$H = h/l_A$	$m = d_p/l$	y_p/b	S_{Apex}/S_{ref}
A 10	0	0.10	0.291	0.460
A 25	0	0.25	0.251	0.452
A 40	0	0.40	0.208	0.442
B 25	+0.167	0.25	0.307	0.618
C 25	-0.167	0.25	0.195	0.312
D 40	-0.333	0.40	0.092	0.191

Figure 3.

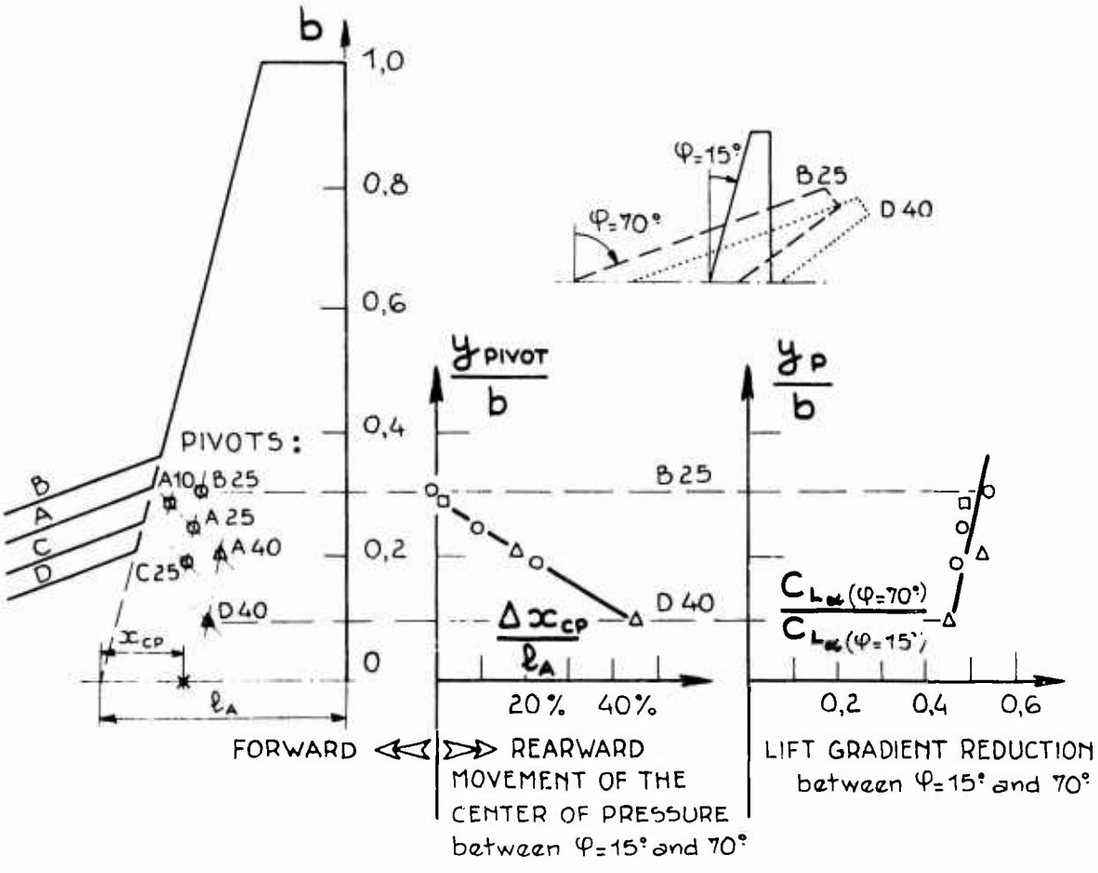

Figure 4.

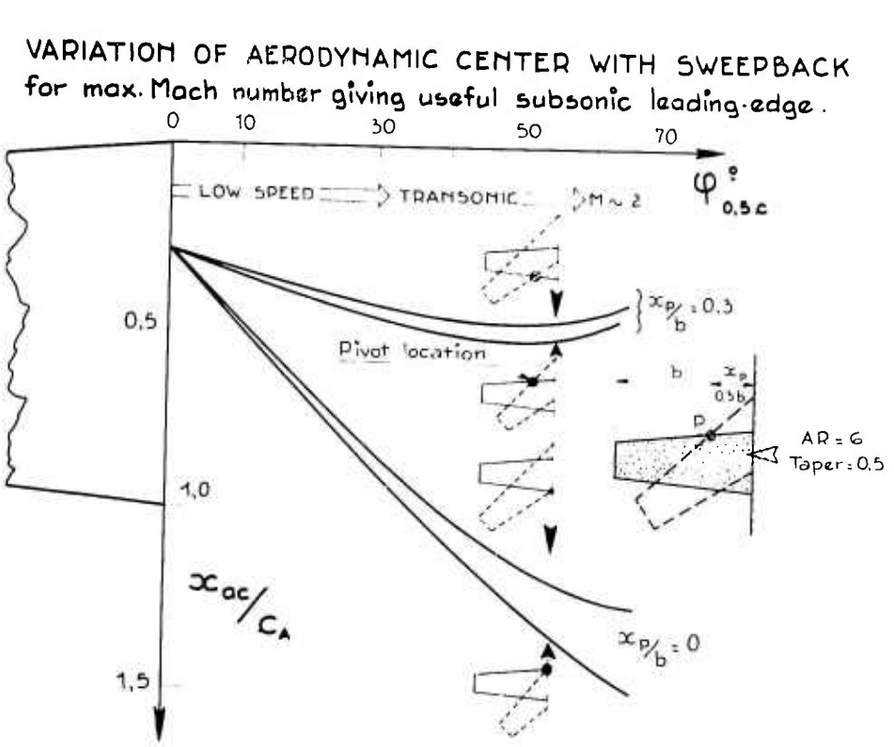

Figure 5.

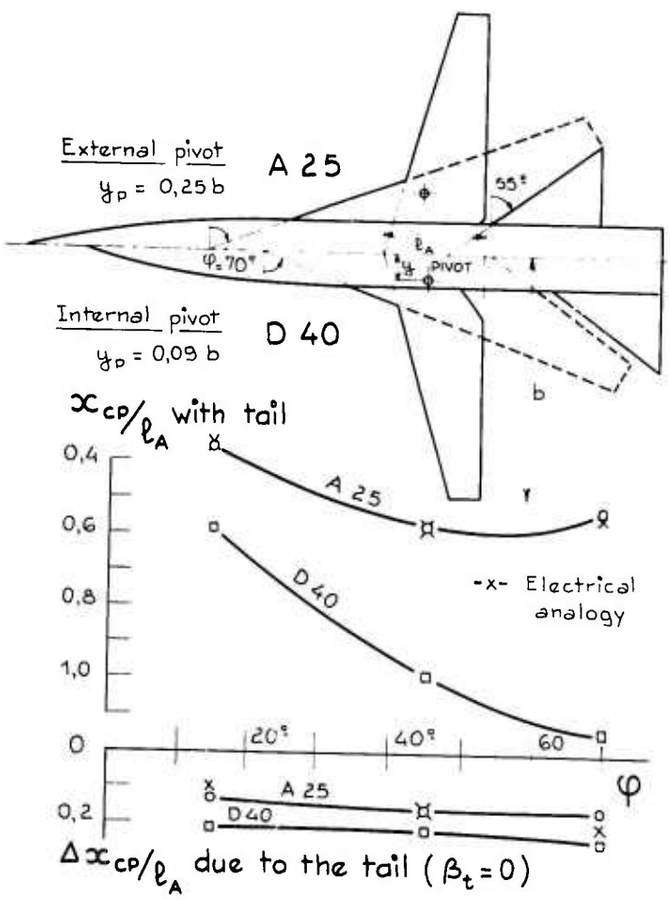

Figure 6.

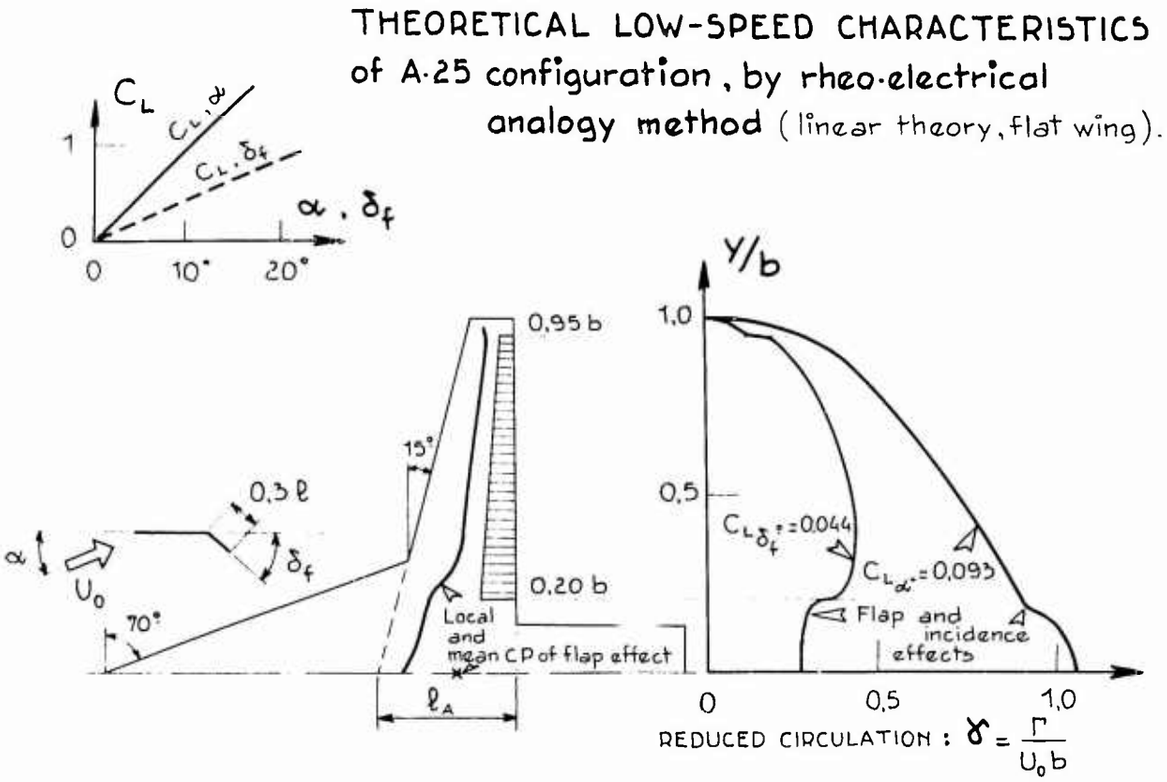

Figure 7.

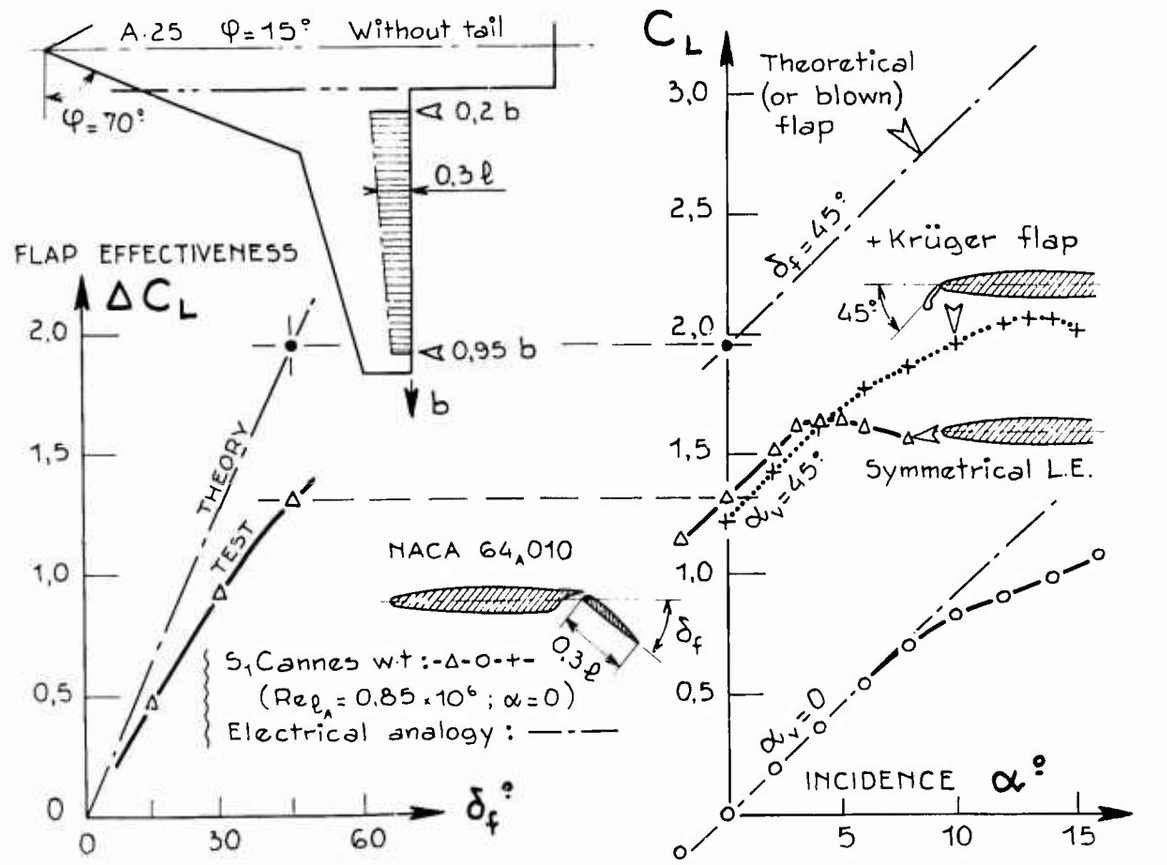

Figure 8.

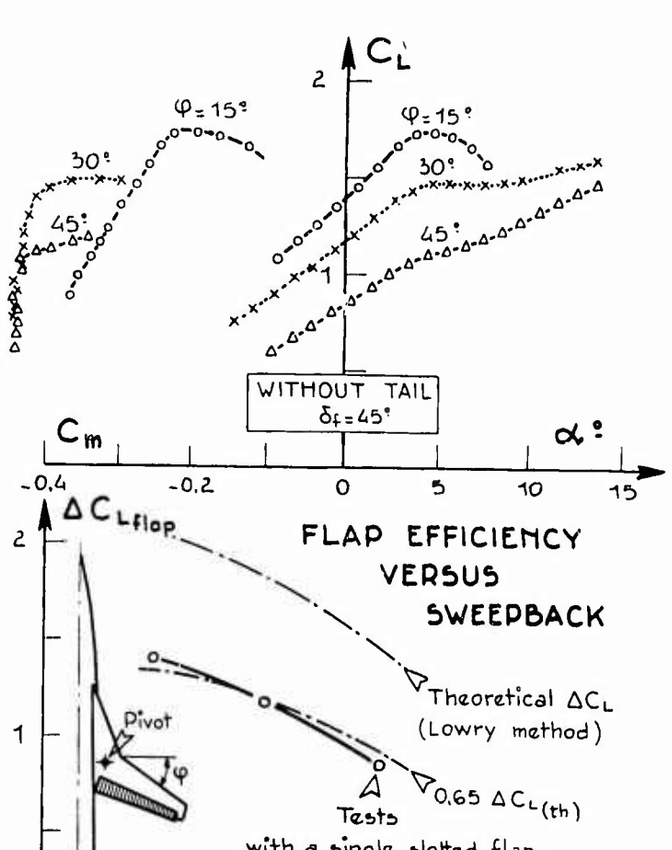

Figure 9.

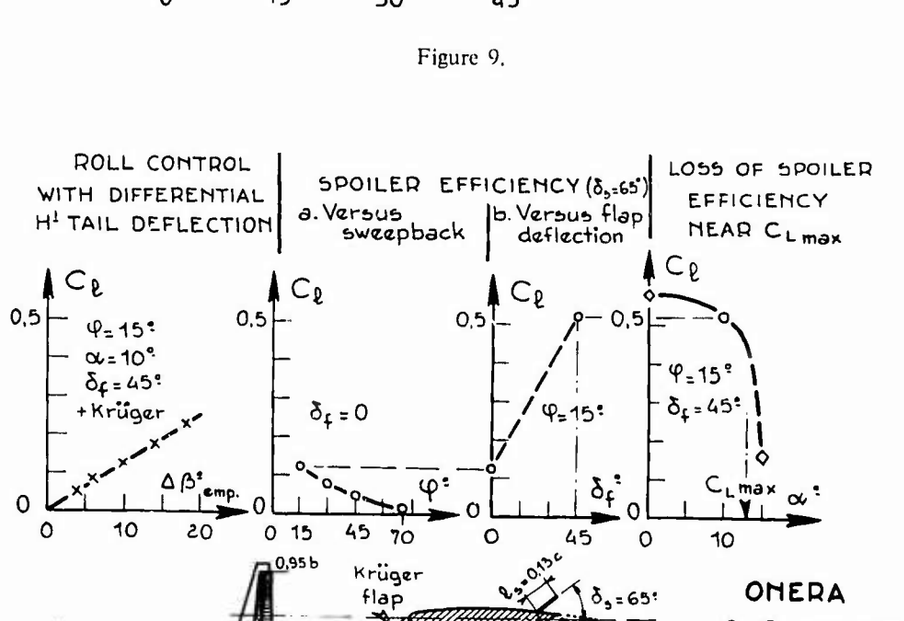

Figure 10.

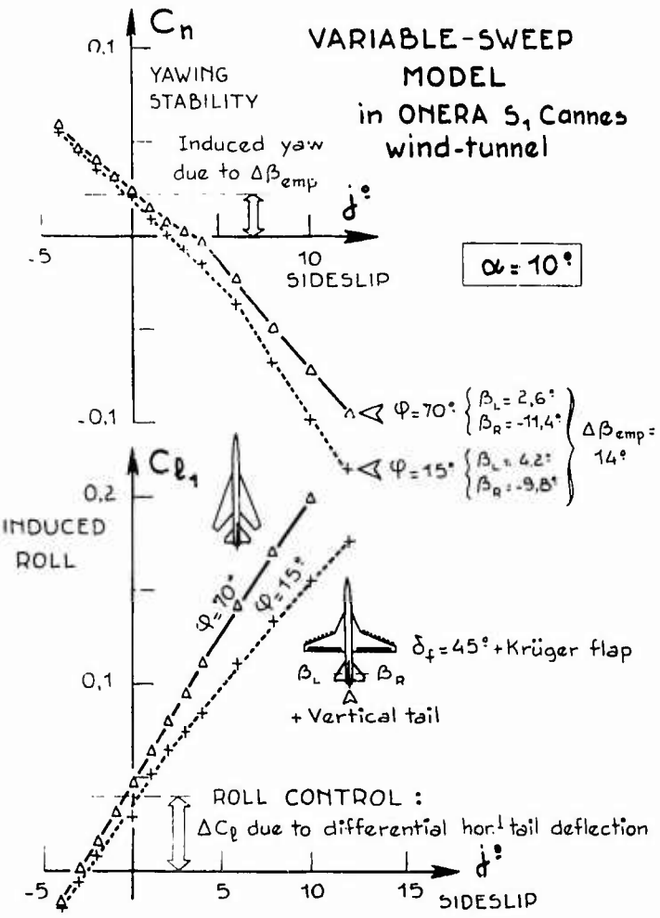

Figure 11.

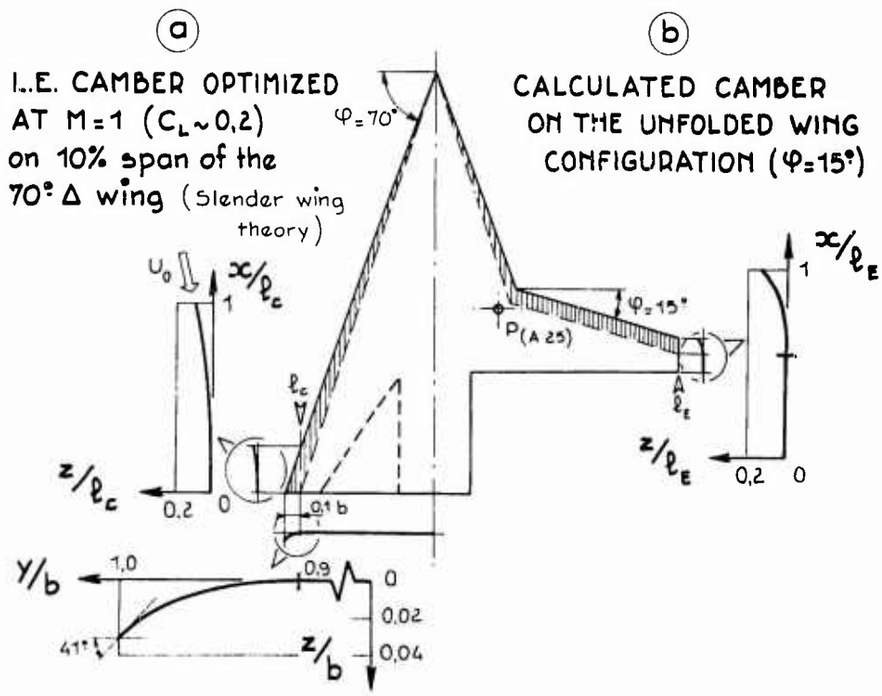

Figure 12

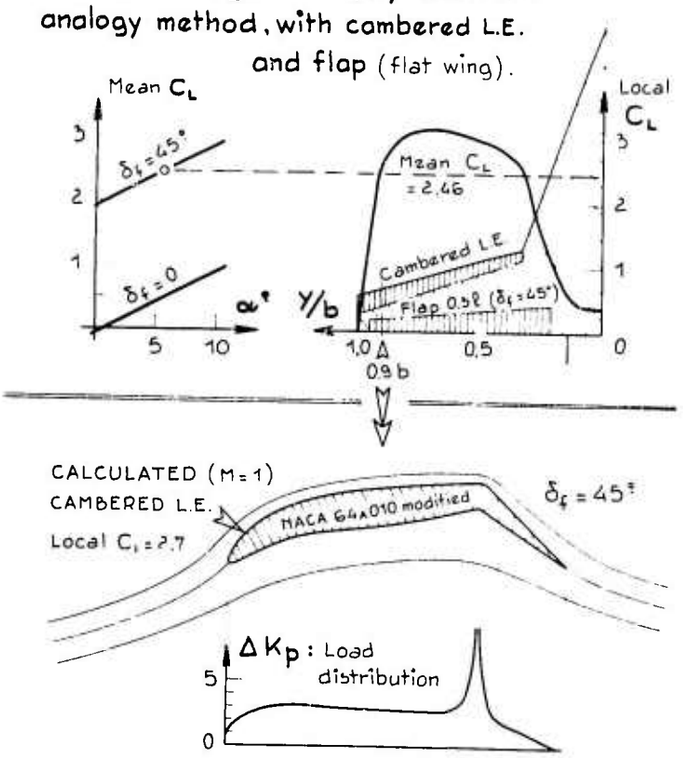

Figure 13.

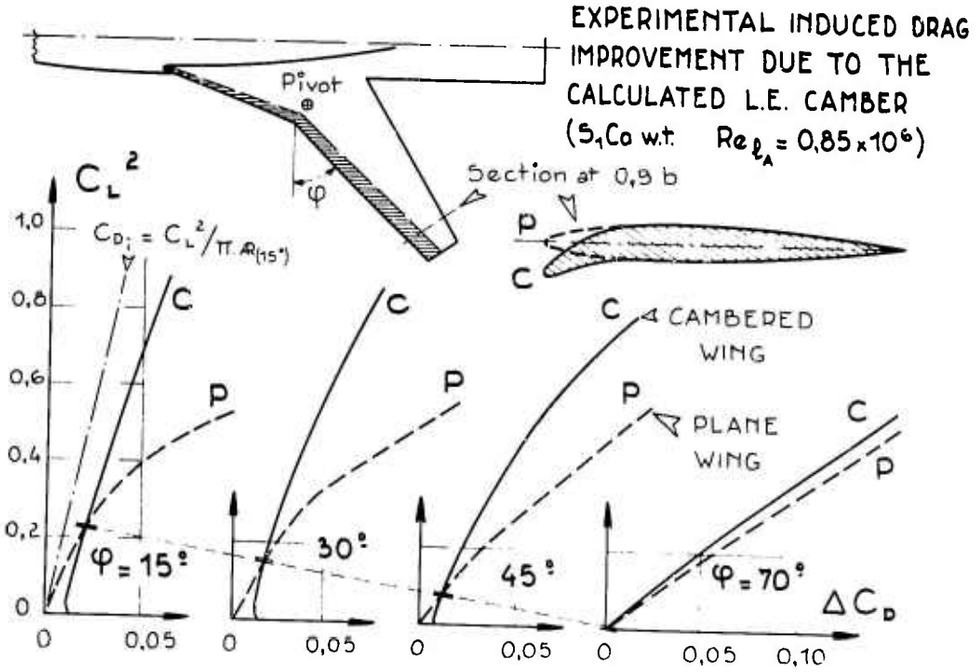

Figure 14.

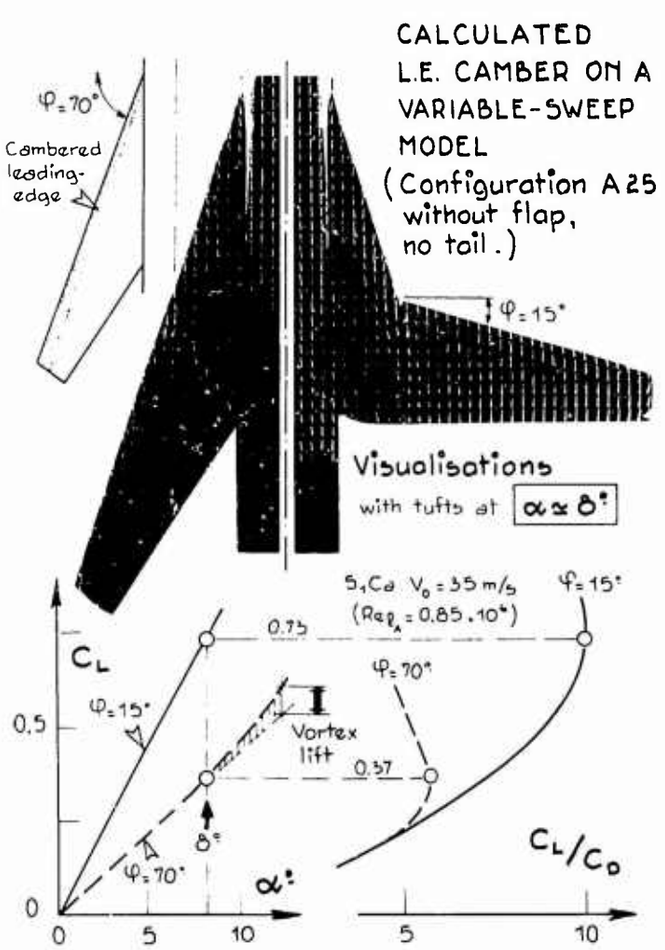

Figure 15.

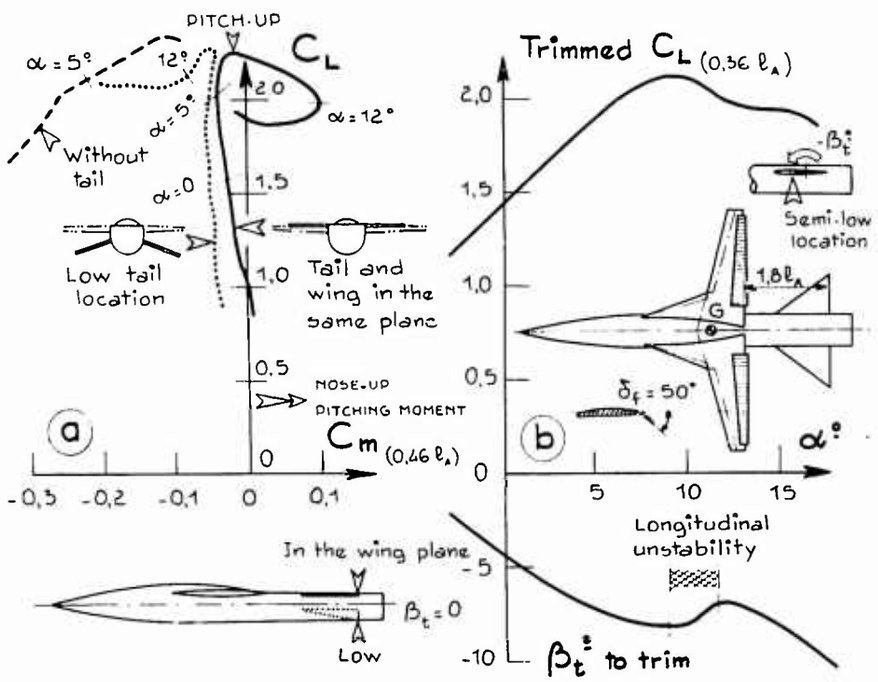

Figure 16.

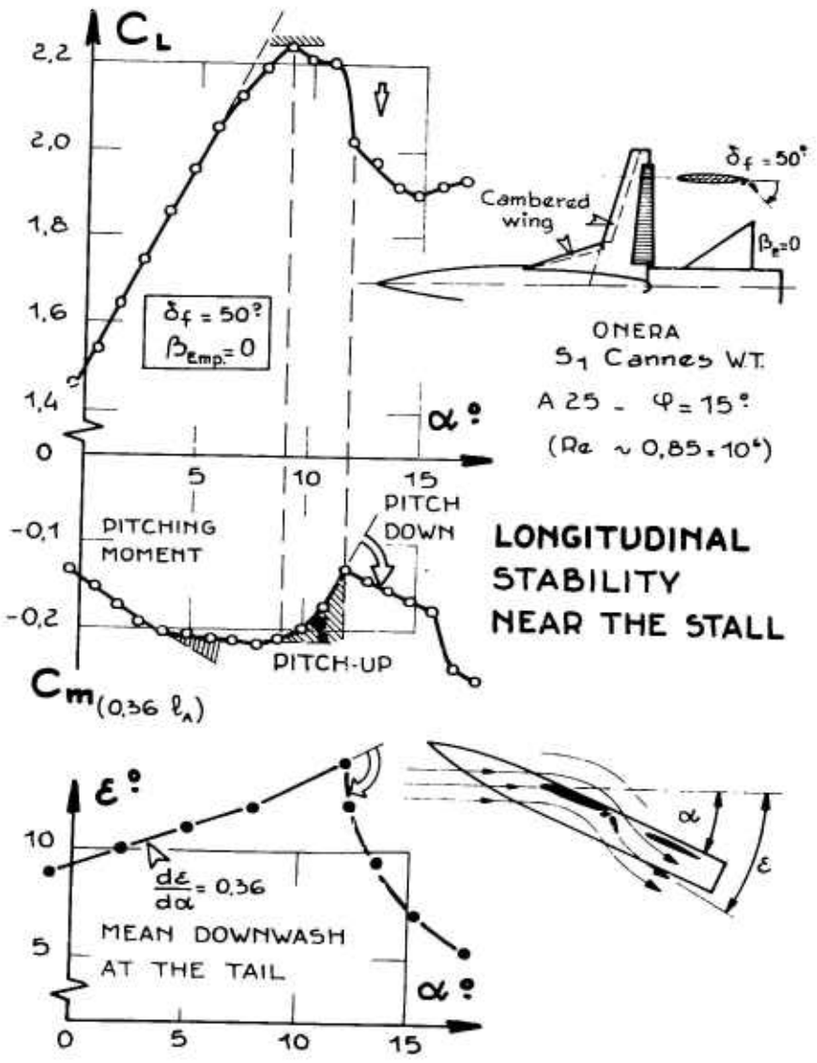

Figure 17.

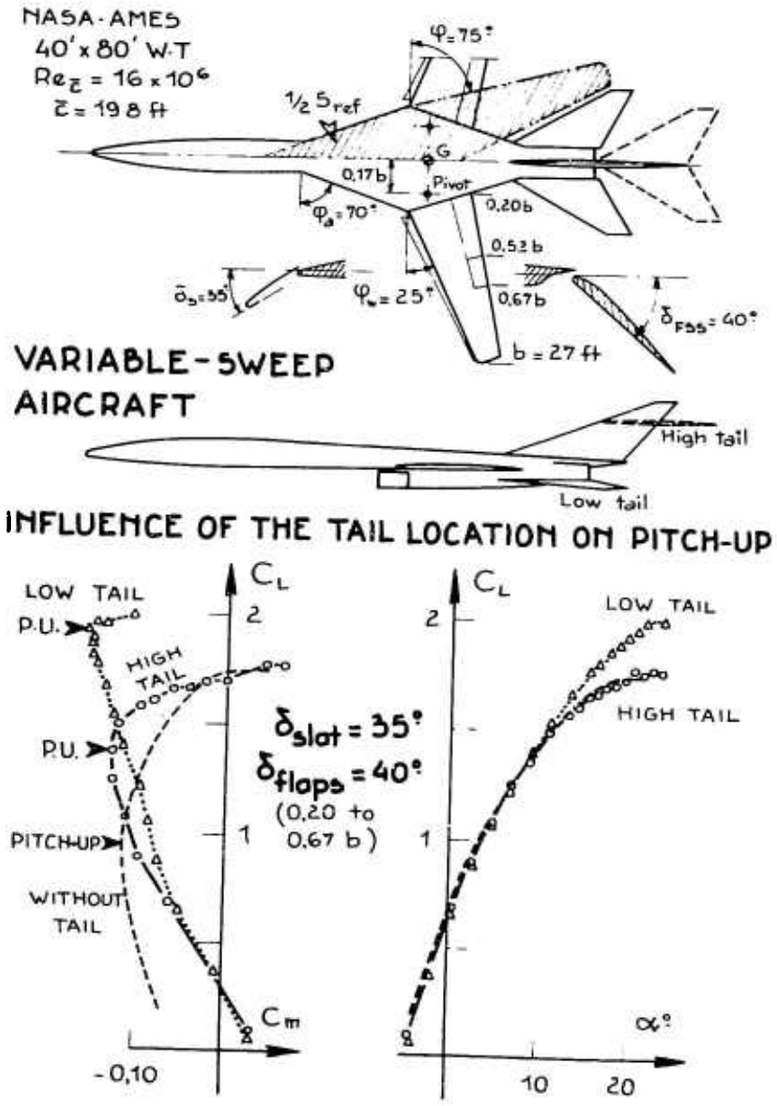

Figure 18.

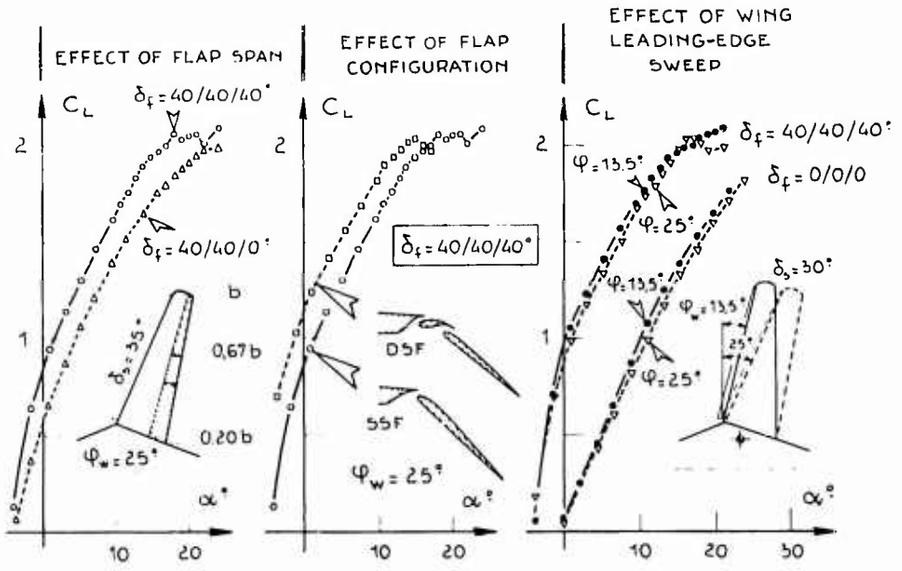

Figure 19.

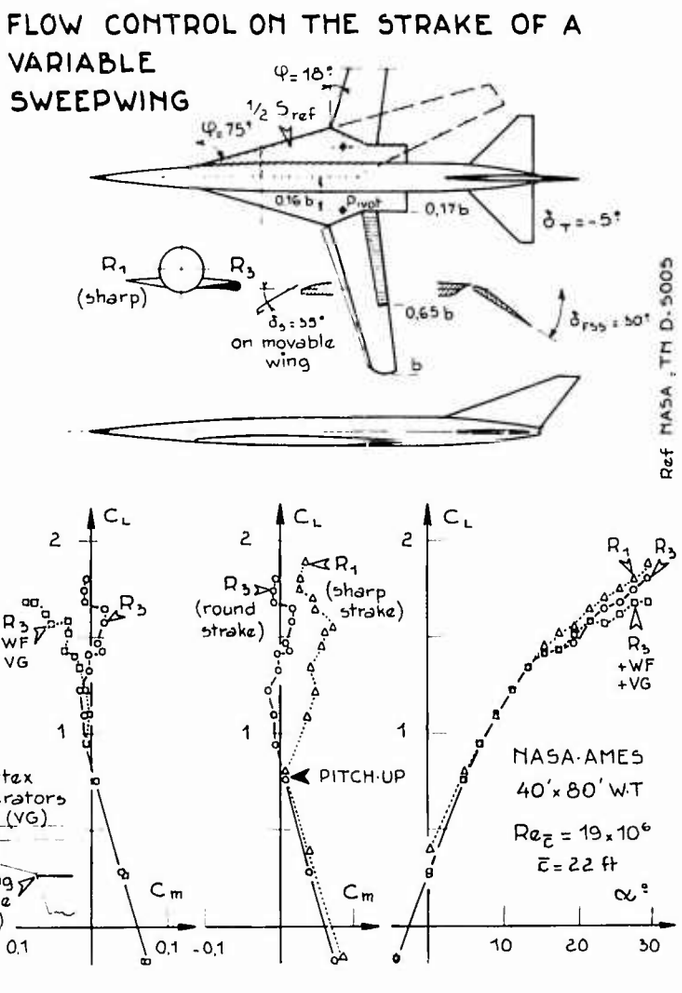

Figure 20.

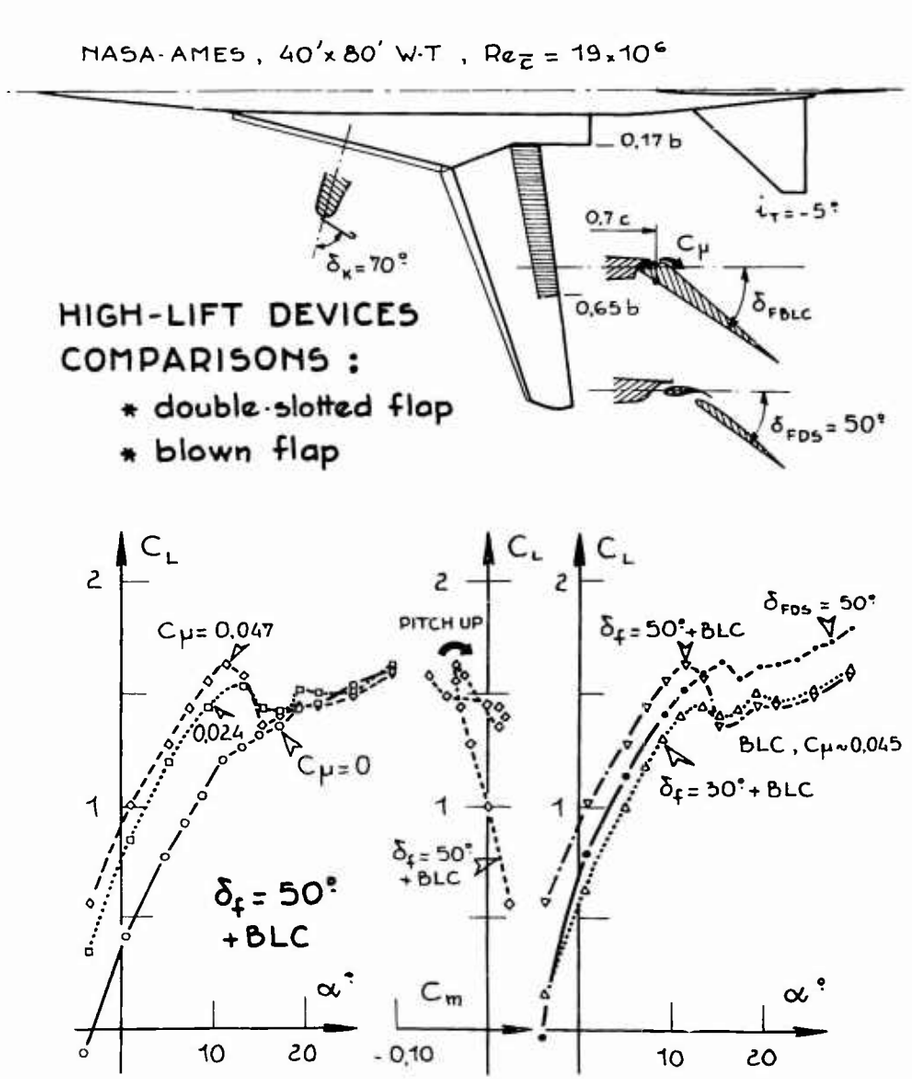

Figure 21.

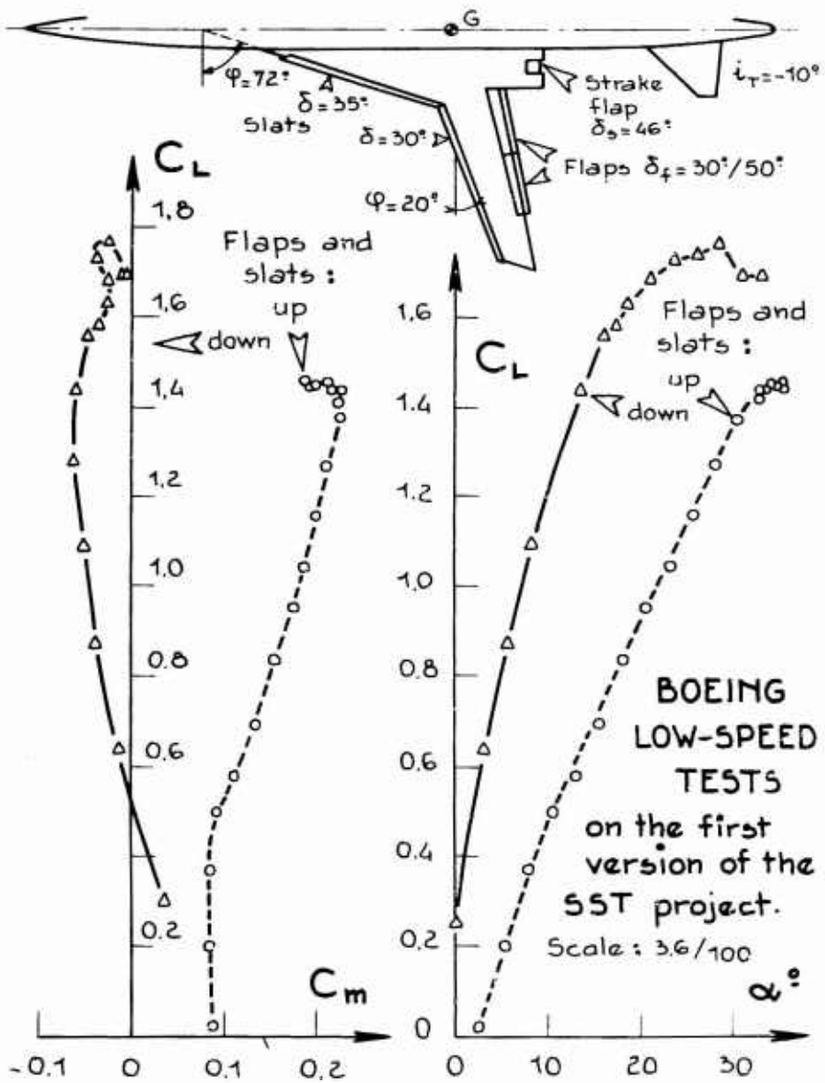

Figure 22.

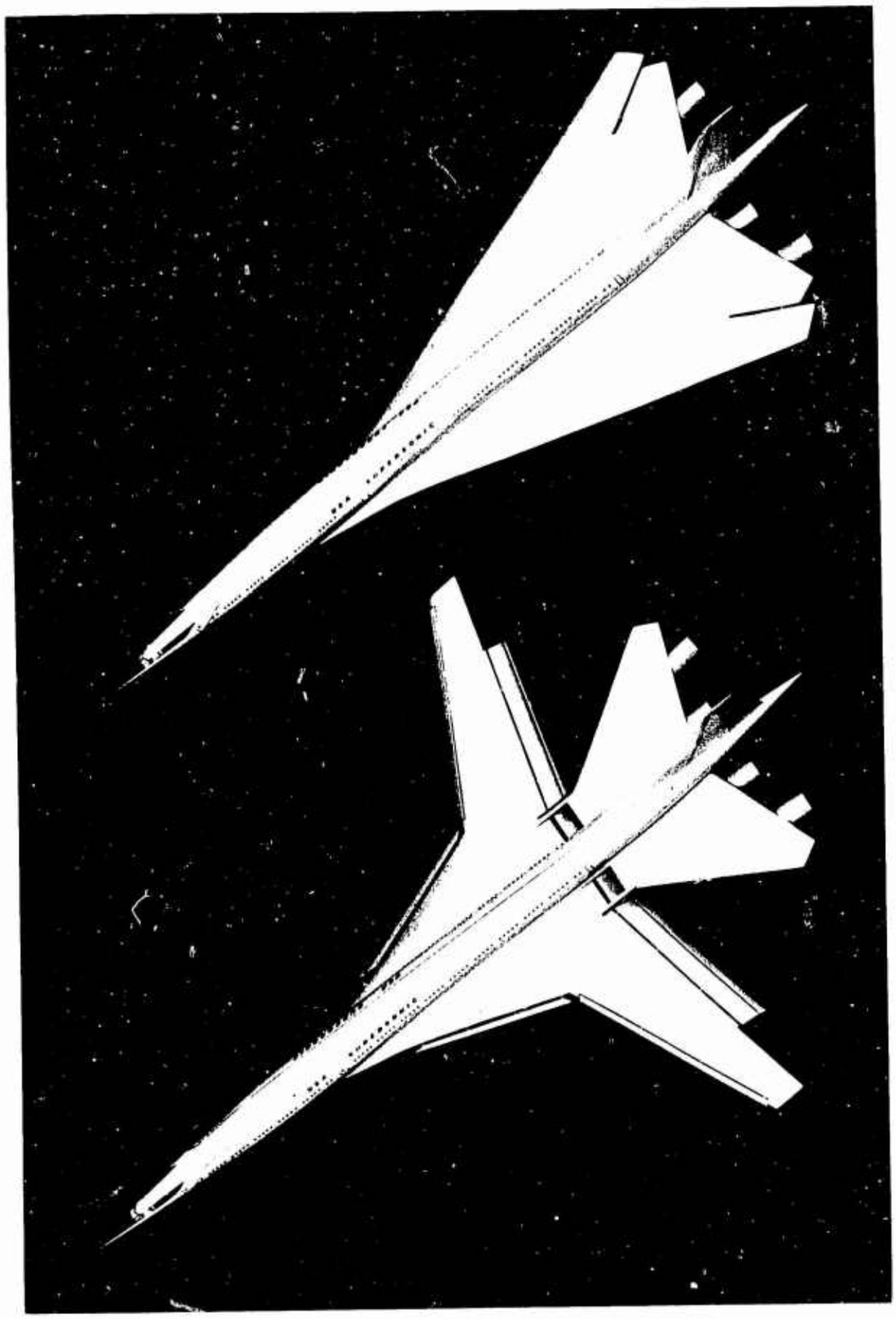

Figure 23.

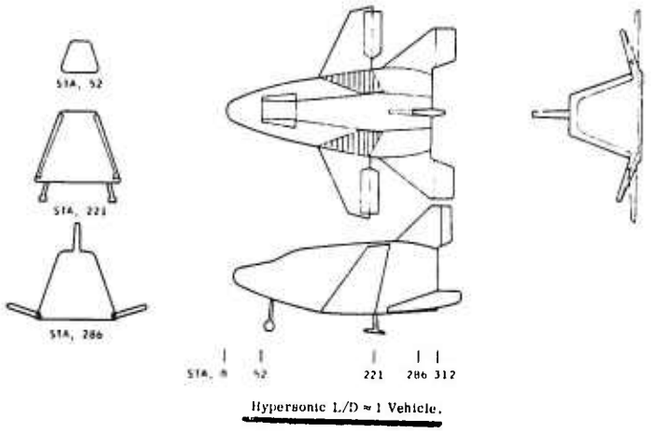

Hypersonic L/D ≈ 1 Vehicle.

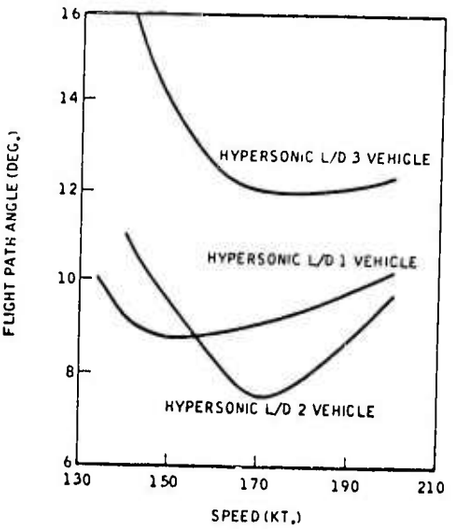

Equilibrium Glide Flight Path Angle Versus Speed.

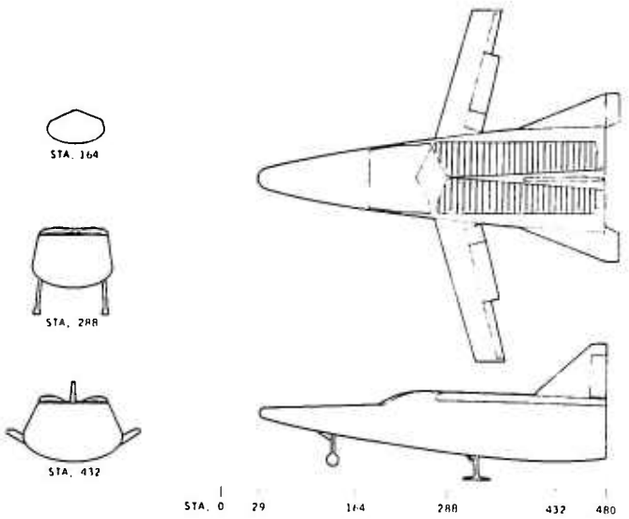

Hypersonic L/D ≈ 2 Vehicle.

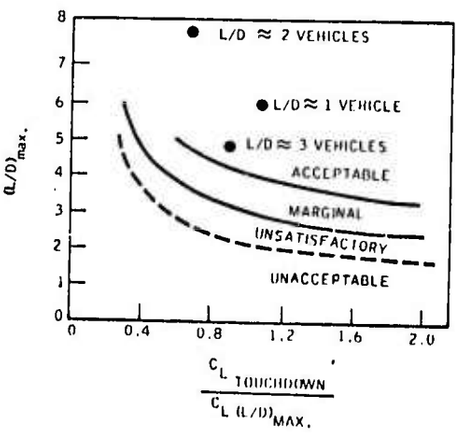

L/D Versus C_L/C_L (L/D max.) Requirements.

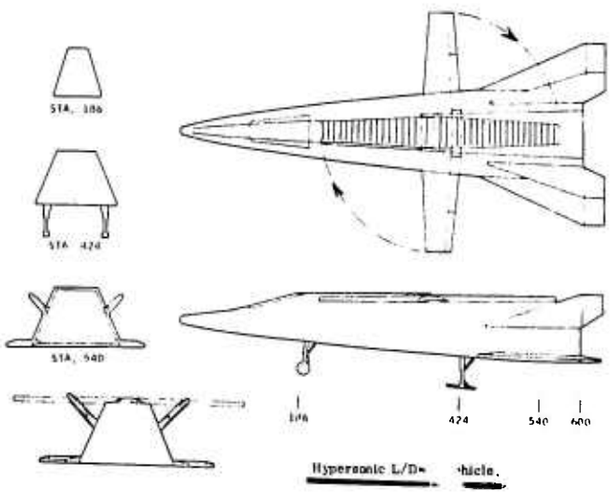

Hypersonic L/D= ·hicle.

LANDING CHARACTERISTICS

OF 3 VARIABLE GEOMETRY ENTRY SPACECRAFT with hypersonic $L/D = 1, 2$ and 3

Figure 24.

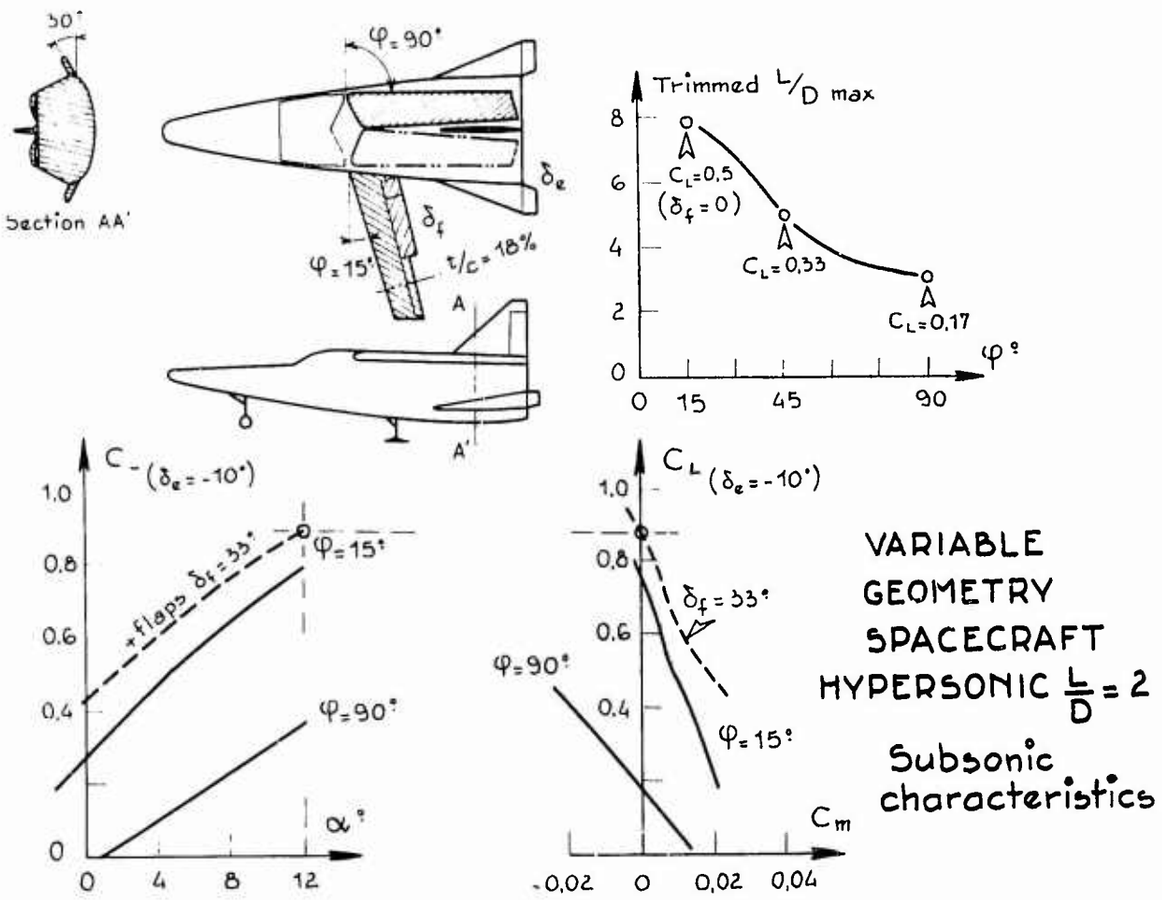
50°
Section AA'
φ=90°
δe
δf
φ=15°
t/c=18%
A
A'
Trimmed L/D max
8
6
4
2
0
CL=0,5
(δf=0)
CL=0,33
CL=0,17
φ°
0
15
45
90
CL (δe=-10°)
1,0
0,8
0,6
0,4
0
flaps δf=33°
φ=15°
φ=90°
α°
0
4
8
12
CL (δe=-10°)
1,0
0,8
0,6
0,4
δf=33°
φ=90°
φ=15°
Cm
-0,02
0
0,02
0,04
VARIABLE
GEOMETRY
SPACECRAFT
HYPERSONIC L/D = 2
Subsonic
characteristics

Figure 25.

FUNDAMENTAL ASPECTS OF FLOW SEPARATION UNDER HIGH-LIFT CONDITIONS

by

H.P.Horton

von Kármán Institute for Fluid Dynamics
Brussels, Belgium

NOTATION

$H = \delta^* / \theta$	boundary-layer shape parameter
Me	external Mach number
p	static pressure
u,v	velocity components in the boundary layer in the x,y directions
ue	velocity at outer edge of boundary layer
x,y	orthogonal coordinates on surface
z	ordinate normal to surface
β	inclination of a streamline to the x direction
βw	inclination of limiting streamline to the x direction
γ	ratio of specific heats of gas
δ	boundary-layer thickness
δ^*	boundary-layer displacement thickness
θ	boundary-layer momentum thickness
μ	viscosity of gas
ν	kinematic viscosity of gas
λ	pressure gradient parameter
τ_w	surface shear stress
ϕ	angle between dividing streamline and surface at separation

FUNDAMENTAL ASPECTS OF FLOW SEPARATION UNDER HIGH-LIFT CONDITIONS

H.P.Horton

1. INTRODUCTION

The aim of any lift augmentation device, whether it be mechanical or pneumatic, is to enable a larger proportion of the hypothetical inviscid lift of a wing to be achieved than would otherwise be possible. The loss of lift due to viscosity is comparatively small when the viscous effects are confined to thin boundary layers on the body surfaces, but when a boundary layer becomes detached from the surface, other than at the trailing-edge, very large losses of lift usually occur. Lift augmentation devices are, therefore, means by which body shapes and boundary conditions may be achieved which prevent undesirable boundary-layer separations from occurring. It is accordingly appropriate to discuss here the basic types of separation which may occur in high-lift conditions, to try to gain an idea of what we are attempting to control.

We commence with a brief description of the processes by which laminar and turbulent boundary layers are caused to separate.

2. BASIC CONCEPTS OF TWO-DIMENSIONAL LAMINAR AND TURBULENT SEPARATION

Boundary-layer separation from a smooth two-dimensional surface always occurs as a result of a rise in the static pressure of the external stream, which is transmitted through the boundary layer to the surface because the pressure gradient normal to the surface, $\partial p/\partial z$, is zero according to the boundary-layer approximations.

However, the magnitude of the pressure rise which may be sustained by a boundary layer before separation takes place, as well as the details of the separation process, depend upon whether the boundary layer is laminar or turbulent. We shall, therefore, discuss laminar and turbulent separation separately, noting that in practice turbulent separation is the case of greater interest in subsonic high Reynolds-number flow.

2.1 Laminar Separation

The mechanism of laminar separation is shown in Figure 1. The boundary layer, through which the velocity "u" rises from zero at the surface $z = 0$ to the external stream velocity u_e at the outer boundary-layer edge $z = \delta$, enters the region of rising pressure at the streamwise position $x = x_a$. Because the same pressure gradient acts on the slowly-moving inner region as on the outer region, the fluid near the wall is retarded more than that at the edge (viscous forces maintaining the velocity at the wall to be zero). The value of $\partial u/\partial z$ at the wall, and hence the wall shear stress $\tau_w = (\mu \partial u/\partial z)_w$, therefore falls as the boundary layer progresses until it finally changes sign at the separation point x_s . A flow in the reverse direction then occurs near the wall, and from the separation point a single streamline is emanated dividing the fluid in the original boundary layer from that flowing upstream. According to Oswatitsch[1], this dividing streamline leaves the surface at an angle ϕ given by

$$\tan \phi = -3 \frac{\partial \tau_w / \partial x}{\partial p / \partial x} .$$

Although $\partial \tau_w/\partial x$ is continuous through the separation point, it falls off rapidly after separation and the skin friction, as well as the reverse flow velocities, appear to be generally very small in the separated region. According to the ideas of Maskell[2], the dividing streamline may be thought of as consisting of the merging of two "limiting streamlines" infinitesimally close to the surface, one coming from upstream of S and the other from downstream. This is indicated in Figure 1.

The strongly inflected nature of the velocity profiles in the vicinity of separation and thereafter results in hydrodynamic instabilities except at very low Reynolds numbers, and transition therefore usually occurs a short distance behind separation. The consequences of this are discussed in Section 4.

There are many methods available for calculating the position of laminar separation, given the inviscid pressure distribution. Probably the most popular method is that of Thwaites[3], which was extended to compressible flow by

Rott and Crabtree[4]. In terms of the external Mach number, M_e, the method gives the separation point to be determined by:

$$\frac{1}{Me}\frac{dMe}{dx}\frac{1}{N}\cdot\int_0^{x_s} N\,dx = 0.2\,, \quad \text{where} \quad N = \frac{Me^5}{\left[1+\frac{\gamma-1}{2}Me^2\right]^4}\,,$$

and $x = 0$ corresponds to the stagnation point. This formula is valid for the case of zero heat transfer only. It should, however, be remarked that some recent papers[28,29,30] cast doubt on the validity of the assumption implicit in this formula that the pressure gradient parameter $\lambda = (\theta^2/\nu)(due/dx)$ at separation is constant. For greater accuracy, the method of Reference 28 (a simplification of Reference 31) is to be recommended.

Accurate numerical procedures for solving the compressible laminar boundary-layer equations, which will accurately predict the separation point for a given pressure distribution, have been developed by Sells[5] and Smith and Clutter[6]. However, because there is always in practice a slight interaction between the boundary layer and the external flow upstream of separation, it is doubtful whether the use of these more sophisticated methods is justifiable unless this interaction is taken into account.

For rough estimates, laminar separation may be taken to occur when the external velocity has dropped to 94% of its peak value.

2.2 Turbulent Separation

Separation of a turbulent boundary layer occurs as a result of the same basic mechanism as laminar separation; that is, slowly moving fluid close to the surface is retarded by a positive pressure gradient and finally reversed. However, as shown in Figure 2, the shape of the turbulent velocity profile is such that only very close to the wall is the velocity in the layer greatly different from that of the external stream; furthermore, the process of turbulent mixing provides a powerful mechanism for exchanging energy from the outer region to the inner. As a result, a turbulent boundary layer is able to withstand a much larger rise in pressure than is a laminar layer.

The balance between the kinetic energy of the mean motion and that of the turbulence is extremely complicated in the inner region, and is only imperfectly understood. Since this effectively determines under what conditions the layer separates, our ability to predict turbulent separation is severely limited. The main difficulty lies in the observed fact[7] that, before complete detachment of the boundary layer occurs, a region exists in which intermittent streaks of back-flow are formed near the surface as shown in Figure 2. In this region, the temporal-spatial mean of the skin friction is very small but positive; locally and intermittently it changes sign, however. It is, therefore, evident that any two-dimensional, steady model of turbulent separation must be in general inadequate. (Of course turbulence itself is unsteady and three-dimensional – but the unsteadiness and three-dimensionality near separation are outside the spectrum of turbulence.) For instance, the usual representation of mixing length and eddy viscosity obtained from "healthy" boundary-layer data predict unrealistic behaviour when the mean skin friction vanishes (mixing length gives a zero skin-friction profile with an infinite value of $\partial u/\partial z$ at the wall); probably these concepts should be applied separately to the forward and intermittently reversed flows. An interesting discussion of these problems is given by Sandbord and Liu[8].

Amongst the most important conclusions of this work is the observation that the region of intermittent separation is that region previously identified as turbulent separation by most experimenters. This explains the discrepancy between the value of the shape parameter $H = \delta^*/\theta$ at separation of about 2.3 (or even as low as 1.8) quoted in many works, and the value of $H = 3.5$ found by Stratford[9] in a flow which had not yet reversed. It appears that the real separation criterion should be the attainment of a value of H between 3.5 and 4 *unless* the pressure gradient is very severe, when separation will occur at much lower values of H. Sandbord and Liu define complete separation as the point at which the flow near the surface is forward and reversed for equal periods of time.

We must observe, however, that no existing methods are capable of predicting the flow development in the intermittent separation region. So, for the present, we must content ourselves with the prediction of the start of the region – the "separation point" given by most theories. Methods of predicting the development of turbulent boundary layers in adverse pressure gradients are too numerous to discuss here – but we might perhaps mention the "finite difference" method of Bradshaw et al.[10], as being probably the most reliable; a compressible version of this programme also exists.

3. TYPES OF SEPARATED FLOW ON SINGLE TWO-DIMENSIONAL AEROFOILS

When the incidence of a single two-dimensional aerofoil with no high-lift devices is increased towards that of maximum lift, regions of separated flow are formed whose position and mode of development determine both the maximum lift which may be achieved and the way in which the lift subsequently falls. These separated regions are usually situated near the leading or trailing-edge; a useful classification of stalling behaviour into *three* basic

types by McCullough and Gault[12] sheds some light on the relative roles of leading and trailing-edge separation. This classification is: -

3.1 **Trailing-Edge Stall**: (preceded by movement of the turbulent separation point forward from the trailing-edge with increasing incidence).

This is characteristic of most thick sections; the peak of the lift curve is usually rounded, and the loss of lift after stall is gradual (Fig.3). The extent of the separated flow region at maximum lift may be as large as 50% of the aerofoil chord: prediction of the maximum lift would require a solution of the separated flow problem and is therefore difficult.

Some qualitative estimate of the stalling behaviour may, however, be made by examining the shape of the pressure distribution on the suction surface at the incidence at which turbulent separation is predicted at the trailing-edge, as suggested by Young[13] in his useful review of the stalling problem. Referring to Figure 4, in case (a), the concave, near-equilibrium type of upper-surface pressure distribution leads to values of the boundary-layer shape parameter H which are large over much of the rear of the aerofoil; turbulent separation will, therefore, spread very rapidly forward from the trailing-edge with increase of incidence, leading to a sudden stall. In case (b), the convex shape of the pressure distribution results in low values of H except near the trailing-edge; the point of separation will move only slowly forward from the trailing-edge and the stall is gradual.

3.2 **Leading-Edge Stall**: (caused by abrupt flow separation near the leading-edge, usually without subsequent re-attachment).

This type of stall is often exhibited by moderately thin sections, and is a sudden stall in which there is little or no rounding of the lift curve before the stall (Fig.5).

The abrupt separation near the leading-edge may occur in two ways, both associated with the existence of a very small region of separated flow near the leading-edge prior to the stall, usually called a "short separation bubble". Such a bubble is characterised by a laminar separation, followed by transition in the separated boundary layer and subsequent turbulent re-attachment. In the first mechanism of leading-edge stall, this bubble suddenly "bursts" into a large separated region occupying most of the aerofoil chord, due to a very small increase of incidence. In the second, the turbulent boundary layer a short distance behind the bubble separates (because of its weakened state) and again a large separated region occurs. These two mechanisms appear to be characteristic of the low and high Reynold number regimes respectively, with a smooth transition between the two; however, the evidence for the second mechanism is rather indirect[14,15]

Separation bubbles will be discussed in more detail in the following section.

3.3 **Thin Aerofoil Stall**: (preceded by flow separation at or near the leading-edge with re-attachment at a point which moves progressively rearward with increasing incidence).

This stall occurs on all sharp-edge aerofoils, and on thin aerofoils with rounded leading-edges. In the case of sharp-edge aerofoils, the flow separates at the leading-edge (except at very small incidence), and re-attaches some distance aft, the re-attachment point moving progressively rearward with increase of incidence until, at approximately maximum lift, it reaches the trailing-edge. As shown in Figure 6a, the stall is not so abrupt as the leading-edge type.

On thin rounded aerofoils, a short bubble usually forms at low incidence which bursts into a long bubble at an incidence well below that of stall, resulting in the characteristic kink in the lift curve shown in Figure 6b. This long bubble is, however, much smaller than the aerofoil chord, but grows until the maximum lift incidence is reached, in the same way that the bubble on a sharp-edge aerofoil grows.

It should be remarked that the distinction between leading-edge and thin aerofoil stall is not clear-cut, and that different stalling behaviour may be exhibited by an aerofoil at different Reynolds numbers. Also combinations of stalling behaviour may occur with separations arising both at the trailing and leading-edge.

Increase of camber can radically effect the stalling behaviour of an aerofoil; leading-edge camber will generally have the effect of suppressing a leading-edge stall, whilst trailing-edge camber (for instance, the deflection of a flap) increases the leading-edge suction peak and thereby increases the tendency to leading-edge stall.

4. SEPARATION BUBBLES

When a boundary layer separates from the surface of an aerofoil, and subsequently either re-attaches to the surface or merges with another shed boundary layer, a closed "bubble" containing fluid circulating with low velocity is formed; examples of such bubble flows are shown in Figure 7. Because the re-circulation velocity is low, the static pressure is generally nearly constant in such bubbles except in the region of re-attachment, where a pressure rise occurs.

Since such bubbles have a large influence on all types of stall, as we saw in the preceding section, we now discuss bubble flows in more detail.

Figure 7a shows a leading-edge bubble of limited extent; as previously stated, the separation is usually laminar followed by transition and a turbulent re-attachment. However, two basic types of bubble have been observed, usually called "short" and "long". The short type is extremely small compared with the aerofoil chord, contracts in length with increase of incidence and only disturbs the surface pressure distribution significantly in its immediate vicinity. Long bubbles on the other hand have lengths comparable with the chord length, grow with increase of incidence and strongly perturb the overall pressure distribution.

The bursting phenomenon previously mentioned is a sudden change-over from the short to the long bubble mode, and may occur either as a result of an increase of incidence or a decrease of Reynolds number. It was until recently believed that bursting occurs as a result of a sudden change in the mechanism and position of transition, but careful experiments shows this to be unfounded[16]. By considering the problem as one of viscous-inviscid interaction, it has since been shown[17] that bursting occurs when the boundary layer and inviscid external flows become incompatible, when the re-attachment process fails and the whole flow field has to adjust itself until re-attachment is possible. Reference 17 provides a method for estimating the conditions under which a bubble will burst, whilst the prediction of the pressure distribution on an aerofoil with the resulting long bubble has been treated by Norbury and Crabtree[18] and Woods[19]. The latter considers only the potential flow part of the problem, and requires in supplement information about the separated turbulent shear layer development, which could be obtained by using an adaption of the Korst[32] model used in supersonic flows.

Figure 7b shows a long bubble which has grown to the stage where the point of re-attachment is no longer on the aerofoil but has become a point of confluence of the dividing streamlines from the upper and lower surfaces, whilst Figure 7c shows a rather similar type of bubble arising from a rear separation.

5. FLOW SEPARATION ON MULTI-AEROFOIL SYSTEMS; WAKE-BOUNDARY LAYER MIXING

In its most general sense, separation may be thought of as occurring when a boundary layer leaves a surface at any point, and hence the smooth flowing-off of the boundary layers from a trailing-edge is a form of separation. Thus any multiple system of aerofoils (for instance a main aerofoil with slat and slotted flap), in which the components are sufficiently close together for the shed wake from one component to be able to impinge on another component, represents essentially a separated flow system.

Additionally, of course, each component may have regions of separated flow on it in the same way as a single isolated aerofoil, and the resulting flow fields can be exceedingly complex and not amenable to any existing type of analysis.

As an example, consider the flow around an aerofoil with a slat, shown schematically in Figure 8. Boundary layers are formed on the upper and lower surfaces of the slat which are shed at its trailing-edge as a wake; the momentum thickness of this wake is governed by the drag of the slat, whilst its width increases with downstream distance. Depending on the relative positions of the slat and aerofoil, this wake may or may not mix with the boundary-layer aerofoil upper surface. If no mixing occurs, the effect of this wake upon the pressure distribution and the boundary-layer development on the main aerofoil will be small; but if mixing does occur, the boundary layer of the main aerofoil will be thickened and the tendency to separate at the trailing-edge will increase.

Although little work has been done on the wake-boundary-layer mixing problem (some recent work of interest is in Reference 27), we may tentatively identify the various stages which may be expected to occur in such a mixing process. Referring to Figure 8a we have:

1. A pre-mixing region, where the boundary layer and wake develop separately;

2. A blending region, where the inner edge of the wake diffuses towards the surface through the boundary layer and the outer edge of the boundary layer diffuses through the wake. Since the behaviour of the turbulence is basically hyperbolic[16], the inner boundary layer and outer wake will be unaffected until the edge of the diffusion region reaches the point in question;

3. A relaxation region, in which the high level of turbulence introduced into the boundary layer by the wake, and the distortion of the velocity profiles, die down, until finally a normal turbulent boundary layer is reached, increased in momentum thickness by an amount approximately equal to the momentum thickness of the wake, as compared with the momentum thickness which the boundary layer alone would possess.

In order to be able to predict the separation of such a thickened boundary layer in the general case, we need to be able to predict these stages of development; no suitable method exists, but Bradshaw's method[10] might conceivably be extended to this situation once the necessary empirical functions used in the method have been established.

In practice, a slat is usually used in conjunction with a trailing-edge flap, probably slotted, which lead to additional difficulties, as shown in Figure 9. If the full free-stream dynamic pressure is to be utilized in the slot, the whole main aerofoil lower-surface boundary layer must pass through the slot, join with the upper-surface boundary layer and finally may mix with the new boundary layer developing on the flap. Prediction of the separation point on the flap then becomes a formidable problem.

6. THREE-DIMENSIONAL SEPARATED FLOWS

The subject of three-dimensional separation and separated flows is a difficult one and we can give here only an outline. More detailed information is to be found in References 1, 2 and 20 to 25. Most of this work is concerned with laminar layers, but since turbulent boundary layers contain an essentially laminar region near the wall, all conclusions concerning surface flow patterns are valid for turbulent flows also, whilst the qualitative descriptions of post-separation flow behaviour are not dependent upon the state of the boundary-layer.

As we saw in Section 2, two-dimensional separation occurs when the skin friction (which in this case has only one component) changes sign; i.e. when $\mu(\partial u/\partial z)_w = 0$. In a three-dimensional boundary layer, on the other hand, there are two components of the skin friction $\mu(\partial u/\partial z)_w$ and $\mu(\partial v/\partial z)_w$, where u,v are velocities measured in the x,y direction and x,y are orthogonal coordinates in the surface. Only at special "singular points" will these components vanish simultaneously, but to restrict a definition of separation to such points would be too restrictive since it is a matter of observation that three-dimensional separation can occur along lines on which the parallel skin-friction is non-zero. For example, on a yawed wing of infinite span the flow separates along a line parallel to the leading-edge at which the spanwise skin friction is non-zero. Hence, a more general criterion for three-dimensional separation than the vanishing of skin friction must be sought.

The concept of limiting streamlines[2] is useful here; these we define as the limit of streamlines as the surface is approached, and we may easily show that such streamlines are coincident with lines tangential to the skin-friction direction (skin-friction lines). For if a streamline near the surface makes an angle β with the x direction, we have

$$\tan\beta = \frac{v}{u}.$$

Hence the limiting streamline angle βw is given by

$$\tan\beta w = \lim_{z\to 0}\left(\frac{v}{u}\right) = \lim_{z\to 0}\frac{(\partial v/\partial z)_w}{(\partial u/\partial z)_w},$$

the differentiation being necessary because both v and u are zero when $z = 0$.

Hence,

$$\tan\beta w = \frac{\mu\left(\frac{\partial v}{\partial z}\right)_w}{\mu\left(\frac{\partial u}{\partial z}\right)_w},$$

which is the inclination of skin-friction lines to the x direction. The limiting streamline direction can be entirely different from the external streamline direction, particularly in strong pressure gradients, because of cross-flow in the boundary-layer induced by curvature of the external streamlines.

We now see that in the infinite yawed wing case, if x,y are respectively perpendicular and parallel to the leading-edge, $\tan\beta w$ becomes infinite if the x component of skin friction vanishes. Hence the skin-friction lines become tangential to the separation line, as shown in Figure 10a. The pattern of the separation streamlines is shown in Figure 10b; the limiting streamlines upstream and downstream of separation merge at the separation line as two-dimensional separation.

The streamline pattern at a line of re-attachment is like that at separation with all the arrows reversed in direction. Again considering an infinite yawed wing, a closed bubble may be formed between lines of separation and re-attachment as shown in Figure 11. A vortex with a spanwise velocity component is formed within the bubble[26].

Closed bubbles are one of two basic types of flow which result from three-dimensional separation, the other type being free vortex sheets, the two being distinguished by whether the particle paths are closed or open. A well-known example of a free vortex sheet is that arising from the leading-edges of a slender delta wing, Figure 12; part-span vortex sheets may also be formed on finite swept wings at, for example, the junction between attached flow on the inboard part of a wing and separated flow on the outboard part, as shown in Figure 13. Mixed flows often

occur when two surfaces of separation meet, as for example in the case of separation from a body of revolution at incidence, shown in Figure 14.

7. THEORETICAL POSSIBILITIES

In the preceding discussion, we have of necessity been limited to a qualitative description of separation problems because of the lack of analytic techniques except in certain specialized cases. We briefly discuss now the possibility of applying theoretical techniques to the simplest problem of interest here — that of the prediction of the maximum lift and the drag of an aerofoil.

To accomplish this, we must be able to:

1. predict the *onset* of flow separation;
2. predict the subsequent development of the separated flow region(s) up to the maximum lift incidence.

The first problem is by far the easier, and by using any modern method of laminar and turbulent boundary-layer prediction together with a short separation bubble analysis (if necessary), a reasonable degree of accuracy may be achieved. When the stage is reached that either a trailing-edge separation, a short bubble burst or a turbulent re-separation is predicted, we are faced with the second problem.

The analysis of separated flow problems in subsonic flow by free-streamline theory is a very old branch of fluid mechanics; the usefulness of the results is, however, extremely limited because the inviscid nature of the analysis necessitates the use of empirical data to close the solution. Thus, for example, the flow about a bluff body with an extensive region of separated flow may be predicted with reasonable accuracy (e.g., Reference 19, p.452) but only if the pressure in the wake is known. This pressure can only be predicted by means of separated boundary-layer theory, and until recent years such a theory was non-existent. However, considerable progress has been made in the analysis of separated turbulent boundary layers in supersonic flows; the resulting ideas have, however, been applied in only one or two simple sub-sonic cases. Two of the most important contributions to the study of supersonic separated flows are the mixing theory of Crocco and Lees[34], which is basically an entrainment method, and the theory of Korst[32] which considers separated regions of essentially quiescent fluid bounded by mixing layers; the conservation of total pressure on the dividing streamline is a basic premise of the theory. The basic theory is applicable only to cases in which the boundary layer at separation is infinitesimally thin, but later developments such as that of Nash[33] include the effect of an initial boundary layer. Green[35] has used an entrainment method to calculate the development of a subsonic base flow.

The main difficulty in calculating subsonic separated flows is the need for iteration between calculations of the inviscid and viscous flows until convergence is achieved; it is not a simple matter to choose an initial pressure distribution or displacement surface which will lead to convergence.

REFERENCES

1. Oswatitch, K. — I.U.T.A.M. Symposium on Boundary-Layer Research, Freiburg, 1957. Springer Verlag, Berlin, 1958.
2. Maskell, E.C. — *Flow Separation in Three Dimensions.* RAE Tech. Note Aero 2565, 1955.
3. Thwaites, B. — *Approximate Calculation of the Laminar Boundary Layer.* Aero. Quart. Vol.1, 1949, p.245.
4. Rott, N.
Crabtree, L.F. — *Simplified Laminar Boundary-Layer Calculations for Bodies of Revolution and for Yawed Wings.* J. Aero. Sci., Vol.19, 1952, p.553.
5. Sells, C.C.L. — *Two-Dimensional Laminar Compressible Boundary-Layer Programme for a Perfect Gas.* ARC R & M 3533, 1968.
6. Smith, A.M.O.
Clutter, D.W. — *A General Method for Solving the Compressible Boundary-Layer Equations.* Douglas Aircraft Engineering Paper 1699, 1963.
7. Sandborn, V.A.
Kline, S.J. — *Flow Models in Boundary-Layer Stall Inception.* J. Basic Eng., Trans. A.S.M.E. Series D, Vol.83, September 1961, p.317.

8. Sandborn, V.A. Liu, C.Y. — *On Turbulent Boundary-Layer Separation.* J. Fluid Mech., 32 Pt.2, 1968, p.293.

9. Stratford, B.S. — *An Experimental Flow with Zero Skin Friction Throughout its Region of Pressure Rise.* J. Fluid Mech., Vol.5, 1959, p.17.

10. Bradshaw, P. et al. — *Calculation of Boundary-Layer Development Using the Turbulent Energy Equation.* J. Fluid Mech., Vol.28, Pt.3, 1967, p.593.

11. Bradshaw, P. Ferriss, D.H. — *Calculation of Boundary-Layer Development Using the Turbulent Energy Equation. II Compressible Flow on Adiabatic Walls.* N.P.L. Aero Report 1217, 1966.

12. McCullough, G.B. Gault, D.E. — *Examples of Three Representative Types of Airfoil Section Stall at Low Speed.* NACA TN.2502, 1951.

13. Duncan, W.J. — *The Principles of the Control and Stability of Aircraft.* (See Chapters 11 and 14 by A.D.Young). Cambridge University Press, 1952.

14. Wallis, R.A. — *Boundary-Layer Transition at the Leading Edge of Thin Wings and its Effect on General Nose Separation.* Advances in Aero Sci., Vol.3, Pergamon Press, London, 1962. pp.161–184.

15. Evans, W.T. Mort, K.W. — *Analysis of Computed Flow Parameters for a Set of Sudden Stalls in Low-Speed Two-Dimensional Flow.* NASA TN.D-85, 1959.

16. Woodward, D.S. — *An Investigation of the Parameters Controlling the Behaviour of Laminar Separation Bubbles.* RAE TM. Aero.1003, 1967.

17. Horton, H.P. — *A Semi-Empirical Theory for the Growth and Bursting of Laminar Separation Bubbles.* ARC C.P.1073, 1967.

18. Norbury, J.F. Crabtree, L.F. — *A Simplified Model of the Incompressible Flow Past Two-Dimensional Aerofoils with a Long Bubble Type of Flow Separation.* RAE Tech. Note Aero 2352, 1955.

19. Woods, L.C. — *The Theory of Subsonic Plane Flow.* Cambridge University Press, 1961, p.359.

20. Küchemann, D. — *Types of Flow on Swept Wings with Special Reference to Free Boundaries and Vortex Sheets.* J. Roy. Aero. Soc., Vol.57, 1953, p.683.

21. Legendre, R. — *Séparation de l'Ecoulement Laminaire Tridimensionnel.* Rech. Aero. No.54, 1956, p.3.

22. Eichelbrenner, E.A. — *Décollement Laminaire en Trois Dimensions sur un Obstacle Fini.* O.N.E.R.A. Publication No.89, 1957.

23. Cooke, J.C. Brebner, G.G. — *The Nature of Separation and its Prevention by Geometric Design in a Wholly Subsonic Flow.* Boundary Layer and Flow Control, (Edit. G.V.Lachmann), Vol.I, Pergamon Press, London, 1961, p.158.

24. Lighthill, M.J. — *Introduction: Boundary-Layer Theory.* Laminar Boundary Layers, (Edit. L.Rosenhead), Oxford University Press, 1963, p.72.

25. Brown, S.N. Stewartson, K. — *Laminar Separation.* Annual Review of Fluid Mechanics, Annual Reviews Inc., 1969, pp.45–72.

26. Horton, H.P. — Ph.D. Thesis, Queen Mary College, University of London, 1968.

27. Deeb, S.D. — Ph.D. Thesis, University of Birmingham, 1969.

28. Head, M.R. Hayasi, N. — *Approximate Calculations of the Incompressible Laminar Boundary Layer.* ARC 28507, FM 3783, 1966.

29. Liu, C.Y. Sandborn, V.A. — *Evaluation of the Separation Properties of Laminar Boundary Layer.* Aero. Quart., Vol.XIX, Pt.3, 1968, p.235.

30. Curle, N. — *A Two-Parameter Method for Calculating the Two-Dimensional Incompressible Laminar Boundary Layer.* ARC 28113, FM 3718, 1966.

31. Heid, M.R. — *An Approximate Method of Calculating the Laminar Boundary Layer in Two-Dimensional Incompressible Flow.* ARC R & M 3123, 1959.

32. Korst, H.H. — *A Theory for Base Pressure in Transonic and Supersonic Flow.* J. of Appl. Mech., Vol.23, 1956, pp.593–600.

33. Nash, J.F. — *An Analysis of Two-Dimensional Turbulent Base Flow Including the Effect of the Approaching Boundary Layer.* ARC R & M 3344, 1963.

34. Crocco, L.; Lees, L. — *A Mixing Theory for the Interaction between Dissipative Flow and Nearly-isentropic Streams.* J. Aero Sci., Vol.19, 1952, pp.649–676.

35. Green, J.E. — *Two-Dimensional Turbulent Re-Attachment as a Boundary-Layer Problem.* AGARD C.P.No.4, 1966, pp.393–428.

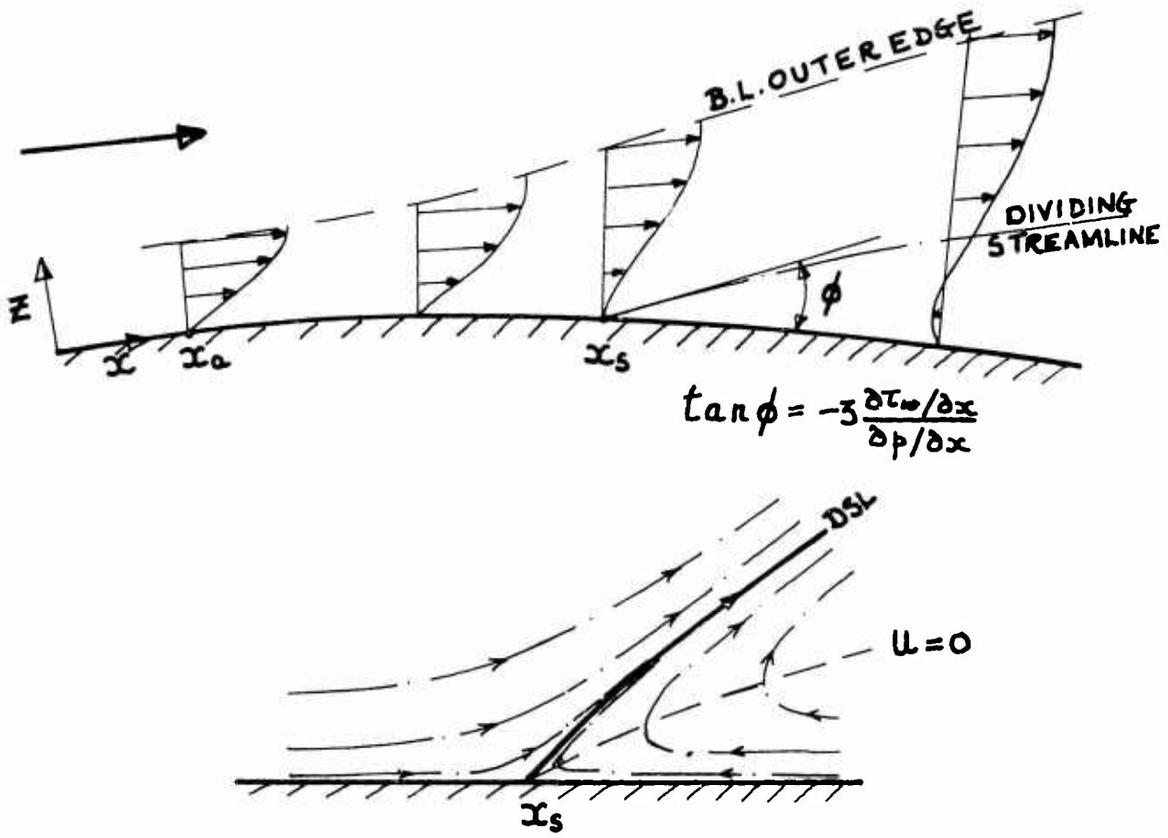

Fig.1 Laminar separation

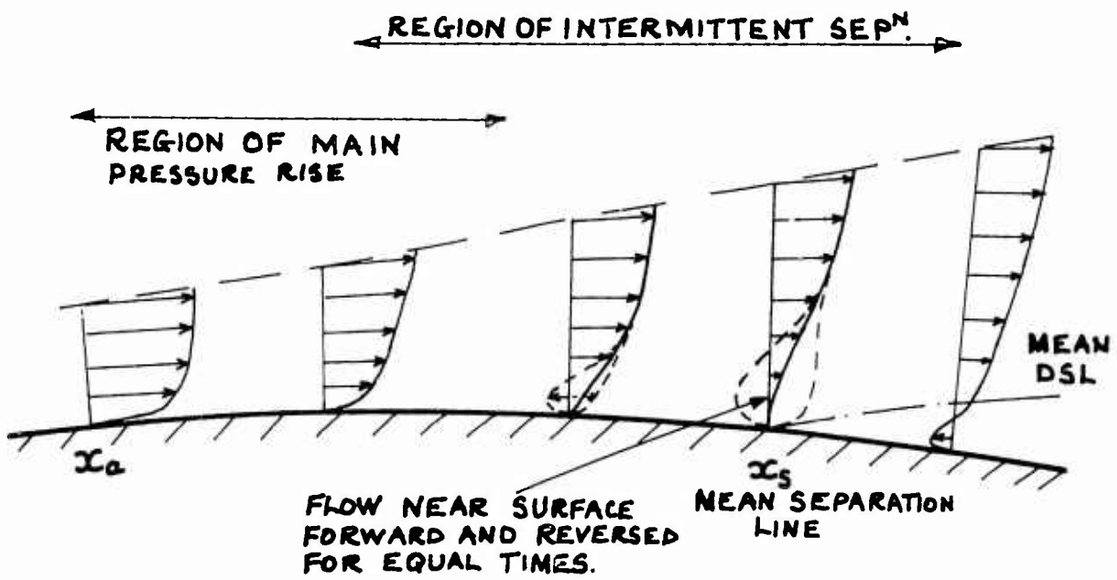

Fig.2 Turbulent separation

——— Mean velocity profiles
— — Intermittent velocity profiles

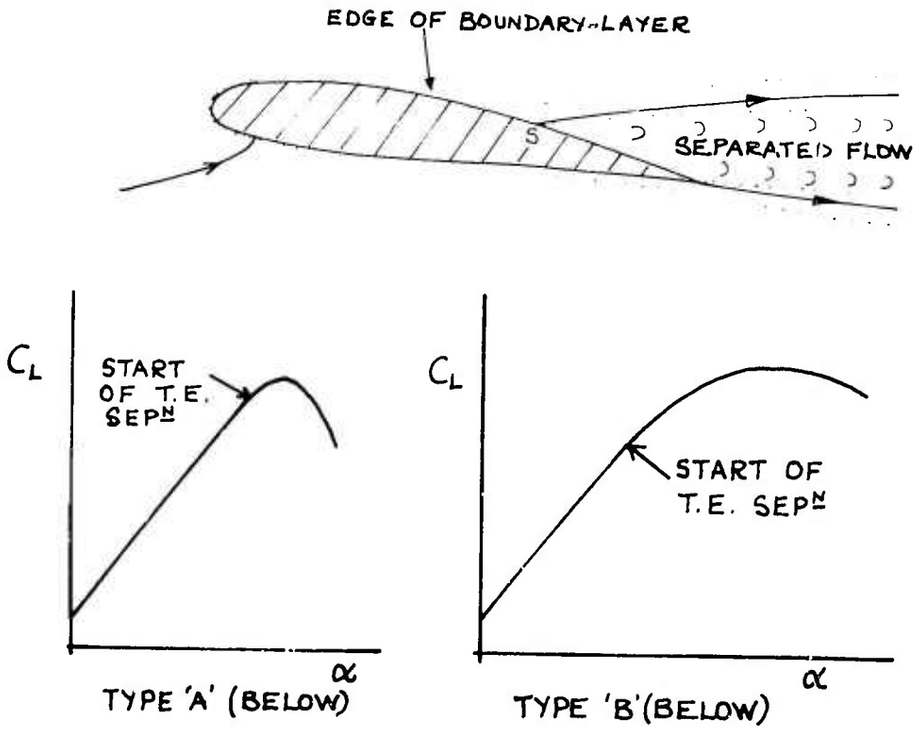

Fig.3 Trailing-edge stall

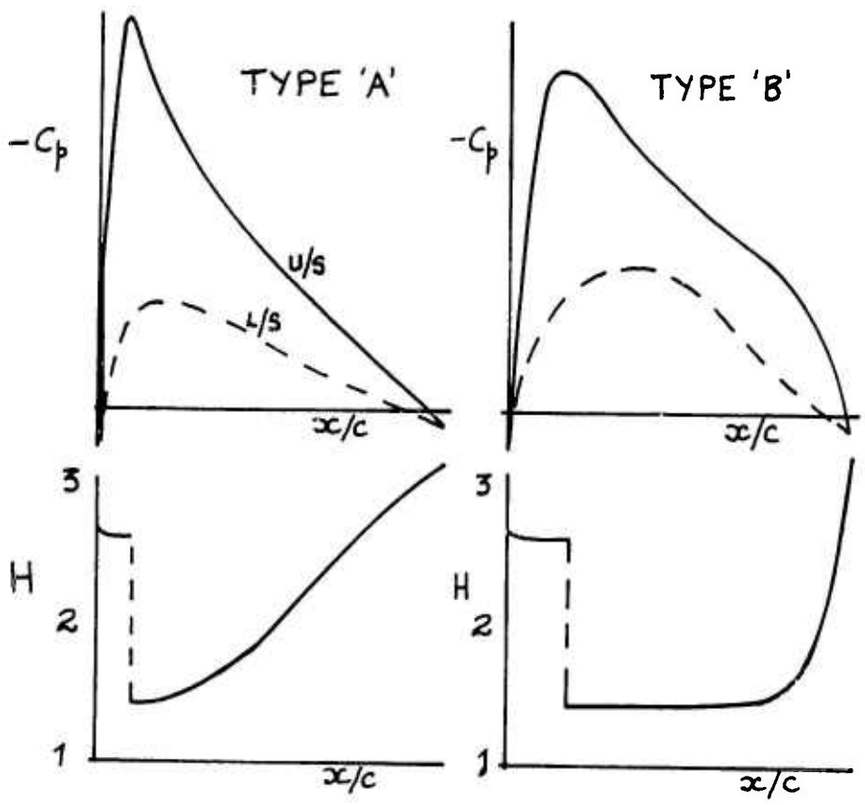

Fig.4 Pressure distributions and shape parameters for 2 types of trailing-edge stall

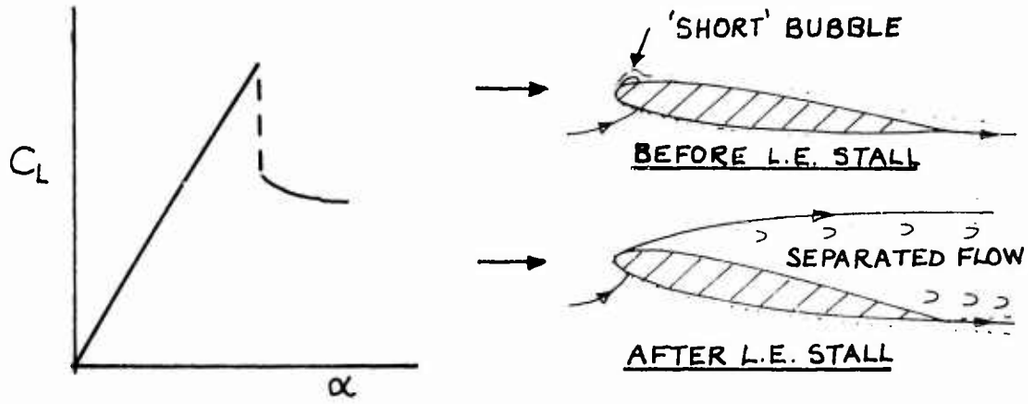

Fig.5 Leading-edge stall

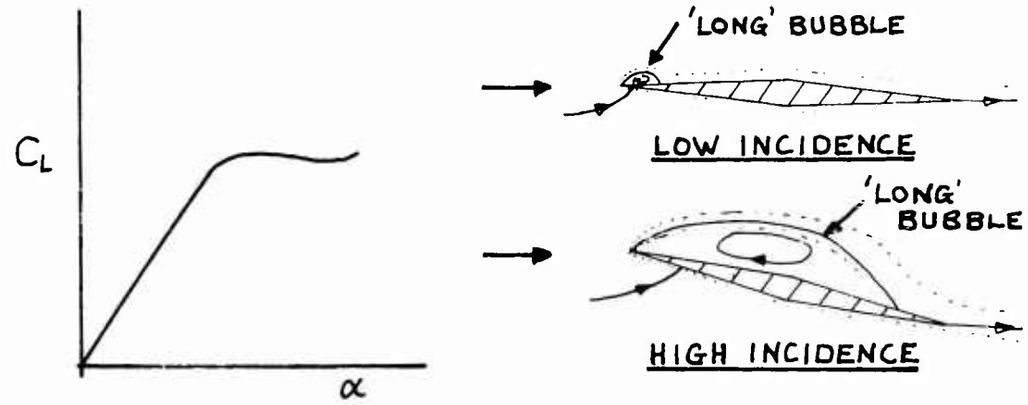

Fig.6(a) Thin aerofoil stall — sharp leading-edge

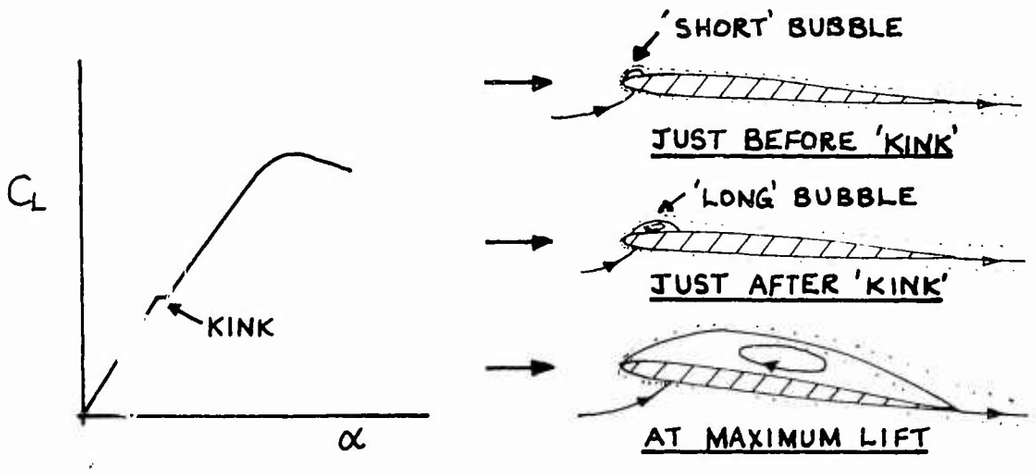

Fig.6(b) Thin aerofoil stall — rounded leading-edge

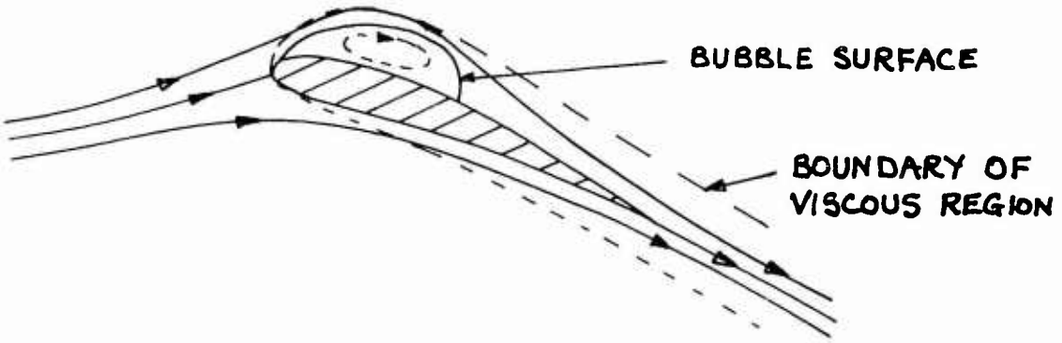

SMALL LEADING-EDGE BUBBLE.

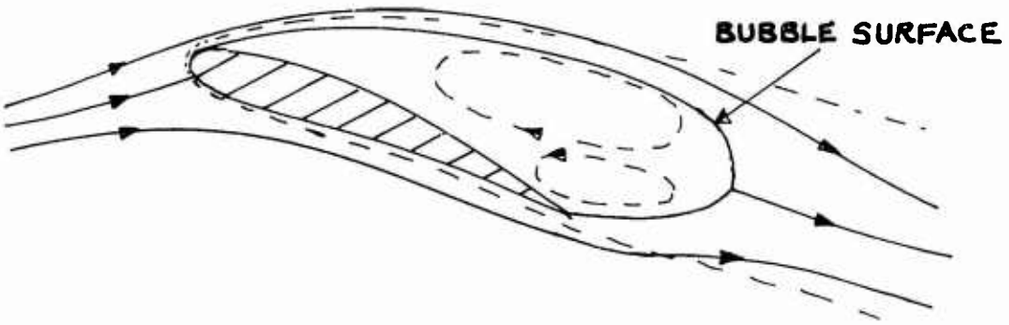

L.E. BUBBLE EXTENDING BEHIND T.E.

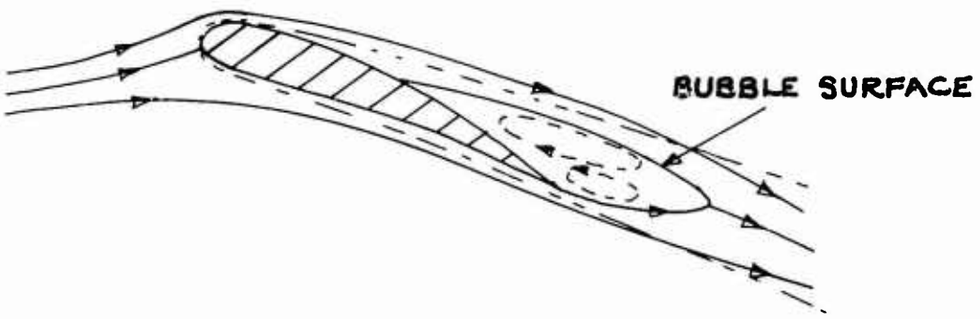

TRAILING-EDGE BUBBLE.

Fig.7 Examples of two-dimensional bubbles

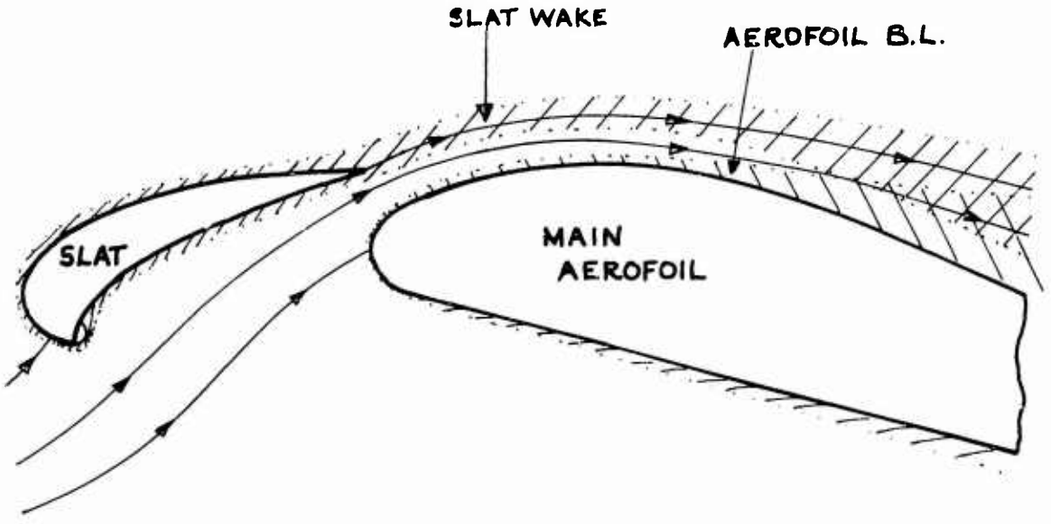

Fig.8 Flow round a slatted leading-edge

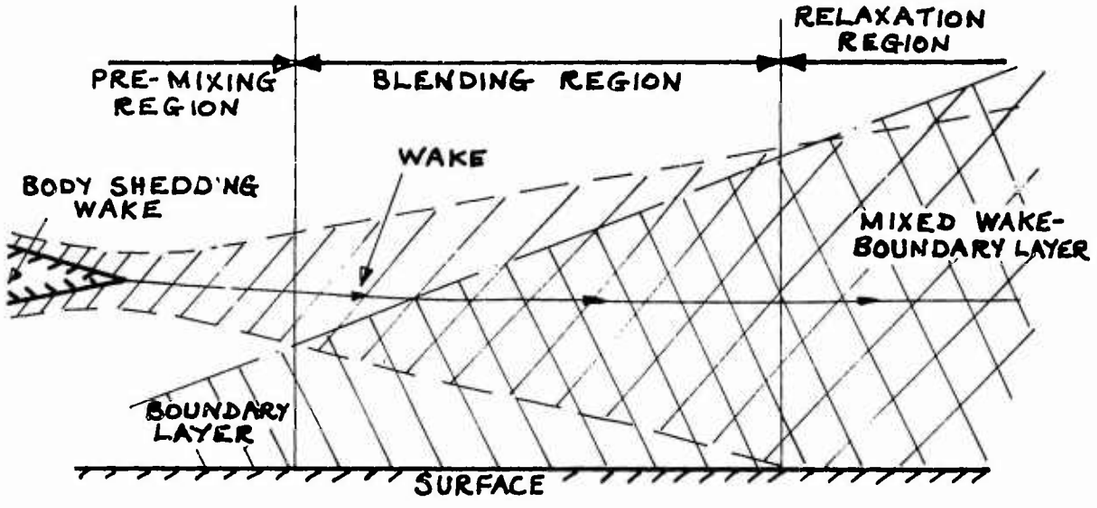

N.B. VERTICAL SCALE EXAGGERATED.

Fig.8(a) Regions of wake-boundary layer mixing

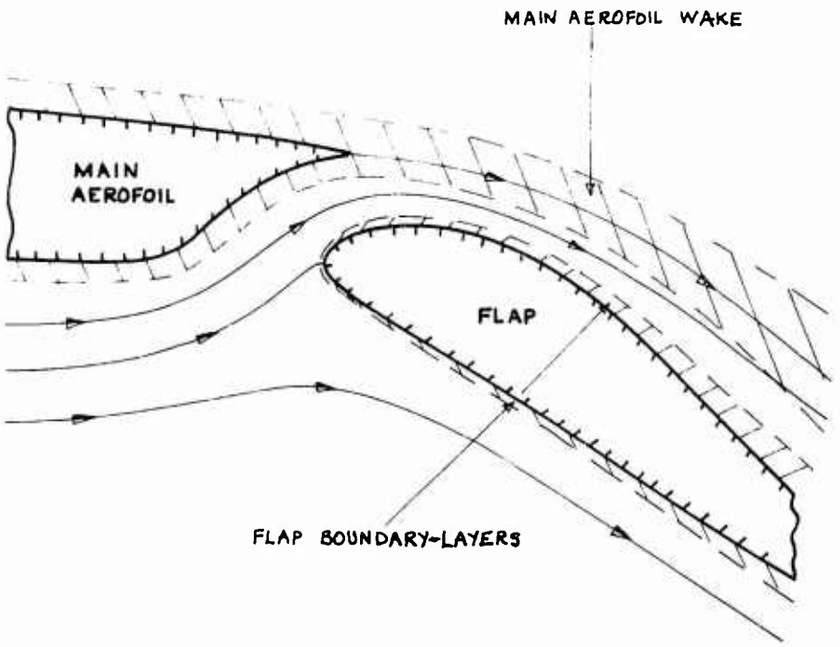

Fig.9 Flow round a slotted flap

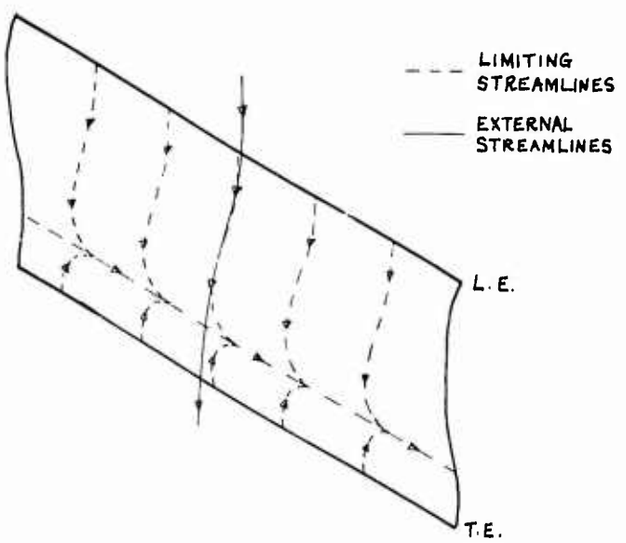

Fig.10(a) Separation from an infinite yawed wing

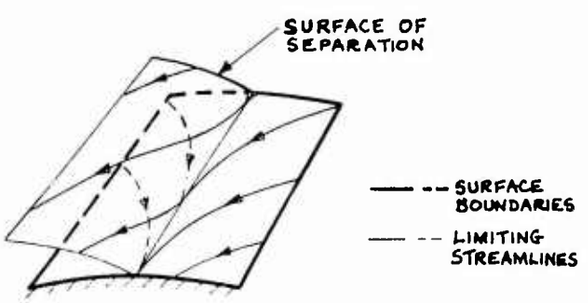

Fig.10(b) Streamline pattern at a line of three-dimensional separation

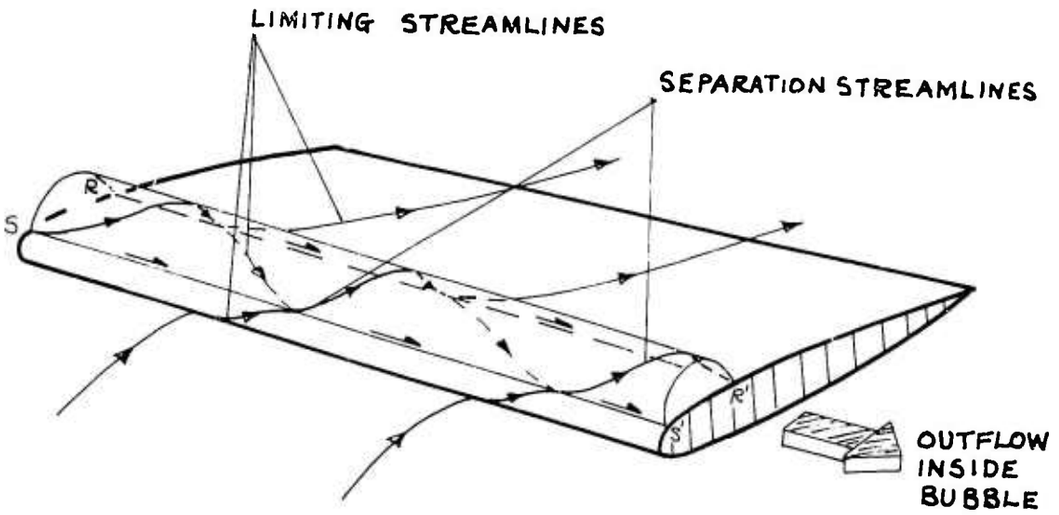

Fig.11 Leading-edge bubble on a swept wing, containing a trapped vortex with outflow

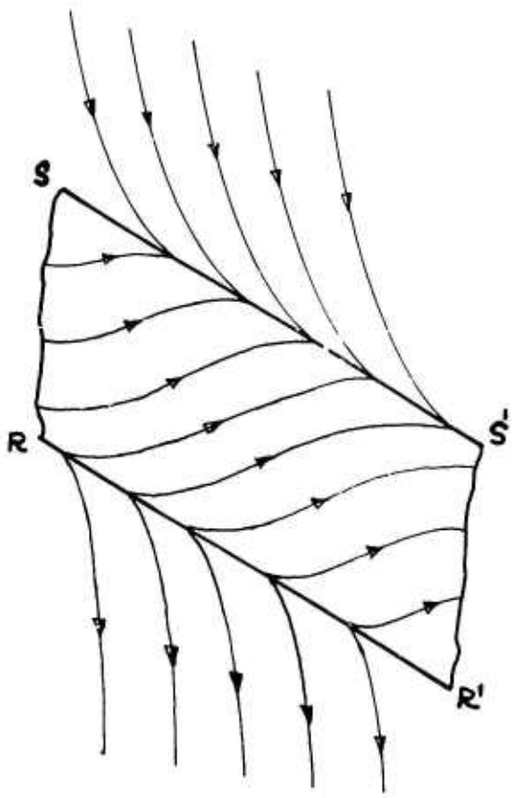

Fig.11(a) Corresponding limiting streamlines

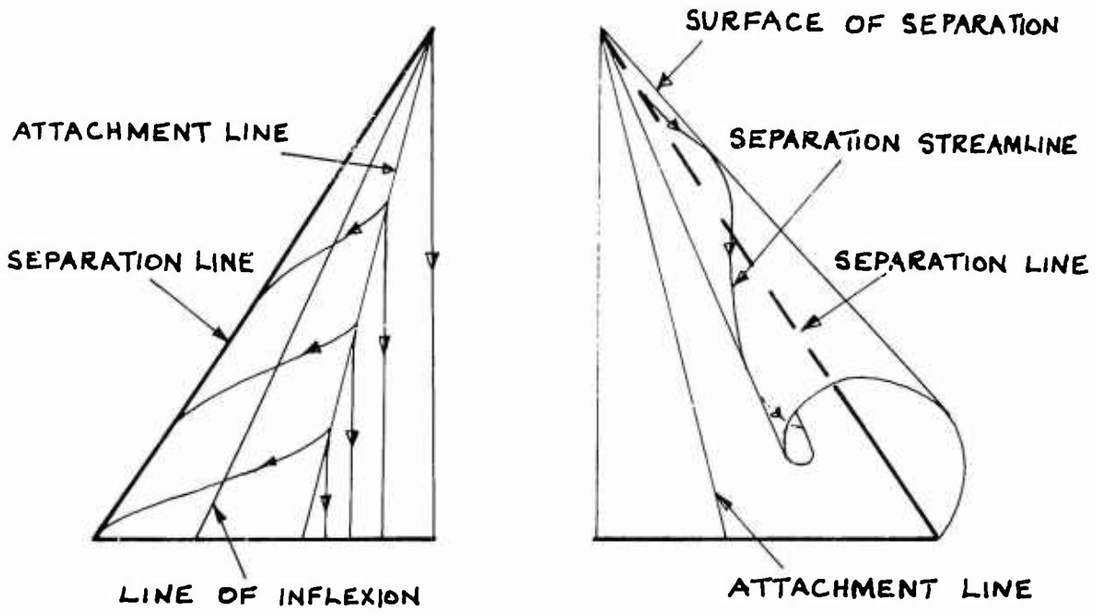

Fig.12 Formation of a vortex sheet at the leading-edge of a slender delta wing

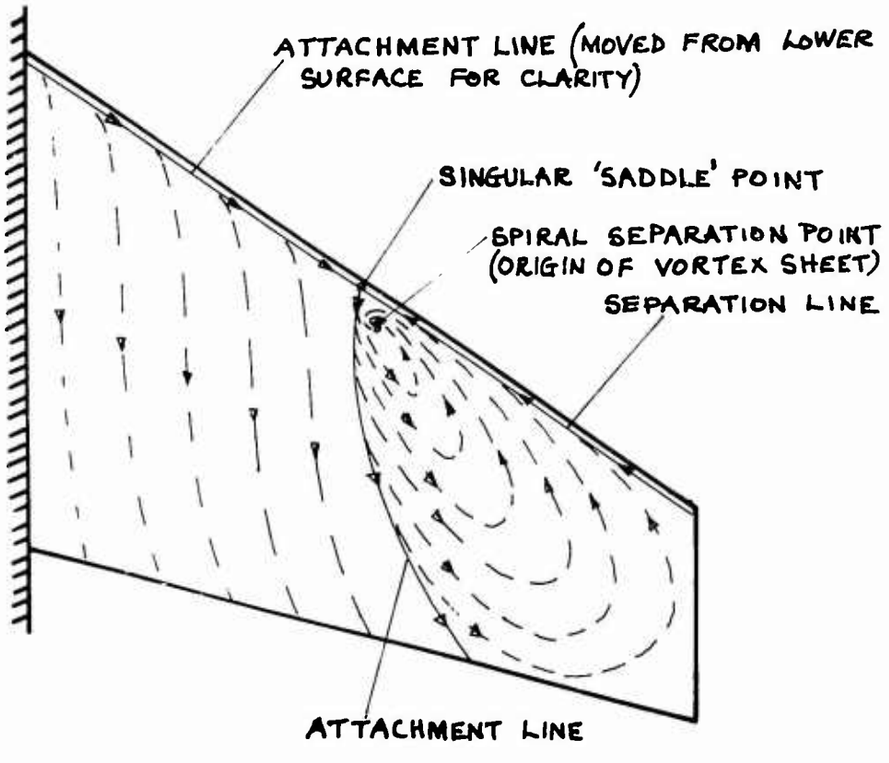

Fig.13 Formation of a part-span vortex sheet on a swept wing

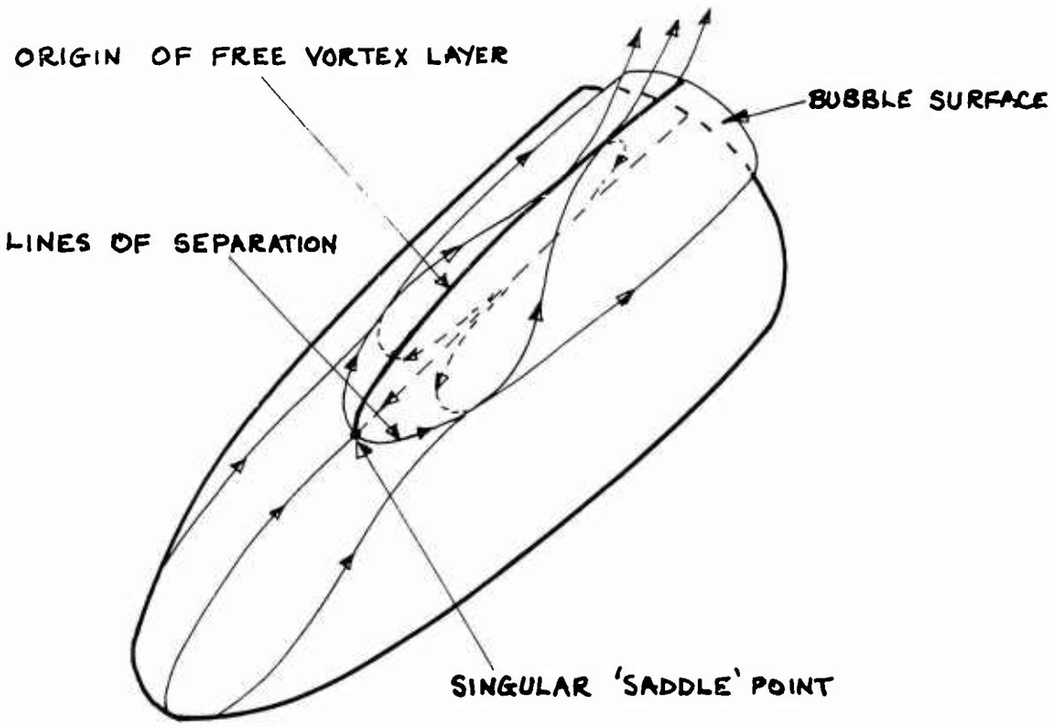

Fig.14 Mixed bubble and vortex layer flow on a body of revolution at incidence

SOME NOTES ON

TWO-DIMENSIONAL HIGH-LIFT TESTS IN WIND-TUNNELS

by

B. van den BERG

Nationaal Lucht-en Ruimtevaart Laboratorium (NLR);
Amsterdam, Netherlands.

SOME NOTES ON TWO-DIMENSIONAL HIGH-LIFT TESTS IN WIND-TUNNELS

B. van den Berg

1. INTRODUCTION

Though two-dimensional flows never really exist on aircraft wings, two-dimensional wind-tunnel tests on aerofoils with high-lift devices may be very instructive, since the essential features of the three-dimensional wing usually are well represented by the two-dimensional flow. Two-dimensional wind-tunnel tests have several advantages as compared with three-dimensional tests. The most obvious advantage is that the models are cylindrical and therefore comparatively easy to make. This is of particular importance, since high-lift models usually are very complicated due to the flaps and slats, which should all be movable and rotatable relative to each other. With two-dimensional models the width of the flap and slat slots is constant across the span, which simplifies the adjustment of the slot widths considerably. For aerofoils with boundary-layer control by blowing or suction and for aerofoils equipped with a jet-flap, the transport of air to or from a two-dimensional model is easy to realize. Apart from the advantage of a simple model construction, another important advantage of the use of two-dimensional models is that in a wind-tunnel of given size a model with a substantially larger chord can be installed than when a three-dimensional model is used. This means that a higher Reynolds number can be achieved in the same test facility with a two-dimensional model.

The main disadvantage of two-dimensional tests is of course that the results must be translated into three-dimensional circumstances. The conversion of the measured two-dimensional data to the corresponding data for a three-dimensional wing is never very reliable. This is in particular true for the maximum lift, since no simple relations exist between the two- and three-dimensional values for this case. Uncertainties in the conversion of the data exist even more with swept wings. This manifests itself in the difficult question which aerofoil section of a swept wing should be chosen for the two-dimensional model, the streamwise section or the section perpendicular to the wing quarter-chord line? When the section perpendicular to the quarter-chord line is chosen, the flow around the two-dimensional aerofoil is similar to that around an infinite sheared wing according to potential theory. The boundary-layer flow on a swept wing, however, suggests that a streamwise section might be a better choice for the two-dimensional model. The importance of a correct conversion of the two-dimensional data to three-dimensions is not so great as one might think, since it is common that the two-dimensional tests are followed by three-dimensional tests with a complete aircraft model. The main goal of two-dimensional tests is usually to compare the effectiveness of various high-lift devices, so that a device can be chosen for application on the complete model.

When the wing sweep angle is very large or the aspect-ratio is very small, two-dimensional tests are senseless. This is clearly true for instance for swept wings which exhibit a vortex flow along the wing leading-edge at high incidences. It is difficult to state generally above which sweep angle, or below which aspect-ratio, two-dimensional tests become of little value. The important thing to keep in mind is that the essential features of the three-dimensional flow should be represented reasonably well by the two-dimensional flow.

In the following, some problems associated with two-dimensional high-lift tests will be discussed. First, something will be said about the test set-up in the wind-tunnel, the design of the models and the methods to determine the forces on the model. Then the tunnel wall interference effects will be discussed. These include the effect of the constraint which the tunnel walls impose on the flow as well as the danger of boundary-layer separations on the tunnel walls. The necessity of boundary-layer control at the model tunnel wall junctions will be demonstrated.

2. TESTING TECHNIQUES

2.1 Test Set-Up and Model Construction

A two-dimensional test set-up is obtained by placing a finite span of the aerofoil between reflection planes. When the aerofoil model spans the tunnel, the tunnel walls will form the reflection planes. Two-dimensional tests are performed often in general-purpose wind-tunnels, but wind-tunnels also exist that are specially designed for two-dimensional work. The height/breadth ratio of the test section of these special tunnels usually is relatively large. In this test section the model is mounted horizontally. Due to the large height of the tunnel, large chord models can be applied without an inadmissible large constraint of the flow around the aerofoil by the horizontal tunnel walls. The geometrical aspect-ratio of these models is small, however, so that there is a great risk that the boundary

layer on the tunnel side walls will affect the test results appreciably. The influence of the presence of the tunnel side walls on the nominally two-dimensional flow will be discussed extensively in Section 3.2. It may be remarked in advance, that the effects should not be underestimated. For that reason very large test-section height/breadth ratios are not advisable for two-dimensional high-lift tests generally.

In Figure 1 some possible test set-ups in a wind-tunnel with a normal test-section height/breadth ratio are shown. The most simple possibility is a model that spans the tunnel completely from wall to wall. In Figure 1 a horizontal model is shown spanning the larger dimensions of the test section; but the model may be mounted also vertically, of course. In fact, with a vertical model that spans the smaller dimension of the test section, generally a better compromise is obtained between the magnitude of the interference effects of the tunnel walls parallel to the model and those perpendicular to the model. Moreover, from model strength considerations, a smaller model span is an advantage. The principle drawback of a model spanning the tunnel is that the boundary layer on the tunnel walls is usually thick, so that the wall boundary-layer interference effects may be quite severe. To avoid this, large false walls from tunnel roof to floor may be installed with the model mounted horizontally inbetween (see Figure 1). The boundary layers on the false walls will be much thinner than on the tunnel walls. An important drawback of this test set-up, however, is that the false walls divide the test section into three separate channels. The distribution of the mainstream flow between the three channels depends on the resistance in the three channels. The velocity in the centre section is therefore not necessarily equal to the mean velocity in the test section. As a matter of fact, the velocity in the centre section has been found to differ considerably from the mean velocity. The difference varies when the model drag alters. It will be evident that in these circumstances the calibration of the velocity in the centre section will give rise to large troubles. In practice, it appears often impossible to avoid important uncertainties in the determination of the free-stream velocity for the model. An improvement is achieved when dummy models are mounted between the false walls and the tunnel walls, since the resistance in the three channels will be approximately equal in that case. At large incidences the dummies will stall earlier than the centre section, however, so that again the determination of the free-stream velocity presents difficulties.

Another possible test set-up consists of a model between end-plates that do not span the tunnel (Fig.1). To preclude the test section being divided effectively into three channels, the height of the end-plates should not exceed half the tunnel height[1]. With end-plates a chordwise loading independent of the spanwise position is soon obtained, but very large end-plates are necessary to obtain a lift-incidence curve slope near the two-dimensional value. This is predicted also by the theory of Mangler[2]. For instance, with a geometrical aspect-ratio $A = 3$ and end-plates of a height three times the model chord, the effective aspect-ratio is only $A = 8.3$ according to Mangler's calculations, which means that the lift-incidence curve slope is still 20% below that in really two-dimensional conditions.

From the three test set-ups that have been discussed, the most simple one, with the model spanning the tunnel, appears to be the most advisable. A primary reason is that a reduction of the boundary-layer thickness on the walls connected to the model, which is the main advantage of the other test set-ups, does not seem to lead to substantial reductions of the wall boundary-layer interference effects. It appears that the mere presence of a wall at the model ends is more important than the thickness of the boundary layer on that wall. The fact that the velocity diminishes to zero at the wall is apparently most essential, while the way the velocity diminishes to zero seems to be a second order effect.

Figure 2 gives a photograph of a two-dimensional aerofoil model mounted vertically between the upper and lower turntable of the wind-tunnel. The incidence of the model can be adjusted by rotating the turntables. The forces on this model were deduced from static pressure measurements on the surface at the mid-span section. If the forces are measured with a balance, the test arrangement is not so simple. The model forces may be measured with the external balance of the tunnel or with an internal strain-gauge balance. In both cases it is advisable to divide the model into a centre section and two outboard sections and to measure only the forces on the centre section, so that a direct influence of the wall boundary layer on the test results is avoided. Figure 3 shows a typical test arrangement, which employs an external balance to measure the model forces[3]. The centre section is connected to the tunnel floor balance with struts. The main difficulty with such test arrangement is to keep the displacement of the centre section relative to the dummy sections within acceptable limits. The small gaps between the centre section and the dummies should be sealed, since any appreciable leakage of air from the lower to the upper surface may result in local lift losses. This can be done with little balance constraint by fitting an inflatable rubber seal or by filling the gap with soft felt. When the model forces have to be measured with an internal balance, a simple solution for a two-dimensional test set-up might be to use two strain-gauge balances, one between each dummy and the centre section. Such an arrangement is less advisable, however, because of the large effects that deformations of the tunnel structure (e.g. by temperature changes) have on the balance readings. One is forced therefore to use one internal balance, preferably in the middle of the centre section. This balance must be connected to "earth" via a supporting beam inside the model centre section, but nowhere touching it. Figure 4 shows an example of a test arrangement with an internal strain-gauge balance[6].

The models are usually made out of metal or out of a metal frame with a covering of synthetic resin such as araldite. The construction of two-dimensional models gives no great trouble generally. Some difficulties may occur with the construction of leading-edge slats, since these slats are thin and the loads on the slats are high. The lift on a slat may well be as large as a quarter of the total lift on the airfoil. A construction with an acceptable stiffness can usually be attained by applying a sufficient number of slat brackets. The design of a good flap or slat

bracket is not so easy, since it is a normal requirement that the flaps and slats will be rotatable and movable in horizontal and vertical direction, while the brackets should also disturb the flow as little as possible. Figure 5 gives a sketch of a flap bracket, which is kept very thin to minimise flow disturbances. If the size of the brackets is very small, which will often be the case with flap vane brackets for instance, the only solution may be to use a set of alternative brackets for every position to be investigated. When boundary-layer control by blowing or suction is applied or when a jet-flap is employed, attention should be paid to the uniformity with which the air is blown or sucked over the span. A satisfactory spanwise distribution is not easily achieved sometimes with jet-flaps, because of the large amounts of air that have to be supplied. It is profitable in such cases to utilise excess pressure air, so that the required duct areas in the model may be reduced by increasing the airfeed pressure. When the forces on the model are determined by balance measurements, the air must be fed into the model without significant balance constraints. An extensive discussion of the possible methods of minimising constraints from airfeeds to models, is given in References 1, 3, 4 and 5.

2.2 Measuring Methods

The forces on the model may be measured directly with a balance or may be deduced from pressure measurements. The use of a balance has the advantage that the reduction of the test data is straightforward and quick, but the model construction is complicated, as discussed earlier. When the forces are measured by pressure-plotting of the model, the model is much easier to make, notwithstanding the numerous pressure tubes that have to be installed. An important advantage of pressure-plotting measurements is that a partition of the model in a centre section and two outboard dummy sections is not necessary. This means that there are no gaps between the sections, and thus there is no risk of air leakage through the gaps and of discontinuities in the model surface. Pressure-plotting should not be regarded simply as an alternative to the use of a balance, as pressure measurements give a great deal of fundamental information, besides the overall forces. This information might be very useful if a new flap or slat shape has to be designed, when the investigated flap or slat proves to be unsatisfactory. The loads on the flap and slat, which are needed for the structural design of the actual aircraft, can also be deduced from the pressure measurements. A practical drawback is that each model modification has consequences also, for some pressure tubing, and that pressure tubes have to be installed in each new model part.

The number of pressure holes required for an accurate integration of the pressure varies generally between 60 and 130, depending on the complexity of the high-lift devices. Relatively many pressure holes should be placed in regions with large pressure variations, i.e. near the leading-edges of the wing, the flap and the slat. The pressures can be recorded quickly with automatic scanning devices and pressure transducers. With a modern data processing equipment and an electronic computer, the integration of the pressures to the overall forces should not cause much trouble.

The scanning speed may be severely limited by the large resistance of the pressure tubes between the holes in the model surface and the transducer. This can be avoided by putting a buffer volume near the scanning device at the end of each tube. In this volume, the pressure will adjust itself to the pressure on the model surface before the pressures are scanned. The buffer volume must be very much larger than the pressure transducer volume, since otherwise the measured pressure will depend on the previous pressure applied to the transducer. A multi-manometer may be helpful to indicate leaks in the pressure tubes during the tests and gives an immediate impression of the pressure distribution over the aerofoil. If the multi-manometer is placed near the scanning device, its volume may serve as the buffer volume mentioned earlier. For an aerofoil near stall, it is possible that the flow over the aerofoil is intermittently attached and separated. Such a change of flow condition should not occur during the time needed to scan the pressures, since otherwise the recorded pressures belong partly to a separated and partly to an attached flow, and consequently unrealistic results are obtained. In these circumstances it is necessary to shut off the pressure tubes just before scanning the pressures.

The forces on a two-dimensional model can not only be determined by pressure-plotting of the model, but also by pressure-plotting of the tunnel walls facing the model. The resultant force on these walls should be equal to the total lift of the aerofoil. A kind of mean lift over the full model span is obtained in this way, even when the pressures on the tunnel walls are measured only along the centre-line. An accurate value for the pitching moment of the aerofoil is difficult to achieve from the tunnel wall pressures, so that for the determination of the pitching moment a balance is still needed. Also no drag data are obtained.

From pressure measurements on the model surface, only the pressure drag of the aerofoil is obtained, not the friction drag which may constitute a large part of the total drag. When performing pressure-plotting measurements, the total profile drag must be obtained in another way, usually from measurements of the total-head and static pressure in the wake behind the model. In principle, the fact that the drag must be determined from wake traverses should be considered as one of the drawbacks of pressure-plotting measurements. In practice, however, it proves to be nearly impossible to obtain reasonably accurate drag data from balance measurements as well. This can be shown plausible as follows.

Suppose that the effective aspect-ratio of the model has a finite value A. The induced drag-coefficient C_{di} at a lift coefficient C_l may be written in the form $C_{di} = C_l^2/\pi A$. The order of magnitude of the profile drag to be measured is $C_d \approx 0.03$. If an accuracy of 10% is demanded for the profile drag measurements, the induced

drag coefficient must be less than $C_{d_1} < 0.003$. To meet this requirement at a lift coefficient $C_l = 3$, the effective aspect ratio of the model must be larger than $A > 1000$. It will be evident that this is a very high effective aspect-ratio for a practical two-dimensional test set-up in a tunnel. Even when there are no flow separations near the model tunnel wall junctions, the circulation will decrease in the boundary layer on the tunnel wall connected to the aerofoil. This will be discussed more extensively in Section 3.2. Since deviations from the two-dimensional condition are inevitable near the tunnel walls, it is unlikely that really high effective aspect-ratios can ever be realized in practical cases.

From the foregoing it must be concluded that there is little hope of a reasonably accurate determination of the profile drag by balance measurements. Wake traverses appear to be the only way to obtain accurate values for the drag. Essentially the cause of the problem is that the drag is so small compared with the lift. In the case considered earlier, the lift is hundred times the drag, so that a difference in the model incidence $\Delta\alpha = 0.001$ rad $\approx 0.06°$ already leads to an error of 10% in the drag, if measured with a balance.

Wake measurements can be carried out most conveniently at a distance of a half to one chord behind the trailing-edge of the aerofoil. The rake used for the wake traverses should be suitable for small wakes as well as for large wakes, since the drag may differ considerably at various incidences and for various model configurations. This means that numerous total-head tubes will be necessary in general. The wake pressures can be measured also by a pressure transducer with a scanning device and the data can be integrated to the drag by a computer. In that case it is important to chose an intelligent criterion for the wake boundaries, where the integration must start and finish.

Also with the wake traverse method, problems may arise in connection with the two-dimensionality of the flow. Usually wake traverses are made only at one spanwise station, assuming that the wake behind the model will be precisely two-dimensional. It appears that this is not always true. Substantial spanwise variations in the size of the wake have been found in certain cases. Figure 6 gives an example of the magnitude of the variations that have been measured. The drag deduced from wake traverses has been plotted there against the spanwise position at which the wake traverse was made. All wake traverses were made here at approximately one chord distance behind the aerofoil trailing-edge. It is apparent that the measured drag varies considerably over relatively small spanwise distances. There is no clear correspondence between the drag variations and the position of the flap and vane brackets. Behind the vane bracket the wake drag is smaller and not larger than the mean wake drag, which can be explained by secondary flows, however. Between the vane bracket and the model centre the wake drag increases twice without apparent cause. The drag variation seems to be almost periodic with a wave length in the order of 10% to 15% chord. The results suggest that wakes may be inherently unstable in certain circumstances. It should be realized that a row of rather weak streamwise vortices is sufficient to obtain the observed variations in wake size. It is not clear under which circumstances spanwise variations are likely to occur. The available evidence up to now suggests that non-uniform wakes become more probable at high lift coefficients, but in any case the particular flap configuration that is investigated plays an important part too.

It is evident from the foregoing that it is always necessary to check the two-dimensionality of the wake if reliable drag data are demanded. This may be done by employing two or three rakes at different spanwise positions. When the wake drag does vary appreciably, still more wake traverses are needed to obtain a good mean value for the drag.

3. TUNNEL WALL INTERFERENCE EFFECTS

3.1 The Effect of the Walls Parallel to the Model

Due to the presence of the tunnel walls the flow around the model will be distorted to some extent, so that the forces on the model in the tunnel will not be precisely equal to the forces in an unlimited stream. Therefore, corrections must be applied to the test data for tunnel interference effects. One distinguishes between the interference effects due to blockage of the flow by the model (and the wake of the model) and the effects associated with the lift on the model. The latter is the most important for high-lift tests and therefore the discussion will be limited here to the tunnel wall interference effects due to lift.

The magnitude of the tunnel wall corrections is normally obtained by calculating the difference between the inviscid flow around the model in the tunnel and that in an unlimited stream. The flow around a two-dimensional model in the presence of the two tunnel walls below and above the model may be determined by considering the flow around an infinite series of alternately inverted and erect images of the model. The interference effect is then given by the influence of the infinite series of images on the flow at the model. In practice, it is customary to introduce a simplified representation of the actual model. When the model is represented by one single lifting vortex on the centre-line of the tunnel, the contributions of the infinite series of vortices of alternating sign cancel each other at the position of the vortex, so that there is no tunnel wall interference effect to a first order approximation. However, the images do induce a curvature of the flow, which also affects the model forces, if the model chord is not vanishingly small. The influence of the flow curvature can be translated into a change of aerofoil camber and incidence and in this way a tunnel wall correction to the lift and pitching moment can be determined, as discussed for instance in Reference 7. The corrections may be written in the form:-

$$C_l = \frac{\pi^2}{24}\left(\frac{c}{h}\right)^2 . (C_l + 2C_m) ,$$

$$C_m = \frac{\pi^2}{192}\left(\frac{c}{h}\right)^2 . C_l$$

where C_l and C_m are lift and pitching moment coefficient and c/h is the aerofoil-chord/tunnel-height ratio. These formulae are correct to the order $(c/h)^2$ and are valid only at small model incidences and small flap angles, since the model is assumed to lie entirely on the tunnel centre-line.

From the given formulae, it might be concluded that fairly large chords can be applied for two-dimensional models in wind-tunnels without an unacceptable tunnel wall constraint. The state of things is less favourable than it seems to be, however. The main reason is that the presence of the tunnel walls does not lead simply to an overall change in the stream direction, but to an induced flow curvature, so that the pressure distribution over the aerofoil will be essentially different from that in an unlimited stream. It is evident that the influence of the tunnel wall constraint on the maximum lift is not really predictable in these circumstances. Besides this, the assumption that the incidence and the flap angle are small appears to be rather restrictive in practice. In Figure 7, the approximate tunnel wall correction to the lift is compared with the correction for a flat plate with a plain flap according to exact inviscid theory. Exact solutions are given at zero flap deflection and varying incidence (Ref.8) and at zero incidence and varying flap angle[9]. In the first case the differences between the approximate and exact tunnel wall corrections are small, but it is apparent that large discrepancies occur when the flap is deflected. For flap angles exceeding 30° the approximate tunnel wall correction formulae given earlier appear to be not valid anymore. The approximate formulae overestimate the corrections substantially at larger flap angles. At very large flap angles, the correction even changes sign according to the exact theory for a hinged flat plate.

The large discrepancy between the results of the exact and the approximate theory is somewhat surprising. It should be realized, however, that the approximate theory is based on the induced flow curvature, leading to corrections of the order $(c/h)^2$, because for a model placed centrally in the tunnel there are no corrections of the order c/h. When the model does not coincide exactly with the tunnel centre-line, as happens when a flap is deflected, corrections of the order c/h will be introduced, which may well cause large differences in the corrections to be applied. This does not yet explain why the deviations from the approximate corrections for the flat plate without flap are so small compared with the deviations with deflected flap. It is important to note that it is assumed that when an incidence is applied, part of the plate moves upwards and part of it downwards, so that the effects of the off-centre position of both parts will cancel each other to some extent. Since the larger portion of the load is on the forward part of the plate, which moves in a direction contrary to that of a deflected flap, the deviations from the approximate corrections must be opposite to those due to flap deflection. This is in accordance with Figure 7. Another reason for the comparatively small deviations due to incidence is that only incidences up to roughly 20° are considered. For flap angles of this magnitude the deviations from the approximate corrections are also not large.

It will be clear from the foregoing that the use of relatively large two-dimensional models is not recommended for high-lift tests. The model-chord/tunnel-height ratio should never be chosen larger than $c/h = 0.30$. If large flap angles are applied, a model chord/tunnel height ratio $c/h = 0.25$ is more advisable. When very high lift coefficients are achieved, it is possible that the boundary layers on the tunnel walls below and above the model will separate due to the presence of the model. This may also set a limit to the model size, as will be discussed next.

Though the pressure gradients on the tunnel walls parallel to the model are much smaller than the pressure gradients on the model, it is still possible that flow separation occurs first at the tunnel walls, because the boundary layer on the tunnel walls is very much thicker than the model boundary layer. At high lift coefficients the model may induce quite substantial pressure gradients on the tunnel walls, even with moderate model-chord/tunnel-height ratios. In Figure 8, the variation with streamwise distance of the pressure coefficient C_p on the tunnel walls is given for a lift coefficient $C_l = 4$ and a model-chord/tunnel-height ratio $c/h = 0.30$. The pressures on the tunnel walls have been calculated theoretically, assuming that the high-lift model may be replaced by one vortex of the correct strength. It is apparent from Figure 8 that there is a risk of flow separation on both tunnel walls. On the tunnel wall at the pressure side of the model the flow may separate upstream of the model, while on the wall at the suction side the flow is in danger of separation downstream of the model. Of course, such flow separations will affect the model test results substantially. Flow separations on these tunnel walls must be avoided therefore.

The magnitude of the pressure gradients on the tunnel walls parallel to the model is determined to a first order approximation by the parameter $\Gamma/U_0.h$, for a model with a circulation Γ at a tunnel speed U_0 and a tunnel height h. This parameter may also be written in the more convenient form $C_l.c/h$. Tunnel wall boundary-layer calculations that have been carried out for one case, gave separation at $C_l.c/h \approx 2$ according to D.N.Foster, RAE (private communication). In practice, he found that separation occurred at a somewhat higher value of $C_l.c/h$. To meet the requirement $C_l.c/h < 2$ for a model with a chord/tunnel-height ratio $c/h = 0.25$, the lift coefficient should not exceed $C_l = 8$. This means that large risks of separation on the tunnel walls parallel to the model only exist if extremely high lift coefficients are achieved, at least for models with a normal chord tunnel-height ratio. It should be realized, however, that the admissible value of the parameter $C_l.c/h$ will depend on the relative thickness

of the boundary layer on the tunnel walls, δ/h. In tunnels with comparatively thick wall boundary layers, separations will occur much earlier. Therefore the possibility of flow separations on the tunnel walls parallel to the model should always be kept in mind.

3.2 Effect of the Walls Perpendicular to the Model

The interference effects of the tunnel walls perpendicular to the model are due completely to the boundary layer on these walls. The boundary-layer interference effects may be very severe, however, in particular at large incidences near the stall of the aerofoil. Also, at small incidences the effects of the boundary layer are not negligible. A simple example is the effect on the position of the transition from laminar to turbulent flow near the walls. On a flat plate the turbulence has been found to spread from the tunnel walls with an angle of roughly 10°. When pressure gradients are present, the flow mechanism near the wall junctions becomes very complicated due to the strong secondary flows that are generated. If there is a lift on the model, the related circulation must decrease in the tunnel wall boundary layer. At the wall, circulation (not the lift) is zero, so that vortices with a total strength equal to the circulation around the aerofoil must extend to infinity. It is difficult to establish along which paths the vortices actually leave the model and go to infinity, since this depends on the secondary flows that are generated at the model tunnel wall junction. The vortices that leave the model will in general affect the two-dimensionality of the flow. Since the vortices are situated very near the tunnel wall, the reflected vortices will partly compensate the effects. The results of early theoretical calculations on the effect of the vortices on the two-dimensionality of the flow[10,11] did not at all agree with the experimental results[12]. The main reason for this probably is the much too simple assumption that was made in the theories about the position of the vortices leaving the model. It was assumed that the vortices are concentrated behind the model tunnel wall junctions, while in fact they will be distributed in all directions over the tunnel walls. It will not be easy to solve this interference problem theoretically, because viscous effects play an essential rôle. As long as now flow separations occur, the interference effects are not very large generally. In that case they will seldom lead to great errors in the test data, provided that only the forces on a centre section of the model are measured and the drag is determined by wake traverses. This is not true anymore, however, if premature flow separations occur at the model tunnel wall junctions, as will be discussed next.

The boundary layer at the model tunnel wall junction will separate with a smaller adverse pressure gradient than the boundary layer on the model itself. If no measures are taken, separated regions are usually found near the walls at incidences well below the stalling incidence of the model centre section. These separated regions spread spanwise in triangular wedges with an angle of the order of 45°. This means that for a model with a geometrical aspect-ratio $A < 2$, flow separations may exist at the centre section, which originate from the tunnel walls. At larger geometrical aspect-ratios, there is a very considerable indirect influence of the flow separations near the walls on the measured forces at the mid-span section. This indirect influence is due to the large local lift losses that are associated with the flow separations. The local lift losses near the walls lead to a reduction of the effective aspect-ratio of the model, so that the geometrical incidence of the model in the tunnel will increase faster than the effective incidence at mid-span. It is possible that the effective incidence even decreases with increasing geometrical incidence. This has been made plausible by De Vries in an analysis of the results of a two-dimensional investigation[13]. It seems worthwhile to summarise the analysis here.

For this investigation a 12% thick aerofoil model was used with a geometrical aspect-ratio $A = 3.5$, and mounted between the tunnel walls. Drag data of this model were obtained from pressure measurements on the model surface and from wake traverse measurements. An estimate of the induced incidence at mid-span can be made by considering the difference between the results of both methods of drag measurement, since the drag determined by pressure-plotting of the model includes an "induced drag" term, while the drag deduced from wake measurements does not. In general the drag may be written in the form:–

$$C_d = C_d(0) + K.C_l^2 \quad .$$

It is the last term in the equation, which is of interest here. One may divide the term $K.C_l^2$ into three parts; a part due to the induced drag, $K_i.C_l^2$, a part associated with the profile pressure drag, $K_p.C_l^2$, and a part associated with the profile friction drag, $K_f.C_l^2$. The last two parts, $(K_p + K_f).C_l^2$, constitute together the profile drag, which is measured when wake traverses are carried out. The sum of the first two parts, $(K_i + K_p).C_l^2$, is obtained by pressure plotting measurements. In order to calculate the induced incidence, two different assumptions are possible. It is possible to assume that the increase of the drag determined by pressure plotting with lift is completely due to the induced drag. This means that it is supposed that $K_p = 0$. The induced incidence thus found will overestimate the real value. It may also be assumed that only the difference between the drag determined by pressure-plotting and by wake traverses is due to the induced drag. In that case, it is supposed in fact that $K_f = 0$. The obtained induced incidence will now be an underestimate of the real value.

In Figure 9, the maximum and minimum value thus estimated of the induced incidence α_i at mid-span is plotted against the geometrical incidence α_g for a typical case. The difference between the maximum and minimum value appears to be sufficiently small to draw conclusions from the results. The induced incidence is seen to be rather small at small and moderate geometrical incidences, but the induced incidence increases fast at large geometrical incidences, when severe flow separations occur near the tunnel walls. It is particularly important to note that the rate of increase of the induced incidence then soon exceeds the rate of increase of the geometrical incidence, which

means that the effective incidence of the model decreases with increasing incidence. The geometrical incidence, at which the rate of increase of the induced and the geometrical incidence are equal, $d\alpha_i/d\alpha_g = 1$, coincides practically with the incidence at which the maximum lift was measured at mid-span. Consequently, the conclusion must be drawn that the stalling incidence never was attained at mid-span. What actually happens is shown clearly in Figure 10, where the measured lift coefficient C_l at mid-span is plotted against the geometrical incidence α_g and also against the effective incidence α_e (the maximum value, obtained by subtracting the minimum value of α_i from α_g). Though the plot against the geometrical incidence shows a normal lift curve with a more or less rounded peak, the plot against the effective incidence demonstrates that actually the lift increases first nearly linearly with increasing incidence and then decreases because the incidence decreases. The pressure distributions on the model at geometrical incidences before and beyond maximum lift were also found to be almost identical at the same lift.

The results given in Figures 9 and 10 were deduced from tests with an aerofoil with retracted flap. Similar results were obtained at a flap deflection of 25° and 45°. In all these cases the measured maximum lift at mid-span was determined completely by the features of the flow at the model tunnel wall junctions, together with the geometrical aspect-ratio of the model. There is not necessarily any relation with the maximum lift in a truly two-dimensional flow. It is evident that two-dimensional tests in such circumstances must be regarded as very unsatisfactory.

It is not so easy to avoid premature flow separations at the model tunnel wall junctions. Simple modifications, like fairings at the model ends or fences on the model near the walls, do not lead to significant improvements generally. The only effective way to cure the wall separations seems to be the application of boundary-layer control by suction or blowing. The first successful attempt to avoid the wall separations by boundary-layer control was probably made by Boeing[14]. Both blowing and suction at the tunnel walls were applied with good results. At the RAE, tests have been carried out with suction of the tunnel wall boundary layer adjacent to the model[15]. At the NLR, a blowing boundary-layer control system has been developed to prevent flow separations near the walls. In the following, mainly the NLR investigations in this field will be discussed, because the author is most familiar with them.

At the NLR, a cylindrical aerofoil model was available with blowing slots for boundary-layer control at the aerofoil nose and at the knee of a trailing-edge flap. These slots were divided into several separate spanwise sections, so that in a two-dimensional test set-up blowing could be applied only over the parts adjacent to the walls. Though blowing slots in the tunnel walls near the model are to be preferred, of course, to slots in the model near the tunnel walls, it was believed that experiments with this model could be instructive. In Figure 11 some results are given of these experiments[16]. In the example given, uniform blowing was applied over the flap deflected 30°, but blowing at the nose was applied exclusively through the two slots adjacent to the walls. The variation of the lift measured at mid-span with incidence is given for various blowing momentum coefficients C_μ at the nose. The momentum coefficient is defined as $C_\mu = mV_j/q_0 c$; where m equals the mass flow of blown air per unit length of the slot, V_j equals the blowing jet velocity, q_0 equals the free-stream dynamic head, and c equals the model chord. It is evident that nose blowing only near the walls leads to considerable increments of the maximum lift at mid-span. Visualization of the flow over the model with tufts demonstrated that the lower blowing momentum coefficient at the nose was already sufficient to ensure that the flow separated first near the model centre. A doubling of the nose blowing momentum coefficient near the walls does not lead to appreciable further increments of the maximum lift at mid-span. Apparently the effect of nose blowing near the walls becomes small as soon as the blowing quantity exceeds the amount needed to avoid the onset of flow separation at the model tunnel wall junctions. This is not an unreasonable result since, once separations are avoided by blowing, further blowing will lead only to small local lift increases and consequently will alter the lift at mid-span very little. Substantial discrepancies due to excess blowing near the walls should be expected only after stall, since then the flow is kept artificially in an attached condition, while it ought to be separated. Discrepancies beyond stall are regarded as less important usually, however. It is a very encouraging result that the test data at mid-span are relatively insensitive to excess blowing near the walls, since this means that it is not necessary to adjust in each case the blowing quantities carefully to get the best possible two-dimensional stall pattern. It should be realized further that, with blowing slots in the tunnel walls, the sensitivity to excess blowing very probably will be even much less than in the case considered here with slots in the model.

After this preliminary investigation, tests were carried out on a two-dimensional aerofoil model with a double-slotted flap mounted between the tunnel walls with boundary-layer control at these walls[17]. Blowing slots were installed flush in both tunnel walls near the model nose and just ahead of the flap. The width of the blowing slots is 2 mm and the length is 300 mm for the slots near the nose and 500 mm for the rear slots, which extend above and below the shroud of the model (chord 600 mm). The local forces on the model were determined by pressure-plotting at a mid-span section and at a section very near a tunnel wall. In Figure 12, the measured lift at mid-span and near the wall without and with blowing along the walls are compared for a typical case. The flap was deflected 40° and the same amount of blowing was applied through all slots ($C_\mu \approx 0.14$). Without blowing, the lift near the wall is seen to be much smaller than the lift at mid-span. When blowing is applied, the lift at mid-span and near the wall increase both and become nearly equal. It may be assumed therefore that, with blowing along the walls, the two-dimensionality was maintained over the whole incidence range. In Figure 13, some more results of this investigation are given. The measured maximum lift at mid-span has been plotted there against the blowing momentum coefficient C_μ, defined earlier. It is apparent that first the maximum lift increases fast with increasing amount of blowing along the walls, but that above a certain blowing momentum coefficient the maximum lift remains constant within the experimental scatter. On account of the results of the preliminary investigation, it was already

expected that the effect of blowing would become small as soon as the blowing quantity exceeds the amount needed to avoid premature flow separations near the model tunnel wall junctions. The maximum lift remains constant here for blowing momentum coefficients above C_μ = 0.03 to 0.06 , but these values will depend on the particular model configuration and test set-up. In view of the small influence of excess blowing, one will apply generally blowing momentum coefficients that well exceed the minimum value, in order to ensure that early flow separations near the walls will not occur in any condition.

In Figure 13, results are given for two different positions of the tunnel wall blowing slots relative to the model. With blowing configuration A the slots are placed approximately in their optimum position, that is very near the regions with large adverse pressure gradients. With blowing configuration B the slots are situated at some distance ahead of the model nose and the flap. No difference is seen to exist between the results obtained with the two blowing configurations. In some cases during the investigation it was found that with a less favourable blowing configuration a somewhat larger amount of blowing was needed to obtain the constant maximum lift region, but for the rest the measured maximum lift at mid-span seems to be very insensitive to the position of the blowing slots. In practice it is very profitable to situate the blowing slots at some distance ahead of the flap, since in that case the flap position and flap angle may be altered without changing also the position of the slots in the tunnel walls. A fundamental advantage of boundary-layer control by blowing is that flow separations are prevented over a large area behind the slot, so that the position of the slot is not very critical. Suction must be applied usually rather close to the areas with large adverse pressure gradients, so that the suction arrangements at the tunnel walls must be adapted frequently to the particular model configuration tested. For that reason blowing might be more practical than suction for routine measurements.

4. CONCLUSIONS

The following recommendations may be made with regard to two-dimensional high-lift tests:

1. The model chord/tunnel height ratio should not exceed c/h = 0.3 .
2. Boundary-layer control should be applied at the model tunnel wall junctions.
3. Only the forces on a centre section of the model should be measured.
4. The drag should be determined by wake traverses; however, the two-dimensionality of the wake must be checked.

REFERENCES

1. Anscombe, A. Williams, J. — Some comments on high-lift testing in wind-tunnels with particular reference to jet-blowing models. J. Roy. Aero. Soc., Vol 61, pp 529-540; 1957.

2. Mangler, W. — Die Auftriebsverteilung am Tragflügel mit Endscheiben. Luftfartforschung, Band 14, p.564; 1937.

3. Butler, S.F.J. Williams, J. — Further comments on high-lift testing in wind-tunnels with particular reference to jet-blowing models. Ae. Quart., Vol XI, pp 285-308; 1960.

4. Williams, J. Butler, S.F.J. — Recent developments in low-speed wind-tunnel techniques for V/STOL and high-lift model testing. Z. Flugwiss., Vol 13, pp 73-89; 1965.

5. Lachmann, G.V. (Editor) — Boundary layer and flow control. Pergamon Press, London; 1961.

6. Van den Berg, B. — Wind tunnel investigation with a two-dimensional aerofoil on the effect of blowing over a flap and over a control surface. WGLR Jahrbuch 1962.

7. Pankhurst, R.C. Holder, D.W. — Wind tunnel technique. Chapter 8. Pitmans, London; 1952.

8. Tomotika, S. — The lift of a flat plate placed in a stream between two parallel walls and some allied problems. Aero. Res. Inst. (Japan) Rep. 101; 1934.

9. De Jager, E.M. Van der Vooren, A.I. — Tunnel wall corrections for a wing-flap system between two parallel walls. N.L.R. Rep. W.7.; 1961.

10. Preston, J.H. — The interference on a wing spanning a closed tunnel, arising from the boundary layers on the side walls. A.R.C. R. & M. 1924; 1944.

11. Loos, H.G. — Enige beschouwingen over de grenslaaginterferentie bij de aansluiting van een draagvlak en een wand. N.L.L. Rep. A. 1282 (in Dutch).

12. Mendelsohn, R.A. Polhamus, J.A. — Effect of the tunnel-wall boundary layer on test results of a wing protruding from a tunnel wall. NACA TN 1244; 1947.

13. Van den Berg, B. De Vries, O. — Wind tunnel investigation on a two-dimensional model of the Fokker F-28 wing with various types of flaps. N.L.R. Rep. A. 1598; 1969.

14. Wimpress, J.K. Swihart, J.H. — Influence of aerodynamic research on the performance of supersonic airplanes J. of Aircraft, Vol. 1, No. 2; 1964.

15. Foster, D.N. Lawford, J.A. — Experimental attempts to obtain uniform loading over two-dimensional high-lift wings. R.A.E. TR. 68283; 1968.

16. Van den Berg, B. De Boer, E.B. — Windtunnelonderzoek aan een tweedimensionaal vleugelmodel met grenslaagbeinvloeding door uitblazen door spleten in het vleugeloppervlak bij de vleugel-wand aansluitingen. N.L.R. TR. 69089 LI (in Dutch).

17. De Vos, D.M. — Low speed wind tunnel measurements on a two-dimensional flapped wing-model using tunnel wall boundary layer control at the wing-wall junctions. N.L.R. TR. 70050 U; 1970.

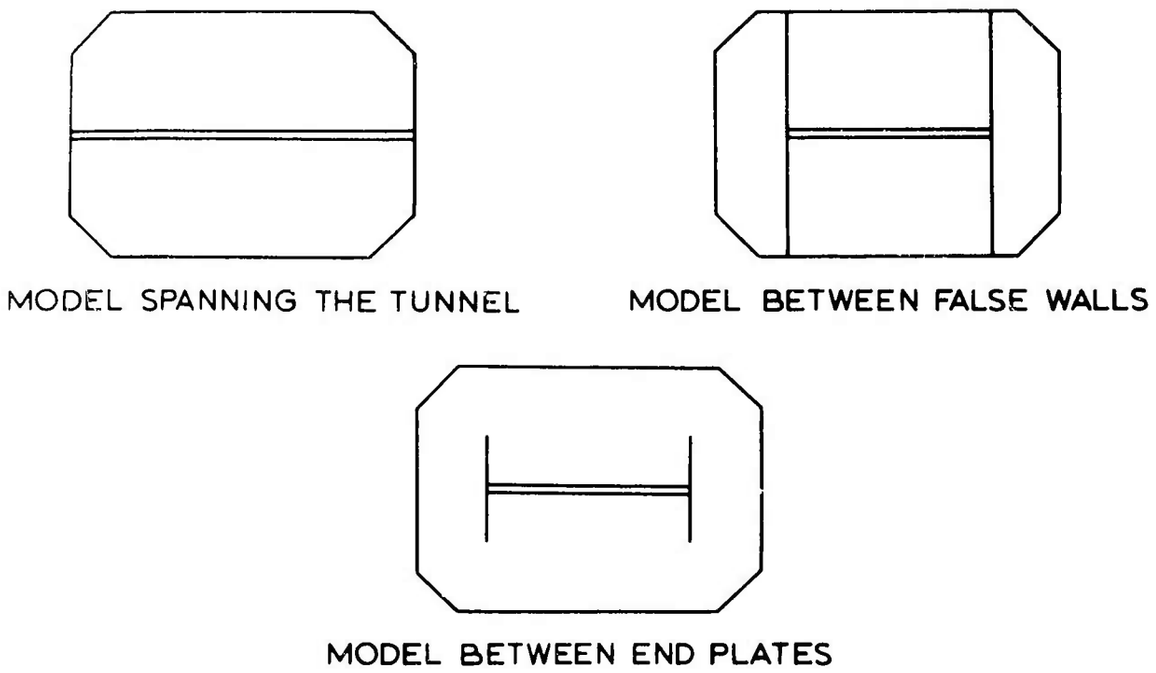

Fig.1 Possible test set-ups

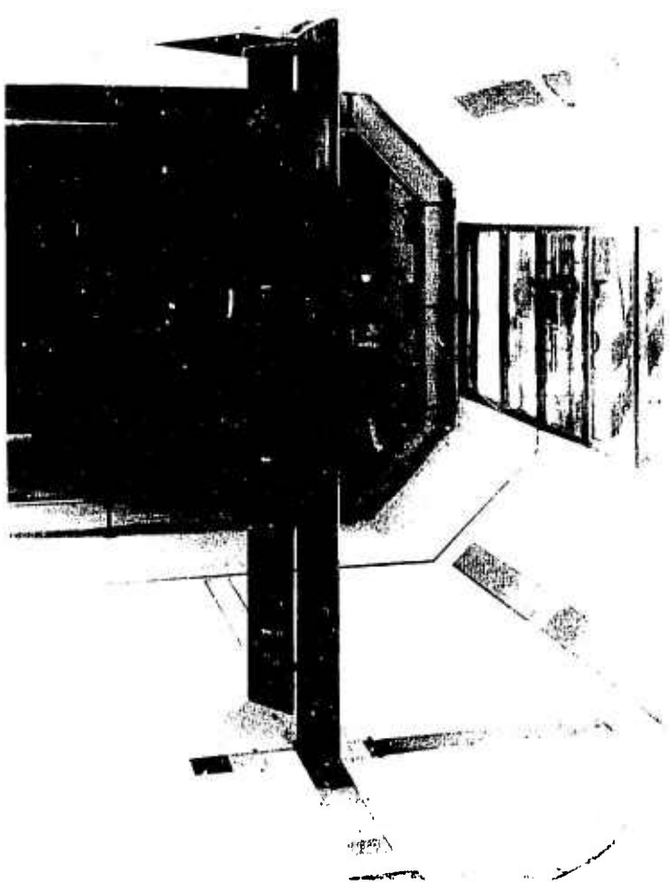

Fig.2 Two-dimensional pressure-plotting model in a wind tunnel

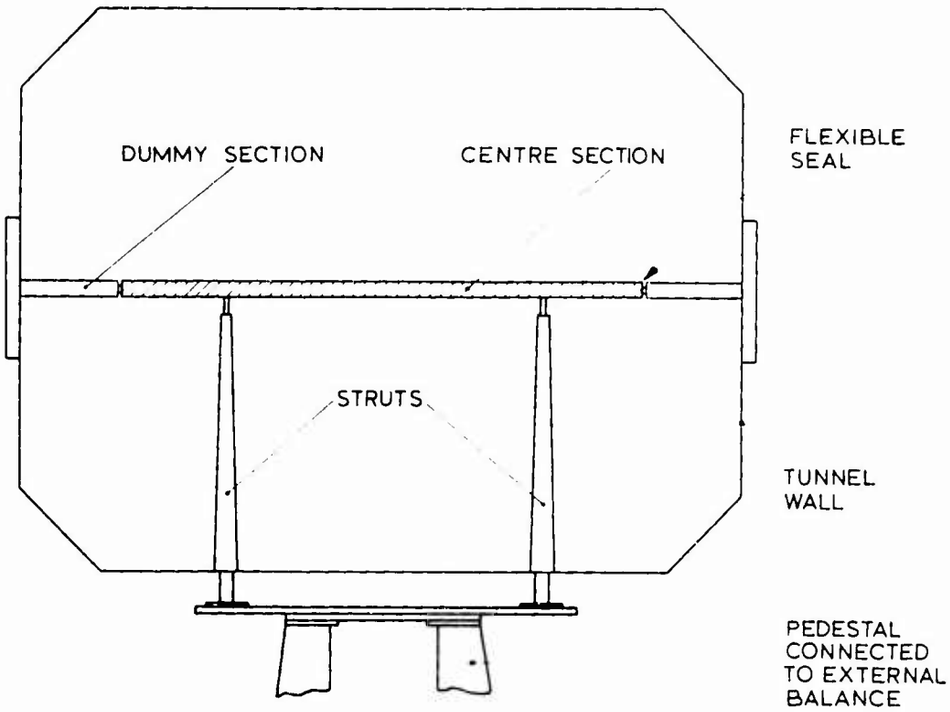

Fig.3 Typical test arrangement for a model, using an external balance

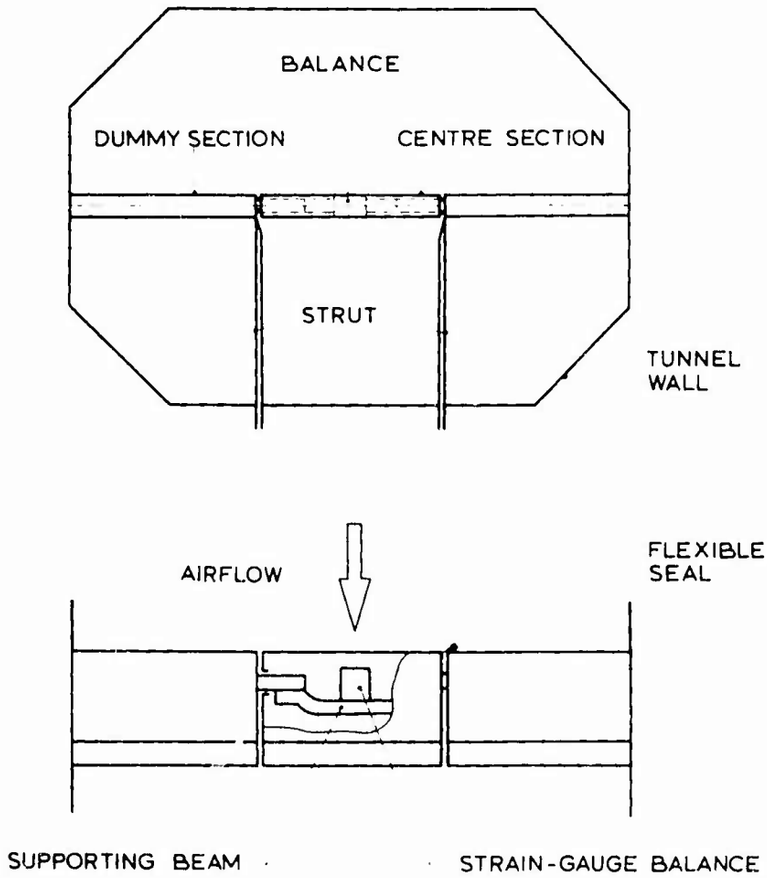

Fig.4 Typical test arrangement for a model, using an internal balance

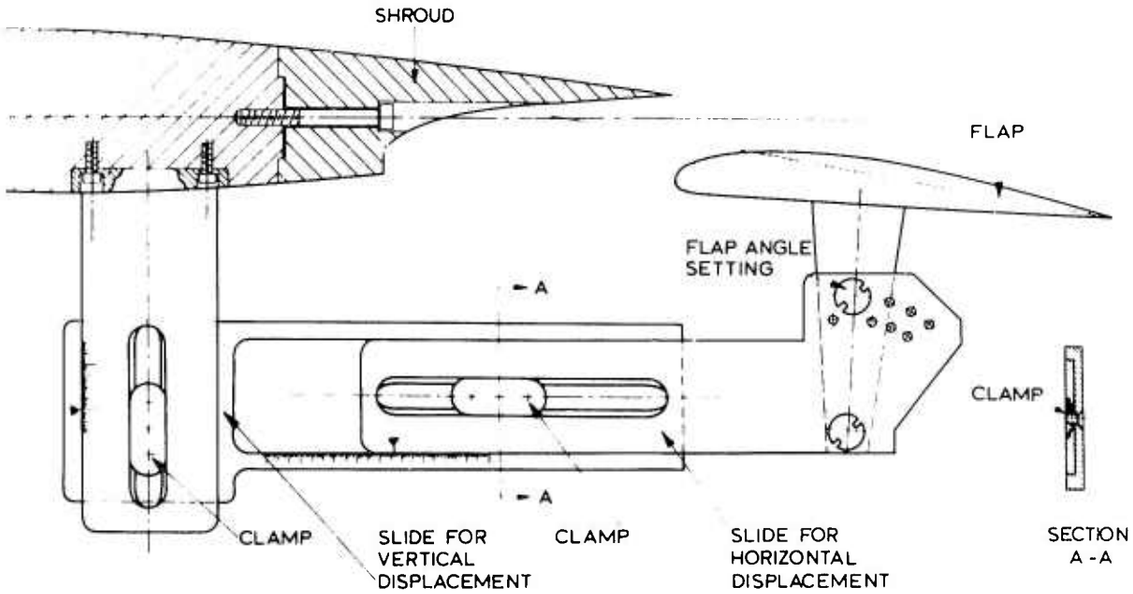

Fig.5 Possible flap bracket design

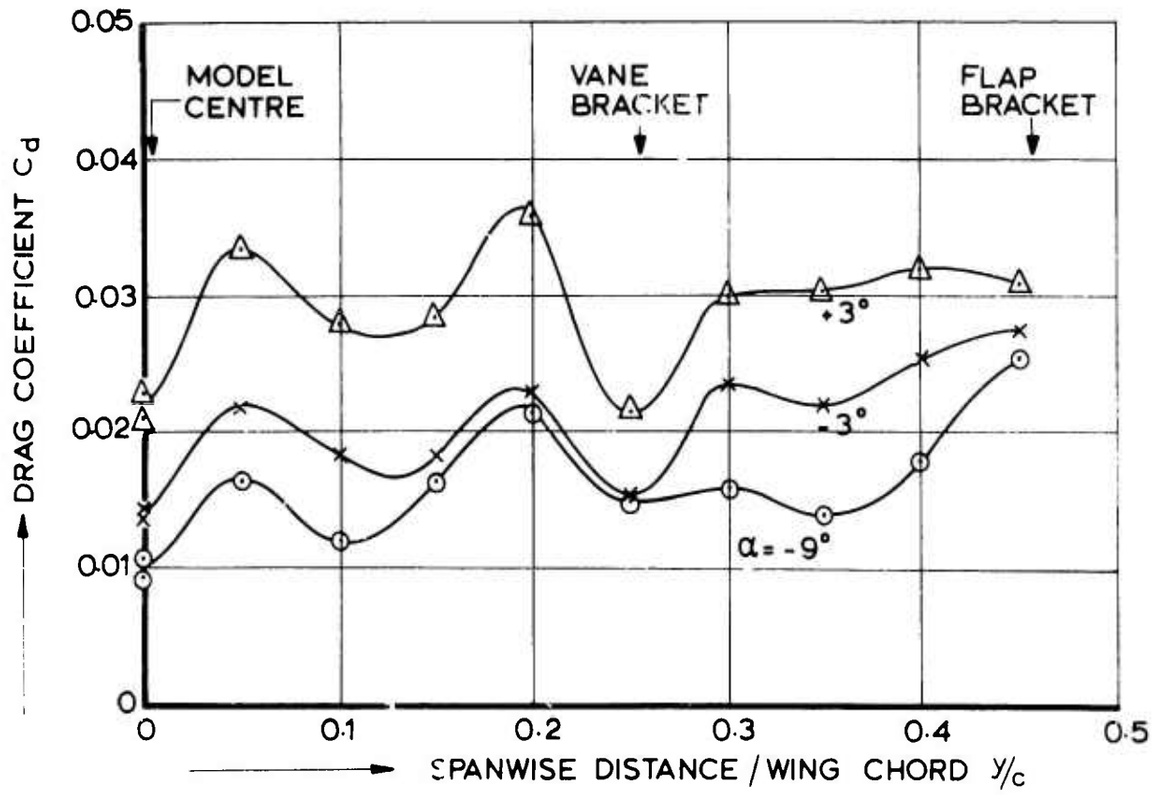

Fig.6 Spanwise variation of the wake drag of an aerofoil with a double slotted flap

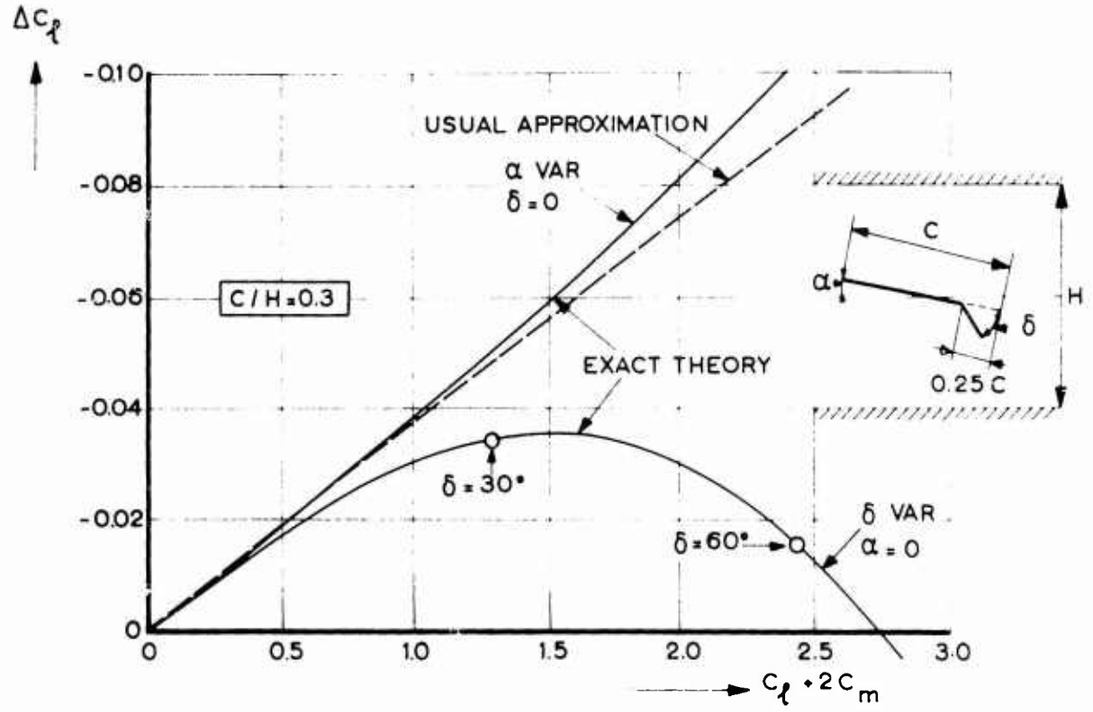

Fig.7 Tunnel wall corrections according to the usual approximation and to an exact theory for a hinged flat plate

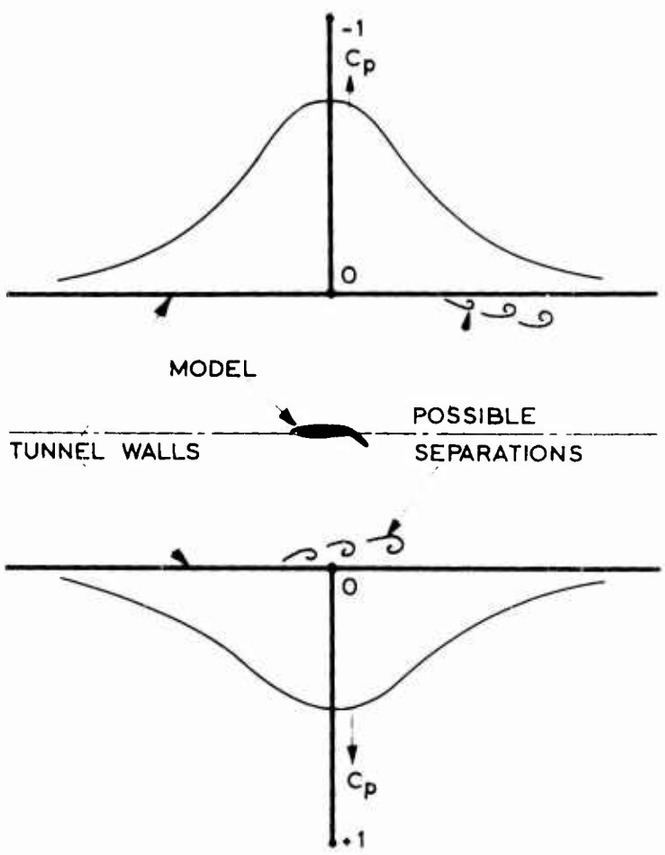

Fig.8 The pressure distribution on the tunnel walls above and below an aerofoil at $C_l = 4$ and $c/h = 0.3$

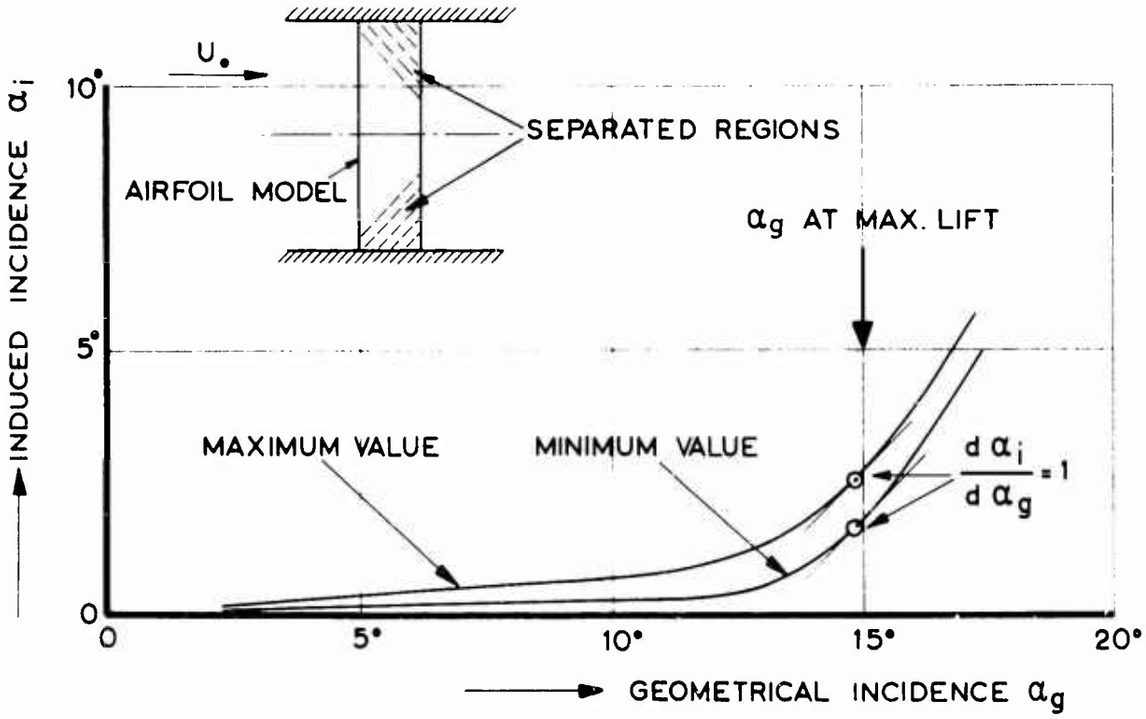

Fig.9 The induced incidence at mid-span due to flow separations near the tunnel walls, estimated from the measured drag data

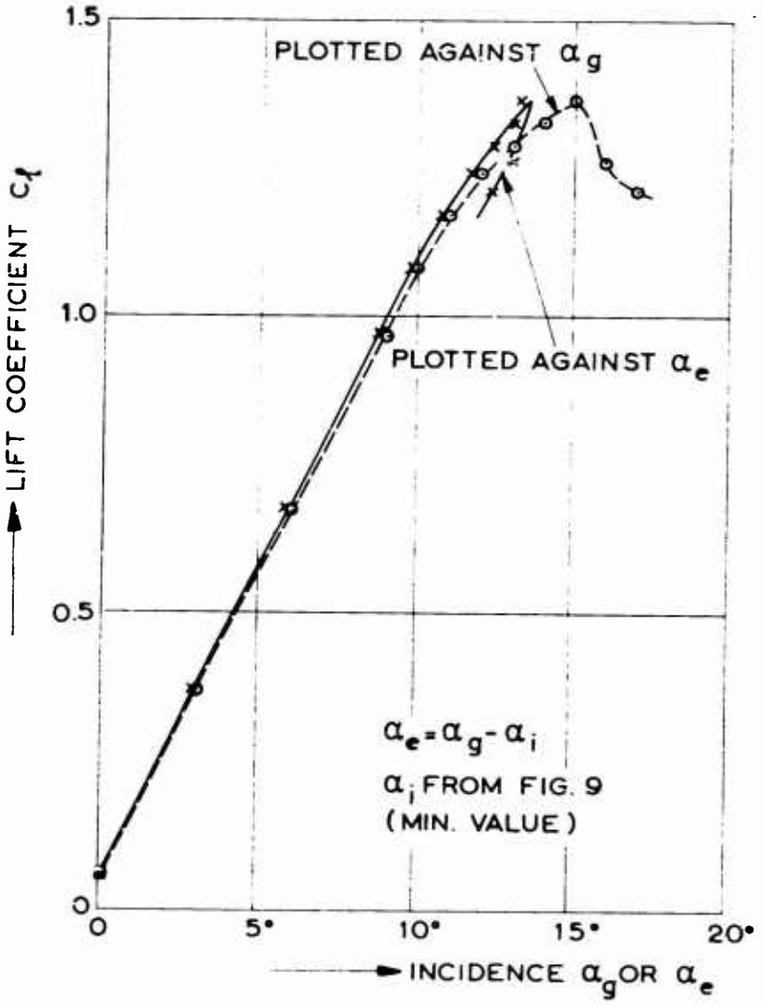

Fig.10 The lift plotted against the geometrical incidence and the estimated effective incidence

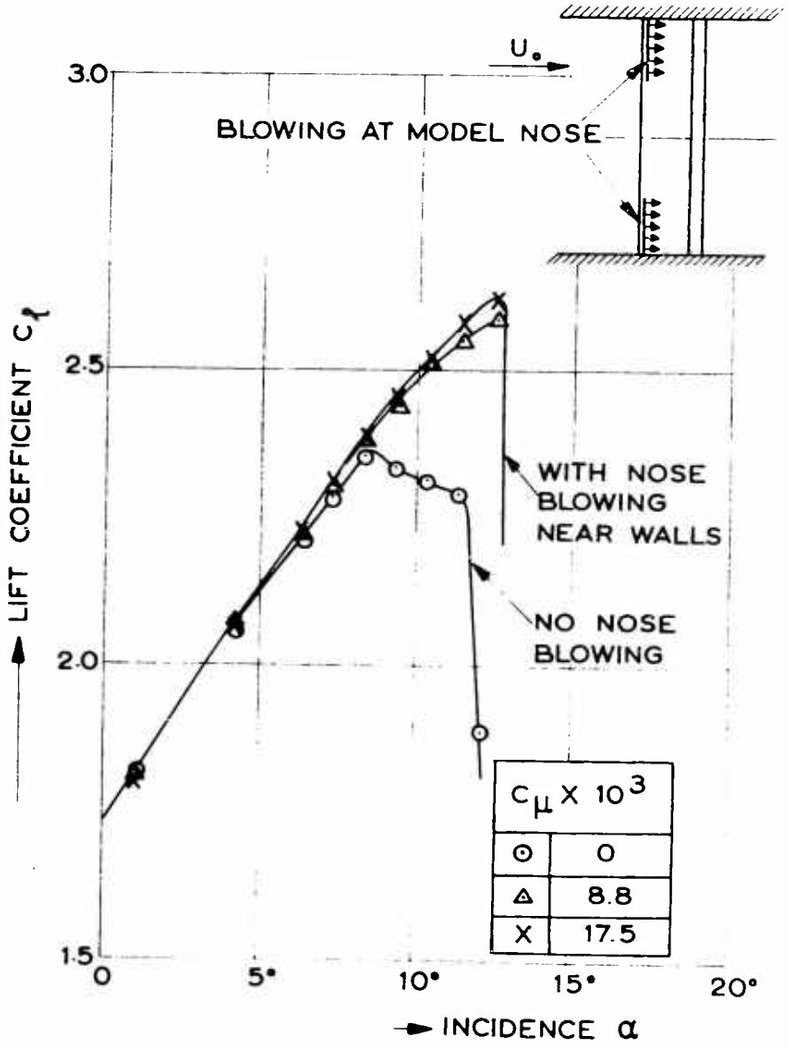

Fig.11 Effect of blowing along the model nose near the walls on the lift at mid-span

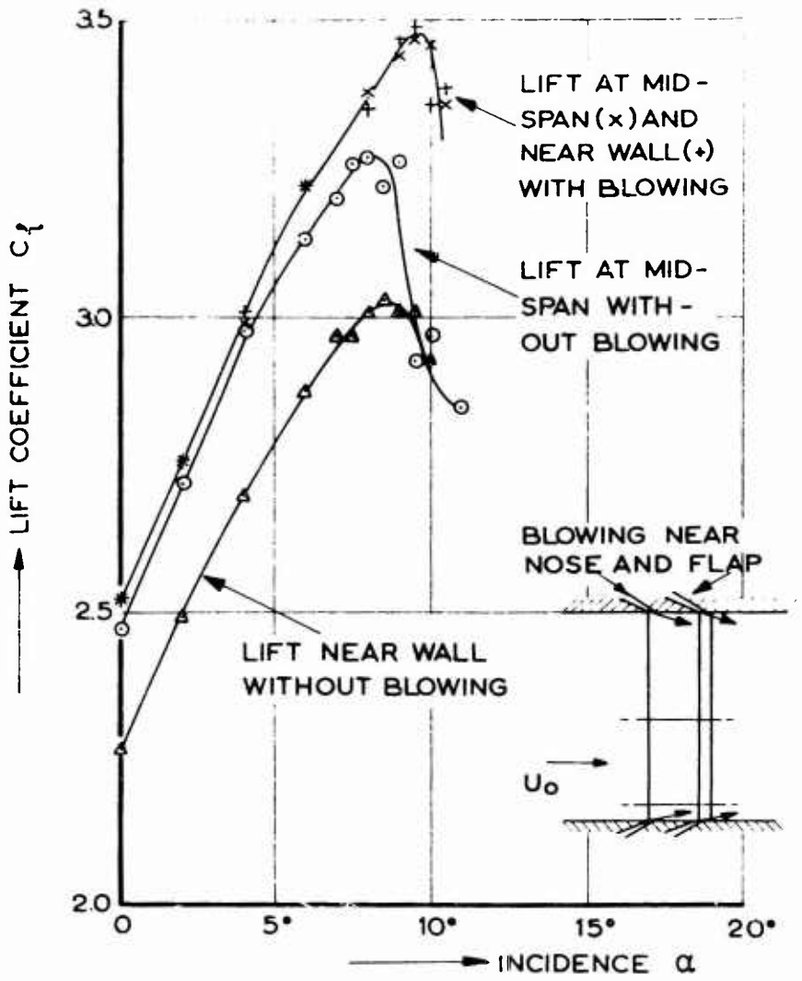

Fig.12 Effect of blowing along the tunnel walls on the lift at mid-span and near the wall

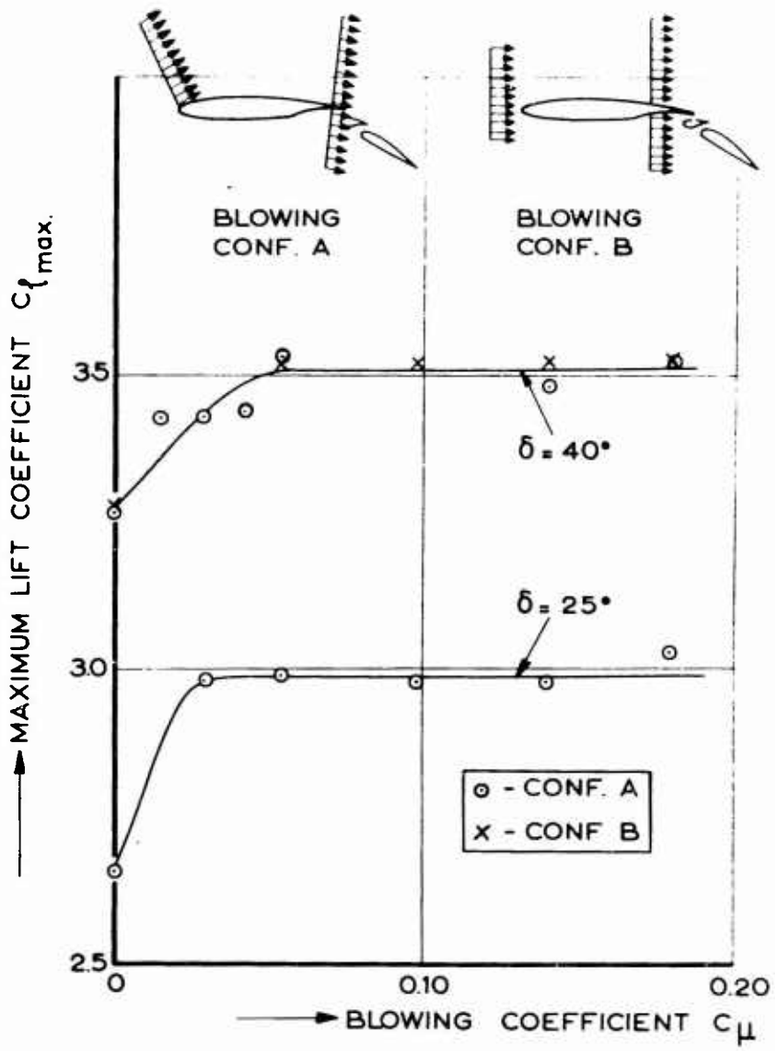

Fig.13 Variation of the maximum lift at mid-span with the rate of blowing along the tunnel walls

SUMMARY OF DISCUSSION

relating to

TWO-DIMENSIONAL MODEL-TESTING TECHNIQUES

1. Spanwise Variation of Wake Drag

Spanwise variations of wake drag had also been measured by Boeing, but had been attributed to spanwise variations of the position of transition. The variations had been much reduced after transition had been fixed. At RAE a current practice was also to fix transition. This decision had been made in order to remove from the drag-lift curves some features which were considered to be associated with rapid chordwise movements of the transition position.

2. Control of the Wall Boundary Layer at the Wing-Wall Junction

A number of contributors to the discussion had had experience of controlling the separations of a wall boundary layer by both blowing and suction. Boeing's had originally used suction but, due to limited plant capacity, had now adopted a blowing system. RAE had found that, for their model with a blown flap, blowing on the wall had resulted in interference with the wing boundary-layer control system; so they had developed a suction system instead. In general, it appeared that either boundary-layer control system could be effective in suppressing the separation of the wall boundary layer; while further reasonable increases in the flow of the boundary-layer control system, above the minimum level, seemed likely to have little effect on the measured forces. However, a warning was given from the Canadair representative that, for short span models, the forces on the wing which would be measured by a balance could vary continuously with changes in the boundary-layer control quantities. Reference was made to Figure 3 of McGill University Report 69-1 by T.Selbohm on "Boundary-layer transition and wake measurements at low Mach number for an aerofoil with single-slotted flap".

MODEL TESTING REQUIREMENTS AND TECHNIQUES FOR HIGH-LIFT SCHEMES: THREE-DIMENSIONAL ASPECTS

by

C. RUSSELL

Principal Engineer, Wind-Tunnel Dept., British Aircraft Corporation;
Warton (Lancs.), U.K.

ACKNOWLEDGEMENT

The author is indebted for the help and advice he has received from colleagues at B.A.C. Warton during the preparation of this lecture.

1. INTRODUCTION

The subject of three-dimensional 'High-Lift' model testing is dealt with from the point of view of the development of a specific full-size project. Various topics and problems are dealt with, in approximately the order in which they would normally arise, from initial concept to data presentation. The number and diversity of possible High-Lift schemes and test procedures is too great to be described fully, but an attempt has been made to examine the most important. Historically, it may be said that the field is still expanding, and that the extension of each end of the speed-range of fixed-wing aircraft is introducing new problems to be solved.

2. THE NEED FOR THREE-DIMENSIONAL TESTS ON HIGH-LIFT SYSTEMS

The optimised flow conditions which may be determined by two-dimensional testing will be modified when three-dimensions are fully represented.

High-speed flight requirements will dictate that the basic 'clean' wing should have a combination of twist and taper, with spanwise variations in section and leading-edge sweepback. The High-Lift System will thus emerge from a complex three-dimensional shape, and then be subjected to non-uniformities across the span from such causes as (Fig. 1):-

(i) wing root and tip effects

(ii) end effects and gaps in flaps, slats, ailerons, spoilers etc.

(iii) support-brackets, and their fairings, for the above

(iv) local induced flow-fields caused by engine intakes and exhausts, and propeller slipstreams

(v) features along the wing such as tanks, nacelles, pylons etc.

(vi) devices such as Boundary-Layer Fences, Leading-edge notches and Vortex Generators.

In order to approach the two-dimensional C_{Lmax} with a three-dimensional wing, it would be necessary to make the whole span reach the stall simultaneously, and this is difficult to achieve due to the variation of effective incidence across the span; nor is it desirable, since conditions would then change very suddenly. The development pattern of the stall must be examined, as large rolling-moments are likely to be generated if the tip stalls first.

Even at low incidence there will be small areas of separated flow, difficult to predict without tests, and as the wing approaches the stall these will increase and there may also be powerful vortices arising from separation at the leading-edge. Fig. 2 illustrates typical differences between two-dimensional and three-dimensional test results.

Three-dimensional tests are needed to establish the variation of C_L with incidence, $C_{L_{max}}$, the pattern of stall development, hysteresis at the stall, and sensitivity to side-slip. As well as these wing characteristics, the three-dimensional flow field behind the High-Lift wing can produce large effects on the tail-unit, and tests on 'complete' models are required to establish the overall longitudinal and lateral stability, and control effectiveness.

An additional bonus arises when an accurate three-dimensional model is drawn and constructed early, as it provides a valuable check on the precise definition of the aircraft geometry and lay-out.

3. THE CHOICE OF TYPE AND SIZE OF MODEL, AND THE TEST CONDITIONS

These questions are often decided by convenience, cost and the availability of test facilities, but a most important factor should be the relationship of the proposed tests to the aircraft timescale and budget.

During the early stages it is vital to be able to quickly compare the effectiveness of alternative High-Lift schemes, whilst the design is 'fluid'. Later on it will be required to check the preferred configuration results against estimates, using the latest definitions of geometry; then to examine the effects of modifications and additions. Fig. 3 shows how three important attributes of a test programme (including manufacture and result analysis), are required to vary during the life of a project. The factors considered are (a) speed of execution, (b) accuracy of the results and (c) total cost. Since there are many alternative ways of examining 'High-Lift' performance, these factors can vary widely. At the onset:- speed is needed to prevent costly mistakes; the tests should be relatively cheap, since there will be greatest likelihood of changes in requirements; and accuracy may be sacrificed in order to achieve the first two, so long as the purposes of the tests are satisfied. As the project progresses:- speed is no longer so important; there will be more point in spending money; and the geometry will be better defined, enabling accuracy to be worth achieving. Towards the very end of the project:- speed and cheapness are again appropriate, as there will be little time or money available.

Bearing the above considerations in mind, the main factors affecting the choice of model and test conditions are shown in Fig. 4, the lines between them indicating inter-dependence. Deciding upon the best model and test conditions involves the examination of many possibilities.

3.1 Reynolds and Mach Numbers

Ideally, in planning a test series we should start by ensuring that Reynolds Number and Mach Number correspond to the aircraft values, i.e. 'take-off', or 'combat' conditions if required, and adjust the

other parameters to suit, finally measuring in the wind tunnel the desired relationships between attitude and load-coefficient. In practice, the range of possible values for V, ρ, and L at the facilities available does not usually allow the correct Reynolds No. or Mach No. to be reached except for small slow-flying aircraft. Testing a small model at increasing velocity can attain the correct Re. No., but the Mach No. may be too high and compressible flow conditions may lead to reduced High-Lift performance. The effects of compressibility may begin at surprisingly low velocity, due to high local velocity and C_p values over slats and flaps etc. producing sonic conditions at low free-stream Mach No (See Fig. 5). Fig. 6 shows a typical result of measuring $C_{L_{max}}$ on a particular high-lift model at increasing velocity, with constant pressure and temperature. As the velocity is increased from very low values, $C_{L_{max}}$ also increases, that is the effect of Re. No. is beneficial, but as the Mach No. becomes significant there is a falling-off in performance (Figs. 7 and 8). In this connection, the work of Gault (1) should also be noted, where the importance of the relationship between aerofoil leading-edge thickness at 1.25% chord and Re. No. is shown to be important in determining the type of stall. This has been substantiated by tests on a high-lift wing on which the leading-edge thickness was progressively increased, and gave an increasing $C_{L_{max}}$.

It has been shown (2) that the performance of high-lift systems near the stall can vary significantly with Re. No. up to a value of six million, and that it is dangerous to extrapolate from tests at lower values. Much useful testing of incremental effects can, however, be done at quite low Reynolds number.

The use of a pressurised tunnel makes it possible to vary Mach No. and Re. No. independently, and to reach high Re. No. at low Mach No., but there is a limit to the air density ρ which can be used, depending upon the strength of the model or its supports, since loads are proportional to air density. Testing over a range of pressure also means that the required load capacity of the model force-measuring system must be greater, and providing adequate resolution becomes a problem. Fig. 9 shows the relationships between Mach No. and Re. No. for various sizes of model, and the effect of pressurisation.

Since the flight-test stall investigation programme will begin at high altitude, it is of advantage to represent this condition in the tunnel, if possible, as well as the sea-level case. This will enable correlation to be checked as soon as possible, and if necessary the model wing-section distorted so as to agree with flight test results, although this is a practice which should only be employed as a last resort.

3.2 Model Strength

For a given geometry, the stresses acting upon a model or full-scale component are proportional to $q.C_F$,

where $q = \frac{1}{2}\rho V^2$ and C_F is some force coefficient.

For example, in the case of wing root bending moment,

$$M = (\text{Lift}).\ y = q.S.C_L.y$$

where y is the spanwise distance of the wing centre-of-pressure and S the wing planform area;

while $$Z = k.c.t^2;$$

where k is a constant depending upon the shape of the cross section, with chord c and maximum thickness t at the root.

But the max. stress, $$p = \frac{M}{Z} = \frac{q.S.C_L.y}{k.c.t^2}.$$

Since y and c are proportional to L (some characteristic length), and S and t^2 to L^2,

$$p \propto \frac{q\ L^2.C_L\ L}{k\ L.L^2}.$$

$$\therefore\ p \propto qC_L.$$

A similar result applies to any section subject to a bending moment, and also to components in pure tension or compression.

When $q.C_F$ is small we may use low strength materials such as wood, 'Tufnol', or dural; but if qC_F is high, steel is required. Fig. 10 gives the relevant physical properties of the most common structural materials. Where the bulk of the load-carrying member must be minimised, such as for slat and flap brackets, or if internal space is needed for some other purpose, we should use more highly stressed components, with a thin shell of weaker material to form the external shape. Increasing use is being made of glass-fibre reinforced resin, and other techniques involving plastic materials.

Since we need only present the correct external shape to the airflow, the internal model structure presents less of a problem than do such items as slat and flap brackets, which will be highly stressed full-scale components in order to minimise their interferences. If such components are to be scaled without distortion, there will thus be a limit to the q which can be utilised. The situation is made worse by the need for higher safety factors for model parts (say 4) than for full scale (typically 1.5), but alleviated by the possibility of using high strength material, and by using 'solid' cross-sections.

However, the attainment of high Re. No. with low Mach No. should be restrained if excessive q is required, due to using a small model, since this will lead to unrepresentative 'external' supports.

The use of a minimum Safety Factor of 4, or greater with timber or other non-uniform materials, is influenced by the following:

(i) The need to avoid stressing procedures as complicated or time-consuming as the methods used on full size aircraft.

(ii) The need to limit deflections of model components to much less than those occurring full size.

(iii) The uncertainties and difficulties of producing adequate joints between small components which need to be often removed or adjusted.

(iv) Provision for loadings due to handling and vibration.

3.3 Model Size

As well as influencing Re. No., model size depends upon the following:

(a) The test facility and equipment, i.e. the size of working section and the load capacity of the load measuring system.

(b) Whether the required tests are to be carried out on a complete, half, or partial model.

(c) The tunnel corrections. It is important that the model is not made so large relative to the tunnel, in order to increase Reynolds No., that the uncertainties of the Tunnel Corrections introduce excessive errors.

(d) Manufacturing facilities and techniques. Depending upon the experience and capacity of the model design and manufacturing organisation, models which are very large will incur extra expense due to being above their normal capacity. On the other hand, High-Lift wings usually have some dimensions which are a very small percentage of the local chord e.g. slat and flap gaps, but which require close tolerances to be set. Small models will thus be difficult to manufacture with sufficient accuracy.

(e) In the case of an aircraft with a long fuselage (and as High-Lift systems develop, fuselages tend to become relatively larger), there may be a limit set by the desired incidence range and fouling of the tunnel roof or wall.

3.4 Test Facilities and Equipment

For High-Lift and other testing, the appropriate facilities and equipment may be judged by their capacity to handle the required values of the parameters shown linked on Fig. 4, but emphasis should also be placed upon the ability to provide a 'quick look' at data as it is produced, so that variations may be introduced into the test programme to accommodate the unexpected. There may not be time to fully compute corrected results, but it should be possible to examine raw data immediately after each run.

3.5 Type of Model and Support

Model types fall into three main categories, - complete, half and partial.

Complete models have the advantage of permitting the effects of sideslip to be investigated, so that measurements of lateral stability in the High-Lift configuration can be made. There may also be important changes in the longitudinal components during sideslip, and it may be found that there is an appreciable loss in $C_{L_{max}}$, especially with swept wings.

The mounting of a 'complete' model in the tunnel may be via a combination of struts and wires, or by means of a sting support with an internal strain-gauge balance, especially if the project has convenient jet pipes (Fig. 11). If struts are to be used, it will be necessary to determine the strut-interference effects, which will vary with the operation of the High-Lift components, and extra runs will be required to determine them. An alternative mounting system to support the model whilst strut-only loads are measured, must be provided if an external balance has been used. (3)

If the aircraft layout permits, sting mounting has advantages for 'Project' work where time is important, although there may be corrections to make for model distortion to accommodate the sting, and sting-support induced flow angularities. The base pressure correction which applies to the sting cavity is usually negligible at the low free-stream Mach Nos. employed for most High-Lift testing.

Sting mounting has the fundamental advantage for High-Lift work that flow disturbances due to the mounting itself are as far distant as possible from the wing, and thus have minimum effect upon it. In addition, the wing is left clear for the fitting of engine nacelles, undercarriage, external stores etc., and in the case of variable-sweep aircraft enables wing-sweep to be varied without having to disturb the mounting.

Half models (Fig. 12) do not permit the representation of sideslip, but their advantages are:-

(a) Higher Reynolds No. in a given tunnel.

(b) By measuring wing root bending moment the spanwise position of the C.P. can be determined. This is very useful in assessing the pattern of stall development.

(c) Power-supplies and wiring etc. can be easily led into the model without the need for exposed pipes or shafts.

(d) No strut or sting interference corrections.

(e) Cheapness, since only one flap and slat etc. is required.

The other objections to the use of half-models concern the nature of the flow at the wing-root and at the fuselage floor junction. In particular:

(a) The wing may suffer from premature root-stall, due to flow separation along the floor, flow in the gap between fuselage and floor, or 'corner-vortices' may occur.

(b) The effective velocity over the fuselage and wing root may be reduced by being immersed in the floor boundary-layer.

A series of comparative tests on a complete and a half model with flaps and slats, using the same wing components for both, have been carried out at B.A.C. Warton, and gave good agreement in $C_{L_{max}}$ and tailplane power.

Some points of interest are:-

(1) A suction-strip, powered by an external fan, was provided across the tunnel floor, just ahead of the model nose. The Boundary-layer at this station was completely removed. With suction off there was a reduction in $C_{L_{max}}$, and a slightly more stable $C_m - C_L$ curve.

(2) The gap between fuselage and floor was made as small as possible (approx. 0.005 root chord), limited by the clearance required to allow model deflection under load and the flatness of the floor. It was found that increasing this gap reduced $C_{L_{max}}$ in a linear manner, over a small range, and the loss in $C_{L_{max}}$ due to the gap used was estimated at about 1%.

(3) There was little sign of premature wing-root separation, or of 'corner vortices'. An additional suction strip (4) on the floor near the wing root, which had been suggested, was found to have very little or no effect with this model configuration.

It should however be noted that the model concerned had a fairly broad fuselage, raising the wing and tailplane away from the floor by about 0.5 root-chord at the wing.

Half models may also employ either a Strain-gauge or an external mechanical balance and, although 'lateral' components will not be plotted, it is advisable to measure all 6 components, in order to be able to plot spanwise C.P. position, and to offer alternative axes definitions for the result data.

Partial models, that is, less than half a complete model (Fig. 13), are used more rarely, and are closely related to two-dimensional models. They have the advantage of enabling even higher Re. No. to be reached, and permit better representation and optimisation of the finer details of such things as flap fairings, pylon attachments, slat, flap and control gaps. Their main disadvantage is that the spanwise loading conditions and local upwash are incorrect, but they do permit comparative testing to be carried out (Fig. 13). End-plates are often used, to avoid the wall boundary-layer.

3.6 Tunnel Corrections

These derive from the size and type of both model and tunnel, as well as the range of coefficients to be explored. The main ones relating to High-Lift testing are:-

(1) Strut or Sting 'tare' and interference effects; 'tare' being that part of the measured loads which comes from the supports themselves, zero in the case of a sting mounted model; and 'interference' being the change in the loads on the model due to the presence of the supports. The determination of these effects can be complex and time-consuming and, in the case of strut mountings, required to be repeated for each change in High-Lift configuration.

(2) Blockage, which may be divided into 'Solid' and 'Wake' blockage components. (3,6) The standard corrections for these effects may be applied. We may write

$$U_F = U_T (1 + \varepsilon)$$

where U_F = equivalent 'free-stream' velocity

U_T = uncorrected tunnel velocity,

with $\varepsilon = \varepsilon_s + \varepsilon_w$

where ε = total blockage correction

ε_s = solid blockage

ε_w = wake blockage.

The usual method of calculating ε_w in a closed tunnel is to use

$$\varepsilon_w = \frac{1}{4}\frac{S}{C} \cdot C_{DT}$$

where S = wing area

C = tunnel cross-section area

C_{DT} = measured drag.

So that ε_w is simply taken as being proportional to the total drag. The above expression can be easily incorporated into the data reduction programme.

However, when there are large areas of separated flow, Maskell (5) has shown that we may more accurately divide C_{DT} into its components, C_{Do} and C_{Di}, and gives

$$\varepsilon_w = \frac{S}{4C}\left[C_{Do} + F(C_{DT} - C_{Do} - \pi\frac{K}{A}C_L^2)\right],$$

C_{Do} and K being deduced from the plot of C_{DT} vs C_L^2 as in Fig. 14.

A value of 5 is suggested for F, when $1 < A < 10$.

Comparative values for ε, for a particular High-Lift wing with slat and flap, are shown in Fig. 15, plotted against α.

It can be seen that the differences only became greater than about 1% after the stall, and in this particular instance it was decided to use the simpler linear expression which did not require determination of C_{Do} or K. This will not always apply, e.g. models with high sweep and/or small nose radius causing a strong leading-edge Vortex.

(3) Tunnel constraint; with a closed working section we may use

$$\Delta\alpha = \delta\frac{S}{C}C_L \text{ due to induced upwash}$$

and hence

$$\Delta C_L = -\delta\frac{S}{C} \cdot C_L \cdot C_{DT}$$

$$\Delta C_D = \delta\frac{S}{C}C_L^2$$

$$\Delta C_m = -\delta\eta \cdot \frac{S}{C}C_m \cdot C_L .$$

$\delta\eta$ is the additional interference at the tail as compared with the average over the wings.(6)

These expressions all require a value for δ, which is generally of the form shown in Fig. 16. So that, provided we maintain Span/Tunnel Breadth <0.8, say, the value of δ is fairly constant and well established. A further model size criterion is to limit the wing area so that $\Delta\alpha$ is less than 2° at C_{Lmax}. Thus a smaller model must be used if high-lift coefficients are envisaged. This will also limit the other constraint corrections, and hence the effect of errors in them.

Greater $\Delta\alpha$ corrections than 2° may be acceptable, but there is more danger of introducing chordwise variations into the incidence constraint correction, so that the effective camber is increased. 'Open' working sections have the disadvantage for high-lift work that the strong downwash behind the model can deflect the jet much more than the deep stream would be deflected in flight. With this excessive jet deflection the effective camber of the aerofoil is much reduced. Slotted working sections (Boeing - Vertol) and variable-geometry working sections are being developed, which may be suited to large high-lift models (7).

Jet-flap models in a closed working section present an extra problem, when considering the size of model which may be tested. This arises from the tendency for the flow along the tunnel floor, beneath the jet, to break down when the ratio of downwash to freestream energy is too high (Fig. 17). Evidence of this can be seen by the use of tufts or smoke on the floor and walls which, as the tunnel speed is decreased, first show agitation of the floor boundary-layer, then the formation of a 'horseshoe' vortex which spreads across the floor and up the walls.

South (8) has produced a simple criterion based on a lift coefficient, C_{Lhb},

where

$$C_{Lhb} = \frac{L}{\frac{1}{2}V^2 h.b}$$

with h = height above floor
b = span

The limiting value of C_{Lhb} is shown to be dependent upon the (Drag/Lift) ratio D/L, and that at negative D/L, $C_{Lhb} \leq 3.0$.

At positive D/L less than 0.6 and h/b greater than 0.6:-

$$C_{Lhb} < \frac{3.0}{1 + 4(D/L)^2} \quad \text{See Fig. 18}$$

These relationships may be re-arranged to give the boundaries shown in Fig. 19, where the height above the floor, in chords, is plotted against C_L for various values of (L/D).

3.7 Ranges of Attitudes and Coefficients

As well as needing to be estimated in advance because of their effects on tunnel corrections, these are also required in order to:-

(1) Ensure that the incidence mechanism is capable of reaching the desired maximum. In some cases, especially with a high set tailplane, up to $\alpha = 45^\circ$ may be required in order to study longitudinal stability fully. Cross-wind landings must be simulated by yawing the model, the max. yaw angle depending upon the lowest landing-speed and greatest cross-wind component to be considered.

(2) Check that the load capacity of the intended balance is adequate. This is not always a simple decision, it depends upon the quality of resolution and repeatability of the overall measuring system, or its safety factors. If the intended load range is smaller than the balance design capacity, then the 'scatter', absolute accuracy, and repeatability will suffer. On the other hand, if the balance is working near to its maximum load limits, the amount of buffet and vibration will be critical and may result in hysteresis or even fatigue failure.

This is especially the case with High-Lift systems near and at the stall. Rolling-Moment is particularly difficult to predict in advance, since it depends upon the type of stall development (Root or tip first) peculiar to the layout being tested, and also can be greatly influenced by any small asymmetries in the model (wing twist, leading-edge radius, the 'fit' of slats, etc.) - or in the tunnel flow.

3.8 Power Supplies to Models

With any type of High-Lift model, i.e. Complete, Half, or Partial, the need may arise to supply power of some kind, as well as to take out signal leads from transducers or pressure-tubes to a measuring system. This causes two extra types of problem which must be taken into account when deciding upon the type and size of model to use, i.e.

(a) Extra blockage and interference; due to the presence of pipes, cables etc., except when a half model is used.

(b) Extra mechanical restraints; stiffness, which will affect the load calibrations of the measuring system; and friction, causing hysteresis in the readings.

Consideration should be given to the probable size of both of the above effects, which will depend upon the type of model, the type of load measuring system, and the form in which power is transmitted. Alternative power transmission systems include -

(i) Electrical; for propeller motors etc. It will be required to find a motor which is sufficiently powerful, small, light in weight, and capable of precise remote control. A balance will need to be struck between the desired duration of each test run and the cooling method employed.

(ii) Compressed air, may be used for jet-engine intake and exhaust simulation via an ejector (Fig. 20), to power a jet or blown flap, or to power a turbine. The air may be fed into the model by means of flexible pipes, or an air-bearing type connector if the restraint and hysteresis is significant (9, 10).

(iii) Hydraulic power, there are motors available which have good power to bulk weight ratios, and needing only relatively small supply pipes. In effect, the hydraulic fluid provides both power and cooling flow.

(iv) Chemical, such as piped Hydrogen Peroxide. Very high powers may be supplied with only small diameter piping, but there are special problems of safety and high temperature.

(v) Mechanical, in certain cases shaft drive to propellers is feasible (11).

3.9 Ground Simulation

An extra consideration, when deciding upon possible test arrangements, is the ability to carry out investigation of the effect of the proximity of the ground. We can simulate the flow conditions around an aircraft flying level close to the ground by the use of a 'ground-board' just beneath the model, extending just ahead of and behind it. The incidence range will be restricted, depending upon the height above ground being tested (Fig. 21).

Points to note regarding ground-board installations are:-

(a) the boundary-layer on top of the ground-board, beneath the model should be minimised, by keeping the leading-edge short, and removing as much of it as possible by means of an extraction system, or by using a belt moving at free-stream velocity.

(b) the possibility of ground-board leading-edge separation should be reduced by using a blunt leading-edge, and minimising the blockage underneath it. Flow visualisation should be carried out on the ground-board at the start of testing to check this.

(c) although the total mass flow through the working section will be known, there will be uneven division of the flow going above and below the ground-board, depending upon the relative total-head losses, and varying with model incidence and configuration. An extra pitot-static tube beneath the ground-board may be used to determine the mass flow above it, and hence the effective tunnel velocity. The usual blockage corrections can then be applied to the cross-section above the ground-board.

(d) tunnel constraint effects are only applicable for the other three walls, and are usually so small as to be negligible.

(e) For jet flap models, where the high velocity wake striking the ground may result in separation of the boundary-layer, Heyson has deduced a criterion which can be expressed as C_{Lhb} max = 3.3 (C_{Lhb} based on span and height above ground).

If tests closer to the ground are required, a moving belt or distributed suction should be used, rather than a fixed ground-board.

4. SPECIAL FEATURES OF THE DESIGN OF HIGH-LIFT MODELS

The materials and method of construction derive from the consideration of accuracy, cost, and speed of manufacture (Section 2) and the strength requirements (Section 3), with a resultant design which may range from a wooden model with simple bent sheet metal fittings, to an all-metal wing with complicated precision machined components. The former will be cheap and quick to build but of low accuracy, whilst the latter will be time consuming and expensive, but highly accurate and give more repeatable results. 'Numerical Control' machining of the main components offers the prospect of some speeding up of the manufacture of the major components, but depends upon the availability of precise geometrical definition. There are countless possibilities and composite methods of construction. Fig. 22 gives an example.

The critical model components affecting time-scales are usually the supports and means of adjustment of slats and flaps etc., especially where there is to be a wide range of settings, and there are many possible designs. Fig. 23 illustrates some flap-bracket designs, each type being appropriate to a particular type of test. Much depends upon the desired tolerances, and these vary widely over the wing and its high lift devices. They should be specified in advance to the Designer wherever possible, in order to avoid needless effort. Target values for a 'precise' model, expressed as a fraction of the local chord, are given in Fig. 24; but often the effects of variation in a particular dimension will not be known until after the tests. Then it may be found that certain dimensions are relatively unimportant until a critical value is reached, when there is a sudden effect, such as flow separation.

The methods of adjustment employed where variable angles and gaps are required fall between two extremes:-

(a) Variable clamps, which require to be set up and measured in the tunnel, can be very time consuming, and subject to the skill of the operator.

(b) Precision made sets of fixed brackets give very repeatable results, so long as the correct bracket is used; i.e. subject to the risk of operator error, especially if there are many variables.

The ideal adjustment is one which can be carried out very quickly with high repeatability of test results, and small chance of incorrect setting. When a complicated set of alternative parts is to be used, it is most desirable to carry out trial assemblies of all possible arrangements, by the tunnel crew, and to have clear rigging diagrams available.

When tests are to be carried out under conditions of low q ($\frac{1}{2}\rho V^2$) and up to high incidence, the importance of minimising model weight should be emphasised if a sting or other internal balance is employed which is sensitive to axial-force, even though the lift-loading on the wings is high and great strength is required. This is due to the fact that most of the axial-force range will come from the axial component of model weight at high incidence, and the desired aerodynamic load to be measured may be very small in comparison (Fig. 25).

5. TECHNIQUES AND REQUIREMENTS AFTER THE MODEL HAS BEEN INSTALLED

Following model installation and check-out of the recording and measuring systems, a tunnel running programme must be prepared. This need not necessarily follow the order in which tests may have been specified from purely aerodynamic considerations. They should be re-arranged and also include measurements of tunnel corrections and 'Tare' effects. The test programme should minimise configuration changes, suit the availability of parts, provide frequent repeatability checks of some basic configuration, and leave scope for the Tunnel Engineer to carry out extra investigations or flow visualisation where appropriate. This implies a quick turn-round of data, or a 'quick-look' facility.

5.1 Possible Measurements

The list of possible measurements will be chosen from:-

(1) Model attitude.

(2) The six components of force and moment. Usually only the static components of output signals are recorded, but increasing attention is being paid to the measurement of fluctuations, such as buffet and the rate of change of rolling moment at the stall.

(3) Supplementary force, or pressure measurements concerned with model power supplies.

(4) Surface pressures at selected stations.

(5) Observations of flow patterns, both surface and three-dimensional.

All except item (5) are commonly recorded via electronic transducers. The recording of flow patterns has been greatly aided by the use of 'Polaroid' materials and equipment which guarantees success on every occasion possible, and reduces the time between observation and dissemination.

5.2 Programme Variables

Tunnel programmes consist of manipulation of the following variables:-

(1) Incidence α and Sideslip β. A 'Run' or 'Traverse' is normally carried out by varying one and holding the other constant.

(2) Control angles, including tail and fin off cases.

(3) Settings of High-Lift system components relative to the wing datum. Each separate component has three variable dimensions if there is negligible spanwise movement; [illegible], and the vertical and horizontal displacements.

(4) The addition of 'loose' items such as stores, fences etc.

(5) Power input to propellers, ejectors etc. There may be two variables, such as Torque and R.P.M., Air Pressure and Mass flow.

(6) Wing sweep, if appropriate.

(7) Reynolds and Mach No., i.e. pressure and velocity.

It can be seen that with so many measurements and variables the data analysis team may soon be swamped, especially with modern data acquisition systems. In the case of a 'complete' model, we could carry out incidence or sideslip traverses at say

Five sideslip angles or incidences.

Six tailplane angles, and tail off.

Slat:- Five angles, three extensions, three gaps.

Flap:- Five angles, Four extensions, three gaps (More if double slotted).

Wing sweep:- Three angles.

i.e. $2 \times 5 \times 7 \times 5 \times 3 \times 3 \times 5 \times 4 \times 3 \times 3 = 567{,}000$ possibilities!

We may also investigate say three velocities, and three pressures if a compressed-air tunnel is used. Also rudder angles, differential tail, bombs and stores, ... We must eliminate most of the above combinations by a systematic approach.

5.3 Programme Planning

A few recommendations when planning test programmes are:-

(a) Before any other tests, carry out flow visualisation on model supports, reflection planes, etc., particularly on new or unusual arrangements; also make any mounting interference measurements first, in order that the data reduction programme may be applied to real cases as soon as they are tested. 'Fabricated' data should have already been tried through the data reduction programme, but it is almost inevitable that some unexpected difficulties will arise, as computing methods are continually developing and changing.

(b) Decide the policy on fixing transition or otherwise as soon as possible.

(c) Test the 'clean' wing first, to examine the basic features of the design and look for trouble. Examine flow visualisation of possible areas of separated flow.

(d) Optimise slat and flap settings, for instance, by starting at the most likely slat position; adjust the flap to find and fix at the best arrangement then do the same with the slat. Go back to the flap and check various positions with the slat at its new chosen setting. Beware interdependence.

(e) Look for non-linearities in force and moment results at small angles of incidence, sideslip, or control deflection, as there may be real flow phenomena to be discovered. Non-linearities at larger angles indicate the possibility of 'fouls' between the 'live' part of a model and its support or support-shroud. The use of an electrical warning system is recommended.

5.4 Flow Visualisation Methods

Wherever possible, flow visualisation should only be carried out as an aid to the interpretation of force measurements. On its own, it can lead to quite erroneous conclusions.

(1) Smoke in the quantity normally available is only useful at low speed, and soon fills a closed return tunnel. Smoke generators using heated oil or expendable smoke cartridges are available.

(2) Tufts are easy to observe and clean to use, but their presence can bring about a premature stall.

(3) A simple method of detecting boundary-layer transition is to smear a dark-coloured model with a thin coating of a China-clay and Kerosene mixture, and to run the tunnel until evaporation of the Kerosene leaves a white deposit beneath the turbulent boundary layer. There will also be some evaporation at the extreme leading-edge.

(4) Surface oil flow is best done using a fluorescent pigment powder suspended in a mixture of oils having the appropriate density, viscosity, and volatility to suit the velocity, temperature, and size of model. A mixture which is too thick will refuse to move where the boundary-layer is sluggish; too thin a mixture and there will be insufficient powder left to photograph well, even in the ultra-violet lighting, which may be used to improve contrast and minimise the effect of variations in the model surface colour. Transition of the boundary-layer may also be observed by the different drying rates which cause a slight colour change.

With any flow visualisation technique, hysteresis may sometimes be observed at the stall, (12); this can be checked by carrying out an incidence traverse which increases, through the stall, then decreases; the C_L/α plot will show a closed loop at the stall (Fig. 26). Thus, if the incidence is set before the tunnel is started up in order to facilitate the production of a surface oil flow pattern, the effect of increasing the Re. No. from zero will be to reach the flow condition corresponding to the lower C_L of the two possible values. This characteristic should be borne in mind when examining surface oil patterns.

REFERENCES

1. Gault, D. E. — Correlation of low speed airfoil section stalling characteristics with Reynolds No. and Airfoil geometry. N.A.C.A. TN3963; 1957. Also Roy. Aero. Soc. Aerodynamics Data Sheets.

2. Williams, J. — Recent Basic Research on V/STOL Aerodynamics at R.A.E. Z. Flugwiss, Vol. 14, pp 257-276; 1966.

3. Pope, A. Harper, J. J. — Low Speed Wind Tunnel Testing. Wiley & Sons; 1966.

4. Ainscombe, A. Williams, J. — Some comments on High-Lift testing in Wind Tunnels, with particular reference to Jet-blowing models. J. R. Ae. Soc., Vol. 61, pp 529-540; Aug. 1957.

5. Maskell, E. C. — A theory of the blockage effects on bluff bodies and stalled wings in a closed Wind Tunnel. R.A.E. Aero. Report 2685; Nov. 1963.

6. Pankhurst, R. C. Holder, D. W. — Wind Tunnel Technique. Pitman, London; 1952.

7. Heyson, H. H. — Theoretical study of the use of variable geometry in the design of minimum-correction V/STOL wind tunnels. N.A.S.A. TR R-318; 1969.

8. South, P. — Measurements of flow breakdown in rectangular Wind Tunnel sections. N.R.C.C. Aero Report LR-513; Nov. 1968.

9. Trebble, W. J. G. — Exploratory investigation of the effects of blowing from the leading edge of a Delta Wing. R.A.E. TR 66126; April 1966.

10. Williams, J. Butler, S. F. J. — Recent developments in low-speed wind-tunnel techniques for V/STOL and High-lift model testing. Z. Flugwiss., Vol. 13, pp 73-89; 1965.

11. Fink, M. P. Smith, C. C. — Pressure distribution of a large semispan tilting wing, with flap and propeller. N.A.S.A. TN D-5481; Oct. 1969.

12. Lee, G. H. — The aerodynamic design philosophy of the Handley-Page Jetstream. Aircraft Engineering; Sept. 1967.

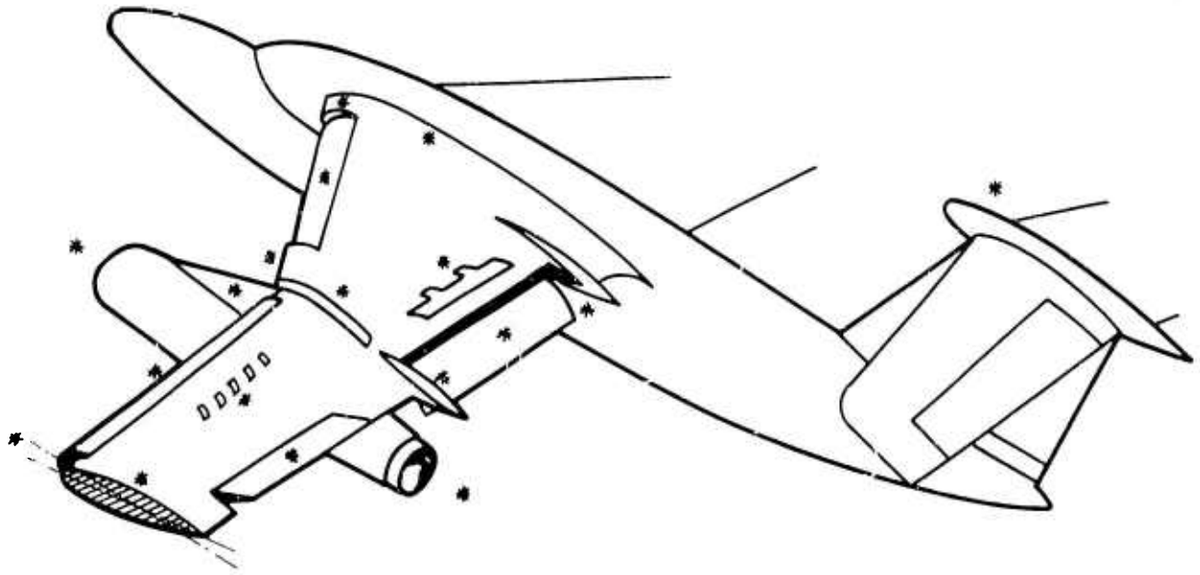

Fig.1 Features requiring 3-D test

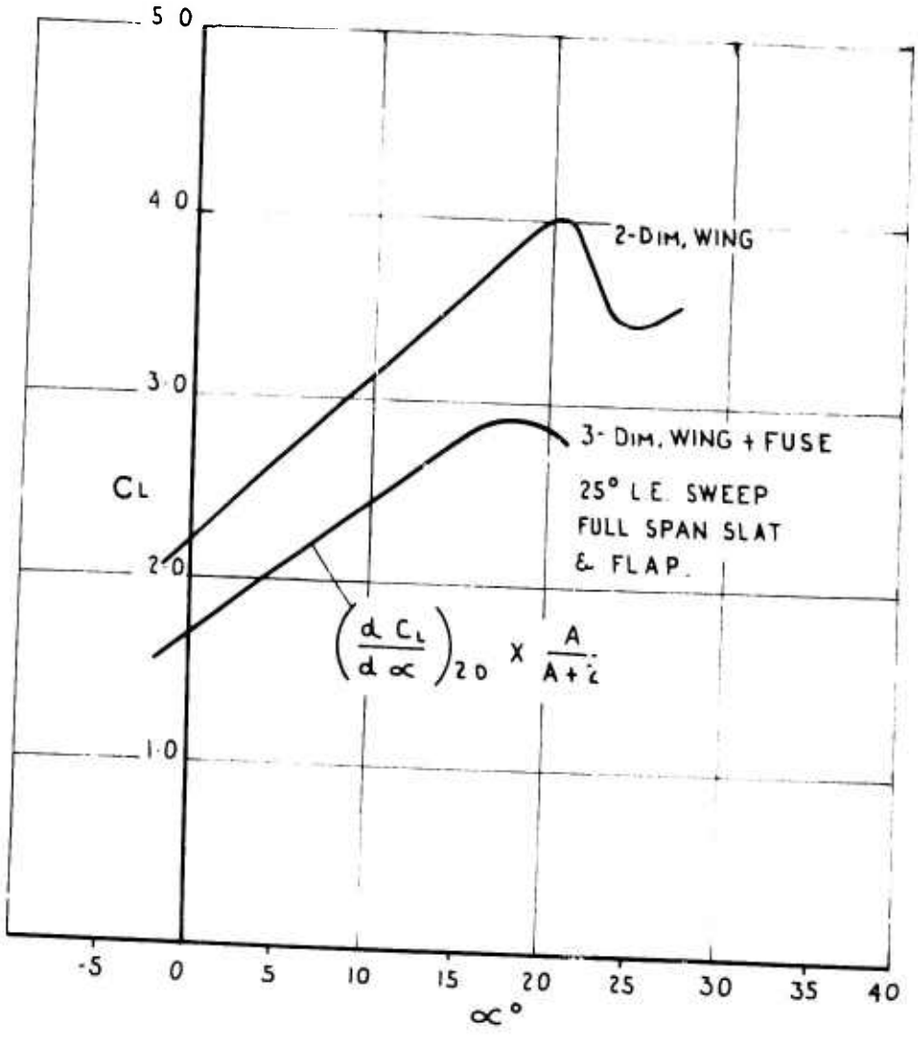

Fig.2 Comparison of 2-DIM and 3-DIM tests with LDG.-edge slat and double-slotted flap

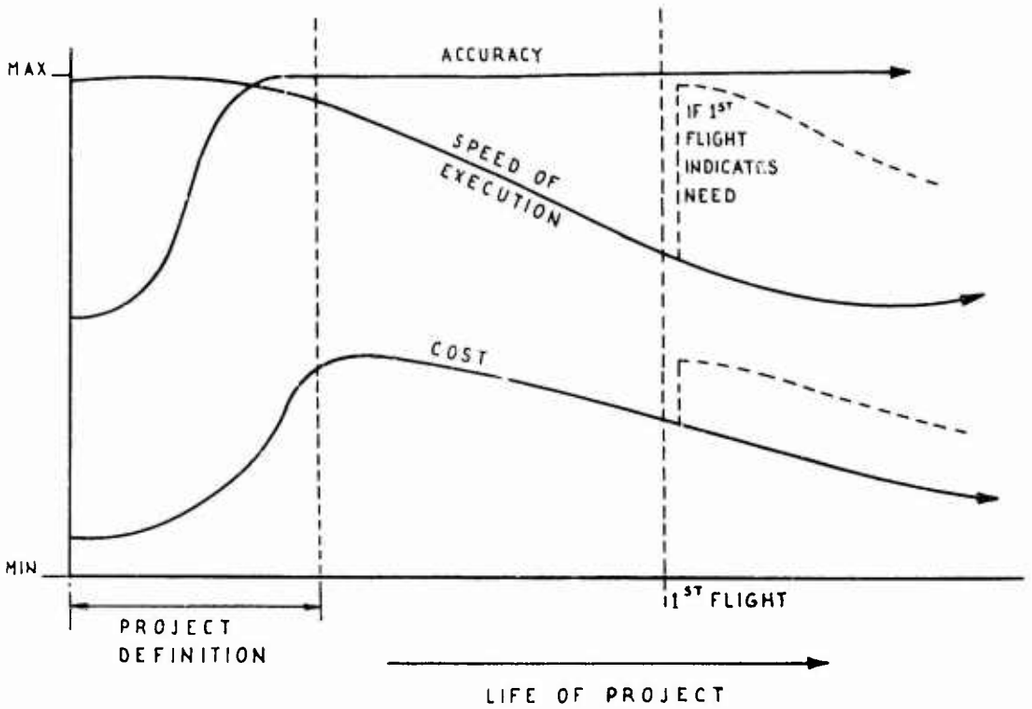

Fig.3 Relative desirability of test attributes

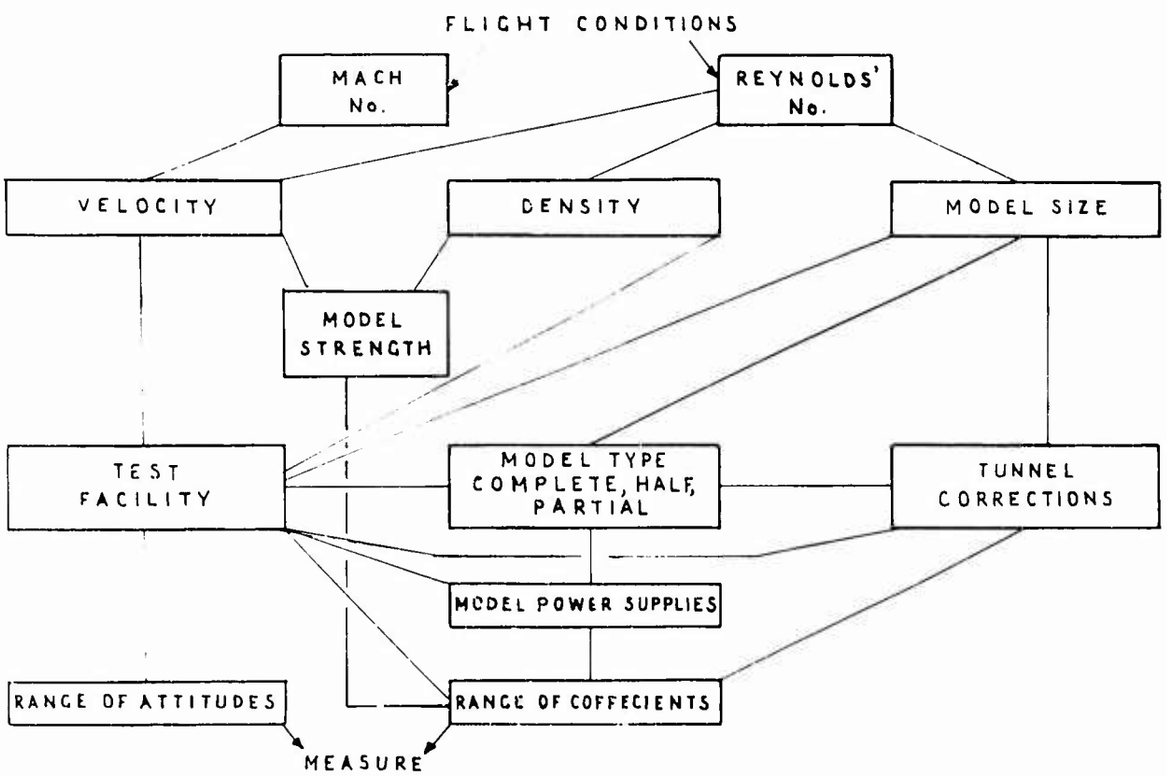

Fig.4 Main test parameters and interactions

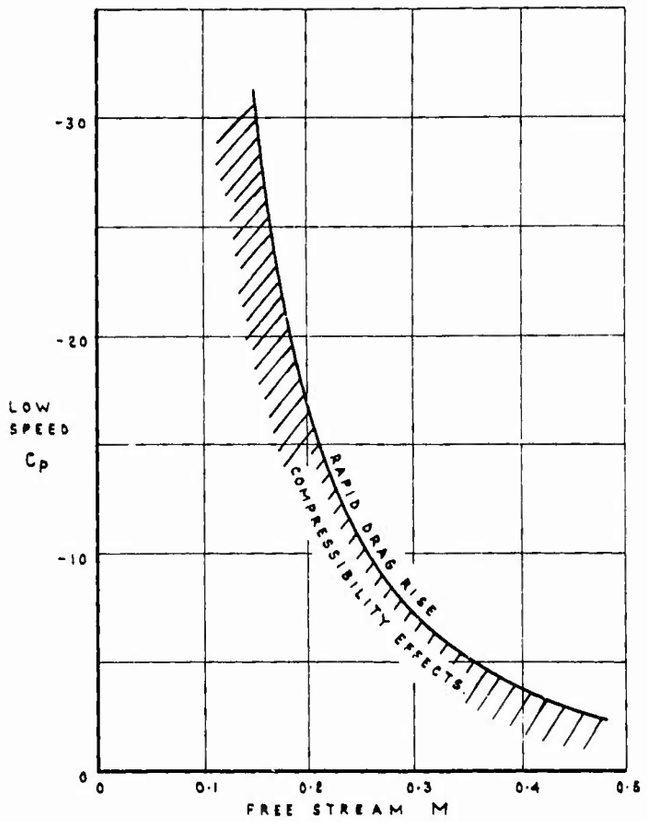

Fig.5 Onset of sonic conditions in peak suction region

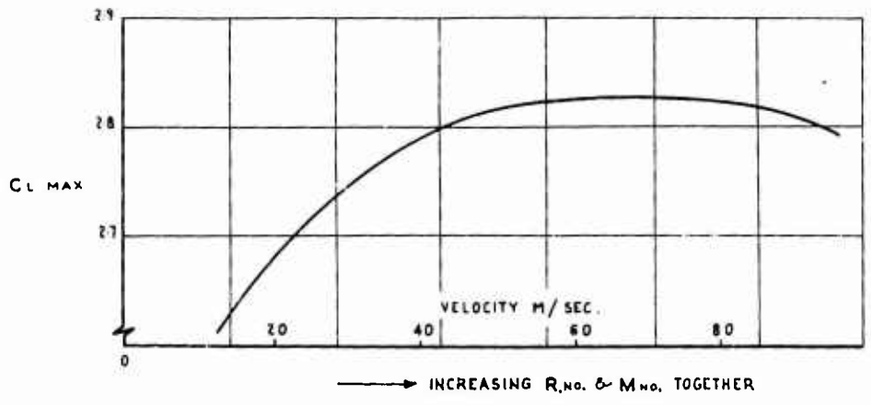

Fig.6 Variation of $C_{L\,max}$ with velocity (constant air density and model size)

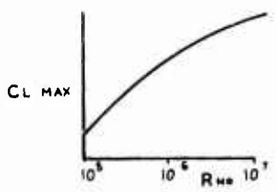

Fig.7 Effect of R.no. alone M constant (subcritical)

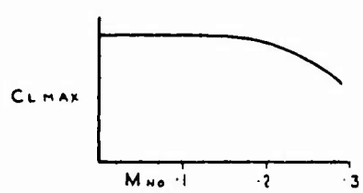

Fig.8 Effect of Mach No. alone R.no. constant

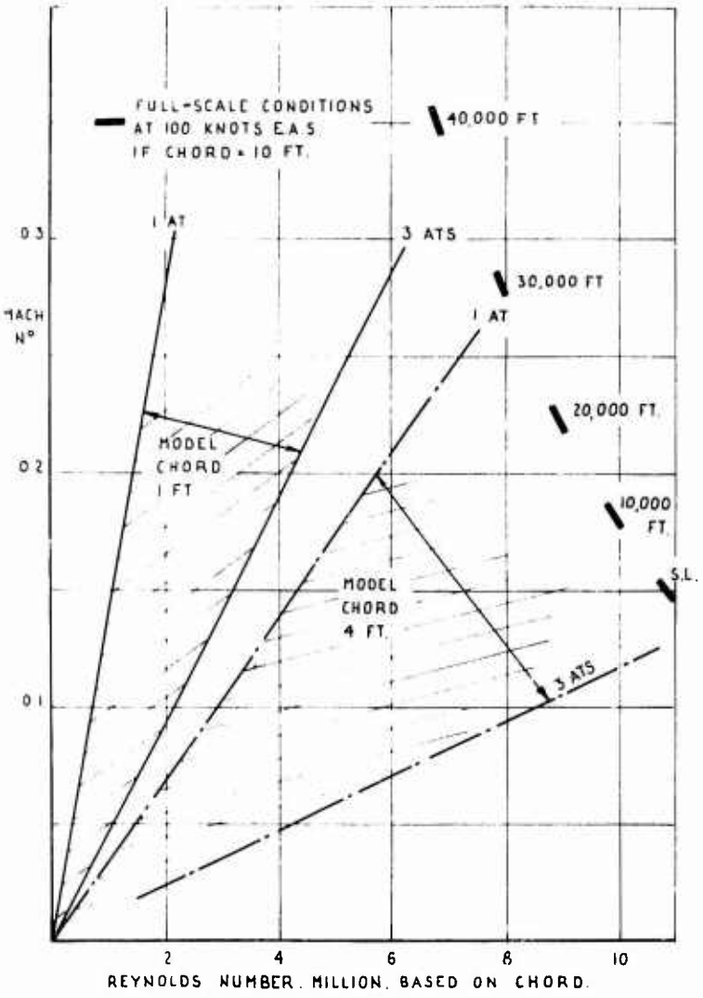

Fig.9 Ranges of Mach and Reynolds' Nos. obtainable in a pressurised tunnel (1 to 3 ats.)

MATERIAL	MAX. WORKING TENSILE STRESS (SAFETY FACTOR > 4)	SPECIFIC GRAVITY	E MILLIONS	COMMENTS
MAHOGANY TEAK WALNUT	1,000 P.S.I	0·7	1·3	EASILY WORKED BEWARE 'GRAIN' AND WARPING. LAMINATE.
'TUFNOL'	5,000 P.S.I	1·3	1·3	EASILY WORKED TAKES A FINE EDGE. MORE STABLE THAN WOOD.
DURAL	10,000 P.S.I.	2·8	12	LIGHT AND STRONG. FAIRLY EASILY WORKED.
BRASS	5,000 P.S.I AND OVER	8·5	12	MALLEABLE
MILD STEEL	10,000 P.S.I.	8	30	STIFF AND STRONG MALLEABLE.
HIGH TENSILE STEEL	UP TO 40,000 P.S.I.	8	30	DIFFICULT TO WORK BUT SUITABLE FOR HIGHLY STRESSED COMPONENTS.

Fig.10 Structural materials for high-lift models

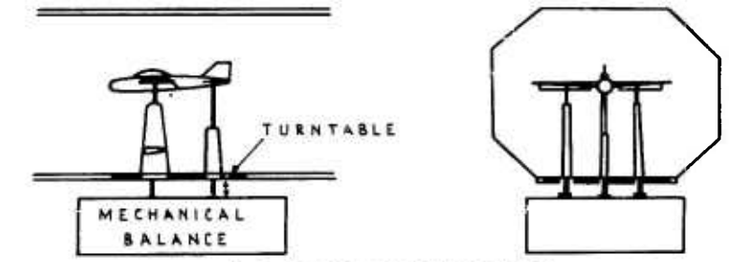

a) 3-STRUT ON MECHANICAL BALANCE

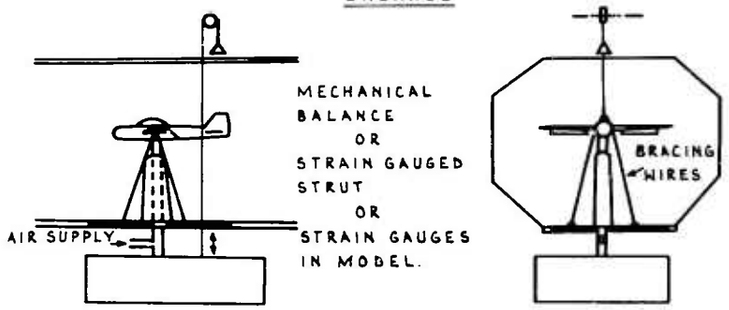

b) SINGLE CENTRE-STRUT, WITH AIR SUPPLY

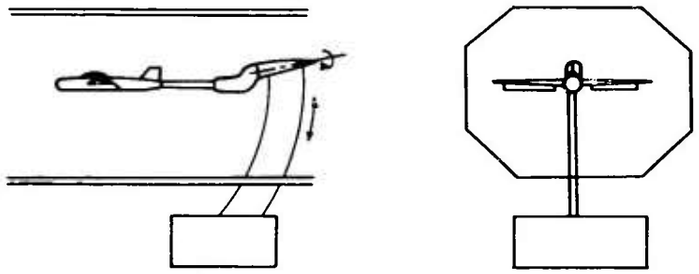

c) 'STING' SUPPORT

Fig.11 Some types of support for "complete" models

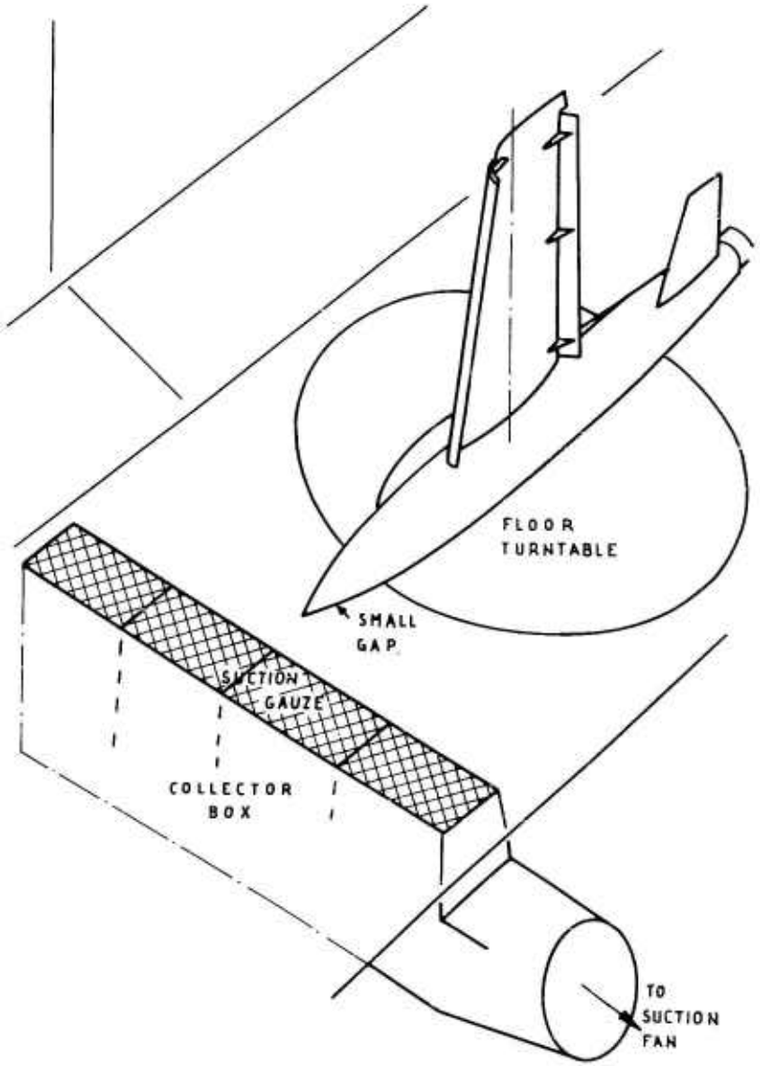

Fig.12 Half-model installation with floor boundary-layer removal

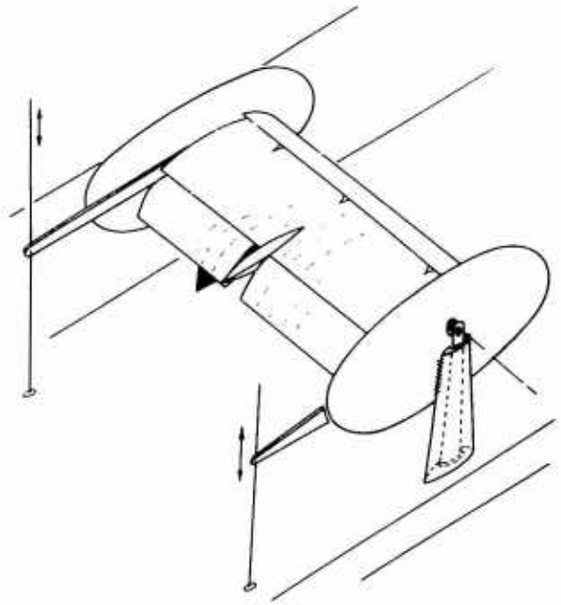

Fig.13 "Partial" model, with end-plates on mechanical balance

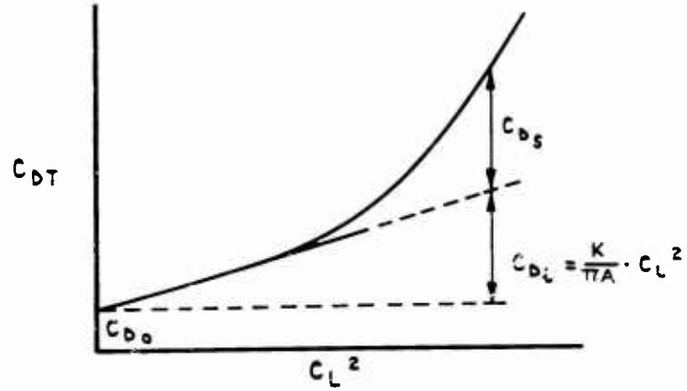

Fig.14 Derivation of C_{Do} and K for use in "Maskell" wake blockage correction

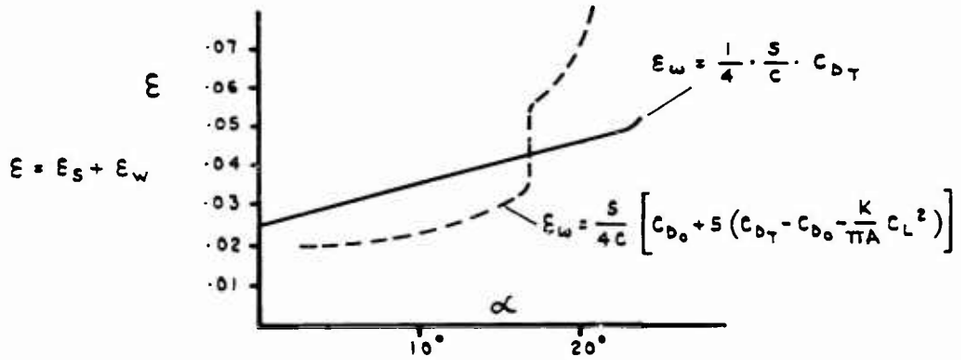

Fig.15 Effect of alternative wake blockage corrections

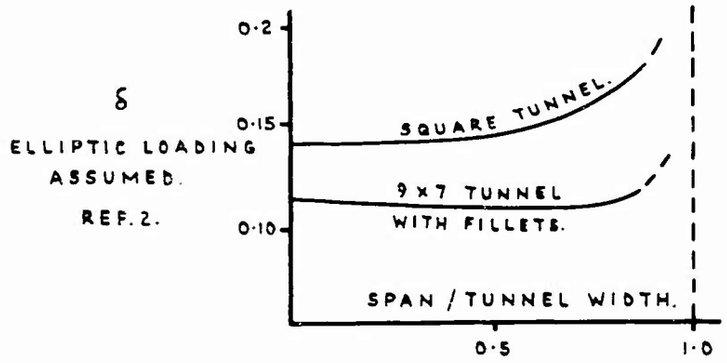

Fig.16 Variation of tunnel constraint factor with model span/tunnel width

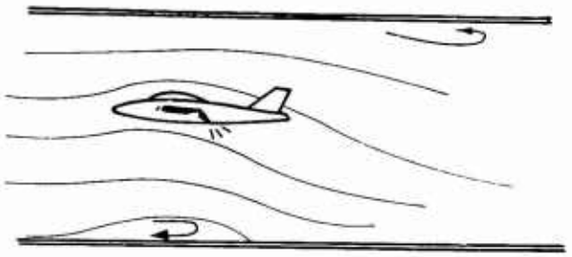

Fig.17 Effect on tunnel flow when $\frac{\text{Downwash Energy}}{\text{Freestream Energy}}$ is too high

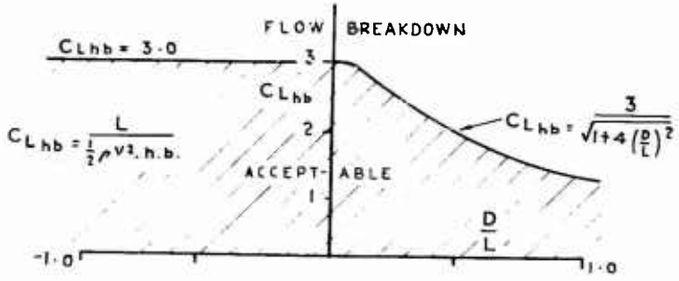

Fig.18 Test limit suggested by south for jet flap models

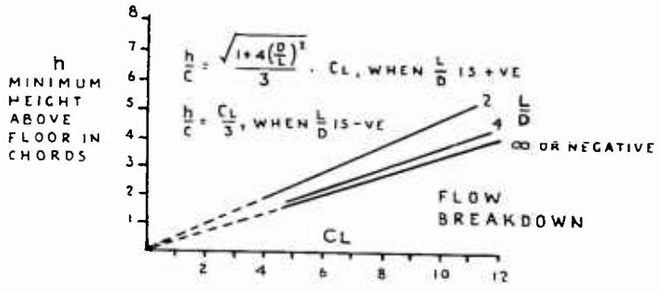

Fig.19 South's criterion in terms of C_L, $\frac{h}{c}$ and $\frac{L}{D}$

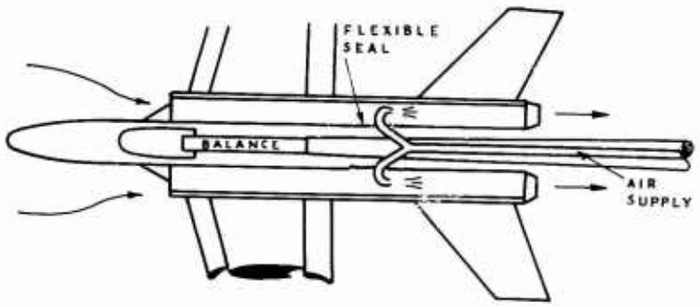

Fig.20 Compressed - air ejectors to induce intake and exhaust flow

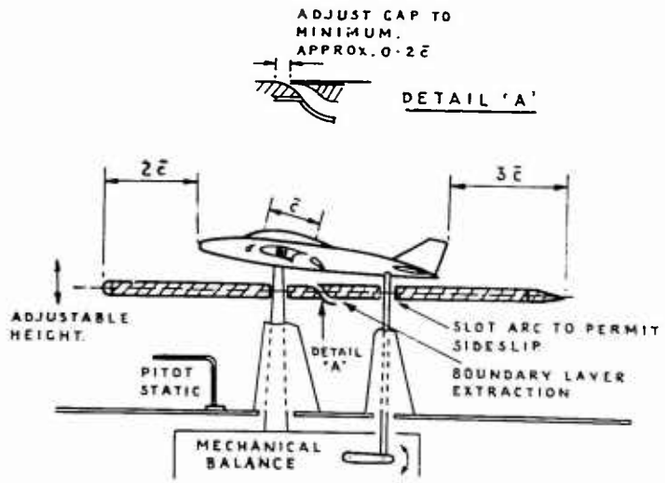

Fig.21 One type of ground board installation

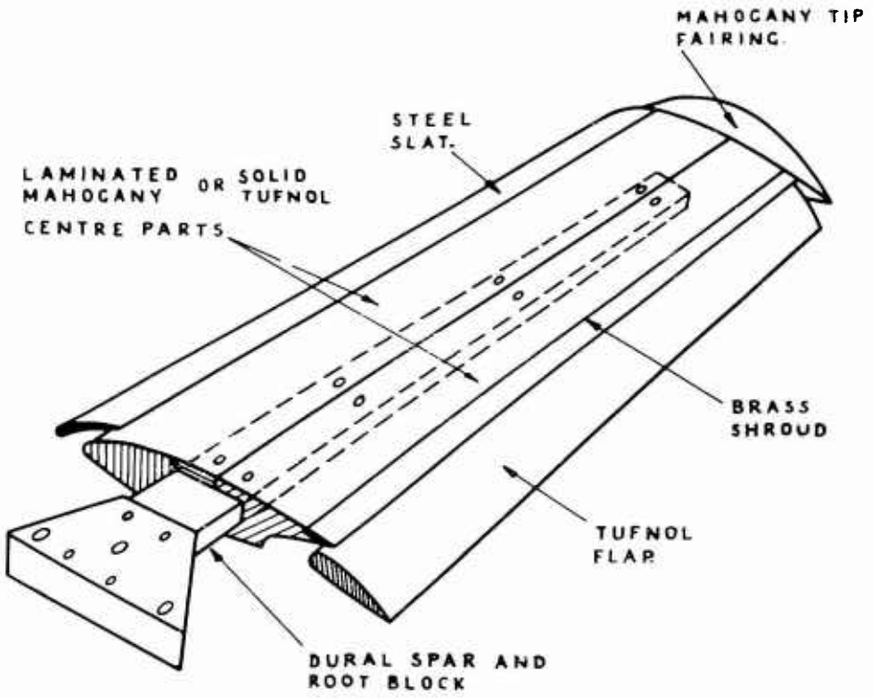

SLAT	: STEEL TO MINIMISE DEFLECTION
CENTRE	: MAHOGONY OR TUFNOL, EASILY WORKED
SPAR AND ROOT BLOCK	: DURAL, STRESSED TO CARRY ALL LOADS.
SHROUD	: SHEET BRASS, FOR FINE EDGE
FLAP	: TUFNOL, EASILY WORKED, STABLE
TIP FAIRING	: MAHOGANY, LIGHT, EASILY WORKED.

Fig.22 Composite wing construction suitable for moderate qC_{Lmax}

a) BENT STEEL STRIP, EX STOCK

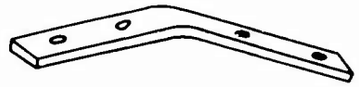

APPROX. 1 MAN HR TO DESIGN & MANUFACTURE.
ANGLE, GAP & OVERLAP SET UP IN SITU

b) MACHINED & BRAZED

APPROX. 10 MAN HRS
ANGLE PRE-SET.
GAP & OVERLAP BY FITTING TO WING DURING MANUFACTURE.

c) ALL PARTS MACHINED.

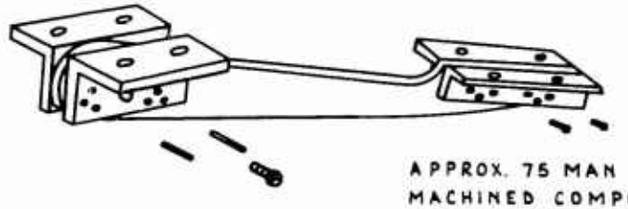

APPROX. 75 MAN HRS.
MACHINED COMPONENTS MADE TO COMPUTED ANGLES AND POSITIONS.

Fig.23 Alternative flap bracket designs

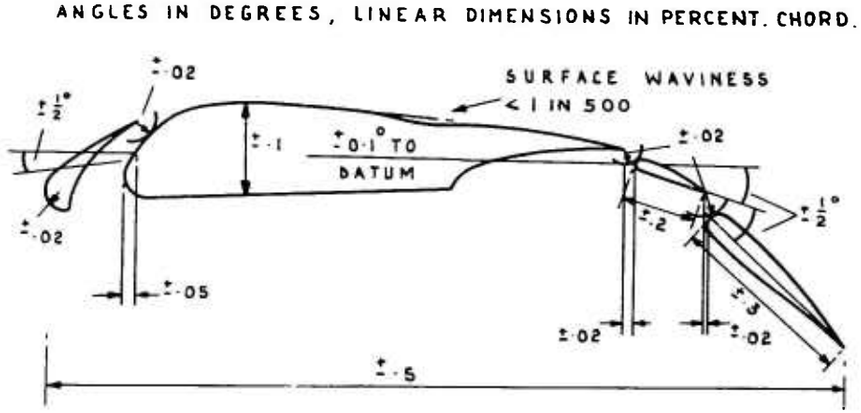

Fig.24 Suggested tolerances for a "precise" model

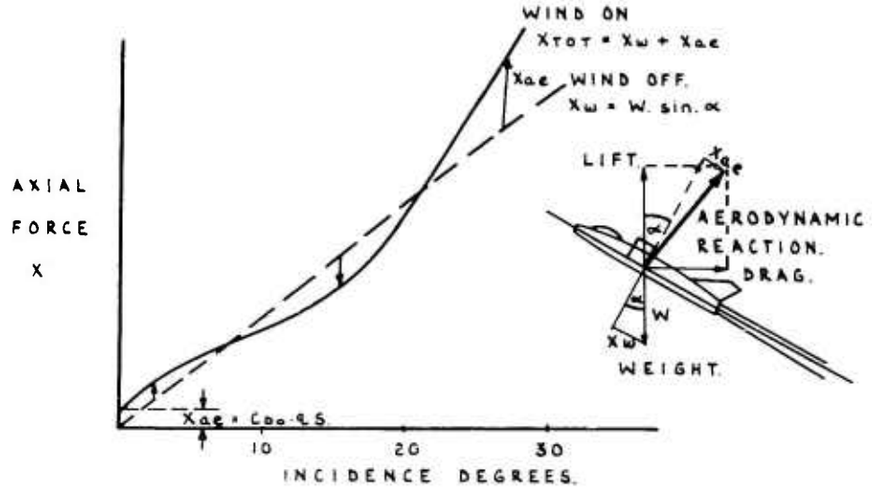

Fig.25 Effect of model weight on axial force measurement

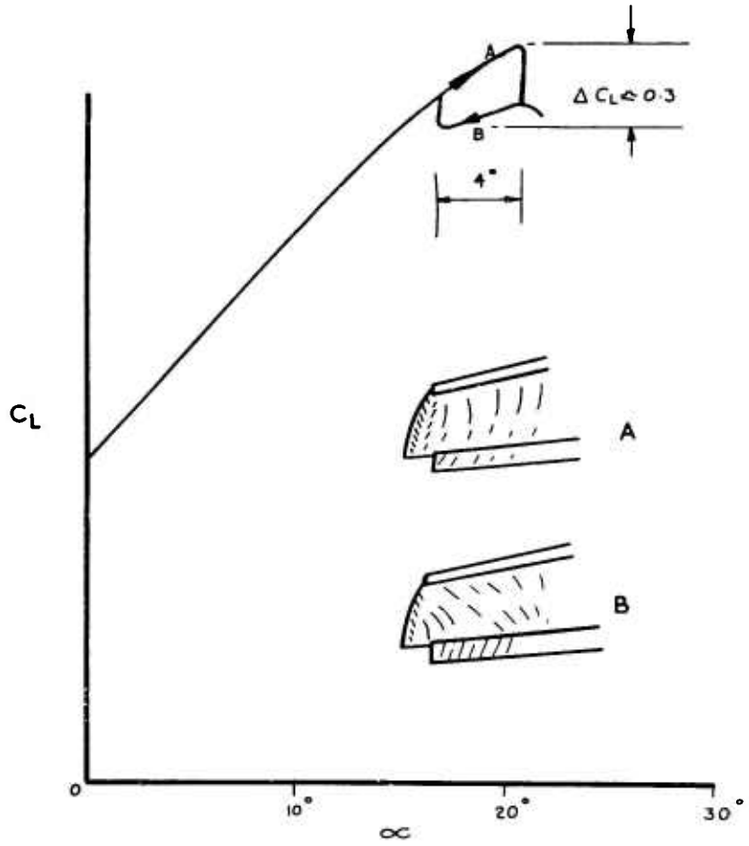

HIGH-LIFT WING WITH SLAT & FLAP

Fig.26 Result of model test showing hysteresis at the stall

SUMMARY OF DISCUSSION

relating to

THREE-DIMENSIONAL MODEL-TESTING TECHNIQUES

1. Ground-effect Testing

It was generally agreed that moving ground-belt rigs are now not currently considered as essential as they had been a few years ago. Nevertheless, for a fixed ground-board, special care must be taken to minimise the effect of the boundary-layer on the ground-board. For example, the pressure distribution on the ground-board should be monitored, to provide an indication of the occurrence of boundary-layer separation. Furthermore, an attempt could be made to remove some of the boundary-layer. An extraction slot (Fig. 21 of Paper) for boundary-layer removal should not be placed too far forward, since the boundary-layer would then have time to thicken before reaching the tailplane; nor so far rearward as to be over-influenced by variation in wing downwash. Adjustments to the slot flow should be made by reference to measurements of a boundary-layer rake on the ground-board downstream of the slot.

2. Usefulness of Half-model Techniques

Experience with the usefulness of half-model techniques varied among the contributors to the discussion. Manufacturing imperfections can apparently play a large part in comparisons of results from half-models and complete-models. For this reason, the lecturer had used the same half-wing in his comparative tests. The good correlation obtained might well be due to the fact that the wing had a tip stall; if the stall had commenced at the root, then the effect of the wind-tunnel boundary-layer on the half- model results might have been more pronounced. Differences in the fuselage surface patterns, and in the values of C_{mo}, had been measured; but the agreement between the tailplane powers was reasonable. It was emphasised that half-models have their special advantages, but that complete reliance on them is not advisable.

ANALYSIS OF TRANSPORT APPLICATIONS

FOR HIGH-LIFT SCHEMES

by

L. B. GRATZER

Chief Aerodynamics Technology, The Boeing Company;

Seattle, U.S.A.

SUMMARY

The aim of the present paper is to review the development of high-lift schemes within the framework of current and possible future applications to transport airplanes. The way in which the design trade-off process affects airplane economics is illustrated in relation to the impact of high-lift system design on the final configuration selection. An assessment of representative high-lift concepts, including boundary-layer control, is given in terms of low-speed performance potential.

For long-range transport airplanes operating from long runways, it is shown that well-designed mechanical flap systems are generally competitive with more sophisticated concepts involving blowing or suction boundary-layer control (BLC). However, assessment of recent progress in high-lift technology indicates that significant performance gains for long-range airplanes may be possible using BLC techniques. The gains for airplanes designed to operate from shorter fields appear attractive and achievable with today's technology. For STOL airplanes the use of BLC to provide high wing lift together with direct lift from the engines, or a more highly integrated form of lift augmentation such as the jet-flap, is mandatory.

The interaction between high-lift system design and problems involving the stability and control characteristics of the airplane are considered. While substantial effects of trim lift and drag penalties, tail sizing and ground proximity exist, the lateral control arrangement has the greatest influence on the selection of flaps and wing geometry. Finally, the need for continued aerodynamic development and design application effort is pointed out and certain areas where substantial payoff may exist are discussed.

1. INTRODUCTION

The success of the high-speed transport airplane which has seen an intensive development over the last decade or more has been due, in a substantial way, to the diligence with which designers have applied new technology and exercised the complex tradeoff of design parameters to achieve well-balanced configurations. Each advance in technology or new design concept has tended to change the relative importance of the fundamental parameters, resulting in sometimes subtle, sometimes revolutionary, changes to the aerodynamic configuration of the airplane. For example, the introduction of the concept of wing sweep at once changed the basic configuration of the airplane and permitted much higher speeds without significant drag penalties. Fortunately, the jet engine was available to permit practical operation in a speed regime for which the piston engine-propeller combination was basically unsuited. Thus the swept-wing and jet engine combination provided the formula for efficient cruise at high subsonic Mach numbers. However, this did not occur without the necessity for some compromises, particularly in low-speed characteristics and field length requirements. Thus the need arose for more effective high-lift devices which could offset the adverse low-speed effects of wing sweep and the higher wing loadings associated with configurations optimized for cruise performance.

With the background outlined above in mind, it will be the aim of this paper to show the way in which the design tradeoff process affects the airplane configuration and to assess the impact of various high-lift concepts on the overall performance potential of the transport airplane.

While there are countless variations on the basic high-lift devices and lift-augmentation concepts developed over the last fifty years, the present analysis will be based on representative configurations considered to have high performance potential and applicable, in a practical sense, to transport airplanes.

2. CRUISE EFFICIENCY VS LOW-SPEED PERFORMANCE

The primary consideration in selecting a transport airplane configuration is the achievement of high cruise efficiency. This is usually accomplished by carrying out trade studies to determine the best combination of geometric, propulsion and other parameters to satisfy the mission requirements with minimum cost. While a large number of design variables (parameters) are used to characterize the configuration, some of the most important are thrust to weight ratio, wing loading, aspect-ratio, wing sweep and thickness. One of the more effective ways of presenting the results of a typical tradeoff process is illustrated in Fig. 1 showing the typical variation of thrust loading, T/W, versus wing loading, W/S, for constant values of takeoff gross weight. In this example, the mission is fixed (i.e. payload, range and cruise Mach number) along with certain design parameters. Since the direct operating cost (DOC) is generally proportional to takeoff gross weight, an attractive selection in this case appears to be a takeoff gross weight near 400,000 lb. with T/W = 0.23 and W/S = 155 lb/ft^2. Similar charts can be constructed for other combinations of design parameters from which an optimum selection could be made. However, to this point, no consideration has been given to field length characteristics in the configuration selection. This can be presented conveniently by augmenting the information shown in Fig. 1.

Before proceeding with this step, it is important to review the basis for field length calculations to highlight the fundamental parameters relating to the performance of high-lift systems as applied to transport airplanes. Fig. 2 illustrates a typical takeoff profile executed according to Federal Aviation Regulations (FAR) requirements. Of particular significance is the lift-off speed V_{LO}, which must be greater than 1.1 times the minimum unstick speed V_{MU}. The latter is determined in test as the minimum speed at which the airplane can fly off at the applicable gross weight on all engines. A further requirement sets the speed V_2 greater than 1.2 times the stall speed V_S, or 1.1 times the minimum control speed V_{MC}, whichever is greater, as the airplane reaches 35 ft. above ground. The stall speed V_S, is also determined in test to be the minimum speed achieved in a prescribed stall maneuver at the applicable configuration and gross weight. The apparent lift coefficient in the stall, C_{LS}, is usually 10 to 12 percent higher than the maximum lift coefficient in 1g flight. Without dwelling on the complexities of these rules, it will be apparent that the design of the high-lift system is crucial in achieving the minimum speeds which relate directly to the lift coefficients and other aerodynamic parameters used for field length calculations. Since the actual takeoff distance is given by the relationship shown in Fig. 2, the presentation of takeoff field length performance on a plot of thrust loading versus wing loading (e.g. Fig. 1) is straightforward.

The typical landing profile, conducted according to the FAR, is illustrated in Fig. 3. Here the approach speed V_{app} is 1.3 times the stall speed, and must be carried out at a weight such that the available climb gradient with one engine inoperative is greater than 0.027. In a situation involving a go-around, the required climb gradient on all engines must be greater than 0.032. Again the importance of high-lift system design to achieve high approach lift coefficient and lift to drag ratio L/D, to minimize field length, is apparent from the actual landing distance relationship given in Fig. 3. Although the landing distance depends only on wing loading, presentation of landing field performance on a chart such as Fig. 1 is still appropriate.

Typical results for a takeoff and landing performance analysis are shown in Fig. 4 superimposed on the plot of Fig. 1. Here it is immediately apparent that an airplane selected for optimum cruise performance will tend to require excessive takeoff and landing field lengths. Compromises necessary to provide acceptable field performance must be made without an inordinate increase in the gross weight required to accomplish the mission. The point indicated by the cirle designatos a choice which keeps the field lengths to 11,000 ft. and 4,800 ft. for takeoff and landing respectively with a moderate increase in takeoff gross weight to about 415,000 lb. This results in a selection of T/W = 0.24 and W/S = 127 lb/ft^2, corresponding to an engine thrust and wing area somewhat greater than those required for optimum cruise performance. Since the airplane in this example is obviously takeoff field length critical, the landing

distance selection is not significant except as it corresponds to a higher value of wing area than necessary to minimize gross weight. This may be desired for future growth potential. It should be recognized that the results of this type of study are influenced substantially by the levels of technology assumed in all areas, including aerodynamics, weights, and engine performance. In particular, high-lift technology has a major impact since improvements in C_{Lmax} and L/D will tend to shift the takeoff field lines downward and the landing field lines to the right permitting a closer approach to the optimum cruise configuration.

More recently, the noise characteristics of airplanes have begun to exert a significant influence on the selection of design parameters, since operating restrictions due to noise can have a serious effect on airplane economics. All new transport airplanes in the United States must now operate under noise regulations imposed under FAR Part 36. The essential features of these rules are illustrated in Fig. 5 which shows typical noise contours generated by an airplane near the airport and surrounding community. For the case shown, the noise on takeoff is just under the FAR limit of 108 EPNDb over a point 3.5 miles from the start of the runway. The noise along a sideline 0.35 N.Mi. from the runway centerline is somewhat less than this limit, while the noise on approach at a point 1 N.Mi. from the runway is somewhat over the FAR limit. Thus, it is probably necessary in this case to invoke the trade rule which permits an exceedence in one category if it is balanced by less noise in others according to the trade rule indicated in Fig. 5. Since engine noise characteristics are influenced by the height over the measuring station, which in turn is determined by engine thrust and airplane L/D, it is apparent that airplane noise characteristics can also be superimposed on the plot of Fig. 1.

This has been done for the takeoff case in Fig. 6 where lines of constant noise relative to the FAR limit are shown. The increments from this limit are also tabulated for sideline and approach noise. The design point selected in Fig. 4 is also shown here and appears acceptable from the noise standpoint when the slight exceedence indicated is offset by the favorable sideline noise increment. However, this would not be true for a design selection closer to the optimum cruise point. Thus, for example, the benefits of a change in high-lift technology which permitted higher wing loading would not necessarily be realized without further efforts to reduce noise. While it is apparent that the design of the high-lift system influences the low-speed characteristics (i.e. C_{Lmax} and L/D) of the airplane, thereby affecting engine thrust required and noise, it is also clear that other design trades such as more attenuated at the source, must be exercised to arrive at the best overall compromise.

3. CHARACTERISTICS OF HIGH-LIFT SYSTEMS

The development of high-lift schemes has had a long history in which the fundamental aims have been to provide practical systems which permit increases in maximum lift, C_{Lmax}, and improvements to the low-speed operating envelope of the airplane; mainly through improvements to airplane L/D. A review of the many approaches used in the past to apply high-lift schemes to airplanes is clearly beyond the scope and intent of the present discussion, particularly since this has been well treated in the literature (cf. Ref. 1). Rather, the objective will be to illustrate a logical approach to the evaluation of various high-lift concepts as applied to transport airplanes. The analysis will be based on relatively recent theoretical and experimental results obtained with mechanical devices and boundary-layer control techniques which are representative of the present state-of-the-art.

3.1 Mechanical Systems

The low-speed polar of the airplane, such as given in Fig. 7, provides the appropriate format for illustrating the fundamental aerodynamic characteristics of high-lift systems. Typical lift and drag characteristics of a transport wing of aspect-ratio 8.0, with 35° sweepback, are shown for a range of trailing-edge flap settings from flaps-up to the landing configuration. The basic lift and drag data are representative of a well-developed mechanical system. Improvement in leading-edge device design can be expected to extend the lift curves to higher stall angles and values of C_{Lmax} while improving the envelope of the individual (δ_F = const.) drag polars, i.e. the envelope polar. Aerodynamic improvements to trailing-edge flaps will generally reduce airplane attitudes at a given lift and increase values of C_{Lmax} while reducing stall angles. Although increases in C_{Lmax} will result in extending the envelope polar, further improvements in the envelope polar can be expected at lower lift coefficients if significant reductions in profile drag are realized. The curve corresponding to flaps-up minimum drag plus elliptic induced drag is shown as an idealized polar to indicate the potential which still remains for improvement. Research on the aerodynamics of high-lift devices in recent years has provided substantial progress toward narrowing the gap between the actual envelope polar and the ideal polar, but intensive efforts in the future will be necessary to close this gap further.

Fig. 8 shows typical effects to be expected for several different types of leading-edge devices. The favorable effect of curvature and flap chord to wing chord ratio on the lift and drag characteristics of the wing are quite apparent. The designer will generally try to obtain these aerodynamic benefits within the constraints imposed by system weight and complexity. The achievement of a totally satisfactory design will also depend to a large degree on the care exercised in arrangement details such as spanwise extent of the flaps, supports, actuators, and eliminating or sealing gaps.

The aerodynamic characteristics of several representative types of trailing-edge flaps are shown in Fig. 9. For flap systems having comparable flap chord to wing chord ratios, with equivalent deflection angles, relatively small differences in aerodynamic characteristics are indicated in the landing configuration. Equivalent flap deflections correspond to the angles required in each case to give the same value of lift at $\alpha = 0$ in potential flow. However, the selection of the trailing-edge arrangement for a particular application will depend on the balance between takeoff and landing field requirements, airplane attitude limits, buffet, as well as general arrangement considerations related to actuation, lateral control, flight path control and others. Weight and complexity tend to play an even more important role in the selection and design of the trailing-edge system than in the case of the leading-edge.

Airplane low-speed performance characteristics are most conveniently understood and evaluated by converting the conventional drag polar to a plot of L/D versus C_L. Fig. 10 shows the data of Fig. 7 in this form, including the envelope polar and the idealized polar represented as $C_{D_o} + C_L^2/\pi A$. In most applications it is important for the designer to consider how improvements to the system may be accomplished and to what extent compromises should be made to achieve aerodynamic gains. The researcher also is interested in finding ways to measure progress and to determine where effort is needed to provide further improvement. At any stage of high-lift system development, the area between the envelope polar and the ideal polar tends to be indicative of the potential for performance improvement. But where should the major effort be concentrated? While the answer to this question is never completely straightforward, the various areas indicated in Fig. 10 generally represent the major drag components attributable to the items noted. It will usually be found that improvement to both the leading-edge and trailing-edge flap shapes offers substantial opportunities for reduction of profile drag. Induced drag can be reduced significantly by eliminating flap cutouts and extending the flap span. However, the trim drag penalty associated with flap span extensions on swept wings tends to reduce the benefit to rather small values. Substantially greater benefits can be shown for a straight wing. Recent tests also tend to indicate that the induced drag penalty due to the fuselage is quite small, even at large flap angles, if reasonable care is taken to provide a clean wing-fuselage juncture. However, some loss in $C_{L_{max}}$ will occur. At the lower flap angles, significant gains could be expected from better airfoil camber shape since the leading-edge and trailing-edge devices do not provide a sufficiently close approach to the desired camber. At higher flap angles, these devices can more nearly match the ideal camber shape. A substantial part of the area labelled "non-ideal camber" represents viscous drag which cannot be completely eliminated even with extraordinary methods such as suction boundary-layer control. The area between the curve labelled "operational limit" and the envelope polar also represents improvement potential. The operational limit curve constitutes the locus of points for which the operating lift coefficient $C_{L_{V_2}}$, at a given flap setting, is equal to an appropriate fraction (in this case, 1/1.60) of the FAR stall lift coefficient C_{L_S}. As discussed previously, this number may not be greater than 1/1.44 and is one of the restrictions which must be observed for takeoff. Thus, any improvement in $C_{L_{max}}$ will tend to move these operating points to the right bringing the operational limit curve closer to the envelope polar. It will be remembered that the lower limit on lift-off speed is related to V_{LOF}, or the corresponding lift coefficient $C_{L_{LOF}}$, so that this also controls the takeoff distance. However, an operating curve corresponding to this limit cannot be shown on the plot since the lift-drag characteristics are substantially changed by ground effects. Because experience shows that an aerodynamic improvement which increases $C_{L_{V_2}}$ tends to increase $C_{L_{LOF}}$ proportionally, it is usually not necessary to consider both limits simultaneously in the evaluation of high-lift systems.

Certain relationships between airplane aerodynamic characteristics and takeoff and landing performance are now considered. Fig. 11 shows the effects of takeoff lift coefficient on takeoff distance, where the flap angle is selected to correspond to the appropriate point on the operational limit curve of Fig. 10. It will be noted that there is a C_L for which the distance is minimum corresponding to the value of C_L above which the air distance increases total distance faster than the ground run reduces it. The dashed curve corresponds to the weight beyond which the second segment climb gradient is less than required; i.e. 0.030 for one engine inoperative. At a given gross weight, improvements in the L/D envelope and/or the operational limit will tend to reduce takeoff distances and to shift the second segment line to the right.

In a similar fashion Fig. 12 shows the effect of $C_{L_{max}}$ on the FAR landing field length where the flap angles can be selected to correspond to the values of $C_{L_{max}}$ indicated. However, at a given gross weight, the field length continues to decrease as $C_{L_{max}}$ increases in contrast to the takeoff case. As the weight increases for a given airplane/engine combination, the landing climbout limit is reached (dashed line) beyond which the all-engine climb gradient is less than required. A field length corresponding to a landing speed of 150 kt. is referenced to indicate an area above which operational problems related primarily to speed may be encountered.

We now consider the impact of the various improvement possibilities previously discussed on airplane takeoff and landing performance. The operational limit curve of Fig. 10 is reproduced in Fig. 13 corresponding to the basic L/D envelope of the airplane. Also shown is an operational limit curve corresponding to the L/D envelope and $C_{L_{max}}$ values associated with the potential improvement level for leading-edge devices. For a given airplane, the variation of L/D with C_L required for constant takeoff distance can be shown with each point on the curve corresponding to a weight at which the second segment limit is reached. Typical values of field length are given in Fig. 13 along with a crossplot for constant values of second-segment-limited weight. Thus, actual field lengths and corresponding weights can be read at points where the airplane operational limit curve crosses the appropriate field length and weight curves. This approach provides a convenient method for determining gains in takeoff performance due to aerodynamic improvements such as those indicated in Fig. 10. For example, the circle indicates the operating point for a takeoff distance of 10,000 ft. for which the takeoff gross weight is 395,000 lb. However, if the potential indicated for leading-edge shape improvements can be realized, the new operating point indicated by the triangle, permits a takeoff weight of 413,000 lb. from the same field. The gain of about 18,000 lb. takeoff weight can be used to provide more range and/or payload capability.

A procedure similar to the above could be followed for the landing case, where lines of constant field length would correspond to weights limited by the landing climbout requirement. However, transport airplanes are not often limited by the climbout requirement due to relatively low landing weights and the moderate values of $C_{L_{max}}$ needed for available fields. These are normally achievable with mechanical devices. Referring back to Fig. 10, the curve corresponding to the climbout limit at the landing weight is shown for a typical situation. For the landing flap polar, an adjustment has been made in the drag level to account for landing gear drag. In this case, the airplane, in the landing configuration, has higher L/D than necessary and improvements to the L/D envelope will not change the landing performance although approach noise could be reduced. On the other hand, improvements to $C_{L_{max}}$ will be necessary if shorter landing distances are required and this could conceivably cause the climb-out limit to be critical for short fields.

The gains in takeoff performance corresponding to the elimination of the various major drag contributors can now be summarized in a plot such as that of Fig. 14. These are plotted versus the efficiency factor, ϵ in the equation, $C_{D_o} + C_L^2/\pi Ae$ which describes an "improved" envelope polar lying in the area between the basic envelope polar and the ideal polar. Such polars can be associated with the curves of Fig. 10 by selecting the appropriate values of e. The related operational limit curves are found corresponding to appropriate values of $C_{L_{max}}$ for each trailing-edge flap setting. It is apparent from Fig. 14 that substantial gains in takeoff gross weight and field length reductions are attributable to the reduction or elimination of the various sources of drag. While the noise reduction associated with improvement in L/D is significant, the possible gain here is not the major reason to seek high-lift system improvements since other means, such as engine noise treatment, are available to reduce noise. The tradeoff possibilities are very complex and beyond the scope of this discussion. While the potential gains indicated here are very attractive, it must be recognized that continued effort in aerodynamics and the development and application of advanced concepts will be necessary to achieve progress in an area which becomes increasingly difficult to exploit as the ideal polar is approached.

3.2 Boundary-Layer Control Devices

Since the first experiments with boundary-layer control (BLC) over sixty years ago, a great many different applications of the fundamental concepts have been tried, alone and in combination with various mechanical devices. Although ideas on suction developed first, the use of blowing at critical areas on aerodynamic surfaces subject to flow separation followed fairly soon thereafter. Periods of research activity in both the United States and Europe led to intensive efforts, particularly following World War II, to apply both suction and blowing BLC concepts to military airplanes. However, owing to practical difficulties and lack of a clear demonstration of decisive advantage, no significant applications of BLC to commercial transports have appeared to the present time. Fundamentally this stems from the following:-

1) Airport runways have continually been extended to permit the operation of larger and heavier airplanes at higher takeoff and landing speeds.

2) Improvements in the design of mechanical high-lift systems have tended to keep pace with the trend toward higher wing loading so that benefits from the use of BLC techniques have not appeared sufficiently attractive.

However, the developing trend toward STOL airplanes will almost certainly make the use of some form of lift augmentation mandatory.

3.2.1 Blowing Boundary-Layer Control

For purposes of the present discussion, the possibilities for the application of BLC techniques to transport-type airplanes will be explored on the basis of some of the more promising practical approaches. Fig. 15 illustrates several basic ways in which the blowing BLC principle can be applied to the leading-edge and trailing-edge of a wing. At the leading-edge, the incorporation of single or multiple blowing slots has been shown to be very effective in increasing $C_{L_{max}}$. Normally it is expected that increasing the momentum coefficient C_μ will lead to higher stall angles and $C_{l_{max}}$. However, the leading-edge develops high peak pressures at moderate angle-of-attack, thus leading to the early onset of local sonic flow. This tends to limit the BLC effectiveness to fairly low values of C_μ corresponding to the angle-of-attack at which strong shock waves begin to appear. This situation can be alleviated by incorporating a leading-edge device such as a Krueger flap, but maximum effectiveness is obtained with a curved flap. At the trailing-edge, blowing from the shroud over a simple flap has been the subject of extensive research. It is an effective way to increase the lift capability of a flap system featuring mechanical simplicity and low weight. On the other hand, certain advantages can be shown for flap blowing on an otherwise conventional single-slotted flap. The ejector nozzle arrangement achieves the same effect as shroud blowing, with substantially less power, due to ejector augmentation. Ref. 2 discusses the application of this concept to the Boeing 707 prototype and the corresponding wind-tunnel and flight results. Obviously this principle has potential in any application where high pressure air is available.

Fig. 16 shows representative two-dimensional data for leading-edge BLC configurations. Blowing on a plain leading-edge is highly effective at low C_μ although effectiveness levels off beyond $C_\mu = 0.03$ due to the onset of sonic flow at the leading-edge. The added effectiveness of two or more slots tends to be marginal. The Krueger flap maintains BLC effectiveness to somewhat higher values of C_μ, although it also shows a tendency to level off as the peak pressures at the flap-wing intersection become too high. The curved flap, in addition to having somewhat higher effectiveness at low C_μ, maintains BLC effectiveness up to substantially higher values of C_μ than shown in the plot.

Fig. 17 shows lifting characteristics for several training-edge BLC configurations. Blowing over a trailing-edge flap deflected to high angles, reduces the tendency for the flap to separate as C_μ is increased. For example, with shroud blowing, the lift coefficient at $\alpha = 0$ increases with C_μ until the point is reached at which the flow is completely attached. Beyond $C_\mu \approx 0.03$, the lower rate of lift gain is associated with the jet-flap regime of operation. The single-slotted flap becomes fully attached at a substantially lower C_μ since it has less separation initially. Beyond $C_\mu \approx 0.015$, BLC effectiveness is characteristic of the jet-flap regime. The ejector nozzle in this case appears about equivalent to shroud blowing except that it produces significantly higher values of $C_{L_{max}}$. Full-scale results (2) show somewhat greater advantage for the ejector nozzle concept.

The evaluation of various high-lift concepts using blowing BLC can be carried out in a manner which is analogous to that used for mechanical systems, provided the weight penalties of the BLC system are properly accounted for. The performance potential for a representative system incorporating leading-edge blowing combined with a double-slotted trailing-edge flap is first examined in comparison with the

mechanical flap system previously used. The latter polars are reproduced in Fig. 18 along with the corresponding operational limit line. In performing this assessment, it must be recognized that the problem is really one of optimization to select the appropriate level of C_μ and flap angle for each field length. For present purposes it will be assumed that the BLC air is supplied by auxiliary power units (APU) installed in the airplane. The mechanical flap airplane will be compared with a BLC configuration for which the weight of the APU and the BLC system (i.e. ducting valves, etc) is compensated by a corresponding reduction in the weight, and therefore thrust, of the main propulsion system. The drag polar data from the wind-tunnel includes the residual thrust from BLC nozzles and careful analysis shows that a large fraction of the theoretical nozzle thrust is usually recovered, appearing as excess momentum in the wing wake over a large range of C_μ, including static conditions. Thus it is appropriate to credit the APU with the full BLC nozzle thrust. The equivalent drag of the airplane is then represented by $C_{De} = C_{DB} + C_\mu$ where C_{DB} is based on the measured balance force in the wind direction.

To carry out the optimization process, the polar set for the complete range of flap angles is plotted for several values of C_μ and the corresponding operational limit lines determined. Furthermore, the mapping for constant field length and second-segment-limited weight is plotted to correspond to the new level of total thrust for each C_μ. Even though full credit is taken for the APU thrust, the total thrust for the BLC airplane is less than that of the mechanical flap airplane by an increment given by the relation, $\Delta T/W = -1.2\ C_\mu/C_L$, corresponding to the installed weights and cycle characteristics of the BLC system, the APU and engines. Fig. 18 shows the results of the evaluation process, where the dashed polar corresponds to the C_μ level and flap angle associated with the 10,000 ft. takeoff distance. The adjusted field length lines correspond to the reduced total thrust available at each field length with tick marks indicating the noted values of takeoff weight. The composite operational limit line is also shown as the locus of points corresponding to the optimum C_μ and flap angle for each field length considered, where the optimum is determined by the maximum gain in takeoff gross weight at a given field length. Again, choosing an example for 10,000 ft. takeoff distance, it is seen that the BLC system will permit a takeoff weight of 403,000 lb. corresponding to the point indicated by the square in Fig. 18. Since the basic flap system allows only 395,000 lb. on takeoff, a gain of 8,000 lb. takeoff weight can be credited to the leading-edge BLC system. At a weight of 410,000 lb. the corresponding reduction in takeoff field length would be about 600 ft. While these gains may not be sufficiently attractive to introduce the additional complication of BLC, into the high-lift system design, the sensitivity of the performance gains to the available technology and the developing state-of-the-art requires continued reappraisal of blowing BLC applications. For airplanes designed to operate from smaller fields, the performance gains would begin to appear quite attractive.

Where the emphasis is on takeoff performance, the results of studies based on wind-tunnel tests tend to show that BLC applied to the trailing-edge has marginal potential. This is strongly implied by the two-dimensional data shown in Fig. 17 which indicates that a well-designed double-slotted flap produces a lift coefficient at zero angle-of-attack, $C_{l_{\alpha=0}}$ quite close to the potential flow value. The application of BLC to such a flap would be expected to yield a lift variation with C_μ typical of the jet-flap regime, resulting in low BLC effectiveness. Similarly the variation of $C_{l_{max}}$ with C_μ should reflect the fact that little mixing of the jet with the wing upper surface boundary-layer can take place at low values of C_μ. Complete airplane model tests in the wind-tunnel confirm these expectations, so that there appears to be no advantage to trailing-edge BLC for takeoff.

For applications where landing performance is more important, particularly for STOL operation, the use of trailing-edge BLC may be attractive; e.g. in cases where airplane attitude is restricted or the overall scheme depends on maintaining flap effectiveness to very high angles. In most transport applications, however, it is difficult to overcome the advantages of leading-edge BLC with curved flaps combined with large, effective trailing-edge mechanical flaps.

3.2.2 Suction Boundary-Layer Control

We now turn to a discussion of the possibilities for suction BLC applications. While considerable research has been devoted to suction BLC concepts in the past and some flight work accomplished, these efforts have been quite meager in comparison to the extensive work with blowing BLC. Most of the suction BLC concepts have been based on the principle of continuous removal of a portion of the boundary-layer through porous surfaces, such as illustrated in Fig. 19. More recently there has been interest in the use of multiple suction slots at either the leading-edge or on trailing-edge flaps to keep the boundary-layer attached. Combined suction and blowing BLC is a fairly old concept which has seemed attractive where a high pressure source of air is available. Fig. 19 shows one variation of this idea where suction of the main flap surface is accomplished by ejector action. The mixed stream is then ejected tangentially over the second segment. It is apparent that this principle can be applied in a variety of ways at either the leading-edge or trailing-edge.

Fig. 20 shows some typical two-dimensional results obtained with leading-edge suction in combination with a 13% chord curved flap. The dashed curves are estimations based on known levels of $C_{l_{max}}$ at $C_Q = 0$. The effectiveness of the suction BLC measured in terms of power required to achieve a given increment in $C_{L_{max}}$ can be three or four times that of blowing BLC. However, there is no easy way to generalize this relationship since the system details are very important in such a comparison. Also, the suction BLC system is inherently limited since a cutoff in effectiveness occurs at the C_Q corresponding to complete removal of the boundary layer at the last downstream slot.

The results of tests on a single-slotted trailing-edge flap with multiple suction slots are shown in Fig. 21. The effects of several combinations of slots on $C_{l_{\alpha=0}}$ are found for an arrangement where all slots are vented to the same plenum. The slot widths were selected to provide the desired inflow distribution. It is apparent that the first two slots are most effective in producing attachment although the results at higher C_Q are better with more slots. The dashed line indicates the envelope of the curves

shown and represents the maximum suction effectiveness obtained for this type of flap. The curve of $C_{l_{max}}$ versus C_Q demonstrates that trailing-edge suction is about 60% as effective as suction applied at the leading-edge over the range of C_Q shown here.

The application of suction BLC to high-lift system design is generally considered to be more difficult than for blowing BLC, because of the need to provide a highly-integrated well-balanced air distribution and power system. Since there is relatively little experience with this type of BLC in practical installations, it is probably too early to assess the ultimate potential of suction BLC for high-lift applications. Nevertheless, it is possible to carry out studies based on existing data and to evaluate suction BLC on the same basis used for the other high-lift schemes.

Typical results for a system using suction BLC in combination with a curved leading-edge flap and a double-slotted trailing-edge flap are illustrated in Fig. 22, where the lift-drag characteristics of the basic mechanical flap system are shown for comparison purposes. As in the blowing case, the correct approach is to assess the performance of the system at several BLC levels corresponding, in this case, to appropriate values of C_Q. Again the mechanical flap airplane is compared with the BLC configuration for which the weight of the APU and the BLC system is compensated by a corresponding reduction in the weight, and therefore thrust, of the main propulsion system. In this assessment, the power for suction is assumed to be supplied by an APU which exhausts the suction flow at the freestream velocity for the climbout condition on takeoff. Therefore, only the primary thrust plus an amount corresponding to the suction flow at an appropriate lower speed is credited to the APU for takeoff. The drag polars are based on the results of limited wind-tunnel tests, with adjustments to measured drag to account for the inflow momentum of the suction flow, but no correction for suction power required. The optimization and evaluation process is carried out in the same fashion as for the blowing BLC case. Again the total thrust of the suction BLC airplane is less than that of the mechanical flap airplane by an increment given by the relation, $\Delta T/W = -6.5\ C_Q/C_L$, which corresponds to the installed weights and cycle characteristics of the BLC system, the APU and engines. Fig. 22 shows the results of the evaluation process where the dashed polar corresponds to the C_Q level and flap angle associated with the 10,000 ft. takeoff distance. The adjusted field length lines correspond to the reduced total thrust available at each field length with the noted values of takeoff weight indicated by tick marks along these lines. The composite operational limit line is the locus of points corresponding to the optimum C_Q and flap angle for each field length, where the optimum is determined by the maximum gain in takeoff gross weight at a given field length. The difference between the composite operational limit line and the mechanical flap operational limit line is indicative of the potential for gain in takeoff weight which becomes larger as the field length decreases. At a takeoff distance of 10,000 ft., the takeoff weight for the suction BLC airplane is found to be 410,000 lb. corresponding to the point indicated by the square in Fig. 22. Since the mechanical system permits a takeoff weight of 395,000 lb., the gain due to suction BLC for this comparison is 15,000 lb. The reduction in takeoff field length at a weight of 400,000 lb. is about 1100 ft.

The performance gains quoted are quite attractive and indicate substantially better potential for suction BLC than for blowing BLC. However, it should be remembered that the relationship can change depending on advances in the technology and experience in actual application of BLC concepts. For airplanes designed for shorter field operation, suction BLC appears to be less attractive than blowing because of the inherent limitations discussed earlier.

The potential for the application of suction BLC to trailing-edge devices appears to be limited for reasons similar to those which apply for blowing BLC. However, there is evidence that trailing-edge suction is not subject to the same limitation at high C_Q as in the leading-edge case. This is related to the fact that trailing-edge suction, properly applied, can work on the boundary-layer generated on the wing ahead of the suction location. This may be important for application to short field designs.

4. POWERED LIFT

For some time, there has been a developing interest in the possibilities for the application of high-lift concepts coupled with the direct use of engine thrust to achieve really short takeoff and landing (STOL) performance for commercial airplanes. A number of different concepts combining both high wing lift and deflected engine thrust in various ways have been studied in the past (e.g. Ref. 3) to evaluate overall suitability of such schemes for commercial application. These include:-

1) The high-lift wing using BLC at either the leading-edge or trailing-edge combined with cruise engine thrust deflection.

2) The jet-flap concept (4) which uses a major portion of the engine flow distributed along the trailing-edge and exhausting over the flap. The more recent augmentor-wing concept (5) is an extension of the jet-flap idea incorporating the ejector principle.

3) The externally-blown flap (6) in which the cruise engine exhaust flow is directed at the undersurface of the trailing-edge flap.

4) The direct-lift concept which incorporates separate lifting engines (either turbofan or turbojet) with a high-lift wing. The deflection of the cruise engine thrust may be optional depending on the wing lift level achieved.

However, no STOL configuration has yet emerged which clearly demonstrates all the essential features necessary for successful operation in a viable transportation system using such aircraft. Clearly, this will depend to a large degree on the penalties (e.g. operational, weight, cost, etc.) which must be accepted to achieve STOL capability, and meet stringent noise requirements at close-in fields.

Some of the fundamental problems and important performance and design parameters related to STOL aircraft can be examined conveniently by considering a somewhat idealized configuration which includes the essential elements of most STOL concepts. The aim will be to explore some of the basic requirements and limitations of STOL aircraft.

Fig. 23 shows the thrust requirements in level flight for an airplane incorporating cruise engines which can be vectored to any desired angle. It is also assumed that the envelope drag polar of such an airplane is parabolic with $C_{D_o} = 0.065$, $A = 8.5$, and $e = 0.85$. Each of the solid lines corresponds to a given thrust deflection angle for the total installed thrust. The minimum thrust requirement corresponds to the envelope of the constant deflection curves which indicates a steady increase in T/W to a value of 1.0 as the speed decreases to zero. It is significant that thrust deflection of 20 degrees is very nearly optimum over a large range of speed down to at least 50 knots.

The landing performance of a STOL airplane with deflected thrust can be examined more conveniently by plotting T/W versus speed for constant values of C_L. This has been done in Fig. 24 which also includes a landing distance scale along the abscissa. The landing distance calculations are based on a 6^o approach path over a 60 ft. obstacle and an average braking coefficient μ of 0.4. The performance envelopes are shown for $\gamma = -3^o$, 0^o, and $+3^o$, to indicate the sensitivity of thrust requirements to the flight path. Although the constant C_L lines are given only for level flight, for small values of γ they essentially expand (or shrink) vertically relative to the point $T/W = 1.0$. It is apparent that for landing distances approaching 1500 ft., very high values of C_L are required in order to minimize thrust requirements. On the other hand, if C_L is limited, for example to a value of 4.0, the thrust required is nearly twice the minimum and the required thrust deflection (cf. Fig. 23) is about 80^o. However, even this level of lift would require substantial BLC levels to provide the required operating margin. For field lengths below 1500 ft., the minimum thrust requirements rapidly increase and the thrust increments required because of aerodynamic lift limitations become even larger.

An alternative scheme for a STOL configuration could involve the use of the jet-flap concept, which has been the subject of considerable research in the past. The curve represented by the large dots shows the performance envelope ($\gamma = 0^o$) corresponding to wind tunnel data from NASA research (7) in this area. A close approach to the ideal performance envelope indicates the potential of the jet-flap concept for STOL provided practical schemes can be developed for application.

An analysis of the takeoff situation for STOL operation can be carried out on a basis similar to that illustrated above in the landing case. However, the problem is slightly more complex since the takeoff distance is not a simple function of takeoff speed. Using the previous format, the results of this type of analysis are presented in Fig. 25 for a four-engine airplane. The required T/W is shown for different wing lift levels and also for several values of takeoff distance corresponding to an engine failure at the critical speed. The performance envelope for each value of takeoff distance corresponds to the minimum installed T/W required at any speed. As expected, there is also an optimum takeoff speed and lift coefficient for each field length case. The analysis also shows that the relationships between required thrust deflection and lift coefficient are very similar to those found for the landing situation, indicating little need for thrust deflection when operating on the envelope below a lift coefficient of 4.0. Thus, in either the takeoff or landing situation, several fundamental conclusions become evident:-

1) It is important to achieve the proper wing lift levels in order to minimize the installed T/W for STOL airplanes.

2) When optimum lift levels can be obtained, thrust deflection is relatively unimportant.

3) When the wing lift is limited, increased thrust levels along with thrust deflection must be used to provide STOL performance capability.

5. STABILITY AND CONTROL CONSIDERATIONS

It is not unusual in the initial development of high-lift systems to find that problems related to stability and control are considered to be of secondary importance. Certainly there are few instances where such considerations will compromise the selection of effective high-lift schemes. Nevertheless, factors directly related to high-lift system design often have a critical influence on the selection of those aspects of the airplane geometry and systems which determine its stability and control characteristics. These can be very critical for STOL airplanes where low speeds and engine-out conditions introduce severe control effectiveness requirements.

Fig. 26 illustrates in a fairly general way, the important effects of trim requirements on lift. These are given in terms of the ΔC_L required to trim the airplane in the approach condition as a function of trimmed $C_{L_{max}}$. Increasing values of $C_{L_{max}}$ generally correspond to increased flap angles requiring substantial increments in down tail-load to balance the wing pitching moments. Trailing-edge BLC appears somewhat more difficult to trim than mechanical flaps. On the other hand, leading-edge BLC requires relatively little incremental tail-load since the lift is derived basically from increased wing angle-of-attack. The lines labelled "L.E. BLC" in Fig. 26 start from points on the general trend line for mechanical trailing-edge flaps corresponding to different flap angles.

An earlier discussion of trim requirements pointed out some of the adverse effects on airplane L/D. Fig. 27 shows general trends in L/D for different kinds of high-lift devices. Tendencies exist for the adverse effects of trim to level out and decrease somewhat at higher values of $C_{L_{max}}$ corresponding to large-chord trailing-edge flaps deflected to high angles. This trend can be demonstrated by theoretical analysis and is attributable to the polar shape at high values of C_L. Increments in L/D due to leading-edge BLC appear slightly favorable because of the significant favorable effect of blowing on trailing-edge flap effectiveness and the relatively small pitching moments due to angle-of-attack increments.

The arrangement of the lateral control system almost inevitably interacts strongly with the high-lift system layout. One arrangement which has been used extensively, includes an inboard aileron to provide a spoiler backup and lateral trim surface which will not reverse at high speed. The induced drag penalties associated with such a device are indicated in Fig. 28 and have been discussed previously in relation to possible performance gains. The incorporation of the outboard aileron which is used only for low-speed operation is compatible with the use of part-span flaps. For moderate to large wing sweep, little or no penalty in drag results since any reduction in induced drag attributable to the use of full-span flaps is largely cancelled by a trim drag increment.

While many factors must be considered in selecting the size of the horizontal tail, the impact of the high-lift system design is evident in Fig. 29. The line corresponding to the aft C.G. stability limit sets one requirement for tail size. A further requirement to trim at the forward C.G. limit of the airplane depends substantially on approach speed or lift coefficient. Since airplane loading requirements result in a specified C.G. range, a lower design approach speed has the effect of increasing the required tail volume. Reductions in tail size can be achieved by increasing the operating tail lift coefficient, but this again must be obtained by more sophistication in the airfoil sections used on the tail or by incorporating high-lift devices.

The effect of ground proximity on the aerodynamic characteristics of the airplane becomes increasingly important as lift levels increase. This phenomenon continues to be the subject of considerable research, particularly in relation to the development of practical STOL and VTOL configurations. However, the results are complex and highly configuration dependent rendering them beyond the scope of the present discussion. The effects of ground proximity on conventional transport airplanes, while significant, are generally not critical. Fig. 30 illustrates the range of aerodynamic characteristics to be expected between free-air conditions and a height corresponding to touchdown. Of particular importance is that a significant margin between $C_{L_{app}}$ and $C_{L_{max}}$ at $h/\bar{c} = 0.8$ exists for the landing case. Adequate margins are frequently lacking for operation in the STOL regime particularly for configurations using large amounts of deflected thrust. Also sufficient elevator or stabilizer deflection must be available to compensate for the reduction in downwash at the tail as the ground is approached. For the takeoff case, ground effect can have an important influence on the V_{MU} that the airplane can demonstrate. An unfavorable impact on takeoff performance during abuse tests can also be expected, particularly if the geometry of the airplane permits rotation to angles which result in high drag.

6. REQUIRED RESEARCH AND DEVELOPMENT

It has been pointed out that the technology of high-lift is still a developing one and that substantial low-speed performance gains may be achieved with continued emphasis on research and development. Although it is difficult to foresee all the areas of research which will provide substantial payoff, the following are considered to be of major importance:-

1) Mechanical devices have been extensively developed and refined in the past. Nevertheless, substantial opportunity for performance improvement still exists if ways can be found to increase section L/D and $C_{l_{max}}$. This will most likely follow from the application of advanced aerodynamic analysis methods which are capable of predicting the flow about complex wing and flap geometries. Further progress may also be expected from the imaginative application of sound aerodynamic principles to the development of new concepts with subsequent evaluation and improvement in the wind-tunnel.

2) Boundary-layer control schemes have been the subject of intensive research for many years and their potential in transport applications is only now beginning to appear attractive. Even though blowing BLC has to this point received major emphasis, there may still be possibilities for further improvement in terms of the power required to achieve a given lift level. Suction BLC, on the other hand, has received relatively little attention. From a fundamental standpoint, it appears to offer more potential than blowing in transport applications. However, much more effort in aerodynamic research and design application is needed to realize the inherent advantages of this technique.

3) Reynolds number effects have always introduced unknowns into the process of predicting full-scale airplane performance on the basis of model tests. In certain instances they have been cited as the cause of serious unanticipated performance deficiencies. While it is difficult to make a hard case in most instances, substantial evidence exists pointing to relatively large variations of aerodynamic characteristics (e.g. L/D, $C_{L_{max}}$, C_M) over the range of Reynolds number between wind-tunnel and flight conditions. As long as these variations are fairly predictable on the basis of theory, wind-tunnel test, or previous flight experience, the inherent technical risks may be acceptable. However, as new high-lift concepts and techniques evolve, it becomes increasingly important to test at Reynolds numbers approaching full-scale. If this is not done, uncertainty regarding the risks involved introduces a substantial lag between concept development and application. Increasing recognition of the need for data at high Reynolds numbers had led to some development and adaptation of existing facilities as well as the construction of several new tunnels in the United States and elsewhere. A need still exists for research facilities which can provide Reynolds numbers approaching those of today's large aircraft.

4) Theoretical methods for analysis and design of aerodynamic configurations have seen extensive development and use during the last ten years or more. This has been possible because of the general availability of high-speed digital computing equipment. Such methods usually apply to the potential flow about two- or three-dimensional shapes and are extremely useful in predicting flow characteristics under a wide variety of conditions. Also, methods of analyzing the boundary-layer have been developed, particularly for predicting two-dimensional flow characteristics. While some progress may still be achieved using present approaches, more effective theoretical techniques are

essential to permit the aerodynamic analysis of complex shapes. To achieve realistic results, new methods must treat the interactions between the potential flow and the boundary-layer essentially on a unified basis in which the three-dimensional aspects of the boundary-layer flow are accounted for.

7. CONCLUSIONS

A review of contemporary applications of high-lift schemes to transport airplane design has shown that the development of mechanical devices has tended to keep pace with the need for better high-lift systems. However, parametric design studies involving the match between airplane cruise-efficiency and low-speed performance generally indicate that more effective high-lift systems could lead to lower direct operating cost through lower design gross weight. Examination of the possibilities for aerodynamic improvement shows that substantial low-speed performance gains may still be achieved if research and design efforts are appropriately directed.

An assessment of various high-lift concepts including suction and blowing BLC has been given in terms of their respective low-speed performance potentials. It is shown that the best of today's mechanical systems are quite well-adapted to meet the requirements of long-range transports operating from long runways. The use of BLC techniques, particularly suction, may provide significant performance gains if proper application of current technology can be made. However, a continuing reappraisal of the potential of competing schemes is necessary, as high-lift technology continues to develop and improvements in one area change the basis for comparison with others.

On the other hand, it can be concluded that the application of BLC techniques in high-lift system design becomes quite attractive when the airplane must operate from shorter fields. For very short field lengths characteristic of STOL operation, the use of BLC appears mandatory along with some form of direct lift. Alternate schemes involving lift augmentation such as the jet-flap, or external blowing on the trailing-edge flap may also be attractive.

A discussion of stability and control problems related to high-lift system development has touched on the more important interfaces. From the design standpoint, the selection of tail size and the arrangement of the lateral control system interact most directly with the high-lift system. Ground effect is not usually a substantial factor in the configuration development of the high-lift system as long as the operating lift coefficient is not too high. However, at lift coefficients necessary for STOL operation, large adverse effects may result, particularly if some form of direct-lift is involved. These effects are highly configuration dependent, making it difficult to carry out general studies which can be used in a specific application.

REFERENCES

1. Lachmann, G. V. — Boundary Layer and Flow Control. Vol. I. Pergamon Press, New York; 1961.

2. Gratzer, L. B.; O'Donnell, T. J. — Development of a BLC High-Lift System for High-Speed Airplanes. J. Aircraft Vol. 2, No. 9; Nov.-Dec. 1965.

3. Fitzsimmons, R. D. — A Boeing View of Commercial STOL. Presented at the Air Force V/STOL Technology and Planning Conference; 23-25 Sept. 1969.

4. Davidson, I. M. — The Jet Flap. J. Roy. Aero. Soc.; Jan. 1956.

5. Whittley, D. C. — The Augmentor-Wing Research Program; Past, Present and Future. AIAA Paper No. 67-741; Oct. 1967.

6. Wimpress, J. K. — Aerodynamic Technology Applied to Takeoff and Landing. Annals of New York Academy of Sciences Vol. 154, Art. 2; Nov. 1968.

7. Lockwood, V. E.; Turner, T. R.; Riebe, J. M. — Wind Tunnel Investigation of Jet-Augmented Flaps on a Rectangular Wing to High Lift Coefficients. NACA TN 3865; Dec. 1956.

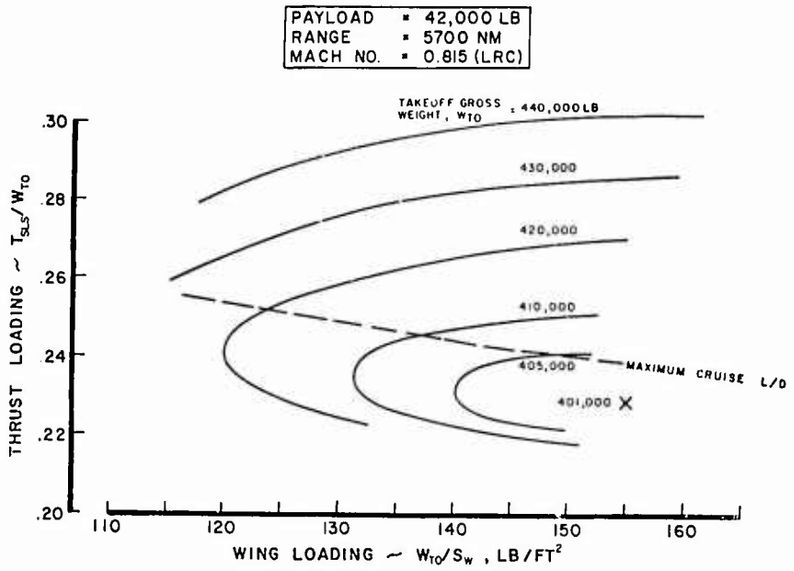

Fig.1 Cruise performance

$$\text{DISTANCE} \doteq K\frac{W/S}{\rho g C_L T/W} + f\left(\frac{T}{W}, \frac{W}{S}, \frac{L}{D}\right)$$

(GROUND) (AIR)

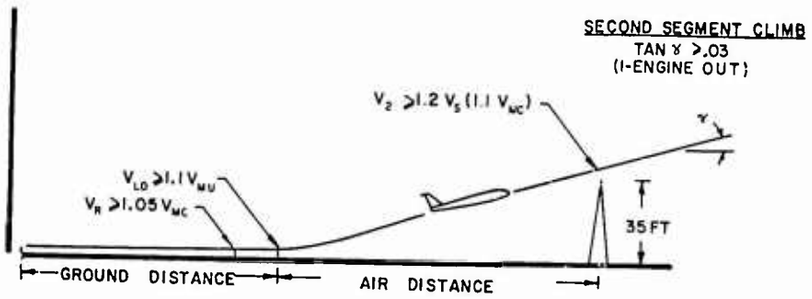

Fig.2 Takeoff profile

$$\text{DISTANCE} \doteq K\frac{W/S}{\rho g C_L \mu} + f(h, \tan\gamma_1)$$

(GROUND) (AIR)

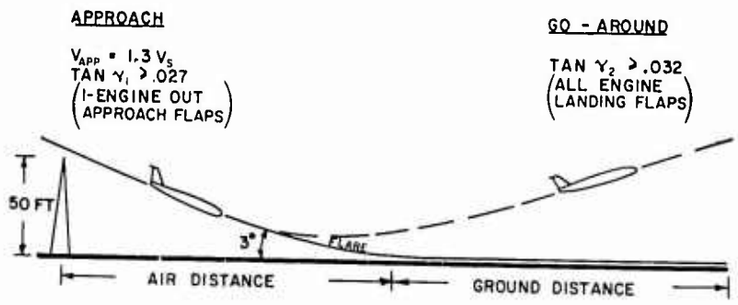

Fig.3 Landing profile

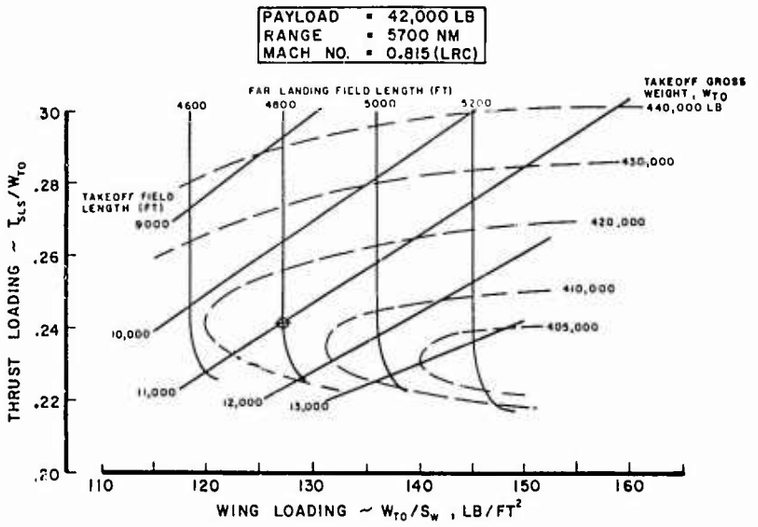

Fig.4 Low-speed performance

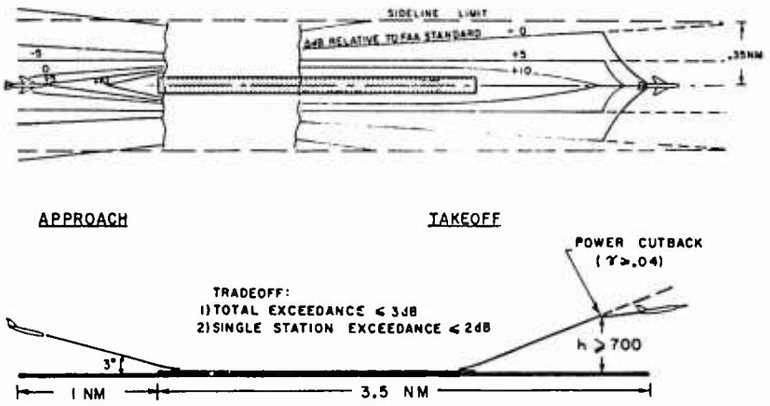

Fig.5 Noise requirements

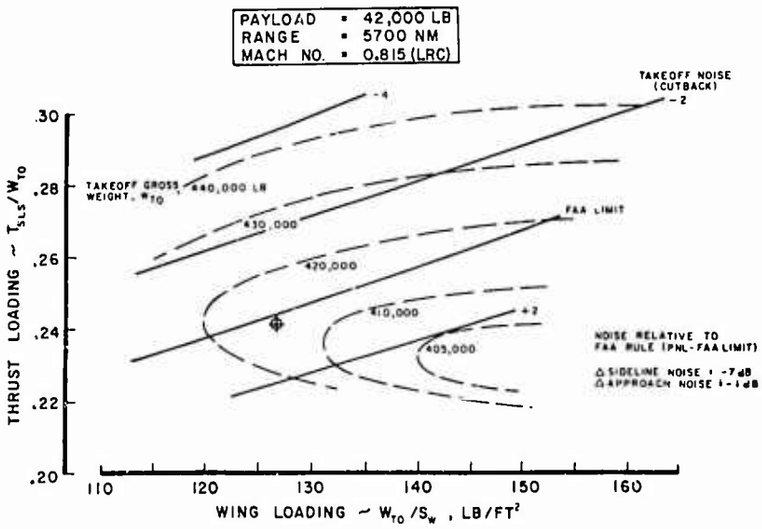

Fig.6 Noise characteristics

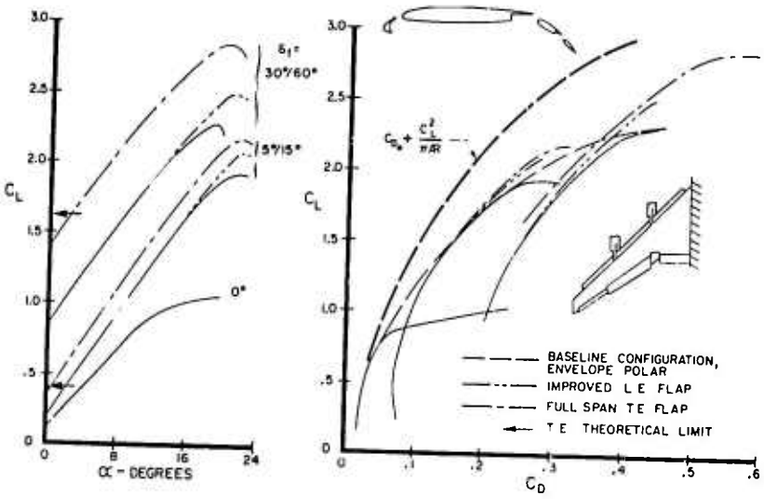

Fig.7 Low-speed drag polar

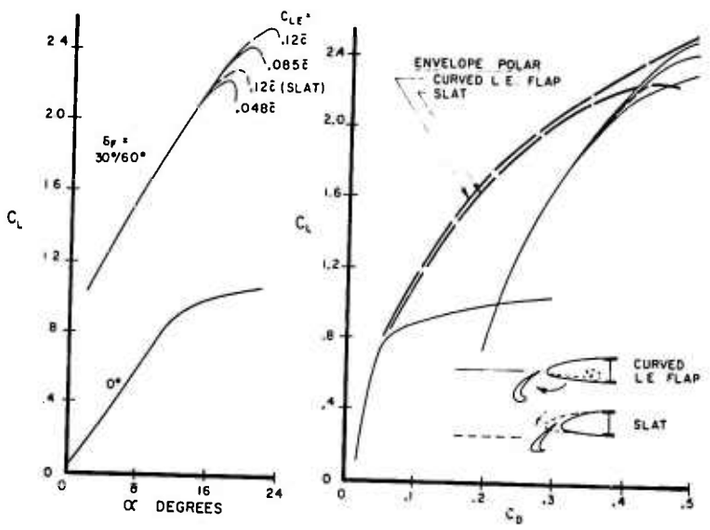

Fig.8 Leading-edge effects

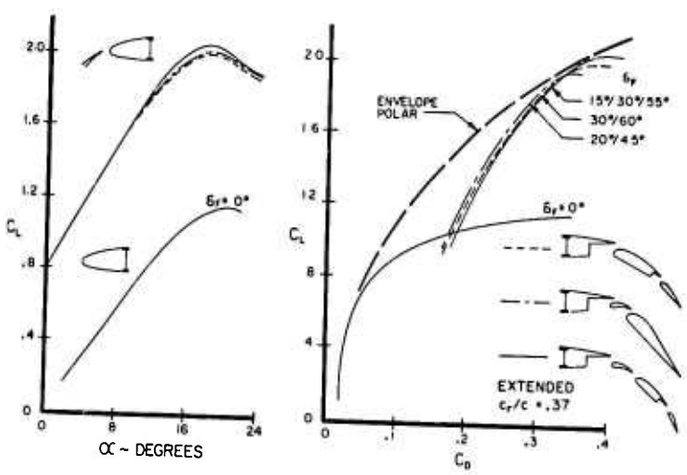

Fig.9 Trailing-edge effects

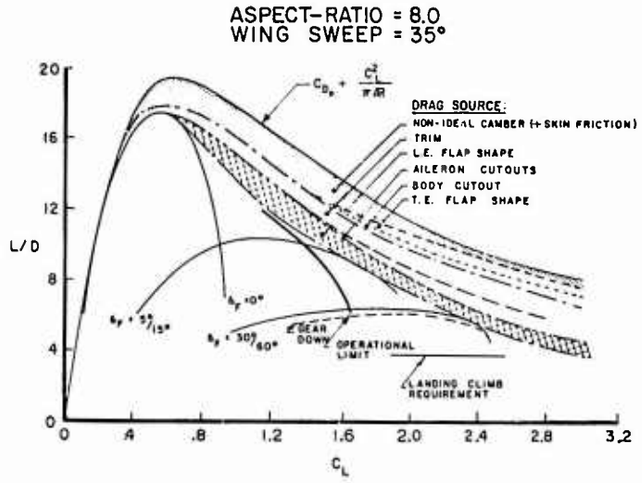

Fig.10 Lift-drag characteristics

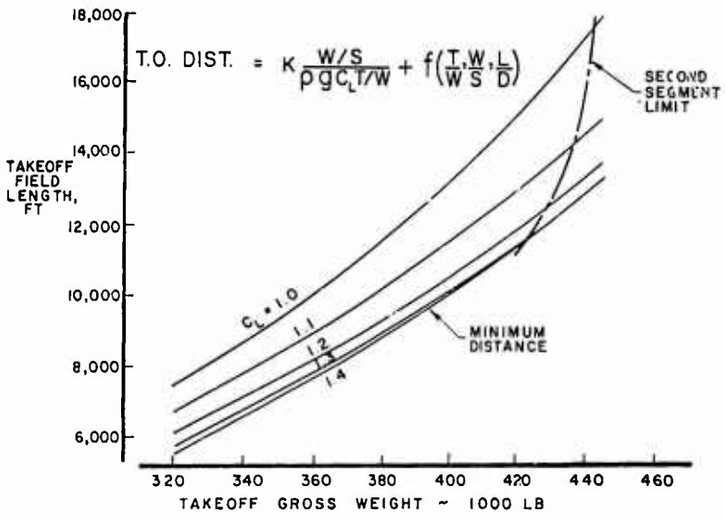

Fig.11 Takeoff performance

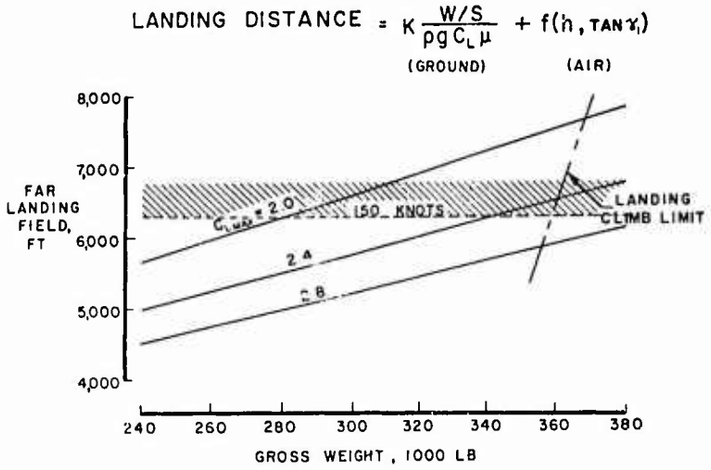

Fig.12 Landing performance

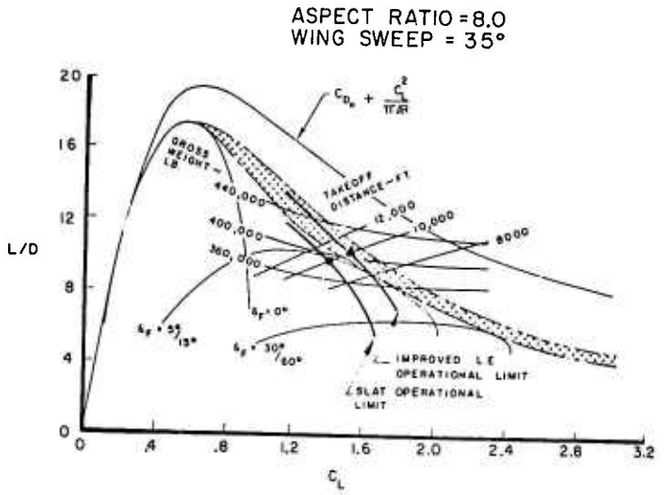

Fig. 13 Performance potential

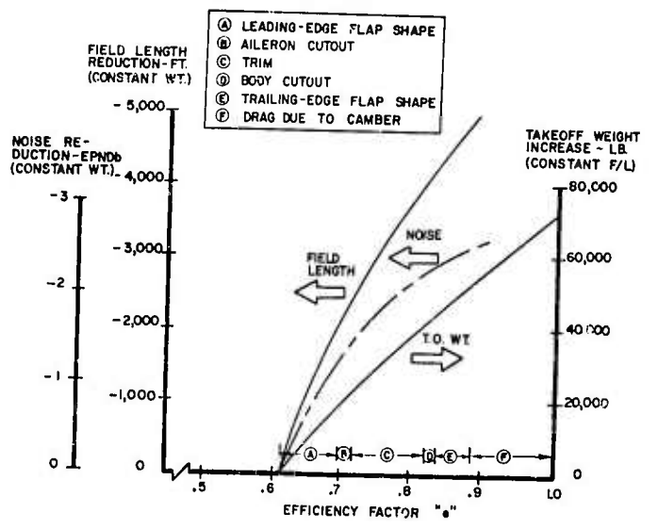

Fig. 14 Takeoff performance gains

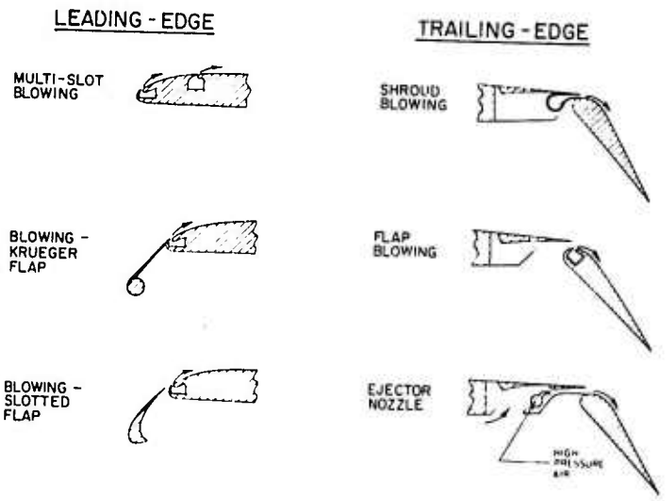

Fig. 15 Blowing BLC concepts

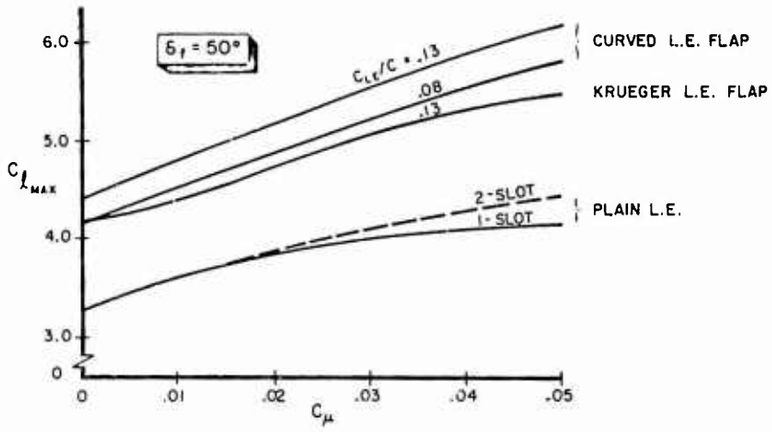

Fig.16 Leading-edge blowing two-dimensional data M = .165

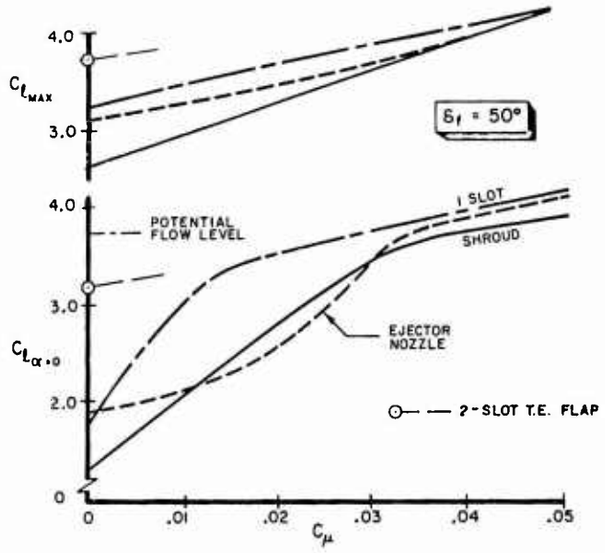

Fig.17 Trailing-edge blowing two-dimensional data M = .165

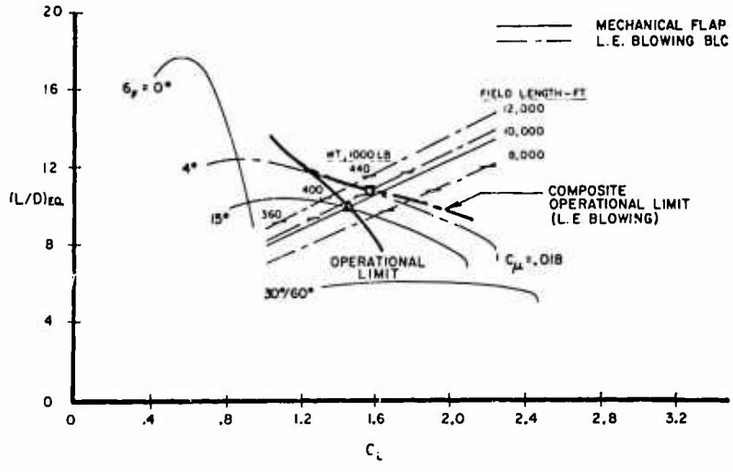

Fig.18 Performance potential leading-edge blowing

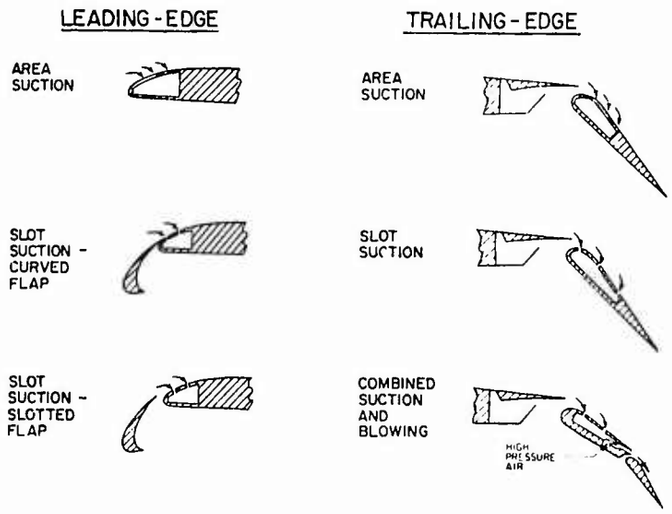

Fig.19 Suction BLC concepts

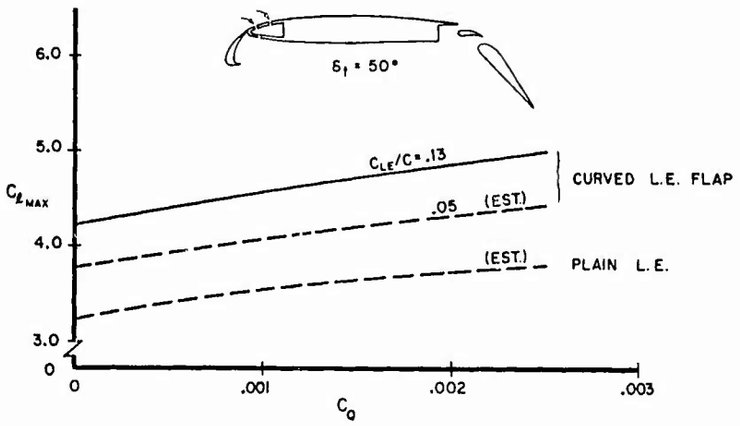

Fig.20 Leading-edge suction two-dimensional data M = .165

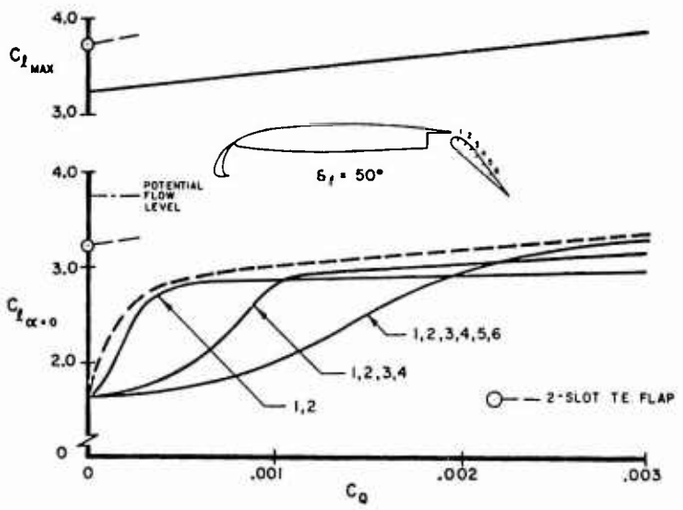

Fig.21 Trailing-edge suction two-dimensional data M = .165

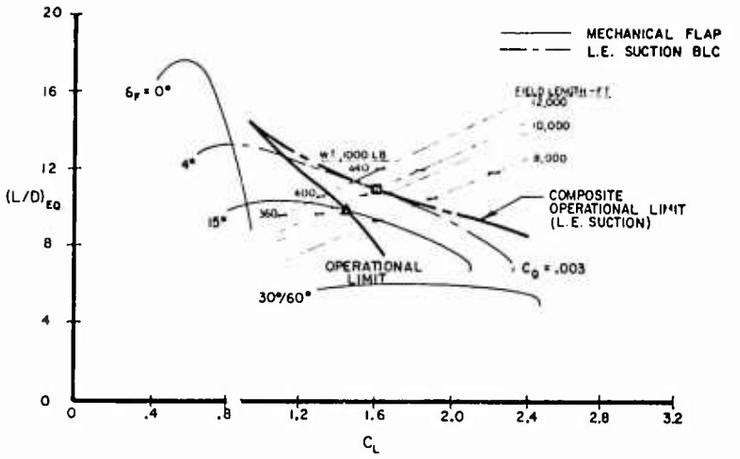

Fig.22 Performance potential leading-edge suction

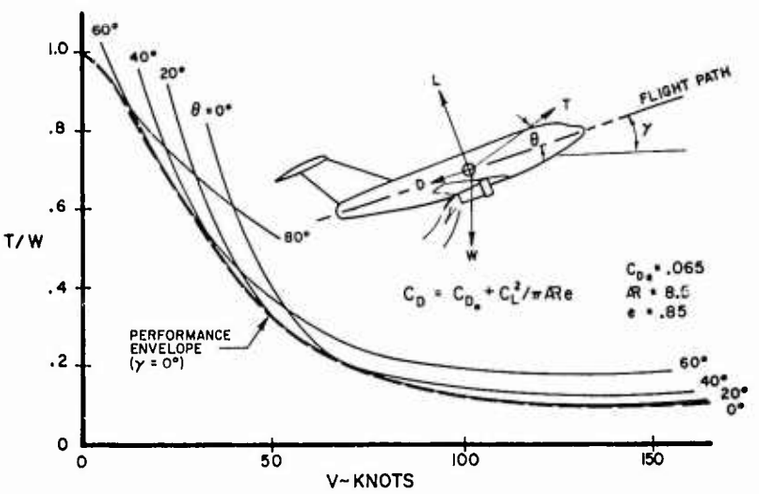

Fig.23 STOL thrust requirements. Wing loading = 80 PSF (landing)

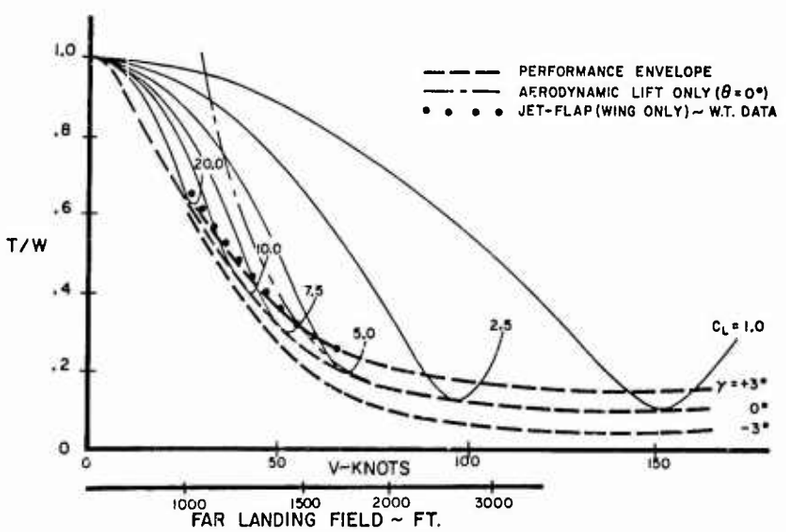

Fig.24 STOL landing performance. Wing loading = 80 PSF

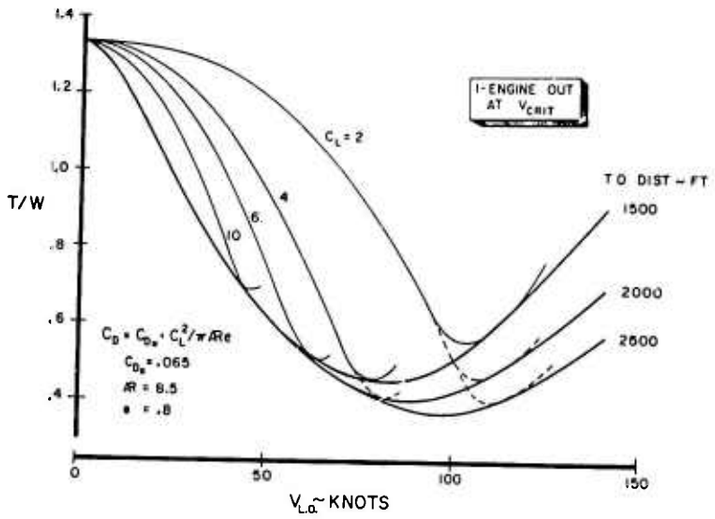

Fig.25 STOL takeoff performance. Wing loading = 90 PSF

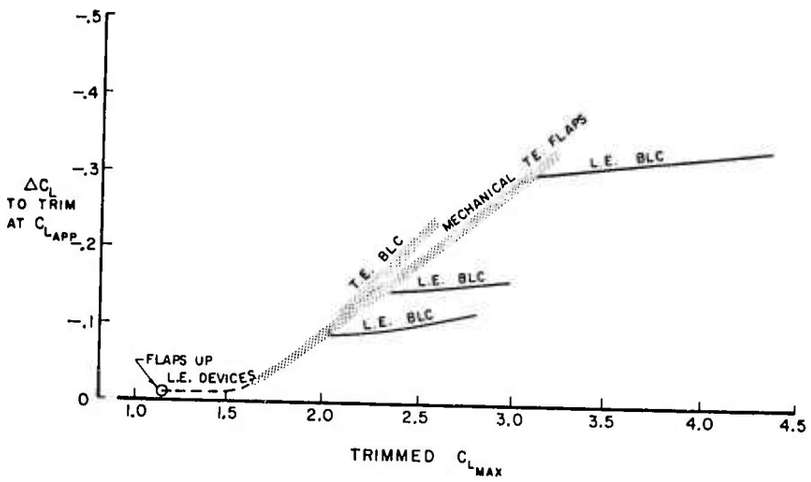

Fig.26 Effect of trim on lift

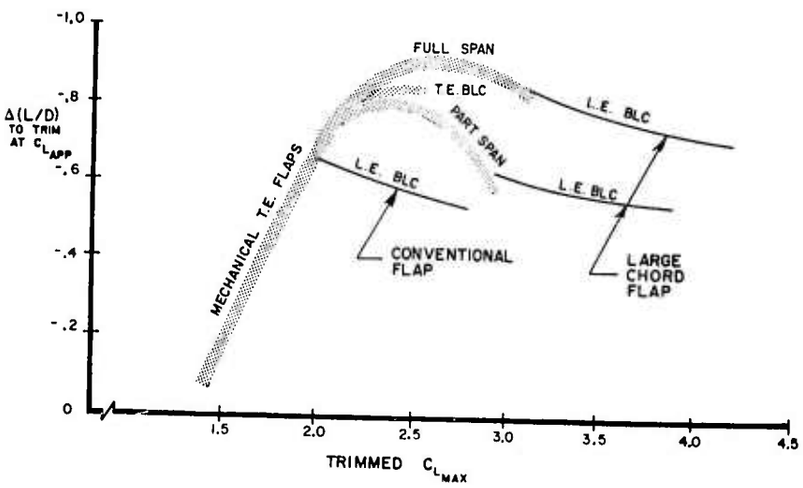

Fig.27 Effect of trim on L/D

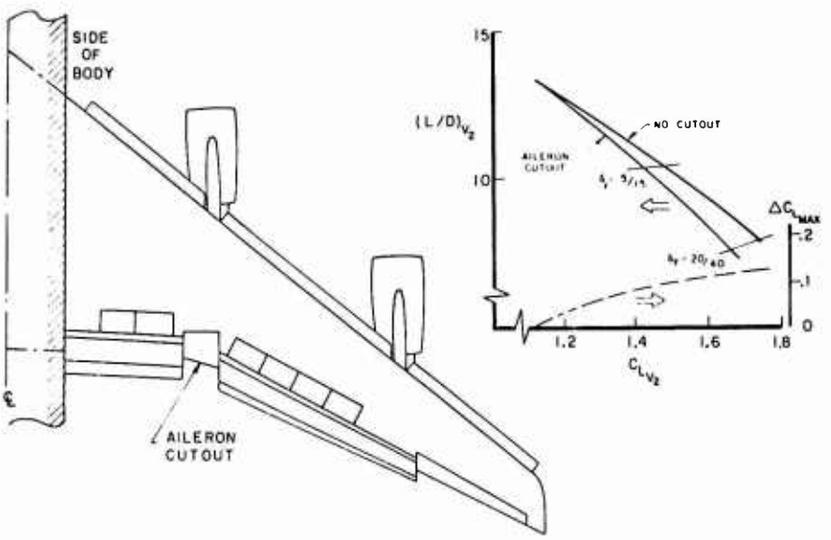

Fig.28 Lateral control

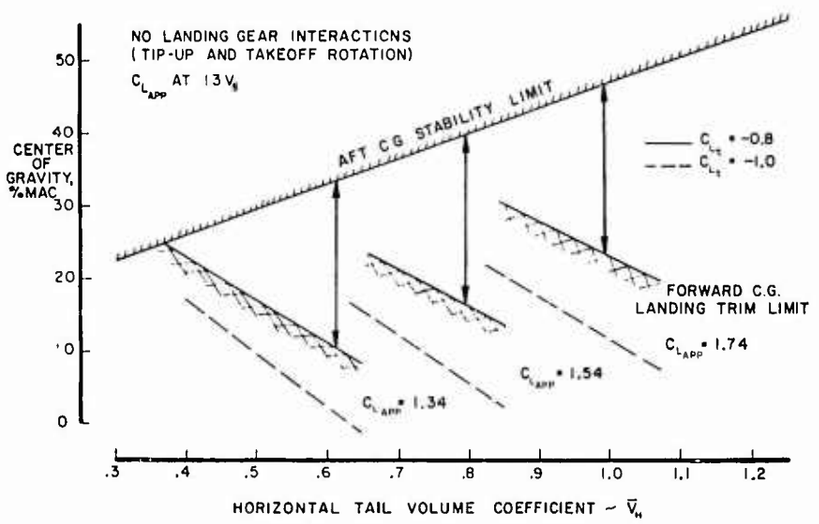

Fig.29 Tail sizing for high-lift flaps

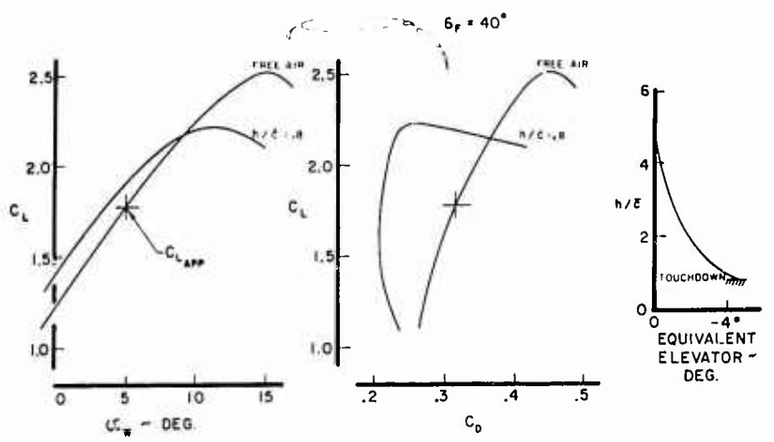

Fig.30 Ground effect. Tail on, $s_{FRI} = -10°$

SUMMARY OF DISCUSSION

relating to

TRANSPORT APPLICATIONS FOR HIGH-LIFT SCHEMES

1. Take-off and Landing Design-point Distances (Fig. 4 of Paper)

The take-off distance of 11,000 ft. was chosen here as being representative for a contemporary long-range jet transport. Since the aircraft in this particular example is obviously take-off field length critical, the prescribed landing distance of 4,800 ft. is not significant here except that it corresponds to a somewhat higher value of wing area than would be necessary to minimise gross weight while meeting the take-off distance requirement. This would be desirable to provide growth potential.

2. Difference between the Slat and L.E. Flap Configurations in Fig. 8 of Paper

Since the slat is a device which is deployed from the upper surface of the wing, its shape cannot easily conform to the ideal contour necessary to achieve the highest $C_{L_{max}}$. Experience shows that a L.E. flap which is deployed from the lower surface can be made flexible and incorporate a rotating nose-piece. These features taken together provide the ideal surface contour needed. The values of $C_{L_{max}}$ shown in Fig. 8 for these two devices are representative of the landing configuration for a wing with 35 degrees sweep.

3. Accentuation of High-speed Buffet Problems by High Wing Loading

Some contributors argued that, since high-speed buffet problems tend to be accentuated by high wing loading, it would appear difficult to justify a design point selection close to the optimum indicated in Fig. 1 of the paper. It was asked also whether this offset the importance of high-lift system improvements. The lecturer agreed that buffet considerations were indeed important and could limit the wing loading of a particular aircraft design. However, he considered that there is still considerable pay-off for improved high-lift systems in the example given, without going all the way to the cruise optimum. Also, this situation served to indicate the importance of further wing design effort to improve high-speed buffet margins.

4. Limits Corresponding to Lift Curves for Improved Mechanical Flaps in Fig. 7 of Paper

The improvement levels shown for leading-edge flaps correspond to recent experience at Boeing's in the analytical design of a series of devices based on keeping the peak pressures to a minimum. The trailing-edge levels are for full-span double-slotted flaps developed from similar considerations and adjusted to the final configuration on the basis of wind-tunnel tests. The value of $C_{l_{max}}$ ($\alpha = 0^{\circ}$) for the landing configuration is about 85 per cent of the potential flow value.

5. Basis of T.E. Flap System Selection in Fig. 9 of Paper

Since the aerodynamics of the flap systems shown in Fig. 9 were said to be nearly equivalent, it was asked how other considerations such as weight, complexity, etc. enter into the final selection of the system. The lecturer commented that experience with the above types of flaps indicates that chord extension can be largest for the triple-slotted arrangement, thus providing a significant lift advantage. Obviously, the complexity of the system as well as its suitability for take-off (and even cruise) depends on the ingenuity of the designer, so that it is difficult to generalise on the relative merits of the various types. However, in situations where landing performance (i.e. distance, speed, attitude) is critical, the triple-slotted flap is considered usually to have the overall advantage, in spite of small weight penalties and perhaps others.

ANALYSIS OF COMBAT AIRCRAFT APPLICATIONS FOR LIFT-AUGMENTATION DEVICES

by

R.Taisseire

Division Aerodynamique, Bréguet Aviation
Vélizy, France

SUMMARY

This paper presents a general review of the more impor' ant problems associated with the design of high-lift systems for combat aircraft. These problems are often very complex and their satisfactory solution always implies a compromise between the high and low-speed characteristics. It must also be stressed that performance and flying qualities cannot be considered separately as any modification of one will have an effect on the other.

Low-level high-speed flying requires small wing thickness to chord ratio (about 5 to 7%), high sweep angle (35° to 45°), small aspect-ratio (3 to 4) and high wing loadings (about 400 to 500 kg per sq. meter). With such a wing, it is particularly difficult to provide good take-off and landing performance for short field operation while maintaining good flying qualities at low speeds.

Very effective high-lift devices are needed to achieve the low stalling speeds required for short take-off and landing distances and their design must be such as to provide a satisfactory level of control in the low-speed flight range.

The following review is intended to clarify the problems encountered in achieving these aims and to indicate ways of solving them.

ANALYSIS OF COMBAT AIRCRAFT APPLICATIONS FOR LIFT-AUGMENTATION DEVICES

R.Taisseire

1. DEFINITION OF THE MAXIMUM PERMISSIBLE C_L

It is generally accepted that, with the kind of aircraft we are considering, the speed, when clearing a fifty foot obstacle, must be at least equal to $1.2V_s$, both for take-off and for landing.

V_s is the stalling speed, defined by: $W = \frac{\rho}{2} . V_s^2 . S . C_{L\,max}$.

For a given configuration, the maximum usable $C_{L\,max}$ is defined as being that value of C_L beyond which the control of the aircraft is no longer possible. This control loss can occur as a deterioration in either longitudinal flying qualities (pitch-up), or in lateral flying qualities (loss in roll control, uncontrollable motions in roll or yaw). One thus has to look first at the flap configuration which can produce, at a given angle of attack, the highest possible value of C_L. Then, one must adapt this basic shape to the aircraft configuration in order to maintain, at these high angles of attack, acceptable longitudinal and lateral flying qualities.

2. CHOICE OF A HIGH-LIFT DEVICE CONFIGURATION GIVING, AT SOME ANGLE OF ATTACK, THE HIGHEST POSSIBLE INCREASE IN C_L

2.1 Choice of the Trailing-Edge Flap

First it must be stated that blown flaps will not be considered here. It would certainly be feasible to consider the use of blowing for certain cases, in particular on carrier-based aircraft where the deck landing problem necessitates very high maximum C_L's. But we think that the loss in thrust involved is only acceptable when very high T/W is available, and that it is possible to obtain very high $C_{L\,max}$ even with highly swept wings without the complications of blowing. This means that considering the overall balance between thrust, weight and maximum permissible C_L, classical high-lift devices compare favourably with devices involving Boundary-Layer Control.

Now we consider the type of flap which is most suitable for fighters. Our choice is the slotted flap with vane (see Figure 1). In two-dimensional conditions it is able to give substantially higher C_l's than the single flap (up to a 50% increase) and it does this without any great mechanical complications.

The use of a triple-slotted flap would theoretically result in a two-dimensional supplementary C_l of the order of 0.4 to 0.5 (Fig.2), which reduces to about 0.2 when taking the sweep and aspect-ratio into account (Fig.3). But in the overall balance, this gain would be reduced on wings of such small dimensions, because of very definite problems:

- external fairings, resulting in high drag at high speeds;
- cut-outs at the level of the rails and jacks, cancelling part of the gain in C_l ;
- big increase in weight;
- maintenance problems due to the complexity of the device.

Even on transport aircraft, where there is much more room for jacks, rails and rollers, the problem of the use of such flaps has not been easily solved. Thus for fighter aircraft, the solution of the problem can be considered impossible.

Our choice of the type of flap thus being justified, we now consider the determination of its relative chord, of the slot's shape and height, of the leading-edge radius, and of the flap's optimum rearwards position. This can be done in various ways (see Figure 1). Some of the lecturers have spoken to your about such an optimization by theoretical methods. From a practical point of view, I think that the final and definitive choice has to be made in the wind-tunnel, using models on which these parameters are varied. A rectangular wing model allows an approximate choice to be made, and the final adjustments are made on a model representing the aircraft.

Experience shows that the optimum characteristics of the flaps on such planes, are, on the average, as follows:

relative chord of the order of 30 to 35%;

maximum deflections of 40 to 45 degrees;

backwards position from 6 to 9% of the total chord.

One can obtain similar results with main and secondary slots of various heights, but these slots must have a sufficiently converging shape to be really effective. Any divergence of the slot is unacceptable (see Figure 3).

A model built in order to determine the final configuration must have variable flap and vane positions, with both longitudinal and vertical movement; it would also be worthwhile to test various types of vane, considering as a basic parameter the leading-edge radius.

2.2 Choice of the Wing Leading-Edge Modification

In parallel with the definition of the trailing-edge flap, one also has to define a type of leading-edge slat. If one has a very effective trailing-edge flap, the $C_{L\,max}$ will be determined not by stall of the flap itself, but by stall of the wing in front of the flap (see Figure 4).

Correct modification of the leading-edge can delay the beginning of this phenomenon. This can be achieved in various ways. One can camber the leading-edge, which is the less effective solution, or fit it with a movable slat, of which the most effective kind is the slotted one.

In two-dimensional cases, such a slat can result in a $C_{L\,max}$ increase of the order of 0.3 to 0.4. Also, if well designed, it can give a $C_{L\,max}$ increase of 0.15 to 0.20 on the swept wing (see Figure 5). However, a slotted slat is more complex than other types of leading-edge device: jacks, rails and rollers are necessary. But, taking into account the resulting increase in maximum lift, and the slat's favourable effect on the longitudinal and lateral flying qualities, the complication seems to be fully justified.

2.3 Maximum C_L in Two-Dimensional Flow

Finally, the system of flaps and slats we have defined can give, in the two-dimensional case, a value of the maximum C_L of the order of 3 to 3.5.

3. FITTING THE HIGH-LIFT DEVICE ON THE AIRCRAFT TO OBTAIN THE MAXIMUM PERMISSIBLE C_L

The type of flaps and slats now having been defined, one has to incorporate them efficiently on a wing whose general characteristics, flaps up, have been determined by performance and flying quality considerations at high speeds.

Let us recall once more the average wing's characteristics:

low relative thickness (5% to 7%);

low aspect-ratio (3 to 4);

high sweep (35° to 45°).

Before optimising a given type of high-lift device on such a wing, one first has to analyse its stalling mechanism, flaps fully down: this will give an understanding of the adverse changes which occur at high angles of attack, both in longitudinal motion as well as in lateral and transverse motion. This analysis will allow us to look at the appropriate procedures for avoiding these changes and to obtain the best possible efficiency from the high-lift system.

3.1 Mechanism of the Stall of a Highly-Swept Wing Developing High Lift

The stalling mechanism of such a wing, with (or without) high-lift devices working, is roughly as follows. Starting from a given angle of attack, leading-edge stall begins at the wingtips. With increasing angle of attack, this stall extends towards the wing root, and the lift becomes increasingly concentrated on the inner part of the wing (see Figure 6). This produces a variety of effects as follows.

In the stalled part, the lift is decreasing, giving (due to the sweep) some pitch-up tendency. The smaller the aspect-ratio, the more limited this tendency, due to the fact that the aerodynamic centre moves rearwards in the stalled zone (see Figure 7). On the other hand, due to the lift concentration in the central zone, the rate of change of downwash $d\epsilon/d\alpha$ behind this part of the wing is increasing with angle of attack. We will see later what conclusions concerning the tailplane position are to be deduced from this fact. Lastly, the stall at the wing-tip produces asymmetrical phenomena (wing drop) and also some loss of control effectiveness in roll due to the tip location of ailerons or spoilers. Further, these troubles are accompanied by buffeting, the severity of which increases with the amplitude of the observed phenomena.

All of these factors – which one can establish in wind-tunnel tests on models without tailplanes – can contribute to limiting the maximum usable C_L. One has therefore to reduce their effect before considering the configuration of the complete aircraft (i.e. the aircraft with tailplane on).

3.2 Solutions for Limiting the Effect of Wing-Tip Leading-Edge Stall on the Maximum Permissible C_L

The most obvious way to limit the wing pitch-up and the asymmetric phenomena involved in stalling is to modify the wing-tip leading-edge in order to prevent the wing-tip stall.

With the exception of the deflection of the slat itself, several complementary means can be used:

- some leading-edge extension on part of the span ("Crusader" type leading-edge);
- leading-edge camber;
- wing wash-out (but not too much, because of the corresponding increase in the wing's angle of attack at a given C_L).

Figure 8 shows all of these modifications. The spanwise extent of the leading-edge slat and of the local modifications we have enumerated will obviously depend on the particular case being considered, and one cannot state general rules.

From the very beginning of the design it must be ensured that various combinations of slat span and chord, camber and degrees of wash-out can be obtained on the wind-tunnel model. In the same way, flap and slat deflections and slots must be capable of being modified if necessary.

An additional method of limiting the effects of leading-edge stall of the wing-tip is by differential deflection of the trailing-edge flaps – deflecting them less over the outer part of the wing. This method will be increasingly efficient with increasing extension of the flaps over the wing span, and is therefore most useful when full-span flaps are used. It is advisable – right from the beginning – to split the flaps at some spanwise locations, and also to incorporate some possible adjustment of slots and, of fore-and-aft position on the wind-tunnel model.

Finally, it is also possible to improve stalling conditions by using some complementary means such as leading-edge notches, or better, fences whose chordwise extent will be systematically varied, as will be their height and spanwise location (see Figure 9). Roughly speaking, the effect of such a device is to divide the flow into two parts of limited aspect-ratio, and so to reduce the intensity of the lateral flow and of the leading-edge separation.

The measurements made while varying these parameters must, in all cases, be guided by flow visualization, which is a very direct and quick means for choosing the configurations to be considered.

Summing up, tests without a horizontal tailplane generally permit the choice of a configuration of slats and flaps which is as good as is possible. But such tests are obviously insufficient for the estimation of the maximum permissible C_L of the complete aircraft. This value also depends on the shape and position of the horizontal tailplane.

3.3 Influence of the Height of the Horizontal Tailplane on the Maximum Permissible C_L of the Aircraft

Even taking as much care as is possible, one can only delay the angle of attack at which the leading-edge tip separation finally occurs. On the model without a tailplane, it is in fact acceptable that at a very high angle of attack, a certain tendency for pitch-up exists. Its effect is to limit the nose-down C_m to be trimmed near the $C_{L\max}$, and thus to decrease the loss of C_L due to the trimming in the vicinity of the stall (see Figure 10). But obviously, this pitch-up has to be cancelled and transformed into a pitch-down on the complete aircraft. This can be achieved by accurately positioning the horizontal tailplane.

When the angle of attack is increasing, it has been seen that the lift is concentrated towards the plane of symmetry and that, due to this fact, $d\epsilon/d\alpha$ is increasing behind this part of the wing. If the tailplane is located within the vortex centre zone, where $d\epsilon/d\alpha$ is the most intense, it will result in some destabilization, which will become increasingly stronger as the angle of attack is increased. In this case, the effect of the tailplane will be to increase the pitch-up.

Let us recall that the increase in stability due to the tailplane can be written:

$$\Delta\left\{\frac{\partial C_m}{\partial \alpha}\right\}_H = \frac{q_H}{q_0}\left\{\frac{\partial C_L}{\partial \alpha}\right\}_H \cdot \left(1 - \frac{\partial \epsilon}{\partial \alpha}\right) \cdot \frac{S_H L_H}{Sc} .$$

This stabilization is thus higher as $d\epsilon/d\alpha$ is smaller.

Now, on one hand, the tailplane will tend to enter the vortex zone when the angle of attack is increasing, if it is in a high position with respect to the wing. On the other hand, it will have a tendency to go away from the vortex, if it is in a low position. Note that when the tailplane turns through an angle α, the vortex line turns only through ϵ (see Figure 11).

Thus, one can say that the high position increases the pitch-up tendency, while the low position decreases it and can be expected to give some pitch-down. This is confirmed by many experimental results, and Figure 12 illustrates this influence of the relative position in height of the tailplane and the wing.

The practical conclusion is finally that, for a given wing-fuselage configuration, the maximum permissible $C_{L\,max}$ will be greater with a low tail than with a high one, because in the latter case it will be limited by pitch-up.

3.4 Buffeting Problems

Buffeting problems are connected partly with the stall of the wing and partly with that of the tailplane.

It is obviously difficult to determine the intensity of in-flight buffeting from the usual test results giving overall force and moment measurements. The buffet due to the wing can be related to the beginning of wing-fuselage pitch-up (see Figure 13). Further, concerning the part due to the tailplane, it is possible to try and determine by flow visualization the angle of attack at which the lower surface of the tailplane is stalled, and so approximately define the part of the polar curve where the buffet will start in flight (see Figure 14).

One can also determine the buffeting in the wind tunnel through a harmonic analysis. However, one has to wait for flight results to define, not the onset of the phenomenon, but its exact intensity. Naturally, it will be less intense if the flow on the wing has been improved by the procedures already described and if the tailplane is in the most favourable position with respect to separation over the lower surface of the tail which means that the tailplane is in a low position.

3.5 Lateral Control Problems of High-Lift Aircraft at High Angles of Attack

The main stability and lateral control problems occurring at high angles of attack for a high-lift aircraft, which put a limiting value on the maximum permissible C_L, are the following:

- asymmetries in roll near the stall;
- loss in effectiveness of the control system in roll;
- loss in efficiency of the vertical fin;
- adverse yaw.

These various problems will now be successively examined.

3.5.1 Asymmetries in Roll near the Stall

These asymmetries are obviously due to the fact that stall is occurring at the tip of the wing, and that the losses in lift on the two sides are not absolutely symmetrical.

This results in the appearance of unacceptable rolling moments, which can be relatively high due to the size of the moment arm, which is practically equal to the semi-span. The remedy obviously consists in delaying these phenomena and in minimising their magnitude. The solutions we have talked about to improve the flow on the wing are thus also effective in solving this problem; namely, leading-edge camber, wing wash-out, well designed slats, differential flap deflection, wing fences, etc.

It is possible, in the wind tunnel to combine flow visualization with rolling moment measurement. One can thus define the angle of attack at which the trouble occurs. Due to scale effect, this angle will generally be 2° to 3° higher in flight, but the methods used to decrease the rolling moment on the model and to delay its onset till a higher angle of attack is reached will also be effective on the actual aircraft.

3.5.2 Loss in Roll Effectiveness at High Angle of Attack

Due to wing-tip separation, the parts of the roll control devices (ailerons and spoilers) which are located in that zone will progressively lose their efficiency as angle of attack is increased. It is thus essential, in order to avoid a total loss in control efficiency, to locate as much of these control devices out of the stalled zone as is possible. From this point of view, a roll control system consisting only of ailerons appears impractical on an aircraft with a highly swept wing. In order to maintain adequate efficiency at high angles of attack, one would have to use ailerons extending over such a large part of the span that the effectiveness of the high-lift system (being limited in span) would be considerably lowered.

One therefore has to specify either

spoilers alone, located in the best spanwise position, and allowing full-span flaps to be used;
or a combination of ailerons and spoilers, the proportion of each being accurately determined by low and high speed considerations.

From the point of view of the maximum permissible C_L, each of the configurations can be envisaged. But the former may, in fact, result in a somewhat higher value of $C_{L\,max}$. While its practical realization is a bit more difficult, experience proves that it is achievable. However, a very high lift effectiveness which results in a high permissible C_L can lead to a number of other problems which we will look at in Section 4.

3.5.3 Adverse Sideslip Problems on Entry into a Turn near the Stall

This problem concerns all of the aircraft of the type we consider, at very low speeds. In a low-speed entry into a turn the lateral component of the weight causes the aircraft to acquire some adverse sideslip (see Figure 15). This sideslip tends to decrease the roll rate according as to how effective the high-lift system is, because of the increased dihedral effect. (We recall that l_v increases with ΔC_L due to the flap deflection).

The sideslip tendency is aggravated by the fact that n_v tends to decrease when the angle of attack is increased. Figure 16 shows the variation of l_v and n_v as functions of the flap setting and of the angle of attack.

The situation may be improved by using the rudder, or by incorporating some roll-yaw coupling. A very good solution results from using differential deflection of the horizontal tailplane. At high angles of attack, the main effect of such a device is to give direct yaw (and very little roll). Its use then increases the roll rate, not by its direct roll effect (because it is not increasing l_ξ by very much), but by the cancellation of the adverse sideslip by its resulting high values of n_ξ. If such a system is adopted, obviously its amplitude must be decreased at higher speeds. But this is not the subject of this lecture.

3.5.4 Loss in Effectiveness of the Vertical Fin at High Angles of Attack: Variations in Yaw

The maximum permissible C_L can be determined in certain cases by the loss in fin efficiency at high angles of attack. When the flaps are strongly deflected, the decrease in n_v is less sensitive to incidence change than it is for the clean aircraft (see Figure 16). Most of the n_v is due, in that case, to the wing itself; induced drag being bigger on one side than on the other. Nevertheless, n_v finally decreases at high C_L, which is enough to produce some loss of yaw control in certain cases. This kind of trouble can, in some cases, define the maximum permissible C_L. Improvement of the situation results from:

the best possible design of the slats and flaps;

the use of a big enough fin and also a fairing between the fuselage and the fin (allowing some retention of the lateral lift at high angle of attack), or a ventral fin;

giving the same kind of effect (see Figure 17).

The use of such devices obviously depends on the general configuration. One has to test these in the wind tunnel, and to retain the best design.

3.6 Recapitulation

The methods of achieving the maximum permissible C_L and thus the minimum approach and take-off speeds have been examined (expected max. C_L from 1.6 to 1.8). This problem being solved, we will now look at the problems arising at normal approach and take-off angles of attack due to the realization of such high values of the maximum C_L.

4. PROBLEMS CONNECTED WITH HIGH-LIFT SYSTEM DEVICES AT NORMAL OPERATING ANGLES OF ATTACK OF THE AIRCRAFT

4.1 Problems Connected with the High Values of C_m due to Flap Deflection

Summarising, high flap deflections produce two opposite effects on all kinds of aircraft:

a direct effect, which is the nose-down moment due to the deflection of the flaps themselves;

an indirect effect, due to the change in flow direction over the horizontal tail, giving some nose-up moment and tending to compensate the first effect.

It may be easily seen that, on a highly swept wing aircraft, the former of these two influences tends to be dominant. It becomes more important as the spanwise extent of the flaps becomes larger. Effectively, the high

C_l values existing at the tip of the wing located behind the C.G. position have a tendency to contribute a very important nose-down moment. The result is that the full effect due to the deflection of the flaps on such an aircraft generally results in a pitch-down tendency.((See Figure 18, showing the order of magnitude of the ΔC_m due to the flaps with the horizontal tailplane off). The several consequences of this result will now be analysed.

4.1.1 Lift Loss due to C_m Trimming

If, at a given incidence, ΔC_m is the pitching moment coefficient without a tailplane, this nose-down ΔC_m must be trimmed by a tail ΔC_l (based on wing area); namely

$$\Delta C_l = + \Delta C_m \cdot \frac{c}{L} ,$$

c being the reference chord (mean aerodynamic chord) and L the distance between the C.G. and the horizontal tailplane aerodynamic-centre.

It is then obvious that the larger the magnitude of the nose down ΔC_m, the larger is the loss in C_l due to the trim. For this reason, one can see that it is possible to find some compromise by limiting the wing span or, better still, by limitng the external flap deflection.

4.1.2 Trim Change During the Flap Deflection Phase

The obvious aim is to have no trim change when changing the flap deflection. However, due to the fact that ΔC_m is more negative when the flap effectiveness is bigger, the total ΔC_m for the entire aircraft starting from a given trim position (flaps up) and keeping elevator angle constant when deflecting flaps will remain negative, and will increase with increasing flap effectiveness (see Figure 19). This means that there will be a change of elevator angle to trim during the flap deflection. A change of more than 5° or 6° is unacceptable, and one has to limit it to the minimum level, for a given desired value of ΔC_L due to the flaps.

In fact, it is possible to have some coupling between the flap and elevator deflection, but this is an additional complication to be avoided as much as possible. One has, in any case, to get the rate of trim compatible with that of the flap movement itself, this generally being of the order of 5 to 10 seconds for the total travel. The best way to limit the trim change is to adjust the fore-and-aft position of the tailplane. Putting the tailplane as close as possible to the wing's trailing-edge is very favourable from that point of view. This is obviously due to the fact that the downflow behind the flaps is more intense as one goes closer to them, so that the nose-up moment due to the horizontal tailplane becomes larger. However, to counteract this advantage, it is necessary to increase the tail plane area in order to maintain a tail volume sufficient to give adequate longitudinal stability. The compromise between these two conditions is obviously not easy to realise.

Finally, we point out that differential flap settings also help the trim problem, the reason being the same as explained before. We also note that a kinked trailing-edge, giving less trailing-edge sweep just in front of the tail-plane, also gives some benefit.

4.1.3 Forward C.G. Problems at Take-Off and Landing

For the type of aircraft we are considering, the forward C.G. limit is generally defined by take-off or landing conditions.

(a) The critical problem concerns the lifting of the nosewheel at take-off. At the ground roll incidence, the speed for nosewheel lift is that at which the aerodynamic moment (with flaps at the optimum setting and maximum up-elevator) becomes high enough to compensate the nose-down moment due to the reaction on the main wheels and the friction forces (see Figure 20). The aerodynamic moment, with maximum up-elevator, decreases with increase of flap efficiency. Furthermore, the aerodynamic moment becomes less positive, and the nosewheel lifting speed therefore increases, as the C.G. position moves forward.

For a given flap efficiency, it is thus necessary to scale the horizontal tail plane so that this speed, using the envisaged maximum up-elevator, remains low enough (for example 1.1 V_s) for the most possible forward C.G. position at take-off. It should be noted that it is imperative to take ground effect into account in this evaluation. Its adverse effect will be analysed in the paragraph concerning the approach and landing, but the philosophy is the same at take-off. In other words, the decrease in downwash near the ground, at a given angle of attack, tends to increase the nose-down moment due to the flap deflection, and thus also to increase the elevator deflection necessary to give the required nose-up moment.

One can say finally that, in some cases, nosewheel lifting can determine the limiting forward position of the aircraft's C.G.

(b) *At approach and landing conditions*

As a general rule, the flare problem at landing still defines the forward C.G. limit of the aircraft. In order fully to utilise the high-lift possibilities of an aircraft, one has to assume the maximum value of the final approach and landing C_l in flare for all possible C.G. positions at landing. One then has to remember

that, during the flare, the substantial reduction of downwash at the tailplane produces an additional nose-down moment. This results in an increase in the elevator deflection needed to trim the aircraft. With the C.G. forward of a certain position, the trimming of the expected C_L becomes impossible (Fig.21). This C.G. position then becomes the forward limit, if no other condition is more stringent. One has, in any case, to arrange the balance of the aircraft in such a way that the C.G. is aft of this position.

4.2 Problems Concerned with Drag

The high drag due to an effective high-lift system results in some problems at landing as well as at take-off. These are well known and it is not necessary to debate them very much here.

4.2.1 Take-Off

We consider the most general case of a multi-engined aircraft. Two possibilities have to be considered:

(a) *Short take-off conditions*

In this case, engine failure or safety at take-off are not to be taken into account. For a given weight, one has then to look at the best compromise between a high take-off C_L and a value of $C_D - C_L$ giving as high an acceleration as possible. For relatively low weights, the decrease in acceleration due to high flap deflections is generally compensated by the resulting decrease in the take-off speed. With increasing weight (and in particular in overloaded take-offs) the effect of the drag becomes preponderant, and above a certain value of the weight one has to decrease the flap deflection (see Figure 22).

(b) *Take-off with engine failure – determination of minimum runway length*

Considering the engine failure case, one has to select a take-off speed such that the vertical speed with the remaining engine working (and if necessary after release of the external stores) is large enough to clear 50 ft. This speed must, in any case, be larger than $1.1\ V_S$. If this speed has not yet been attained, one has to wait for $1.1\ V_S$ as a minimum for the lift-off, and the speed at the time the obstacle is cleared has to be $1.2\ V_S$. In any case it may be worthwhile to decrease the flap deflection (see vertical speeds vs flap deflection in Figure 23).

The lift-off speed having been so defined, one now determines the critical speed; should an engine failure occur at the critical speed, the runway length required to carry on with the take-off and clear the 50 ft obstacle or to stop the aircraft will be the same. This length is obviously the minimum allowing for safety. In the case of high overloads this speed would occur after the lift-off speed, and in that case, the minimum runway length will be defined by the acceleration stop. Figure 24 illustrates such a situation and shows the 50 ft clearing and the acceleration stop distances. It is supposed that in the case of failure occurring after take-off, the external stores will be released at a given altitude (of the order of 15 ft).

4.2.2 Approach and Landing

For approach and landing conditions, the most critical problem in connection with drag is that of engine failure on a two-engine aircraft, and chiefly at high weights. This problem is even more critical when the descent slope is specified (GCA or ILS approaches), and yet even more when the approach speed is limited to a maximum (carrier landings). The aircraft must then have enough thrust to ensure adequate vertical speed variations around the mean slope as well as possibly at the given speed. In the case of ILS or GCA approaches, one generally considers that the thrust and lift-drag ratio must be high enough for the aircraft to be able to maintain level flight, flaps and under-carriage down. This is not always possible with flaps fully down (Fig.25); for example, just after take-off and in high temperature conditions.

One has thus to pay particular attention to this problem, right from the beginning of the design, and always to consider a flap configuration which permits the performance described.

4.3 Problems Connected with Lateral and Transverse Flying Qualities

4.3.1 Rolling Efficiency

At normal approach and take-off angles of attack and speeds, the control system in roll must be designed to be very efficient, especially in the case of flight in a cross-wind. This problem is particularly critical with a high-lift device of high efficiency, due to the large rolling moments with sideslip resulting from it. But, in addition to the high rolling efficiency, one also requires rolling moment to increase steadily with control deflection, so as to avoid pilot induced oscillations. To sum up, high values of l_ξ and $l(\xi)$ curves as linear as possible have to be obtained.

(a) *Realisation of effective roll control devices*

It is possible to obtain effective roll control by using an aileron-spoiler combination, or spoilers alone, in order to have the benefit of high-lift devices extending over the full span. To obtain adequate efficiency from ailerons alone requires that they should be of excessive spanwise extent, thus limiting flap efficiency

except if the aileron itself is also used as a flap. The remarkable effectiveness of the spoiler-ailerons or spoilers alone can be illustrated by giving the order of magnitude of the obtainable l_ξ. For the clean aircraft, a reasonable value of l_ξ is of the order of 0.0005. Flaps down, values three times higher can be expected, which could not be obtained with classical ailerons.

(b) *Linearity of the $l(\xi)$ curve*

This point particularly concerns spoilers. It has been seen that the efficiency of these increase as the flap deflection increases. This is due to the destruction of the flap slot effect by the spoiler (see Figure 26), resulting in high losses of local C_l and thus in a large rolling moment, which in many cases does not increase steadily enough with deflection.

If one wants to avoid P.I.O.S. on the approach, one has to pay particular attention to the problem. It can be completely solved by suitable choice of the following parameters:

spoiler chordwise and spanwise location;

geometry of the flap slope itself;

differential deflection of the flaps;

occasional use of non-linear gearing between the stick and the elevator.

No general rule can be recommended, because the choice of a solution is a matter of compromise between low and high speeds, and because the longitudinal stability and maneuverability problems we have previously discussed must also be taken into account.

4.3.2 Dynamic Stability

The use of a very effective high-lift device results in significant variations of the aerodynamic derivatives, compared with those obtained on the clean configuration. The order of magnitude of these variations can be indicated; for example, l_v and n_v can be doubled when flap deflection increases from zero to the maximum value; the dynamic derivatives, except l_r, which can be doubled, do not vary much. Typical variations of these derivatives are tabulated for an average angle of attack (of the order of 5°):

Flap setting	0°	*Full deflected*
l_v	.10	.20
n_v	.15	.30
l_p	.30	.30
n_r	.50	.60
l_r	.15	.30
n_p	0	0

Consider the lateral stability equations:

(i) $$\frac{d\beta}{dt} + r \quad p\alpha = \frac{Y}{mV}$$

(ii) $$\frac{dp}{dt} \quad \frac{E}{A}\frac{dr}{dt} = \frac{l}{A} L$$

(iii) $$\frac{dr}{dt} \quad \frac{E}{C}\frac{dp}{dt} = \frac{l}{C} N$$

where A is the principal roll inertia;
C is the principal yaw inertia,
E is the x z product of inertia.

When their solution is obtained as a function of the speed, this being correlated with the angle of attack, one finds that the terms having the most effect on the damping ratio are those which are dependent on the angle of attack, and also (to a lesser extent) those depending on the product of inertia term E.

These effects are, in fact, increased by the large value of l_v.

The variations are as follows:

the damping decreases with decrease of α, i.e. with increase of speed;

the effect is most important when E is large, i.e. when the principal axis of inertia in roll is pitched nose-down.

Figure 27 shows these effects in the (ξ,ϕ/v) plane; also shown are handling assessments based on the Cooper scale.

We see that an effective high-lift device combined with a nose-down principal axis of inertia can lead to dutch roll instability when the speed increases. The problem is then to choose a flat deflection and inertia axis position such that this instability can only occur at a speed higher than the design speed of the flaps.

4.4 Wave-Offs (Overshoots)

Although not directly connected with the flap configuration, the problem of overshoot at landing has enough importance to be noted as one of the main problems associated with flying qualities at low speeds. It must be ensured, as far as possible, that during this manoeuvre no moment variations occur, especially in the pitching-down direction. It is therefore necessary to eliminate the reasons giving rise to such a tendency as early as possible in the design. We recall the two main reasons:

(a) *The first one is the C.G. position with respect to the thrust axis.* It is imperative that the thrust axis position be as near as possible to the C.G.

(b) *The second one can be the jet-elevator interaction.* Such an interaction essentially depends on the configuration of the rear of the aircraft, and can be determined by direct measurements. These measurements must be performed and the necessary modifications made as soon as possible, in order to avoid later modifications arising from prohibitive elevator deflections during overshoots.

5. ADDITIONAL PROBLEMS

These problems will only be mentioned because the solutions to them are not always required. They are interaction problems and may generally be solved using the results of wind-tunnel tests.

5.1 External Stores Effect

These problems due to the presence of external stores are essentially stability ones. They may be more or less critical when the flaps are down, but one can say, in general, that if they have been solved for the clean aircraft then the effect in the high-lift condition will be very small. Nevertheless, the fact that this is true and that no significant rear C.G. limitation is imposed for take-off and landing should be checked by wind-tunnel tests.

5.2 Problems Due to the Landing Gear

These problems concern:

- the drag;
- the longitudinal stability;
- the longitudinal trimming.

It is necessary to optimize, in particular, the configuration of the undercarriage doors. When the undercarriage is down, as much as possible these doors must be closed. In order to be representative enough, the models being used in wind-tunnel tests must be provided with the cavities existing on the aircraft when the landing gear is down.

5.3 Problems Concerned with Deflection of the Airbrakes

The aircraft behaviour in the high-lift condition when the airbrakes are in use must be considered, with particular attention to the longitudinal stability. One must check that the interactions between the airbrakes, the flaps and the tailplane in the approach configuration do not result in any instability or any important increase in the trim deflection of the elevator. This check must be performed in the presence of ground effect.

5.4 Miscellaneous

In fact, all the problems mentioned in Sections 5.1 to 5.3 also affect the lateral stability and some care must be taken to consider this aspect. In all cases, the effect of thrust must if possible be considered, both far from the ground and near to it.

On carrier-based aircraft, flight path optimization must be very accurately determined using analogue computers or simulators, and taking into account the various effects described above.

The problems of control forces are also important. The way to avoid P.I.O.'s for example, is not only to obtain the best dynamic qualities of the aircraft but also to achieve a good compromise between the stability characteristics and the displacements and forces on stick and pedals. But, if the aircraft is good in itself, this kind of problem is generally solved by adjustments in flight, so will not be considered in this lecture.

Some other problems, concerning the behaviour of the engines at take-off or landing, for example, must also be considered. The effectiveness of the auxiliary doors, in particular, must be very carefully optimized, but it has not been possible to develop them further.

Technological problems of much interest concern the visibility, the methods of achieving flaps and slats without large interruptions at the level of the rails and jacks, the landing parachute behaviour, etc. We can only mention them as being of some particular interest.

6. CONCLUSIONS

As has been stated at the beginning of the paper, the choice of a configuration solving all the problems involved with high-lift devices is very difficult. It must be done mainly by experimental methods. The main problems have been examined and qualitatively discussed with the intention of presenting their most important aspects. In fact, it is possible to enter into quantitative details and experimental results only when speaking of some particular aircraft. It seems to me that the most important thing is to be aware of the questions that have been raised, and not to neglect any of them.

If one takes care in solving these problems, and treats them as interdependent, never losing sight of the repercussions they have on one another, then it will be possible to achieve an aircraft having good performance and good flight qualities in both take-off and landing.

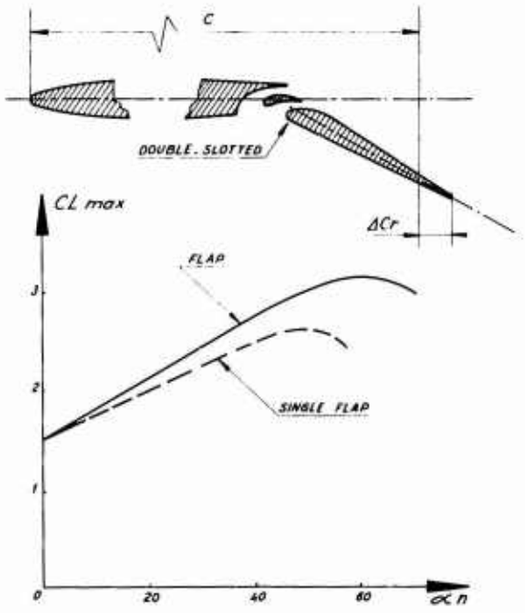

Fig.1 Comparison between the double-slotted flap and the single flap (two-dimensional)

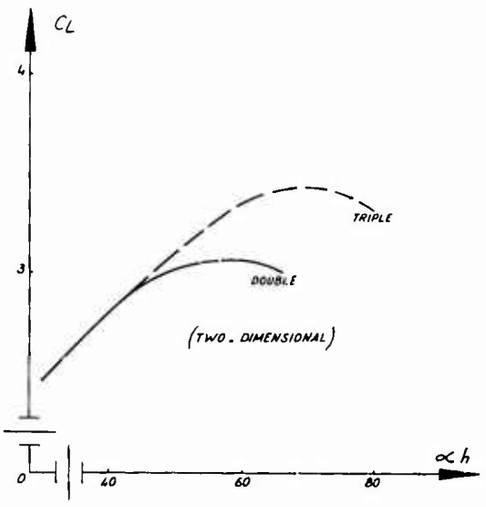

Fig.2 Comparison between double and triple slotted flap efficiency

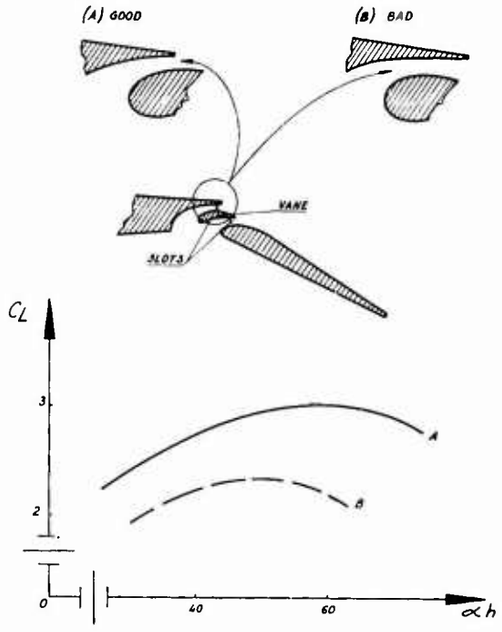

Fig.3 Convergence effect of the slot

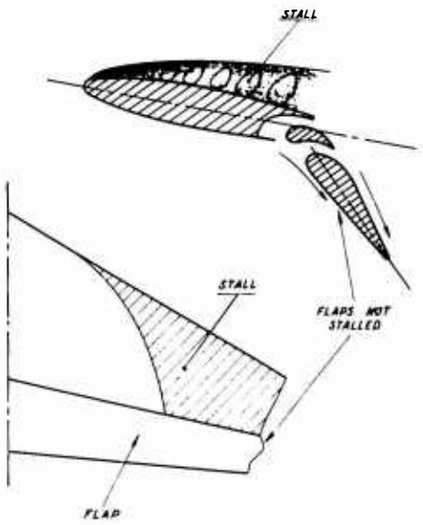

Fig.4 Wing stall, flaps down, no leading-edge device

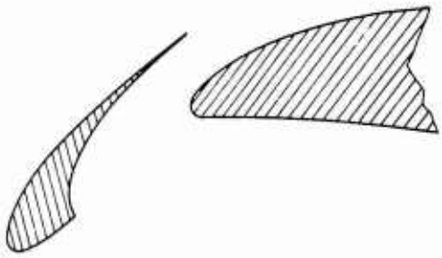

Fig.5(a) Leading-edge slat

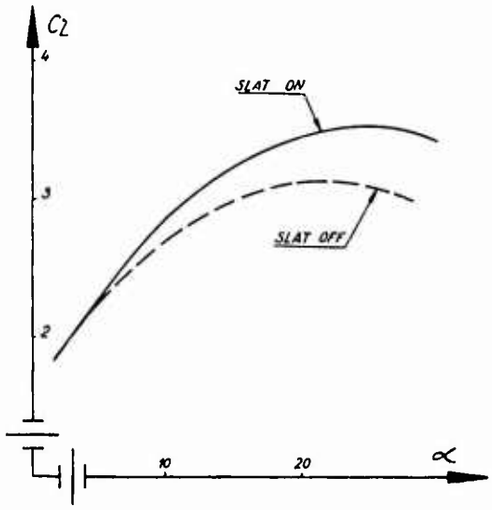

Fig.5(b) Slat effect in two-dimensional conditions

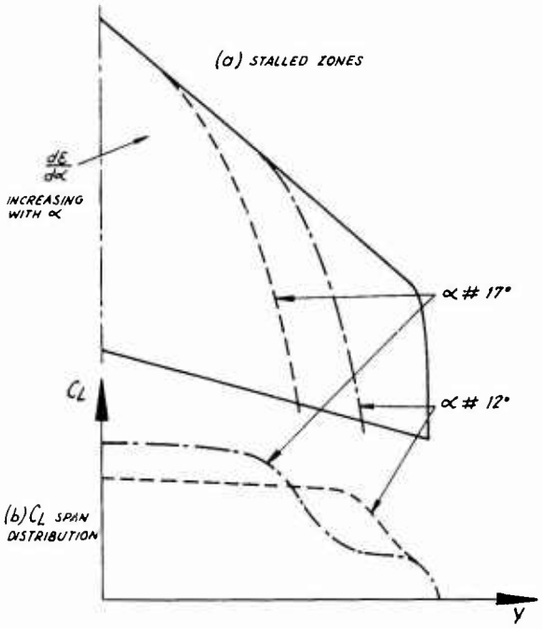

Fig.6 High swept wing stall

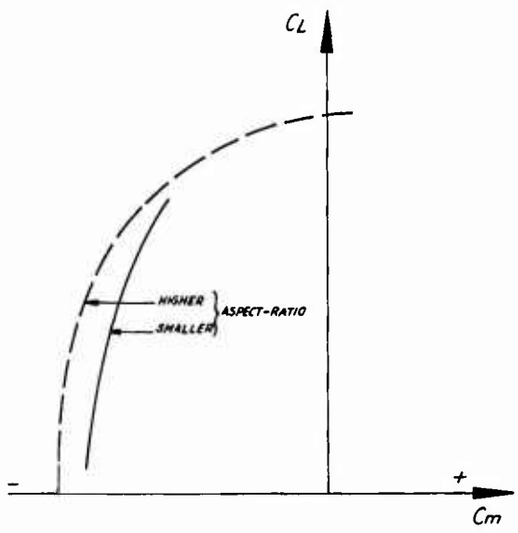

Fig.7 C_L (Cm) curves at given sweep horiz. tail off

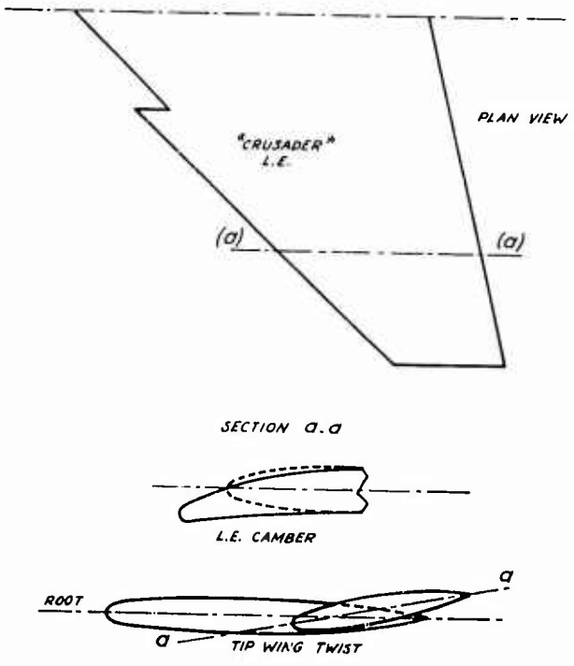

Fig.8 Local modifications to limit the tip leading-edge stall

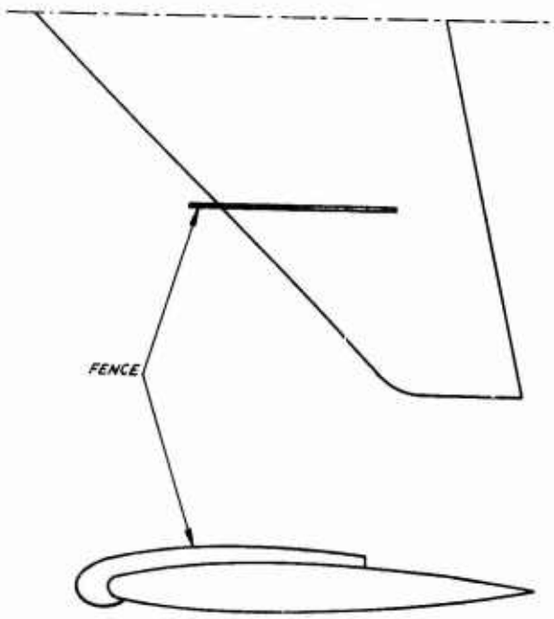

Fig.9 Wing fence

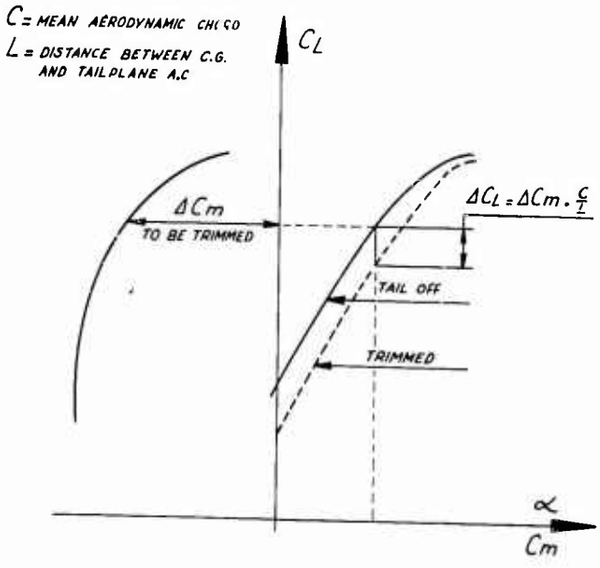

Fig.10 $C_L(\alpha)$ curves tail off and trimmed

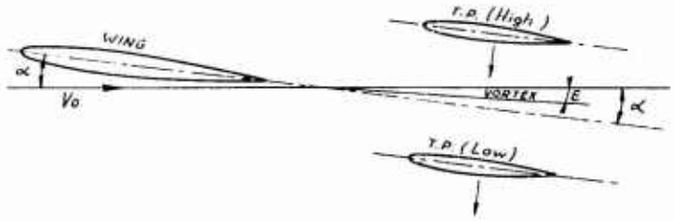

Fig.11 Relative positions of the tail plane and the vortex center zone versus α

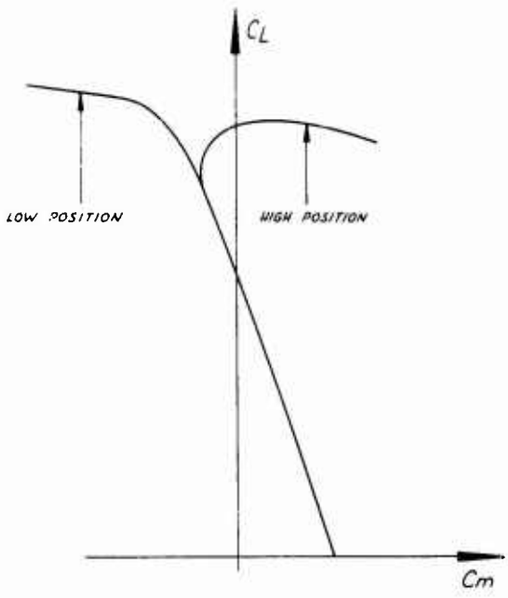

Fig.12 C_L (Cm) curves at a given value of η with high and low tailplane position

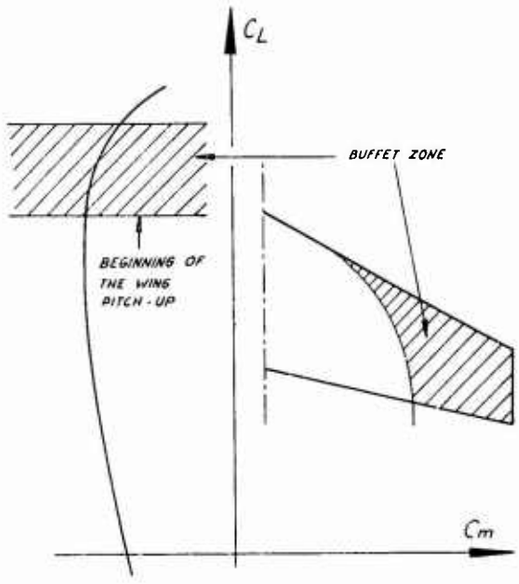

Fig.13 Buffet correlated with wing fuselage pitch-up

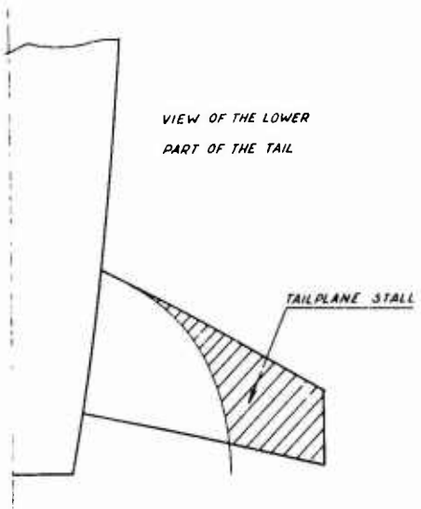

Fig.14 Stall of the lower part of the tailplane (tail buffet) at the trim position

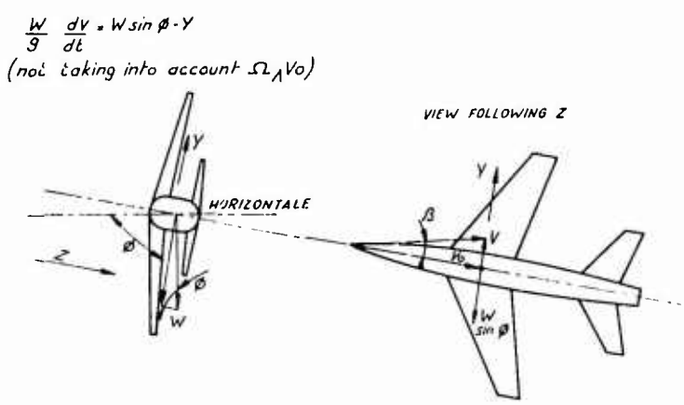

Fig.15 Adverse aerodynamic lateral speed V and sideslip β due to the lateral weight-component

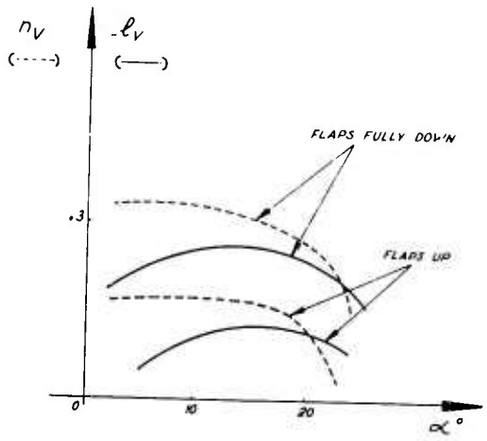

Fig.16 n_v and l_v variations with the angle of attack and the flap deflection

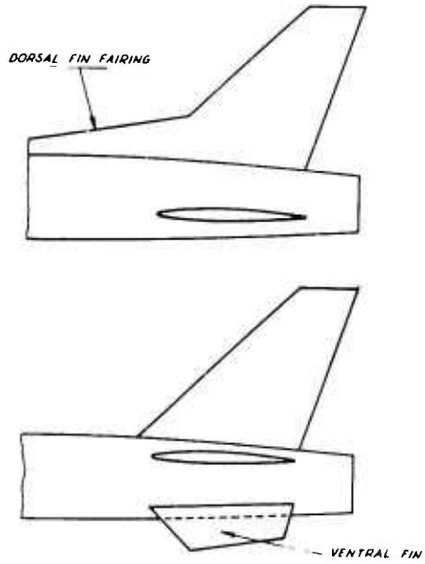

Fig.17 Fin fairing ventral fins

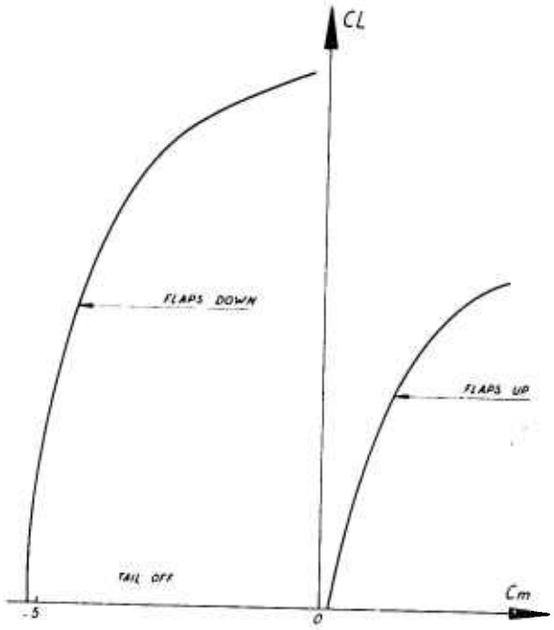

Fig.18 ΔCm due to the flaps deflection, horizontal tail off

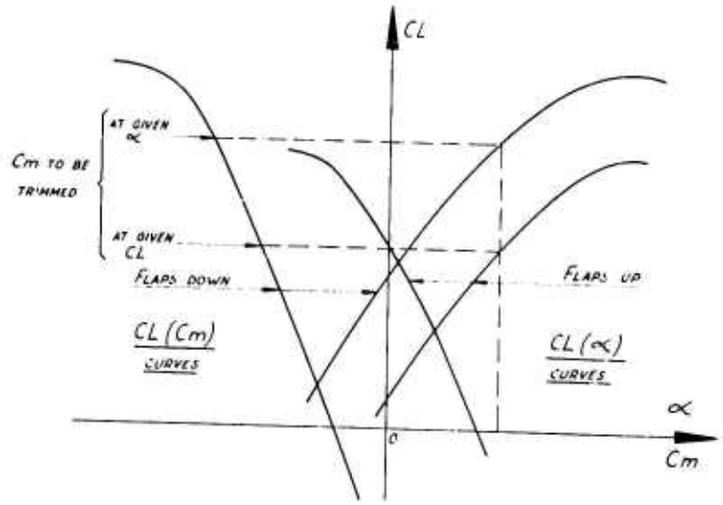

Fig.19 Cm due to flaps deflection at given η value

(1) $R_2 = W - L$
(2) $M = R_2 x + f(W-L)h$
} abs. values

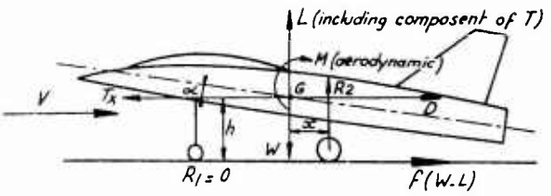

Fig.20 Forces and moments equilibrium at nosewheel lifting

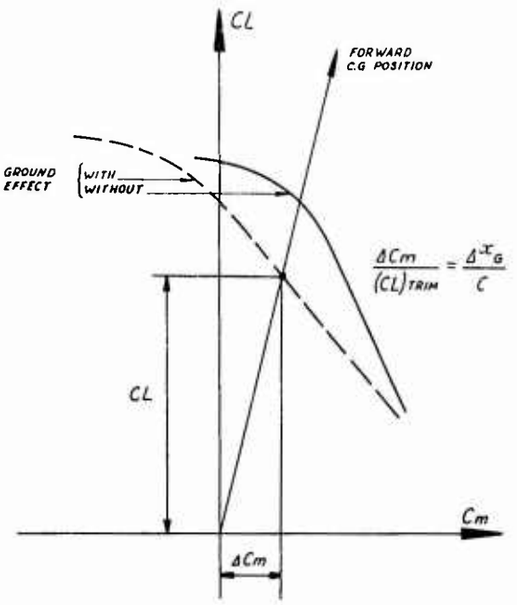

Fig.21 Definition of the most forward C.G. position to be trimmed at a given CL, with a given η

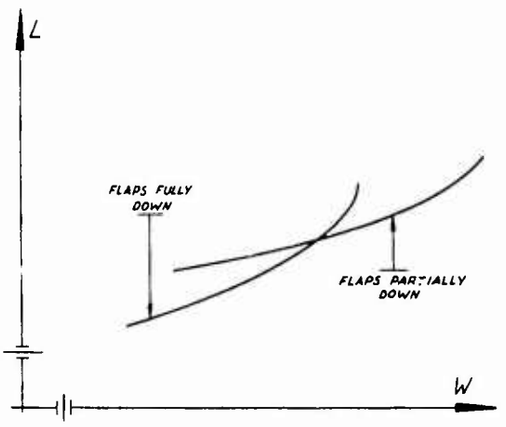

Fig.22 Effect of flap deflection on the take-off length versus weight

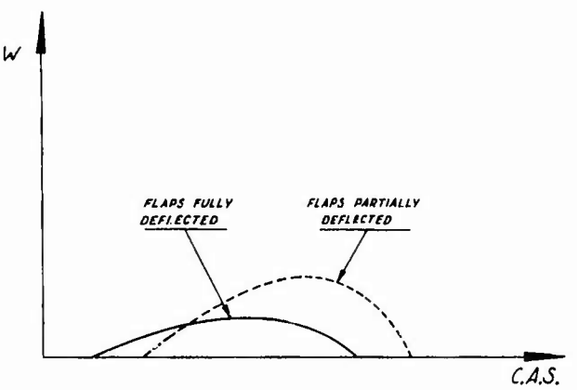

Fig.23 Effect of the flap deflection on vertical speed, one engine out (stores released)

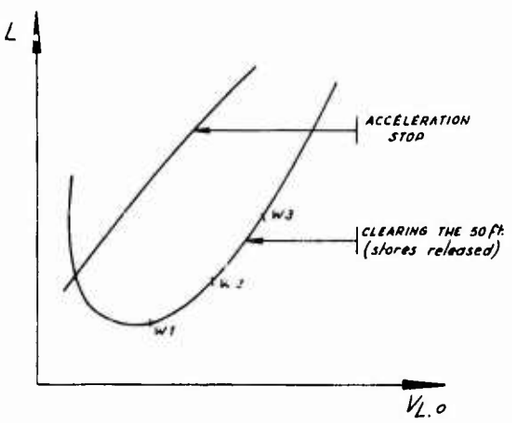

Fig.24 Acceleration stop and 50 ft clearing distances, with failure at take-off

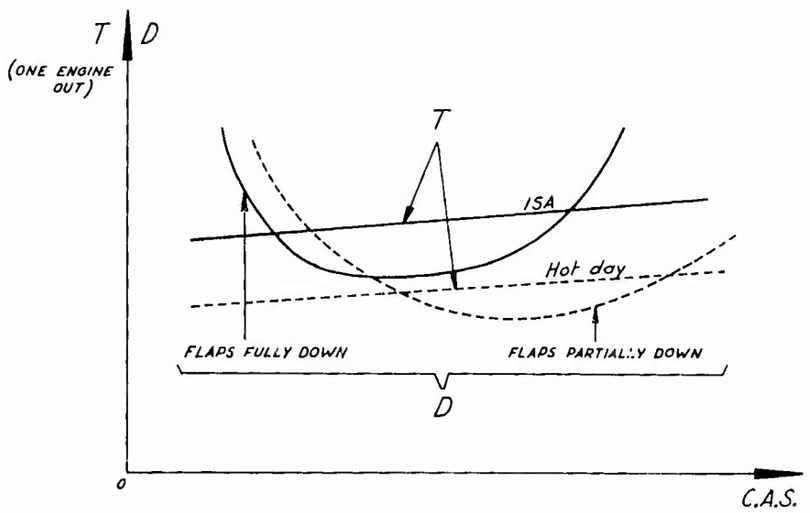

Fig.25 Level flight with one engine failed at maximum weight, flaps down

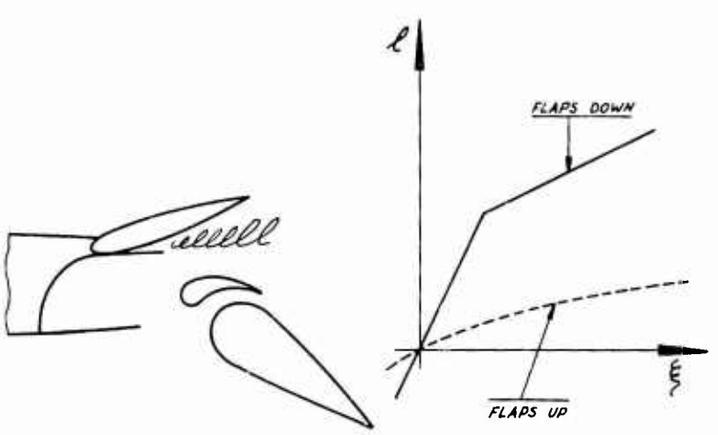

Fig.26 Spoiler efficiency, flaps down

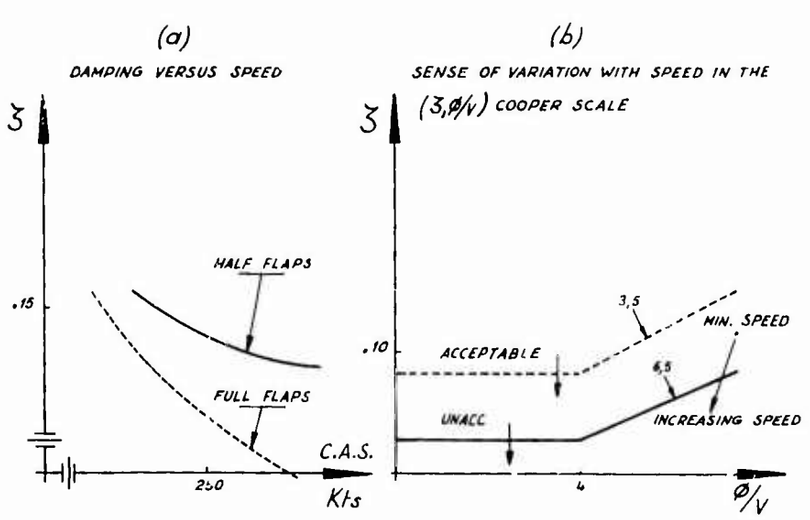

Fig.27 Dutch roll characteristics versus speed flaps fully down

[illegible] OF THE WING

[illegible] AIRCRAFT APPLICATION OF LIFT-AUGMENTATION DEVICES

1. Compromise between Design of High-lift Devices for Low and High Speeds

The leading-edge devices can be used to improve margins and the manoeuvre limits at high speeds. The form of the wing (relative thickness, camber, twist, 'Crusader' extension of L.E. having been chosen mainly from high-speed considerations, one can attempt then to improve the manoeuvrability of the aircraft by selecting a suitable deflection of L.E. devices (e.g. slats) these latter having themselves been optimised primarily for conditions of landing and take-off.

2. Influence of Fences on High-speed Manoeuvrability

Fences, suitably sized and positioned, can have like slats a favourable influence on high-speed manoeuvrability. However, the dimensions and the position then most appropriate are not the same as those for the improvement of flight qualities at low speeds.

3. Influence of Mach Number on the Lift due to Slats

The use of slats for flight at high subsonic speeds can improve the flight qualities at large incidences. Thereby, even for Mach numbers of the order of 0.9, one can hope to increase the incidence limit by one or two degrees.

4. Use of Lower Surface Camber on the Leading-edge of the Horizontal-Tailplane

By the use of such a camber (or by a slatted nose like on certain 'Phantoms'), the separation on the tailplane can effectively be delayed and thereby improvements made to the longitudinal control and buffet limits at high incidence. However, it is essential to verify that the aircraft drag does not suffer too much at high Mach numbers.

5. Limiting Speed for the Use of Partially-deflected Trailing-edge Flaps

The normal speed limits have to be defined by structural analysis. However, restriction to the corresponding flight domain is strictly a piloting question.

6. Value of Flares at Take-off

The possibility is perfectly feasible on multi-engined aircraft, since in particular the flares are largely inert then and do not present an explosion risk.

7. Influence of Wing Height on Maximum Lift

In principle, the high position is the most favourable and can give an appreciable gain in the maximum lift coefficient C_{z_m}.

8. Reversal of Spoiler Efficiency at Take-off

[illegible] experiences by the lecturer, he agrees that this reversal phenomenon [illegible] actually possible with certain special wing profiles. Actually, it would be [illegible] important to take account of the possibility of such a phenomenon at the large [illegible] with in the spin, as well as at take-off and landing.

9. Variation of Lateral Damping with Speed

The proposition according to the text of the paper is not general. It depends essentially on the relative importance of the aerodynamic derivatives in comparison with each other. However, it does exist in certain cases and the possibility must not be [illegible].

10. Trim Change due to Flaps

It is true that with numerous aircraft, particularly those with smaller sweepback, [illegible] configuration and lower tail arms than those of combat aircraft, the moment

due to flap deflection is nose-up, the influence of the flap deflection on the tailplane in this case more than outweighing the nose-down moment from the flaps themselves.

FLIGHT TESTING MILITARY TRANSPORT AIRCRAFT FOR CLEARANCE IN THE STOL ROLE

by

K. P. EYRE

Performance Division, Aircraft & Armament Experimental Establishment,

Boscombe Down, U.K.

1. INTRODUCTION

This paper gives an indication of the type of tests which are likely to be required in the United Kingdom to clear an aircraft from handling and performance aspects for military S.T.O.L. applications. Tests made to clear the Andover C. Mk. 1 are given as an example.

No special consideration is given to particular high-lift devices each of which may of course introduce individual problems. However it is considered that in the case of S.T.O.L. aircraft generally the problem of variability in behaviour may require more than usual attention due to the rapid manoeuvres and short distances involved with considerable dependence on pilot technique.

2. OBJECT OF TESTS

(a) To ensure that the basic flying characteristics and techniques recommended by the aircraft manufacturer are safe.

(b) Using the approved technique to measure the average performance for comparison with the requirement and provisional operating data.

(c) To obtain a reasonable estimate of the scatter in performance in order to assess whether or not the operational safety factors should be increased in relation to those normally used.

3. GENERAL HANDLING TESTS

On the assumption that the aircraft has to be cleared over its whole practical flight envelope, then the following aspects would usually be checked over the full range of weight, centre of gravity, speed, altitude and likely configurations prior to making a specific S.T.O.L. assessment. A minimum of two and usually three or more pilots make qualitative appraisals.

I. Qualitative

Pilots' assessment of overall suitability for role including assessment of control friction and backlash, cockpit appraisal, ground handling on both wet and dry runways, effects of turbulence, crosswind, rain, poor visibility day and night, best speeds, configurations and techniques.

II. Longitudinal stability and control

(a) Static stability margins stick free and fixed. (Stick force to change speed and control-surface angle to trim at different speeds.)

(b) Short period oscillations.

(c) Trim authority and changes of trim with power, flaps, undercarriage, airbrakes, sideslip and mis-set trim.

(d) Stick force per g.

(e) Aircraft response on stick release after speed change.

(f) Minimum unstick and threshold speeds.

III. Lateral and directional stability and control

(a) Sideslips.

(b) Short period oscillations.

(c) Trim authority and changes of trim with power, speed, etc, including effects on one or more engine failures.

(d) Rates of roll.

IV. Flight envelope

(a) Lowest flight speeds and warning margins.

(b) Highest flight speeds or Mach numbers.

(c) Limiting speed/Mach number/g combinations.

(d) Limiting lift conditions with variation of Mach number.

V. Engine handling

(a) Engine cuts and relights.

(b) Engine accelerations and decelerations.

(c) Manoeuvres with one or more engines out.

VI. Autopilot and auto-stabilisers

VII. Instrument approaches

VIII. Single failures other than engines

(P.F.C., flaps, pilot mis-selections, etc.)

Two of these basic types of test which are particularly relevant for a S.T.O.L. aircraft are the assessment of the behaviour at the minimum flying speed and the minimum speed at which an engine failure can be controlled in the case of a multi-engined aircraft. In order to illustrate typical tests made in more detail, a rough breakdown of the specific tests made on these aspects is given in the following two paragraphs.

3.1 Minimum Flying Speed (V_S)

This is defined as the lowest practicable speed at which the aircraft can be flown.

Tests are usually made at high and low weight with extreme forward and aft centre of gravity positions, at an altitude of about 10,000 ft for the initial tests and subsequently at lower or higher altitudes if considered appropriate for the operational role. An area free from cloud and turbulence is selected. At each loading condition in the appropriate aerodynamic configuration with the engines at idling conditions, the speed is reduced with the wings level from an initial trimmed speed of approximately 1.3 x the estimated lowest practicable speed at which the aircraft can be flown. For the majority of the tests the rate of speed reduction is approximately 1 kt/sec, but slower and faster rates are also checked (order of 0.5 to 3 kts/sec). The following aspects are noted:

(a) Whether there is any warning of approach to a stall or other limiting condition; the nature of the warning and the speed and incidence at which it occurs.

(b) The position of the control column at the limiting condition, the forces required and the nature of the force/speed/incidence relationship, e.g. whether the force reduces considerably just prior to a stall.

(c) The behaviour of the aircraft at the limiting condition; especially whether a wing drops and, if so, how suddenly and whether it can be raised by ailerons alone.

(d) Whether there is any tendency to spin.

(e) The method of recovery from a stall or other condition and the height lost during recovery.

(f) Whether or not the aircraft can be prevented from reaching the limiting condition if recovery action is initiated at the warning stage.

For all minimum flying speed checks, incidence and sideslip indications are normally presented to the pilot and, if a stall or loss of lateral control is not achieved at some incidence reading agreed prior to the flight on the basis of the Firm's flight tests and tunnel tests, the test is discontinued to avert the danger of a super-stall or other known hazard.

The wings level tests are repeated with power on; but it is not always practical to carry out tests with take-off power applied, because of the dangers inherent in the excessively steep attitudes which can result even with the reduced power available at a reasonable test altitude.

Checks are also made in turning flight, either with the turn progressively tightened at a constant speed of about 1.2 x the lowest practical flight speed, or in the case of large aircraft at an angle of bank of about 30° with the speed reduced at a rate of up to about 3 kts/sec. A brief check is made of the characteristics with an engine failed when appropriate but only usually in wings level flight.

Normally the characteristics at the limiting conditions are considered acceptable if on average there is no violent behaviour; i.e. wing drop not exceeding the order of 30°, no rapid pitch up or down, no tendency to spin, height loss of the order of 200 or 300 ft and the recovery can be made with the normal use of the controls.

The warning of the approach to limiting conditions is considered acceptable if the stick-force gradient up to the limiting condition is positive and there is natural buffet or artificial warning with sufficient margin from the limiting condition to make a satisfactory recovery (minimum usually of the order of 7 kts or 7% E.A.S. or I.A.S., or 6° incidence).

Stalling or limiting low-speed handling characteristics worse than those described as normally acceptable may be accepted, depending on the role, if the warning system is very obvious (e.g. audio plus stick shaker) and has a high integrity (e.g. duplicated) with more than the minimum warning margin.

If the case of a limiting incidence being prescribed in order to avert a superstall then ideally a stick pusher or other artificial recovery device should be fitted but, depending on the role, this would not necessarily be considered essential for a military aircraft if the warning of approach to the dangerous situation and the margin from the dangerous situation are considered adequate. If however an aircraft is likely to operate for long periods near the ground or sea, then the requirements are interpreted more severely.

3.2 Minimum Speed for Control Immediately After an Engine Failure (V_{mca})

This is defined as the lowest speed at which a sudden complete engine failure can be controlled when initially in wings level flight.

Centre of gravity is not usually considered an important variable for these tests, but checks are sometimes made at high and low weight if it is practicable, in order to cover the different lateral inertias. The lowest safe height is normally used in order to obtain the greatest assymetry due to power, but extreme care in testing is required if the power-off stalling speed in particular is of the same order as the minimum control speed and, for this reason, tests are often only a practical possibility at very light weight.

The tests are made using all likely configurations for take-off, cruise and approach and the engine giving the most asymmetric effect is used to simulate a failure.

The normal test procedure is to throttle the critical engine at a speed well in excess of the estimated minimum control speed (20 kts plus) and then, with the maximum appropriate power on the other engines, to slowly reduce the speed (1 kt/sec) until with wings level and either full rudder or a foot force of the order of 180 lb the aircraft can be maintained on a steady heading. The speed is then further reduced until a steady heading can be no longer maintained with about 5° of bank applied.

The aircraft is then flown with all engines at the appropriate power at the minimum speed determined from the previous test, or 5 to 10 kts above this speed initially if considered prudent, and the critical engine is quickly throttled back. If possible no recovery action is taken for 2 seconds or until 20° of bank is achieved whichever occurs first. The 2 second time delay for pilot appreciation plus reaction is rather arbitrary, being based on experience, and is sometimes modified if not considered realistic on a particular aircraft. For some aircraft conditions it may not be possible to obtain a steady speed of the order required using a practical technique, due to the high acceleration (e.g. at low altitude in the take-off configuration.) In this case, a further final check would be made failing an engine on an actual take-off at the highest practical weight to give the lowest forward acceleration, or at the lowest practical altitude at an acceleration appropriate to a normal take-off.

During the recovery manoeuvre it is considered acceptable if, by not using excessive skill, height can be maintained without exceeding a change in heading in excess of 20° or the attainment of an attitude which would be dangerous near the ground (e.g. allowable bank angle determined by possibility of wing tip touching the ground). During the transient manoeuvre and after regaining straight steady flight, the rudder force should not exceed the order of 180 lb (Note:- pilot is capable of 600 lb) with an aileron control force of about 35 lb on a stick or 50 lb on a wheel. After regaining straight steady flight, the associated angle of bank should not exceed 5° and the direction of flight should not diverge by more than 10° from the original direction.

Further checks may subsequently be required if at the speed chosen these requirements are over met or under met.

In determining a minimum safe flight speed for scheduling to the operator at which an engine failure can be controlled, it is normal to factor the test minimum control speed by 1.1 (e.g. safety speed $V_2 \nmid 1.1\ V_{mca}$) to provide a reasonable margin over the real critical speed in addition to the hidden safety built in by the tests, in that a pilot can physically apply the order of 500 to 600 lb foot force when suitably strapped in and an angle of bank of up to 10° can possibly be used in extreme cases. The extra foot force will of course be of no help if full rudder is obtained with the 180 lb used in testing as a reasonable value that can be sustained over a period before trimming out at the safety speed V_2.

4. S.T.O.L. HANDLING TESTS

There are no laid-down military requirements in terms of numbers in the United Kingdom, as such a large number of parameters must be specified in the requirements in order to take account of the particular aircraft characteristics and the appropriate operational risk acceptable. However, to illustrate the tests likely to be required and the standards of acceptability used in the United Kingdom recently, the Andover C. Mk. 1 assessment is given as an example.

On this aircraft because of the large variability in behaviour obtained, primarily due to differences in pilot technique, it was necessary to assess critical handling aspects on a statistical basis instead of the more normal method of making a small number of checks at limiting conditions.

4.1 Description of Andover C. Mk. 1

The Hawker Siddeley Andover C. Mk. 1 (Fig. 1 and Fig. 2) is a tactical transport designed for the carriage of passengers or freight, airborne and air-landed assault, supply dropping and aeromedical evacuation. The normal maximum take-off weight is 50,000 lb. It was developed from the Avro 748 transport which was designed to civil standards. Brief details of dimensions and loading are given in Appendix 1.

The basic flying controls are conventional, being a mixture of geared and spring tabs manually operated. The flaps are Fowler type, but for flap positions in excess of $22\frac{1}{2}$° an additional trailing-edge tab moves downwards to modify the lift/drag characteristics considerably in the short landing setting of 30° (Fig. 3). No spoilers are fitted. The settings are:-

10°-- Normal take-off and supply dropping

$22\frac{1}{2}^{\circ}$-- Normal take-off and normal landing

27° with 42° tab-- Short take-off and normal landing

30° with 80° tab-- Short landing

The aircraft is powered by two Rolls-Royce Dart RDA 12 engines, each developing a nominal maximum power of 2930 propeller shaft horsepower using water methanol injection. Using the normal landing technique the flight fine-pitch stops are withdrawn on the ground and the resultant fining of the blades gives an increased propeller drag. Reverse thrust may be selected in the air or on the ground, but when it is used in the air the prior selection of reverse intent results in a higher idling thrust than in the normal case.

4.2 Handling Requirements Applied

4.2.1 General

Ideally, the clearance standard should be tailored to the acceptable risk of a particular operation. However, in the absence of specific guidance from the operator as to what risk is acceptable for particular operations and in order to keep the clearance as simple as possible, only two standards of clearance are normally recommended by A&AEE for this type of aircraft. One standard is intended to give civil safety standards for normal military operations in passenger or freight roles, and the other is the highest risk standard considered reasonable for a particular role. The following requirements are for the highest risk standard applied to the Andover, and the general assumption is made that in the worst aircraft loading condition the chance of reaching a disastrous situation during any particular manoeuvre should not exceed the order of 1 in 1000 occasions (e.g. if there is only one critical parameter and a normal distribution applies then a margin of approximately 3 standard deviations is required from its mean value to its limiting value). The overall accident rate for the fleet of aircraft will of course depend on how often the aircraft are operated at an aft centre of gravity and if there are any other significant variables.

4.2.2 Take-off

(a) The chance of a single engine failure can be ignored below the final steady climb out condition.

(b) The rotate speed and unstick technique should be such that at a margin of at least 3 standard deviations of incidence is available from the average condition to the stall in the worst loading case. (Aft centre of gravity).

(c) The lateral control should be adequate in cross winds of the order of 15 kts. Minimum rate of roll about 10°/sec.

(d) In the average take-off case in calm air, the stall warning should not operate either in the initial unstick manoeuvre or in the initial climb out (mid centre of gravity). Stall warning set with approx 6° incidence or 7 kts or 7% E.A.S. or I.A.S. margin from power-off stall.

4.2.3 Landing

(a) On the final approach, the chance of a single engine failure on overshoot can be ignored.

(b) The lateral control should be adequate in cross winds of the order of 15 kts. Minimum rate of roll about 10°/sec.

(c) The flare and land manoeuvre should be such that a margin of at least 3 standard deviations of vertical velocity is available from the average value to the ultimate design value in the worst loading case (forward centre of gravity, high weight).

4.3 Tests Made

4.3.1 Take-off

In order to minimise scatter in behaviour, the Firm's recommended technique was to apply rapid full back stick at the appropriate rotate speed V_R ($V_R \approx 0.95\ V_S$ power-off, or $1.0\ V_S$ with 35% wet power on). At aft centre of gravity it was essential to apply a programmed stick input (i.e. not wait for clues from the aircraft's actual response before applying forward stick). The stick input shape was triangular in this case (Fig. 4).

For maximum effort climb out, the aim was to go for $V_C \approx (V_R + 10$ kts) until clear of obstacles ($V_C \approx 1.1\ V_S$ power-off or $1.15\ V_S$ power on. V_{mca} = 85 kts I.A.S. At 40,000 lb AUW, V_C = 76 kts I.A.S: and at 50,000 lb AUW, V_C = 89 kts).

Tests were made using 4 pilots, varying the weight and centre of gravity over most of the practical ranges in various weather conditions, off different airfield surfaces in the United Kingdom and overseas to ascertain the likely variability in behaviour. A total of 175 S.T.O.L. take-offs were made with 85 at the critical aft centre of gravity position. Not all of these tests were made solely for handling checks off normal runways and some were made during the assessment of limiting airfield surfaces in terms of softness and undulations.

In order to assess the risk during the initial take-off manoeuvre, incidence was measured using an A.D.D. (Airstream Direction Detector) (Fig. 5), which was calibrated during the trials by measuring pitch attitude by an internal gyro and flight path using external cameras. Wind velocity was measured using a sensitive anemometer with a trace recorder on the ground near the take-off position.

Fig. 6 shows the results of the initial tests at A&AEE and, as a result of these tests, the clearance was restricted to centre of gravity positions no further aft than the mid position. The C_L plotted is the maximum achieved during the take-off manoeuvre and is based on the basic wing area. The difference between I.A.S. and E.A.S. although believed to be small is difficult to measure in this condition. Consequently, the absolute values of C_L are rather dubious and the main intention of the Figure is to show the maximum values of the incidence achieved at the different centre of gravity positions in relation to the stall warning and the probable stall. After further experience however with a more precise technique, the statistics were improved; it was found that at aft centre of gravity with an experienced pilot, the mean maximum incidence could be reduced to about 11° with a standard deviation of about 1.2°, with 95% confidence, thus giving the order of 15° at the 3 standard deviation level (Fig. 7). (It should be noted that in all the Figures where standard deviation values are quoted these are as measured and not factored for a given confidence level.) It was apparent from the results, however, that a small variation in technique could produce a considerable increase in the maximum incidence achieved. The stall warning operated in the range 11° to 13° and hence at aft centre of gravity was of some nuisance value for this transient manoeuvre, where the aircraft was virtually out of control depending on the right programmed stick input for a safe return to the climb out incidence.

As the stalling incidence was estimated to be of the order of 18°, the revised technique was considered acceptable on a military operational necessity basis. However, it was emphasised in Pilots Notes that the safety depended primarily on pilot training and that the training must include experience at aft centre of gravity in good weather conditions before real operations, especially at night.

The initial climb out speed ($V_C = V_R + 10$ kts) was considered to be acceptable only in calm weather conditions as the margin to the stall warning was of the order of 3 kts. In turbulent conditions, in order to prevent frequent nuisance operation of the stall warning system and to maintain a reasonable margin from the stall, it was considered that the initial climb out speed should be increased. On the assumption that the maximum horizontal gust increment does not often exceed 0.6 x the mean wind strength, and ignoring aircraft speed response, a reasonable increment in climb speed for this aircraft is now considered to be 0.5 x the mean wind strength.

e.g.

Mean wind strength w	10	20	30	
Gust increment 0.6 w	6	12	18	
Speed increment required to prevent stall warning (0.6 w - 3)	3	9	15	(As $V_C - V_{SW} \approx 3$)
Suggested increment $\frac{1}{2}$ w	5	10	15	
Speed increment required to prevent stall (0.6 w - 10)		2	8	(As $V_C - V_S \approx 10$)

This increment in speed should be applied irrespective of wind direction in order to cover lateral as well as longitudinal control problems.

4.3.2 Landing

The Firm's recommended technique was to make the final approach at 1.2 x power-off stalling speed using the V.S.I. (Vertical Speed Indicator) as the primary indication of rate of descent, flaring on visual clues and selecting ground fine pitch and full reverse thrust whilst still in the air just prior to touch-down. As for take-off, tests were made over the weight and centre of gravity range in various weather conditions, onto different airfield surfaces in the United Kingdom and overseas. During the trials off a normal runway surface, 120 landings were made with 4 pilots and of these 65 were at a forward centre of gravity position, which was considered likely to be the most critical case from handling aspects in the flare. Some of these tests were made to measure performance in addition to handling qualities.

In order to assess the risk during the final landing manoeuvre, the vertical velocity at touch-down was measured and readings were also taken of undercarriage loads from strain gauges. The vertical velocity was measured using two types of external cameras, undercarriage closure rate and an internal aircraft camera photographing a light spot projected from the aircraft onto the ground. It was found from the early test results that the average vertical velocity was about 4.5 ft/sec with a standard deviation of 2.5 ft/sec at a 95% confidence level. (Fig. 8). From later tests with better instrumentation, these results were modified to a mean of 6.2 ft/sec with a standard deviation of 2.1 ft/sec at forward centre of gravity. Hence at the 3σ level the vertical velocity would be $(6.2 + 3 \times 2.1) = 12.5$ ft/sec. Because operations were required on semi-prepared surfaces however, it was considered that a further allowance for a mean 1 in 50 slope should be taken into account, which is equivalent to about 2 ft/sec at the approach speed of this aircraft. The ultimate strength vertical velocity requirement for the undercarriage was therefore 14.5 ft/sec and the aircraft landing weight was limited to the value meeting this requirement; i.e. 42,000 lb. In measuring vertical velocity at touch-down, considerable differences in measurements were obtained with the different forms of instrumentation. The early test results, giving a low mean value and a high standard deviation, were obtained using a relatively slow speed external camera (2 frames/sec). The later results were obtained using a higher speed camera (44 frames/sec) and the light spot which was considered to be the best method. The undercarriage initial closure speed appeared to be about 40% less than the aircraft vertical velocity, probably due to tyre deflection.

In judging the landing manoeuvre considerable reliance has to be placed on the V.S.I. and, as the standard pressure instrument fitted was subject to considerable lag, pilots were initially reluctant to maintain a steep approach near to the ground without an external glide path aid (Fig. 9). It was found that, after training using a glide path aid, more confidence was achieved in the use of the V.S.I. and steeper approaches were achieved more consistently without an external aid. It was considered however that whenever possible an external glide path aid should always be used to assist judgement of rate of descent. An upper limit was placed on the glide path angle of 6° and a rate of descent of 1000 ft/min. The 6° would give an average rate of descent of about 900 ft/min and could not be increased greatly because of the fairly high idling thrust associated with the selection of the reverse thrust facility in the air. Even if it had been possible to increase the approach angle, however, pilots were not happy in judging the flare with rates of descent much above 1000 ft/min and as this figure allowed some use in tail winds or at high altitude a restriction of 1000 ft/min was considered reasonable.

The threshold speed law of $1.2\ V_S$ was adequate for flaring in calm air and over most of the centre of gravity range; but at extreme forward centre of gravities, only obtainable at low weight, it was necessary to limit the threshold speed to a constant minimum value of 80 kts.

For adequate lateral and pitching control and also to cover the chance of hitting the stall due to a random gust, it was considered that the threshold speed should be increased in turbulent conditions. An increment of half the total average wind present is now considered to be of the right order, on similar reasoning to that given for the climb out case.

5. GENERAL PERFORMANCE TESTS

As for handling, a considerable number of routine measurements would be made to clear the normal transport role, but in this case none of these tests are very relevant for S.T.O.L. operations near the ground and will not be described.

6. S.T.O.L. PERFORMANCE TESTS

In order to illustrate typical differences in performance between initial estimates and that obtained from flight tests, and the sort of scatter obtained in the appropriate environment using a practical technique, the Andover is again given as an example.

6.1 Take-off

In I.S.A. conditions the average distances agreed reasonably well with predictions at high weights, but in tropical conditions the distances achieved were considerably longer than predictions - - approx 25% on ground run or about 300 ft (Fig. 10). The difference between the techniques indicated in Fig. 10 was not in stick input but included small changes in rotate and climb-out speed and, for these small changes (order of 5 kts), the effect on the mean overall distances was small at these limiting flight conditions. This would not be true in general for speeds well removed from the minimum practical values, of course, and the distances are probably more nearly proportional to V^2 at rather higher speeds.

There appeared to be two effects, firstly the slope of distance against weight was less than predicted and secondly the effect of temperature was more than predicted. The weight effect can possibly be explained as maximum power could not be applied at forward speed due to propeller limitations and consequently a ramp input of power was applied along the initial part of the ground run. In predictions the power output was assumed to be constant and the errors would thus be expected to be more at light weight where the power had sometimes not stabilised in the very short time before unstick (order of 20 secs). In the tropics, however, if the power build up was similar the tendency would have been to have reduced the effect of temperature. The power pattern was also affected by the use of methanol water, however, and consequently it was difficult to assess the overall situation. The stabilised engine performance appeared to be as predicted and, as engine power is usually the main source of doubt in predicting change of take-off performance with temperature or altitude, it is difficult to explain the discrepancy unless transient effects were significant.

There also appeared to be a tendency for the time between rotate and unstick to increase more than would be expected, possibly due to the lower elevator power with less slipstream effect, especially at Nairobi with the higher altitude and lower engine power. This effect however on subsequent checks did not appear to be very large and probably not more than one second (approximately 100 ft in distance).

The measured standard deviation of the ground run was 10% and on the air distance 30%. There was however considerable variation in technique during the airborne phase and, although pilots were briefed to carry out a maximum effort manoeuvre consistent with clearing real limiting obstacles, it is likely that this was not always done and on other experience the scatter in the presence of real limiting obstacles might be reduced considerably. Generally speaking, for most conventional aircraft using normal techniques, the standard deviation of total take-off distance to the screen height varies from 5 to 10% and as expected the S.T.O.L. technique gives a higher than normal scatter.

6.2 Landing

Considerable variability was experienced in the air distances measured and the parameter with the most marked effect was the approach angle through 50 ft. (See Fig. 12).

Using the V.S.I. to set up a 6° approach angle without glide path aid experience the mean angle was 4.5° with a standard deviation of 1.1° (43 landings). After having used a glide path aid, or when using the aid, the mean angle achieved was 5.7° with a standard deviation of 1.0° (41 landings); see Fig. 13.

The other main variable affecting the air distance was the point of flare initiation.

Overall the mean air distance without glide path aid experience was 850 ft with a standard deviation of 25% and after experience with an aid, 710 ft with a standard deviation of 15%.

Tests were also made at R.A.E. Bedford using a water barrier to simulate a real obstacle (1). Landings were made using 4°, 6° and 8° glide path aiming to clear the 50 ft barrier by 15 ft. In order to achieve an 8° glide path, reverse thrust was not selected in the air, thus enabling a lower idling thrust to be used but of course increasing the total air distance at a given glide path angle.

Three types of approach were made:-

(a) No barrier but a bar on the ground.

(b) With barrier and bar on the ground.

(c) With barrier with ring and bar sight.

Fig. 15 shows the performance achieved in terms of height at the barrier, and Fig. 16 shows the distance to touch-down from the barrier for the three glide path angles. It will be noted that, when using the barrier, the average distance to touch-down reduces as the glide path angle increases without any appreciable change in the scatter for the small sample tested.

In I.S.A. conditions the measured average ground run was 1.04 x the estimated distance, but in the tropics the factor was 1.13. The only variable which was found to be possibly significant was the speed loss during the flare and, although there was a very big scatter in this, the average value was 13 ft/sec in I.S.A. and 7 ft/sec in the tropics. This is not understood. The standard deviation of ground roll distance was 14%. At a given approach angle, the most important single variable affecting total distance to stop is likely to be speed at the screen height, and the normal standard deviation to be expected on landing distance from the screen height for most conventional aircraft varies from 10 to 20%. Using a glide path aid the results are in the middle of this bracket but without an aid are likely to be at the high end.

6.3 Interpretation

For military operational necessity type of operations the normal method of presenting the performance, when reduced to standard conditions of zero wind, level dry runway of stated surface, appropriate altitude and appropriate temperature, is to quote the average achieved by A&AEE pilots using the agreed representative technique in reasonably good weather conditions (measured in conditions of under 10 kts wind strength) and to give guidance on the operational safety factor that should be applied to cover the scatter.

As a result of these tests, it was suggested that a margin of 3 x the standard deviation measured under test conditions is probably reasonable for initial operations. This means that, under the test conditions, roughly 1 in 1000 cases will be outside the factored distances. Only experience of actual operations will of course show whether or not this order is satisfactory as there are so many variables to be considered for the real case. (Weather, pilots, different aircraft, training, enemy action, terrain, deterioration with time, etc.) As an illustration of how the recommended factors could be used in order to obtain a strip length, Appendix 2 gives examples for an unobstructed site having two types of surface prior to the main strip.

Results from Service trials so far have given similar or greater scatter than obtained during the A&AEE tests, as would be expected with the larger number of pilots and aircraft and less certainty on the test data.

7. CONCLUSIONS

It will be seen from the test results on the Andover that, because of the possible large variability in behaviour, then from both handling and performance safety aspects it is essential to define the pilot procedures as precisely as possible and to emphasise to the pilot the importance of using a constant procedure. This applies both during testing and when promulgating limitations and procedures to the operator.

In the design stage also, there is little point in spending a lot of time on detailed optimisation if the finished product has handling and performance characteristics which are very dependent on pilot technique, as large safety factors will have to be applied in both these areas thus reducing or cancelling altogether any design advantage. The use of simulators at an early stage may give some insight into the likely variability and the use of automatic control systems in the actual design can possibly help to minimise the problem.

As weather conditions have such a large effect on both handling and performance, the best possible means of continuous wind velocity recording should be used during testing.

Take-off and landing tests should if possible be made over a simulated barrier to obtain more realistic performance data and, if sufficient tests cannot be made during the clearance trials to establish the variability with reasonable assurance, then further data should be obtained from the operator from specific in-service trials.

A glide path aid should be used wherever possible to improve the consistency of touch-down performance.

REFERENCES

1. O'Leary, C.O.
Slatter, N.V. Flight tests to investigate the problems of steep approaches by S.T.O.L. aircraft. R.A.E. TR.69277 ; 1969.

APPENDIX 1

ANDOVER C. MK. 1
BASIC DATA RELEVANT TO THE STOL ROLE

1. WEIGHTS

Maximum take-off weight	50,000 lb
wing loading	60.2 lb/sq ft
Maximum landing weight	42,000 lb
wing loading	50.5 lb/sq ft

2. CENTRE OF GRAVITY

Aft limit	80" 0.36$\bar{c}$
Forward limit	57" 0.133$\bar{c}$

3. WING

Area	831 sq ft
Span	98 ft 3 ins
Aspect-ratio	11.6
Section root	NACA 23018
tip	NACA 4412
Standard mean chord	8.48 ft
Quarter-chord sweep	2.92°

4. FLAP

Fowler type with auxiliary tab

Area	79.9 sq ft per side, or total flap area is 19.2% of wing area.
Span	27.7 ft per side from 12% to 67% semi-span.
Mean total chord	2.88 ft
Flap tab chord/total flap chord	37.2%

5. STALL WARNING SYSTEM

Safe-Flight system with vanes on each wing. The system operates at vane forces tabulated below

0° Flap	15 grammes
10° Flap	15 grammes
22½° Flap	17 grammes
27° Flap	19 grammes
30° Flap	23 grammes

NOTE: As a small force is required to operate the vane, the warning is not independent of ($\frac{1}{2}\rho V^2$) and consequently the stall warning margin varies over the weight range; (approx 2°).

APPENDIX 2

SUGGESTED STRIP LENGTH REQUIREMENTS

The following two examples show how the required strip length can be estimated for the particular case where obstacles in the undershoot and overshoot are not critical. The same principles can be applied to cases where obstacles are critical.

ASSUMPTIONS

1. Firm hard surface with similar friction characteristics to dry asphalt, tarmac or concrete.

2. No obstacles in undershoot or overshoot, i.e. any approach path can be used.

3. Order of major accident rate allowable due to adverse take-off or landing performance about 1 in 1000 take-offs or landings when operating at the limiting conditions.

Strip A

Undershooting or overshooting will produce a major accident.

(a) Take-off case (Standard deviation of ground run 10%)

Allow say 50 ft. for turn at end.

$$\text{Strip length} \approx 1.3 \times \begin{pmatrix}\text{Average basic}\\ \text{ground run}\end{pmatrix} + 50 \text{ ft.}$$

(b) Landing case (Standard deviation of ground run 14%)
(Standard deviation of touch-down position 100 ft.)
(Average touch-down position beyond aiming point 100 ft.)

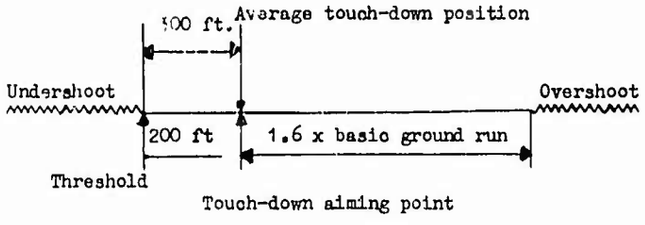

$$\text{Strip length} \approx 300 \text{ ft.} + 1.6 \times \begin{pmatrix}\text{Average basic}\\ \text{ground run}\end{pmatrix}$$

The factor 1.6 allows for some variability in touch-down position, but not the full effect of combining the scatter in ground run with the scatter in touch-down position, as the two are not completely independent; i.e. short touch-down will be associated with high speed and long ground run in some cases.

The factor is also only applicable for nominal ground runs of the order of 700 ft. Any large variations from this will require a modified factor.

Strip B

Undershoots and overshoots can be permitted in say 1 in 20 operations at limiting conditions; e.g. surface in undershoot and overshoot can be used occasionally without serious damage for distances equal to the difference between the lengths of Strip A and Strip B.

(a) Take-off case

$$\text{Strip length} \approx 1.2 \times \begin{pmatrix}\text{Average basic}\\ \text{ground run}\end{pmatrix} + 50 \text{ ft.}$$

(b) Landing case

$$\text{Strip length} \approx 200 \text{ ft.} + 1.4 \times \begin{pmatrix}\text{Average basic}\\ \text{ground run}\end{pmatrix}$$

SEE DIAGRAM ON NEXT PAGE

The evidence for touch-down position and variability of position is based on trials on the Hercules C. Mk. 1, Argosy C. Mk. 1, and Andover C. Mk. 1, when attempting to touch-down at the beginning of a membrane. The average touch-down position was about 100 ft. down the membrane with a standard deviation of about 100 ft. The distribution was slightly skew with the shortest touch-downs not more than 100 ft. short of the threshold and furthest down being 400 ft. from threshold.

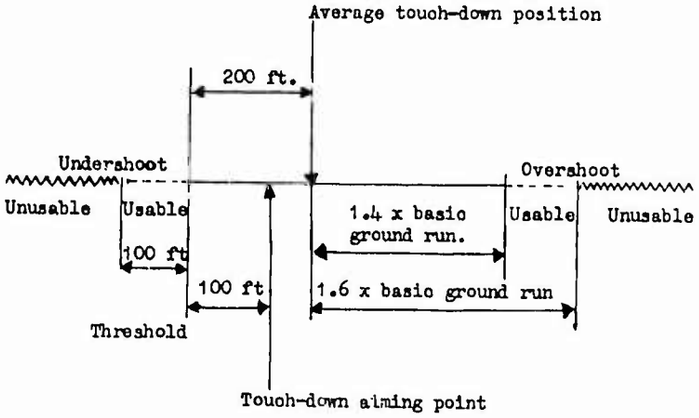
Average touch-down position
200 ft.
Undershoot
Overshoot
Unusable
Usable
1.4 x basic ground run.
Usable
Unusable
100 ft
100 ft
1.6 x basic ground run
Threshold
Touch-down aiming point

Fig. 1 Andover C. Mk. 1

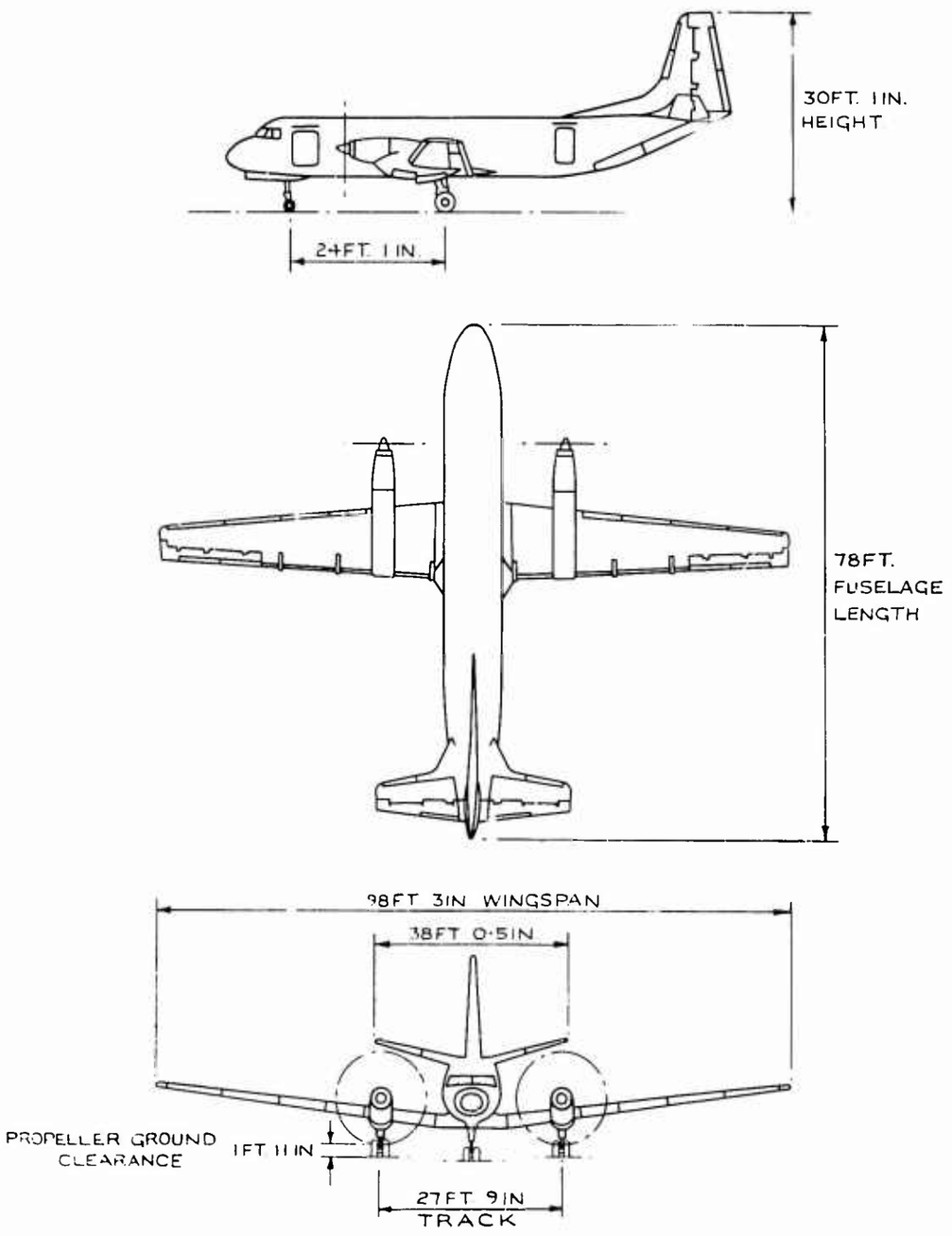

Fig. 2 General arrangement Andover C. Mk. 1

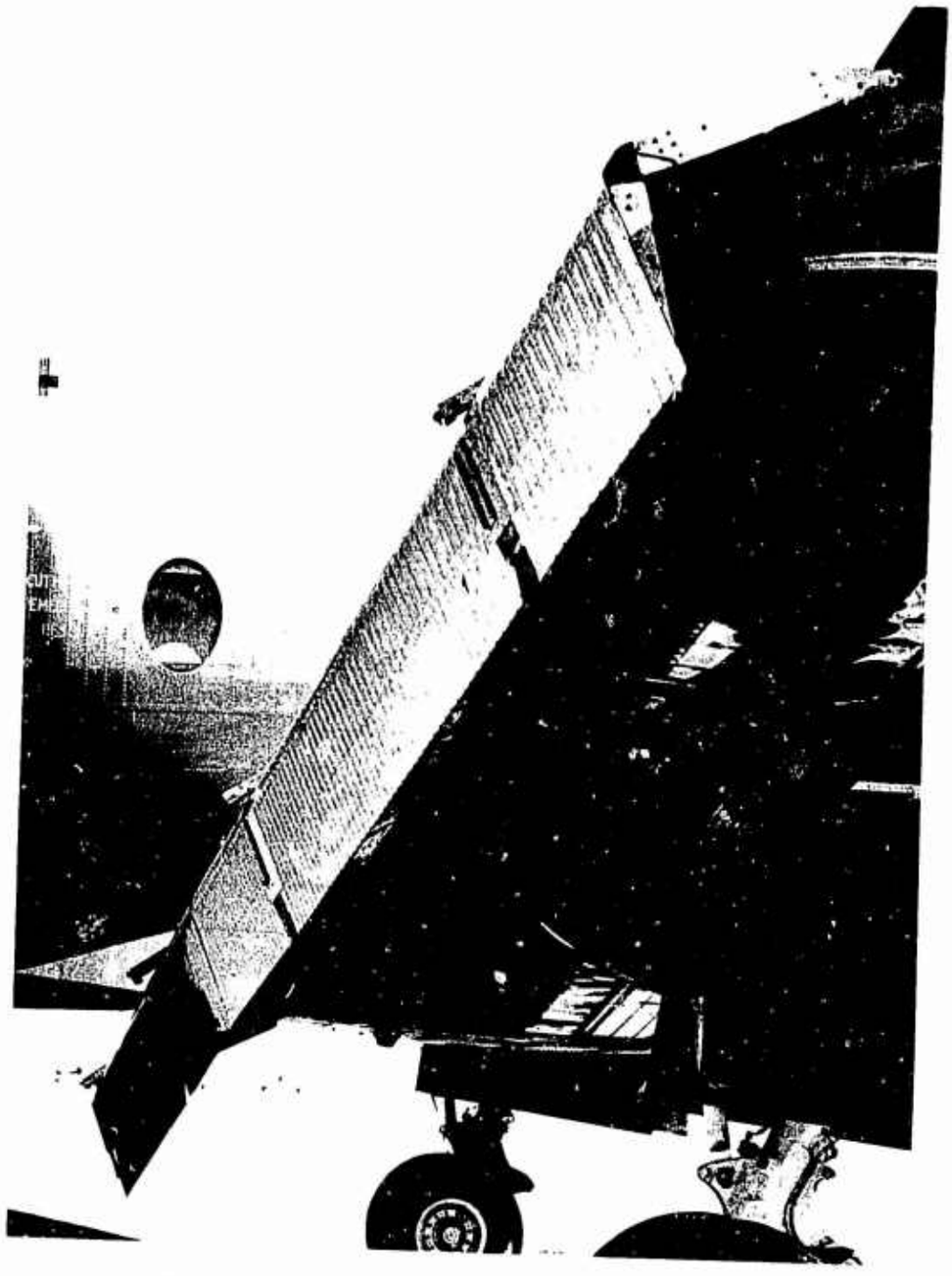

Fig.3 Andover C. Mk.1. Flap/tab in S.T.O.L. landing position

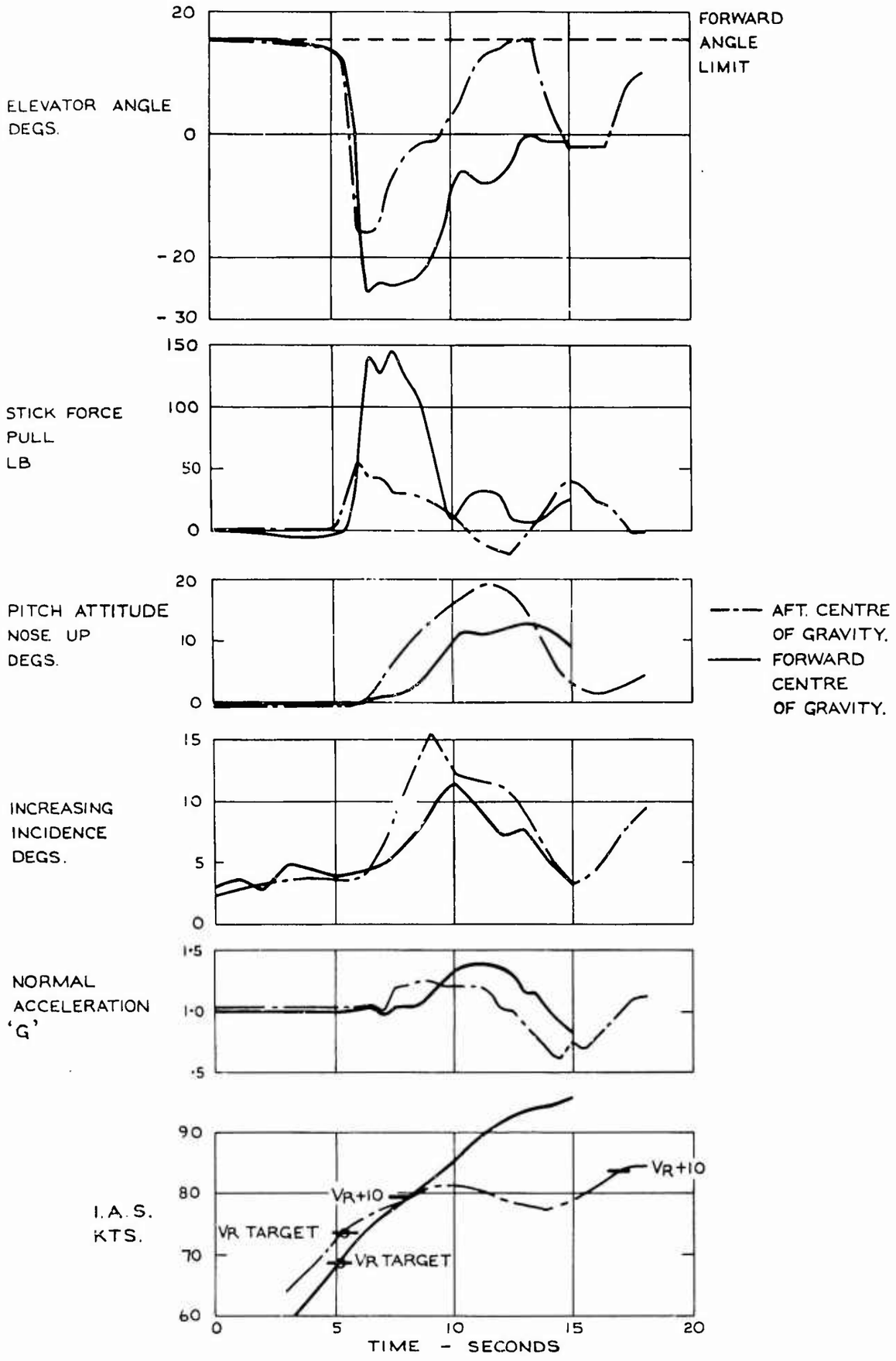

Fig.4 S.T.O.L. take off

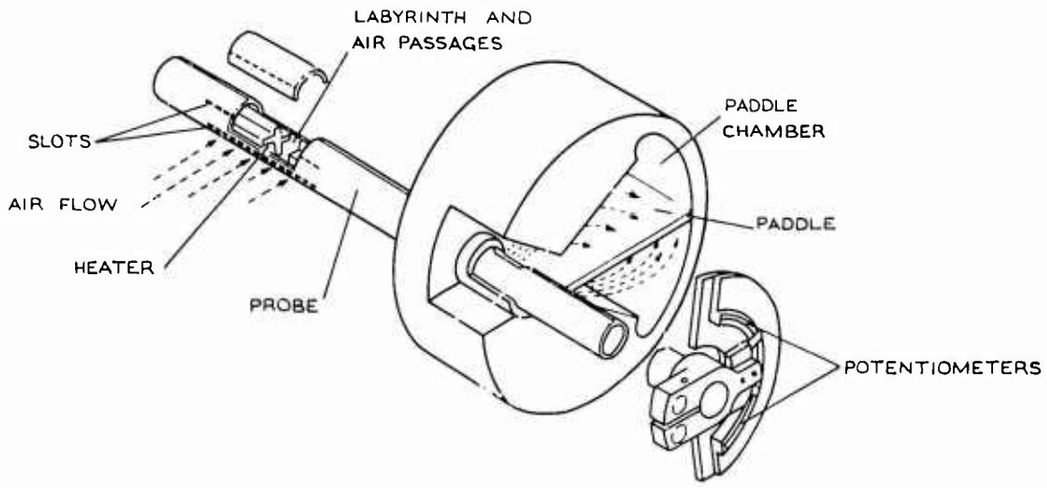

Fig.5 Specialities attitude direction ic ctor

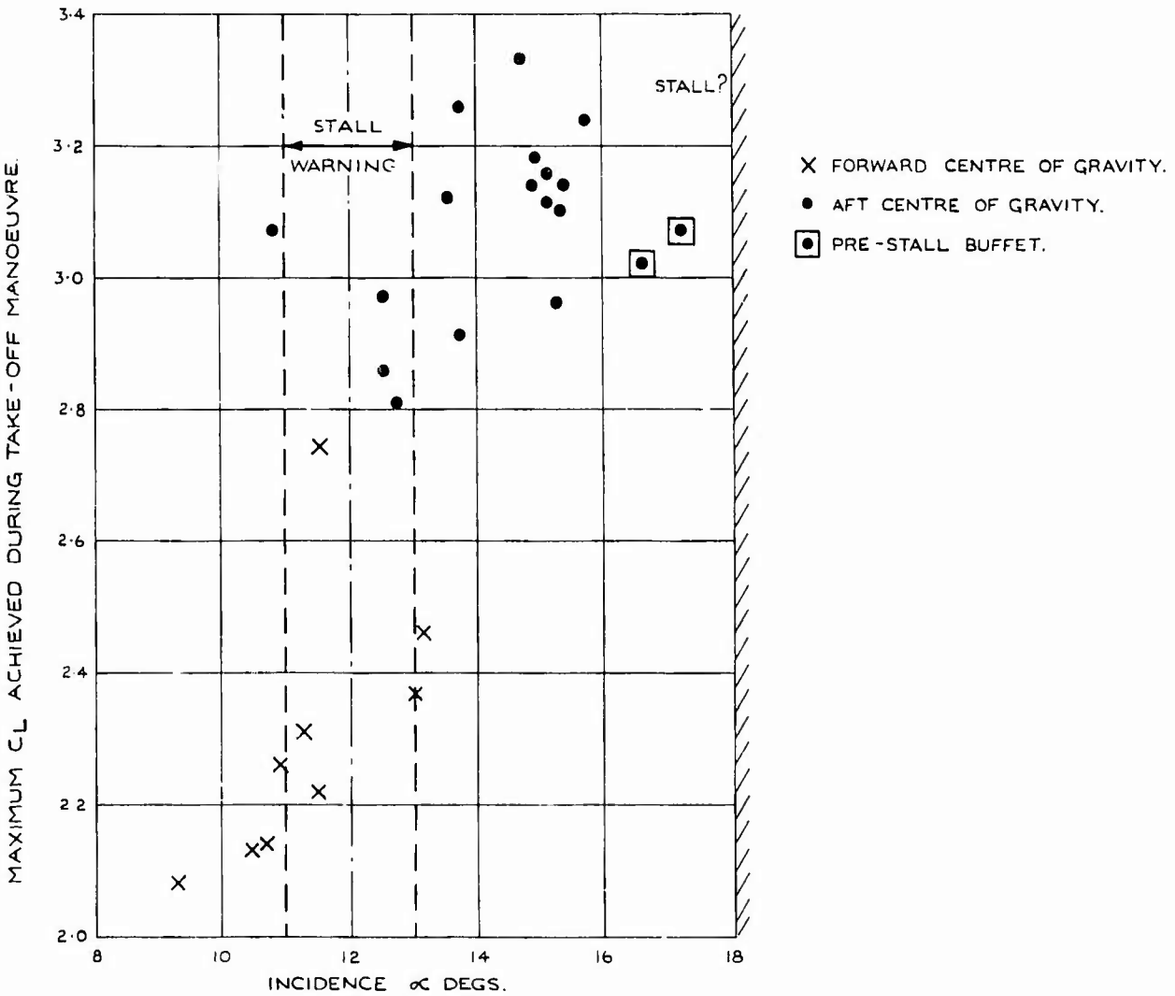

Fig.6 S.T.O.L. take off (early tests)

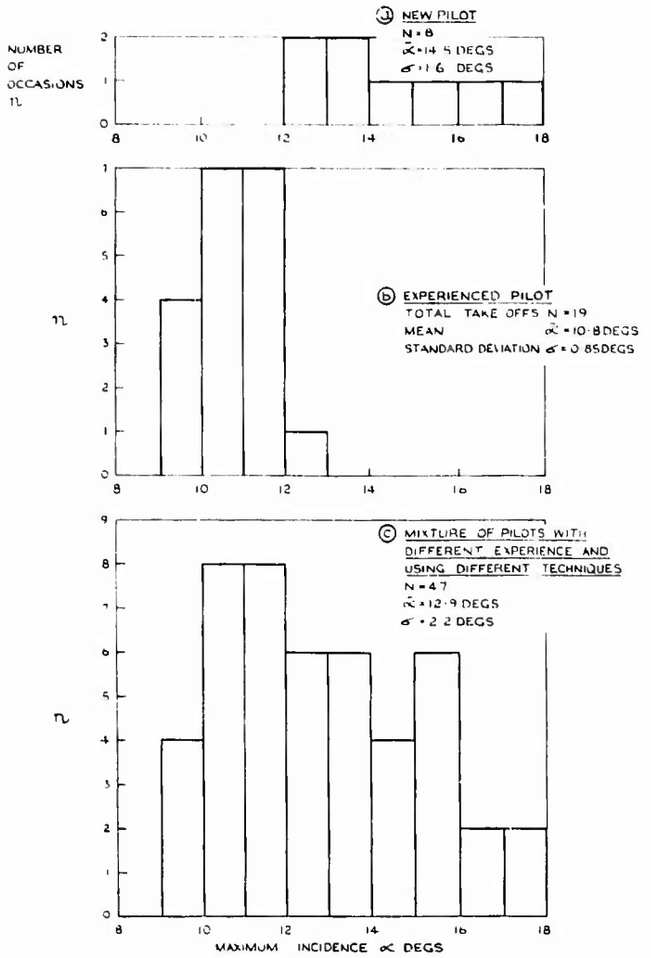

Fig.7 Maximum incidence on S.T.O.L. take off at aft centre of gravity

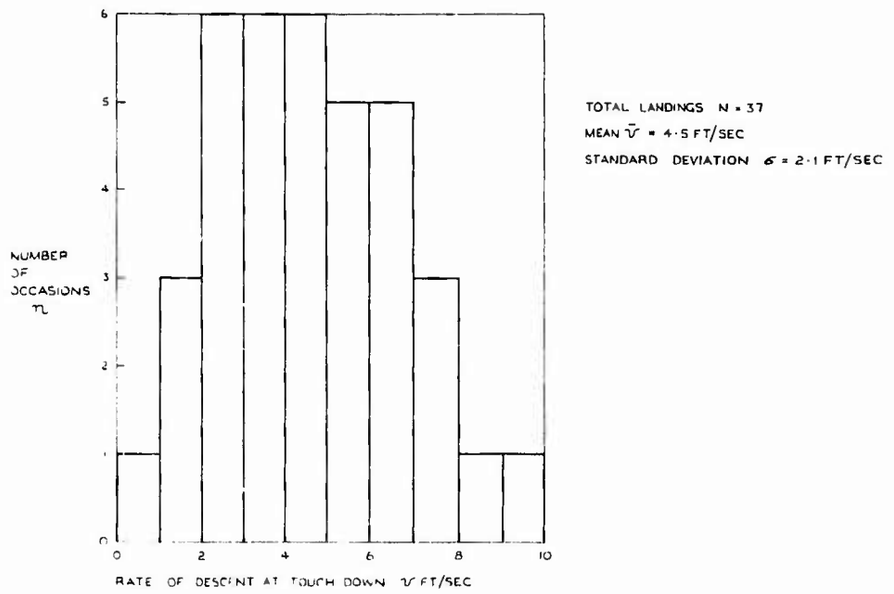

Fig.8 Rate of descent at touchdown for S.T.O.L. landings. Range of centre of gravity position

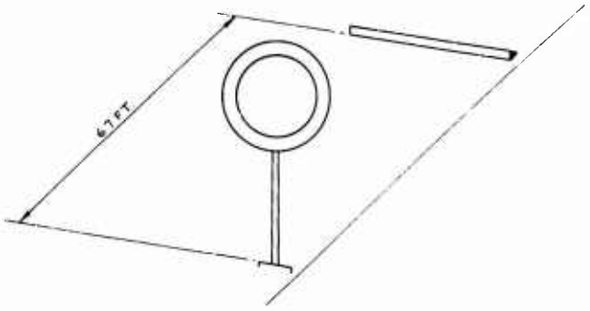

Fig.9 Sketch of ring sight and bar set up for 6° approach

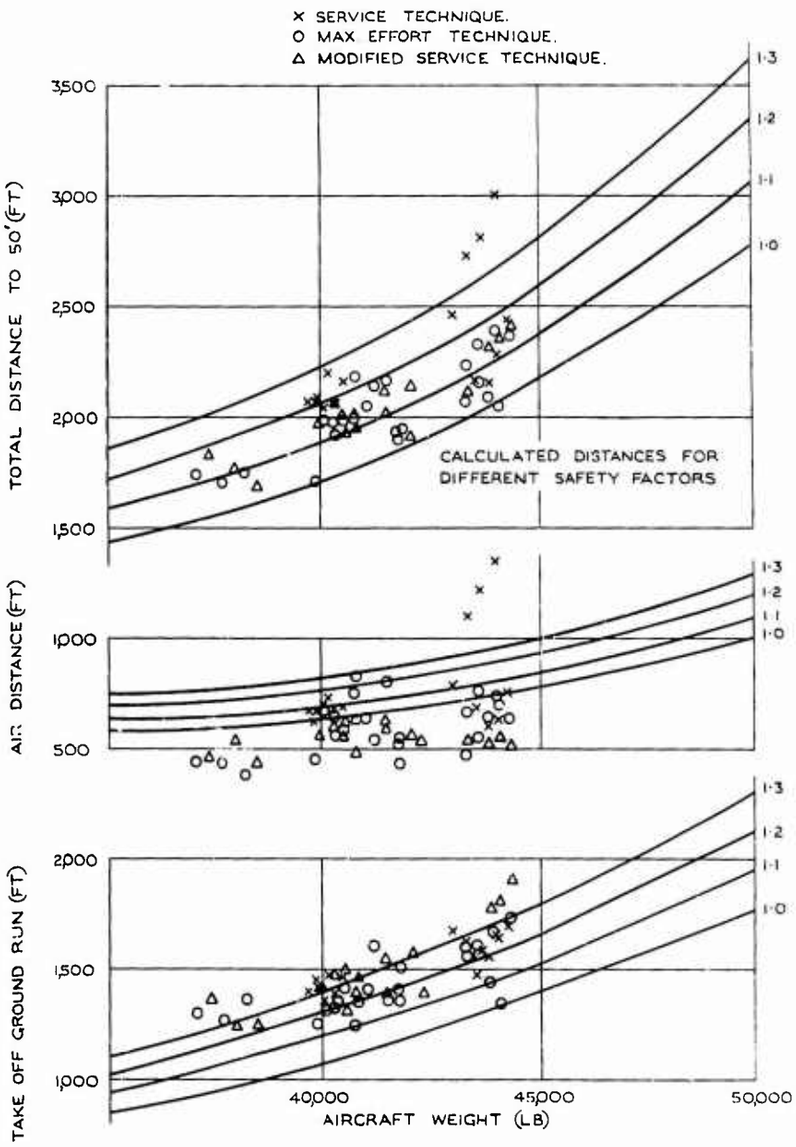

Fig.10 Short take off performance I.S.A. + 20 ° 90 ft. Comparison of test points with calculated distances

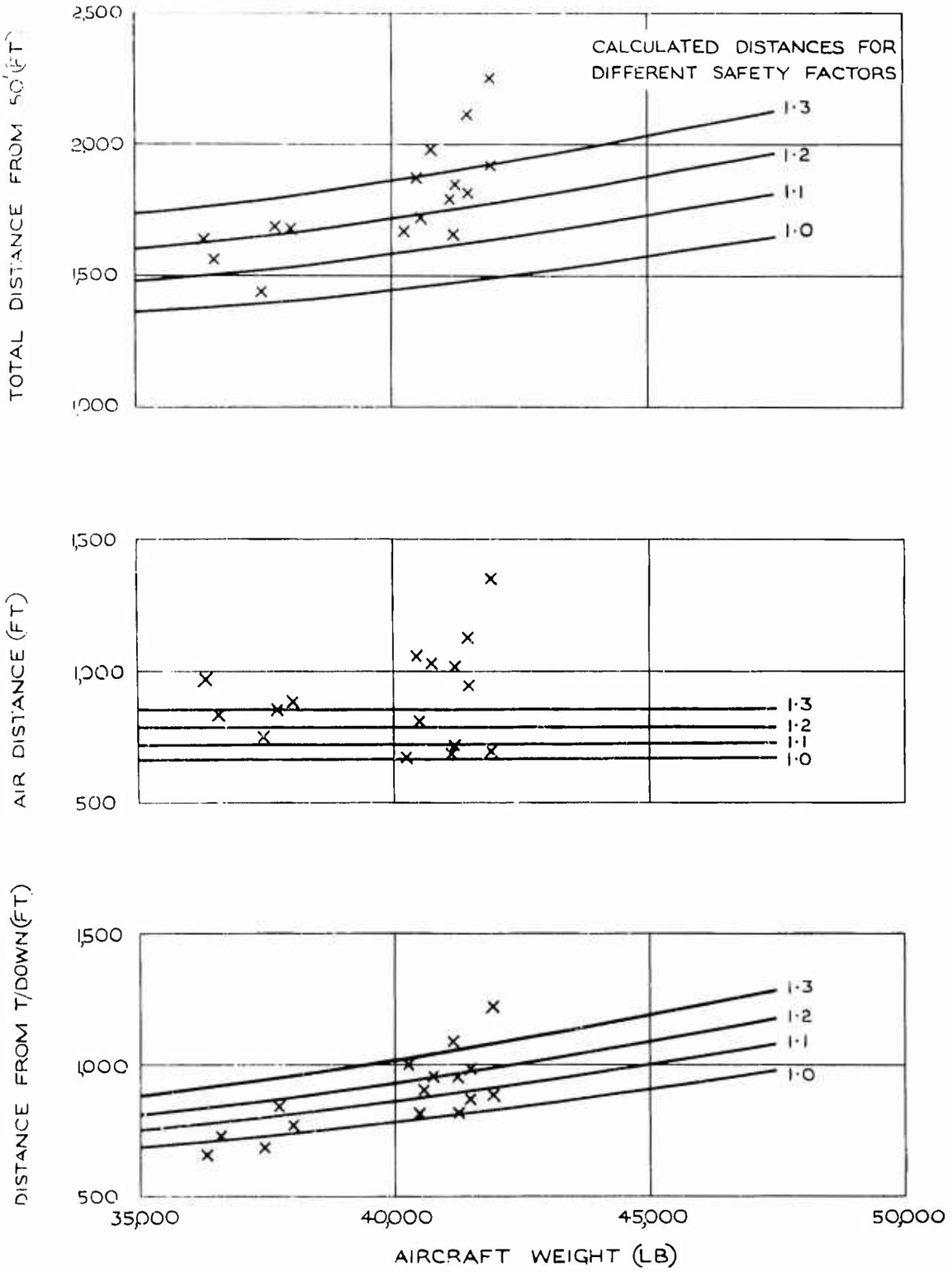

Fig. 11. Short landing performance. U.S.A. + 20° C. 5,000 ft. Comparison of test points with calculated distances

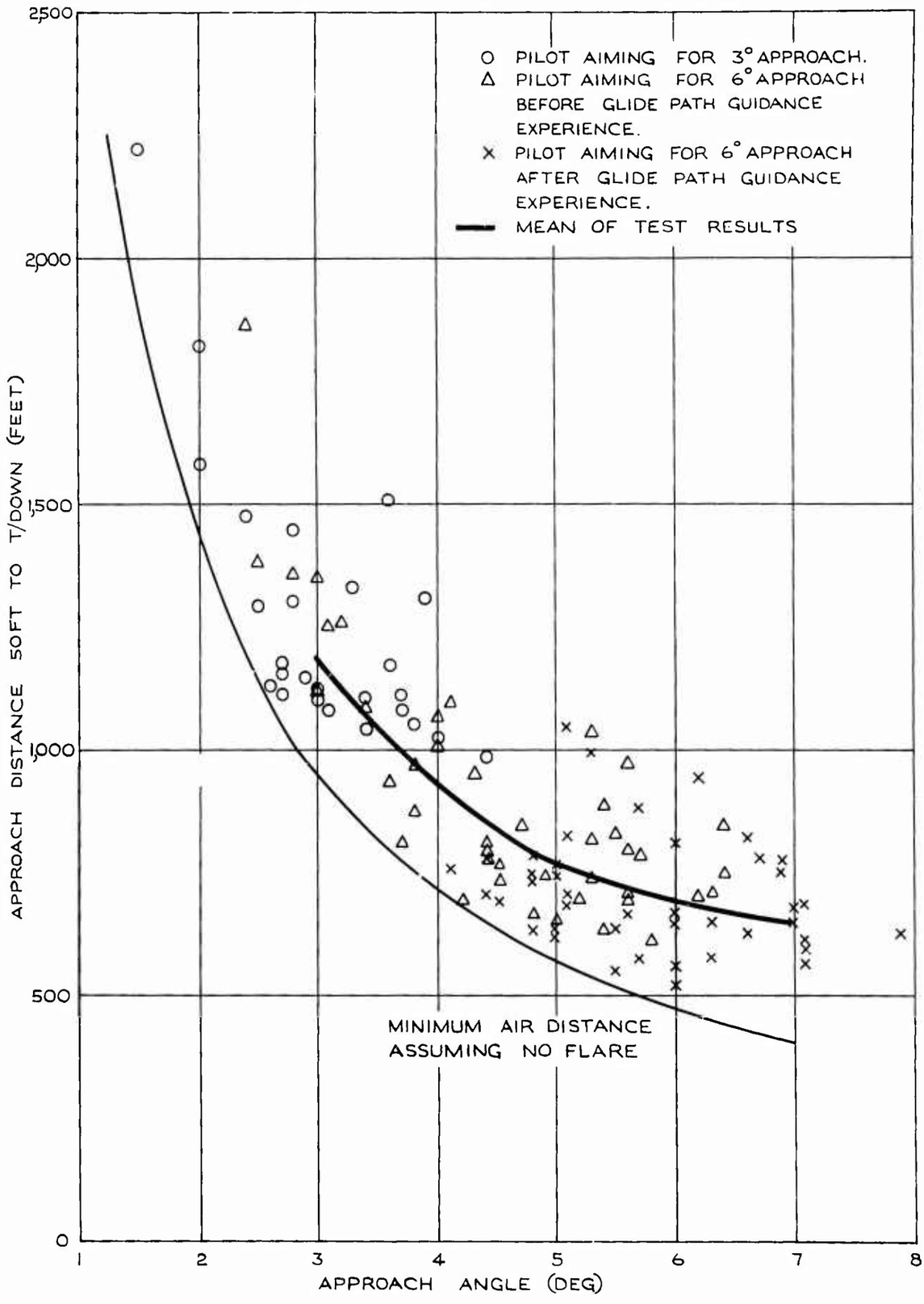

Fig. 12 Approach distance → approach angle

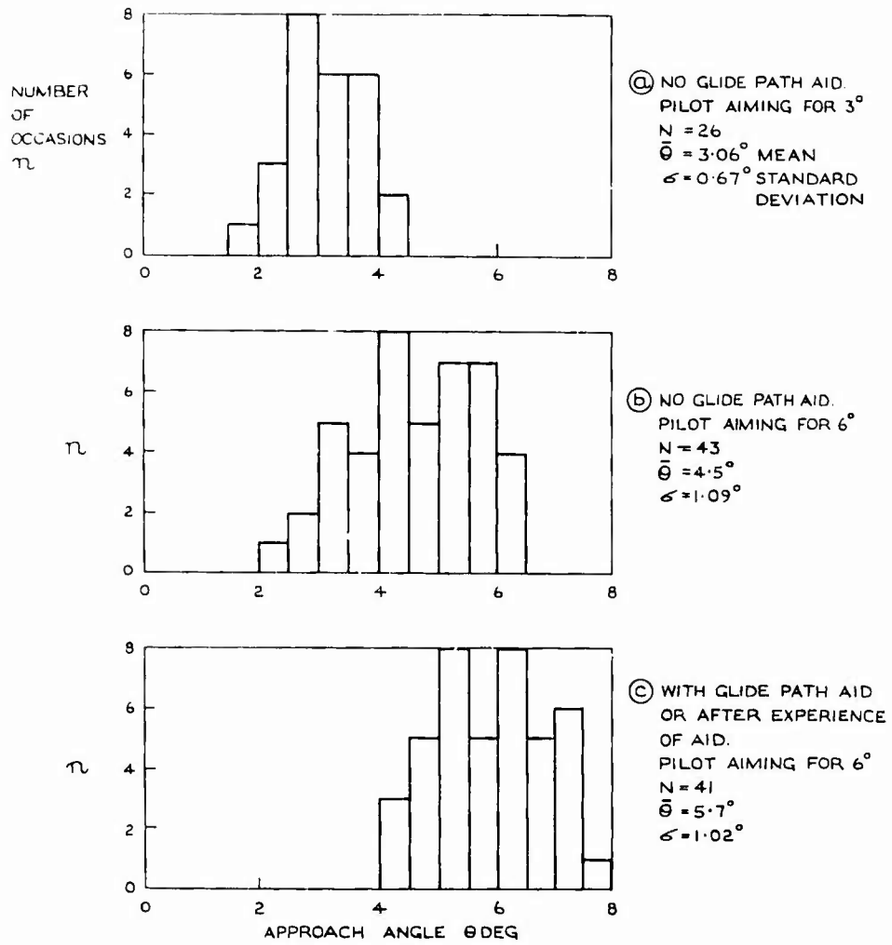

Fig.13 Approach angle through 50 ft. for S.T.O.L. landings

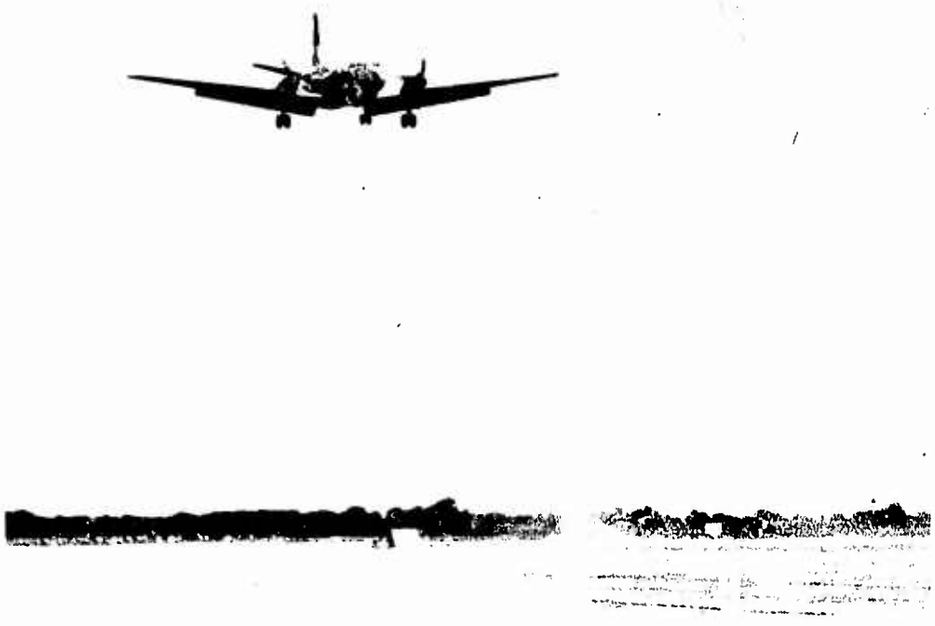

Fig.14 S.T.O.L. landing over water barrier

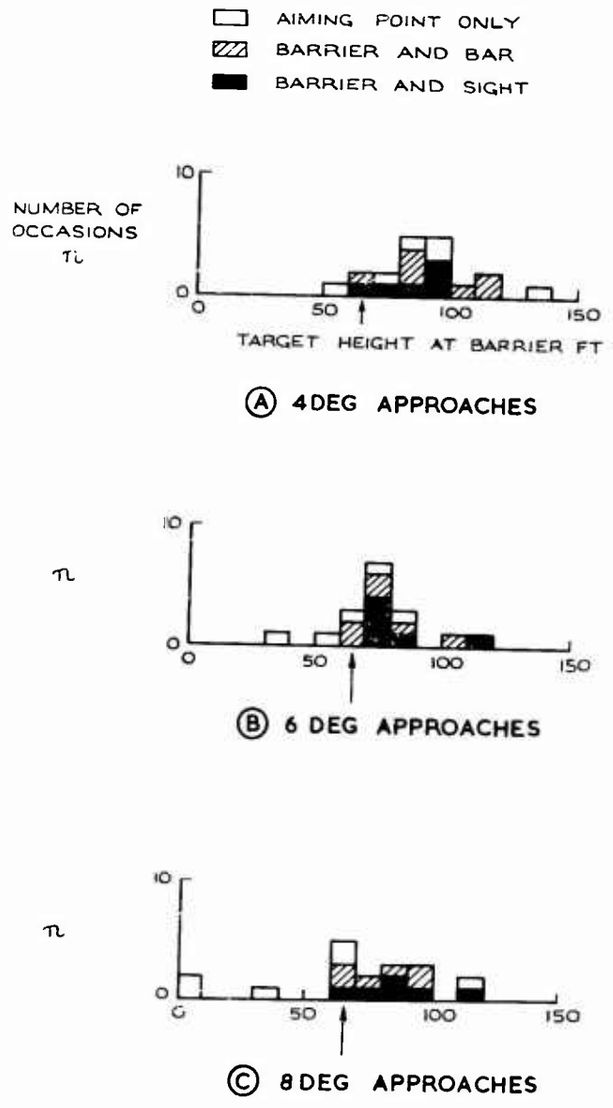

Fig.15 Height at 50 ft. barrier

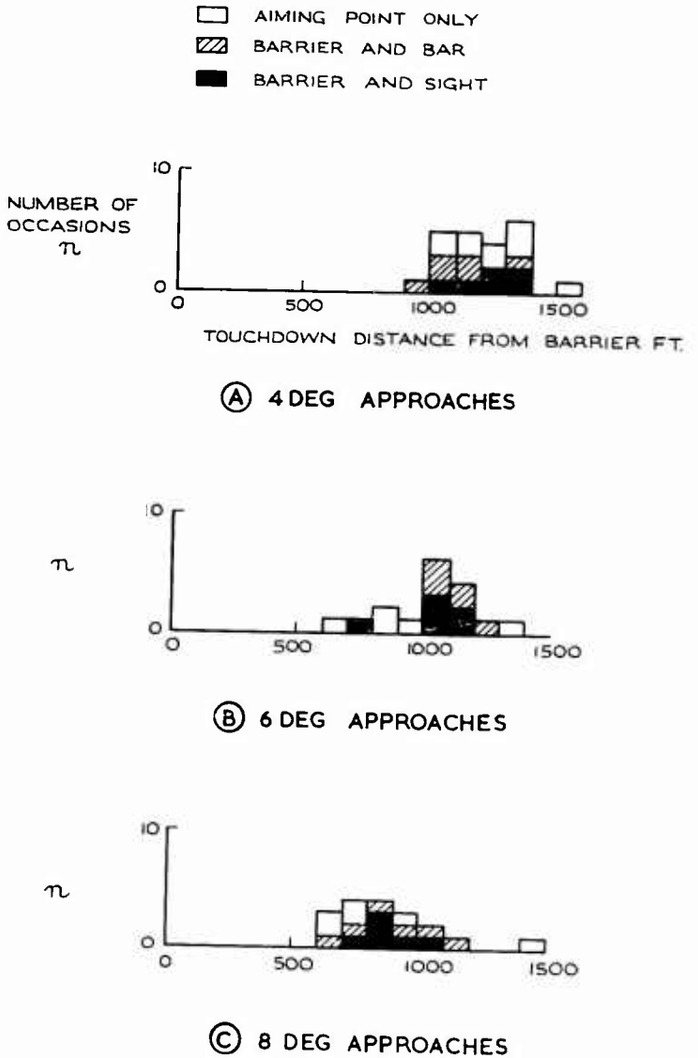

Fig.16 Touchdown distance from 50 ft. barrier

Paper No. 5

FLIGHT TESTING TRANSPORT AIRCRAFT

1. Difference between tasks of A. & A.E.E. (Military) and A.R.B. (Civil)

R.A.F. are only interested in airworthiness aspects and generally sit in on Firm's flying. A. & A.E.E. are interested in both airworthiness and operational aspects, and most clearance trials are done by flying an aircraft at Boscombe Down or Wyton or RAE.

In connection with the handling measurements made at A. & A.E.E., unless specifically requested it is not normal to make detailed comparisons between results achieved and theory or tunnel tests. The results are in the main assessed against standards of acceptability based on past experience and on the average behaviour and the variability of the aircraft under test in relation to its particular role.

2. Comparison of Performance Factors in Appendix 2 of Paper with B.C.A.R. Factors

It is difficult to compare directly as the philosophy of measurement of the basic distances is different, and allowance is made for additional variables such as wet surface and particle clearance in the B.C.A.R. factors.

Basically military performance data presented in an O.D.M. (Operating Data Manual) represents the average achieved by a good Service pilot (as measured at A. & A.E.E. in reasonably good environmental conditions). Because of the need for the Service to vary their operational risk, it is left to the operator to apply an appropriate safety factor to cover scatter and variation from this average standard due to operational or in-life differences from the test conditions. Specification performance is normally based on the A. & A.E.E. unfactored average standard. In the case of performance measured by Firms for incorporation in Civil Flight Manuals when suitably factored by the fixed mandatory factors it is usual to apply considerable effort to produce minimal distances consistent with the defined technique, and on some occasions this technique will require more than the usual standard achieved in the Service unless specific attention is drawn to this aspect.

Removing the factor in B.C.A.R.'s for the effect of a wet surface on ground roll, the required runway length based on landing performance would be about double using B.C.A.R. factors and performance measurements compared with the military standard and factors given in Appendix 2 (Strip A) for the Andover at a weight of 45000 lb.

3. Optimum Flight Path Control

On conventional aircraft it is normal to fly the flight path on the elevator and to control speed using the throttle. This system appears to give generally the best overall control, but particular aircraft and systems must be assessed theoretically and preferably on a simulator to check the optimum technique.

4. Possible Handling Improvements

To reduce air distance scatter, then in addition to using external glide path guidance, it would be possible to fly straight in but one would have to consider the weight penalty with stronger undercarriage apart from possible passenger discomfort aspects. Radio altimeter call-out or HUD presentation could be used to give pilot better indication of precise flare height. A large part of the scatter on the total distance to run from the screen height is due to speed variability and this could probably be improved with an auto-throttle system. Complete auto-pilot system may give more precise control of take-off manoeuvre but could be worse from a handling scatter point of view with similar systems to those at present in use. Director is no use for Andover type situation, as manoeuvre is too rapid, but could be of use for slower type of manoeuvre.

5. Distance Factor of 1.7 in Strip A Landing Case

This covers touch-down variability combined with variability in ground stopping distance.

6. Pilot Technique Aspects Affecting Performance Factors

Includes any complex technique demanding a high degree of training to ensure repeatability; the pilot should not be required to make selections during a very short time take-off run without very precise information on when to make selections (e.g. deflecting flaps or nozzles), or make rapid manoeuvres without the ability to monitor the effect of his inputs continuously. Also, judgement aspects with inadequate visual or other references; (e.g. approach path assessed without external glide path, flare height without accurate height information, etc).

7. Instrument Presentation of Glide Path, e.g. On Head-up Display

The glide path could be given to the pilot on instrument presentation, possibly by measuring ground speed and vertical velocity; but this is more complex than with an external aid because of wind effects and extra head down or up instrument required.

LIFT AUGMENTATION DEVICES

AND THEIR EFFECT ON THE ENGINE

by

J. A. HOOPER, Head of Aircraft Project Studies Dept.

E. A. WHITE, Head of Engine Project Studies Dept.

H. C. HILLIER, Engine Project Studies Dept.

Rolls-Royce Ltd., Bristol Engine Division, Filton, U.K.

SUMMARY

In Part 1, interface problems between engine and airframe associated with the achievement of short field performance are described. Civil and military aircraft are treated with the main emphasis on civil STOL. A range of possible lift augmentation devices is considered, and their effect on engine design is shown. The associated problems of noise and performance are also considered.

In Part 2, optimum engine designs and their particular characteristics for various systems are then described in some detail.

ACKNOWLEDGEMENTS

The authors wish to express their gratitude to members of the New Projects Area of Rolls Royce, Bristol Engine Division for their help in preparing this paper.

The authors also wish to thank Rolls-Royce Limited for permission to publish this paper and emphasise that the views expressed therein are their own and do not necessarily reflect the views of the Company.

PART 1:- INTERFACE PROBLEMS BETWEEN ENGINE AND AIRFRAME

by J. HOOPER

1. INTRODUCTION

This paper is divided into two parts.

Part I considers the interface problems between engine and airframe associated with the achievement of short field performance. Civil and military aircraft are treated, but the main emphasis is on civil S.T.O.L.

Current civil S.T.O.L. requirements are considered, and the need for some form of engine powered lift augmentation device is demonstrated. Lift augmentation devices are treated in a fairly wide meaning of the term, in the sense of any means of providing more lift ranging from blown flaps to direct jet lift. Various possibilities of providing engine power for lift augmentation are considered. Propulsion and lift may be provided by a single multiple-function power unit, or by separate propulsion and lift units. The minimum safe number of engines, and of course, minimum number of types of engine must clearly be a design aim. The problem is therefore approached by first considering the propulsion engine, optimised for S.T.O.L. from the point of view of performance and noise considerations. The compatibility of this engine with the demands imposed by forms of lift augmentation systems such as external and internal-blown flaps is then considered. Having thus investigated the possibility of a multiple function engine, other systems such as separate engine blowing units and separate lift engines are considered. The results of this analysis lead to four separately identifiable engine/airframe combinations, and the establishment of certain basic engine design criteria.

Military aircraft requirements are treated fairly briefly, following much the same approach.

Part II of the paper considers the effect of the design criteria established in Part I on the thermodynamics of the engine, and describes various engine solutions appropriate to the engine/airframe combinations arrived at in Part I. Multiple function powerplants are described, and the penalties associated with non-optimum designs compromised for special purposes are shown. Single function powerplants are then considered, and engines optimised for propulsion, direct lift and blowing air supply are described in detail.

2. CIVIL S.T.O.L.

2.1 Basic Requirements

Because of increasing air and ground congestion, particularly in the United States, increasing attention is being paid to the possibilities of V/STOL. This has led in both the U.K. and Germany to government issued requirements for V.T.O.L. In the U.S. where the problem is much more pressing than in Europe, the emphasis has been placed on S.T.O.L.

Eastern Airlines, a major U.S. carrier that operates in the NE Corridor area issued a draft specification in mid-1969 for a STOL aircraft. Most major airframe companies responded with design proposals. Rolls Royce engines were included in these proposals, and a separate RR response was also made. The results of Eastern's analysis of these proposals are expected to be made public to the participants within the next month or so.

The basic Eastern STOL aircraft requirement is shown in Fig. 1.

The main points to note which are significant in this context, are the 1500 ft. field length and the 95 PNdB noise requirement. These two items provide the main technical difficulty in the requirement.

2.2 Field Performance

In order to understand the demands likely to be made on the engine, it is first necessary to consider STOL field performance.

Some possible lift augmentation devices are shown in Figs. 2 and 3. Fig. 2 shows aerodynamic lift systems representative of the three main types, namely mechanical flap, internal-blown flap, and external-blown flaps. Fig. 3 shows two representative direct lift systems, characterised by vectored thrust and lift fan.

Fig. 4 shows F.A.R. take-off distance versus thrust/weight ratio for these various systems. Internal or external blown flap systems require a total installed thrust/weight ratio of up to 0.55, mechanical flaps with thrust vectoring a thrust/weight ratio of 0.57, and mechanical flaps and lift engines a total installed thrust/weight ratio of approximately 0.62.

Fig. 5 shows landing performance. This figure shows that landing performance rather than take-off is critical. It is not possible to achieve 1500 ft. landing field length with mechanical flaps alone.

Fig. 6 illustrates this more clearly, showing that the shortest practicable field length available with mechanical flaps is of the order of 2000 ft. plus. To achieve shorter field lengths than this, some form of engine augmented lift is necessary.

Figs. 4 - 6 assume an initial aircraft take-off wing loading of 70 lb/ft^2 as being compatible with acceptable ride characteristics.

It is concluded that additional lift must be supplied other than that available from conventional aerodynamic means in order to achieve 1500 ft. field length. The energy required to produce this lift must be generated by some type of engine system. This may take the form of high pressure air for internal flap blowing, engine exhaust air for external flap blowing, or a direct lift thrust input.

2.3 How is this Additional Lift Obtained From the Engines and how is the Propulsion Unit Affected

There are various possibilities, of which the following are considered:

(a) Bleeding HP, IP or LP air.)
(b) High mass flow engine exhaust.) Propulsion Engine.
(c) Vectored thrust.)

(d) Separate bleed engine.

(e) Separate lift engine.

Items (d) and (e) do not significantly affect the propulsion engine; in the next sub-section 2.4 therefore, only (a) (b) and (c) are considered.

2.4 The STOL Propulsion Engine

In considering the propulsion engine it is not sufficient to consider performance alone; noise is of equal if not greater importance. In this section, the ability of the conventional engine design to supply flap blowing air is compared with the capabilities of propulsion engines designed (a) for optimum performance and (b) for minimum noise.

2.4.1 Blowing Air Supply Capability

It is first necessary to consider how much bleed air is likely to be required. Fig. 7 shows a typical curve of C_μ* against ΔC_L. The actual value of ΔC_L for a particular value of C_μ will obviously vary according to the particular flap configuration etc. The band of C_μ shown on the Figure is taken to be representative of that required to achieve the C_L necessary for 1500 ft. field performance. Clearly there is a possible trade-off between mass flow and pressure ratio in order to achieve a desired mV. Fig. 8 shows an important consideration which must always be borne in mind when considering pressure ratio, namely the wing volume which will be taken up by ducting.

Fig. 9 shows the areas from which bleed air is typically extracted and the order of pressure ratio and temperature likely to be encountered.

Fig. 10 shows the approximate limits of bleed air which may be taken and the effect on thrust for a bypass-ratio 3 engine. The gas generator cannot in general supply more than about 15% of its total flow, either IP or HP bleed. It is possible to rematch the engine to take up to about 25% IP bleed at the expense of some performance penalty. There is no effective limit to the amount of bypass air which can be taken. However, low pressure ratio bypass air may be a problem at high λ,s. This question is dealt with more fully in Part II of the paper.

Fig. 11 shows the maximum bleed flow available from the engine for a range of bypass ratios, compared with the flow required as shown previously in Fig. 7. This Figure assumes a fixed overall thrust (including bleed thrust) at 0.7 unstick speed. It is clear that conventional engines of bypass ratio of 3 or above are unable to supply sufficient high pressure air from IP or HP compressors. Only bypass air can be used.

Turning now to externally-blown flaps, higher bypass-ratio is clearly advantageous in lowering exhaust gas velocities and temperatures on the flaps. Fig. 12 shows jet core temperatures versus λ for a flap 12 ft. from the jet nozzle. Below a bypass-ratio of 9 approximately, a steel flap structure is probably required, with consequent weight penalty.

The conclusion reached is therefore that, for internal flap blowing, sufficient HP or LP bleed is only available up to bypass-ratio 3 or so. Bleed is unrestricted from the LP. For external flap blowing, bypass-ratios of above 9 are desirable.

2.4.2 Engine Optimised for STOL from Performance Considerations

This section considers a propulsion engine optimised for STOL solely from the point of view of providing minimum aircraft take-off weight and direct operating costs. For the purposes of arriving at representative weights in the study, it is assumed that lift augmentation is provided by internally-blown flaps supplied with air by separate blowing engines. Thus, propulsion engine design is not compromised by flap blowing considerations. Fig. 13 shows the typical flight profile assumed for STOL operation in this study. Fig. 14 shows a typical STOL aircraft design as used in this study.

---

* $C_\mu = \frac{mV}{qS}$ where M = blowing mass flow, V = expanded jet velocity at blowing slot, q = dynamic pressure, S = Gross wing area

STOL aircraft will tend to be more expensive to operate than CTOL aircraft. Therefore, achievement of minimum possible direct operating costs is of great importance.

Fig. 15 shows the optimum cruise speed for minimum direct operating costs plotted against stage length. Sensitivity is also shown. This Figure was obtained by designing a series of aircraft at each stage length for the speed range shown, and then calculating direct operating costs. For STOL operations the main stage-length is likely to be of the order of 200 nm with some routes up to 500 nm. This is typical of both the U.S. and U.K. A cruise speed of 0.72 is therefore considered to be a reasonable compromise for STOL operation for minimum D.O.C.

Fig. 16 shows the ratio of take-off to cruise thrust required for 1500 ft. and 2000 ft. field length, and the way in which the ratio available from the engine varies with bypass-ratio. A cruise height of 25,000 ft. is assumed. The engine ratio is shown as a band rather than a line, because the choice of engine T.E.T. can affect this ratio. For optimum thrust match for 1500 ft. STOL and 0.72 M cruise, bypass-ratio should clearly be of the order of 9 to 12. Bypass-ratio will reduce if increased cruise speed is required.

Fig. 17 shows the variation of sfc with bypass-ratio, both bare engine and installed (including a factor of 1.5 for aircraft installation effects). Fuel carried is approximately 13% of aircraft T.O.W. Fig. 18 shows the overall result in terms of relative take-off weight and relative direct operating costs versus bypass-ratio, for an aircraft designed to fulfill the 500 nm stage-length Eastern mission. Again bypass-ratios between 9 and 12 are indicated for minimum take-off weight and direct operating costs. No great sensitivity to bypass-ratio is shown, there being only some 2½% difference in D.O.C. between $\lambda = 6$ and $\lambda = 10$.

It is therefore concluded that performance considerations indicate a bypass-ratio of between 9 and 12 for minimum direct operating costs. However, D.O.C.'s are relatively insensitive to bypass-ratio in the region $\lambda = 4$ to 12.

2.4.3 Engine Optimised for Minimum Noise

Noise is becoming increasingly important in dictating engine design. The community in general is beginning to react against all forms of pollution of the environment - to which noise is a significant contributor. In the case of civil vehicles designed for STOL or VTOL, which by implication will operate inside or very close to densely populated areas, it is of over-riding significance. This is reflected in the target noise levels proposed by various bodies for V/STOL compared with conventional aircraft.

Fig. 19 shows target noise levels for CTOL and STOL aircraft. The CTOL levels shown are the latest U.S. Unilateral Regulations (FAA Document Docket 9337, Nov. 3rd. 1969) and are referred to a 1000 ft. sideline distance for comparative purposes. The STOL level is a tentative FAA proposal; Eastern suggest this level at 500 ft. sideline. The main point to note is that the proposed STOL noise levels mean, in simple terms, about half the annoyance noise level of the CTOL. Since many present aircraft are above the CTOL levels shown, the magnitude of the step forward in technology that is required can be appreciated. This section gives a very simplified description of some of the noise reduction methods possible.

In order to understand the problem of engine noise reduction it is first necessary to identify the main source of noise. Fig. 20 shows noise sources for a turbojet and high bypass-ratio turbofan engine. The main sources of noise in the turbofan are the fan, the turbine, and the jet exhaust. Fig. 21 shows the variation with bypass-ratio of the noise produced by these sources for a representative range of engine designs.

The present state of art is such that turbine noise production is imperfectly understood and is therefore difficult to silence for that reason. Jet silencing other than by reductions in jet velocity is difficult if only because of the gas temperatures encountered. This leaves the fan noise as the most amenable to treatment at the present time. In designing for minimum noise there are many factors which must be considered. There are for example, design considerations such as rotor/stator spacing, blade chord, tip speed and number of fan stages as shown in Fig. 22.

Fig. 23 is very important in its influence on STOL engine design. This shows jet velocity versus noise, with turbine and fan noise levels superimposed. It is clear from this Figure, making allowance for possible improvements in fan and turbine noise attenuation, that jet velocities of less than 900 ft/sec should be aimed for. This ensures that the noise source probably least amenable to treatment is under control. The fan noise is left dominant and this can then be reduced by using noise attenuating linings in the areas as shown in Fig. 24. The aim is thus to obtain a balanced minimum noise solution. Typical noise contributions of the three main sources and the effect of noise attenuation is shown in Fig. 25 for a high λ engine.

Fig. 26 shows the effect of bypass-ratio on 1000 ft. sideline noise for both unsilenced and silenced engines. This Figure assumes present day technology in noise attenuation, and shows little difference in noise between $\lambda = 6$ and $\lambda = 12$. However, there are believed to be possibilities of further improvements in state of art of fan attenuating materials, having an effect as indicated by the tentative dotted lines shown in Fig. 26 and showing the possibility of perhaps a further 5 PNdB reduction in noise at $\lambda = 10$ to 12.

Since at present it is exceedingly difficult to meet target STOL noise levels, this is of considerable significance. The conclusion is therefore drawn that the optimum bypass-ratio for minimum noise is of the order of 10 to 12.

2.4.4 Thrust Vectoring

Thrust vectoring will be mentioned only briefly here, since it is discussed more fully in Part II of the paper which deals with some of the detailed engine problem areas. As bypass-ratio is increased, fan pressure ratios decrease in order to maintain the optimum thermodynamic cycle. This in turn means that duct losses become much more important, and results in significant increases in cruise sfc due to nozzle losses as bypass-ratio is increased. In addition nozzle sizes tend to become very unwieldy, and can give rise to significant drag and weight penalities.

For bypass-ratios of the order of 10 or 12 therefore, thrust vectoring does not at present appear to be a very attractive solution.

2.4.5 Optimum Propulsion Engine for STOL

Bringing the conclusions of 2.4.1, 2.4.2, 2.4.3 and 2.4.4 together therefore gives the following results.

For a minimum noise and best operating economics the propulsion engine should have a bypass-ratio between 10 and 12. To minimise installation problems this should clearly be biased towards 10 rather than 12.

If bleed air is required from the propulsion engine, only LP air is likely to be available in the quantities required. Because fan pressure ratio is fairly low (Fan P.R.≈1.5 at these high bypass-ratios for optimum thermodynamic efficiency), some compromise in engine design and efficiency will be necessary to provide the bleed pressure ratios of the order of 2.5 or more which are likely to be required. This is discussed more fully in Part II of the paper.

Gas generator exhaust velocities must be kept below 900 ft/sec.

2.6 Lift Engines

Lift engine requirements are fairly clear and can be stated much more simply. They should be as high a thrust/weight ratio as possible, have low specific fuel consumption, and have noise levels compatible with the requirements specified above. Most people will be familiar with the Rolls Royce RB 202 lift fan engine which is designed to fulfill these requirements, and it is described more fully in Part II of this paper. In essence it is very similar to the propulsion concept described above, in that it has a bypass-ratio of about 10, a single-stage fan, and low exhaust velocity. Because of the emphasis on thrust/weight ratio it has, however, a much lower pressure ratio.

2.7 Blowing Engines

Blowing engine requirements are as for lift engines in terms of high thrust/weight ratios, low sfc and low noise levels. They should also, however, provide air at a pressure ratio consistent with a reasonable duct size i.e. PR = 2.5+.

2.8 Possible STOL engine/airframe Combinations

From the above considerations it is possible to rationalise four types of engine (derived from three basic types) which in correct combination would provide the STOL solution.

These are shown in Fig. 27.

(1) Single Function propulsion unit optimised for performance and minimum noise.

(2) Multi-function unit compromised to provide LP bleed air as well as propulsion.

(3) Single function optimised lift unit.

(4) Single function optimised blowing air supply unit.

Possible engine/airframe combinations (with the minimum safe number of engines quoted) are then as shown in Figs. 29 to 32.

1. External-blown flap using 4 optimised propulsion engines.

2. Internal-blown flap

using (a) 2 optimised propulsion and 2 separate blowing units.

or (b) 4 multiple function propulsion units.

3. Fan lift aircraft using 2 optimised propulsion and 4 optimised lift engines.

3. MILITARY STOL

3.1 Introduction

Military STOL will be mentioned only very briefly since problems of national security intrude when discussing military aircraft. On the subject of transport aircraft present indications are that any military STOL vehicle is likely to be a derivative of a civil machine. The comments given above on

civil aircraft therefore apply. Combat aircraft will be treated very superficially. At the present time noise considerations are not important, performance being the main consideration, so that many constraints affecting civil STOL no longer apply.

3.2 Combat Aircraft Field Performance

Following the approach used in civil STOL, Fig. 28 shows the areas in which engine powered lift augmentation is required, for fixed wing and variable geometry aircraft. This shows that, down to roughly 1000 ft. ground run, the average fighter can be served fairly adequately by mechanical devices. The apparent difference between this result and the civil STOL results is due entirely to the different rules of operation and safety factors involved between civil and military operation. There has been little pressure to reduce these distances in conventional fighters, probably because the high installed thrust/weight ratios of around 0.8 to 1.0 now common in advanced designs give a fairly balanced T.O./landing field performance of around 1000 ft. ground run.

Recent combat aircraft which have used boundary-layer control by flap blowing for various reasons are Phantom, F104, and Buccaneer. Bleed air extraction has caused various detail problems which have been solved satisfactorily in practice.

V/STOL Combat Aircraft

When very short or vertical take-off and landing performance is required then the simplest solution so far proposed is engine lift provided by the vectored thrust engine. The Hawker Siddeley Harrier is the well-known and very successful example of this concept.

A further development of this concept has been proposed, when supersonic capability or high specific excess power are required. This envisages the adoption of a further lift augmentation device known as plenum chamber burning, in which the cold flow from the LP fan is burnt in the front vectoring nozzles to provide considerable thrust or lift boost. This can typically augment lift off thrust by some 30% and has a significant effect on specific excess power.

Combinations of vectored thrust engine and lift engine have also been proposed, as in the German VAK 191 prototype now under construction.

In a combat aircraft, lift engine volume and thrust/weight ratio are all important. Low noise levels and low specific fuel consumption are relatively unimportant, and this leads to the adoption of a turbojet design such as the RB 162 or the XJ99, in contrast to the $\lambda = 10$ RB 202 civil design.

PAYLOAD	100-200 PASSENGERS.	
DESIGN STAGE LENGTH	500 N.M.	
FIELD LENGTH	1500 FT. (S.L. 90°F)	
CRUISE SPEED	350-500 KTS. T.A.S.	ISA+10°C
CRUISE ALTITUDE	15,000 - 30,000 FT.	
NOISE	95 Pndb.	
TIMESCALE	1973-1975	

Fig.1 Typical STOL requirement (Eastern Airlines US)

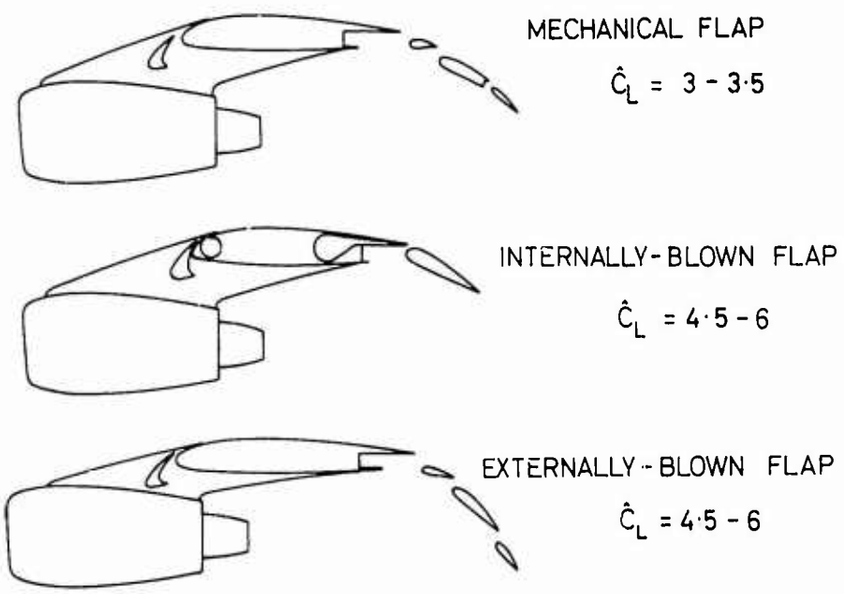

Fig.2 Aerodynamic lift systems

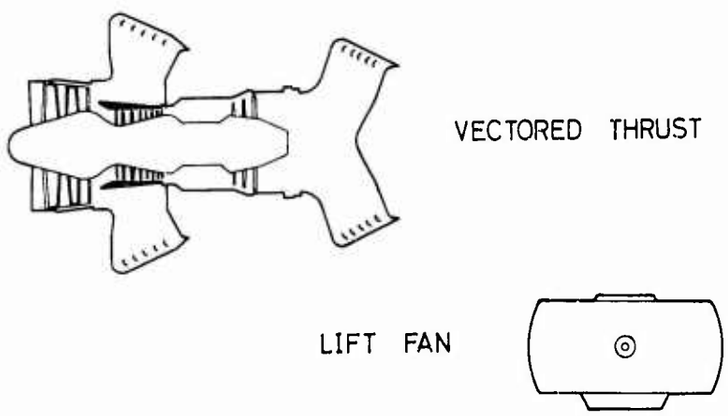

Fig.3 Direct jet lift systems

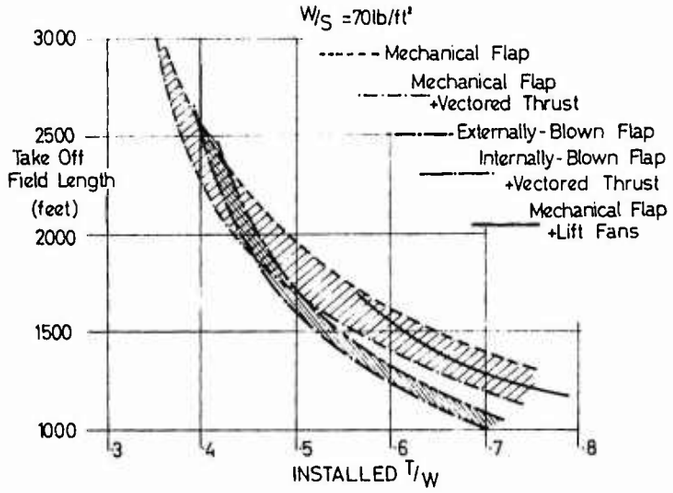

Fig.4 Take-off performance

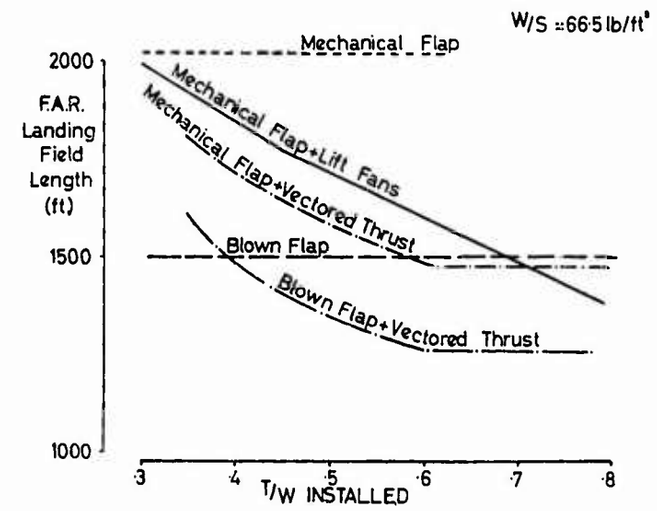

Fig.5 Landing performance

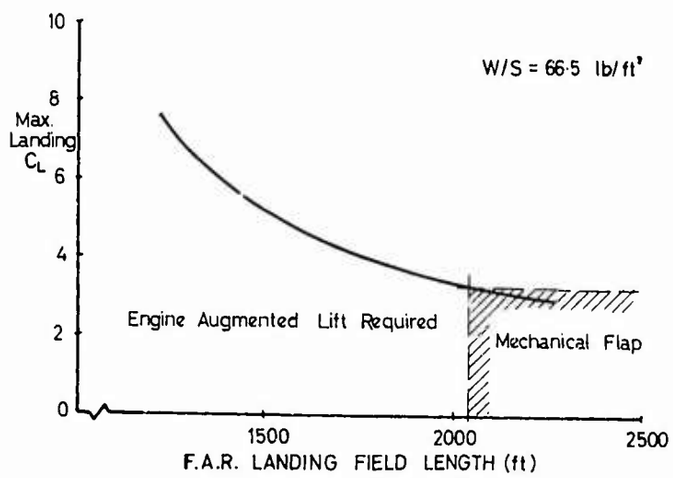

Fig.6 Effect of C_{Lmax} on landing performance

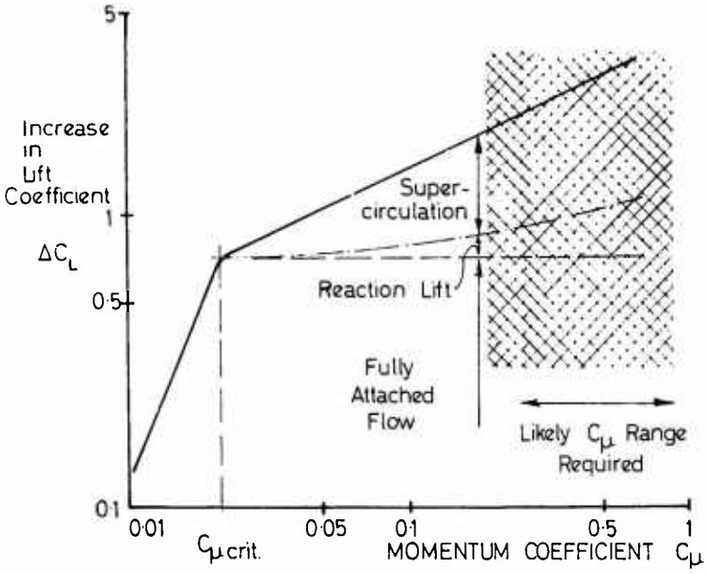

Fig.7 Additional lift generated by blowing

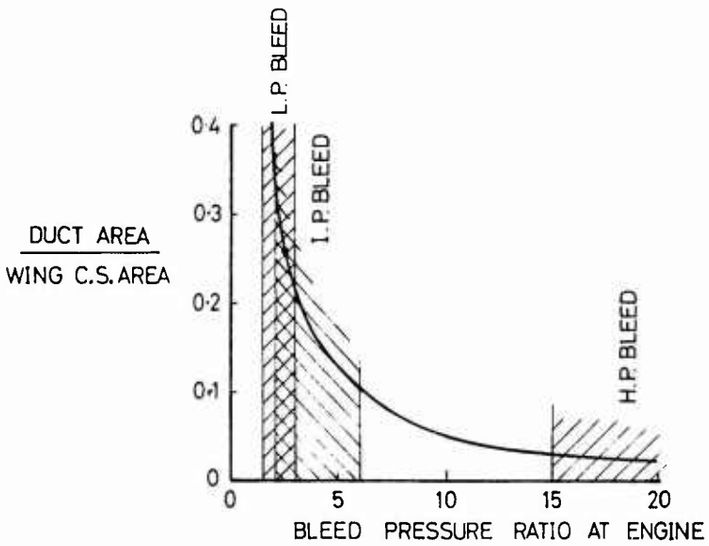

Fig.8 Influence of pressure ratio on duct area

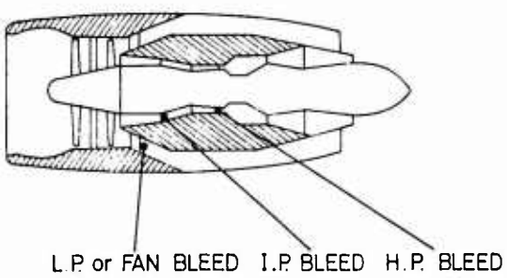

	L.P. or FAN BLEED	I.P. BLEED	H.P. BLEED
PRESSURE RATIO	1·2 - 3	2 - 6	15 - 25
TEMPERATURE °K	310 - 470	375 - 575	700 - 900
% GAS GEN. FLOW (MAXIMUM)	100 x Bypass Ratio	10 -15%	5 -10%

Fig.9 Bleed sources bypass engines

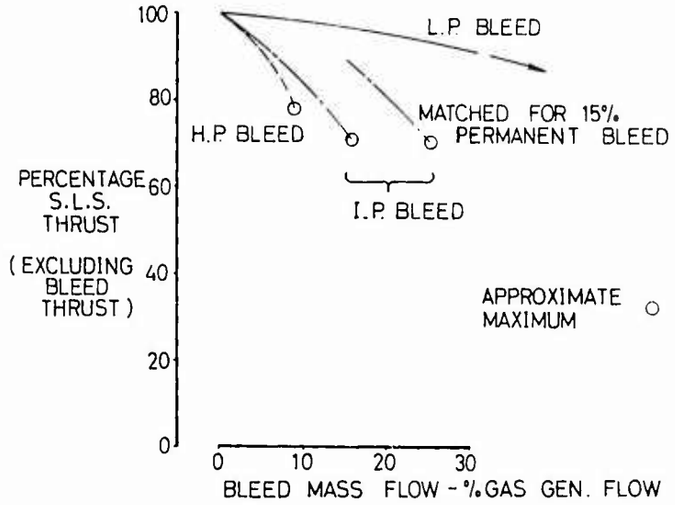

Fig.10 Effect of bleed on static thrust

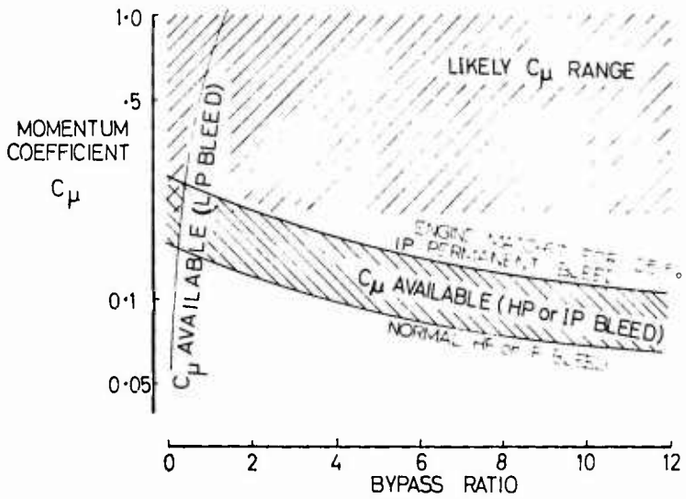

Fig.11 Momentum coefficient available

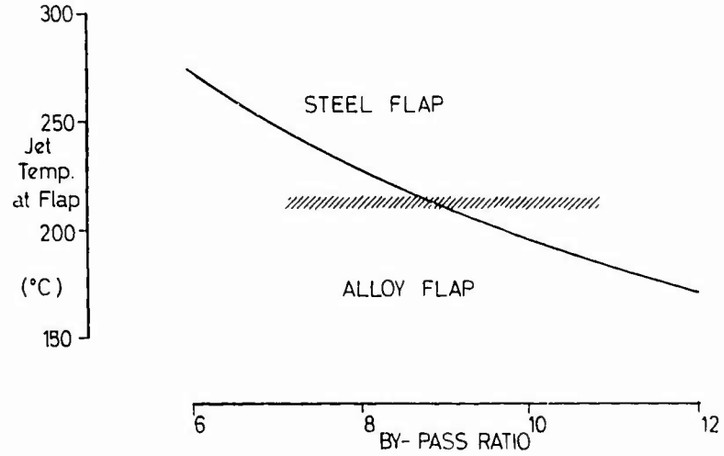

Fig.12 Jet temperature at externally-blown flap

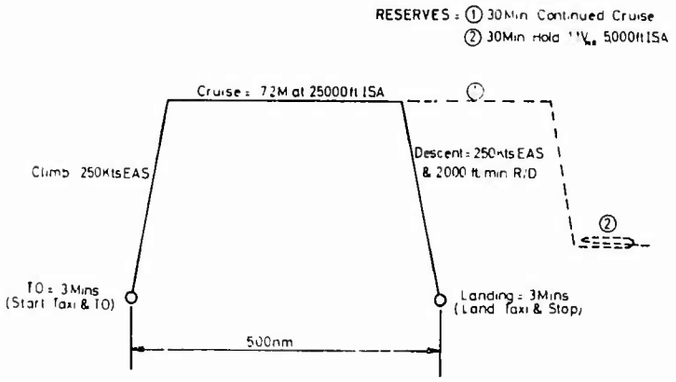

Fig.13 Typical STOL flight profile

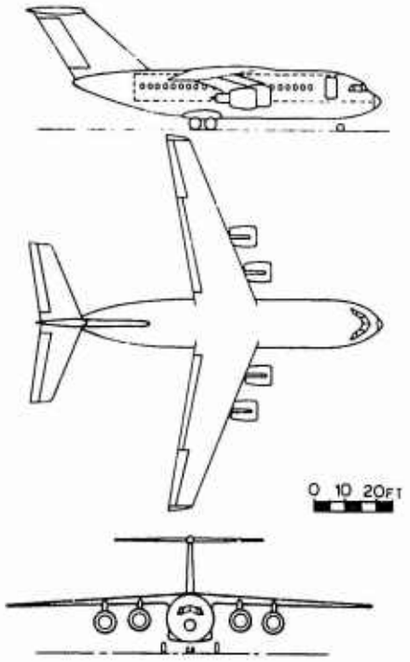

Fig.14 Typical STOL design

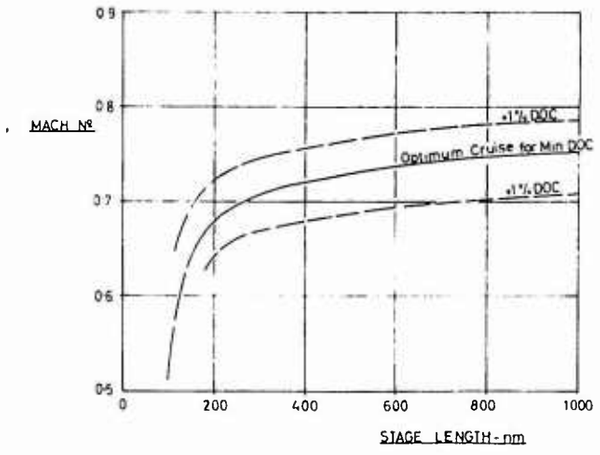

Fig.15 Cruise speed for minimum DOC

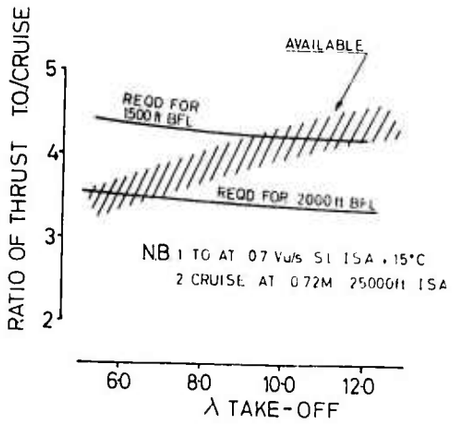

Fig.16 Effect of bypass ratio on thrust matching

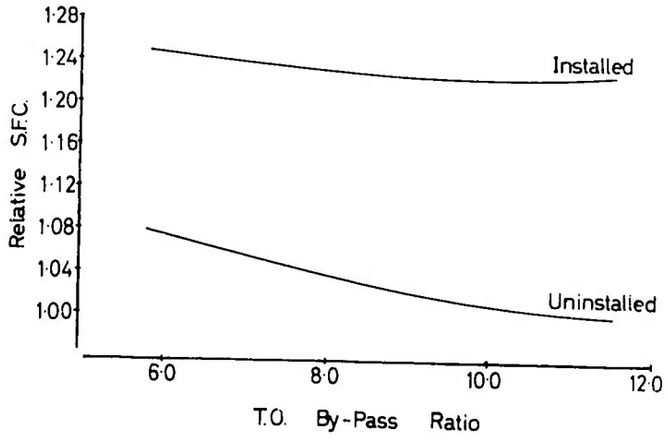

Fig.17 Effect of bypass ratio on SFC

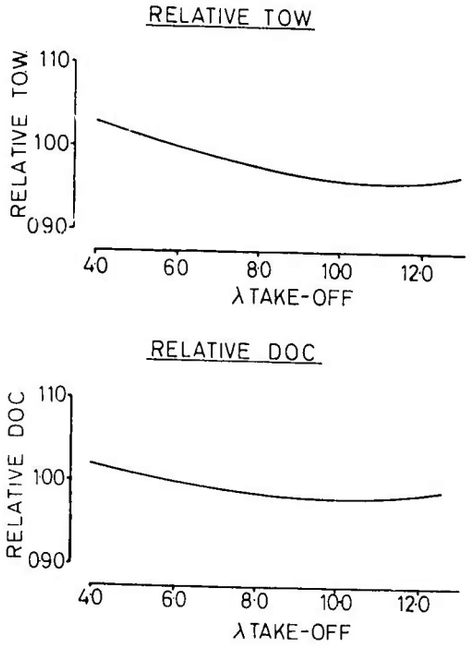

Fig.18 Effect of bypass ratio

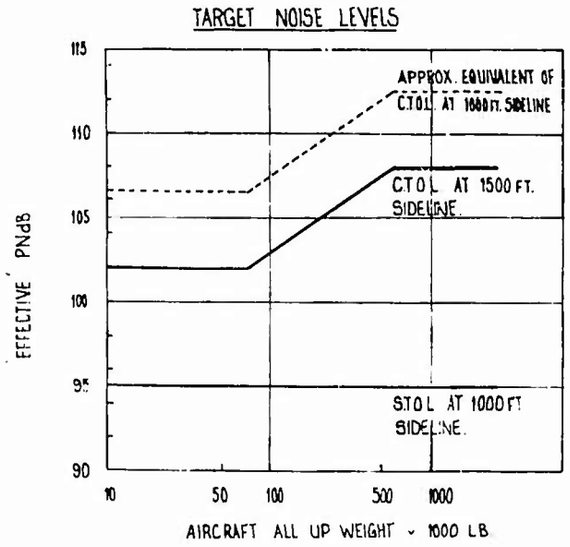

Fig. 19 Target noise levels

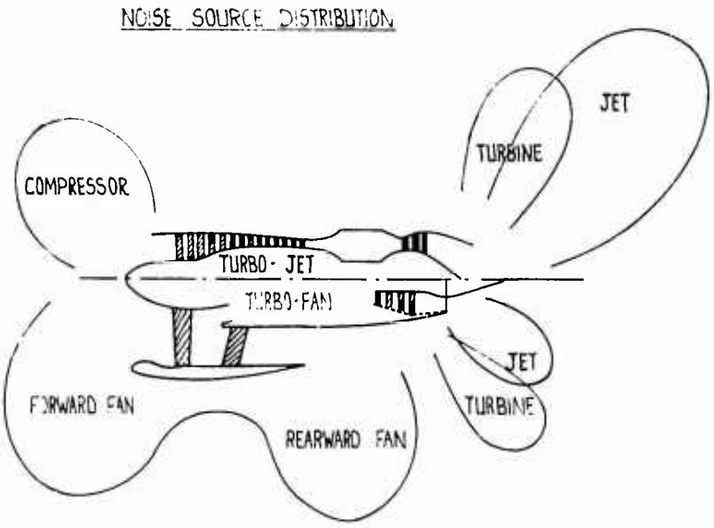

Fig. 20 Noise source distribution

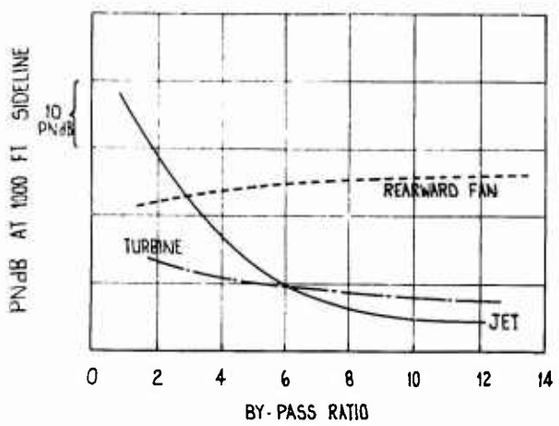

Fig. 21 Effect of bypass ratio on noise components

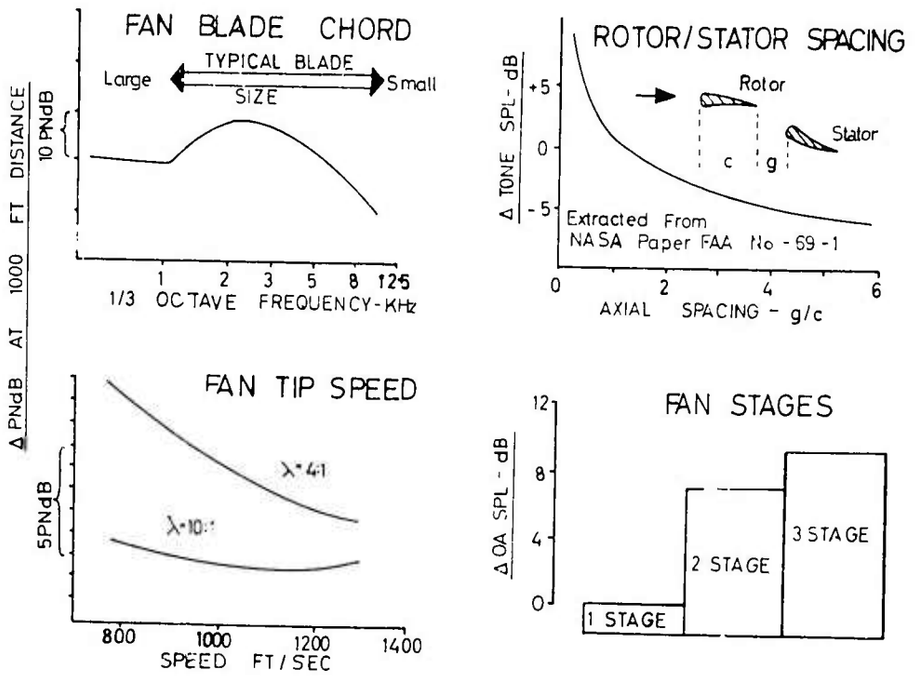

Fig.22 Effect of fan design parameters on noise

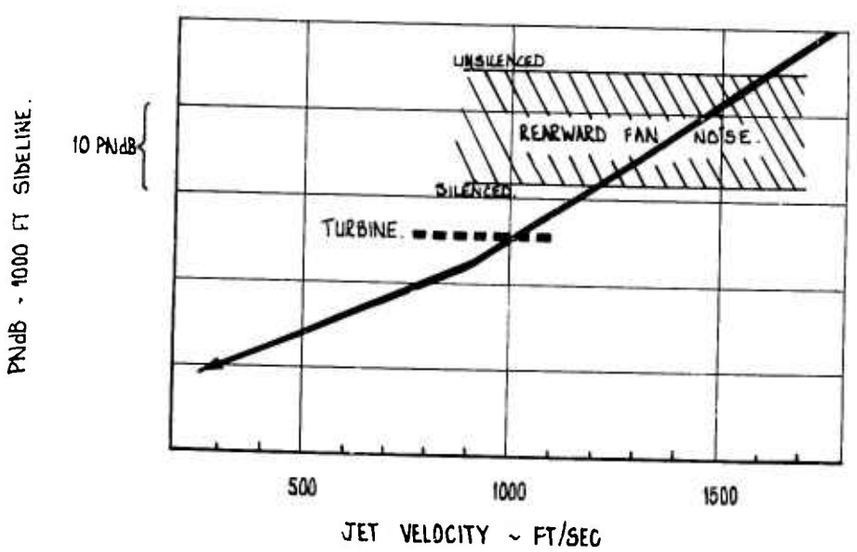

Fig.23 Effect of jet velocity on noise

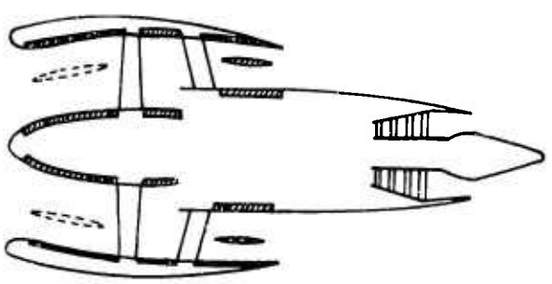

Fig.24 Acoustic lining

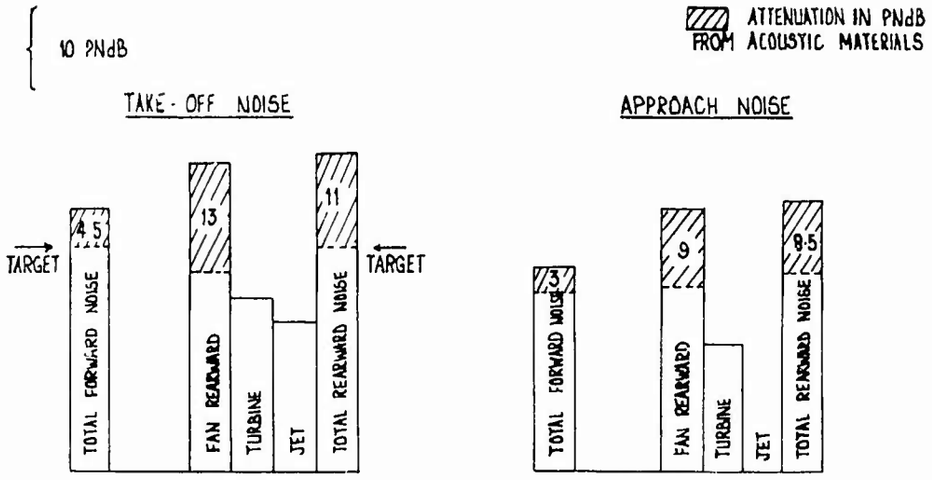

Fig.25 Effect of acoustic materials on total forward and rearward noise

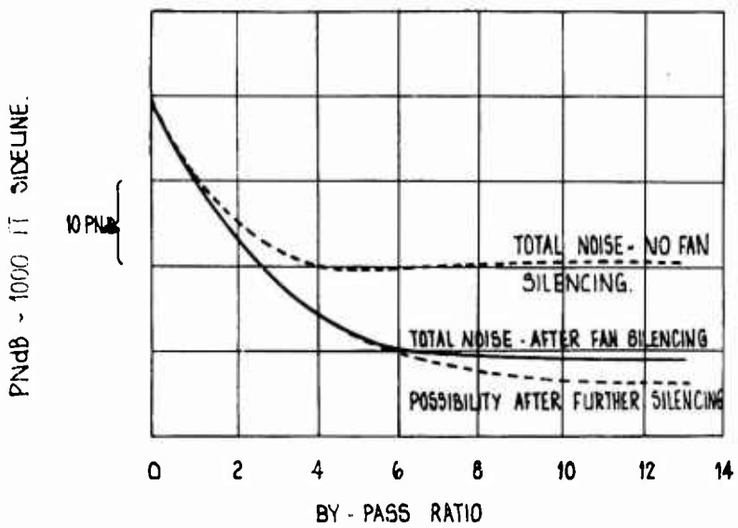

Fig.26 Variation of noise with bypass ratio

1 SINGLE FUNCTION PROPULSION UNIT OPTIMISED FOR PERFORMANCE AND NOISE

2 MULTI-FUNCTION PROPULSION UNIT COMPROMISED TO PROVIDE L.P. BLEED AIR

3 SINGLE FUNCTION OPTIMISED LIFT UNIT

4 SINGLE FUNCTION OPTIMISED BLOWING AIR SUPPLY UNIT

Fig.27 STOL engine types

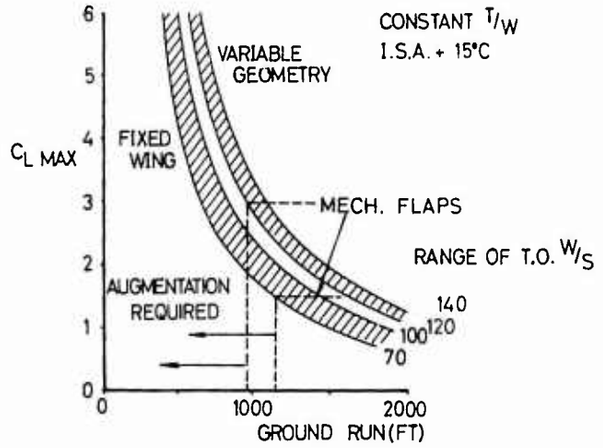

Fig.28 Landing performance of combat aircraft

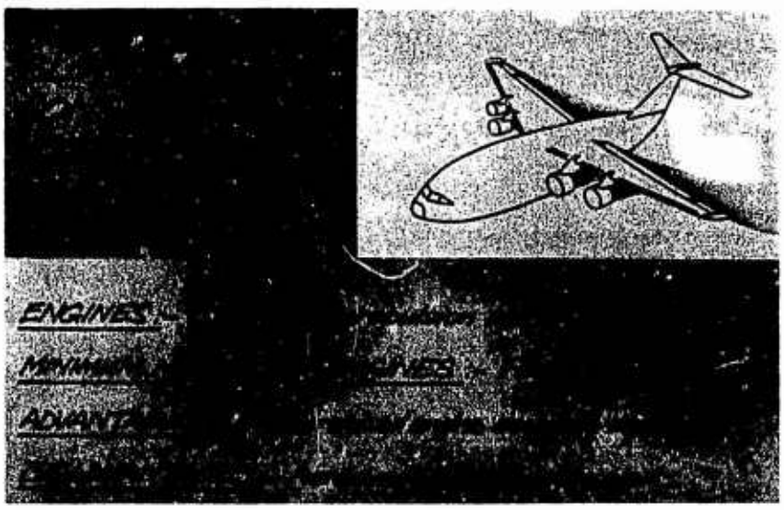

Fig.29 External-blown flap configuration

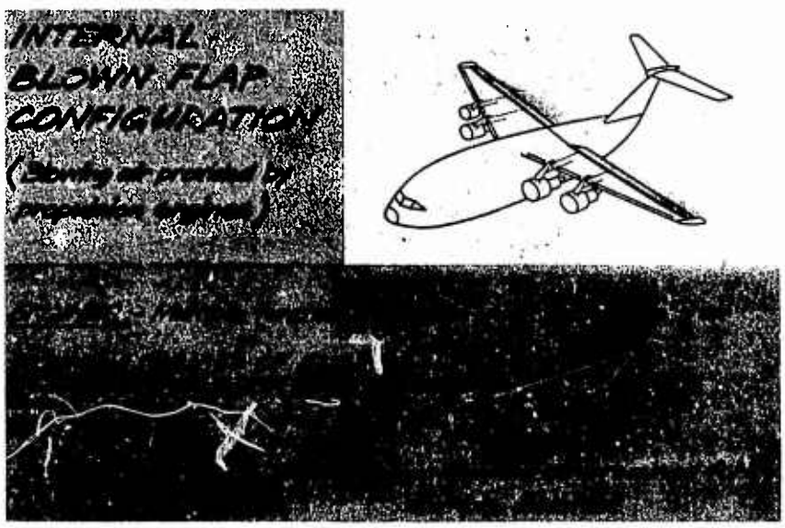

Fig.30 Internal-blown flap configuration (blowing air provided by propulsion engines)

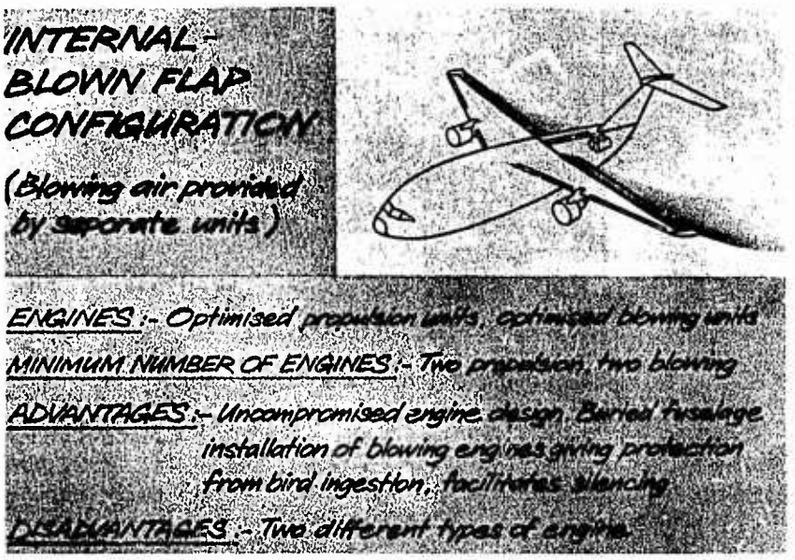

Fig.31 Internal-blown flap configuration (blowing air provided by separate units)

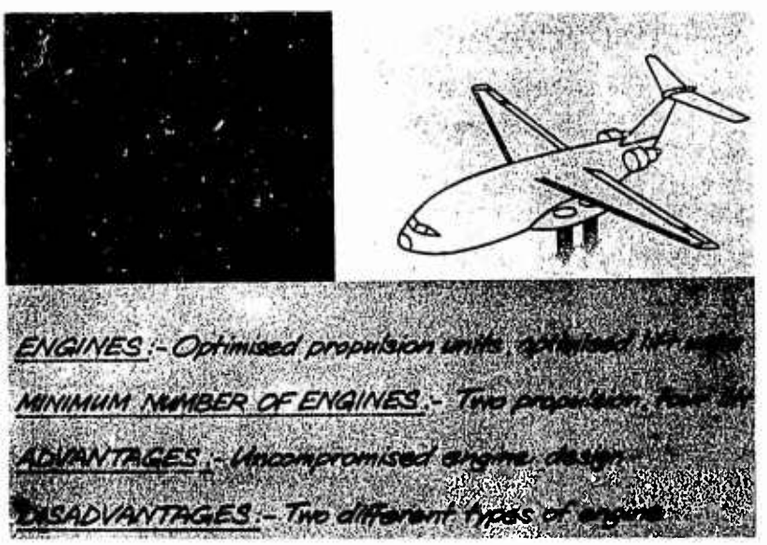

Fig.32 Lift fan configuration

PART 2 - THERMODYNAMIC PROBLEMS AND SOME POSSIBLE SOLUTIONS

by E.A. WHITE and H.C. HILLIER

1. INTRODUCTION

This part of the paper takes up the design criteria established in Part I on the thermodynamics of the engines for STOL applications, and leads in to descriptions of several possible engine solutions with their associated advantages and disadvantages.

2. PROPULSION ENGINE WITH BLEED AIR CAPABILITY

Part I of the paper has already indicated that the penalties associated with providing large quantities of bleed air from a conventional propulsion engine are severe, the severity increasing with bypass-ratio.

Fig. 1 shows the take-off thrust penalty for IP delivery bleed up to 25% of the gas generator flow and Fig. 2 shows similar data for HP delivery bleed, for an engine of 15000 lb. thrust. These show that, for a given aircraft bleed requirement in actual pounds/second (typically 15 lb/sec. for a four engined 100 seat aircraft), the penalties at quite modest bypass-ratios are unacceptable. Bleeds above 15% could in any case give rise to flow matching problems, losses in compressor efficiency arising from poor velocity profiles, and design problems in physically extracting the bleed air. Fig. 3 shows how the gas generator air flow falls at a given thrust size with increasing bypass-ratio and hence illustrates why the bleed penalties are so crippling.

The question therefore arises of utilising bypass bleed air. There is virtually no restriction on the amount available, certainly where the primary and secondary streams are unmixed. However, it has already been said that a bleed air pressure ratio in excess of 2.5 is desirable in order to minimise the flow requirements and duct sizes. Fig. 4 shows optimum fan pressure-ratio against bypass-ratio and above a bypass-ratio of about 2:1 the bypass air pressure-ratio is inadequate. The engine cycle could be compromised in the interests of maintaining the bypass pressure-ratio at the required level but the performance penalties are again severe. Fig. 5 shows the losses in thrust and Fig. 6 the increases in specific fuel consumption, stemming from this compromise at various bypass-ratios. Above a bypass-ratio of around 3.5 the cycle becomes thermodynamically impossible owing to an insufficiency of energy in the core flow.

It is reasonable to conclude that these penalties are unacceptable at the high bypass-ratios required for optimum cruise performance. Hence the dilemma facing the engine designer. At the high bypass-ratios required for cruise the penalties associated with bleed from the gas generator are high and the bypass bleed air pressure-ratio is inadequate, whereas the optimum engine with a high enough bypass pressure-ratio has an unattractively low bypass-ratio for cruise. The latter also suffers from another drawback, namely, a fundamentally high jet noise level arising from the high velocity of the primary stream efflux. Fig. 7 summarises these efflux conditions and indicates the typical sideline jet noise level of 110 PNdB, 1000 ft. lateral distance with an aircraft speed of 200 knots.

However, a neat solution to all these problems is possible. Fitting an aft fan to the primary stream will not only drop the hot jet velocity and therefore jet noise levels to acceptable values, but will increase the thrust of the complete powerplant and produce an overall bypass-ratio giving low levels of cruise specific fuel consumption. Fig. 8 outlines the design parameters of an aft fan unit for such an engine, and shows that it is possible to achieve a hot exhaust velocity of 900 ft/sec with local bypass-ratios around 4:1 and fan pressure-ratios around 1.45. Fan matching problems, the desirability of a single stage fan turbine for mechanical simplicity and the need for a low fan tip speed (around 1100 ft/sec) from machinery noise considerations will together dictate the actual choice of aft fan parameters. These are summarised in Fig. 9.

The typical layout of a complete powerplant is shown in Fig. 10 and the performance of such an engine is summarised in Figs. 11 and 12. The engine will provide a propulsive thrust at take-off of 16500 lb., together with a total bypass bleed airflow of 80 lb/sec. at a pressure ratio of 2.75, assuming a basic engine total intake air mass flow of 200 lb/sec. At a typical cruise condition of 0.75 Mach number, 25000 ft., the total propulsive thrust assuming the bleed air is expelled from a separate propelling nozzle is 4660 lb. and the resultant specific fuel consumption is 0.75 lb/lb/hr.

The engine noise levels would still be unacceptably high without acoustic treatment owing to the gas generator fan and aft fan machinery noise components. However, suitable treatment will reduce the noise levels to values of around 100 PNdB at the three measuring points as is shown in Fig. 13. These values, whilst meeting F.A.A. regulations for conventional aircraft, are still higher than the F.A.A. proposals for STOL aircraft which will be extremely difficult to meet with any engine.

3. PROPULSION ENGINE WITH BLEED AIR CAPABILITY 'DESIGNED IN'

Hitherto, we have been considering the penalties and problems of large air bleeds at take-off on engines without a basic bleed capability inherent in the original design and with an optimised cruise performance, without bleed as a prime consideration. An alternative solution to the choice of a suitable engine which appears to have several advantages is the high bypass-ratio turbofan with an oversized IP compressor fundamentally capable of providing large airbleeds. Such an engine would avoid the compressor mis-matching problems mentioned earlier and the performance penalties are considerably reduced.

Fig. 14 shows the losses in take-off thrust at various bypass-ratios with IP compressor delivery bleeds up to 25% of the primary flow for engines designed to this concept. Fig. 15 highlights the benefits of this approach compared to the engines described earlier. At a bypass-ratio of 6:1, for example, the loss in take-off thrust is improved from 35% to 25% by this technique. Fig. 16 shows the layout of a typical three-shaft engine designed on these principles. Such an engine would naturally embody the levels of technology to be anticipated in the next generation of large civil subsonic transport propulsion engines. In particular the fan tip speed would be kept down to around 1100 ft/sec. or less, to minimise the fan machinery noise and the hot jet velocity would be intrinsically low. The engine configuration would lend itself to conventional acoustic treatment of the fan inlet and outlet ducts.

4. PROPULSION ENGINES WITH NO BLEED REQUIREMENTS

We now consider the choice of a STOL propulsion engine where there is no requirement for large air bleeds. Clearly, in this case, the provision of additional lift during take-off and particularly landing would result from the use of separate blowing engines or direct lift engines both of which are described in a later section of this paper.

It is worth reiterating a conclusion from Part I of the paper, that for low noise levels the hot jet velocity of any engine must be kept to 900 ft/sec or so and in order that acoustic treatment of the fan will produce a balance between jet and machinery noise generation. Fig. 17 shows hot jet velocity against bypass-ratio for a range of turbofans with optimum fan pressure-ratios and indicates that bypass-ratio must be around a value of 10:1 in order to achieve the desired aim. Part I went on to conclude that a bypass ratio of around 10:1 will be optimum for STOL aircraft when all considerations are taken into account and we now examine the problems encountered in the design of such an engine.

Fig. 18 illustrates a number of possible engine arrangements embracing two-shaft and three-shaft layouts, both with directly driven fans and with fans driven through a reduction gear. It is evident that some configurations have distinct disadvantages. A two-shaft engine with directly driven fan has a large number of LP turbine stages at a very large mean radius. Since the fan tip speed must be kept down to around 1100 ft/sec or less the IP compressor, which is connected to the same shaft, would either have to be designed at very high hub:tip ratios to achieve adequate blade speeds or a low loading be accepted and hence a low pressure-ratio. A directly driven three-shaft engine would escape the latter problem, but would require a five stage LP turbine even when the mean radius is nearly double that of the IP turbine. (If the IP turbine mean radius is maintained, the LP turbine would require more than 10 stages).

Hence we are drawn to the attractiveness of the geared fan solutions. These have the virtue of few LP turbine stages and by a suitable choice of reduction gear ratio (around 3:1) the fan tip speed may be kept down to the desired levels without compromising the design of the IP compressor. The three-shaft geared fan engine would encounter shaft whirling problems and seems mechanically unnecessarily complex, whereas the two-shaft engine retains the advantages without the mechanical drawbacks and appears the best layout. The advantages of the two-shaft geared fan concept are summarised in Fig. 19.

Having established the virtues of the geared fan engine a further possibility now emerges. With comparatively little additional complexity, a fan variable pitch mechanism may be incorporated ahead of the reduction gearbox and within the same outside diameter. Such a concept has the merits of achieving optimised fan operating conditions throughout the flight envelope, without recourse to a variable area fan nozzle which could otherwise be required at high bypass-ratios, and of modulating thrust during the aircraft approach. It also offers the possibility, with a suitable design of fan blading, of reverse pitch operation enabling fan thrust reversal to be obtained down to zero aircraft speeds during landing. The latter feature is highly attractive for STOL operations where, as has been shown in Part I, the achievement of a short landing field length is critical. Conventional thrust reverser operation is typically not possible below aircraft speeds of 60 knots owing to re-ingestion problems. Further, because at bypass-ratio 10 the fan thrust is some 8 times the primary thrust it is possible that fan thrust reversal would itself be adequate without recourse to hot thrust spoiling and the overall result is a weight saving compared with a conventional powerplant.

The choice of a variable pitch geared fan, however, does impose several constraints on the designer, not least in the achievement of a high enough fan pressure-ratio for optimised cycle performance with blading suitable for reversed pitch operation. Current technology suggests that these constraints will limit the fan pressure-ratio to a value around 1.25, but Fig. 20 shows that this is, in the event, very near optimum for bypass-ratios of around 10 to 12.

It would not be true, at this point in time, to say that all the problems associated with variable pitch fan blading with reversal capability have been solved and research programmes are even now under way to obtain the solutions. Nevertheless, the concept holds out real advantages for STOL applications which are summarised in Fig. 21.

Fig. 22 illustrates a typical engine arrangement based on the use of M45H gas generator components, the latter engine being a joint Rolls Royce/SNECMA turbofan now under development. This figure shows the basic engine layout with no acoustic treatment as might be used in military applications. The noise levels are fundamentally low, but the engine configuration lends itself readily to additional treatment for civil applications as is shown in Fig. 23. With this layout, the single engine noise levels will meet F.A.A. STOL proposals as is shown in Fig. 24 with typical values at sideline, approach and flyover of 88 PNdB, 93 PNdB and 89 PNdB respectively. However, for a four engined aircraft the total noise levels will be 6 PNdB higher than these values and will not quite meet the proposals at approach.

Fig. 25 shows the uninstalled performance of a bypass-ratio 10 engine using M45H components, giving a take-off thrust of 15,000lb. and a typical cruise specific fuel consumption of 0.60 lb/hr/lb. Part I of this lecture has already established the good take-off to cruise thrust match of such an engine for

STOL aircraft. We have said uninstalled performance on this Figure advisedly, since engines of such high bypass-ratio are critically dependent on good powerplant design for optimum installed performance. As bypass-ratio increases, the influence of losses in gas generator component efficiencies on engine performance become increasingly less critical since the fan makes such a large contribution to the total performance of the engine. On the other hand, the degradation in performance stemming from intake and fan duct pressure losses become more severe the greater the bypass-ratio, as is shown in Figs. 26 and 27 at take-off and cruise respectively. The onus is therefore on the aircraft and engine designers to collaborate at an early stage in the achievement of a clean powerplant design which is essential for good installed performance for engines of this type. Fig. 28 shows some typical installation losses for an engine of bypass-ratio 10 assuming the acoustic treatment shown earlier and including the total powerplant drags. These values forcibly underline the requirement for good powerplant design.

5. BLOWING ENGINES

Part I of this paper concludes that, in order to operate from airstrips of 2000 ft. and under, some form of blown lift or direct lift augmentation is necessary. This section describes a typical blowing engine designed to produce the large quantities of air required for flap blowing.

Fig. 29 illustrates the layout of one such arrangement in which a low weight, low volume engine is used to drive an axial blower. Weight and volume of the complete assembly are all the more important because the engine is used during take-off and landing only and is shut-down for cruise. Typical engine cycle, performance and weight data are given in Fig. 30.

6. DIRECT LIFT ENGINES

As with Blowing engines, weight, volume and noise are of paramount importance for direct lift engines. The characteristics of lift fans are generally well known and it is not intended to dwell on this subject in any great detail other than to point out that the cycle is largely dictated by the need to achieve low noise and hence a low jet velocity.

7. CONCLUDING REMARKS

This paper has described the interface problems between aircraft and aero-engine manufacturers resulting from the need for lift augmentation. Part II has outlined some solutions to the problem, but it is emphasised that no attempt has been made to draw any conclusions on the merits of one solution over another.

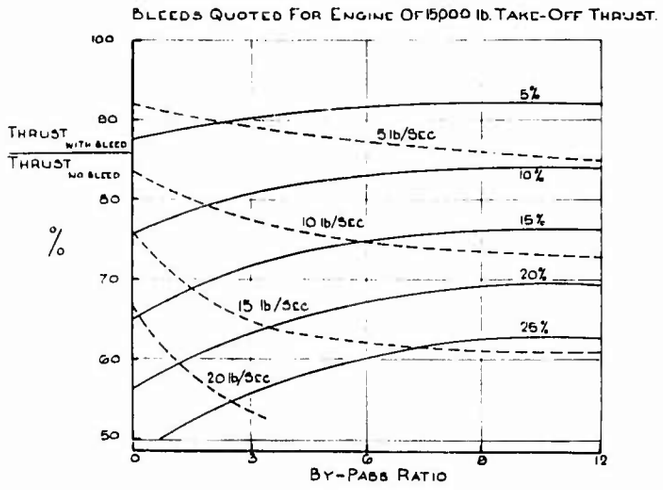

Fig.1 Performance penalty for taking large bleeds from IP compressor

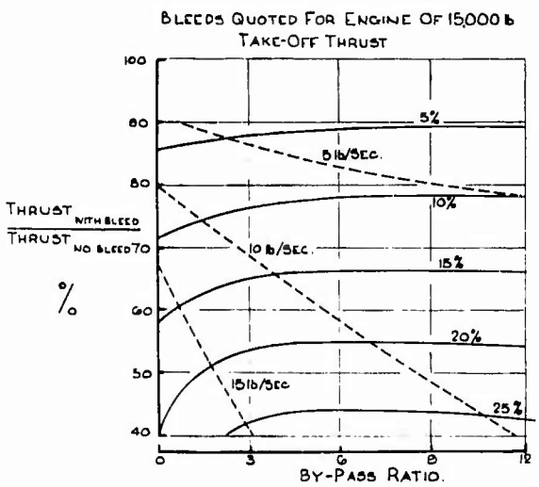

Fig.2 Performance penalty for taking large bleeds from HP compressor

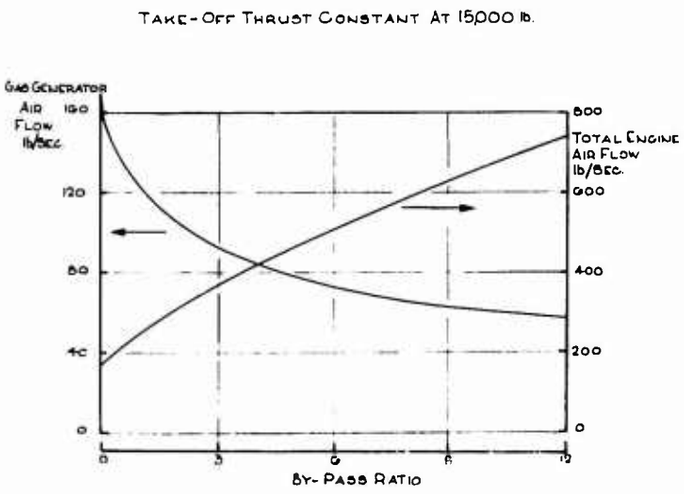

Fig.3 Typical variation of total engine airflow and gas generator airflow with bypass ratio

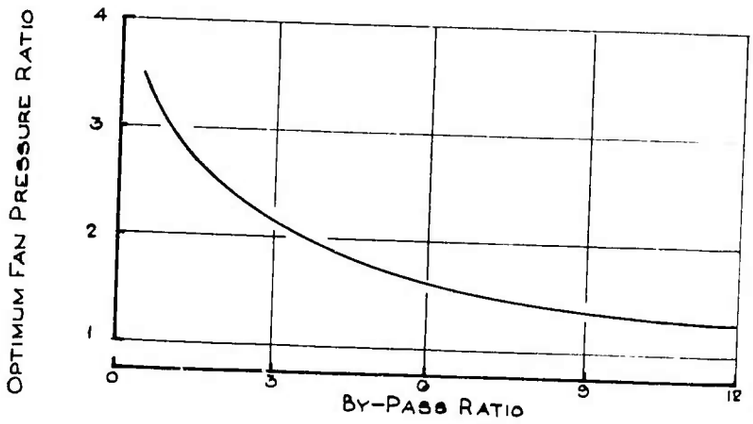

Fig.4 Optimum fan pressure ratio versus bypass ratio

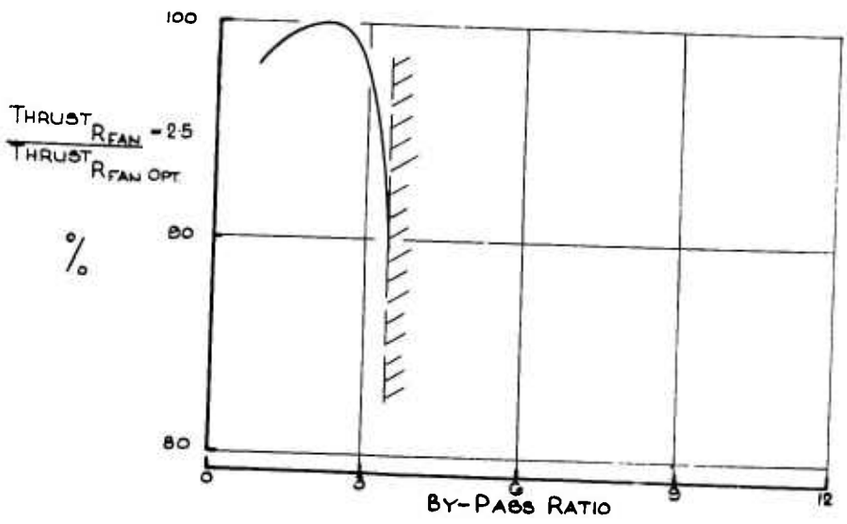

Fig.5 Performance penalty for maintaining fan pressure ratio constant at 2.5

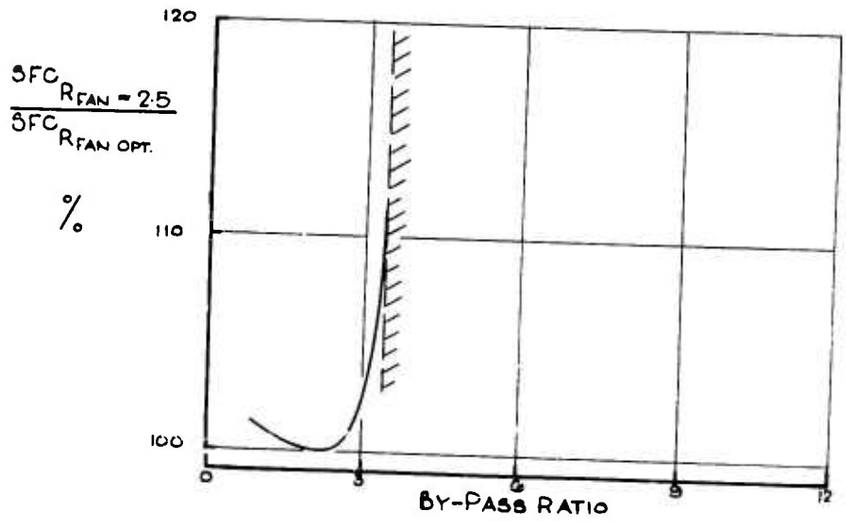

Fig.6 Performance penalty for maintaining fan pressure ratio constant at 2.5

BY-PASS RATIO = 0·62

HOT JET VELOCITY 1800 FT./SEC.
HOT NOZZLE PRESSURE RATIO 2·5
HOT JET TEMPERATURE 910 °K

TYPICAL SIDELINE NOISE LEVEL. 110 PNdB
1,000FT NO GROUND EFFECTS
200 KTS A/C SPEED

Fig.7 Hot jet conditions for engine with optimum fan pressure ratio = 2.75

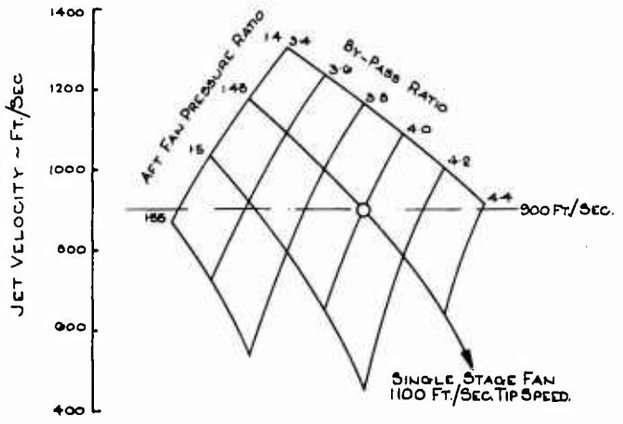

Fig.8 Aft fan required to produce hot jet velocity of 900 ft/sec

AFT FAN TIP SPEED = 1100 FT./SEC.
AFT FAN BY PASS RATIO = 4·0
AFT FAN PRESSURE RATIO = 1·45

RESULTANT HOT JET VELOCITY = 900 FT/SEC.
RESULTANT HOT NOZZLE PRESSURE RATIO = 1·2
RESULTANT HOT JET TEMPERATURE = 780 °K

Fig.9 Aft fan required to produce hot jet velocity of 900 ft/sec

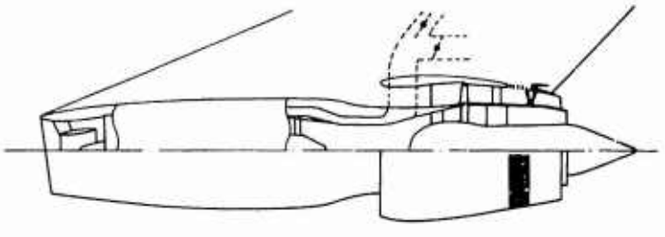

Fig.10 Typical layout of a split flow aft fan engine

PROPULSIVE THRUST AT TAKE OFF	16,500
BLEED AIRFLOW (BY PASS AIR)	80·0 lb/SEC.
PRESSURE RATIO OF BLEED AIR	2 75
TEMPERATURE OF BLEED AIR	400° K

Fig. 11 Performance of typical split flow aft fan engine

CRUISE THRUST AT 0·75 M 25,000 FT ISA +10 = 4660 lb
(WITH BLEED AIR PROPELLING)

SPECIFIC FUEL CONSUMPTION = 0·75 lb/hr/lbF

Fig. 12 Performance of typical split flow aft fan engine

	SPLIT FLOW AFT FAN ENGINE	F.A.A. PROPOSALS FOR STOL.
SIDELINE	92 PNdB 1000 FT. TO SIDE	95 PNdB 1000 FT TO SIDE
APPROACH	97 PNdB 500 FT. ALTITUDE ABOVE MEASURING POINT	95 PNdB 2000 FT FROM THRESHOLD OF RUNWAY
FLYOVER	92 PNdB 1000 FT ALTITUDE ABOVE MEASURING POINT.	95 PNdB 4000 FT FROM START OF ROLL

Fig. 13 Estimated noise levels of typical split flow aft fan engine

BLEEDS QUOTED FOR ENGINE OF 15,000 lb TAKE-OFF THRUST DESIGNED FOR LARGE BLEEDS

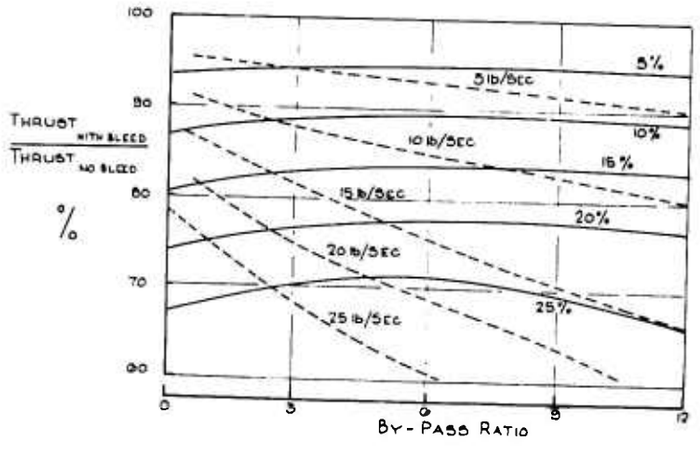

Fig. 14 Performance penalty for taking large bleeds from IP compressor

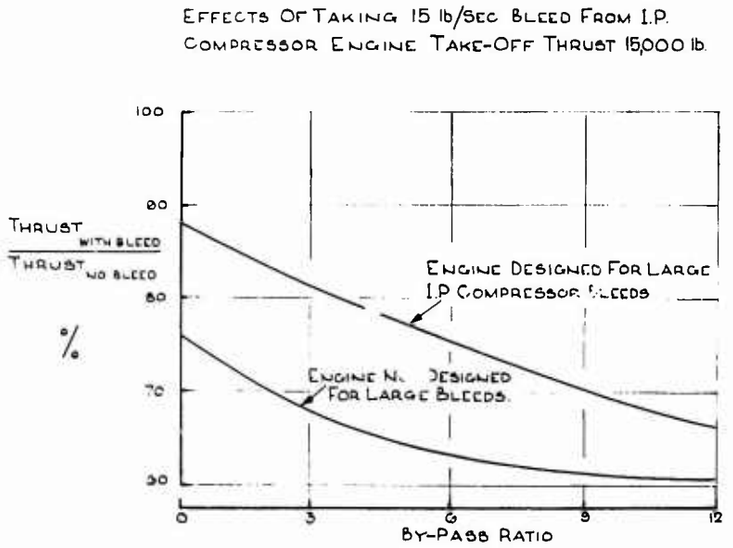

Fig.15 Comparison of performance penalties for taking large bleeds from IP compressor

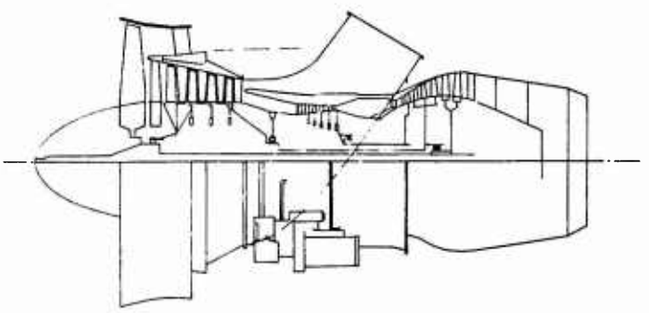

Fig.16 Typical layout of a 3-shaft engine designed for high IP compressor bleeds

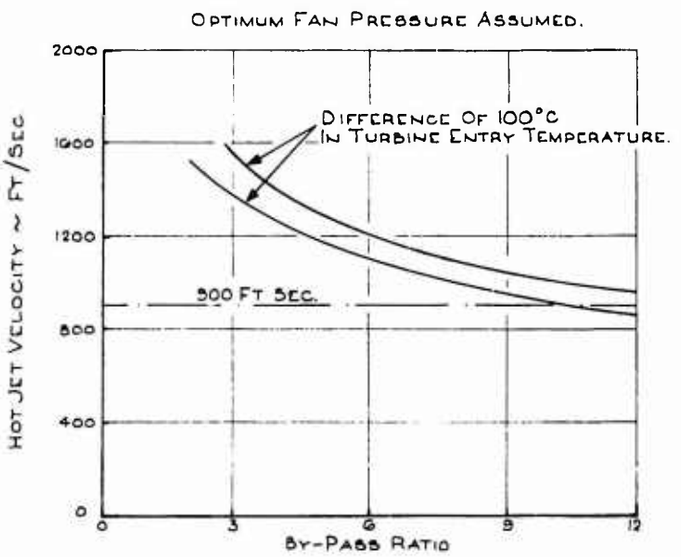

Fig.17 Variation of hot jet velocity with bypass ratio

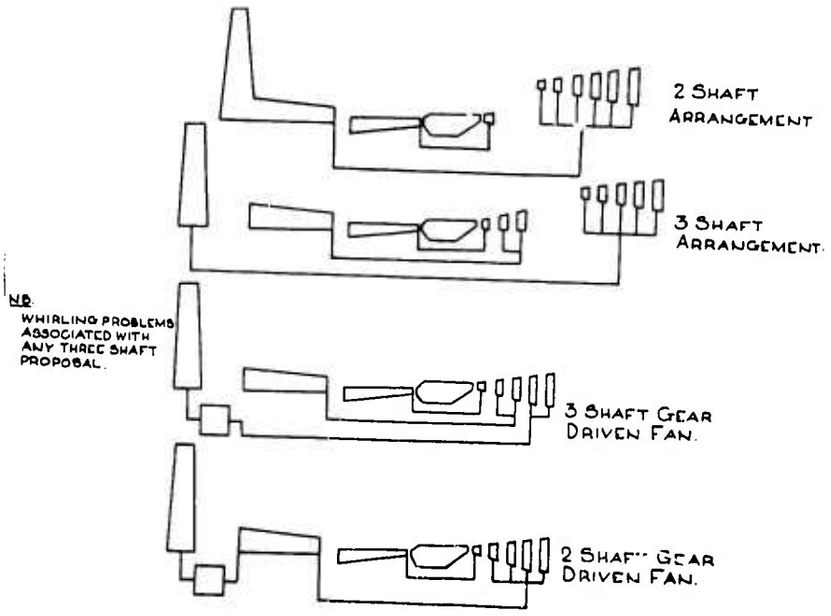

Fig.18 Some possible engine arrangements for bypass ratio 10 engines

* FAN SPEED NOT COMPROMISED BY TURBINE REQUIREMENTS

* I.P. COMPRESSOR SPEED NOT COMPROMISED BY FAN REQUIREMENTS.

* L.P. TURBINE SPEED NOT COMPROMISED BY FAN REQUIREMENTS RESULTING IN MINIMUM NUMBER OF STAGES AT MINIMUM DIAMETER.

* NO SHAFT WHIRLING PROBLEMS.

Fig.19 Summary of advantages of two spool geared fan engine

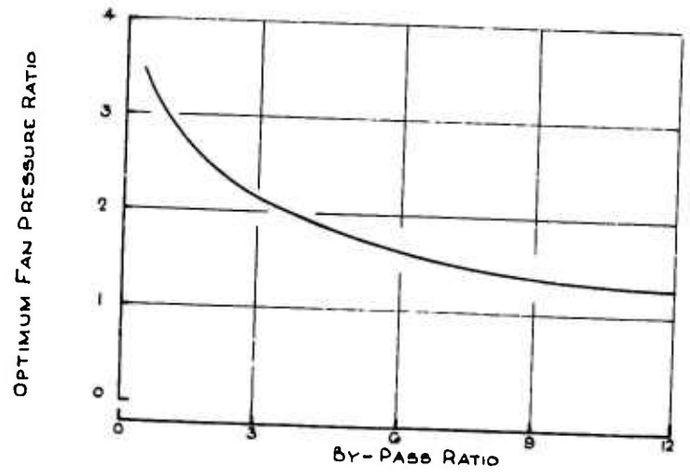

Fig.20 Optimum fan pressure ratio versus bypass ratio

* Facilitates Control Of The Fan Operating Conditions And Eliminates Necessity For Variable Cold Nozzle

* Can Be Used To Produce Reverse Thrust Down To Zero Forward Speed.

* Thrust Reversal Possible With Low Weight Penalty Compared With Conventional Systems.

* Can Be Used To Modulate Thrust On Approach While Maintaining High Engine RPM

* Can Be Used To Minimise Noise At Part Thrust Conditions (On Approach Or After Take Off)

Fig.21 Advantages of variable pitch fan blading

Without Acoustic Treatment

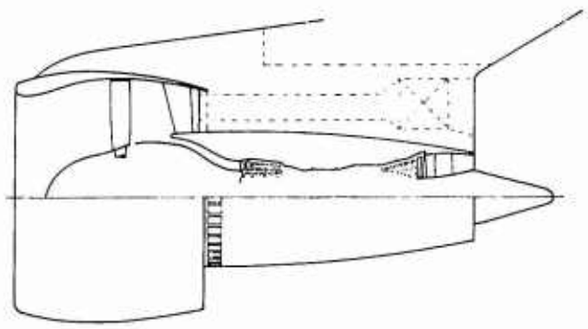

Fig.22 Typical layout of bypass ratio 10 engine with geared fan and variable pitch blading

After Acoustic Treatment

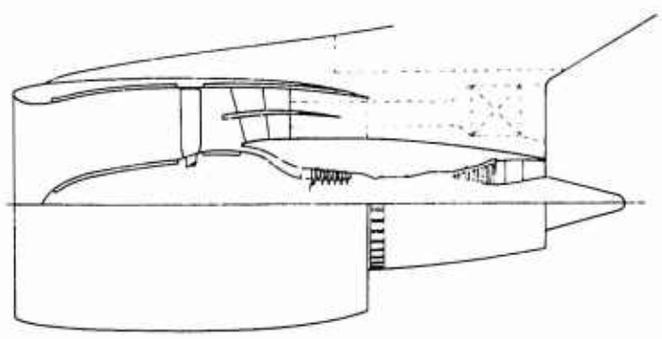

Fig.23 Typical layout of bypass ratio 10 engine with geared fan and variable pitch blading

	B.P.R. 10 Noise Levels	F.A.A. Proposals For STOL
SIDELINE	88 PNdB 1000 FT. TO SIDE	95 PNdB 1000 FT. TO SIDE
APPROACH	93 PNdB 500 FT. ALTITUDE ABOVE MEASURING POINT	95 PNdB 2000 FT. FROM THRESHOLD OF RUNWAY
FLYOVER	89 PNdB 1000 FT. ALTITUDE ABOVE MEASURING POINT	95 PNdB 4000 FT. FROM START OF ROLL

Fig. 24 Typical noise levels of bypass ratio 10 engine with acoustic treatment

TAKE-OFF THRUST AT SEA-LEVEL STATIC ISA ..... 15000 lb

MAXIMUM RECOMMENDED

CRUISE THRUST AT ·72M 25000 FT ISA ..... 3650 lb

SPECIFIC FUEL CONSUMPTION AT CRUISE ..... ·60 lb/hr/lbf

Fig. 25 Performance summary of typical bypass ratio 10 engine

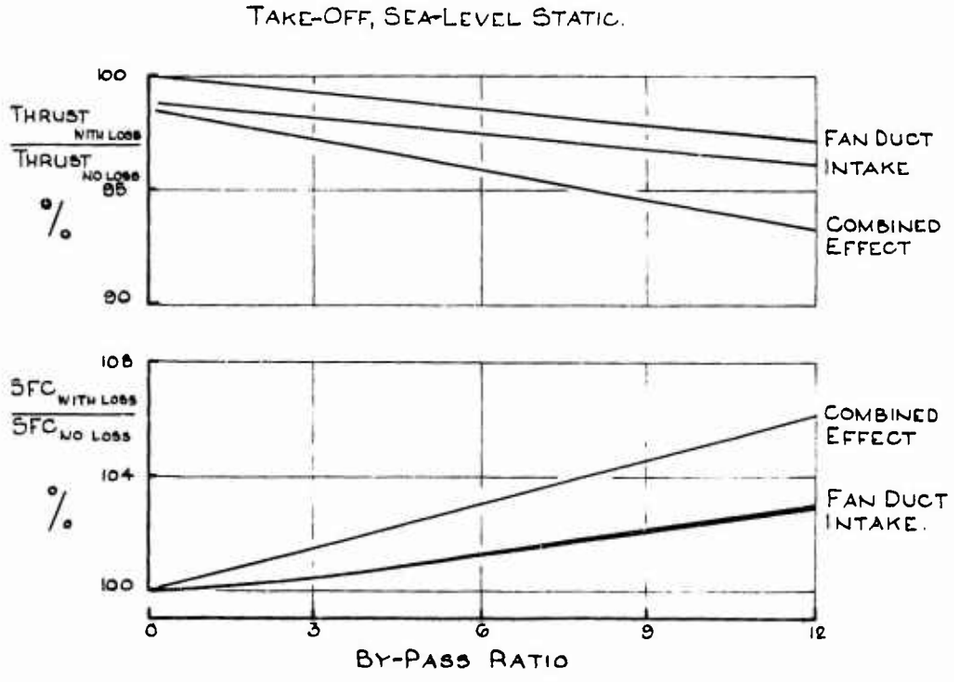

Fig. 26 Effects on performance of intake and fan duct losses of 1%

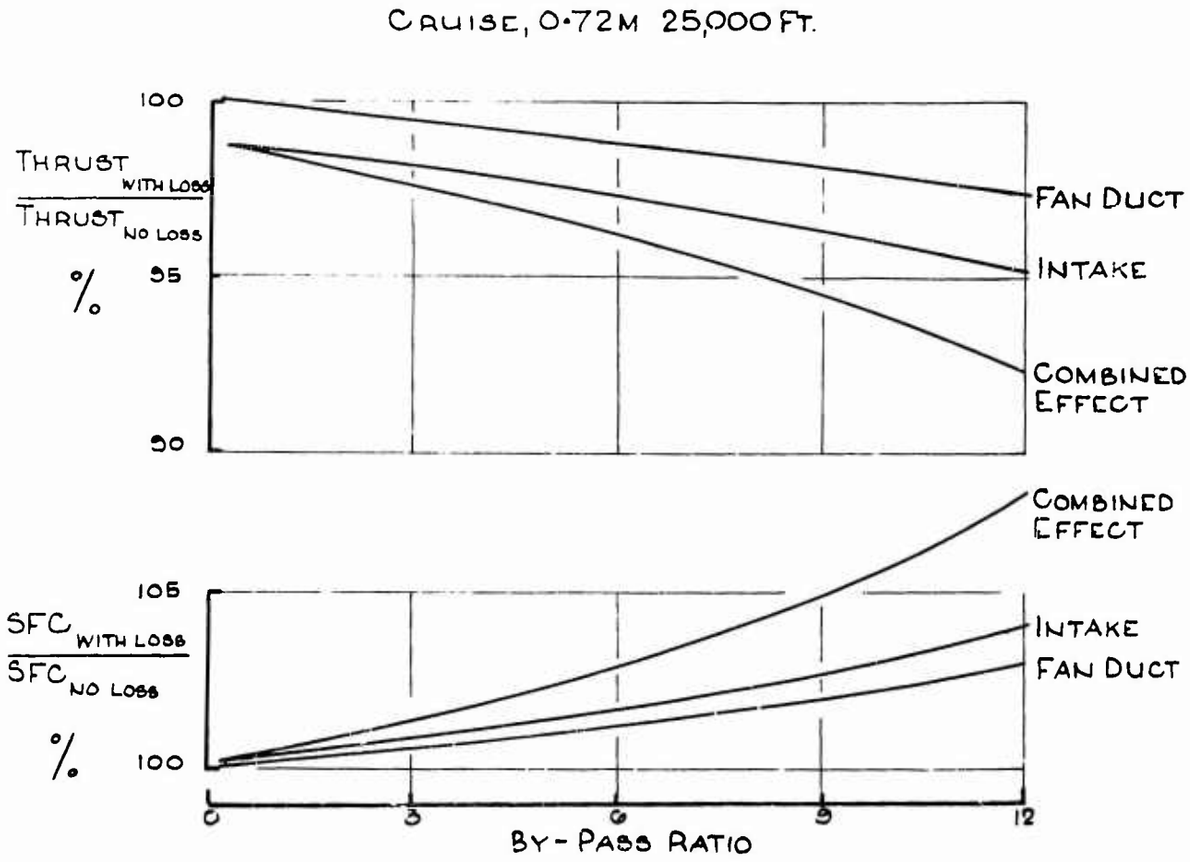

Fig.27 Effect on performance of intake and fan duct losses of 1%

	% LOSS IN NET THRUST	% INCREASE IN S.F.C.
TAKE OFF SEA LEVEL STATIC		
1. BASIC INTAKE AND DUCT LOSSES WITH ACOUSTIC TREATMENT	2·5	1·5
2. POWERPLANT DRAGS	1·0	1·0
3. TOTAL	3·5	2·5
CRUISE MACH 0·72 25000FT.		
1. BASIC INTAKE AND DUCT LOSSES WITH ACOUSTIC TREATMENT	4·0	3·5
2. POWERPLANT DRAGS	8·0	8·0
3. TOTAL	12·0	11·5

Fig.28 Typical installation losses for bypass ratio 10 engine with acoustic treatment

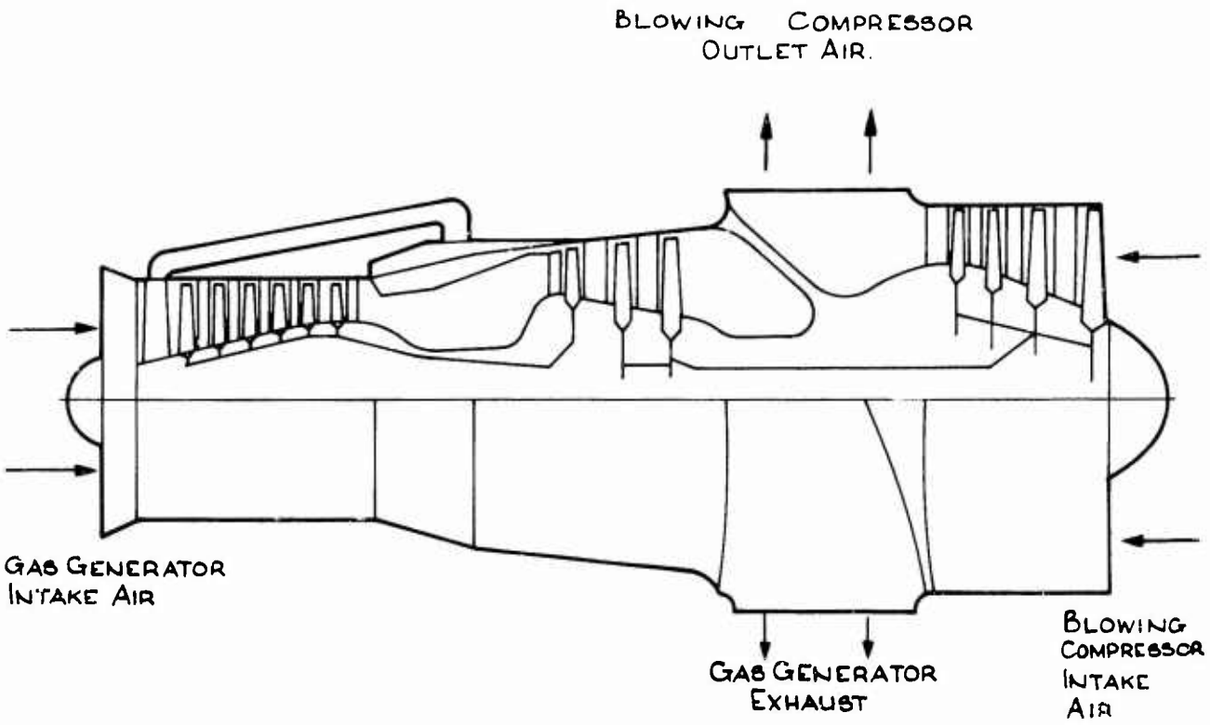

Fig.29 Typical layout of blowing engine

GAS GENERATOR AIR MASS FLOW	85 lb/sec
GAS GENERATOR PRESSURE RATIO	4·5
BLOWING COMPRESSOR PRESSURE RATIO	2·8
BLOWING COMPRESSOR AIR MASS FLOW	105 lb/sec
TYPICAL ENGINE DIAMETER	36 ins
TYPICAL OVERALL LENGTH	120 ins
TYPICAL OVERALL WEIGHT	1370 lb

Fig.30 Typical cycle parameters and performance of blowing engine

OPTIMISING THE PROPULSIVE/LIFT SYSTEM FOR TURBOFAN STOL AIRCRAFT CONSIDERING COST EFFECTIVENESS

by

H.T.Bowling

Senior Aerodynamics Engineer, Lockheed-Georgia Company
Marietta, USA

ACKNOWLEDGEMENT

The author wishes to extend credit and appreciation to C.H.Hurkamp and R.M.Thornton of Lockheed-Georgia Company who made major contributions to this paper.

OPTIMISING THE PROPULSIVE/LIFT SYSTEM FOR TURBOFAN STOL AIRCRAFT CONSIDERING COST EFFECTIVENESS

H.T.Bowling

1. INTRODUCTION

There is now and will be a continuing need for cost effective STOL aircraft suitable for either cargo or passenger transportation. This need exists for both military and commercial applications. There have been successful STOL aircraft designed using turboprop propulsion combined with a deflected slipstream high-lift system; however, the development of an aircraft which integrates the thrust and economical fuel consumption characteristics of a high bypass-ratio turbofan engine with an efficient high-lift system remains as a goal for the aircraft and propulsion industries. It is generally agreed that high bypass-ratio turbofan engines must be considered for new STOL aircraft especially when high thrust levels, high altitude, and high-speed cruise is required. It is the primary purpose of this paper to present the results of a comparison of three STOL high-lift concepts which have been integrated with bypass-ratio turbofan engines. Transport aircraft configurations have been optimized using these concepts and will be compared along with significant characteristics of each system.

The purpose of this comparison was to provide possible insight for future studies and testing. None of these systems have been subjected to a highly detailed analysis and do not represent completely optimized concepts. Every effort has been made to make the comparison as consistent as possible.

In the highly competitive environment of both commercial and military markets, it has become necessary to consider cost effectiveness even in very preliminary design studies. A secondary purpose of this paper is the discussion and demonstration of a study methodology which has been developed to integrate cost effectiveness into the early technical development of new airplane concepts. This methodology will be primarily applied to a military STOL development program. However, there will be some examples shown of considerations of commercial cost effectiveness.

2. SYSTEM DESIGN

There are a number of alternatives for developing STOL performance, such as low wing loading with conventional flap system, high thrust to weight ratio, and exotic mechanical high-lift systems. Low wing loading is perhaps one of the most straightforward of the approaches but exacts penalties in speed, weight and ride comfort. A promising alternative is to incorporate an effective high-lift system which utilizes the propulsion system as the source of energy. As shown in Figure 1, the combined actions of the wing and power plant to achieve high lift can take several forms. All of these are based on thrust vectoring and blowing over aerodynamic surfaces, either singly or in combination. Some have achieved flight status, while others have not yet progressed beyond the wind-tunnel and the drawing board. They include the types of system listed in the central column. The first two systems consider the pure vectored thrust approach differing only in the source and angularity of the thrust vectoring and blowing. Each system has its own advantages, i.e. the lift engine approach utilizes the lighter weight of pure lift engines. The last three systems depend heavily on blowing over aerodynamic surfaces. Boundary-layer control, particularly by blowing over trailing-edge flaps, has been used extensively for lift augmentation. The internally-blown jet-flap represents an extension of BLC to higher energy levels. The externally-blown flap provides the combined action of thrust vectoring and blowing.

The scope of this investigation was limited to promising systems which were determined to be both practical and within the present state-of-the-art. Three systems were selected for comparison. They represent the BLC and Jet-Flap Systems previously discussed combined with vectored thrust to take full advantage of the propulsion system in the attainment of high-lift, and the Externally-Blown Flap System. The takeoff condition was found to be most critical for the determination of aircraft size for a given field length considering the ground rules utilized in military STOL studies. However, in this study recognition was given to techniques for attaining the shortest possible landing distance.

In most commercial STOL studies, experience has shown that landing field length is the critical design factor. What landing safety factors are finally adopted in design criteria and the use of reverse thrust in commercial STOL design have a significant impact on aircraft size and cost. All of the candidate systems include the same type of highly effective thrust reverser, which is designed to minimise inlet contamination in the form of temperature rise at low forward speeds.

The investigation presented in this paper is the result of a part of a continuing inhouse study at Lockheed-Georgia to determine the optimum configuration for a STOL transport aircraft designed to perform short range STOL missions. Figure 2 presents a table of the design constraints used in this particular comparison. These constraints are arbitrarily postulated for the purposes of this comparison; however, they do represent realistic criteria. Figure 3 shows the baseline aircraft design as configured for the Externally-Blown Flap System. A high wing position was selected for ease of cargo loading and minimization of lift losses due to ground effect. The four turbofan engines have a bypass-ratio of 6 and represent current state-of-the-art in the 40,000 to 60,000 lb. thrust category. For this study, an upper thrust limit of 68,000 lb. was established based on the maximum engine size presently proposed by any engine manufacturer. The large fuselage cross-section was optimized for military cargo combination, including large vehicles and double rows of pallets or containers. Moderate sweep and aspect-ratio were selected from prior analysis, and the tee-tail arrangement followed from consideration of high downwash angles generated by the lift systems. The multi-wheel landing gear reflects the need for flotation on soft terrain. Figure 4 presents a cross-section of the wing and nacelle as designed for the Externally-Blown Flap System. The engine is positioned close to the wing for efficient interaction with the double-slotted trailing-edge flap. The configuration shown here is the result of analyzing both earlier NASA tests and more recent tests in the Lockheed-Georgia V/STOL Wind-Tunnel. Two features shown in this illustration are common to all three candidate systems. One is the Krüger type leading-edge flap, which provides a 10% extension of the wing chord, and the other is the thrust reverser. The latter provides a forward vector of the fan thrust, inclined at 30° upward from the horizontal, by opening a scoop-type door and simultaneously closing a blocker in the fan duct. All of the trailing-edge flap systems are full span and utilize 30% to 40% of the wing chord. This arrangement is not necessarily optimum but should provide a reasonable and consistent basis for this comparison.

Figure 5 is a similar cross-section which represents the combination of thrust deflection and blowing BLC. The thrust deflector is a hinged extension of the mixed flow duct, which at its horizontal setting discharges the entire flow through its rectangular nozzle. Any downward deflection angle opens up a passage for the flow of exhaust bleed into a spanwise duct for distributed blowing. The high location of the feeder duct assures the passage of a low temperature fluid, consisting primarily of fan air. The flow quantity is governed by the area of the spanwise discharge flow and is limited by an amount sufficient to create flow attachment. The thrust reverser differs from that of the previous example in that the two blockers, one in the deflector and one in the feeder duct, permit all of the exhaust flow to become reversed. Figure 6, representing the combination of thrust deflection with an internally-blown jet-flap, is quite similar to the foregoing system and differs only in the quantity of exhaust bleed and the design configuration of the flap. Approximately 35% of the fan discharge is fed to the flap, limited to that amount only by the available duct area. The latter is created by the flap itself, the upper and lower elements of which separate progressively with flap deflection. An upper BLC slot is provided at the "knee" and a main jet slot near the trailing-edge, located below a narrow auxiliary control flap. The auxiliary flap is used for both flight path angle and roll control by deflecting the main jet sheet.

Figure 7 shows the wing and nacelles of the foregoing system in planform to illustrate the flow patterns of the ducted fluid as shown by the arrows. Of particular interest is the fact that a cross-duct is provided, connecting the right and left wings. This is accomplished by use of a flexible duct element between the flap and a fixed duct across the top of the fuselage. In the event of an engine-out condition, the rolling moment due to asymmetrical deflected thrust can be counteracted by further opening the slot on the dead engine side, while closing it on the other side and thus equalizing the total lift vectors on each side. Differential slot opening can also be used to augment roll control. While the BLC system can function in a similar manner, it is not capable of providing the same magnitude of roll control.

There are of course many other combinations of thrust deflection and lift augmentation but only these three systems will be discussed in more detail here.

3. METHODOLOGY

It is not practically feasible for one particular technical discipline (i.e. aerodynamics, propulsion, structures, design etc.) to perform a meaningful analysis of a total aircraft design such as the one just described. In any successful study the talents of all groups must be utilized in a systematic manner. The study methodology discussed here demonstrates how the various disciplines contribute to a preliminary comparison of candidate high-lift systems for a STOL aircraft powered by turbofan engines. Figure 8 presents a block diagram which shows how the various study inputs are coordinated. For this study, Operations Analysis/Research provided the operational inputs to this study scheme to include such items as mission profile, payload/cargo compartment matching, and field length requirements. Preliminary design, aerodynamics, propulsion, and structures share in the initial development of possible designs. There is a continuous interaction between these disciplines as noted by the dashed line on Figure 8. This development work continues until sufficient confidence is achieved in a particular design for its inclusion as a candidate system. The aerodynamic, propulsion, and weight characteristics of each system are then input into parametric computer programs which size configurations to simultaneously satisfy the requirements of payload, mission profile and airport performance. Utilizing a rubberized engine concept permits a wide range of combinations of thrust and wing area all satisfying the requirements discussed above. These combinations are then costed and the minimum cost is considered in final configuration selection.

4. AERODYNAMICS

The lift, moment, and horizontal force characteristics (including power effects) of these systems have been estimated and correlated with a significant amount of data from various sources including tests conducted at Lockheed-Georgia. These characteristics are typical of each system, but are not intended to represent the maximum that could be achieved by a complete optimization of such parameters as flap span, chord, engine location, etc.

The lift (C_L) and horizontal (C_X) characteristics of the externally-blown flap system have been estimated using the equations shown on Figure 9. The aerodynamic characteristics of the boundary-layer control/deflected thrust system have been estimated using the equations shown on Figure 10; in this system, which utilizes full-span blowing at the knee of a simple slotted flap plus vectored thrust from quick acting nozzles, only the flow required for flow attachment is bled from the main propulsion engines. The aerodynamic characteristics of the jet-flap deflected thrust system have been estimated using the equations shown on Figure 11.

Figure 12 presents a comparison of the trimmed aerodynamic lift characteristics of these three systems for typical takeoff and landing flap nozzle settings. The trim effects incorporated in these data are calculated from moment data estimated in a consistent manner with the lift and drag data. These data show that the jet-flap system develops higher maximum lift coefficients for a given thrust coefficient than the other systems. An additional comparison is presented in Figure 13 where an aerodynamic/propulsive efficiency factor for each system is shown as a function of thrust coefficient. In this comparison, recognition is given to the ability of each system to produce both lift and horizontal force. The actual efficiency factor is defined as the resultant aerodynamic force vector developed by power input to the system. As shown, both the externally-blown and jet-flap systems are significantly more efficient in producing lift and thrust simultaneously than the BLC system.

4.1 Takeoff Performance

Generalized takeoff performance data have been computed and optimized using the aerodynamic data previously described. For this particular comparison, a military type takeoff distance (total distance over a 50 ft. obstacle) of 1500 ft. was used consistent with the profile and speed margins shown in Figure 14. Ground roll is minimized by keeping the flaps retracted during the ground roll and than rapidly extending them at liftoff for the externally-blown flap system. With the BLC system, quick deflection, quick deflection of the thrust nozzles at liftoff is used; and with the jet-flap system, quick action of both flaps and nozzles are used. The results of these takeoff computations are presented in Figure 15 where thrust/weight ratio is shown as a function of wing loading for each propulsive system.

Each point on these curves represents an optimized combination of flap deflection and/or thrust nozzle deflection for minimum takeoff distance. This comparison reflects again the efficiency of these propulsive lift systems. As shown, both the externally-blown and jet-flap system require a lower thrust/weight ratio than the BLC system. In turn, the jet-flap system requires a slightly lower thrust/weight ratio than the externally-blown flap system.

5. CONFIGURATION SIZING

The next step in the aircraft sizing process is the simultaneous consideration of both airport and cruise requirements of aircraft which employ these systems. The weight aspects of each system will significantly influence the size of each aircraft and parametric weight equations were developed for each concept. Empennage sizes were selected, based on a brief analysis of stability and control power requirements. Cruise-matched configurations were developed as a function of wing loading and cruise power setting. From these configurations, selected aircraft were chosen which also meet the 1500 ft. airport requirement. This matching process is illustrated in Figure 16 where T/W required and available is presented as a function of wing loading.

Figure 17 presents a summary of the characteristics of those aircraft (as a function of wing loading) which satisfy both cruise and takeoff requirements for all three systems. For this study a wing loading range of 60-140 lb/ft^2 was selected. Significant problems in obtaining acceptable levels of control power and ride qualities are encountered with very low wing loadings, while very high wing loadings result in thrust levels in excess of practical consideration. In observing these results, the expected trends of decreasing weight and increasing thrust with increasing wing loading are noted. Application of the externally-blown flap system results in lower weights and thrust than either of the two internally-blown systems. The jet-flap system has higher weights but lower thrust requirements than the BLC system. Noted on this figure is the maximum available thrust restriction previously discussed. There are three major factors that influence these results:- the aerodynamic characteristics (as indicated by Figure 12); the weight of the wing and mechanical portion of the high-lift system; and the weight of the propulsion system and related control system. Because of loads and temperature effects, the externally-blown flap system has a higher wing weight per square foot of wing area.

The jet-flap wing is next heaviest followed by the lighter BLC wing. However, the higher wing weight of the externally-blown flap is more than offset by lower propulsion system weights. Conversely, the higher propulsion system weights of the BLC and jet-flap system offset the lower wing weights. The inter-relationship of these factors

essentially determine the results shown in Figure 17. A configuration for each system must be selected from these data. However, in the methodology used in this study, the final selection of a configuration for each propulsive lift system is made only after considering cost.

6. COST-EFFECTIVENESS

The particular costing procedure used in this study was developed in response to requirements of the US military services where life cycle cost is the basic economic criteria. Most studies in response to commercial studies use direct operating cost as the economic measure. A typical example of this process will be shown later on. All aircraft evaluated in this comparison have the same design maximum payload, cargo compartment size, airport performance, and cruise speed. Inasmuch as each of the systems have equal capability, the effectiveness is the same excluding relatively small differences in reliability, and survivability. Thus, the measure of cost effectiveness to be used in comparing these aircraft can then be taken as the life cycle cost for a fixed fleet size. The most cost effective design is the one with the lowest life cycle cost.

Life cycle cost as used in this study includes costs for Research, Development, Testing and Evaluation (RDT & E) plus Acquisition plus 10 years of Operating and Maintenance (O & M). The (O & M) costs shown in this paper are for 10 squadrons or 160 aircraft. The acquisition costs are for 208 aircraft, or 30% more than the operational squadron level to account for command support, training and attrition aircraft. The life cycle costs represent total costs to the government, including all support costs. These costs were calculated using a computerized cost model in conjunction with a Value Engineering analysis of airframe manufacturing and tooling cost differences. The cost model incorporates Cost Estimating Relationships (CER's) taken from three sources:-

(a) A RAND study on airframe costs.

(b) A cargo aircraft cost model developed by the Advanced Systems Cost Analysis Group within the Air Force Aeronautical Systems Division.

(c) Lockheed experience on previous transport aircraft.

The model has been validated for that portion of aircraft life cycle costs which include airframe development plus production costs, by comparing model results with Lockheed historical cost data on the C-130A and C-141A aircraft. The model results were lower than the actual costs on both aircraft, but by less than 10%. The STOL turbofan aircraft in this study depart significantly from the conventional construction methods and in distribution of weight among the various airframe components, therefore a modification in the model is required to properly account for this added complexity. To account for this, an analysis was performed to determine "complexity" or "cost increase" factors to multiply times the basic code-generated costs.

This study showed that these STOL aircraft differ significantly in construction cost from conventional aircraft in the wing trailing-edge fixed structure and in control surfaces. These differences are primarily in the quantity of mechanism and the temperature environment in which the structure operates. The complexity factors for this study were derived by dividing the estimated production cost (considering the above factors) by the estimated production cost the cost model would predict for a conventional aircraft of the same size. Tooling cost factors were estimated considering required construction methods. The derived factors are not universal, but should be reasonably accurate for a range of aircraft sizes near the point designs evaluated. The results of this Value Engineering Study were airframe manufacturing cost factors of 1.5 to 1.7 and tooling cost factors of 1.3 to 1.4.

For each of the propulsion/lift system concepts examined, life cycle cost as a function of design wing loading was computed using the design characteristics shown in Figure 17. Figure 18 presents the results of this study. These cost curves are used to aid in the selection of the preferred point design among the several generated for each of the three propulsion/lift systems considered. The three driving factors in determining the shape of these curves are airframe weight, fuel consumption rate and engine thrust requirements (see Figure 17). As wing loading increases, aircraft weight decreases while engine size increases. While airframe and propulsion costs are not linearly related to weight and thrust, respectively, they do increase as these two parameters increase. The behavior of the fuel consumption rate vs. wing loading curve depends on engine thrust requirements, while fuel costs are, of course, linearly related to consumption rate.

In Figure 18, the cost curve for the externally-blown flap system is minimum at approximately 110 lb/ft^2 while the jet-flap/deflected thrust system cost is minimum at approximately 95 lb/ft^2. However, the curve for the BLC/deflected thrust system does not show a well-defined minimum within the wing loading range considered. The behavior of the externally-blown flap and jet-flap curves can be understood by referring to the variations of airframe AMPR weight, engine size and fuel consumption rate in Figure 17. For the externally-blown flap system, the weight decreased in going from 90 to 112 ft/lb^2, while the engine size increased and the fuel consumption decreased slightly. When the costs driven by these three aircraft characteristics are combined, a minimum occurs at 110 lb/ft^2. For wing loadings greater than this, the increase in propulsion costs combines with an increase in fuel costs to overcome a slight decrease in airframe costs. For wing loadings less than 90 lb/ft^2, the large increase in airframe costs is the controlling factor.

For jet-flap system a minimum cost occurs, but at a lower wing loading than for the externally-blown flap system. Primarily, this is because the reduction in weight as wing loading increases is not as pronounced as for the externally-blown flap.

The lack of a well defined minimum cost for the BLC system is due to the fact that the airframe weight does not decrease rapidly with increasing wing loading as it does for the other two systems. This, in turn, increases engine thrust requirements. The net result of these changes is that life cycle cost for the BLC system is fairly insensitive to wing loading, at a cost level slightly higher than the minimum costs of the other two systems.

7. SELECTION

A configuration for each high-lift concept has been selected and significant characteristics of each configuration are presented on Figure 19. Several criteria were considered in this selection process, including stability, control, control power, ride qualities, and thrust availability as well as cost. In this particular comparison, selection of minimum cost points represented a reasonable compromise with other criteria and minimum cost was used to make the final selection for each component. A comparison of the major cost components for each configuration is presented in Figure 20. From this final comparison the Externally-Blown Flap System is selected as most promising concept. This final selection is the result of an overall comparison of the three systems in several categories, with associated ratings in order of merit as shown on Figure 21.

Life Cycle Cost comparisons show the Externally-Blown Flap System with a cost approximately 2.5% lower than the Jet-Flap System and 3.5% less than the BLC System. The number of unknowns and assumptions inherent in a cost analysis such as this lessens the importance of the absolute value of these cost results, and the total spread between the absolute cost data is only 3.5%. However, this could represent a difference in 300-400 millions of dollars in relative cost and it is in this context that these data are most meaningful.

Handling Qualities include stability and control characteristics, and the ranking is based on very limited test data and analysis. One-engine-out operation is the major consideration in this ranking and favors the Jet-Flap System because of the cross-ducting feature, which enables the pilot to trim the aircraft laterally by differential adjustment of the blowing slot areas. This operation can be performed manually or made automatic by a pressure-sensing device. The control margin of the Jet-Flap System, after trim, is considerably higher than that of the other two systems.

Operational Qualities include reliability and maintainability. Here, the ranking is based on apparent complexity differences. Although the Externally-Blown Flap is ranked highest in both categories, the effect of engine exhaust impingement on the wing and flap structure is largely unknown. Even though heavily reinforced in the blast areas, the structure will be subject to sonic and lower frequency fatigue cycles. The other two systems are faced with possible failure of the ducts and thrust deflectors. Short of operational experience, studies in much greater depth are required to achieve credible ranking.

Associated Engine Development Risk is ranked in the reverse order of thrust required. Although an upper limit was established on the basis of engine manufacturer's proposals, the risk involved in developing a new engine is inversely related to the degree of thrust extrapolation required over that of the highest rated, present generation engines.

Finally, the matter of available test data must be considered. Since BLC systems have been extensively tested in flight and in the wind-tunnel, the data credibility can be considered very good. Externally-Blown Flap configurations have been tested in the wind-tunnels of NASA and aircraft manufacturers. Jet-Flap Systems of various types have had extensive wind-tunnel testing, but only limited flight evaluation. The Jet-Flap System described in this paper has not been tested but appears to have very promising lift augmentation effects. This system is scheduled for testing at NASA Ames within the next year.

Recommendation as to which system should be selected depends on the operational time frame. For operation in two to four years, the Externally-Blown Flap System would be a logical choice. Beyond this point, however, analysis and development testing in greater depth may well point to the Jet-Flap System. This particular study is presently being refined to incorporate recent wind-tunnel test results and expanded to consider other concepts. Cost effectiveness will surely be considered in these studies.

8. OTHER APPLICATIONS

As previously mentioned, cost effectiveness for commercial STOL application uses another approach than the military procedures just discussed. Direct, indirect, and total operating costs are essential to the determination of system economic feasibility. It is therefore necessary for an aircraft manufacturer to consider these costs even in the early stages of aircraft development. The indirect operating costs are related to the service an airline choses to offer its customers and therefore is difficult to consider in a parametric analysis. However, direct operating costs can be related to configuration studies.

Figure 22 presents a summary of those items which go to make up direct operating cost. The equations which permit the calculation of these costs are generally based on historical data with the exception of the airframe and engine costs. The airframe cost is a function of the airframe weight and the estimated production run, whereas the engine cost is a function of the engine thrust and the estimated number of engines to be produced. All of these factors can be made a part of early parametric studies.

A recent study was made of a commercial passenger STOL aircraft in which direct operating cost was considered from the beginning of the program. This study considered such variables as number of passengers, field length, cruise speed, and range. The externally-blown flap high-lift system previously described was chosen as the basic lift system. In this particular study the cost effectiveness aspects of the design were carried to an even greater depth. Data was generated to compute the indirect operating costs as well as the direct operating costs.

A particular passenger demand was established in order to provide a revenue model. With a method now established to predict both cost and revenue, the analysis could now be extended to analyze profit. Figure 23 presents some typical results of this study which shows aircraft weight, direct operating costs, and finally profit as a function of design cruise speed and field length. These data are relative just as was the life cycle cost discussed earlier. The absolute level may not be extremely accurate, but if the selection of aircraft characteristics can be related to profit the exercise is well worth while.

9. CONCLUDING REMARKS

A comparison has been made of various high-lift systems integrated with turbofan propulsion. In selecting a configuration for each concept and in the final comparison, consideration was given to the aerodynamics, propulsion, weight, and complexity aspects of each system as well as cost. A specific study methodology was used in this comparison which introduces cost effectiveness into the early phases of system development. This work is really just begun and much testing, analysis, and development must occur before a system is evolved and manufactured.

The cost of an efficient STOL system will be fantastic and such a system will have a widespread effect on the environment in which it must operate. There are indications that any STOL system developed in the United States will have to recognize the requirements of the military and commercial customers simultaneously. This will mean that the cost effectiveness of such a system will have to be analyzed using both approaches just discussed. However, this system will come and the development of an operational turbofan STOL transport which utilizes a well integrated propulsive high-lift system must be considered as one of the real challenges to the airframe/propulsion industries.

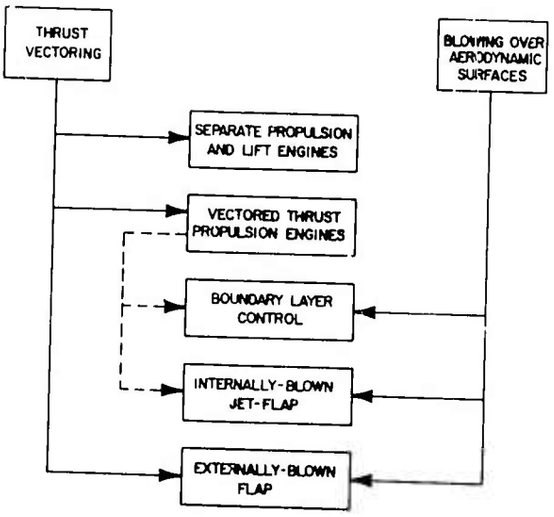

Fig.1 Propulsion/lift systems for turbofan aircraft

o PAYLOAD	64,000 LBS.
o RADIUS	230 N MI
o CRUISE SPEED	MACH 0.75
o T O AND LANDING OVER 50' OBST	1500 FT
o T O AND LANDING ENVIRONMENT	2500 FT., 93.7°F
o AIRFIELD TERRAIN	CBR 4 (200 PASSES)
o CARGO COMPARTMENT SIZE	16'-8" WIDTH 11'-8" HEIGHT 50'-0" LENGTH

Fig.2 Design constraints for an intra-theater cargo transport

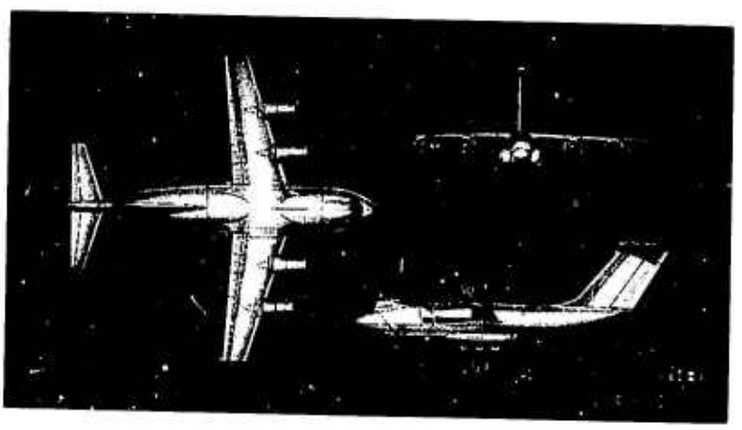

Fig.3 STOL intra-theater transport 32 ton payload

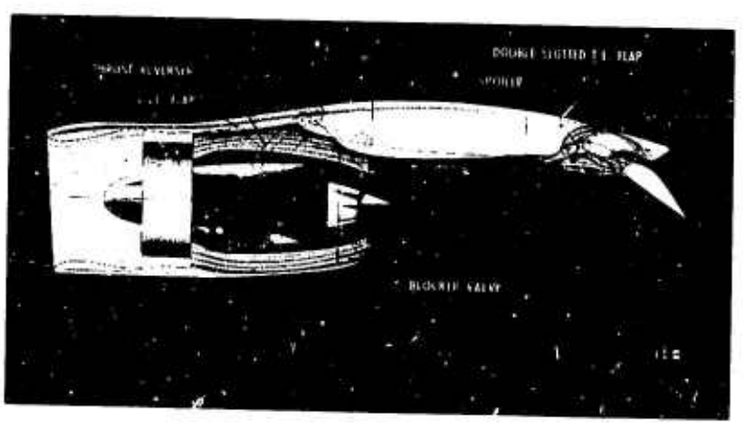

Fig.4 Externally-blown jet-flap

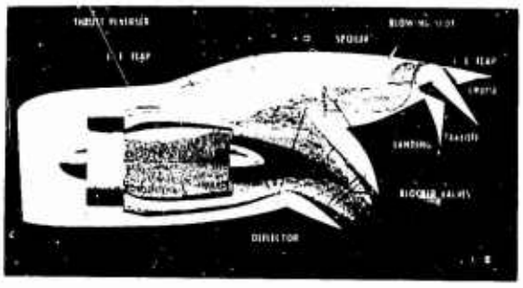

Fig.5 Thrust deflection with BLC

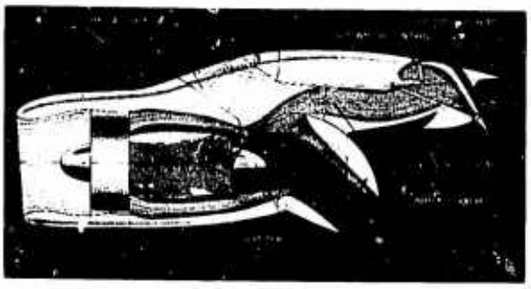

Fig.6 Thrust deflection with jet-flap

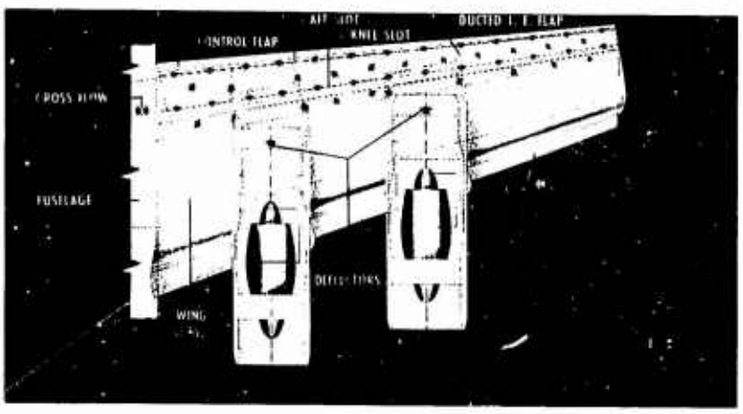

Fig.7 Jet-flap ducting system

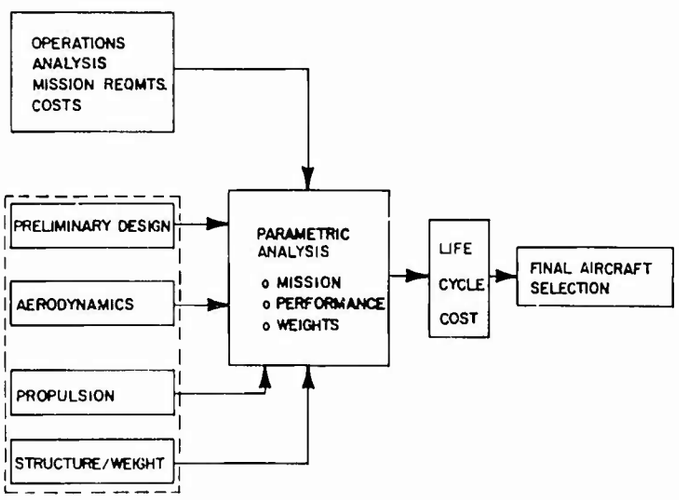

Fig.8 Study methodology

LIFT

$$C_L = C_{L_O} + C_{L_r} + \eta C_T \sin(\alpha + \delta_f) - C_{L_{trim}}$$

WHERE C_{L_O} = POWER OFF LIFT COEFFICIENT

C_{L_r} = ADDITIONAL LIFT DUE TO SUPER-CIRCULATION

η = FLOW TURNING EFFICIENCY

C_T = THRUST COEFFICIENT, T/q_S

δ_f = FLAP DEFLECTION

α = ANGLE OF ATTACK

HORIZONTAL FORCE

$$C_X = \eta C_T \cos(\alpha + \delta_f) - \frac{(C_{L_\alpha} + C_{L_r})^2}{\pi AR e} - C_{D_O} - C_{D_{trim}}$$

WHERE C_{D_O} = POWER OFF PROFILE DRAG COEFFICIENT

Fig.9 Externally-blown flaps

LIFT

$$C_L = C_{L_O} + \Delta C_{L_{C_\mu}} + \eta_1 (C_T - C_{\mu^*}) \sin(\alpha + \delta_V) - C_{L_{trim}}$$

WHERE C_{L_O} = POWER OFF LIFT COEFFICIENT

$\Delta C_{L_{C_\mu}}$ = INCREMENTAL LIFT DUE TO FLOW ATTACHMENT, $f(\delta_f)$

C_T = THRUST COEFFICIENT, T/q_S

C_{μ^*} = BLOWING COEFFICIENT REQUIRED FOR FLOW ATTACHMENT

δ_V = EXHAUST NOZZLE DEFLECTION ANGLE

η_1 = EXHAUST NOZZLE TURNING EFFICIENCY

HORIZONTAL FORCE

$$C_X = \eta_1 (C_T - C_{\mu^*}) \cos(\alpha + \delta_V) - \frac{(C_{L_\alpha} + \Delta C_{L_{C_\mu}})^2}{\pi AR e} - C_{D_O} - C_{D_{trim}}$$

Fig.10 Boundary-layer control/deflected thrust

LIFT

$$C_L = C_{L_O} + C_{L_r}(\text{BASED ON } C_{T_1}) + \eta_1 C_{T_2} \sin(\alpha + \delta_V) - C_{L_{trim}}$$

WHERE $C_{T_1} = (0.35)(\eta_2) C_{T_{total}}$

η_2 = EFFICIENCY OF JET-FLAP SYSTEM (SYSTEM LOSSES)

$C_{T_2} = (0.65) C_{T_{total}}$

HORIZONTAL FORCE

$$C_X = \eta_1 C_{T_2} \cos(\alpha + \delta_V) - \frac{(C_{L_O} + C_{L_r})^2}{\pi AR e} - C_{D_O} - C_{D_{trim}}$$

Fig.11 Jet-flap/deflected thrust

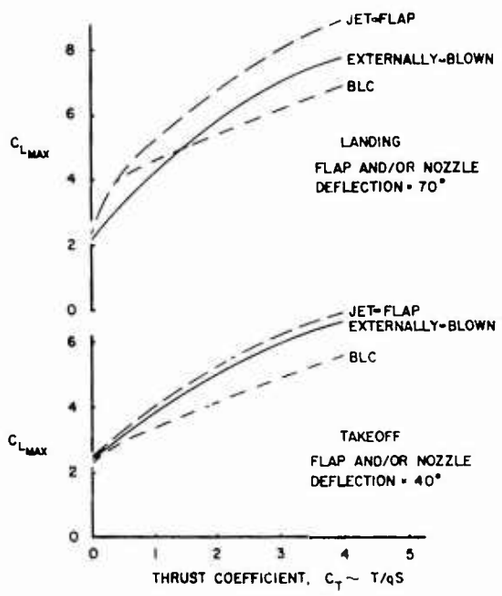

Fig.12 Comparison of aerodynamic lift characteristics

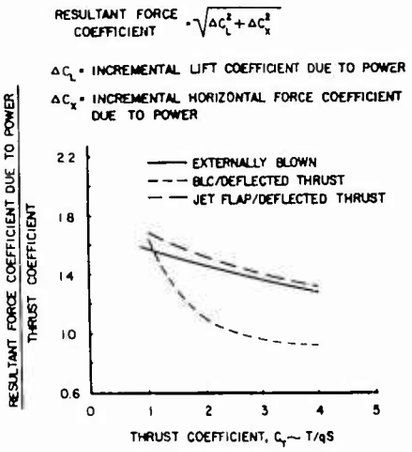

Fig.13 Aerodynamic/propulsive efficiency

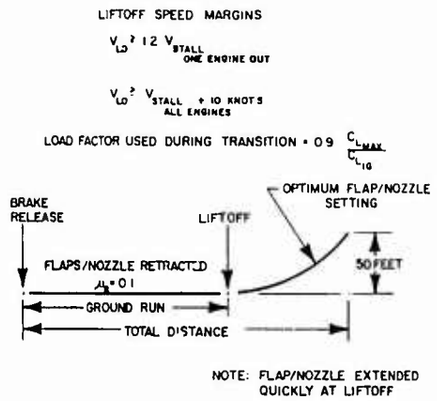

Fig.14 Takeoff profile

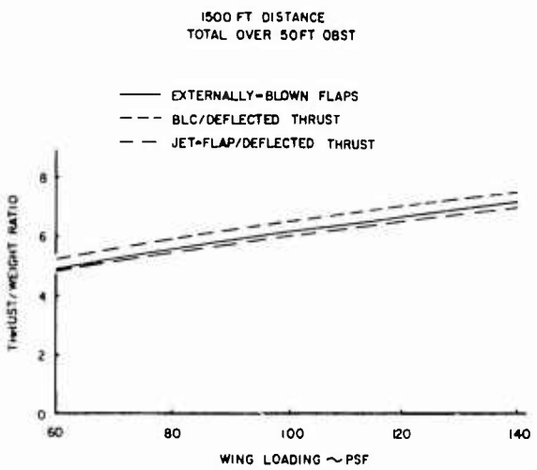

Fig.15 Summary of takeoff requirements

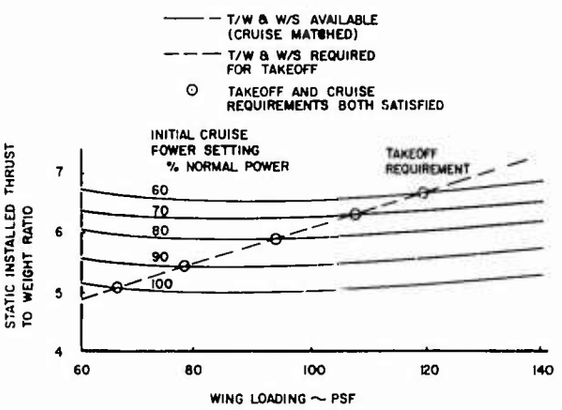

Fig.16 Thrust/weight and wing loading. Required and available

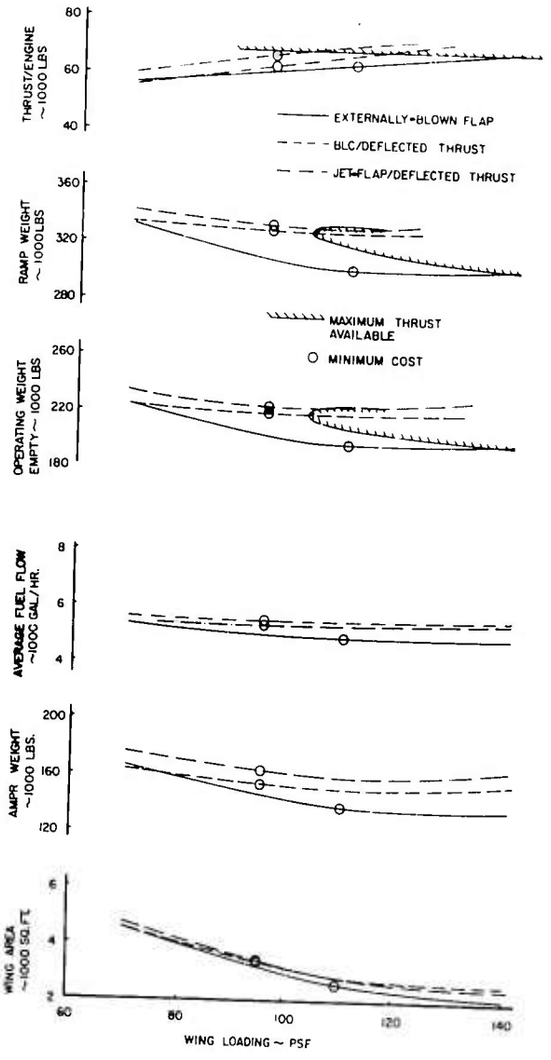

Fig.17 Effect of wing loading

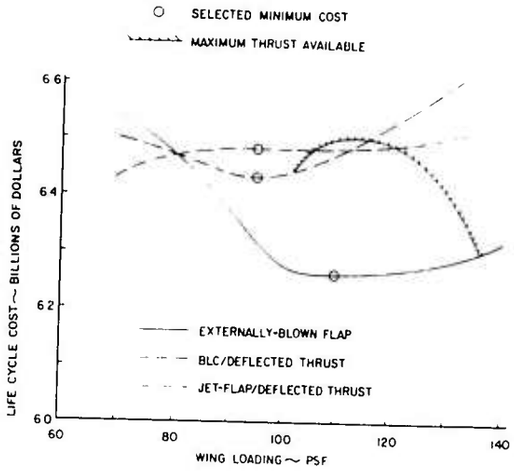

Fig.18 Cost comparison

	UNITS	EXTERNALLY-BLOWN FLAP	JET-FLAP DEFLECTED THRUST	BLC DEFLECTED THRUST
GROSS WEIGHT	LBS	303,800	333,400	330 700
OPERATING WEIGHT EMPTY	LBS	198,800	223,800	219,600
THRUST/ENGINE (S.L.,STD DAY)	LBS	61,570	62,180	66,800
WING AREA	FT^2	2,680	3,370	3,380
T O WING LOADING	(LB/FT^2)	112	98	97
T O THRUST/WEIGHT		0 65	0 60	0 65
$C_{L_{MAX}}$ AT LIFTOFF(PWR ON)		5 45	5 38	4 91
LIFTOFF SPEED	KTS	98	91	97
GROUND RUN	FT	870	860	940
LIFE CYCLE COST	MIL	6261	6436	6482
THRUST COEF AT LIFTOFF		2 3	2 2	2 0

Fig.19 Comparison of selected configurations

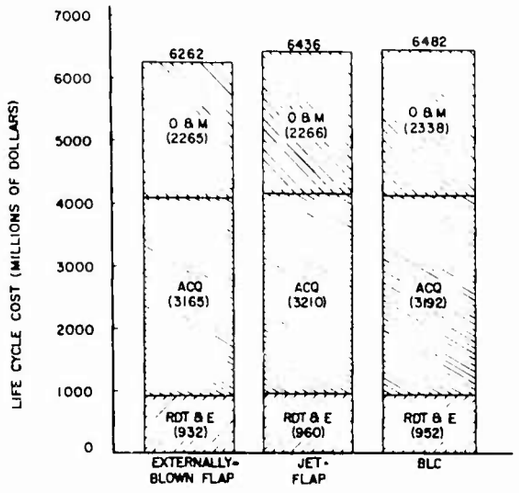

Fig.20 Life cycle cost for selected designs

CHARACTERISTIC	EXTERNALLY-BLOV FLAP	BLC/THRUST DEFLECTION	JET-FLAPY THRUST DEFL
LIFE CYCLE COST	1	3	2
HANDLING QUALITIES	3	2	1
OPERATIONAL QUALITIES — RELIABILITY	1	2	3
OPERATIONAL QUALITIES — MAINTAINABILITY	1	2	3
ASSOCIATED ENGINE DEVELOPMENT RISK	1	3	2
AVAILABLE TEST DATA	2	1	3

Fig.21 Comparison of lift/ propulsion systems

FLYING OPERATIONS

- FLIGHT CREW COST
- FUEL AND OIL COST
- INSURANCE COST

DEPRECIATION ON FLIGHT EQUIPMENT

DIRECT MAINTENANCE ON FLIGHT EQUIPMENT

- LABOR
  - AIRCRAFT
  - ENGINES
- MATERIAL
  - AIRCRAFT
  - ENGINES

MAINTENANCE BURDEN

Fig.22 Direct operating costs

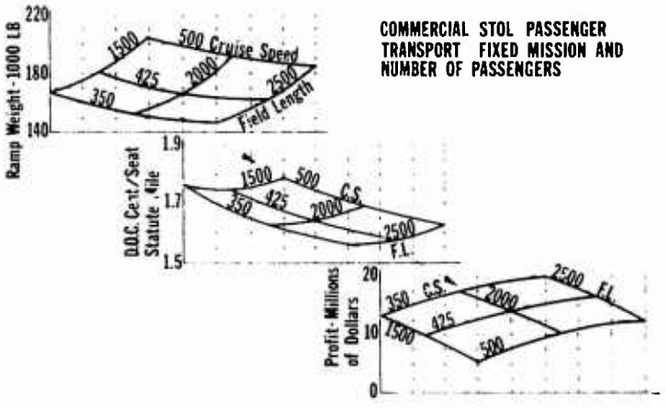

Fig.23 Typical parametric results

SEMINAR CONTRIBUTIONS

12. **A NEW TECHNIQUE FOR AEROFOIL LEADING-EDGE STUDIES**

by J.Monnerie, ONERA, France

13. **SOME COMMENTS ON CHARACTERISTICS OF HIGH-LIFT WINGS**

by D.N.Foster, RAE, UK

14. **THE HUNTING H.126 JET-FLAP RESEARCH AIRCRAFT**

by K.D.Harris, HSA, UK

15. **AERODYNAMIC RESEARCH ON HIGH-LIFT SYSTEMS**

by F.Mavriplis, CANADAIR Ltd, Canada

A NEW TECHNIQUE FOR AEROFOIL LEADING-EDGE STUDIES

by

J. MONNERIE; O.N.E.R.A., Chatillion-sous-Bagneux, France

The connection of flow separation bubbles which develop near an aerofoil leading-edge with the behaviour of a wing at large angles of attack is now well known. To study in detail such bubbles and more generally all flow configurations occurring in the nose region, a special type of mounting base has been developed recently by Erlich and Cabot (1) at O.N.E.R.A., following a suggestion by Poisson-Quinton. They have exploited as far as possible the old idea that the flow near the leading-edge is primarily governed by the location of the stagnation point, and therefore by the circulation around the model.

In the upper half of Fig. 1, we have drawn the whole of the aerofoil profile whose leading-edge is to be studied. The aerofoil total chord is three-quarters of a metre, i.e. the maximum size normally tested at high angles of attack in our Cannes wind-tunnel. This corresponds to a maximum Reynolds number of 2×10^6 when referred to the chord. In the lower half of Fig. 1, the leading-edge region of the profile has been enlarged nearly by a factor of 4, to make up a new model; the circulation around this truncated profile is produced by a jet-flap or a blown flap, while an appropriate outline joins the fore and aft parts.

The similitude of the two models has been verified firstly in the rheo-electric tank; the velocity diagram in Fig. 2 shows the identical nature of the two distributions for the case of a profile with a Handley Page slat. Secondly, the similitude has been also established in the Cannes wind-tunnel; the comparison presented in Fig. 3 for two incidences shows that the correspondence is quite good, despite the difference in Reynolds numbers. The theoretical curve corresponding to a calculation of the potential flow at zero Mach number, together with the typical plateau of short bubbles on the experimental curve, can also be usefully noted. This tool of research has not yet been used very intensively, but the following results may be of interest.

(a) Fig. 4 demonstrates that surface-flow visualisation at the large scale can furnish valid information about the flow near the leading-edge, provided that a cautious interpretation is made.

(b) Fig. 5 confirms that the bubble region can be traversed very accurately with probes; the upper diagram shows the iso-velocity curves in this region; the lower diagram shows the typical development of the form factor H which is the ratio between the displacement-thickness and the momentum-thickness. H varies from the value 2.6 in the laminar region to a value near 1.4 after transition, passing through a maximum value associated with the separation.

(c) Fig. 6 summarises complementary studies in the water-tunnel; first, the model with its blown flap which we call a 'Tetard', i.e. a "tadpole" in English; then a longer bubble with laminar reattachment; a short bubble with transition; and finally a perspective view showing the reverse flow and the reattachment flow.

REFERENCE

Erlich, E Exemples de Recherches sur les profiles dans la soufflerie S.10 du CEAT à Toulouse.
O.N.E.R.A. TP 766; 1969.

ONERA PROFILE "D"

I. FULL PROFILE

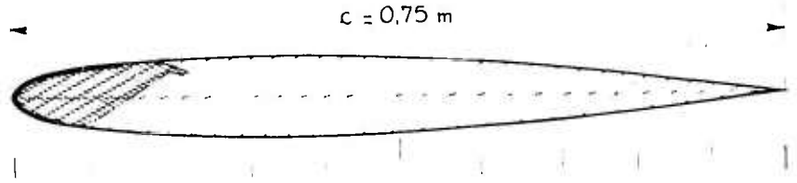

II. CURTAILED PROFILE

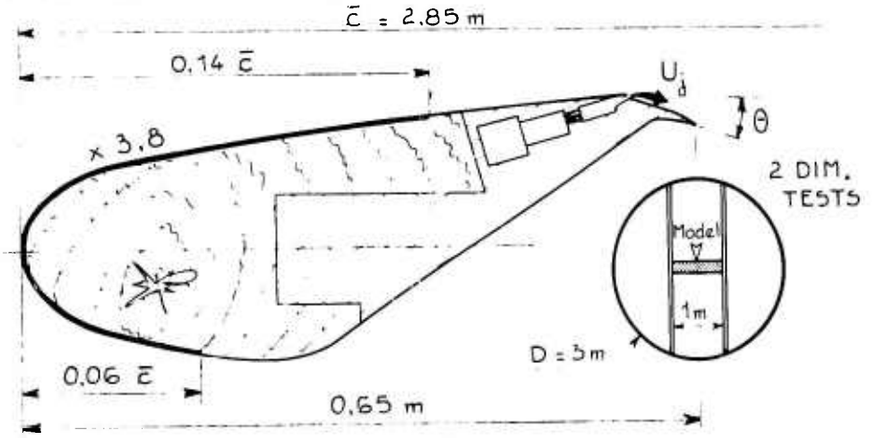

Fig. 1

RHEOELECTRICAL TANK MEASUREMENTS

—o— FULL PROFILE ($\delta_f = 36,2°$ $\alpha = 4°$)

····+···· CURTAILED PROFILE ($\delta_f = 60°$)

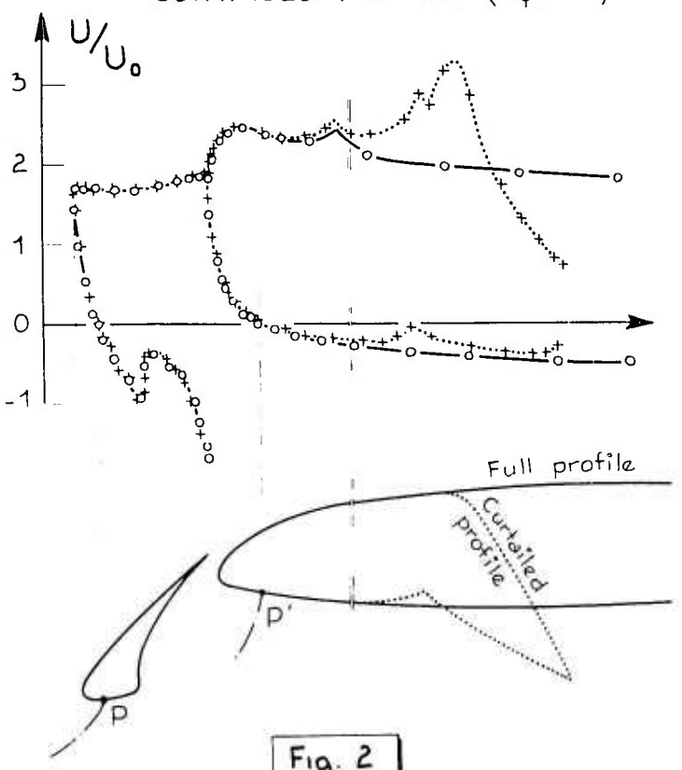

Fig. 2

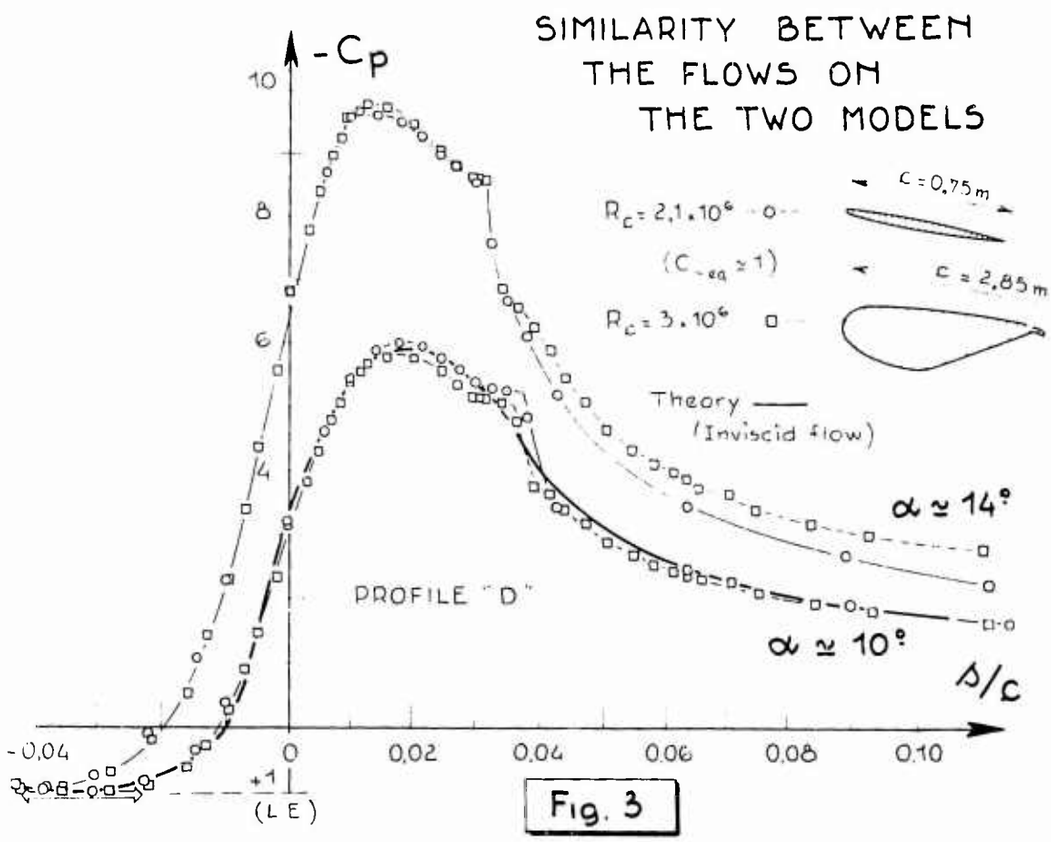
SIMILARITY BETWEEN
THE FLOWS ON
THE TWO MODELS
-Cp
10
8
6
4
$R_c = 2,1.10^6$
$(C_{-eq} \simeq 1)$
$R_c = 3.10^6$
c = 0,75 m
c = 2,85 m
Theory
(Inviscid flow)
$\alpha \simeq 14°$
$\alpha \simeq 10°$
PROFILE "D"
s/c
-0,04
0
0,02
0,04
0,06
0,08
0,10
+1
(L E)

Fig. 3

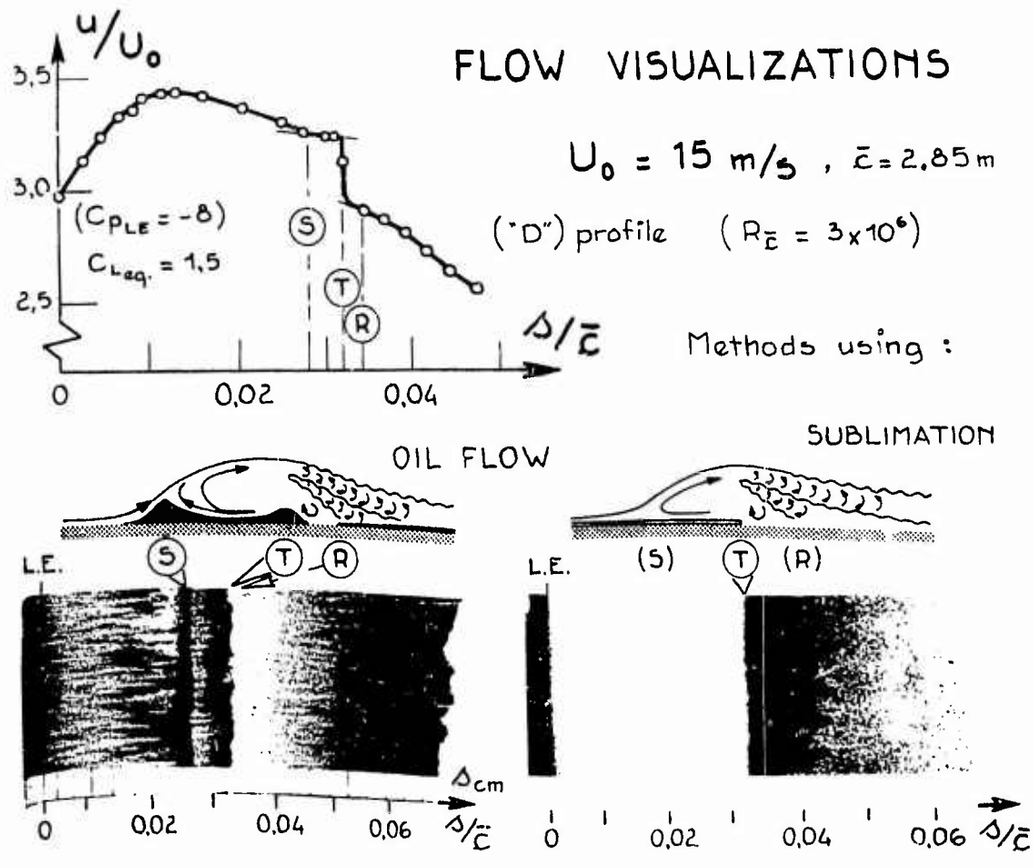
u/U₀
3,5
3,0
2,5
$(C_{PLE} = -8)$
$C_{Leq.} = 1,5$
S
T
R
s/c̄
0
0,02
0,04
FLOW VISUALIZATIONS
$U_0 = 15$ m/s , $\bar{c} = 2,85$ m
("D") profile ($R_{\bar{c}} = 3 \times 10^6$)
Methods using :
OIL FLOW
SUBLIMATION
L.E.
(S)
(T)
(R)
Δcm
0
0,02
0,04
0,06
s/c̄

Fig. 4

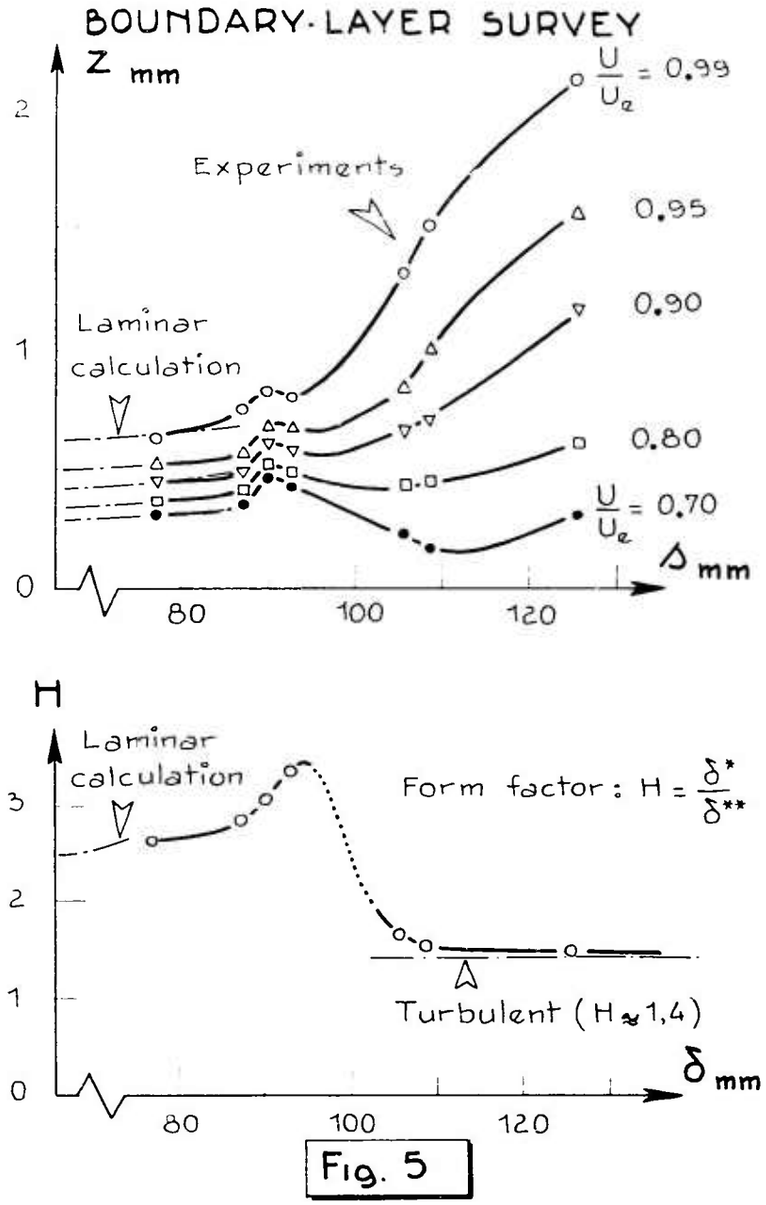

Fig. 5

WATER-TUNNEL VISUALIZATION

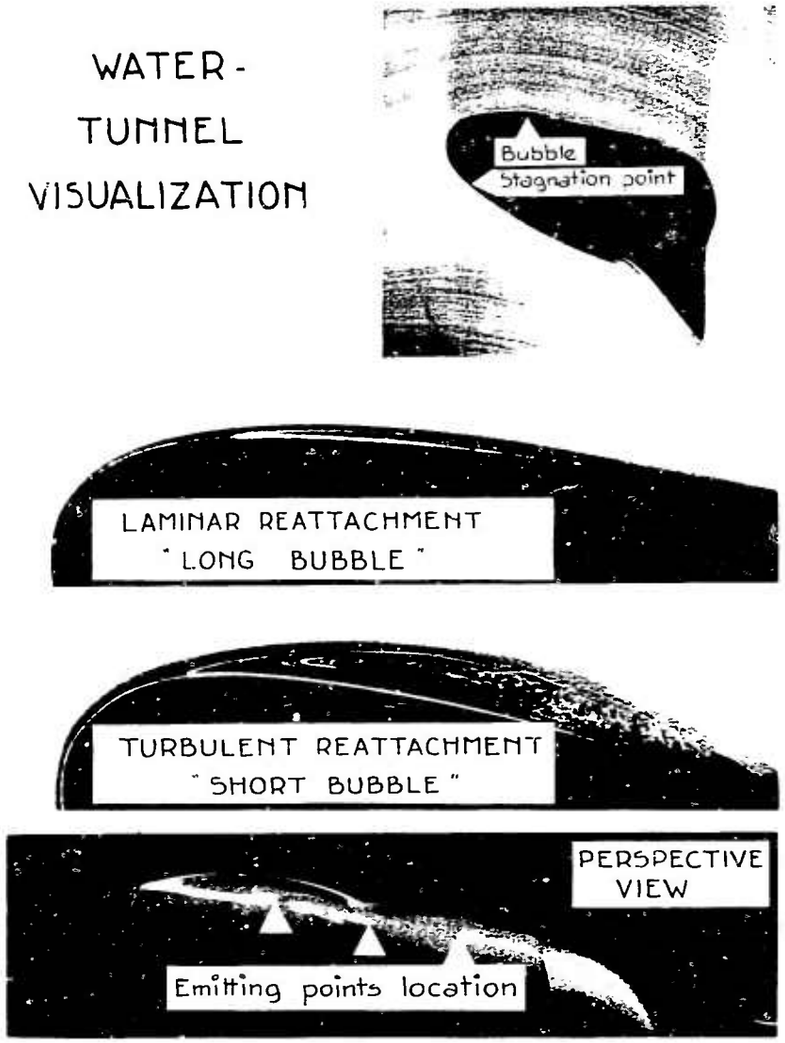

Fig. 6

SOME COMMENTS ON CHARACTERISTICS OF HIGH-LIFT WINGS

by

D. N. FOSTER; R.A.E., Farnborough, U.K.

1. WING WITH PLAIN HINGED FLAPS WITH BOUNDARY-LAYER CONTROL

Wind-tunnel tests, under as near to two-dimensional conditions as possible, have been carried out on a wing section with plain leading and trailing-edge flaps having boundary-layer control by blowing at the flap knees. A range of flap deflections were tested; results are presented here for the condition with no leading-edge flap deflection and with the trailing-edge flap deflection 20°. In addition to inviscid flow calculations of the pressure distribution around the isolated wing section at zero Mach number, calculations have been made for the isolated wing at the Mach number of the wind tunnel tests (0.13) by the method of Sells (1), and for the section in the presence of the tunnel walls, since the ratio of wing chord to tunnel height (4:13) was large. The effect of compressibility on lift was found to be small, although large suction peaks ($C_{p,min} \approx -15$) were measured at the leading-edge at high angles of incidence. The tunnel wall effect was, however, of some significance, and therefore the results calculated with wall effects have been taken as representing the inviscid values for comparison with the wind-tunnel results.

This comparison has been made in Fig. 1, where these results have been superimposed on some of a series of experimental results for different momentum coefficients. Even with boundary-layer control, the experimental lift-curve slopes are lower than the inviscid values, so that the momentum coefficient to achieve the inviscid lift increases with angle of incidence. Fig. 2 shows a typical comparison of the inviscid pressure distribution with that measured experimentally. The agreement is very good, except near the flap knee where the contour considered in the inviscid calculation is of necessity different from the actual contour. Fig. 3 shows the results of measurements of the sectional drag by the wake survey technique. These curves suggest an almost constant thrust recovery of 70% of the momentum coefficient. Also superimposed on the carpet is a line corresponding to the values of angle of incidence and momentum coefficient at which the inviscid lift coefficient was achieved; this line is seen to lie close to zero wake drag throughout.

To summarise, these results would suggest that the inviscid lift is achievable with a momentum coefficient which is dependent on the angle of incidence (or the lift); that under these conditions a pressure distribution will be measured which is very similar to the inviscid predictions; and that sensibly zero drag will result.

2. DRAG WITH HIGH-LIFT DEVICES EXTENDED

For a given wing at a given angle of incidence and with a given flap deflection, planar theory (2) can predict a total lift coefficient C_L and a total vortex drag coefficient C_{Dv}. These can be expressed as

$$C_L = \Delta C_{L\alpha} + \Delta C_{Lf} \qquad (1)$$

$$\pi A\, C_{Dv} = K_1 C_L^2 + K_2 . \Delta C_{Lf}^2 + 2 K_3 C_L . \Delta C_{Lf} \qquad (2)$$

where $\Delta C_{L\alpha}$ is the lift increment due to wing incidence change from the zero lift angle

ΔC_{Lf} is the flap lift increment,

and K_1, K_2 and K_3 are constants, all dependent on the wing planform,

with K_2 and K_3 also dependent on the flap planform.

It can be shown that, within the same linearized framework, the profile drag may be expressed as

$$\frac{C_{Dp}}{C_{Do}} = 1 + J_1 C_L^2 + J_2 . \Delta C_{Lf}^2 + 2 J_{12} C_L . \Delta C_{Lf} \qquad (3)$$

where C_{Do} is the profile drag coefficient due to the thickness distribution, without incidence or camber,

and J_1, J_2 and J_{12} are constants related to the chordwise velocity perturbations due to incidence and flap deflection.

Equation (3) may be rewritten as

$$C_{Dp} = \breve{C}_{Dp} + J_1 C_{Do} (C_L - \breve{C}_{Lp})^2 \qquad (4)$$

Whilst the validity of applying the results of the linearized approximation to a real case is, perhaps, in question, it is of interest to consider what follows from their application to some existing test data (1).

The configuration to be considered is shown in Fig. 4. The wing, of aspect-ratio 8.0 and quarter-chord sweep-back 25° was tested with and without a fuselage, and had Fowler flaps extending from the fuselage side (10% semi-span) to 65% semi-span. The experimental results have been analysed by subtracting from the measured drags a vortex drag derived from equation (2), using predicted values of K_1, K_2 and K_3, and measured values of C_L and ΔC_{Lf}. For the wing + fuselage cases, any contribution to the lift and drag from the forces on the front and rear fuselage sections has been ignored, and only the lift and drag due to the loading across the wing and fuselage at the wing-fuselage junction has been considered. The difference between the measured drag and the theoretical vortex drag is shown (Fig. 6) in the form suggested by equation (4), i.e. relative to a lift coefficient for a minimum value of this difference. The value of $\breve{C}_L$, and the slopes of the lines shown in Figs. 5 and 6 were derived by fitting a "least-squares" parabola to that portion of the data which was considered to correspond to well-attached flow.

Fig. 5 shows results for the wing with the flaps retracted. Two points are noteworthy: first that the lines with and without fuselage are parallel, and secondly that at the take-off condition, ($0.7\ C_{Lmax}$) the departure of the experimental points from the straight line is insignificant. Fig. 6 shows the results of the analysis when the flaps are extended and deflected 15°. Again the lines with and without fuselage are parallel, the increment due to the addition of the fuselage ($\Delta[C_D - C_{Dv}] = 0.0115$) being slightly larger than for the flaps-up case ($\Delta[C_D - C_{Dv}] = 0.0100$). The slopes of the lines on Fig. 6 are some 20% higher than for the flaps-up case, and now the take-off condition is well within the points lying on the line.

The main inference that can be drawn from these results is that, at least to the point $C_L = 0.7\ C_{Lmax}$, the drag can be adequately described by equations (2) and (4).

REFERENCES

1. Sells, C.C.L. Plane subcritical flow past a lifting aerofoil. R.A.E. T.R. 67146; 1967.

2. McKie, J. The estimation of the loading on swept wings with extending chord flaps at subsonic speeds. R.A.E. T.R. 69034; 1969.

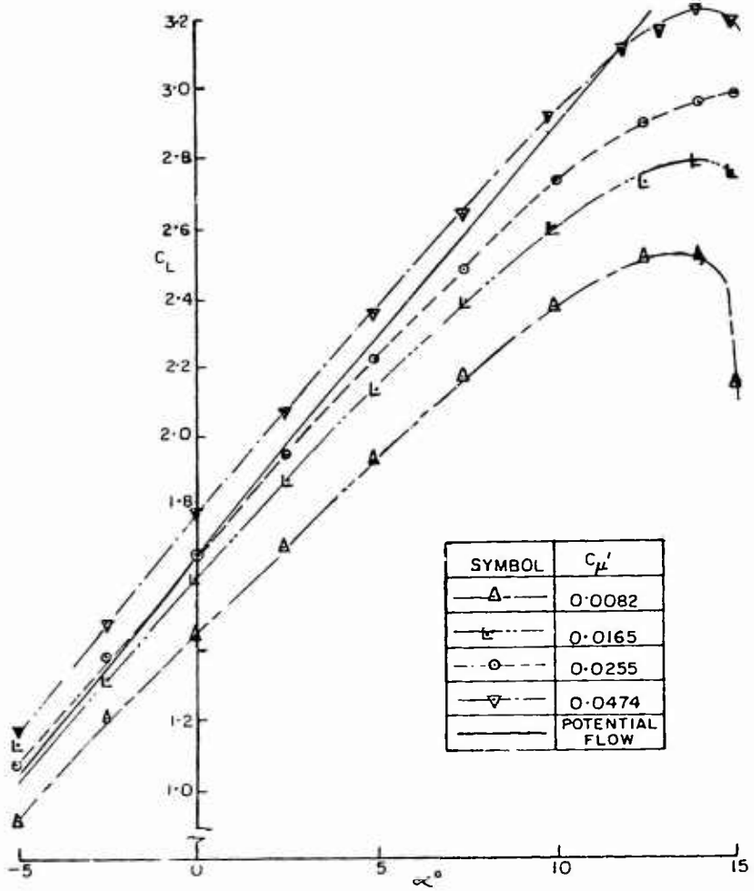

Figure 1 (Crown Copyright)

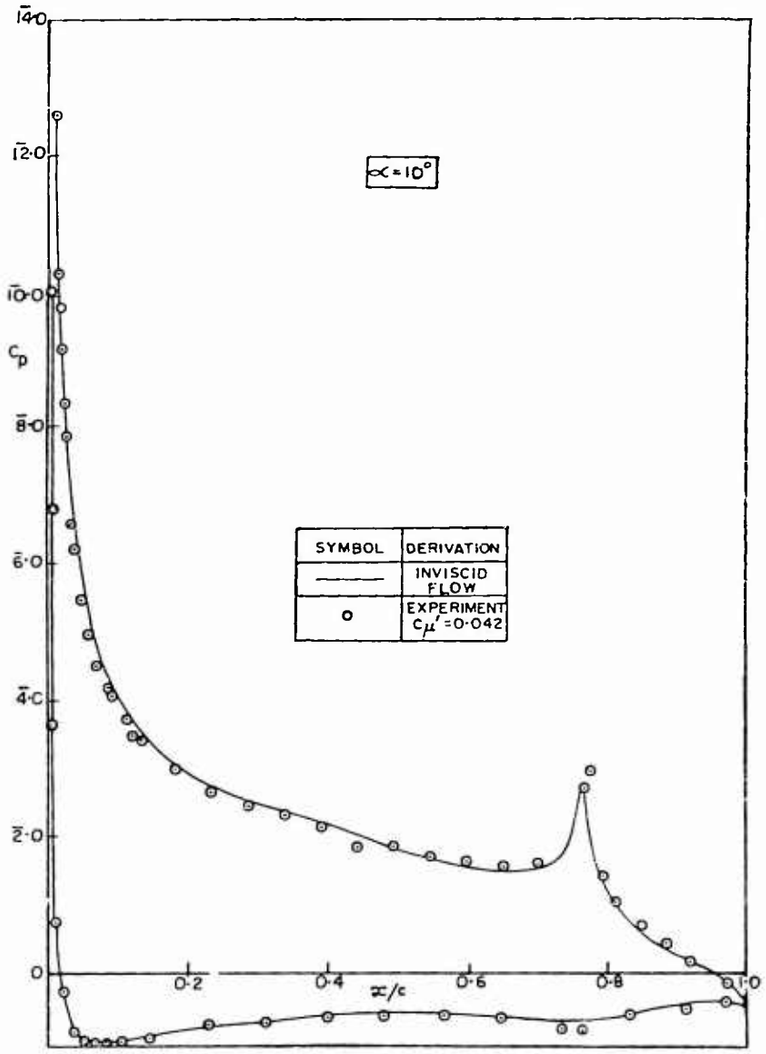

Figure 2 (Crown Copyright)

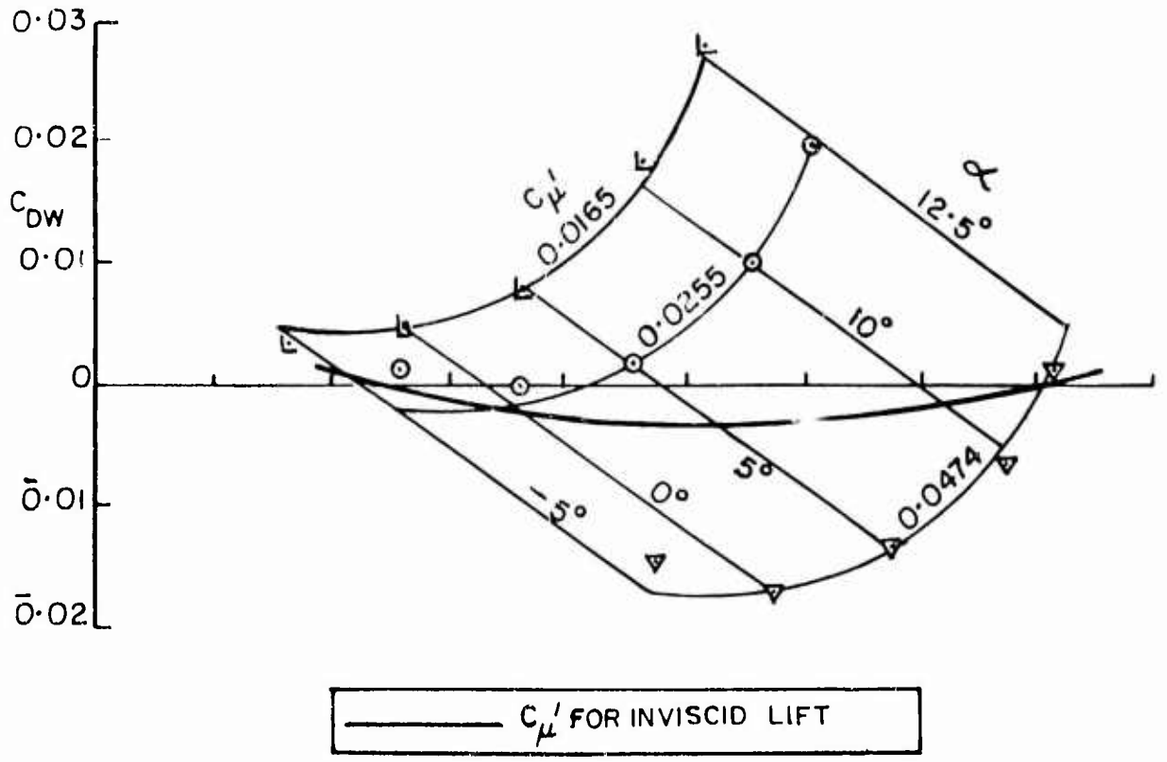

Figure 3 (Crown Copyright)

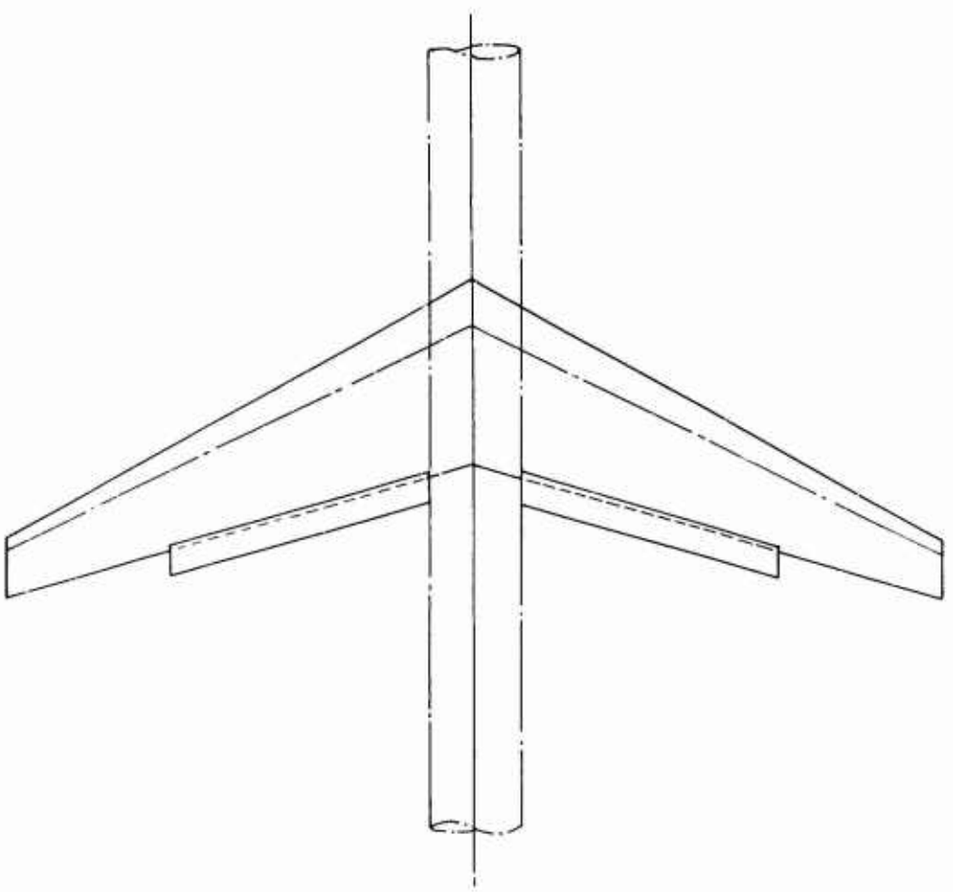

Figure 4 (Crown Copyright)

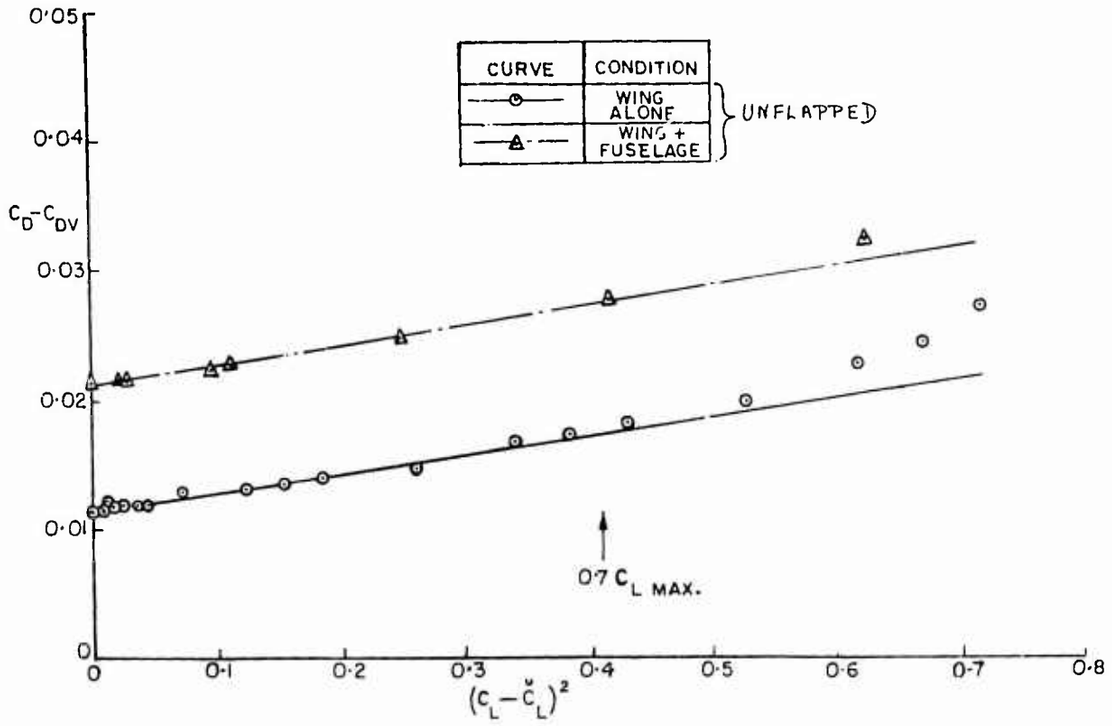

Figure 5 (Crown Copyright)

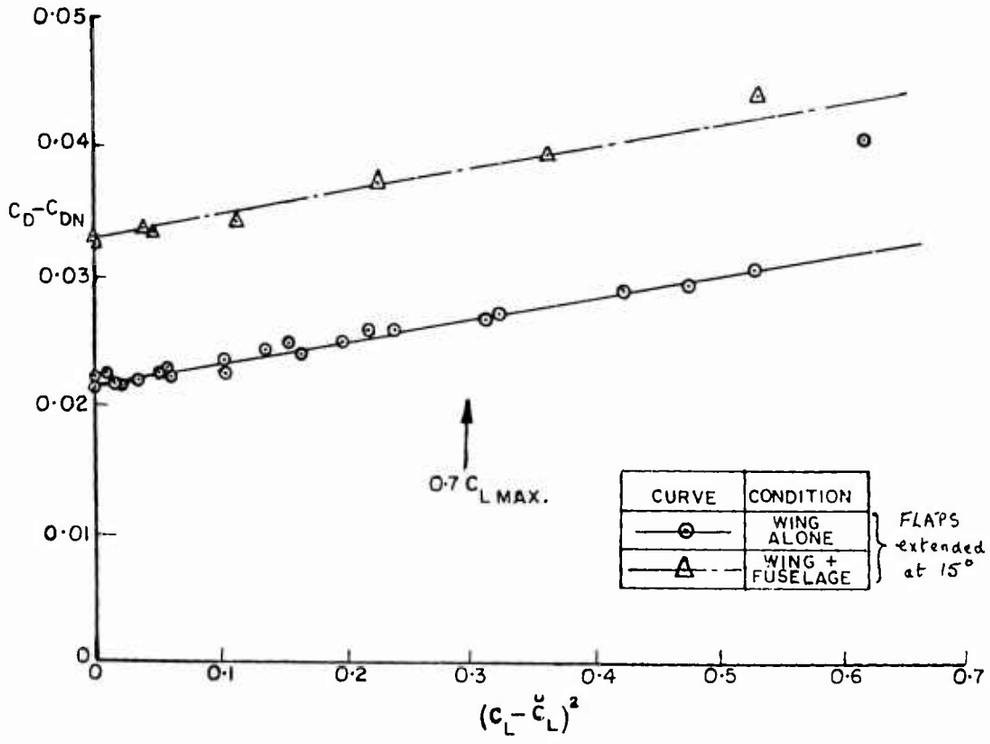

Figure 6 (Crown Copyright)

THE HUNTING H.126 JET-FLAP RESEARCH AIRCRAFT

K.D.Harris

1. FUNDAMENTAL CHARACTERISTICS OF THE JET-FLAP

The jet-flap principle, and the possibilities of applying this principle to a jet-propelled aeroplane, were first conceived at the National Gas Turbine Establishment, UK, in 1952. The concept was made public in 1955 in a lecture to the Royal Aeronautical Society by I.M Davidson, the leading protagonist of the scheme. The pioneer investigations at NGTE and NPL during this early period were followed over the next decade by extensive experimental and theoretical studies, in Britain particularly at the RAE and Huntings. (A comprehensive list of *published* British References has been added for completeness at the end of this Seminar Contribution — *Editors*).

The aerodynamic characteristics which in principle made the jet-flap attractive to the aircraft designer, particularly the designer of STOL aircraft, are of course:-

(i) the ability to develop very large lift coefficients and

(ii) the high level of thrust recovery which is 100% in ideal inviscid flow however great the jet deflection angle to the direction of flight.

It is beyond the scope of the present contribution to discuss these characteristics at length. However, many wind-tunnel tests have substantiated that very high lift-coefficients can indeed be generated. With regard to the thrust recovery hypothesis, it should be mentioned that the division of the streamwise force into thrust and drag components must always be arbitrary, and this inevitably introduces difficulties into the question of how much thrust recovery is obtained. If the jet flux is taken as that leaving the trailing-edge of the wing, and appropriate allowance is made for the trailing-vortex drag and the profile drag, then experiment shows that full recovery of the jet momentum flux as propulsive thrust is obtained quite closely at least for moderate jet angles. However, from the point of view of the aircraft designer it must be remembered that owing to ducting/slot losses, and to skin-friction/turning losses over the mechanical flap which forms an essential part of any practical system, the jet momentum flux leaving the trailing-edge will be appreciably less than that which would be obtained from a conventional engine installation with a short jet-pipe. Indeed, if all or a large percentage of the total engine efflux is discharged in the form of a jet-flap, these losses will inevitably be fairly large. It is these viscous ducting and jet deflection thrust losses, together with the space occupied by the ducting system, which reduces the otherwise attractive properties of the jet-flap to such an extent that it no longer remains an obvious choice for even a STOL aircraft.

2. DECISION TO BUILD A PILOTED RESEARCH AIRCRAFT

The exceptionally high lift-coefficients that the jet-flap offered, together with the remarkable promise of substantial thrust recovery, led to the early decision in 1956 by the British Ministry of Aviation to order a piloted research aircraft. The H.126 jet-flap research aircraft was then designed and built by Huntings (Luton UK) under contract, for a flight research programme at the Royal Aircraft Establishment. This work was intended not only to ensure essential flight research to complement wind-tunnel and theoretical studies, but also to provide flight-handling experience of value more generally for STOL aircraft with high-lift wings.

The desirability of a piloted vehicle was obvious, if only because of the very large C_L-range that would be made possible. However, it was also envisaged that novel means of aircraft control entailing deflection of the jet-flap and variation of the jet-flap thrust might be investigated, and these considerations made a piloted vehicle essential.

In the 1950's by-pass engines had not been developed, and it was quickly realised that a major problem would be met in ducting the very hot and relatively low-pressure gas from the engine(s) to the trailing-edge of the wing. In view of the extreme cost of developing a new type of engine, it was decided that the research aircraft would have to be powered by an existing unit of proven reliability. This meant that the aircraft would inevitably have a very poor overall performance when judged against contemporary aircraft. This fact must always be kept in mind, and no deductions regarding the potential performance of the jet-flap should be drawn from the H.126 without making full allowance for this very severe handicap imposed on the research aircraft.

3. PERFORMANCE SPECIFICATION OF THE RESEARCH AIRCRAFT

When the specification for the research aircraft was being drawn up, the highest landing C_L for most jet aeroplanes was about 1.5, a value not greatly exceeded even today. The bold decision was taken to aim for a usable C_L of 7 to 8, to exploit fully the research possibilities. Eventually, when the difficulties attendant on using an existing pure turbo-jet engine were better appreciated, it was specified that the aircraft should be capable of developing a usable lift coefficient of at least 6 with:-

(i) a 20% speed margin from the 1g stall, and

(ii) the ability to vary the flight path from at least level flight to an angle of descent of at least 5°

The flight control system was to be designed so that the trailing-edge flaps could be geared to the control column, thus permitting investigation of the novel form of control already referred to in Section 2.

4. BRIEF DESCRIPTION OF THE AIRCRAFT

4.1 General Arrangement

A general arrangement drawing of the aircraft is shown in Figure 1. The main features are the fairly large aspect-ratio, shoulder-high wing; the large fin and high-set tailplane; and the rather deep fuselage housing an Orpheus turbo-jet engine under the single seat cockpit. The tricycle undercarriage was not made retractable because interest was mainly in low-speed flight.

With a maximum all-up weight of about 10,700 lb. (47,600 newtons) and a wing area of 217 ft² (20.1 m²), the wing loading is about 50 lb/ft² (2,370 N/m²). To keep the engine jet temperature to not more than 620°C, the basic Orpheus engine had to be de-rated from a test-bed thrust of about 5,000 lb (22,200 N) to about 4,300 lb (19,100 N). However, since 15% of the engine efflux is continuously used for control and autostabilisation purposes, and because of the large thrust losses incurred in ducting the efflux through the fuselage and wings, the effective propulsive thrust from the nozzles is slightly less than 3,000 lb (13,300 N).

The use of only a single engine in an aircraft so vitally dependent on powered lift calls for some comment. In all the early project work two engines were used, but lack of availability of suitable engines coupled with the difficulties of designing a suitable ducting system led ultimately to the decision to use a single engine. Safety for the pilot was to be assured by provision of a "zero-zero" ejector seat; whilst the risk of losing the aircraft, in the event of an engine failure during critical stages of the landing and take-off manoeuvres, was accepted as a necessary price to pay for the other advantages in using a single engine.

4.2 Wing

A high wing configuration was chosen to minimise the loss of $C_{L\max}$ and other adverse interference effects produced by ground effect under high-lift conditions. The aspect-ratio of about 9 was estimated to be the optimum compromise between a high aspect-ratio to minimise trailing-vortex drag, and a low aspect-ratio to minimise ducting losses. Zero sweepback on the flap hinge line was chosen since interest was primarily in low-speed flight.

The most abnormal characteristic of the wing is the thickness of the aerofoil section. The section is NACA 4424, having a thickness-chord ratio of 24%. One major reason for such a high thickness was to accommodate the large diameter ducts which are required to keep the ducting losses to an acceptable level. The large thickness-ratio and camber were also favoured to permit the development of very high lift-coefficients without the additional need for leading-edge devices such as a slat and/or boundary-layer control by nose blowing. A further advantage is the large nose radius of the trailing-edge flap which reduces the losses incurred in turning the jet sheet.

4.3 Ducting System

The ducting system is illustrated in Figure 2. Division of the engine efflux is as follows:-

Jet-flap	55%	i.e. 85% for propulsion
Direct thrust nozzles	30%	
Pitch control jets	5%	used for control purposes
Yaw control jets	5%	
Roll control jets	5%	used for auto-stabilisation

In the early project schemes all the propulsion was to have been supplied in the form of a jet-flap, as in the original NGTE concept. However, it was found that the overall propulsive efficiency could be much improved by restricting the jet-flap to a strength just sufficient to generate the specified lift-coefficient. The jet flow released by this was ducted to direct thrust nozzles positioned at such a distance below the centre of gravity that a nose-up pitching moment was produced approximately cancelling out the nose-down moment of the jet-flap.

5. THRUST LOSSES

Despite the use of the largest possible ducts that could be accommodated in the thick wing, the loss of gross thrust from the engine turbines exit to the jet-flap nozzles amounts to about 22%. A further substantial loss occurs owing to skin friction over the 14% chord mechanical flap.

Whilst this very severe loss of gross thrust arising from viscous ducting and turning effects is not necessarily typical of jet-flapped aeroplanes, it nevertheless seems likely that this will always remain a major problem in any design which seeks to exploit the jet-flap to a significant extent.

6. STABILITY AND CONTROL PROBLEMS

Several severe stability and control problems were revealed by analytical and wind-tunnel studies during the design stage. These arose primarily from the very large incidence and lift-coefficient range for which the aeroplane was designed.

The longitudinal problems included the following:-

(i) A large nose-down pitching moment from the jet-flap;

(ii) A large variation in restoring margin over the incidence range owing to the high location of the wing relative to the centre of gravity;

(iii) A strong nose-down change of trim on landing owing to the large reduction of downwash at the tailplane;

(iv) Flight at speeds far below the minimum drag speed.

Had nothing been done to alleviate the large nose-down pitching moment produced by the jet-flap, there would have been a substantial loss in trimmed lift-coefficient. It would also have led to a large static margin in relation to the manoeuvre margin, and to a highly unstable phugoid mode. All of these problems were much diminished by the re-division of the propulsive flow which has already been referred to in Section 4.3. It was planned to fit infinitely variable thrust spoilers to the direct thrust nozzles, so that the propulsive thrust could be modulated to give the required angle of descent for landing, and to control the flight path.

Further improvements in both stability and control were effected by suitable gearing of a pitch jet to the all-moving tailplane and geared elevator.

The lateral and directional problems involved:-

(i) A stongly unstable spiral mode at high C_L's, the time to double amplitude being about 2 seconds at a C_L of 6.

(ii) A large reduction in weathercock stability when spoiling the thrust from the direct thrust nozzles.

(iii) A large adverse yawing moment from the ailerons at high C_l's.

(iv) Low damping in yaw under certain conditions of flight.

(v) Poor entry into banked turns at high C_l's.

With regard to the spiral stability problem it is well known that the criterion for positive stability is

$$l_v n_r - n_v l_r > 0$$

For satisfactory characteristics in the other lateral and directional modes of motion it is necessary that n_r shall be negative, and n_v positive. Now l_r is naturally positive, and this always makes the second term destabilising. Since l_r tends to be proportional to C_L, the destabilising influence increases continuously with increase of C_l. In the normal way, spiral stability is achieved by using wing dihedral to make l_v negative. However, in the present instance l_v tended to become progressively more positive with increase of incidence, flap angle and jet momentum coefficient. Attainment of a sufficiently negative value of l_v at high C_l would have required extremely large dihedral leading to a grossly excessive negative value at low C_l's, and to quite unacceptable characteristics in the other lateral and directional modes.

Theoretical and experimental work showed that the observed tendency for l_v to become positive at high values of C_L is a fundamental feature of wings of high aspect-ratio. It was therefore decided that autostabilisation would have to be used to overcome the spiral instability problem. Essentially this was done by reducing l_r to make the second term in the above criterion less destabilising. Detailed calculations were made to optimise the overall performance of this system, and it was found that the use of a roll jet to provide the required rolling moment would be simpler and much better than using the ailerons.

The reduction in weathercock stability with spoiling of the direct thrust was not studied in detail, but was probably due to a jet efflux interference effect over the rear part of the fuselage and the fin. Positive weathercock stability is usually a fairly fine balance between a stabilising fin effect, and a destabilising fuselage effect. A relatively small interference effect can then have a significant influence on the overall balance of moments.

Compensation for the adverse yawing moment of the ailerons was provided by gearing the yaw jets to the ailerons.

7. STALLING CHARACTERISTICS

The most important single factor to merge from the flight tests was the severity of the stalling behaviour. Early wind-tunnel tests had in fact exhibited abrupt and large decrease in lift at the stall for high momentum and lift coefficients.

With the engine fully throttled the stall was quite gentle, as expected. However, with somewhat increased engine thrust, and a momentum coefficient C_μ of only about 0.1, the stall became very sharp with no natural warning. Wing drops of up to 60° were experienced, with either the port or starboard wing dropping. With further increase in C_μ the stall tended to become even more violent, still with either wing stalling first.

Flow visualisation in flight, by means of surface tufts, showed that the stall commenced with separation of the flow on the inner part of either the port or starboard wing at about mid-chord. The separation then spread almost instantaneously over most of that half of the wing, whilst the opposite wing remained unstalled during the whole of the ensuing motion.

Wind-tunnel tests made to study the stall behaviour showed, despite a low Reynolds number of about 0.5×10^6 (based on wing mean-chord) an almost identical behaviour to that at full scale. An increase of incidence of 2° to 4° was necessary to make the other half of the wing stall. It can only be presumed that the discontinuity produced by the fuselage provided an effective barrier to the spread of the initial separation. The redistribution of the spanwise loading resulting after the stalling of one-half of the wing would then have induced an increase in downwash over the unstalled half of the wing, thus leading to the observed increase in stalling incidence.

When the model stall characteristics were found to be similar to the full-scale characteristics, it was decided to use the model to study how the behaviour could be improved. Devices which caused the flow to separate early over the inboard part of the wing proved useless, as the separation (once provoked) still spread almost instantaneously over the wing on which it started. Fences of various shapes and sizes were tried, but these proved equally ineffective.

Much the most effective device that was found was a leading-edge slat covering the outer 90% of the exposed wing span. A very strong vortex was shed from the inboard end of the slat. This caused the inner unslatted portion of the wing to stall early, but it was successful because it contained the separation for several degrees of incidence. As a result of this the ailerons retained much of their power, and tests showed that they would have been able to overcome the rolling moment due to asymmetric stalling of the inner part of the wing.

8. CONCLUDING REMARKS

It must be stressed that the H.126 aircraft was conceived and designed over a decade ago, essentially for the first flight research on jet-flaps and not for project development. Naturally, it has been possible to discuss only briefly here some of the extensive flight experience obtained by RAE and Hunting Aircraft - BAC during the period 1963-67, as well as to refer only briefly to the extensive complementary studies (wind-tunnel and analytical) conducted during the design, constructional and operational phases.

Unfortunately, the flight test programme had to be curtailed due to financial restrictions and lack of practical interest in jet-flap applications at the time. In particular, although the ultimate fitting of thrust reversers to the direct thrust nozzles had always been envisaged, these were not in fact fitted, so that landing approaches under high-lift conditions and associated ground effects could not be explored in flight. It is worth adding that some full-scale wind-tunnel tests have recently been carried out by NASA on the unmodified aircraft in their Ames 40 ft. x 80 ft. tunnel. Also, it is still to be hoped that the unmodified aircraft may yet be used for flight investigation at the fairly high lift-coefficients which are likely to be employed in the not too distant future with STOL aircraft.

PUBLISHED BRITISH REFERENCES ON JET-FLAP AERODYNAMICS

GENERAL

1. Davidson, I. M. — The jet flap. J. Roy. Ae. Soc. Vol. 60, pp 25-50; 1965.

2. Stratford, P. S. — Early thoughts on the jet flap. Ae. Quart. Vol. 7, pp 45-59; 1956.

3. Stratford, P. S. — Mixing and the jet flap. Ae. Quart. Vol. 7, pp 85-105; 1956.

4. Williams, J. — British research on the jet-flap schemes. Z. Flugwiss. Vol. 6, pp 170-176; 1958.

5. Williams, J. — Some British research on the basic aerodynamics of powered lift systems. J. Roy. Ae. Soc. Vol. 64, pp 413-437; 1960.

6. Williams, J.; Butler, S. F. J.; Wood, M. N. — The aerodynamics of jet flaps. ARC R&M 3304; 1961.

7. Williams, J. — Recent basic research on V/STOL aerodynamics at RAE. Z. Flugwiss. Vol. 14, pp 257-276; 1966.

EXPERIMENTAL

8. Dimmock, N. A. — An experimental introduction to the jet flap. ARC Current Paper 344; 1955.

9. Dimmock, N. A. — Some further jet-flap experiments. ARC Current Paper 345; 1956.

10. Dimmock, N. A. — Some early jet-flap experiments. Ae. Quart. Vol. 8, pp 331-345; 1957.

11. Williams, J.; Alexander, A. J. — Three-dimensional wind-tunnel tests of a 30° jet-flap model. ARC Current Paper 304; 1955.

12. Williams, J.; Alexander, A. J. — Some exploratory three-dimensional jet-flap experiments. Ae. Quart. Vol. 8, pp 21-30; 1957.

13. Williams, J.; Alexander, A. J. — Some exploratory jet-flap tests on a 60° delta wing. ARC R&M 3138; 1957.

14. Alexander, A. J.; Williams, J. — Wind-tunnel experiments on a rectangular-wing jet-flap model of aspect ratio 6. ARC R&M 3329; 1961.

15. Butler, S. F. J.; Guyett, M. B. — Six-component low-speed tunnel tests of jet-flap complete models with variation of aspect ratio, dihedral and sweep-back, including the influence of ground proximity. ARC R&M 3441; 1961.

16. Huggett, D. J. — Ground effect on the jet-flap in two-dimensions. Ae. Quart. Vol. 10, pp 28-46; 1959.

EXPERIMENTAL (continued)

17. Wood, M. N. — Comparative thrust measurements on a series of jet-flap configurations and circular nozzles. ARC Current Paper 616; 1962.

18. Butler, S. F. J., Moy, B. A., Hutchins, C. D. — Low-speed tunnel tests of an aspect-ratio 9 jet-flap complete model with ground simulation by moving belt rig. ARC Current Paper 849; 1964.

19. Cox, A. P., Butler, S. F. J. — Low-speed wind-tunnel measurements of damping in yaw ($n_{\dot{v}}$) on an aspect-ratio 9 jet-flap complete model. ARC Current Paper 869; 1965.

20. Foster, D. N. — Exploratory low-speed tunnel tests of part-span flap and fuselage effects on a high lift wing. RAE TR 65288; 1965.

THEORETICAL

21. Woods, L. C. — Some contributions to jet-flap theory and to the theory of source flow from aerofoils. ARC Current Paper 388; 1958.

22. Maskell, E. C., Gates, S. B. — Preliminary analysis for a jet-flap system in two-dimensional inviscid flow. ARC Current Paper 359; 1955.

23. Spence, D. A. — The lift-coefficient of a thin jet-flapped wing. Proc. Roy. Soc. A. Vol. 238, pp 46-68; 1956.

24. Spence, D. A. — The lift on a thin aerofoil with a jet-augmented flap. Ae. Quart. Vol. 9, pp 287-299; 1958.

25. Maskell, E. C., Spence, D. A. — A theory of the jet-flap in three-dimensions. Proc. Roy. Soc. A. Vol. 251, pp 407-425; 1959.

26. Küchemann, D. — A method of calculating the pressure distribution over jet-flapped wings. ARC R&M 3036; 1956.

27. Ross, A. J. — The theoretical evaluation of the downwash behind jet-flapped wings. ARC R&M 3119; 1958.

28. Thomas, H. H. B. M., Ross, A. J. — The calculation of the rotary lateral stability derivatives of a jet-flapped wing. ARC R&M 3277; 1958.

29. Taylor, A. S. — A theoretical investigation of the longitudinal stability, control and response characteristics of jet-flap aircraft. ARC R&M 3272; 1960.

30. Hancock, G. J. — The ground effect on a two-dimensional jet-flapped aerofoil. Queen Mary College (London).

31. Huggett, D. J. — A theoretical study of the ground effect on a jet-flap. Southampton University Report USAA 112; 1959.

32. Maskell, E. C. — The interference on a three-dimensional jet-flap wing in a closed wind-tunnel. ARC R&M 3219; 1959.

33. Spence, D. A. — The theory of the jet flap for unsteady motion. J. Fluid. Mech. Vol. 10, pp 237-258; 1961.

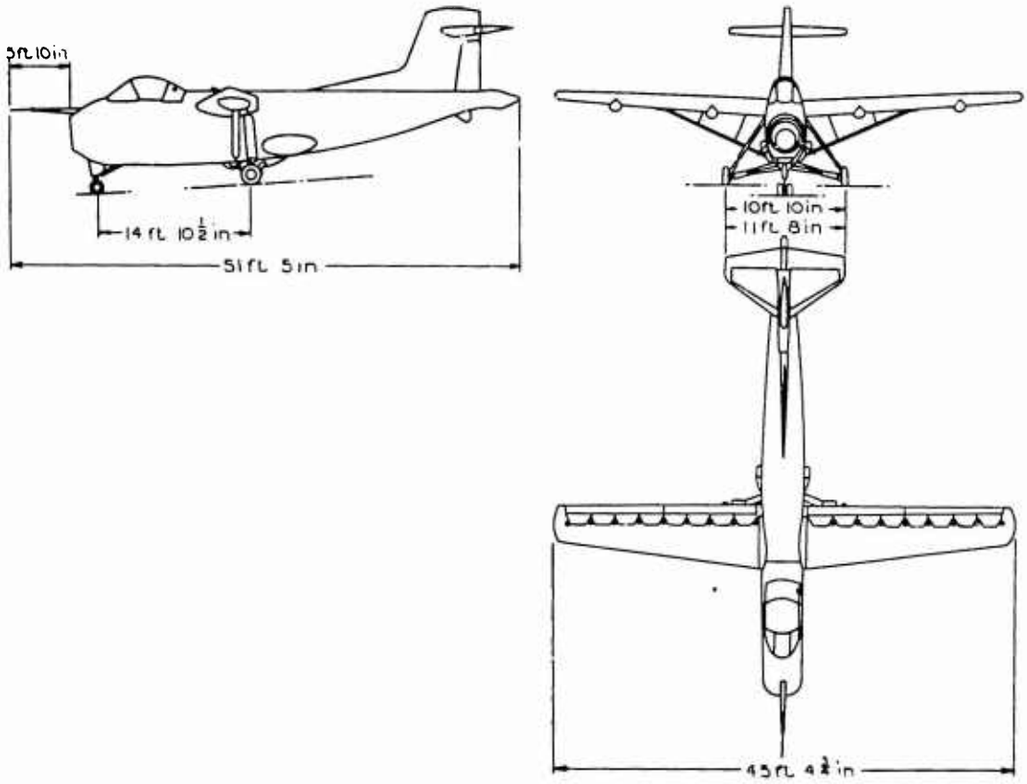

Fig.1 H.126 jet-flap research aircraft

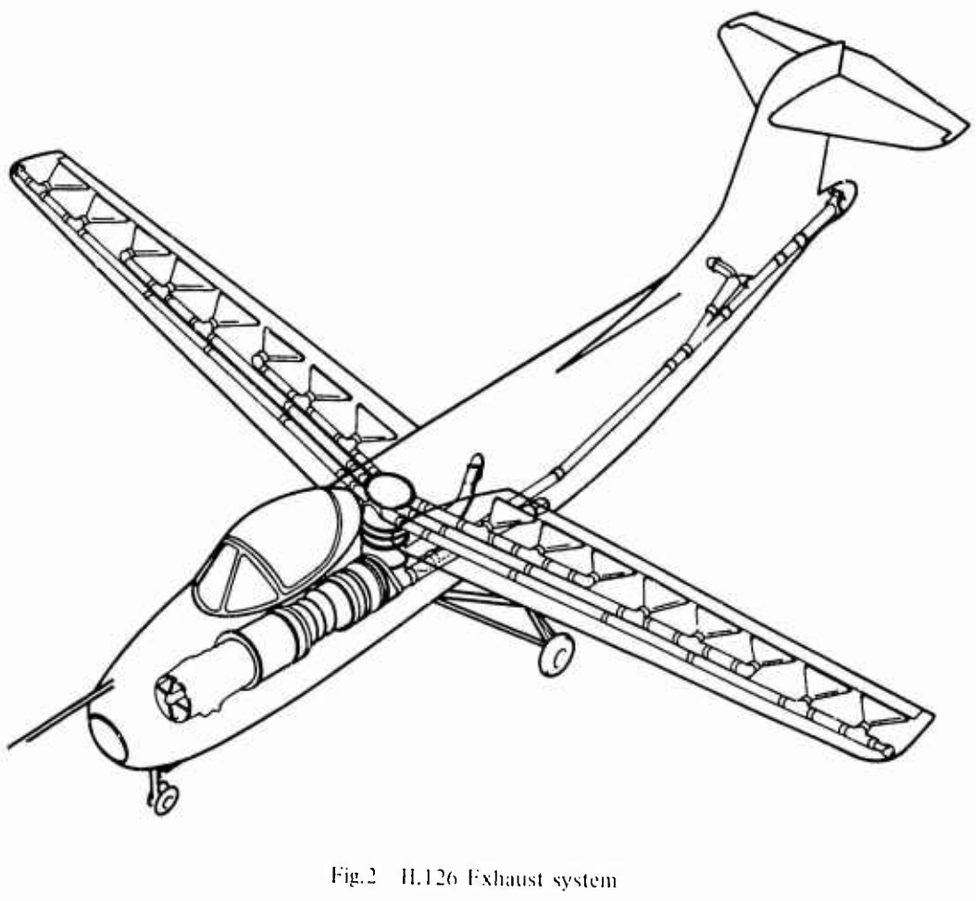

Fig.2 H.126 Exhaust system

AERODYNAMIC RESEARCH ON HIGH-LIFT SYSTEMS

Fotis Mavriplis

1. INTRODUCTION

Research on high-lift systems is part of an overall effort at Canadair to develop aerodynamic technology for future applications to advance aircraft. The objectives of this effort is to develop analytical and experimental methods for dealing with complex aerodynamic problems representative of realistic situations of flight vehicle operations. The work is carried out under two programs which are funded jointly by Canadair and the Defence Research Board of Canada:

(a) Mechanical High-Lift Systems Research and Development DIR Project A-11.

(b) Mathematical Applications in Aerodynamic Design and Analysis Procedures DIR Project A-15.

Some aspects of two-dimensional flow research on high lift systems carried out under these projects are discussed herein.

First, a theoretical method is described which was developed for calculating two-dimensional potential flow about multi-element high-lift airfoils. The method is based on the distribution of vorticity on the airfoil contour.

Second, a wall blowing technique is described which was developed for testing effectively complex high-lift models in the wind tunnel. This technique is essential for obtaining true two-dimensional data for airfoils in the high-lift condition. It was used in a series of tests carried out to study the effect of leading-edge and trailing-edge devices on the aerodynamic characteristics of a 17% and a 10% thick airfoil.

Finally, comparisons of calculated and experimental data obtained on some of the complex configurations tested are presented to demonstrate the usefulness of the methods described here. How these methods can be used to design better high-lift systems is shown by discussing a Krüger leading-edge device which was designed with the aid of the vorticity distribution computer program. As predicted, significantly better high-lift performance was achieved with this device than with a slat which was designed by conventional methods and optimized in the wind tunnel.

2. A VORTICITY DISTRIBUTION METHOD FOR CALCULATING TWO-DIMENSIONAL POTENTIAL FLOW ABOUT MULTI-ELEMENT AIRFOILS

For the study of high-lift systems, a method was developed at Canadair which can calculate potential flow pressure distributions on airfoils of arbitrary thickness and camber with deflected leading-edge devices and multi-slotted flaps[1]. The method uses a continuous vortex distribution on the contour of each airfoil and is basically exact.

The two-dimensional inviscid incompressible flow around the airfoil is represented by superposition of a uniform flow U_∞ at an angle α to the x-axis and the flow induced by an infinitely long closed vortex sheet having the airfoil contour as a cross section (Fig.1). The distribution of vortex density $\gamma(s)$ along the contour is determined so that the resulting velocity from the superposition is tangential to the exterior surface of the contour at all points. The airfoil contour is assumed to be composed of small flat vortex sheet elements, each with a uniform density γ_ν which may vary from element to element.

A solution is obtained by specifying zero internal tangential velocity at the midpoint of each surface element s_μ. This tangential velocity is the sum of three components: the free stream, the integrated effect of all flat vortex sheet elements s_ν on μ and the velocity induced by the vorticity of element s_μ at its own midpoint. Martensen[2] has shown that for a closed body represented by a continuous vortex distribution on the surface, the condition of zero internal tangential velocity is equivalent to that of zero external normal velocity, and that the external tangential velocity $v(s)$ is equal to vortex density $\gamma(s)$. Martensen's approach leads to the following integral equation for the unknown velocity distribution on the airfoil surface:

$$\frac{v(s_\mu)}{2} + \oint v(s) K(s_\mu, s)\, ds = U_\infty \left[\cos\alpha \left(\frac{dx}{ds}\right)_\mu + \sin\alpha \left(\frac{dy}{ds}\right)_\mu \right] . \qquad (1)$$

For the numerical solution of Equation (1), Martensen replaced the continuous vortex distribution by isolated vortices at contour points chosen at equal intervals of an angular parameter. The same approach is used also by Jacob[3] who improved Martensen's method and developed the method for multiple airfoils.

In the present method, Equation (1) is first written as

$$v(s_\mu) + \oint v(s)K(s_\mu,s)\,ds = U_\infty\left[\cos\alpha\left(\frac{dx}{ds}\right)_\mu + \sin\alpha\left(\frac{dy}{ds}\right)_\mu\right] - \frac{v(s_\mu)}{2} \quad . \tag{2}$$

Equation (2) is replaced by a set of M linear equations for M flat vortex sheet elements representing the airfoil contour

$$\sum_{\nu=1}^{M} K_{\mu\nu}v_\nu = R_\mu \quad , \qquad \mu = 1,2,3,\ldots,M \quad , \tag{3}$$

where

$$R_\mu = U_\infty\cos\alpha\left(\frac{dx}{ds}\right)_\mu - U_\infty\sin\alpha\left(\frac{dy}{ds}\right)_\mu - \frac{v_\mu}{2} \quad .$$

$K_{\mu\nu}$ is an influence coefficient which is derived by considering the tangential velocity at the midpoint of element s_μ induced by a flat vortex sheet element s_ν of unit vortex density, $\gamma_\nu = 1$. From Figure 2 we obtain for the tangential velocity

$$v_{\mu\nu} = (v_{\xi\nu}\cos\beta + v_{\eta\nu}\sin\beta)\cos\delta + (v_{\eta\nu}\cos\beta - v_{\xi\nu}\sin\beta)\sin\delta \quad , \tag{4}$$

where

$$v_{\xi\nu} = \frac{\gamma_\nu}{2\pi}(\lambda_1 - \lambda_2) = \frac{\gamma_\nu}{2\pi}\epsilon \quad , \qquad v_{\eta\nu} = \frac{\gamma_\nu}{2\pi}\log_e\frac{r_1}{r_2} \qquad \text{(Reference 4).}$$

For $\gamma_\nu = 1$, Equation (4) gives the influence coefficient

$$K_{\mu\nu} = \frac{1}{2\pi}\left[\left[\log_e\frac{r_1}{r_2}\cos\beta - \epsilon\sin\beta\right]\sin\delta + \left[\log_e\frac{r_1}{r_2}\sin\beta + \epsilon\cos\beta\right]\cos\delta\right] \quad . \tag{5}$$

All the terms of Equation (5) can be calculated from the known x- and y-coordinates of elements s_μ and s_ν. For $\nu = \mu$, the velocity induced by a uniform vortex sheet element at a point close to its interior surface is $-\gamma_\mu/2$, so that the theoretical value of influence coefficient $K_{\mu\mu} = -1/2$. This means that one half of the total external tangential velocity at μ is due to the vorticity of elements s_μ alone. Therefore a simple way of improving the accuracy of the method is to adjust the $K_{\mu\mu}$ values by accounting for the curvature of the elements. By taking the midpoint of the curved rather than the flat element as the control point, we obtain

$$K_{\mu\mu} = -\frac{1}{2} \pm \frac{\theta}{4\pi} \quad , \tag{6}$$

where θ is the subtending angle of circular arc s_μ. The positive sign is for convex and the negative for concave elements.

The system of Equations (3) is solved for three basic flows, two translatory and a pure circulatory flow, i.e.

(a) for $U_\infty = 1$, $\alpha = 0^\circ$ and $v_\mu = 0$ (no circulation)

$$R_\mu^{(a)} = \frac{x_{\mu 1} - x_{\mu 2}}{s_\mu} \quad .$$

(b) for $U_\infty = 1$, $\alpha = 90^\circ$ and $v_\mu = 0$

$$R_\mu^{(b)} = \frac{y_{\mu 1} - y_{\mu 2}}{s_\mu} \quad ,$$

(c) for $U_\infty = 0$, $v_\mu = 1$ (pure circulation, uniform velocity distribution)

$$R_\mu^{(c)} = -\frac{1}{2} \quad .$$

This results in three sets of velocity distributions, i.e. $v_\nu^{(a)}$, $v_\nu^{(b)}$ and $v_\nu^{(c)}$. These are superimposed after being corrected for the proper angle of attack α and proper circulation, to obtain the total tangential velocity distribution

$$v_\nu = v_\nu^{(a)} \cos\alpha + v_\nu^{(b)} \sin\alpha + v_\nu^{(c)} c_{\Gamma} \quad , \tag{7}$$

$$\nu = 1,2 \ldots M \quad .$$

The correction factor c_Γ for the proper value of circulation is determined by satisfying the Kutta condition as follows: the tangential velocities at the midpoints of the upper and lower surface elements adjacent to the trailing edge are set to be equal, i.e.

$$v_1 = v_M \qquad \text{or} \qquad v_1 + v_M = 0 \quad . \tag{8}$$

Applying this condition to the three basic flows gives

$$(v_1 + v_M)^{(a)} \cos\alpha + (v_1 + v_M)^{(b)} \sin\alpha + (v_1 + v_M)^{(c)} c_\Gamma = 0 \quad ; \tag{9}$$

hence

$$c_\Gamma = \frac{(v_1 + v_M)^{(a)} \cos\alpha + (v_1 + v_M)^{(b)} \sin\alpha}{(v_1 + v_M)^{(c)}} \quad . \tag{10}$$

The velocity distribution is then used for calculating the pressure distribution,

$$C_p = 1 - v_\nu^2 \quad , \qquad \nu = 1,2 \ldots M \quad , \tag{11}$$

and the lift coefficient for reference chord $\bar{c}$,

$$C_L = -\frac{2 \sum_{\nu=1}^{M} v_\nu s_\nu}{\bar{c}} \quad . \tag{12}$$

The x- and y-force coefficients and the moment coefficients are obtained by numerical integration of the pressure distribution.

For multiple airfoils the number of flat vortex sheet elements is increased to represent each airfoil by a closed contour and the approximate Kutta condition is applied to each airfoil. In addition one must consider the influence of all the circulations on the Kutta condition of each airfoil.

The method has been programmed in Fortran IV for the IBM 360 digital computer and is now being used for the analysis and design of complex high lift configurations. For input, the program requires only the coordinates of the airfoil contour and the angle of attack. With additional input information, it can also transform, translate and rotate the coordinates of each airfoil to achieve the desired geometry of the configuration. The program output consists of tabulated velocity and pressure distributions, forces and pitching moment and two graphical representations, the input geometry of the configuration and the plotted pressure distribution.

The program can handle problems with up to 8 airfoils and 500 coordinate points. Typical examples are 50 to 70 coordinate points for single airfoils, 130 points for a three-element airfoil and 200 points for a five-element airfoil. Computation time ranges from less than one minute for the first example to two minutes for the last example, and increases only insignificantly if calculation of more than one angle of attack is required.

Figure 3 shows a comparison of the present method with exact theory for a 13% thick, high camber airfoil, derived by Kármán-Trefftz transformation, at a 10° angle of attack. It can be seen that the pressure distribution and the lift coefficient obtained with the present method agree very well with the exact values.

The capability of the computer program to handle up to 8 airfoils is demonstrated in Figure 4 which shows the calculated ground effect on the pressure distribution of a real arbitrary four-element airfoil configuration. The first element consists of a truncated NACA 4417 airfoil with a Krüger flap leading edge device. The remaining elements form a 35% triple-slotted flap deflected 70 degrees. The dotted line shows the pressure distribution calculated for this airfoil configuration alone at zero angle of attack. The pressure distribution for the same airfoil configuration near the ground was calculated by using for input an 8-body system consisting of the four-element airfoil and its reflection in the ground plane.

3. WIND TUNNEL TESTING TECHNIQUE

One of the objectives of the Canadair high lift research was to obtain reliable experimental data, representative of true two-dimensional flow, for airfoils with various leading edge devices and trailing edge slotted flaps. These data were needed for comparison with calculated results in order to check the accuracy of the multi-element analysis method described above and to establish its range of applicability.

Wind tunnel testing of high lift systems presents problems that are caused first by the presence of high aerodynamic loads and second by the complexity of the model. Large pressure gradients created by the airfoil in the high lift condition cause separation of the wall boundary layer. This separation and the resulting system of trailing vortices affect the two-dimensionality of the flow around the airfoil and create a large increase in induced drag, thus making the test data doubtful. Additional problems are introduced when a large span high lift model is used. Slats and vanes of such models being very thin may bend easily under aerodynamic forces, thus distorting the geometry of the gaps and, therefore, the flow in the slots. The alternative is to provide such elements with intermediate supports but these again are undesirable because they obstruct the flow in the slots. Finally large span models which may consist of up to five airfoil elements are difficult to handle and, therefore, time consuming when many configuration changes are to be made in the tunnel. On the other hand, a small span model, although desirable from a practical point of view, is unfavourable for two-dimensional high lift testing because of the wall flow separation problem. By using a blowing technique, it is possible to prevent flow separation from the wall and to obtain good two-dimensional data by using a small span model. For this purpose a wall blowing facility (Figures 5 and 6) was designed and built by Canadair for testing 2-foot chord by 3 foot span high lift models.

The walls are provided with fixed slots ahead of the model and rotatable slots arranged vertically to the upper surface of the airfoil. Compressed air is blown through the slots to help the airflow along the wall into a curved path parallel to the upper surface of the airfoil and prevent it from separating from the wall. With this facility, rapid changes of slot geometry and flap angle can be made in the tunnel so that the effects of such changes on high lift performance can be studied in an efficient manner.

Canadair has conducted extensive wind tunnel testing with the wall blowing facility installed in the test section of the NAE 6-foot by 9-foot Low Speed Wind Tunnel of the National Research Council in Ottawa. Twenty configurations including single, double and triple slotted flaps in combination with leading edge slats, droop noses and Krüger flaps were tested with a modified NACA 4418 and fifty five similar configurations with a NACA 64A210.

Figures 7 and 8 show typical data obtained from these tests. They are balance measurements for two configurations with a triple slotted flap, one with the cruise leading edge (slat in retracted position) and the other with extended slat. The data with no blowing shows a reduction in lift slope and $C_{l\,max}$ associated with a large increase in drag as a result of the wall boundary-layer separation. With wall blowing on, the lift slopes agree well with those of potential flow calculated with the method described above. Also the drag polars display true two-dimensional flow characteristics as they remain vertical over a larger range of C_l with wall blowing.

4. COMPARISON OF CALCULATIONS WITH EXPERIMENT

The capability of the potential flow method and its usefulness as a design tool may be demonstrated by comparing the calculated pressure distributions with experimental data obtained during the wind tunnel tests.

Figure 9 shows how well the present method can predict the real flow pressure distribution at 20° flap deflection. Notice that both theory and experiment show that the changes at the leading edge have practically no effect on the pressure distribution from 40% chord downstream.

For configurations with highly deflected flaps and slats as in Figure 10, the experimental data shows separation from the upper surface of the rear flap, and separation and reattachment at the lower surface of the slat. In the regions of separated flow, the calculated pressure distribution does not agree with the experimental data. Also on the upper surface of the slat there is no agreement between calculated and experimental pressure distributions. Between the slat and the rear flap separation point (approximately at 90% chord), the experimental data follows the potential flow pressure distribution although at a much lower value. The experimental and potential flow lift coefficients for this configuration are shown in Figure 8.

It is difficult to explain the differences between the experimental and potential flow pressure distributions in Figure 10 without examining also the results at various other angles of attack. The analysis of such data indicate that the rear flap flow separation causes a reduction of the effective angle of attack which affects the pressure distribution on the slat and the main section. For the case of Figure 10, for example, the experimental pressure distribution agrees well with that of potential flow at 0° angle of attack. The pressure distribution on the fore flap and the vane, however, is not affected directly by the rear flap flow separation and the associated reduction in effective angle of attack. The difference between experiment and theory in this case may be due to the interaction of the boundary layers of the fore flap and vane with a rather thick wake from the main section.

5. DESIGN OF A LEADING EDGE DEVICE

A specific attempt to demonstrate the usefulness of the Canadair potential flow program as a design tool was successful. A leading edge device was designed which is superior to any other leading edge device designed by conventional methods and optimized in the tunnel. The geometry of this leading edge device was derived by using initially a conventional design of a 20% Krüger flap in conjunction with a 35%-chord double slotted flap deflected at a 55° angle. The velocity and pressure distribution for this configuration were computed for 0°, 5°, 10°, 15°, 20° and 25° angle of attack. The results were then examined to determine the change of peaks, gradients and overall smoothness of distribution with angle of attack. Using an iterative procedure, the camber and leading edge diameter of the Krüger flap were then increased methodically in order to lower the peaks and obtain a reasonably smooth velocity distribution throughout the α-range and particularly at an α of 20°. The final geometry was obtained after eight consecutive computer runs resulting in a configuration with a higher theoretical lift coefficient than the original one. This Krüger flap was tested also as a Krüger slat in the wind tunnel along with a 30° droop nose, a conventional slat and a rotatable nose slat. The latter was derived by rotating the nose of the conventional slat about 60° down in order to increase the camber. Both the conventional and the rotatable nose slats have been developed earlier and are now used on an advanced type aircraft. Figures 11 and 12 show the effect of the various leading edge devices on the lift and drag of a NACA 64A210 with a double slotted flap deflected at 37.5° angle, as measured in the tunnel. As predicted, the Krüger flap and slat designed with the aid of the potential flow method show significantly better high lift performance than the rotatable nose slat which was the best of the leading edge devices developed by conventional methods.

Figure 13 shows a comparison between experimental and computed potential flow pressure distributions for a NACA 64A210 with the Krüger flap described above and a triple slotted flap deflected 40°, at 16.36° angle of attack. The close agreement of the experimental and theoretical pressure distributions at such a high angle of attack and lift coefficient ($C_L \simeq 5.0$) indicates an efficient leading edge and trailing edge flap design. For example, the lift coefficient measured in the tunnel for this case was 94% of that calculated for potential flow, as compared with 81% for the case of Figure 10. At the nose of the Krüger flap, the disagreement of experimental and calculated pressure distributions indicates local flow separation and reattachment, i.e. the formation of a bubble, which has little effect on the pressure distribution and lift coefficient of the entire configuration.

6. CONCLUSIONS

Comparisons of calculations with experimental results show that potential flow agrees well with real flow over a large range of conditions. Viscosity does not significantly affect the surface pressure distribution except in the region of separation. Local flow separation and reattachment has a negligible effect on the pressure distribution of a high lift configuration. Flow separation from the rear flap of a multi-element airfoil appears to cause a reduction of the effective angle of attack which lowers the potential flow pressure distribution on the leading edge element and the main section. The difference between experimental and theoretical pressure distributions on the flap elements upstream from the separation region may be due to the interaction of the boundary layers of these elements with the wake from the main section. Since compressibility effects on the surface pressure distribution are negligible for flight Mach numbers below 0.3, it is concluded that for the range of flow conditions which is of interest to take off and landing, potential flow is a useful approximation. The vorticity distribution computer method described here is therefore a useful means for the analysis and optimization of high lift systems. The method can also be used for the design of high lift configurations as it was demonstrated here with the example of a Krüger flap with which lift coefficients in excess of 5.0 were achieved in the wind tunnel.

Wind tunnel testing of high lift systems requires boundary-layer control of the flow along the walls to assure good quality experimental data. Experience with the Canadair flowing wall facility shows that the wall blowing technique is an essential and effective means for two-dimensional wind tunnel testing of multi-element high lift airfoil models.

REFERENCES

1. Mavriplis, F. *A Vorticity Distribution Method for Calculating Two-Dimensional Potential Flow about Arbitrary Multi-Element High Lift Airfoils.* Canadair Report No.ERR-RAZ-000-303.

2. Martensen, E. *Die Berechnung der Druckverteilung an dicken Gitterprofilen mit Hilfe von Fredholmschen Integralgleichungen zweiter Art.* Mitteilung aus der Max-Planck-Institut für Strömungsforschung und der Aerodynamischen Versuchsanstalt No.23, Göttingen, 1959.

3. Jacob, K. *Die Berechnung der Potentialströmung um mehrere Profile mit gegenseitiger Beeinflussung.* Mitteilungen aus der Max-Planck-Institut für Strömungsforschung und der Aerodynamischen Versuchsanstalt No.27, Göttingen, 1962.

4. von Mises, R. *Theory of Flight.* Dover Publications.

NOTATION

c	reference or chord length
$c_{l'}$	correction factor for circulation
c_l	lift coefficient
c_p	pressure coefficient = $(p - p_0)/(\rho/2)U_\infty^2$
$K_{\mu\nu}$	influence coefficient (matrix element); influence of vortex sheet element s_ν on tangential velocity at control point μ
$K_{\mu\mu}$	influence coefficient (diagonal matrix element); influence of vortex element s_μ on tangential velocity at control point μ
M	number of vortex sheet elements representing the airfoil contour. Number of control points
r	distance between two points
R	righthand member of a system of linear equations
s	distance round the airfoil surface
s_μ, s_ν	lengths of vortex sheet elements with midpoints μ and ν
U_∞	free stream velocity
v_μ	velocity tangential to surface at control point μ (positive direction counterclockwise)
$v_\nu^{(a)}$, $v_\nu^{(b)}$, $v_\nu^{(c)}$	tangential velocity distributions obtained from three basic solutions: (a) parallel to x-axis, no circulation, (b) normal to x-axis, no circulation, (c) pure circulation
v_ν	total tangential velocity distribution
x,y	Cartesian coordinates
α	free stream angle to x-axis
β	angle between x-axis and influencing vortex sheet element (s_ν)
$\gamma(s)$	vortex strength per unit length of perimeter
γ_ν	vortex strength of flat vortex sheet element s_ν
δ	angle between x-axis and surface element of control points (s_μ)
ϵ	angle between the two limiting radii r_1 and r_2 from vortex sheet element s_ν to control point μ (Fig.2)
θ	subtending angle of a circular arc approximating airfoil curved element s_μ
λ_1, λ_2	angles between surface coordinate ξ_ν of element s_ν and radii r_1 and r_2
μ, ν	midpoints of elements s_μ and s_ν
ξ, η	surface coordinates, tangential and normal
ρ	fluid density

Subscripts

∞	free stream
1	first point on airfoil surface starting from trailing edge counterclockwise
2	second point on airfoil surface counterclockwise

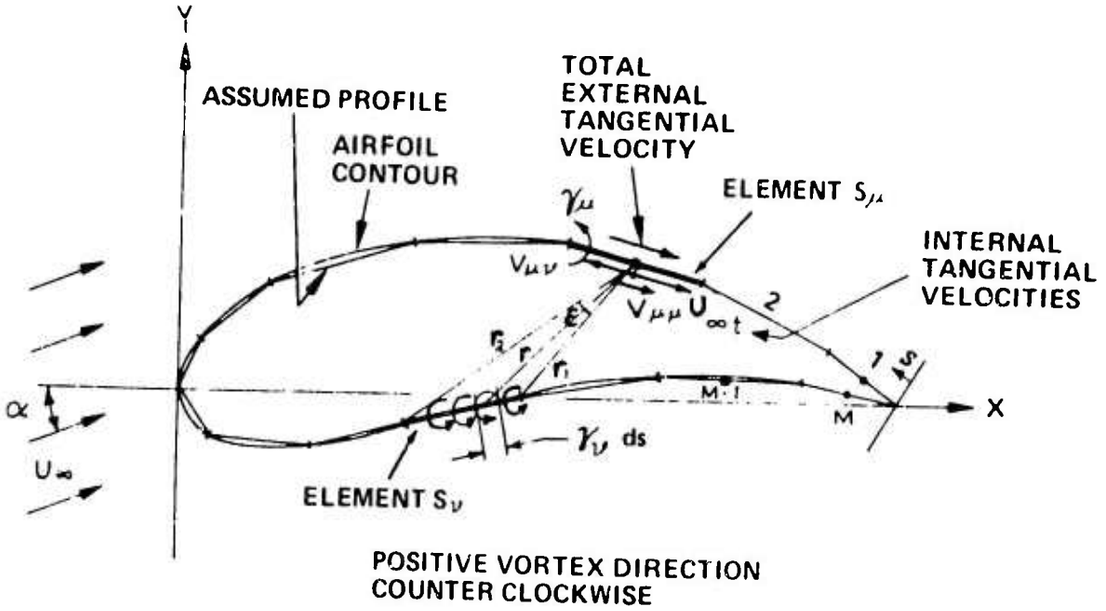

Fig.1 Representation of airfoil section by vortex sheet elements

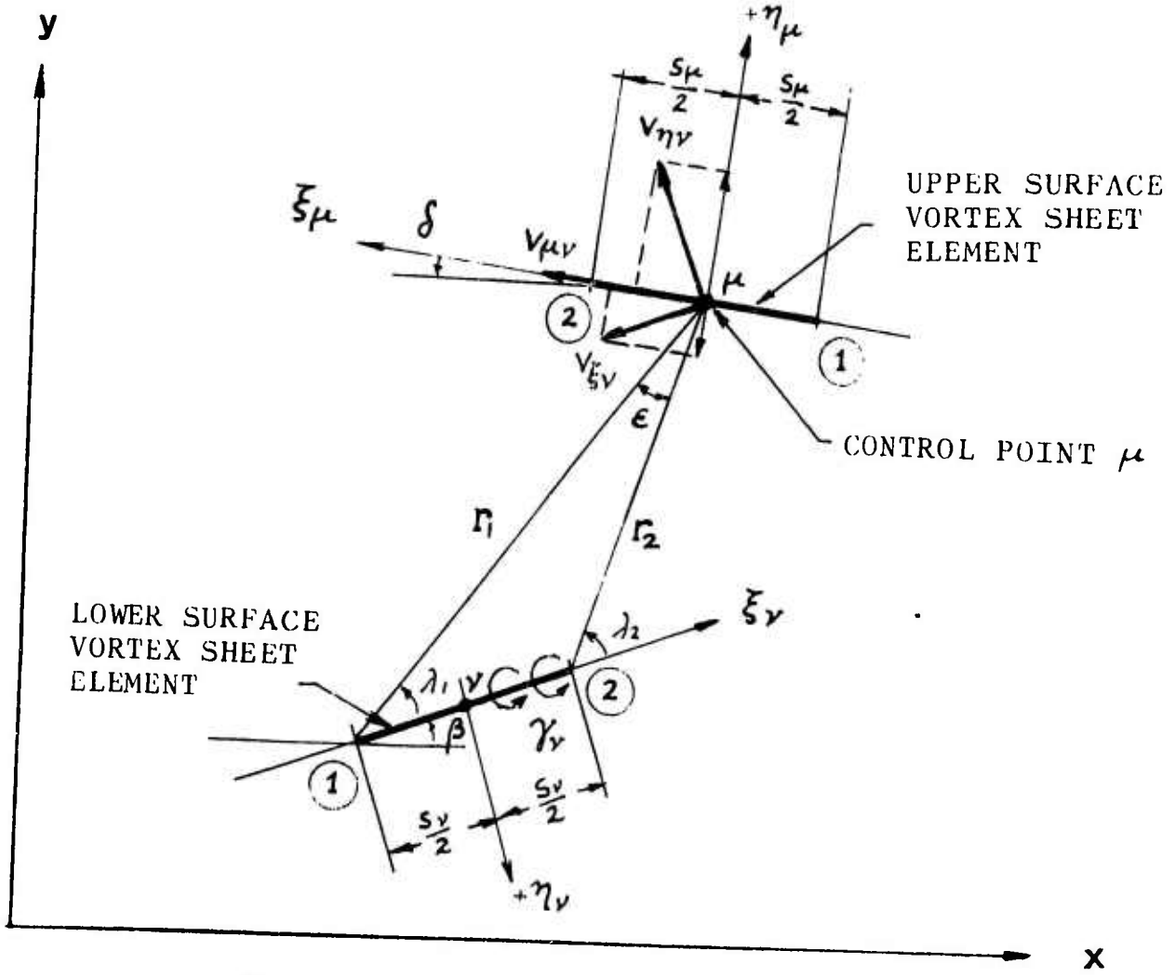

Fig.2 Velocities induced at control point by vortex sheet element

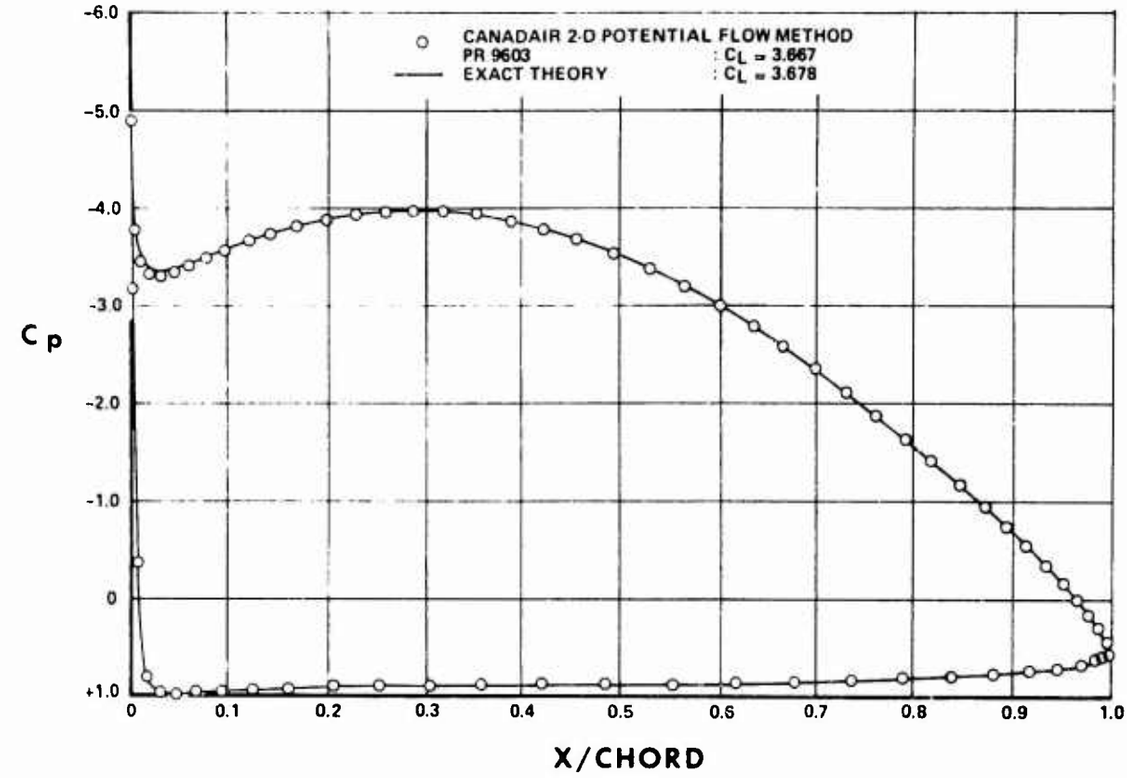

Fig.3 Theoretical pressure distribution on a 13% thick high camber Kármán-Trefftz airfoil, $\alpha = 10^\circ$

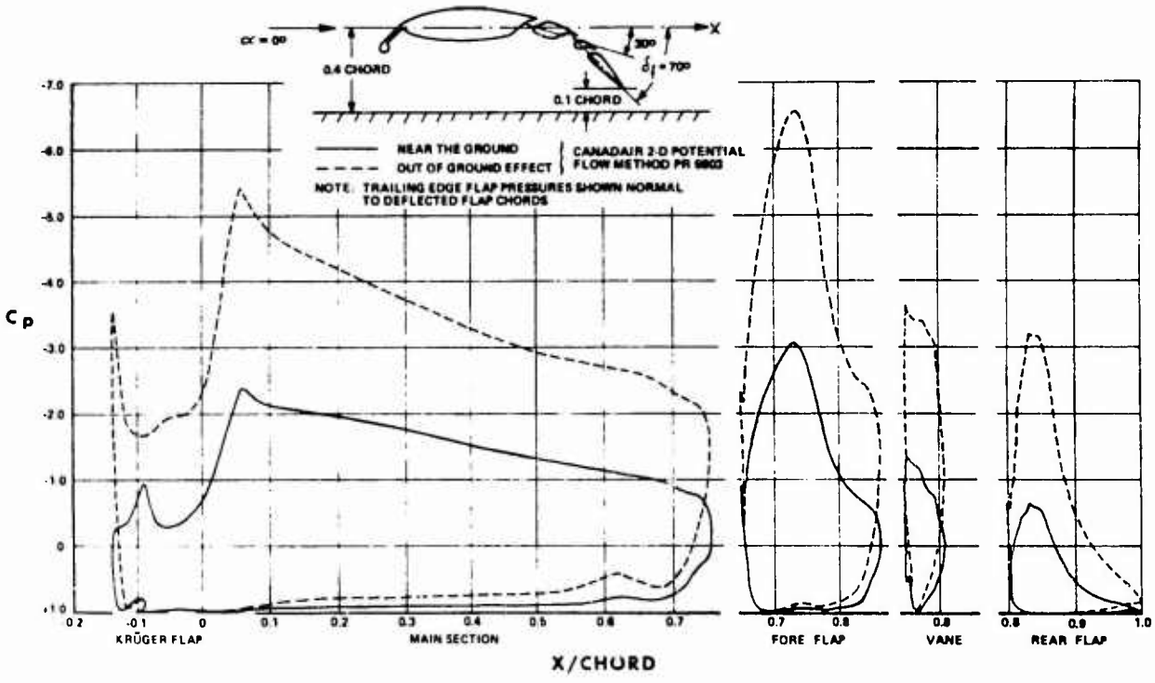

Fig.4 Theoretical pressure distributions on a modified NACA 4418 with deflected triple slotted flap and Krüger flap close to the ground and out of ground effect

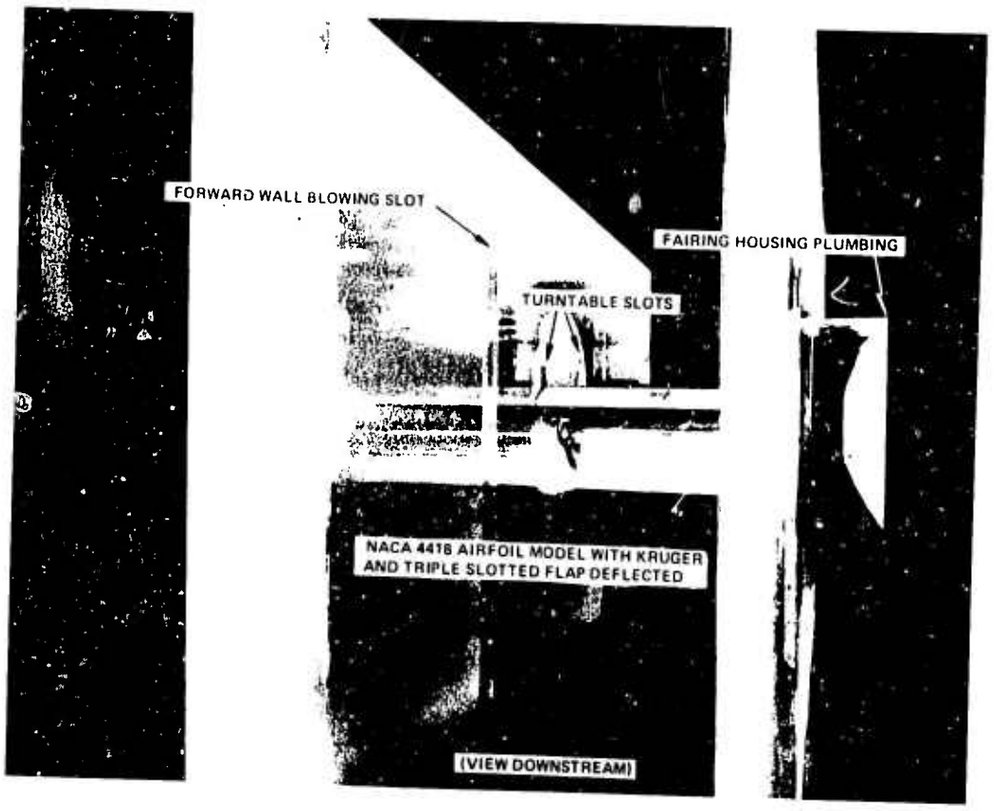

Fig.5 Blowing wall facility with 2-D high lift model

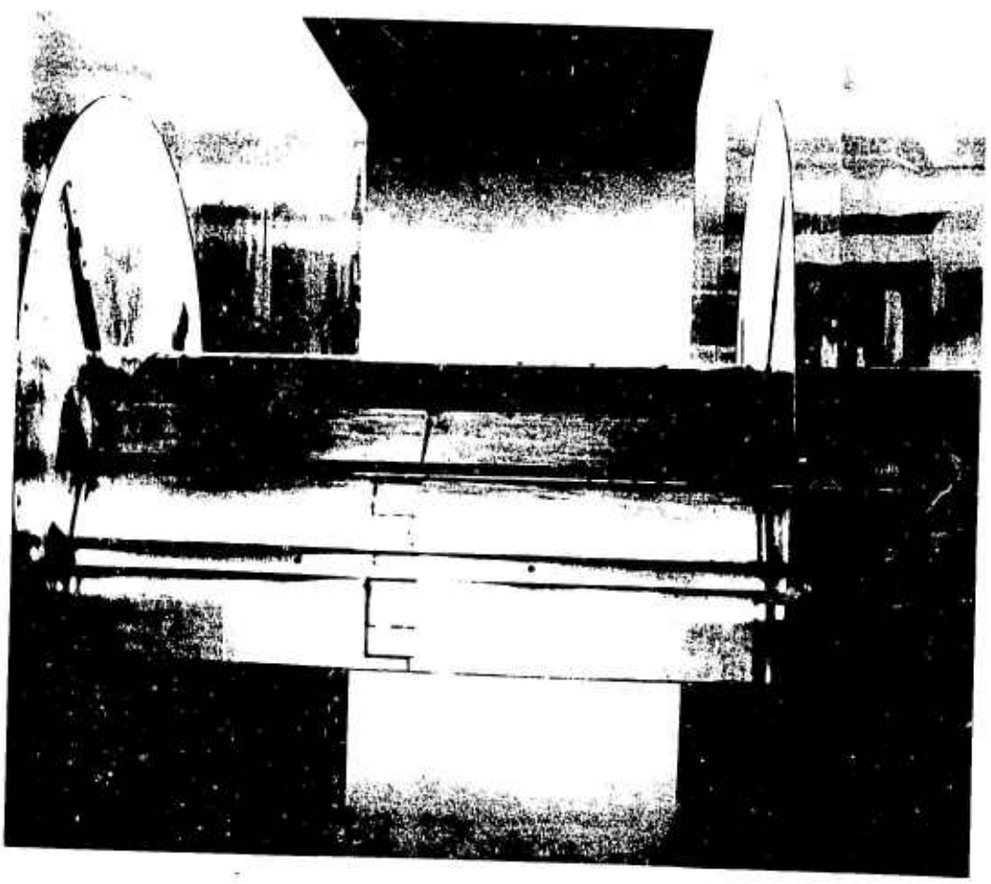

Fig.6 2-D high lift model and wall blowing slot arrangement

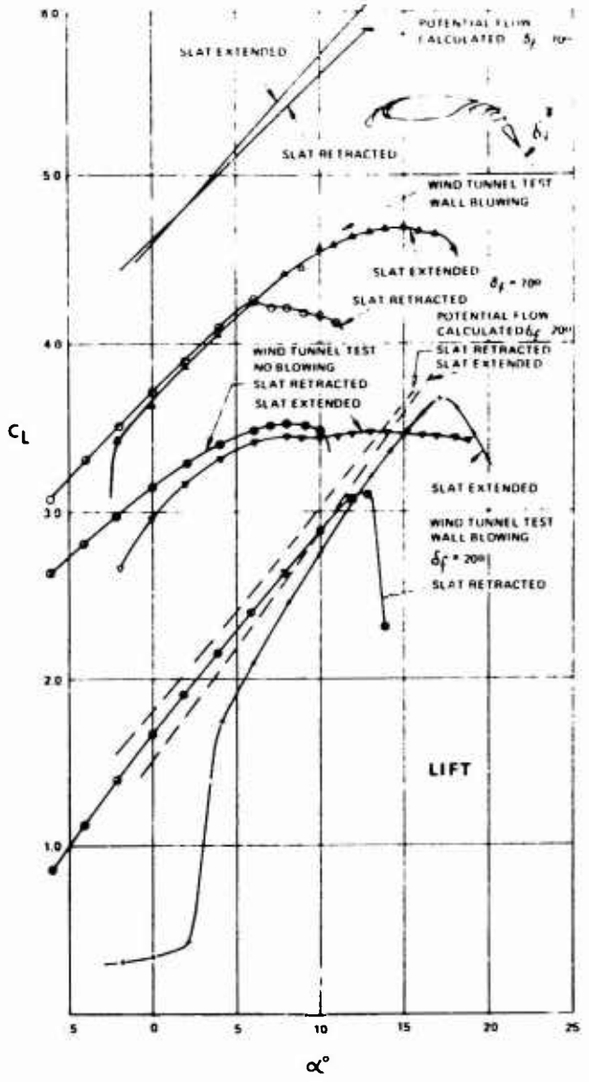

Fig.7 Effect of wall blowing on lift of NACA 4417 with high lift devices

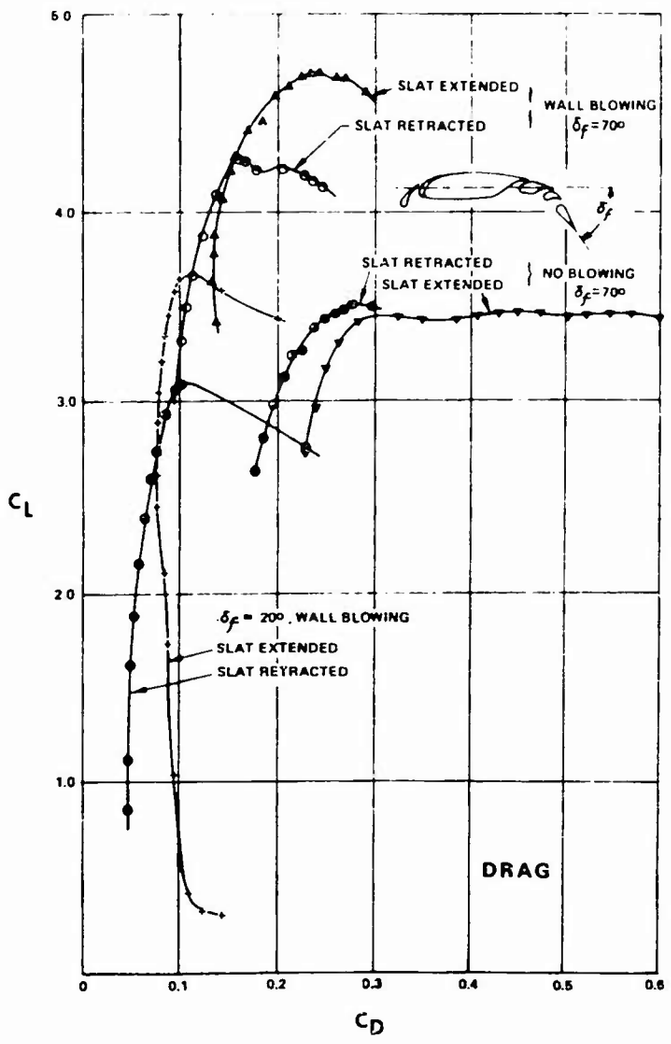

Fig.8 Effect of wall blowing on drag of NACA 4417 with high lift devices

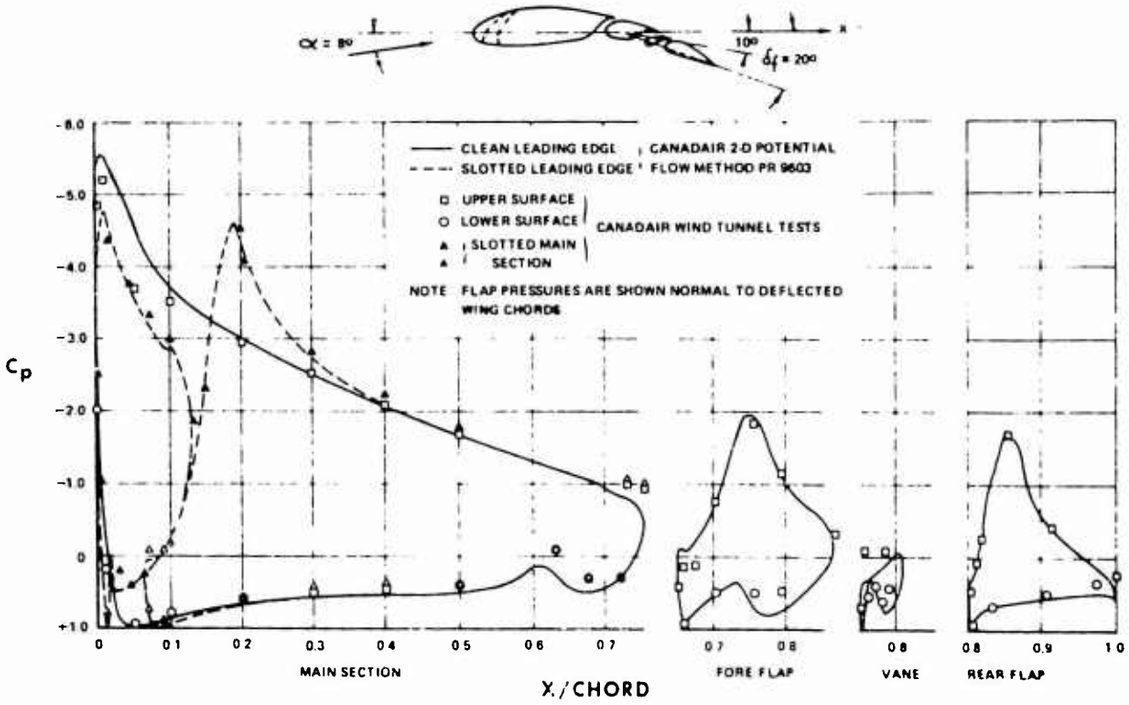

Fig.9 Theoretical and experimental pressure distributions on NACA 4417 with deflected triple slotted flap - Effect of leading edge slot

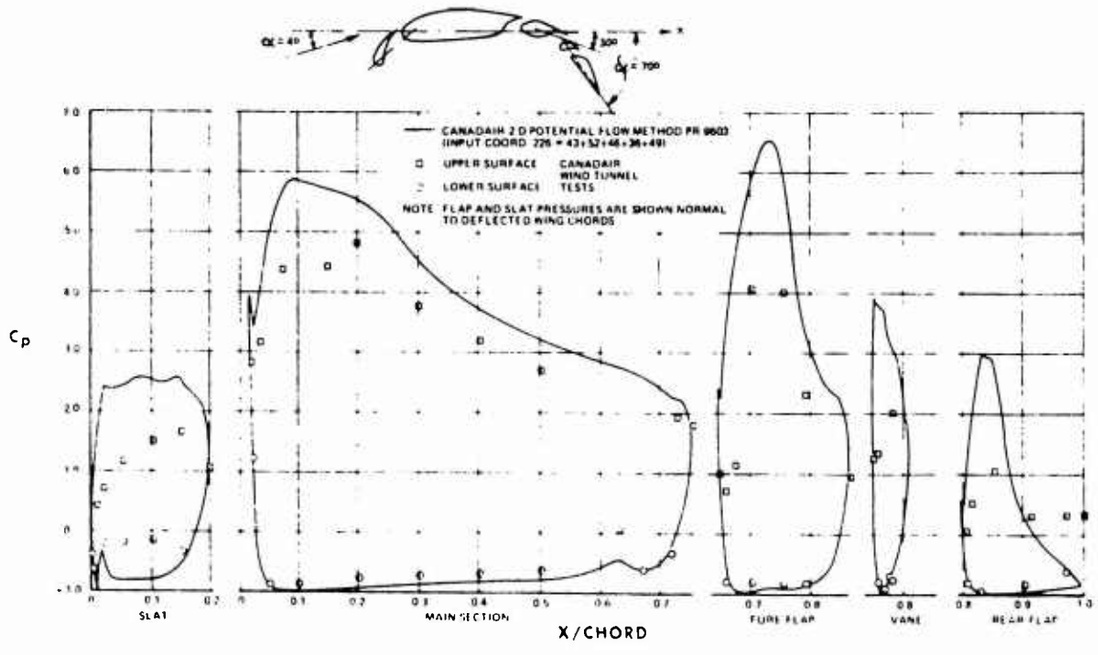

Fig.10 Theoretical and experimental pressure distributions on NACA 4417 with deflected slat and triple slotted flap

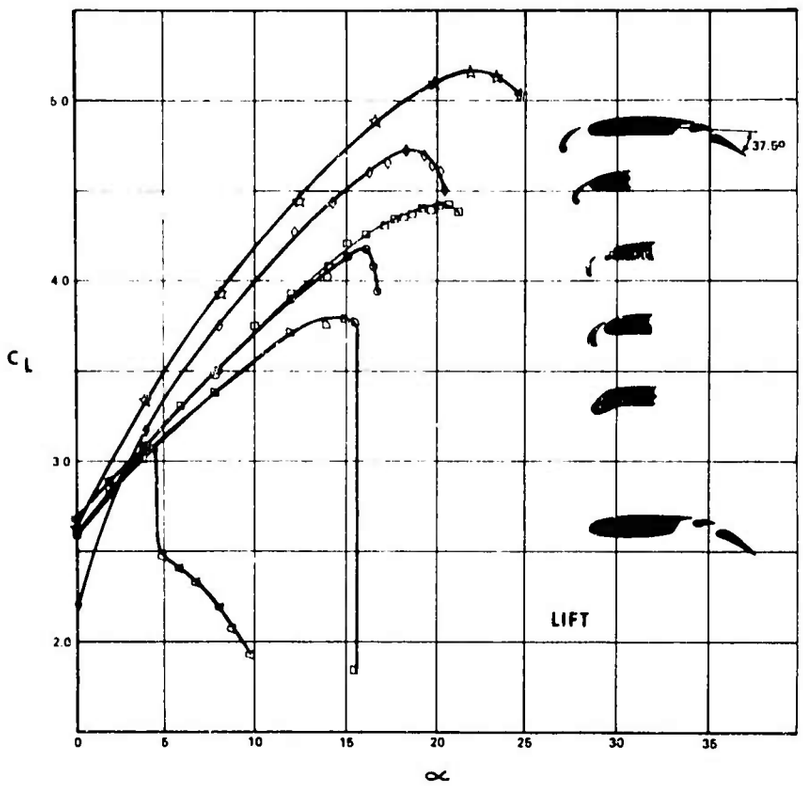

Fig.11 Effect of leading edge devices on lift of NACA 64A210 with double slotted flap. Canadair 2-D wind tunnel test results

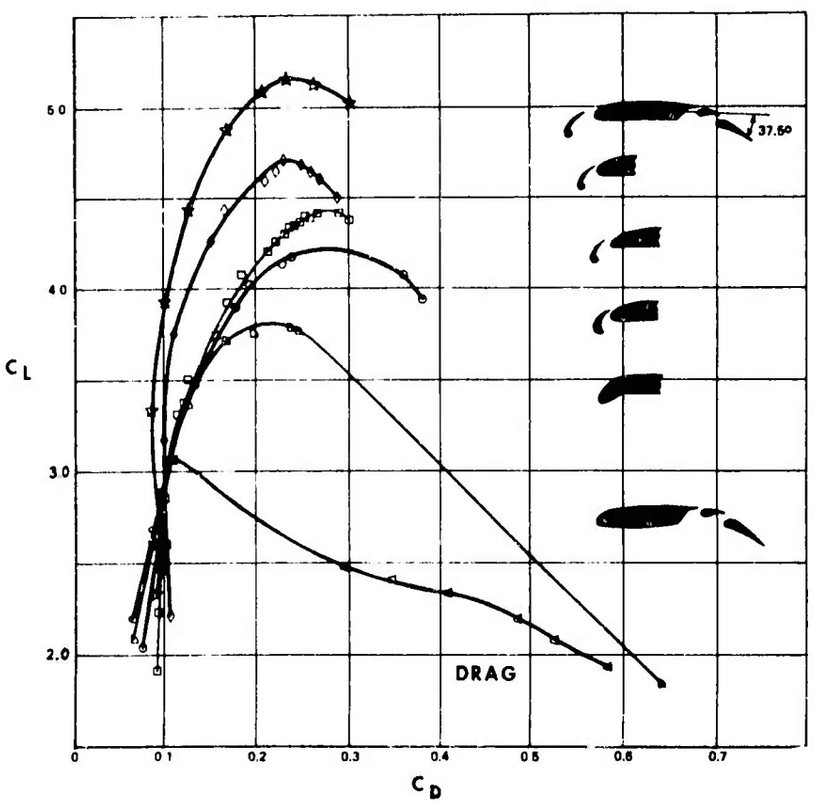

Fig.12 Effect of leading edge devices on drag of NACA 64A210 with double slotted flap. Canadair 2-D wind tunnel test results

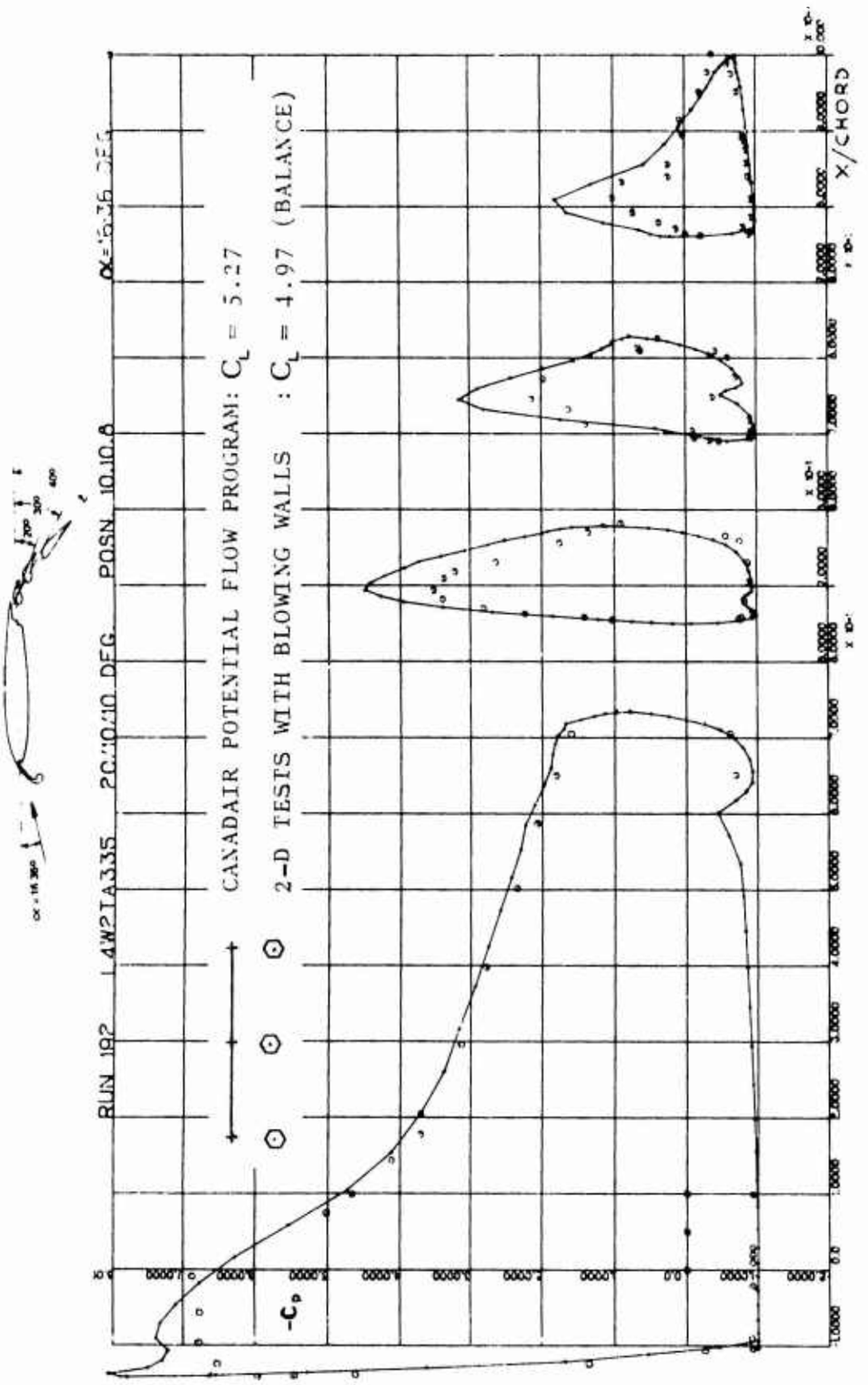

Fig.13 Comparison of theoretical and experimental pressure distributions at α = 16.36 ° of a configuration with Krüger flap and triple slotted flap TA335 deflected 40